

RISØ

DK 990 1377

Risø-R-1114(EN)

MASTER

**Contributions from the Department of
Wind Energy and Atmospheric Physics
to EWEC '99 in Nice, France**

RECEIVED
JUN 04 1999

OST

Edited by Gunner C. Larsen, Kirsten Westermann and Per
Nørgård

DISTRIBUTION OF THIS DOCUMENT IS UNLIMITED
FOREIGN SALES PROHIBITED
al

Risø National Laboratory, Roskilde, Denmark
March 1999

DISCLAIMER

Portions of this document may be illegible in electronic image products. Images are produced from the best available original document.

Database Input

SEND TO: Energy Technology Data Exchange
P.O. Box 1000
Oak Ridge, Tennessee 37831 USA
Atten: Data Control

Date dispatched:

Total number of records in this input file: _____

Total number of records in this input file: _____

Internal label on tape: ☐ yes ☐ no

Date hardcopy dispatched: DK99/09
1999.05.27

Date hardcopy received by OA: _____

NOTE: Please supply a report number and TRN number for each hardcopy document accompanying this input file.

Report Number	TRN	Report Number	TRN
RISO-R-1114(EN)	DK9901377		

Input Acknowledgment: Signature: _____ Date received: _____

Contributions from the Department of Wind Energy and Atmospheric Physics to EWEC '99 in Nice, France

**Edited by Gunner C. Larsen, Kirsten Westermann and Per
Nørgård**

Content

Plenary Sessions

<i>Policy Instruments for Regulating the Development of Wind Power in a Liberated Electricity Market (PLA2.2)</i> P.E. Morthorst	7
<i>Improved Power Performance Assessment Methods (PLB1.2)</i> Sten Frandsen et al.	13
<i>Implementation of Short-Term Prediction (PLD1.2)</i> L. Landberg et al.	17
<i>Status of Standardisation in IEC and CENELEC (PLD1.4)</i>	23
<i>Global Perspectives for Wind Power (PLE1.2)</i> Per Dannemand Andersen	27

Oral Sessions

<i>A Soft Rotor Concept - Design, Verification and Potentials (OB2.2)</i> Flemming Rasmussen and Jørgen Thirstrup Petersen	31
<i>Offshore Wind Farm Bockstigen - Installation and Operation Experience (OB2.6)</i> Bernhard Lange et al.	35
<i>Wind Power and a Liberalised North European Electricity Exchange (OB3.2)</i> Lars Henrik Nielsen et al.	41
<i>Classification of Operational Characteristics of Commercial Cup-Anemometers (OB4.1)</i> Troels Friis Pedersen, Uwe Schmidt Paulsen	45
<i>Is the Nacelle-Mounted Anemometer an Acceptable Option in Performance Testing? (OB4.4)</i> Jan-Åke Dahlberg et al.	51
<i>Harmonisation of Wind Turbine Certification in Europe - JOULE Project EWTC (OC1.5)</i> Christian Nath et al.	57
<i>European Wind Turbine Standards II - EWTS-II (OC1.6)</i> J.T.G. Pierik et al.	63
<i>Experimental Verification of the New RISØ-A1 Airfoil Family for Wind Turbines (OC2.2)</i> Kristian S. Dahl, Peter Fuglsang, Ioannis Antoniou	67
<i>Derivation of Airfoil Characteristics for the LM 19.1 Blade Based on 3D CFD Rotor Calculations (OC2.3)</i> Christian Bak, Niels N. Sørensen, Helge A. Madsen	71
<i>Prodeto, A Computer Code for Probabilistic Fatigue Design (OC4.1)</i> H. Braam, C.J. Christensen, K.O. Ronold, M.L. Thøgersen	75
Risø-R-1114(EN)	3

<i>Experimental Investigation of Ultimate Loads (OC4.2)</i> S.M. Petersen, G.C. Larsen, I. Antoniou, S.O. Lind, M. Courtney	81
<i>Prediction of Induced Vibrations in Stall (OC4.3)</i> Jørgen Thirstrup Petersen, Kenneth Thomsen, Helge Aagaard Madsen	85
<i>Turbulence in Complex Terrain (OD1.2)</i> Jakob Mann	89
<i>Modelling of Extreme Gusts for Design Calculations (NewGust) (OD1.3)</i> Wim Bierbooms, Po-Wen Cheng, Gunner Larsen, Bo Juul Pedersen, Kurt Hansen	93
<i>The Economic Value of Accurate Wind Power Forecasting to Utilities (OD1.6)</i> S.J. Watson, G. Giebel, A. Joensen	97
<i>The Irish Wind Atlas (OD3.2)</i> Rick Watson, Lars Landberg	101
<i>Offshore Wind Resources at Danish Measurement Sites (OD3.3)</i> R.J. Barthelmie et al.	105
<i>A Methodology for the Prediction of Offshore Wind Energy Resources (OD3.4)</i> S.J. Watson et al.	109
<i>Modelization of a Large Wind Farm, Considering the Modification of the Atmospheric Boundary Layer (OD3.5)</i> A. Crespo, S. Frandsen, R. Gómez-Elvira, S.E. Larsen	113
<i>Standards for Measurements and Testing of Wind Turbine Power Quality (OD4.1)</i> Poul Sørensen et al.	117

Poster Sessions

<i>Possibilities for Wind Energy on the Kola Peninsula (PB1.6)</i> J. Wolff et al.	121
<i>Effects of Distributing Wind Energy Generation over Europe (PB2.11)</i> Gregor Giebel	125
<i>Wind Turbines - Facts from 20 Years of Technology Progress (PB2.25)</i> Lars Henrik Hansen, Per Dannemand Andersen	129
<i>European Wind Turbine Testing Procedure Development - Blade Test Methods and Techniques (PB3.17)</i> B.H. Bulder	133
<i>Wind Turbine Certification - The Committee Draft by IEC-TC88-WG9 (PB3.18)</i> Peter Hauge Madsen, William E. Holley	137
<i>HTTP:\WWW.Winddata.com/ (PB4.5)</i> Kurt S. Hansen, Michael S. Courtney	141
<i>Design Off-Shore Wind Climate (PB4.9)</i> Gunner C. Larsen, Hans E. Jørgensen	145
<i>Non-Gaussian Turbulence (PB4.16)</i> J. Højstrup, K.S. Hansen, B.J. Pedersen, M. Nielsen	149

<i>Danish Extreme Wind Atlas: Background and Methods for a WAsP Engineering Option</i> (PB4.17)	
Ole Rathmann, Leif Kristensen, Jakob Mann, Svend Ole Hansen	153
<i>Relative Performance of Different Numerical Weather Prediction Models for Short Term Prediction of Wind Energy</i> (PB4.22)	
Gregor Giebel, Lars Landberg, Kai Mönnich, Hans-Peter Waldl	157
<i>Operational Results from a Physical Power Prediction Model</i> (PB5.5)	
Lars Landberg	161
<i>A New Measure-Correlate-Predict Approach for Resource Assessment</i> (PB5.19)	
A. Joensen, L. Landberg, H. Madsen	165
<i>A Detailed and Verified Wind Resource Atlas for Denmark.</i> (PB5.20)	
N.G. Mortensen, P. Nielsen, L. Landberg, O. Rathmann, M.N. Nielsen	169
<i>WAsP for Offshore Sites in Confined Coastal Waters - The Influence of the Sea Fetch</i> (PB5.21)	
Bernhard Lange, Jørgen Højstrup	173
<i>Model Output Statistics Applied to Wind Power Prediction</i> (PB5.24)	
A. Joensen, G. Giebel, L. Landberg, H. Madsen, H. Aa. Nielsen	177
<i>Wind Resource Modelling for Micro-Siting - Validation at a 60-MW Wind Farm Site</i> (PB5.25)	
Jens Carsten Hansen, Niels Gylling Mortensen, Usama Said Said	183
<i>A Linear Model for Flow over Complex Terrain</i> (PB5.30)	
Helmut P. Frank	187
<i>The Influence of Waves on the Offshore Wind Resource</i> (PB5.37)	
Bernhard Lange, Jørgen Højstrup	191
<i>Optimal Parameters for the FFA-Beddoes Dynamic Stall Model</i> (PB6.10)	
Anders Björck, Murat Mert, Helge A. Madsen	195
<i>Aeroelastic Stability of Airfoil Flow Using 2-D CFD</i> (PB6.11)	
J. Johansen	201
<i>Design of the New RISØ-A1 Airfoil Family for Wind Turbines</i> (PB6.15)	
Peter Fuglsang, Kristian S. Dahl	205
<i>The Influence on Energy Conversion and Induction from Large Blade Deflections</i> (PB6.16)	
Helge Aagaard Madsen, Flemming Rasmussen	209
<i>Study of Blade-Tower Interaction Using a 2D Navier-Stokes Solver</i> (PB6.28)	
Franck Bertagnolio	213
<i>When Real Life Wind Speed Exceeds Design Wind Assumptions</i> (PB7.1)	
Martin Winther-Jensen, Erik R. Jørgensen	217
<i>Variability of Extreme Flap Loads during Turbine Operation</i> (PB7.2)	
Knut O. Ronold, Gunner C. Larsen	221
<i>Grid Impact of Variable-Speed Wind Turbines</i> (PB8.13)	
Åke Larsson, Poul Sørensen, Fritz Santjer	225

<i>Lightning Protection of Wind Turbines</i> (PB8.20) T. Sørensen et al.	229
<i>Improving Transition between Power Optimization and Power Limitation of Variable Speed/Variable Pitch Wind Turbines</i> (PB8.46) Anca D. Hansen, Henrik Bindner, Anders Rebsdorf	233
<i>Experiences and Results from Elkraft 1MW Wind Turbine</i> (PB10.2) Niels Raben, Flemming Vagn Jensen, Stig Øye, Søren Markkilde Petersen, Ioannis Antoniou	237
<i>Keys to Success for Wind Power in Isolated Power Systems</i> (PB11.11) Jens Carsten Hansen, Per Lundsager, Henrik Bindner, Lars Hansen, Sten Frandsen	243
<i>Modelling Supervisory Controller for Hybrid Power Systems</i> (PB11.19) Alexandre Pereira, Henrik Bindner, Per Lundsager, Ole Jannerup	249
<i>Assessment of Wind Turbine Load Measurement Instrumentation</i> (PB9.15) E. Morfiadakis, K. Papadopoulos, N. van der Borg, S.M. Petersen, H. Seifert	253

POLICY INSTRUMENTS FOR REGULATING THE DEVELOPMENT OF WIND POWER IN A LIBERATED ELECTRICITY MARKET.

Senior research specialist P.E.Morthorst
Risø National Laboratory, 4000 Roskilde, Denmark
Ph. +4546775106, Fax. +4546775199, E-mail P.E.Morthorst@risoe.dk

ABSTRACT: Wind power is facing the dual challenge of entering a liberated electricity market and at the same time being one of the main contributors to the reduction of greenhouse gas emissions. The paper analyses the importance of the existing standard payment schemes in the development of wind power, and how this might be affected by the introduction of a liberated electricity market. The existing Danish standard payment scheme has strongly encouraged investments in wind turbines. It has been and still is very effective in promoting a high wind power capacity development, but at a high economic cost to the Danish Government. Different models of conditions for wind power at an electricity exchange do exist, but all seem to introduce a higher risk to the individual wind turbine owner than seen with the present payment scheme. In short it might be stated that going from the existing standard payment system to a market based system, the political uncertainty is converted to a market risk for the individual wind turbine owner.

Keywords: Economics, Energy policies, Energy costs, Electricity market

1 INTRODUCTION

The electricity system in Northern Europe is changing rapidly. In 1996 Norway and Sweden together established the first inter Nordic electricity exchange market (Nord Pool). Through collaboration with the existing Finnish electricity exchange, El-Ex, in 1998 Finland was included in the market. At the beginning of 1999 a specific pricing area has been established for the western part of Denmark, and Danish utility companies are increasingly engaging in pool trading. The Danish legislation on electricity supply opens up for trade in electricity across the borders for consumers with yearly electricity consumption above 100 GWh. The EU-directive on common rules for the internal market in electricity states that each member state has the right of access to the electricity and distribution grids, thus opening the concept of free electricity trade in Europe.

In parallel with this market development a number of countries have committed themselves to considerable reductions of their respective emissions of greenhouse gases (GHG) in relation to the Kyoto protocol. The European Union has agreed on a common GHG-reduction of 8% by the years 2008-12 compared with 1990. The agreed burden sharing within the EU implies that in the mentioned period e.g. Denmark and Germany have to reduce their GHG emissions by 21%.

In the implementation of these targets the development of wind power is expected to play an important role. In its recent White Paper on a strategy for the development of renewable energy the EU-Commission has launched a goal of covering 12% of the European Union's gross inland energy consumption by the year 2010 by renewable sources, that is mainly by biomass, hydro power, wind energy and solar energy. Next to biomass wind energy is foreseen to be the main contributor with regard to future importance. The installed capacity of wind power in EU-countries is proposed to grow to 40 GW by the year 2010 – by the end of 1997 approx. 4.5 GW were installed in the EU [1].

By the end of 1998 approximately 1450 MW of wind turbine capacity had been sited in Denmark, accounting for approx. 9% of total electricity consumption. According to

the governmental plan, Energy21, the utilisation of wind power is targeted to increase to approx. 1700 MW by 2005, including 300 MW offshore turbines. In the long-term perspective wind turbines are expected to play an even more important role; Following the Energy21-plan the total capacity of wind turbines is assumed to increase to approx. 5400 MW by 2030. Should this goal be realised wind-generated electricity would be expected to cover more than 50% of total electricity consumption by 2030 [2].

Until now the Danish Government through a mix of different policy instruments has to a certain extent promoted the development of wind power. But wind power has never faced a liberated electricity market, which expectedly will be a reality in Denmark in the not so far future.

2 WIND POWER AND POLICY INSTRUMENTS

In a national as well as a global perspective wind power is already being developed rapidly. Within the past 7 years the global installed capacity of wind power has increased more than threefold, from approx. 2.3 GW in 1991 to approx. 7.6 GW at the end of 1997, an annual growth of almost 20% [3].

Within Europe the main part of this capacity growth in recent years has been related to relatively few countries, namely Germany, Denmark and Spain. Figure 1 shows the capacity development in these three countries, which together covers approx. 90% of the growth in European installed wind turbine capacity in 1997.

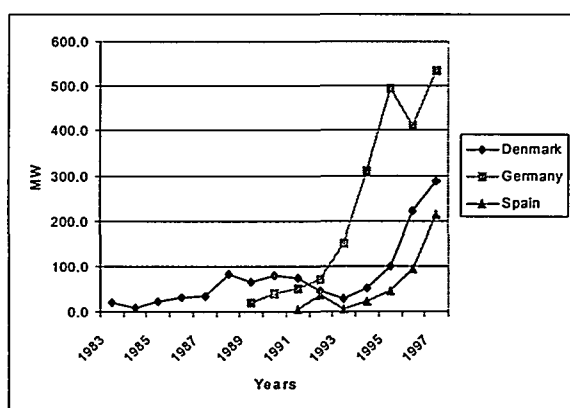


Figure 1: Annual wind turbine capacity development in Germany, Denmark and Spain

As shown in Figure 1 especially Germany has had a rapid development. In 1991 total accumulated capacity in Germany was approx. 100 MW; by now the annual capacity increase exceeds 500 MW and total installed wind power capacity is well above 2000 MW. Similar developments are found in Denmark and Spain, although not to the same extent.

Since the revival of wind turbines in the Danish energy system started back in the late 70s, various policy instruments have been used by the Danish Government to promote and regulate the development of wind power. Among these can be mentioned:

1. *Investment subsidy*, which was used in the 70s and the early 80s. A fixed percentage of total investment cost was subsidised by the Government.
2. *Power purchase agreements*. Utility companies are obliged to buy all power produced by wind turbines, at a buy-back rate equal to 85% of the consumer price of electricity.
3. *Production subsidy*. To promote the development of wind power a general production subsidy is given to all power produced by wind turbines.
4. *Carbon tax*. A general carbon tax is levied on all forms of energy in Denmark. For renewables it affects the price in the same way as the production subsidy. This means that the producers of wind power are refunded the environmental tax.
5. *Tax credits*. Different forms of ownerships have different tax arrangements.

At present, numbers 2 to 5 of the policy instruments above are in use in Denmark [4].

Characteristic for all the above-mentioned three countries - Germany, Spain and Denmark - is that they have introduced some kinds of long-term agreements on (almost) fixed feed-in tariffs, and that these feed-in tariffs are fixed at fairly high levels. Recognising the dominance of these three countries in wind power development in Europe, it might be worthwhile to look more deeply into the importance of the feed-in tariff as one of the main instruments for regulating the development of new wind turbine capacity.

Thus, in the following section the importance of the feed-in tariff will be analysed in more detail, with

Denmark as the specific case. In subsequent sections the challenges for wind power imposed by the liberalisation of the electricity system will be dealt with in relation to the above-mentioned analysis of the feed-in tariff.

3 IMPORTANCE OF FEED-IN TARIFFS AS INCENTIVE TO DEVELOP WIND POWER CAPACITY

At present the feed-in tariff for the Danish private wind turbine owner is approx. 0.60 DKK, or approx. 8.0 cEUR per kWh produced [5]. Of this amount approx. 0.33 DKK (4.4 cEUR) is payment per kWh from the utilities (buy-back rate), while approx. 0.27 DKK/kWh (3.6 cEUR) is refund of energy and environmental taxes from the Government¹.

To analyse the importance of the feed-in tariff an example of a new 600 kW turbine is given. Data for this turbine are shown in Table 1. The 600 kW turbine is typical in size for those erected in 1997 and 1998. The turbine considered is defined as an average one, which is especially important what concerns electricity production and buy-back rate. The buy-back rate is 85% of the consumer price of electricity in the area, where the turbine is located and thus can vary considerably.

Table 1: Characteristics for a new average 600 kW wind turbine in Denmark

Turbine size	600 kW
Turbine Production	1412 MWh/year
Total investment	525.000 EUR
Lifetime	20 years
Buy-back rate (average)	4.4 cEUR
Production subsidy	3.6 cEUR
Total feed-in tariff	8.0 cEUR
Discount rate	3.25% p.a. after tax
Internal rate of return	11.9 % p.a. after tax

Assuming that the existing conditions for feed-in tariff (including subsidies) and taxes are going to continue during turbine lifetime, the internal rate of return after tax (IRR) is calculated for the turbine investment. As shown in Table 1 IRR is almost 12% p.a. after tax and comparing to a normal discount rate after tax of 3.25% p.a., it is obvious that a high profitability is expected from these 600 kW machines. Of course part of this high IRR may be seen as insurance against future changes in the economic conditions but it also points out the presumably main reason for the fast development of turbine capacity in Denmark in recent years.

Two important parameters influence the average calculation given above: The wind regime (and thus the electricity production from the turbine) and the buy-back rate (and thus the total feed-in tariff) which both vary

¹ Throughout this paper 'buy-back rate' is used for the price the utilities pay per kWh for wind-generated electricity, while 'feed-in tariff' is used for the total amount per kWh the wind turbine owners receive, including production subsidies.

considerably from one turbine site to another. Taking these into account gives a more differentiated picture of the IRR of the wind turbine investment.

The variation in the feed-in tariff is shown in Figure 2 for those areas in Denmark, where turbines are erected presently. As seen from the figure the tariff varies from approx. 0.53 DKK/kWh to approx. 0.70 DKK/kWh (7 to 9.3 cEUR), a difference of more than 30%.

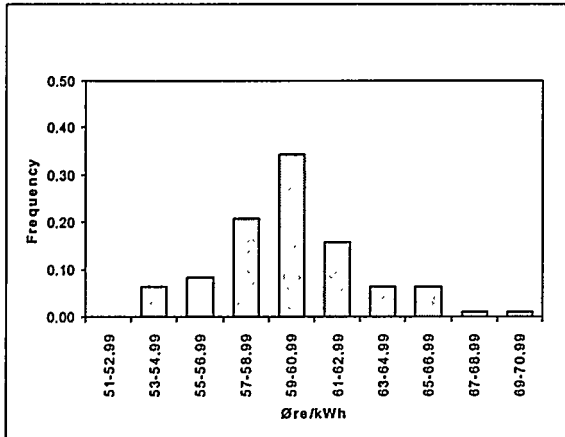


Figure 2: The variability of feed-in tariffs in Denmark
Exchange rate 1EUR = 7.5DKK = 100 øre.

Given the same assumptions as in Table 1 the impact of this variation on the internal rate of return for the 600 kW machine is shown in Figure 3.

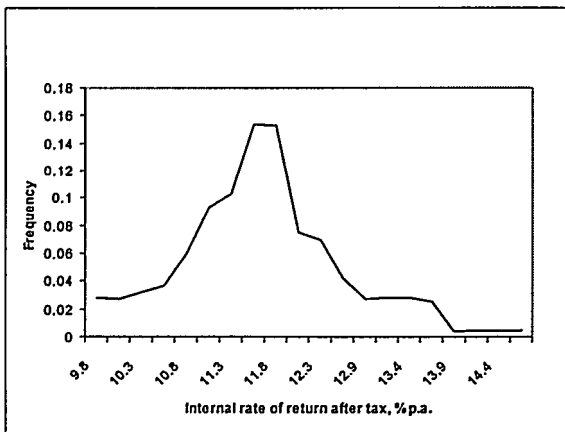


Figure 3: The distribution of the internal rate of return after tax of the investment in a 600kW turbine as a function of feed-in tariff

As shown in Figure 3 IRR varies from approx. 10% p.a. to approx. 15% p.a. A substantial variation but even using the lowest feed-in tariff a high expected profitability is calculated.

Figure 4 shows the IRR of the 600 kW machine when both variations in feed-in tariffs and wind conditions are taken into account². The calculated IRR ranges from approx. 5% p.a. to approx. 22% p.a. after payment of tax.

² The variation in wind conditions is based on those areas where wind turbines are presently erected, only.

So even the turbine erected in an area with the lowest average wind speed and with the lowest feed-in tariff is profitable compared with the normal discount rate of 3.25% p.a.

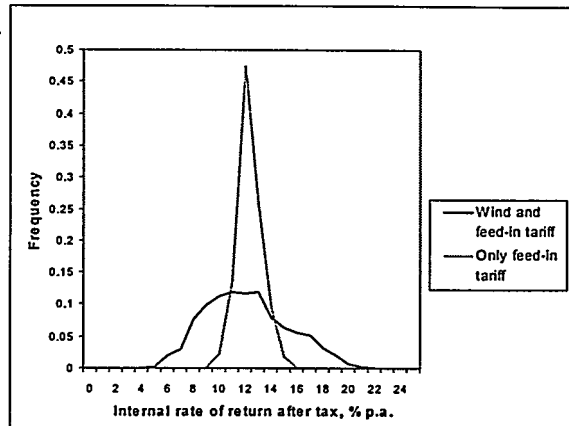


Figure 4: The distribution of the internal rate of return after tax of a 600kW turbine investment as a function of the variation in wind regime and feed-in tariffs.

Thus, it seems that strong incentives in the Danish standard payment system encouraging investments in wind turbines do exist. The Danish model has been and still is very effective in promoting a high wind power capacity development, but presently it is achieved at a high economic cost to society. In 1998 the wind turbine production subsidy paid by the Danish Government amounted to more than 0.5 billion DKK (approx. 75 Mio. EUR). An amount that is rapidly increasing due to the fast turbine capacity development, implying an even more heavy burden on the state budget in years to come.

As mentioned the Danish electricity system is presently being liberalised and different models for including renewable technologies, and among these wind power, are being discussed. A key concern in these discussions is a governmental need of changing the wind power production subsidy from being paid out of the public budget to be paid directly by the Danish electricity consumers. Such models may include wind power participating both in an electricity spot market on the same conditions as conventional fossil fuel fired power plants and in a separate green market, e.g. a green certificate market.

3 WIND POWER IN A LIBERATED MARKET.

Moving into a liberated power market, the conditions for wind power might change dramatically. Using the Nordic power exchange NordPool as an example, a number of characteristics for a power market can be mentioned [4]:

- the spot price for electricity is determined by demand and supply on a daily market (spot market)
- the bidding is performed 12-36 hours in advance
- if it is not possible for a producer or consumer to fulfil his bid, a regulatory premium has to be paid (the Norwegian system)

The NordPool power exchange is geographically bound to Norway, Sweden and Finland, whilst Denmark by now is not a totally integrated part of the exchange. But at the beginning of 1999 a specific pricing area has been established for the western part of Denmark (Jutland and Funen), and Danish utility companies are increasingly engaging in pool trading. The market is dominated by Norwegian and Swedish hydropower.

Demand and supply at the market determine the spot price for electricity. 12-36 hours in advance power plants, distribution companies and other big consumers of electricity are giving their bid to the exchange, stating quantities of electricity supplied or demanded and the corresponding prices. A minor part of total electricity production is actually traded at the spot market. The majority is sold on long-term contracts but the determined spot prices have a considerable impact on prices agreed in these contracts.

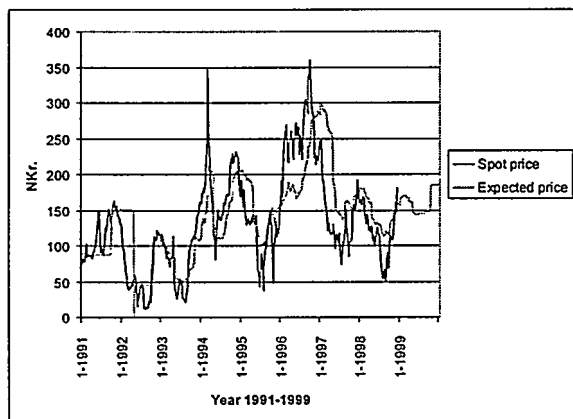


Figure 5: Spot prices and expected prices at the Nordic power exchange from 1991 to 1999³.

Figure 5 shows the determined spot price and the expected long term price at the Norwegian/NordPool³ exchange from 1991 to 1999. As shown the spot price fluctuates considerably, from more than 350 NKK/MWh to less than 50 NKK/MWh. The main reason for this is that price determination is influenced heavily by dry and wet periods. 1992 was dominated by a long wet period, which was the case again at the end of 1993, 1995 and 1998. A large part of 1996 was dry turning into normality at the end of the year. The average price of the considered time period is approx. 140 NKK/MWh. With a few exceptions there is a close correlation between the expected long-term price and the spot price as seen from Figure 5. The long-term price level is expected to be approx. 200 NKK/MWh, corresponding to approx. 0.19 DKK/kWh (approx. 2.5 cEUR/kWh). If this is going to be the ordinary sales price for wind power, some private investments in wind turbines under free market conditions will have a negative rate of return, even if the existing production subsidy and refund of carbon tax are maintained.

³ Until the end of 1995 the electricity exchange covered Norway, only. From 1996 Sweden joined the exchange and the name was changed to NordPool. From 1998 Finland was included as well.

As mentioned electricity producers will have to state their bid to the market 12-36 hours in advance. If wind turbine owners are to supply their electricity production directly to the spot market, this might have a substantial impact on the profitability of wind power [6]. Normally it will be possible to predict the supply of wind power 12-36 hours in advance only to a certain extent. Thus it will be necessary to pay a premium for the difference. Figure 6 shows how the regulatory market functions: If the power production from the wind turbines is higher than the bid, other producers will have to regulate down. In this case the wind producer will get a lower price for the excess electricity produced than the spot market price. If wind power production is lower than the bid, other producers will have to regulate up to secure the power supply. These other producers will get a price above the spot market price for the extra electricity produced; an additional cost, which has to be born by the wind producer. The more the wind producer is off track the higher will be the premium, as shown in Figure 6 by the difference from the regulatory curves to the stipulated spot market price. Using data from the existing NordPool market, the average regulatory premium is expected to be approx. 0.01-0.02 DKK/kWh, or 0.15-0.3 cEUR/kWh [6]. This seems to be a fairly low price to pay for an integration of wind power in the electricity system.

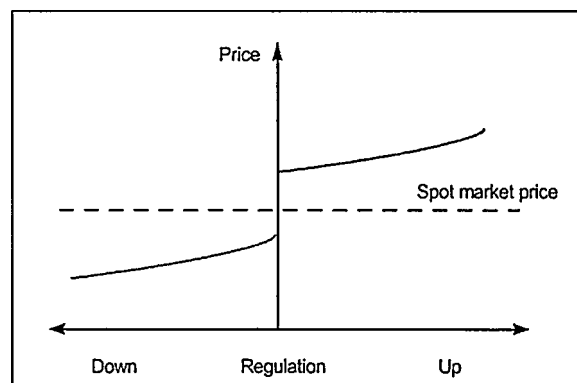


Figure 6: The functioning of the Norwegian regulatory market

4 DIFFERENT MODELS FOR WIND POWER MARKET PARTICIPATION.

In the following three different models for wind power market participation will be analysed to see which conditions appear to be the most appropriate for wind energy.

4.1 Prioritised production – a best case?

Both the Danish Government and the EU-directive emphasise that it might be required of the system operator to give priority to generating installations that use renewable energy sources. For wind power the prioritised production solution might have the following characteristics:

- The wind turbine owners are guaranteed that all electricity generated by the turbines can be sold at the market.
- Electricity production may be sold to a predetermined, market-independent price.
- The additional cost of wind-generated electricity compared to conventional production will have to be born by electricity consumers and not by the public budget.

Depending on the negotiated price, this model might leave wind power as well off as is the case today. In the short run it might protect the development of wind power, but at the same time it does not allow market forces to work.

In the long run it is doubtful if such a solution can be retained. The main reason for this is, that consumers may be willing to pay additional cost for wind produced electricity because they know they get an environmental benefit in return. But if wind power is going to cover a substantial part of domestic electricity consumption, an increasing share will be out of phase with domestic electricity demand. This share will have to be exported at ordinary market conditions, and the consumers will have to pay for an environmental benefit they do not get. Thus it seems doubtful – and to some extent unreasonable – that electricity consumers should pay the extra costs in the long run.

4.2 Wind power at the spot market – a worst case!

Wind-generated electricity may be supplied directly to the spot market at ordinary market conditions as is the case for conventional electricity producing plants leading to the following model:

- All wind-generated electricity is sold at the spot market.
- The expected long-term spot price level will be too low to secure a reasonable rate of return on wind turbine investments.
- The spot market price on electricity may be expected to fluctuate considerably and thus introduce a higher risk on wind power investments.

Thus it can be expected that if wind power must compete on pure market conditions this will totally halt the development of new wind turbine capacity.

4.3 An acceptable model for wind power at the spot market.

In the long run it would be natural if all wind-generated electricity was supplied to the electricity exchange. This would mean that wind-produced electricity could take advantage of the regulatory capabilities of the market to a fairly low price (cf. section 3). But to make wind power reasonably profitable such a model would have to be supplemented by additional payment for the green electricity. An acceptable model could include:

- All wind-produced electricity is sold at the market on ordinary market conditions
- An additional payment is added on top of the spot market price (paid by domestic consumers)
 - Separate green market (green certificates)

- Externality adder (long-term fixed)
- Or the investment subsidy could be reinvented
 - Eventually differentiated according to expected turbine electricity production

To sell wind-generated electricity at the spot market will introduce a price risk that is not present in the existing standard payment scheme. Therefore, to avoid making turbine investments too risky, the additional payment should preferably be fixed on long-term conditions. A possibility would be to introduce a fixed externality adder to be paid by domestic electricity consumers, limited to wind-produced electricity covering domestic demand. But in this case wind turbine owners would get a lower price for exports of wind-generated electricity.

Another possibility would be to introduce a separate green certificate market, which is actually being discussed in Denmark. The supply of green certificates would be tied to the production of wind-generated electricity, while the demand for these certificates would be secured by a governmental requirement that a certain minimum share of total electricity consumption should be covered by green electricity. A green certificate market would be a purely financial market, only restricted by the physical supply and demand for wind-generated electricity on an annual basis. This model would secure that domestic electricity consumers get the environmental benefit from wind power, but at the same time the market determined prices of the green certificates would introduce an additional risk on wind turbine investments.

Finally, an other solution would be to reinvent the investment subsidy. A subsidy of an appropriate size will have the same impact on the internal rate of return as a long-term fixed production subsidy, but to rely on a future production subsidy will of course be much more uncertain. The use of investment subsidies fell into disfavour in US in the 80s, because some turbines were put up on sites with low production possibilities. In retrospect, it seems that those to blame were mainly the US tax conditions, biasing the behaviour of potential wind turbine owners.

5 CONSEQUENCES OF APPLYING THE ACCEPTABLE MODEL

Figure 7 illustrates the possible economic consequences of applying this “acceptable” model to a new 600 kW turbine, given the same average conditions as mentioned in Table 1 (cf. section 2). In Figure 7 the internal rate of return after tax is calculated as a function of the variation in the expected spot market price combined with a fixed production or investment subsidy to achieve an average IRR equivalent to the one obtained with the existing payment scheme. The variation in spot prices is calculated using eight years of data from the Nordic power exchange. The expected long-term price is fixed at 0.19 DKK/kWh corresponding to 2.5 cEUR/kWh. As seen from the figure the variation caused by the existing feed-in tariffs and the spread caused by the expected spot prices are almost identical.

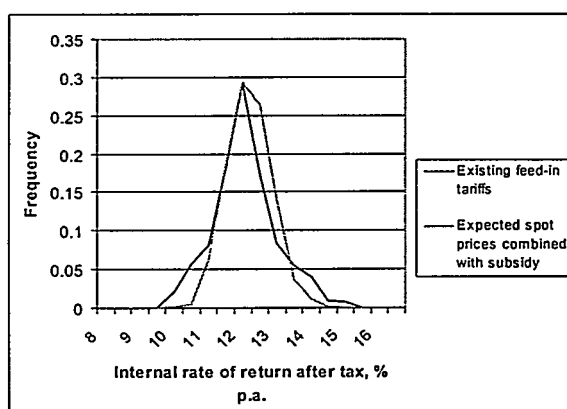


Figure 7: The distribution of the internal rate of return after tax of a 600kW turbine investment as a function of the variation in existing feed-in tariffs and expected spot prices combined with subsidy.

But the two curves are not illustrating the same kind of risk. Looking at the existing system there is a difference in buy-back rates (and thus in feed-in tariffs) from one geographical area to another. But the individual wind turbine owner will know the approximate price he can get by selling his electricity to the power company, and thus the approximate rate of return he can expect on his investment, if the existing conditions continue. He is mainly facing an uncertainty related to the political willingness to retain the standard pricing scheme within the lifetime of the turbine⁴. For the existing feed-in tariffs the figure above is illustrating the economic consequences of the chosen policy, only. Namely that other things being equal one turbine owner will be economically better off than another due to differences in the geographical determined buy-back rate.

In the spot market model the risk of fluctuating spot prices will apply equally to all turbine owners. Referring to Figure 7 the individual turbine owner at the time of the investment will not know where in the rate-of-return interval he might end. Thus with the exception of the wind regime of the potential site, the main factor behind a decision on the development of new turbine capacity might be related to the risk perception of the potential investor to a much higher degree in this model than seen with the previous standard payment scheme.

To summarize the differences between the existing solution and an acceptable market model:

Existing system:

- A high political uncertainty exists: Will existing conditions continue?
- If these conditions actually do continue, the risk for the individual owner is moderate.
- The system is not uniform in pricing.

Acceptable market solution:

- The risk for the individual owner is higher in this model than in the existing payment scheme.
- The policy uncertainty will be lower in this model, although not eliminated.

⁴ This uncertainty is not taken into account in these calculations.

- This solution is uniform in pricing.

In short it may be stated that going from the existing system to a market system, the political uncertainty is converted to a market risk for the individual wind turbine owner.

5 CONCLUSIONS.

The existing Danish standard payment scheme has strongly encouraged investments in wind turbines. The Danish model has been and still is very effective in promoting a high wind power capacity development, but presently it is achieved at high economic cost to society, levying a heavy burden on the state budget due to the production subsidy.

Thus it may be expected that the production subsidy in the near future will be phased out and replaced by a kind of market model, where additional cost of wind-generated electricity will be born by the electricity consumers. Different kinds of market models exist, but all seem to introduce a higher risk for the wind turbine owner. An acceptable model could rely on the spot market supplemented by an additional preferably fixed payment for green electricity. In any circumstances will going from the existing system to a market system imply that political uncertainty is converted to a market risk for the individual wind turbine owner.

6 REFERENCES

- [1] European Commission. Energy for the future: Renewable sources of energy. (White Paper, 26/11/97).
- [2] The Danish Ministry of Environment and Energy, Energy21, Denmark (1995).
- [3] BTM-consult, International wind energy development - World market update 1997, (March 1998).
- [4] Morthorst, P.E., The use of policy instruments in the long-term implementation of renewable energy technologies under liberated market conditions, Renewable Energy, (Special issue September 1998).
- [5] Morthorst, P.E. Independent power production in Denmark - Wind turbines. Ener Bulletin, 18, 66-73 (1996).
- [6] Nielsen, L.H. and Morthorst, P.E (ed.), Fluktuerende vedvarende energi i el- og varmeforsyningen – det mellemlange sigt (System integration of wind power on liberalised electricity market conditions. Medium term aspects (in Danish)), Risø National Laboratory (April 1998).

IMPROVED POWER PERFORMANCE ASSESSMENT METHODS

Sten Frandsen¹, Ioannis Antoniou¹, Jan-Aake Dahlberg², Alan Derrick³, Dimitris Douvikas⁴, P. Chaviaropoulos⁴, R. Hunter⁶, Dimitris Kanellopoulos⁵, George Kapsalis⁵, Rachel Ruffle⁶,

¹Risoe National Laboratory, P.O. Box 49, DK-4000 Roskilde, Denmark,

²Aeronautical Research Institute of Sweden, P.O. Box 11021, S-161 11, Bromma, Sweden,

³National Engineering Laboratory, Birmiehill Roundabout, East Kilbride G75 0QU, Glasgow, UK

⁴Center for Renewable Energy Sources, 19th km Marathonos Avenue, GR-190 09 Pikermi, Greece,

⁵Public Power Corporation, Navarinou 10, GR-106 80, Athens, Greece,

⁶Renewable Energy Systems Ltd., Pilgrims Lodge, Holywell Hill, St. Albans, Herts, AL1 1ER, UK

ABSTRACT: The uncertainty of presently-used methods for retrospective assessment of the productive capacity of wind farms is unacceptably large. The possibilities of improving the accuracy have been investigated and are reported. A method is presented that includes an extended power curve and site calibration. In addition, blockage effects with respect to reference wind speed measurements are analysed.

It is found that significant accuracy improvements are possible by the introduction of more input variables such as turbulence and wind shear, in addition to mean wind speed and air density. Also, the testing of several or all machines in the wind farm – instead of only one or two – may provide a better estimate of the average performance.

Keywords: Performance assessment, wind farm, sensitivity, site calibration, blockage effects, uncertainty.

1 INTRODUCTION

Prior to the initiation of the work, [1] summarised here it was known that the uncertainty – subject to complexity of terrain – of assessment of the production capability of a wind farm would range from 5 to 15% or more, [2] and [4]. Thus, addressing the problem, the purpose is to reduce the financial risk of investment in wind power projects by significant improvement of power performance assessment methods.

The presently used method for assessment of whether a wind farm is meeting the manufacturer's production warranty or not, is to select one or a few wind turbine units for power curve measurement¹. The (standardised) power curve measurement, [3], basically includes measurement of wind speed at hub height some distance in front of the wind turbine and measurement of air density and electric power from the wind turbine. From the measured power curve and a pre-defined wind speed distribution, the annual energy production is calculated and compared to the warranted production. The large measurement uncertainty is expectedly caused by 1) inadequate information of the site wind flow, 2) inadequate anemometry, and 3) lack of control of experimental uncertainties, and last but definitely not least 4) the limited number (two) of flow (input) variables that will affect power. Thus, consider e.g. the influence on power of turbulence intensity, I . In isotropic turbulence, the mean energy flux through a unity area perpendicular to the mean velocity vector is given by

$$e_{flux} = \langle \frac{1}{2} \rho ((U + u_1)^2 + u_2^2 + u_3^2) (U + u_1) \rangle \quad (1)$$

$$\approx \frac{1}{2} \rho U^3 (1 + 5I^2),$$

where $\langle * \rangle$ denotes time average, U is the mean wind speed, u_x are standard deviation of fluctuations in the three orthogonal directions and ρ is the air density. Thus, the energy that potentially may be gathered by the wind turbine is a function of turbulence intensity.

2 METHOD OF IMPROVEMENT

It is presumed that there is a unique power curve to each wind turbine: given that enough input variables are included in the analysis all power variations can be explained. The principal idea of the proposed method is to determine power curves by means of measurement power and of an increased number of flow variables in a met tower. Seeking to measure these unique *reference power curves* has led to definition of the principal test-components

- Site calibration
- Sensitivity analysis
- Wind farm blockage effect

which will be explained below. The result of the assessment will be a number of generalised reference power curves, i.e. measured power curves that have been "corrected" to a set of reference values of the input variables. By means of the reference power curves and a predefined wind speed frequency distribution reference mean power from each wind turbine unit can be calculated. The end-results of the proposed assessment method are thus estimates of the power plant mean and standard deviation of reference mean power.

The components of the proposed extended performance assessment procedure are illustrated in Figure 1, described, and evaluated below.

¹ Also the so-called nacelle anemometry is used; problems related to this technique is reported separately, [5].

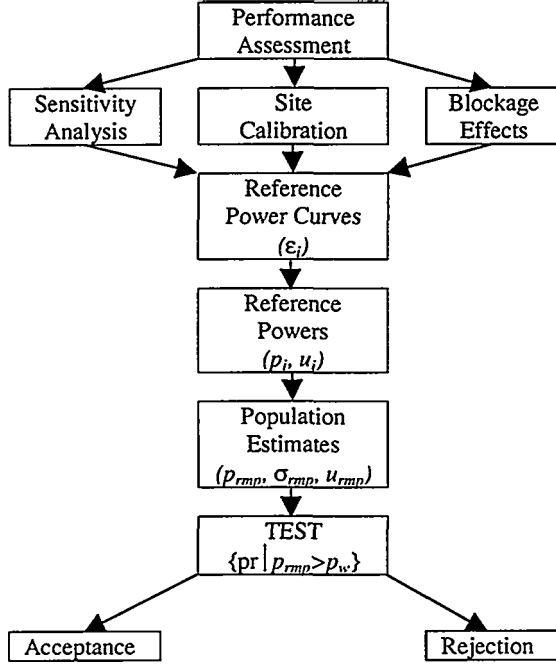


Figure 1: Proposed components in an improved performance assessment procedure.

2.1 Reference power curve

The direct test result of the measurements and data analysis is the generalised power curve with coverage $(\alpha_i; \beta_i)$:

$$p = \mathcal{E}(x) = \mathcal{E}(x_1, x_2, \dots, x_N), \alpha_i \leq x_i \leq \beta_i$$

Should the test covers all possible variations and combination of variations of the variables, the power curve can be said to be fully determined and the coverage complete. Otherwise - and this is always the case in the real world - the test is incomplete. Even if being incomplete, two generalised power curves can be compared without extrapolation, if their coverage ranges are overlapping.

While logical and consistent, the concept is difficult to apply. It is therefore useful instead to define a *reference power curve*. Doing so, it is firstly noted that the along-wind component of the wind velocity is obviously by far the most important. So to devise a reference power curve, hub height wind speed is singled out as reference parameter. Assume next the test data sorted in bins of suitable size according to the reference wind speed (x_i) .

In each bin, the averages of the input quantities are estimated: $u = \bar{x}_1$ and $\{p, \bar{x}_2, \bar{x}_3, \dots, \bar{x}_N\}$ (The overbar denote wind-speed-bin averages of the parameters). Having covered a sufficient range of reference wind speed bins, a *test-average power curve* has been estimated: $\bar{\epsilon} = \bar{\epsilon}(u)$ and $\bar{x}_i = \bar{x}_i(u)$, $i = 2, 3, \dots, N$.

The test-average power curve is different from test to test and from site to site and can therefore not be used for comparison of e.g. a power curve measured at a test site and one measured on an implementation site. If the coverage of two curves are only partly or not at all

overlapping, extrapolation of the measured data to a set of reference conditions will be necessary to make comparison possible. To facilitate extrapolation it is assumed that binwise, power is linear in the independent variables.

Therefore, the analysis is made binwise, thus having levelised the importance of wind speed. Selecting power as the dependent output quantity, the best fit of the data to a hyperplane is found by means of multivariate linear regression analysis (see later):

$$\epsilon_{fi} = \bar{\epsilon} + \sum_{i=2}^N \beta_i (x_i - \bar{x}_i). \quad (2)$$

Here, $\beta_2, \beta_3, \dots, \beta_N$ are the regression coefficients. In principle, one set of regression coefficients is determined for each wind speed bin.

A set of reference values of the input variables has been chosen prior to the test: ${}_R x_i = {}_R x_i(u)$, $i = 2, \dots, N$. The functions could have any shape; however, it seems useful to chose functions that are as representative as possible for as many potential wind farm sites as possible. The reference power curve² derived from the data is

$$\epsilon_{ref} = \bar{\epsilon} + \sum_{i=2}^N \beta_i ({}_R x_i - \bar{x}_i). \quad (3)$$

Introducing a reference frequency distribution of wind speed, the best estimate *reference power* of the unit is

$$p = \int_0^{\infty} f_{ref}(u) \epsilon_{ref}(u) du. \quad (4)$$

From these estimates of reference mean power of the individual units, wind power plant average is determined.

2.2 Sensitivity analysis

Thus, to determine the regression coefficients of Section 2.1, the sensitivity of power to a range of flow variables was investigated. The flow variables included wind speed, flow inclination, turbulence, air density, shear, standard deviation of wind direction and turbulence scale. In multivariate regression analysis techniques one major problem - amongst several - is collinearity (correlation between the independent variables). The method applied for removal of collinearity relates to use of residuals from the independent variables rather than the variables themselves. Each variable in turn is predicted using a linear combination of the remaining variables. The difference between the original variable and the modelled variable (residual) then becomes the new variable for use in the final regression model. These new residual variables then describe the variance of the original variable that cannot be explained by a linear combination of the other independent variables. The method was applied on a number of wind farms/wind turbine units, and the coefficients, β_i , were determined. In figure 2, 3-months mean values of measured power (actual) is plotted together with the power predicted with the result of the regression analysis made on a different machine. It is seen that the prediction model has larger annual variations,

² Note that "reference" refers to reference input variables, and not to fixed power curve.

meaning the machine used for the modelling is more sensitive to the annual variation in the chosen flow variables than the machine used for comparison. If the prediction is scaled to the same mean and standard deviation as actual power, the standard deviation of the difference between predicted and actual power is reduced 30% of the original standard deviation of power.

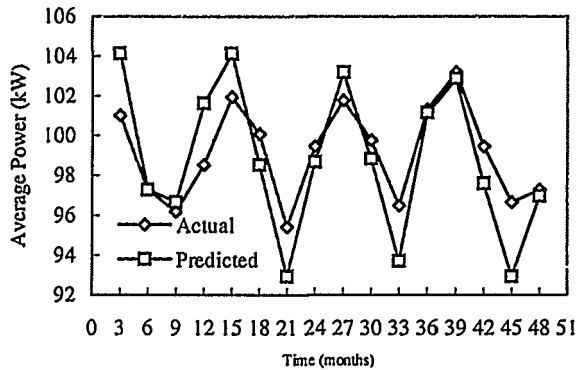


Figure 2 Actual and predicted power, $7 < U < 8$ m/s

In the particular case considered above the most important variable was (of course) wind speed. The next most influential variable was flow inclination (angle between mean wind vector and horizontal) followed by turbulence intensity. First after these came air density.

Numerical sensitivity analysis was also investigated. However, the results were not encouraging, the applied aero-elastic codes predicting variations in power, the only partly matched measurements.

2.3 Site calibration

The phrase "site calibration" covers the activity of establishment of the relationship between the flow variables, measured or computed, at one position in space (reference met mast) with the flow variables at another position (wind turbine).

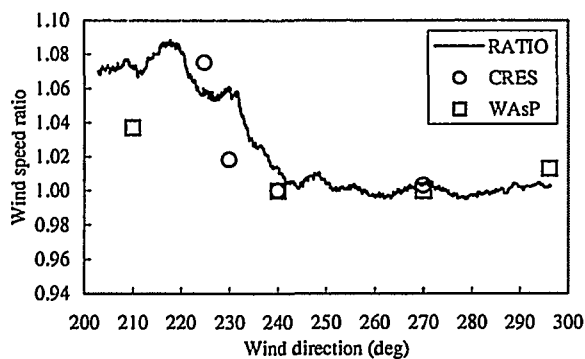


Figure 3 Measured and predicted ratio of wind speeds in two met masts, separated approx. 800m, Vindeby.

Consider N variables (mean wind speed, turbulence etc.) with the values y_1, y_2, \dots, y_N in some reference position. With measurements of these, the target is to be able to estimate the values x_1, x_2, \dots, x_N of the same flow variables in the prediction position. Thus, the generalised problem is to map the functions f_i :

$$x_i = f_i(y_1, y_2, \dots, y_N) \quad i = 1, 2, \dots, N$$

The expression indicates that in general it is to be expected that each predicted variable is a function of all the considered variables at the reference position³. However, with the methods presently available, it has only partly been possible to consider other relations than the relation between the wind speeds at two different positions.

2.4 Blockage effects

The general assumption is that the wind power plant has insignificant influence on the local *climate*, and thus also causes a blockage effect. The plant blockage effect is taken into account in the single-unit performance standard, [3], by demanding that the reference met mast should be placed at least 2 rotor diameters away from the wind turbine under test. A similar - presumably larger - effect would be expected for an array of machines, as illustrated in Figure 4.

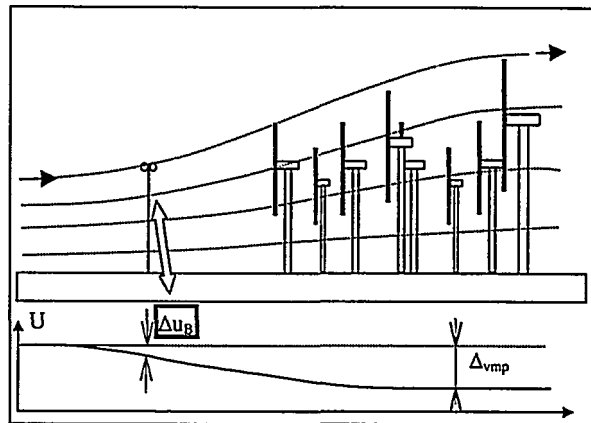


Figure 4 Plant blockage on reference wind speed measurement, wind farm.

The actuator disc concept has been used in the present project as basis for the computation of the flow field near one rotor as well as the influence of multiple rotors. Linearised and simplified solutions for the actuator disc flow have been derived decades ago, but in the present case the full describing equations have been solved by numerical techniques. However, a comparison is also made with simple analytical solutions. The analytical and numerical solutions are in good agreement. With a mast at a distance of 2.5 rotor diameter the blockage is around 1% for a single turbine and around 4% for a row of turbines perpendicular to the wind direction.

3 DISCUSSION

Consider a wind power plant, consisting of M_T wind turbines. Several different measures may be chosen for assessment of the plant's productive capacity. Here, the plant reference mean power - mean of the per-unit reference power - is made the target of assessment. The reference power of wind turbine unit no. i , p_i , is defined

³ I.e. mean wind speed at the prediction position is not only a function of mean wind speed at the reference position, but also turbulence shear etc.

previously. The plant reference mean power and the variance of unit reference power are defined as

$$\mu_P = \frac{1}{M_T} \sum_{i=1}^{M_T} p_i \text{ and } \sigma_P^2 = \frac{1}{M_T} \sum_{i=1}^{M_T} (p_i - \mu_P)^2.$$

Estimators of μ_P and σ_P are assumed derived from a sample of size $M \leq M_T$ of p_i 's, and the specific goal is to determine the uncertainty of the estimators of these two quantities. Employment of the procedures and methods reported opens possibilities for reduction of uncertainties relative to present "common practise". Concerning the upper limit of the ranges of uncertainties (complex terrain), the following would lower the limits.

Rational estimation of reference power of a large fraction or all of the units in the wind farm would potentially lower the uncertainty of the estimate of the *population mean*, the plant reference mean power. The potential improvement depends on to what extent the per-unit estimates can be made independent. Assuming the per-unit uncertainties to be of the same size and uncorrelated, the uncertainty of population mean estimate is reducible to a small number (best case). On the other hand, assuming the per-unit uncertainties to be of the same size but fully correlated, the uncertainty of population mean will be equal to the per-unit uncertainty (worst case).

Numerical site calibration can potentially be improved, by applying numerical tools with the outmost care, and by calibrating the models with to or three met masts at the site. If cost-wise feasible, experimental site calibration would improve results significantly.

Inclusion of a number of input variables in addition to wind speed will - primarily in complex terrain - reduce uncertainty significantly. To obtain that effect, proper regression analysis tools must be applied.

The plant blockage effect is not corrected for in present-day practise. With the typical distance between met tower and wind farm, a correction can be made by means of numerical simulation.

4 CONCLUSIONS

The aim has been to cover all essential issues of power performance of wind power plants. In the following, results that are found the most interesting are outlined.

Different multivariate regression analysis techniques were applied on data from a number of wind farms. It is estimated that the uncertainty in reference power can be reduced by 5-10% percent in complex terrain, by inclusion of more input variables and in turn application of the extended sensitivity analysis.

Two computer codes - the WasP code of Risoe and a code recently developed at CRES - were applied at three test sites of various complexities. Considerable discrepancies between measurements and modelling were revealed in all types of terrain. The analyses disclosed a need to improve methods for site calibration.

It has been found, that for a wind farm the blockage effect is up to 1-2 percent (on wind speed) at a distance of approx. 4 rotor diameters upstream. If not taken into account the productive capacity of the wind farm could for this reason alone be overestimated with up to 3-6%.

An "all wind farm" assessment procedure is proposed. The procedure includes testing of all wind turbines units

individually and forming plant average of the individual results. The advantage is, that an estimate of the *population mean* is obtained - which is not the case when only one or two units are tested as it is often done in presently used assessment procedures.

The concept of nacelle anemometry was investigated as part of the project and reported in [5].

The method presented has the potential in some cases to reduce the assessment uncertainty to half of what it is with presently used methods.

For the future, it is evaluated that the following actions would significantly improve accuracy of performance assessment:

- Identification of ways of assuring the per-unit uncertainties of reference power effectively are uncorrelated.
- Improvement of analytical/numerical methods for site calibration.
- Refining and streamlining sensitivity analysis.
- Improve quality of design, manufacturing and understanding of the operation of the (cup) anemometer.
- Introduction of remote-sensing anemometry, which from the top of each wind turbine can measure wind speed at a freely chosen point in space in front of the machine.

5 ACKNOWLEDGEMENT

The work has in part been financed by the European Union under contract JOR3-CT96-0114.

6 REFERENCES

- [1] Frandsen, S., I. Antoniou, T. Chaviaropoulos, J.A. Dahlberg, A. Derrick, D. Douvikas, P. Dunbabin, J. C. Hansen, R. Hunter, D. Kanellopoulos, G. Kapsalis, L. Kristensen, H. Aa. Madsen and R. Ruffe (1998) *Power Performance Assessment, Project JOR3-CT96-0114, Final Report, 200p., December.*
- [2] Frandsen, S. and C.J. Christensen (1992) *Accuracy of Estimation of Energy Production from Wind Power Plants*; Wind Engineering Volume 16, No. 5, 257-268.
- [3] IEC, 1998, *Wind turbine generator systems, part 12: Power performance measurement techniques*, IEC 61400-12, International Standard, First Edition 1998.
- [4] Pedersen, A.M.J., L.E. Jensen and U.K. Jørgensen, 1994, *Reliability of wind farm production forecasts*, Proceedings EWEC'94, Thessaloniki, Greece.
- [5] Dahlberg, JA, S. Frandsen, TF. Pedersen, R. Hunter, H. Klug (1999), *Is nacelle anemometry and acceptable option in performance testing*, Proceedings of EWEC 1999, March 1-5, Nice, France.

IMPLEMENTATION OF SHORT-TERM PREDICTION

L Landberg, A Joensen & G Giebel
Risø National Laboratory
Meteorology and Wind Energy Department
DK-4000 Roskilde, Denmark
lars.landberg@risoe.dk

SJ Watson, Rutherford Appleton Laboratory (UK)
H Madsen & TS Nielsen, Technical University of Denmark (DK)
L Laursen & JU Jørgensen, Danish Meteorological Institute (DK)
DP Lalas M Trombou & S Pesmajoglou, Observatory of Athens (GR)
J Tøfting, ELSAM (DK)
H Ravn, ELKRAFT (DK)
E MacCarty, WECTEC (US)
E Davis, E Davis Consult (US)
J Chapman, OEM (US)

ABSTRACT: This paper will give a general overview of the results from a EU JOULE funded project ("Implementing short-term prediction at utilities", JOR3-CT95-0008). References will be given to specialised papers where applicable. The goal of the project was to implement wind farm power output prediction systems in operational environments at a number of utilities in Europe. Two models were developed, one by Risø and one by the Technical University of Denmark (DTU). Both prediction models used HIRLAM predictions from the Danish Meteorological Institute (DMI).

Keywords: Short-term prediction, wind farm power output,

1 INTRODUCTION

In many places around the world, but in Europe in particular, the number of wind farms is now so large that the electricity production from these wind farms have (sometimes critical) effect on the running and control of the overall electrical grid.

To fully benefit from these large amounts of wind energy it is therefore necessary to have some kind of idea of the expected production in the next few days.

This will enable the electrical utilities to control the conventionally fueled plants in such a way that fossil fuels will be saved.

2 THE PROJECT

The project consisted of a group of people with skills in many areas: model development and evaluation, utility practices, implementation of models and so on.

2.1 Goal

The goal of the project was to carry out on-line implementation of prediction models developed in earlier projects. The evaluation of the models should be done in economic terms as well as the more traditional ways.

By putting most of the weight on the implementation side and not so much on the actual model development, the project aimed at (and reached) demonstrating that these very sophisticated models can run reliably in a real life operational situation.

2.2 Partners and roles

- Risø National Laboratory (DK): prediction model development, implementation and evaluation, coordination
- Rutherford Appleton Laboratory (UK): model

evaluation using the National Grid Model (NGM) [10]

- Technical University of Denmark, IMM (DK): prediction model development, implementation and evaluation
- Observatory of Athens (GR): model development and evaluation
- ELSAM (DK): model implementation and implementation evaluation, wind farm measurements
- ELKRAFT (DK): model implementation and implementation evaluation, wind farm measurements
- WECTEC (US), E Davis Consult (US), OEM (US): model evaluation for the US cases.

3 OUTCOME

Two prediction models were developed: the Risø and the IMM models. These models were implemented and evaluated in a number of ways described in the following. The two models both use weather predictions from Numerical Weather Prediction (NWP) (here the Danish Meteorological Institute HIRLAM model, cf [5]) models as input. The way this input is used is different for the two models and the differences and the implementation will be described in the following.

The main difference between the two models is that the Risø model was developed with a utility in mind with no on-line access to the wind farm productions, whereas the IMM model was developed with a utility with on-line wind farm productions available. Predictions were made for a number of stations shown in Figure 1. Furthermore, the Risø model was run in an off-line mode for three sites in the US.

The total sum of findings and results form the project can be found in the final report written to the European Commission [11].

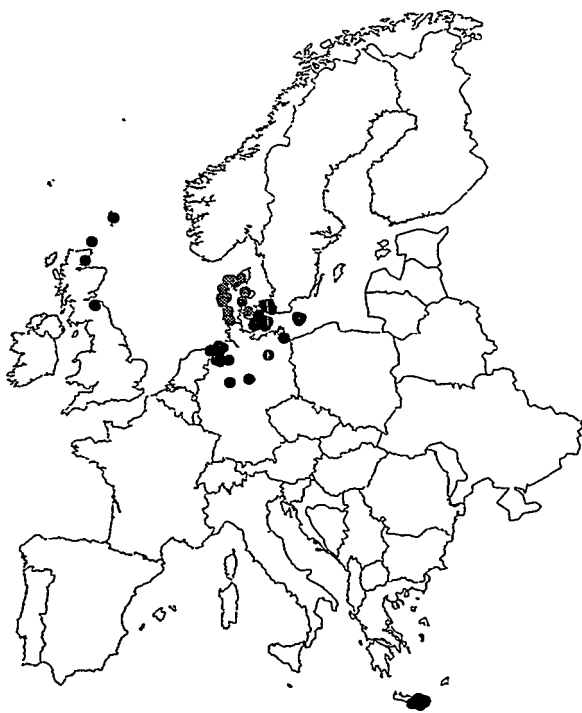


Figure 1: The location of the wind farms. Black dots are the wind farms for which Risø predicts, and gray are the ones IMM predicts for.

3.1 Risø model

The Risø model uses mainly physical relations to transform the predicted wind into predicted power: the overall HIRLAM-predicted wind is transformed to the surface using the geostrophic drag law and the logarithmic wind profile, the surface wind is corrected for local influences using the WASP model [6, 8], and the PARK program [7] is used for calculations of actual wind farm output. The results are corrected using a mathematical filter (a MOS filter). For detailed description and analysis of the model see [2, 3, 4, 1].

The on-line implementation of the Risø model is shown in Figure 2. An example of the predictions as seen of the WWW is shown in Figure 3.

To give an example of the Risø model's ability to predict storms Figure 4 shows the development of a storm and how well the predictions agreed with the observations.

3.2 IMM model

In the IMM model statistical methods are applied for predicting the expected wind power production in a larger area using on-line data covering only a subset of the total population of wind turbines in the area. The approach is to divide the area of interest into sub-areas each covered by a wind farm. Predictions of wind power with a horizon from half an hour up to 39 hours are then formed for the individual wind farms using local measurements of climatic variables as well as meteorological forecasts of wind speed and direction. The wind farm power predictions for each sub-area are subsequently up-scaled to cover all wind turbines in the sub-area before the predictions for sub-areas are summarized to form a prediction for the entire area. The model is described in great detail in [9].

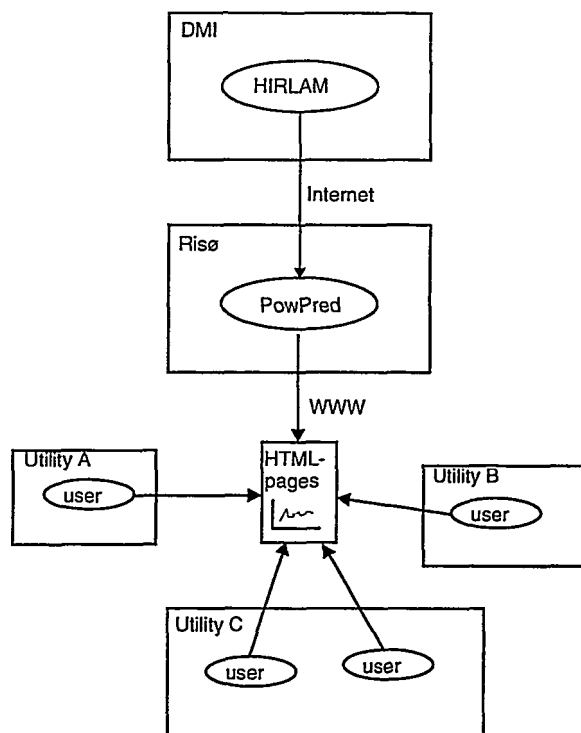


Figure 2: The idea behind the on-line implementation of the Risø model.

The idea behind the implementation is shown in Figure 5. The over-view screen of the prediction system at Elsam is shown in Figure 6

3.3 Elkraft implementation

Elkraft Power Company coordinates energy cooperation in the eastern part of Denmark.

In the Zealand area there are now installed wind turbines with a total capacity of around 300 MW. This figure will double or triple within the next decade. The influence of the fluctuations of the wind power is already being felt in the daily control and operation of the system. Therefore efforts are being undertaken to predict the wind power production.

In the present version of the wind power prediction system the data flows may be sketched as follows. The Danish Meteorological Institute produces predictions of wind speeds for a number of specified locations, 15 in total, where major wind farms are located. The prognoses are represented as values for every third hour, with a time horizon of 36 hours.

The prognoses are transmitted to Risø National Laboratory, where the predictions of wind speed are automatically transformed to predictions of power production, based on WASP analyses of the specific wind farms. These predictions may be seen at the homepage at Risø National Laboratory.

Elkraft Power Company takes the predictions from Risø National Laboratory via the Internet. The predictions are then combined with the available knowledge to produce a prognosis for the whole area of interest. In particular, the wind turbines, for which individual prognoses are not made, are included by using an up-scaling factor. Further, tuning of the prognoses is made, for instance to account for major wind farms

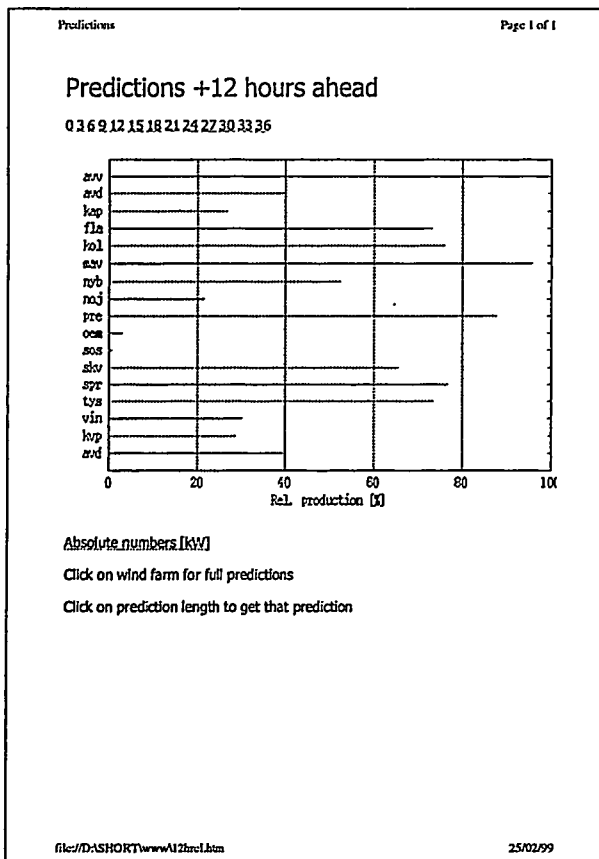


Figure 3: The page viewable on the WWW showing the Risø predictions.

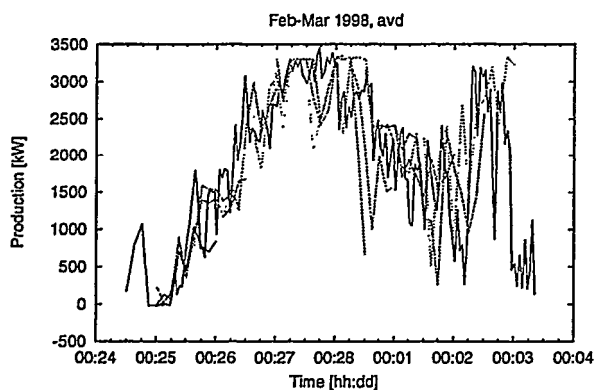


Figure 4: The storm on the 27th February as seen from the Avedøre Wind Farm. Solid line is the observed production and dashed lines are the predictions using the Risø model.

under construction or revision. Longer time biases in the prognoses are detected by comparison with the available measurements, given as hourly or monthly production values.

The prognoses and online measurements are distributed via the local area network to the relevant persons, in particular to those in the control room and to those that trade power on short-term basis.

The system was introduced mid-1998, and has been functional during the last quarter of 1998. An

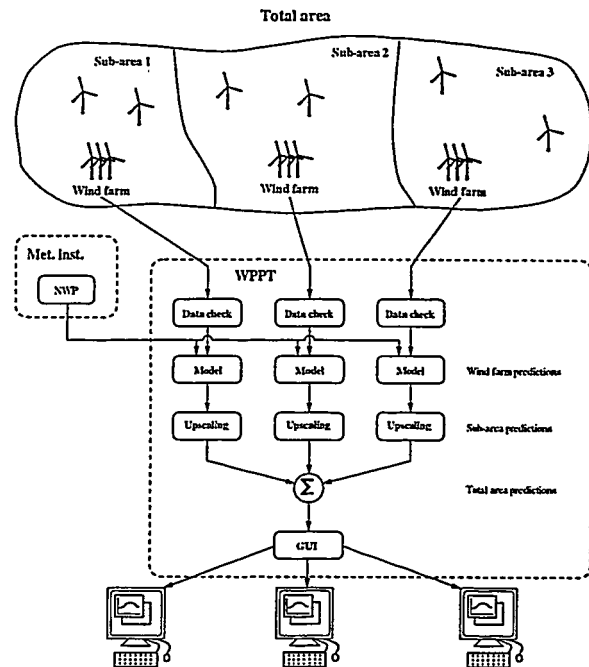


Figure 5: The idea behind the on-line implementation of the IMM model.

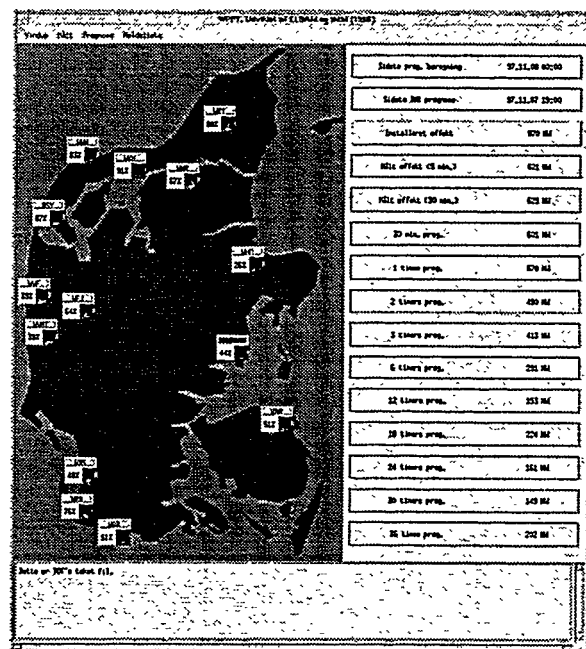


Figure 6: The over-view screen of the IMM model as seen at the Elsam utility

example of the user interface at Elkraft is shown in Figure 7.

3.4 Elsam/Eltra implementation

In the Western part of Denmark Elsam is responsible for the economical load dispatch of the production from the primary power stations, whereas Eltra controls the transmission grid and has the system responsibility. The power production set-up consists of 6 primary power stations equipped with 4250 MW of

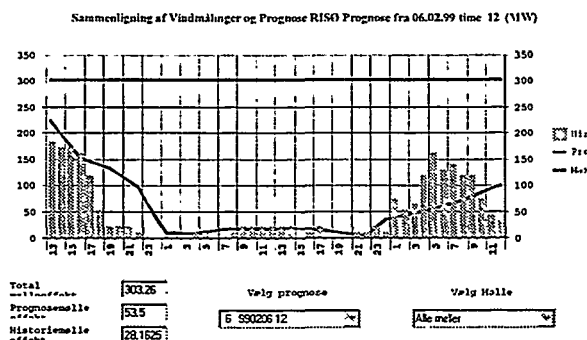


Figure 7: The predictions as displayed in the Elkraft dispatch and control centre. The columns are hourly measured wind power production, the straight horizontal line corresponds to maximum production (i.e. installed capacity) and the curved line is the prediction. It is possible for the dispatcher to choose between current and previous predictions and productions, and which turbines to have displayed.

CHP (Combined Heat and Power) units, a large number of local CHP units with a total installed power of 1400 MW and finally wind turbines with a total rated power of approximately 1000 MW. The production from the local CHP units and the wind turbines is treated as priority production, which implies, that the available power from these sources has to be accepted by the system responsible operator. On a yearly basis the load in the Elsam/Eltra area ranges between 1200 MW and 3700 MW. It is obvious, that the management of 1000 MW of wind power in such a setup will have to rely on the availability of dependable wind power predictions.

The IMM model is implemented in a software package called WPPT (Wind Power Prediction Tool). WPPT was installed in the control centres of Elsam and Eltra in October 1997 and has been used operationally since January 1998. The assessment by the operators is that WPPT generally produces reliable predictions, which are used directly in the economic load dispatch and the day-to-day electricity trade. In periods with unstable weather the operators may choose to modify the predictions (typically smooth the pattern of the prediction) before further usage though. The economical value of the wind power predictions is difficult to evaluate directly mainly due to the problem of assessing the course of action had the predictions not been available. Instead two cases have been analysed in order to illustrate how the predictions are used and with which consequences:

- *Case 1.* On October 17th 1998 the wind power production varied from 600 MW during the morning hours down to 300 MW at 6 pm before increasing to 800 MW at midnight. At 10:30 am the day before WPPT had predicted a wind production around 600 MW during the first half of the day rising to maximum production (930 MW at that time) from 8 pm and onwards. The next wind power prediction based on a new set of meteorological forecasts was available at 4:30 pm October 16th and predicted a different course for the last part of the following day - from 700 MW just before noon down to 350 MW at 5 pm increasing to maximum production at midnight. The first pre-

diction was so different from the actual production, that the running reserve would not have been capable of covering the missing production from 5 PM to 7:30 pm. The missing power would have had to be purchased from NordPool at a total extra price of approximately DKK 16,000. The second prediction was so much better, that the deviation could be countered by the normal means of regulation without any additional costs compared to a perfect forecast. See Figure 8 for details.

- *Case 2.* On November 9th the wind power production varied from 350 MW at midnight 8th increasing up to 800 MW at noon before decreasing down to 100 MW at midnight 9th. This course of the wind power production was accurately predicted the day before and consequently did not imply any costs for the operation.

As indicated by the examples above the operators rely on the wind power production from WPPT in the daily planning since the predictions are markedly better than what can be derived from other sources. This is not to say, that there is no room for improvement, and thus WPPT is subject to continues improvements based on the experiences of the operators.

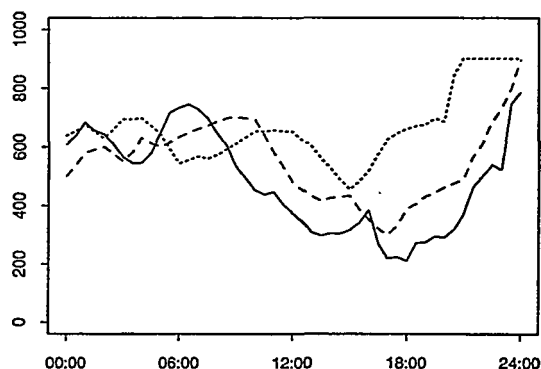


Figure 8: Case 1 (October 17th 1998) predicted by the IMM model. Solid line is the observed production, dashed lines are the predictions.

3.5 RAL calculations

The National Grid Model was run for the England & Wales, Crete and Iowa grids and the results were:

- The forecasts give improved fossil fuel savings over persistence for the England & Wales grid - at least 13% better at 40% penetration (cf Figure 9).
- The results for Crete are poor because the site forecasts are poor.
- Crete has a lot of fast response plant and so forecasting is not so beneficial anyway unless models can significantly improve upon persistence at up to 4 hours ahead. Also a study of Crete would benefit from a hybrid of the RAL NGM and the RAL islands model (which can simulate diesel start-ups on a minute by minute basis).
- The Iowa results are disappointing, this is because of the crude temporal resolution of the forecasts (six-hours).

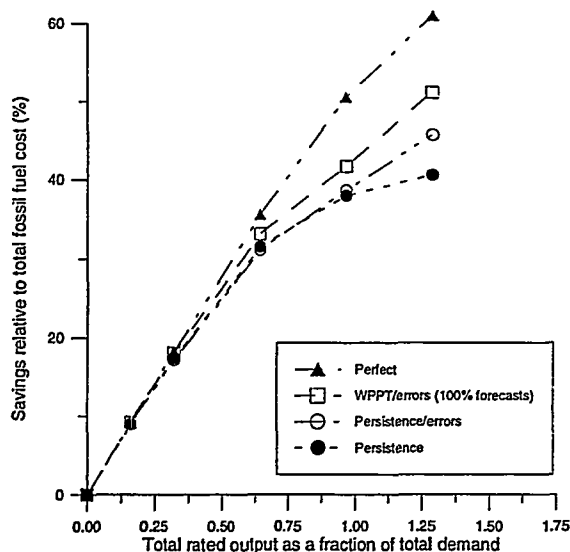


Figure 9: Fossil fuel savings during the calendar year 1994 for different installed wind power capacities into the England and Wales grid using different forecasting methods.

3.6 US results

The Risø forecasting model was applied to selected sites in the US. The general goal of this application was to understand whether the approach used successfully in Europe could be transferred to facilities in the US. When this EPRI program was begun in 1996, it was thought that data either from the EPRI managed eight station North Dakota Wind Resource Assessment Program or the first large EPRI/DOE TVP (Turbine Verification Programme) project at Ft. Davis, Texas would be used. The availability of data from these two projects was limited, forcing EPRI to look elsewhere.

Datasets from regions where wind energy projects were either operational or being considered was a significant consideration in the choice of sites. In addition, areas where the terrain was not too complex, that is, hilly or mountainous, and areas where numerical weather prediction models might have sufficient valid data to perform successfully. The Great Plains was the prime area as the terrain is principally flat or rolling farm- and grasslands. In addition, there is a sufficient observational data base upwind of the Great Plains which should allow for good performance of numerical weather prediction models. The projected development of large wind electric generating facilities in the upper Great Plains of Minnesota and Iowa also focused EPRI on this region.

EPRI obtained data from the first operational wind plant on the Buffalo Ridge in Southwestern Minnesota for use in the forecasting application. This 25MW wind plant came on-line in mid-1994 and power data was made available by the wind plant owner for slightly over a 2-year period. Wind speed and wind direction data was also available for wind resource assessment programs conducted in Iowa during the same time period. These meteorological data were also obtained.

Application of the Risø model requires the use

of numerical weather prediction data. The availability of historical data for the concurrent time period, mid 1994 to mid 1996, was researched. The National Center for Atmospheric Research (NCAR) was contacted and their archives were reviewed. The only complete prediction data set available for the US at that time was for the Nested Grid Model, the operational weather prediction model used by the National Center for Environmental Prediction (NCEP). These data sets were assembled and provided to Risø National Laboratory for testing their modeling approach on US sites.

The Risø model was applied to the Buffalo Ridge Wind Plant, the meteorological site at Alta, and the meteorological site at Sibley. For the wind plant, preparation for application of the model included:

- Creation of a digitized terrain file. This file included all terrain contours within a 10 km radius of the wind plant.
- Creation of a roughness data file. This file included an estimate of the terrain roughness for each of twelve 30 degree sectors.
- Creation of the PARK data files. These files include the power curve for the KVS33, a thrust curve for the KVS33, a meteorological data file consisting of shape, scale and frequency of occurrence of the wind speed in twelve 30 degree sectors, and the location of each (73) KVS33 turbine.

For the two meteorological tower sites, a roughness file is the only required input since these are single sites, wind speed is the predictand, and the files for WASP and PARK are not required.

From the numerical weather prediction data file, the 10 meter, 950 millibar (mb), 850 mb and 700 mb wind speed were extracted. The data for a matrix of four sites, coordinate point 42, 43, 51, and 52 are extrapolated separately to the Buffalo Ridge, Alta, and Sibley sites. This forms the basis for the predicted wind speed. For example, the predictions from the model run of 12159412 (December 15, 1994 at 1200GMT) would consist of wind speed and wind direction values for 8 time periods at six hour intervals, out to 12179412 (December 17, 1994 at 1200GMT).

The model was first applied to the meteorological data at the Alta site. Predictions of average wind speed at eight different time periods in the future twice each day are made using the model. These predictions are based on the numerical weather prediction model. These predictions are then compared to the observed values from the Alta tower. A matrix is then created comparing the predicted and observed values. This matrix is plotted in Figure 10. The poor correlation and pronounced lack of linearity between the predicted and actual values is disappointing.

The reason for this is not yet clear. The data set, consisting of predicted values and actual values, either wind speed (Alta and Sibley) or wind power (Buffalo Ridge) is still being analyzed by staff at Risø. It is possible that the large grid spacing in the NGM model, compared to the smaller grid spacing in the HIRLAM model, could be one of the causative factors.

4 THE FUTURE

This section will describe the different ways the results of this project are planned to be used in future

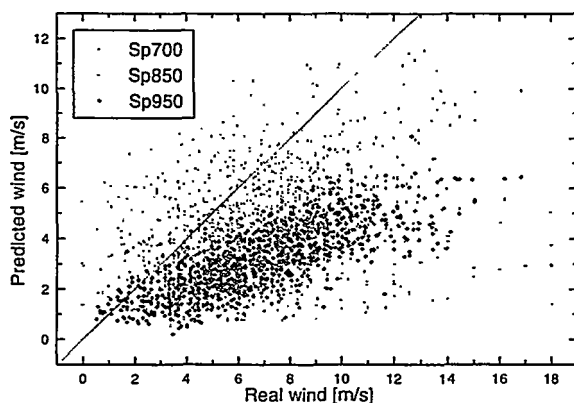


Figure 10: Scatter Plot of the Forecast Wind Speed Versus Actual Wind Speed at the Alta Site.

projects.

In Denmark the Energy Agency via the EFP99 research programme has funded a project where the Danish utilities will be provided with a prediction system which is a combination of the Risø and the IMM prediction systems described in this paper. It is planned that at the end of the project all Danish utilities with a high penetration of wind energy will have this prediction system integrated in the daily dispatch and scheduling.

In the US it is hoped that a EPRI/DOE-funded project will start in 1999. The main goal is to implement the Risø prediction system in the US, predicting for a number of wind farms in the US.

5 SUMMARY

This paper has described the results of a now finished JOULE project, which had as its goal to implement and evaluate in both traditional and economic term models for predicting the power output from wind farms. It was shown that two such models were implemented successfully and that the two major Danish utilities used the predictions in the daily dispatch and planning.

ACKNOWLEDGEMENTS

The project has been funded by the Commission of the European Communities under the JOULE programme, contract JOR3-CT95-0008. The development of the Risø model was as funded by the EFP-programme under the Danish Ministry of Energy and the Environment, contract 1363/94-0005 and JOULE contract JOUR-0091-MB(C). The IMM model was developed in a JOULE II project contract JOUR2-CT92-0083.

REFERENCES

- [1] Landberg, L, 1999: *Operational results from a physical power prediction model*. Proceedings EWEC99, Nice (FR).
- [2] Landberg, L, 1999: Short-term prediction of the power production from wind farms. *J. Wind Eng. Ind. Aerodyn.*, 80, 207-220.
- [3] Landberg L, 1998: A mathematical look at physical power prediction model. *Wind Energy*, 1, 23-28.
- [4] Landberg, L and SJ Watson, 1994: *Short-term prediction of local wind conditions*. *Boundary-Layer Meteorol.*, 70, 171-195.
- [5] Machenhauer, B (ed), 1988: *HIRLAM final report*. HIRLAM Technical Report 5, Danish Meteorological Institute, Copenhagen, Denmark.
- [6] Mortensen, NG, L Landberg, I Troen and EL Petersen, 1993: *Wind Atlas Analysis and Application Program (WASP), User's Guide*. Risø-I-666-(EN)(v.2), Risø National Laboratory, Roskilde, Denmark. 133 pp.
- [7] Sanderhoff, P, 1993: *PARK - User's Guide. A PC-program for calculation of wind turbine park performance*. Risø-I-668(EN), Risø National Laboratory, Roskilde, Denmark. 8 pp.
- [8] Troen, I and EL Petersen, 1989: *The European Wind Atlas*. Published for the CEC by Risø National Laboratory, Roskilde, Denmark. 656 pp.
- [9] Nielsen, TS and H Madsen, 1999: *Experiences with Statistical Methods for Predicting Wind Power*. In proceedings from EWEC99, Nice(FR).
- [10] Halliday, JA, 1988: *Wind meteorology and the integration of electricity generated by wind turbines*. PhD-thesis, Univ Strathclyde, RAL internal report RAL T 075.
- [11] Landberg, L, A Joensen, G Giebel, SJ Watson, H Madsen, TS Nielsen, L Laursen, JU Jørgensen, DP Lalas, J Tøfting, H Ravn, E MacCarty, E Davis, J Chapman, 1999: *Implementing short-term prediction at utilities*. Final report to the European Commission, JOULE project JOR3-CT95-0008.


STATUS OF STANDARDIZATION IN IEC AND CENELEC

Peter Hauge Madsen and Carl Jørgen Christensen
 Risø National Laboratory, P.O. Box 49, DK-4000 Roskilde, Denmark
 Tel: +45 4677 5011. Fax: +45 4677 5970. e-mail: peter.hauge@risoe.dk

RISØ

STATUS OF STANDARDIZATION IN IEC AND CENELEC

Peter Hauge Madsen &
 Carl Jørgen Christensen
 Risø National Laboratory



RISØ

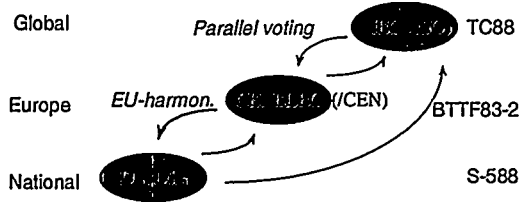
International Standards?

- Trade
- Quality
- Legal requirements
- Technical development
- Safety
 - Loads and load cases
 - Control and protection system
 - Structure
 - Electrical system
 - Installation, O&M
- Testing
 - Performance
 - Noise
 - Blade strength
 - Loads
 - Power quality
- Certification

RISØ

International Standardisation

Levels of standardisation



➔ Trend: More international / less national
 ➔ Initiative (and hard work) remains on a national level

RISØ

IEC Technical Committee 88

Chairman: C.J. Christensen, Denmark
Secretary: A.C. van der Giessen, Netherlands

16 Participating Countries

- China, Czech Republic, Denmark, Egypt, Finland, France, Germany, Greece, Italy, Japan, Netherlands, Russian Federation, South Africa, Sweden, United Kingdom, United States of America

14 Observer countries

RISØ

IEC TC88 Publications (1988-now)

- IEC 61400-1 Ed. 2: WTGS - Part 1: Safety requirements
- IEC 61400-2 Ed. 1: WTGS - Part 2: Safety of small wind turbines
- IEC 61400-11 Ed. 1: WTGS - Part 11: Acoustic noise measurement techniques
- IEC 61400-12 Ed. 1: WTGS - Part 12: Wind turbine power performance testing

(WTGS - Wind turbine generator systems)

RISØ

IEC TC88 working groups

- WG4: Safety requirements for small wind turbine generators
- WG5: Acoustic noise measurement techniques
- WG6: Power performance measurement techniques
- WG7: Safety of wind turbine generator systems
- WG8: Testing of rotor blades
- WG9: Certification procedures
- WG10: Power quality
- WG11: Mechanical load measurements
- PT 61400-23: Lightning protection for wind turbines

IEC TC88 work programme



Committee draft for voting

- IEC 61400-23 TR2 Full-scale structural testing of rotor blades for WTGS's

Committee draft

- IEC 61400-13 TR3 Measurement of mechanical load (TC88 Oct 99)
- IEC 61400-21 Power quality requirements for grid connected wind turbines (TC88 May 99)
- IEC 61400-22 Wind turbine certification (TC88 May 99)

European wind turbine standardization



BTF 83-2 CENELEC Technical Board Task Force

mandated by the European Commission

Chairman: C.J. Christensen, Denmark

Secretary: D. Bakker, Netherlands

Working groups:

- WG1: Engineering integrity
- WG2: Electrotechnical Issues
- WG3: Labour safety
- WG4: Acoustic noise
- WG5: Power performance measurements in complex terrain

CENELEC wind turbine publications



- EN 45510-5-3 Guides for procurement of power system equipment - Part 5-3: Wind turbines (1996)
- EN 61400-11 WTGS Part 11: Acoustic noise measurement techniques (1998)
- EN 61400-12 WTGS Part 12: Wind turbine power performance (1998)
- EN 61400-2 WTGS Part 2: Safety of small wind turbines (1996)
- ENV 61400-1 WTGS Part 1: Safety requirements (1995)
- prEN 50308 (prEN 61400-31) Wind turbines - Labour safety (1998) - CEN/CENELEC Inquiry started
- prEN 61400-1 WTGS Part 1: Safety requirements (1998) - parallel vote reject

International Standardisation Industry's role



- European tradition
 - Standardisation driven by governmental institutions and research centres
 - Industrial participation on national level and through hearings, meetings, etc.
- Atlantic tradition (UK, USA, Japan)
 - Standardisation driven by industry

➡ Trend: more industrial engagement

Status of Standardisation in IEC and CENELEC

Carl Jørgen Christensen, Chairman, IEC/TC88 and CENELEC/BTTF83-2,
Wind Energy and Atmospheric Physics
Risø National Laboratory

A standard for a technical product may serve several purposes. It helps the industry in determining which reasonable requirements a product should live up to in order to satisfy the market. It serves the customer by giving a concise technical description of the product. Exchanging information on a product between seller and buyer is simplified as 'made according to this and that standard' tells much more than long talks. National standards only valid in one country are fine for trade within the country. As a result of the globalisation of industry and trade, it is necessary to develop international standards to replace the many national standards. The national standards tends to develop into trade barriers, as a manufacturer does not like to be forced to produce many variants of a product in order to sell it in many countries with different standards.

The Technical committee IEC/TC88 under the International Electrotechnical Committee is handling worldwide international standardisation of wind turbines. Standardisation in the sense of the harmonisation directives of the EU is handled by the so-called BTTF83-2, which is a 'task force' working for the Technical Board of the European standardisation organisation CENELEC on a mandate from the European Commission.

The main part of the development of standards is being done by the IEC in accordance with the general policy of the CENELEC. A standard issued by the IEC will normally be issued also by CENELEC for parallel voting among the CENELEC member countries. As the memberships in the two organisations are somewhat different and as voting rules are also different, it is not unusual that a standard accepted in the IEC is turned down in the CENELEC. The opposite situation is not quite as likely. This has to do with the fact, that the CENELEC (EN-) standards may be tied into the European technical harmonisation directives and thereby gain considerable legal relevance, whereas the IEC standards are in the first place voluntary, and the member-countries may chose to disregard them.

The IEC/TC88 has been working for 10 years and is now getting to the point where the field of wind turbine standardisation will have reached a reasonably complete coverage. At present, four IEC-standards exist, 3 of them as EN61400 (CENELEC, EU) standards, 1 as non-mandatory European pre-standard (ENV 61400-1, Safety requirements). The EN-standards cover small turbines (part 2), noise measurements (part 11), and power curve measurements (part 12).

Four new topics are being worked on and possibly leading to new standards: Wind Turbine certification, power quality, load measurements and blade testing. These will presumably be finalised in about 2 years.

Three standards are under revision: power performance measurements, noise measurements, and safety requirements. The latter, the pre-standard ENV 61400-1, Safety requirements has just been revised and has been voted on. It has been accepted by the IEC, but was rejected by the CENELEC. The CENELEC/BTTF83-2 will have to discuss what to do with the situation, because according to our mandate from the EU/CENELEC it is mandatory for us to produce a safety standard for the European market. The IEC/TC88 is anyway starting a revision again, as quite a few important technical issues were left unsolved in the last revision, which was just rejected in CENELEC. The outstanding issues mainly have to do with the attitude in the different countries to, how little and how directly, the public should control the industry.

Although we are getting to a point, where our field is pretty well covered with standards, the work does not seem to be coming to an end. The reason is that the wind turbine field is struggling with fast technical progress, which means that the standards are outdated fairly quickly and therefore in constant need of revision. But also needs for new standards that were not envisaged from the beginning

GLOBAL PERSPECTIVES FOR WIND POWER

Per Dannemand Andersen

Risø National Laboratory, P.O. Box 49, DK-4000 Roskilde, Denmark
Tel: +45 4677 5108; Fax: +45 4677 5199; e-mail: per.dannemand@risoe.dk

Global Perspectives for Wind Power

Per Dannemand Andersen
Head of Technology Scenarios Research Programme
Systems Analysis Department
Risø National Laboratory, Roskilde, Denmark
mail: per.dannemand@risoe.dk

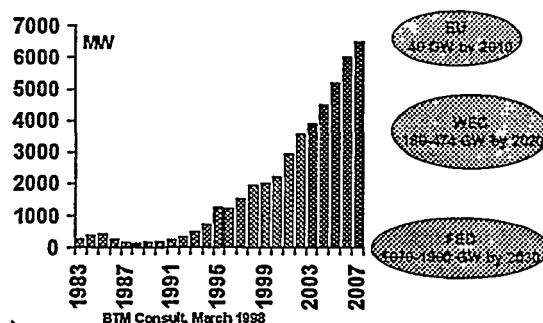
Global Perspective for Wind Power

- ◆ Techniques for looking into the future
- ◆ Market perspectives (near term and long term)
- ◆ Reasons for wind power
- ◆ Energy sector re-structuring
- ◆ Wind energy R&D
- ◆ Changes in technology
- ◆ Costs
- ◆ Concluding remarks

Techniques for Looking into the Future

- ◆ Forecast techniques (short to medium term)
 - based on existing national programmes and national targets such as the World Market Update of BTM Consult (20 GW in 2002)
- ◆ Scenario techniques (long and very long term)
 - predictive type of scenarios such as World Energy Council (180 - 474 GW in 2020)
 - normative type of scenarios (political ambitions) such as EU's target of 40 GW by 2010 or Forum for Energy & Development (1070-1900 GW by 2030)
- ◆ Delphi techniques (broader perspective)
 - based on rounds of questionnaires to expert panels such as the British, the Japanese or the German

Outlook Through Forecasts and Scenarios



Outlook Through Forecasts and Scenarios

Two conclusions

- ◆ Steady market growth in a short term and a medium term perspective
- ◆ Enormous potential in a long term perspective

This Conference

Experiences and planned activities from 37 countries and regions

- | | | |
|-----------------------------|-------------------------|-------------------------------|
| ◆ Algeria | ◆ Finland, arctic areas | ◆ Norway |
| ◆ Antarctica | ◆ France | ◆ Northern Chile |
| ◆ Argentina | ◆ France, Corsica | ◆ Okinawa, Japan |
| ◆ Australia | ◆ Germany | ◆ Russia, Chukotka |
| ◆ Belgium, Flanders | ◆ Greece | ◆ Russia, Kola |
| ◆ Brazil | ◆ Gulf of Botnia | ◆ Russia, Murmansk region |
| ◆ Bulgaria, Black Sea Coast | ◆ India | ◆ Senegal |
| ◆ Croatia | ◆ Italy | ◆ Spain |
| ◆ Cuba | ◆ Korea, Cheju Islands | ◆ Spain, Strait of Gibraltar |
| ◆ Eastern Europe | ◆ Latvia | ◆ Sweden, Suorva |
| ◆ England | ◆ Libya | ◆ Switzerland, alpine regions |
| ◆ Estonia | ◆ Mauritania | ◆ USA |
| ◆ European Union | ◆ New Zealand | |

Outlook Through Delphi Studies



- ◆ **British Study (PREST, 1995)**
 - ➔ Widespread use of commercially competitive wind turbines 1995-2004
 - ➔ Beneficial impact on wealth creation, neutral impact on quality of life
- ◆ **Japanese Study (NISTEP, 1997):**
 - ➔ Practical use MW-class wind power in Japan: 2011
 - ➔ Importance index: low for wind power (44%)
 - ➔ Importance index: high for non-fossil energy sources (94%)
- ◆ **German Study (Frauenhofer ISI, 1998):**
 - ➔ Offshore wind farms larger than 100 MW: 2010
 - ➔ Commercial MW class turbines at a cost in DM/kW as the 750 kW machines of today 2004
 - ➔ Importance index: high (75-79%) for solving environmental problems
 - ➔ Importance index: high (67-68%) for industrial development

Outlook Through Delphi Studies



Three conclusions:

- ◆ The timeframe for the studied break-throughs are the next 10 years - this is not a particular long term perspective
- ◆ Environmental concern is the most important reason for wind power
- ◆ But, industrial development and creation of wealth is also a very important reason for wind power

Changing Reasons for Wind Power



	1970s	1990s	2010s
Context	<ul style="list-style-type: none"> • Energy supply uncertainties • Unstable oil prices • Planned energy sectors 	<ul style="list-style-type: none"> • Cheap Oil • Environmental concerns • Re-structuring energy sectors 	<ul style="list-style-type: none"> • OPEC's safety of demand • Stable fossil prices • New energy sector structure • Diversified supply • ????
Driving factors for wind power	<ul style="list-style-type: none"> • Energy policy issues • Wind energy is a domestic source of energy 	<ul style="list-style-type: none"> • Environment and industry policy issues • Green house gas mitigation technology • New jobs, new technology • Wind energy is clean and safe 	<ul style="list-style-type: none"> • Economical and energy policy issues • Wind energy is competitive • Wind energy is clean and safe • ????

Energy Sector Structure



- ◆ Energy will remain of strategic interest for governments
- ◆ Energy policies will continue to secure
 - ➔ energy to all areas of a country
 - ➔ stable, low energy prices
 - ➔ safety of supply
 - ➔ low environmental impact
- ◆ But energy policies will use other instruments
 - ➔ less detailed planning
 - ➔ less public sector ownership
 - ➔ clear overall targets
 - ➔ more private sector ownership
 - ➔ more market mechanisms

Energy Sector Structure



- ◆ Energy sector restructuring will happen all over the world:
 - ➔ USA
 - ➔ Japan
 - ➔ EU
 - ➔ formerly centrally planned economies
 - ➔ developing countries

Wind power will play an important role under these new market structures. A lot of words must be understood:

- ➔ Power exchanges, power pools, spot markets
- ➔ Financial products such as futures and options for electricity

- ◆ New opportunities, new risks

Perspectives for Wind Energy R&D



R&D spending in the 90s

Future R&D

Overall trend

- ◆ Less government financed R&D
- ◆ More industry financed R&D
- ◆ This trend continues (OECD STI outlook 1998)

Trends for Wind Energy

- ◆ Increased government financed R&D world wide
- ◆ More countries establish R&D programmes
- ◆ Increased in-house industrial R&D

- ◆ Stable governmental funding in a short to medium term
- ◆ More in-house industry R&D
- ◆ More industry financed R&D
- ◆ More R&D within supplying industries
- ◆ Higher specialisation within the research communities
 - ➔ Everybody should not make generic aerodynamics
 - ➔ Specialisation in for example cold climate issues

Some Technology Perspectives



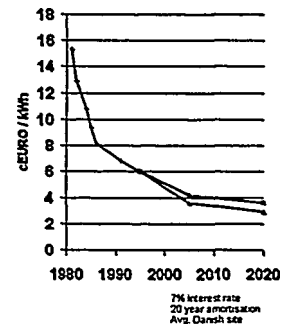
- ◆ Higher flexibility leads to lower costs
 - structural flexibility
 - drive-train flexibility
 - controller flexibility
- ◆ Larger machines, but also higher deviation in "most competitive size"
- ◆ Site and climate specific designs
 - flat terrain
 - mountains
 - offshore
 - arctic conditions
 - deserts
 - high/low wind designs
 - etc.
- ◆ Up-scaling and incremental changes
- ◆ Technology changes are sensitive for the cost of some materials and components
 - carbon fibre for blades
 - neodyn for generators
 - IGBT/MCT for power electronics
 - HVDC transmission

Perspectives for Cost Reductions



Driving factors

- ◆ "progress ratio" = 0.85
based on German and Danish experiences in 80s and 90s
- ◆ A technological potential for reductions exist
- ◆ Increased market volume seems inevitably
- Cost will be cut by 20 - 40 % over the next 20 - 25 year



Concluding remarks



So far, wind power has

- ◆ become a competitive technology for clean energy production
- ◆ become a competitive technology for CO₂ reduction
- ◆ created lots of new business opportunities
- ◆ created tens of thousands of new jobs
- ◆ made one or two handfuls of millionaires

Concluding remarks



In the future wind power will

- ◆ contribute significantly to avoid climate changes
- ◆ provide two digit percentages of many countries electricity supply
- ◆ create numerous business opportunities
- ◆ create millions of jobs
- ◆ maybe create a few billionaires

Conclusion



The perspectives for wind power are good !

Thank you for your attention

A SOFT ROTOR CONCEPT – DESIGN, VERIFICATION AND POTENTIALS

Flemming Rasmussen and Jørgen Thirstrup Petersen
Risø National Laboratory
P.O. Box 49
DK-4000 Roskilde
Denmark
Phone: +45 46775048
Fax: +45 4677 5083
Email: flemming.rasmussen@risoe.dk

ABSTRACT: This paper contains results from development and testing of a two-bladed soft rotor for an existing 15 kW flexible wind turbine. The new concept is characterised as a free yawing down wind turbine with nacelle tilting flexibility and a two-bladed teetering rotor with three-point supported flexible blades with built-in structural couplings. The power and the loads are controlled by active stall and active coning.

The concept has been developed by extensive application of aeroelastic predictions, numerical optimisation and stability analysis in order to obtain optimal aeroelastic response and minimal loads. The flexible blades and the principle of active coning allow the blades to deflect with the wind to such an extent that the loads are reduced to between 25 and 50 % of the loads for a similar rigid rotor.

All conceptual design principles have been focused on application to large MW turbines, and aeroelastic predictions for an up-scaled 1 MW version show that this would have approximately identical characteristics, without being particularly optimised for the actual size.

Keywords: Innovative Concepts, Aeroelastic Stability, Flexibility

1. INTRODUCTION

In parallel to the main research related to the development of the standard three-bladed turbine concept, Risø has for many years been doing research on innovative concepts. The latest work has been the development of a soft rotor for an existing flexible turbine. The soft rotor is the result of an EC Joule-III and Danish Energy Agency supported project that was performed in cooperation between ONERA, LM Glasfiber A/S and Risø.

The idea has been to reconsider some of the fundamental parameters that are not usually taken into account in the rotor design process and to investigate possible potentials by application of new features. However, these features should not necessarily be implemented in the prototype design, but rather be regarded as future options.

The LM 6.1 m blade was defined as the state of the art in blade aerodynamic design and chosen as a starting point for the soft rotor development. All calculations were performed by parametric variations around the characteristics of this blade.

2. AERODYNAMIC DESIGN

Adaptable blade geometry has proven to possess some potentials both with respect to energy production, loads and stability [1]. Adaptable blade geometry could be realised through large deformations with loading or built-in structural couplings between e.g. flapwise bending and blade twist or airfoil shape. These subjects were treated in the project, and some features are built into the final design. The final design is prepared for adaptable airfoil shape with loading in that the blade is designed as a pure shell without spars.

By use of numerical optimisation an investigation [2] was performed of the potentials for energy output increase by applying variable twist distribution with wind speed. An optimum collective pitch setting with wind speed resulted in a yearly energy increase of 2.7 %, relative to fixed pitch

operation. Assuming an optimum twist distribution for all operational conditions resulted accordingly in a 5.5 % increase.

The resulting optimum twist distribution as a function of radial station corresponds to a gradual increase in twist with wind speed, however, only up to 11 m/s. Above this speed the relation is adverse. This would require some kind of active control. The final design has semi-pitchable blades as airbrake system and is thus prepared for active stall regulation, which means that the collective pitch setting is very easy to apply, and the optimum twist distribution is then a realistic option for further developments, but it is not applied for the prototype.

A soft rotor design might give rise to high coning angles and/or large blade deflections. This condition would violate one of the fundamental assumptions in the blade element momentum theory.

An investigation was performed using Navier-Stokes simulations of how the out of plane blade axis shape or swept rotor surface shape affects the rotor efficiency [3].

The investigation revealed the important finding that the induced velocities for straight versus coned or flexible rotors are different at the same radial station, and locally the efficiency can exceed the Betz limit, however, when integrating over the whole rotor projected area, there is no net difference.

A soft rotor that is suited for operation at high coning angles, thus, should be designed e.g. with respect to twist distribution by correction for the lower induced velocities at the inboard blade sections.

The conclusion from the detailed aerodynamic investigations was that optimisations of the LM 6.1 m blade for this particular application were possible, but not necessary in order to fulfil the objectives and demonstrate the feasibility of soft rotor design. This means that the modifications could be limited to the structural dynamic characteristics and structural design.

3. STRUCTURAL DYNAMIC DESIGN

The basis for the structural dynamic design has been an aeroelastic parametric study of the turbine in six different configurations. This represents concepts from rigid hub rotor with distributed flexibility, over hinged rotor to hinged blades with different flap/pitch couplings. All calculations were performed by parametric variations around the characteristics of the LM 6.1 m blade, and numerical optimisation was applied in order to estimate the optimum combination of some of the characteristics.

The conclusion from the evaluation of the overall advantage of the different configurations was that a certain combination of flexibility in both teeter hinge and blade root is most optimal. This means that the concepts have converged towards one with all characteristics integrated: The teetering rotor with blade root flexure and any favourable structural coupling.

The parametric study thus led to the selection of five main characteristics to be used as optimisation variables: The teeter and flex-beam stiffnesses, the amount of $\delta 3$ coupling on the teeter and on the flex-beam and finally the radial position of the hinge simulating the flex-beam.

These optimisations led to the optimal characteristics for the rotor given in Table 1, which was then the precondition for the design and construction work.

Table 1 Optimal and chosen rotor characteristics.

	Teeter stiffness [Nm/rad]	Flap stiffness [Nm/rad]	Teeter $\delta 3$ [°]	Flap $\delta 3$ [°]	Flap radius [m]
Optimal rotor	7000	12000	25	-5	0.4
Final rotor	5000	7000	0	0	0.7

4. DESIGN OF THE SOFT ROTOR

In order to arrive at a realistic (or universal) solution, it was decided to consider the airbrake as a requirement for the soft rotor design. Numerous considerations lead to the decision of using the blade pitch function as a basis for the design of the air brake system. This furthermore gives the opportunity for the concept in the future to include the principle of active stall, which will be advantageous for large turbines.

The design considerations for the blade led to a solution, where the blade practically consists only of the shell, which constitutes the aerodynamic shape, and a flex-beam that is designed to give the optimum blade flapwise stiffness and damping characteristics. This means that the blade has no spar or webs and thus has potentials for light weight and future application of adaptable airfoil geometry.

The flex-beam is a sandwich construction in glass-fibre and rubber, which gives favourable damping characteristics with respect to stall-induced vibrations and yaw-stability.

Alternatively to the traditional blade root flange, the new concept applies a three-point support of the blades, which in principle is applicable independent of wind turbine size. Two of the points constitute flap hinges at the leading and trailing edges, respectively. The hinge angles with the rotor plane and the blade axis determine the flap/edge- and the flap/pitch coupling, respectively. A flap/edge coupling corresponding to a hinge angle of 8° was chosen in order to eliminate stall-induced vibrations. The third point transfers the flapwise bending moment through a flex-beam of well-defined stiffness – the value of which depends on the size of the wind turbine. The principle offers the possibility to

cone the blades 90° so that they are aligned with the wind in order to reduce blade and tower loads at stand still in extreme winds.

The airbrake function is obtained by pitching of the blades approximately 15° negative, which further offers the possibility for adjustable pitch angle and thus active stall-regulation.

In summary the final concept is characterised by:

- Two-bladed teetering rotor.
- Hinged blades with flap/edge-coupling that is controlled by both active stall and active coning.
- Free-yawing downwind turbine.
- Nacelle tilt flexibility.

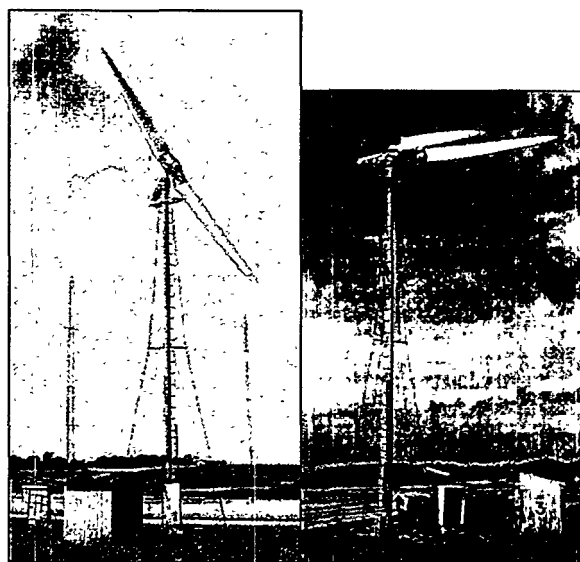


Figure 1 Pictures of the turbine in operation and actively coned at stand still, respectively.

For the actual manufactured turbine, the two control possibilities are only obtained by manual adjustment. Pictures of the final turbine are shown in Figure 1.

5. DESIGN VERIFICATION

During the design phase compromises were made with respect to some of the optimal characteristics, in order to facilitate manufacture and testing. Comprehensive simulations (5 min. series, 12 % turb. int.) were performed once more with HawC [4] with parameter values corresponding to the finally manufactured turbine (Table 1), and compared to measurements. In some cases comparisons were made to calculations for a corresponding teetering rotor turbine with rigid blades. This comparison is illustrated in Figure 2 for the flapwise blade bending moment. It was revealed that blade and tower loads are much reduced for the soft rotor design compared to the stiff teetering rotor.

The yaw stability reflects the important characteristics for the turbine, as it is determined as the resulting response of the sum of the main forces on the turbine. The mean yaw angle is predicted to be very close to zero degrees, except for very low wind speeds, where there is a tendency for positive yawing, as reflected in Figure 3. This was also the case for the measurements, also presented in Figure 3.

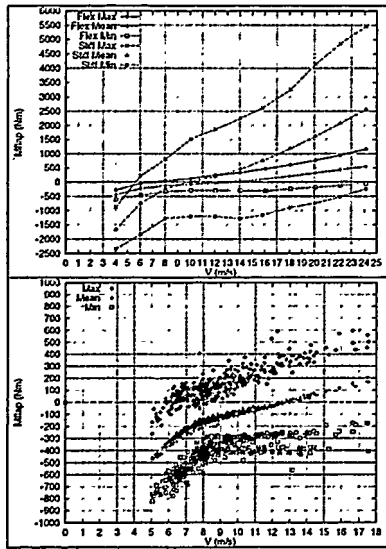


Figure 2 Statistics (30 sec.) for predicted and measured flap moment (prediction for both soft and rigid blades).

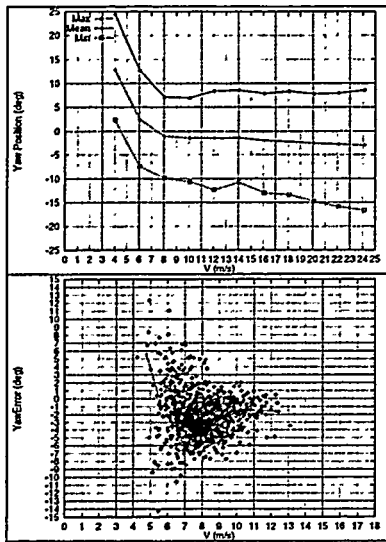


Figure 3 Statistics (30 sec.) for predicted and measured yaw angle in operation.

Teeter instability could be a serious problem, but no such phenomenon has been encountered for the turbine. The statistics for the predicted and measured teeter angle is presented in Figure 4. Both graphs demonstrate that the teeter angles will be limited to $\pm 8^\circ$ in normal operation.

Altogether, the measurements very much verified the estimated optimal characteristics, and the turbine behaved as expected without any need for modifications or adjustments to the design after installation.

6. POTENTIALS FOR UP-SCALING

As mentioned previously the manufactured turbine was considered a scale model of a large MW turbine with respect to design principles. In order to clarify the potentials for up scaling, we look at moments controlling the equilibrium coning angle, θ . A blade segment, assumed to be supported by a mass-less rod and having

length l , mass m , chord c and centered at hinge distance r , is considered. The radial and flapwise position of the segment is determined by r and the coning angle θ , equivalent to the rotation of the hinge at the main shaft, which rotates with angular velocity ω .

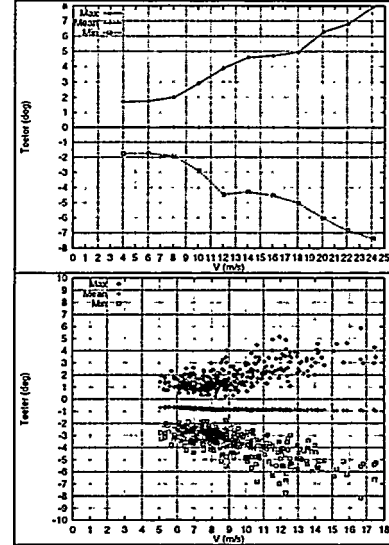


Figure 4 Statistics (30 sec.) for predicted and measured teeter angle in operation.

Expressing equilibrium of the moments from aerodynamic and centrifugal forces with respect to the hinge provides the corresponding coning angle, assuming zero hinge stiffness. The aerodynamic moment yields:

$$M_A = \frac{1}{2} \rho C_L c l \sqrt{r^2 \omega^2 + V^2} \omega r^2 \cos \theta$$

where ρ is the air density, C_L is the airfoil lift coefficient and V is the free wind speed parallel with the main shaft. The moment from the centrifugal force is derived to:

$$M_C = m r^2 \omega^2 \cos \theta \sin \theta$$

Equilibrium of these moments determines the coning angle:

$$\tan \theta = \frac{1}{2} \rho C_L \frac{c r}{m/l} \sqrt{1 + \left(\frac{V}{r\omega} \right)^2}$$

which approximates

$$\tan \theta = \frac{1}{2} \rho C_L \frac{c r}{m/l} \quad \text{for} \quad \frac{V}{r\omega} \ll 1$$

This equation shows that the coning angle θ – with good approximation – is independent of the rotational speed, ω , and also independent of size, assuming similarity scaling, and that the mass per unit length is scaled with the radius squared.

In general, when up-scaling a wind turbine applying similarity and constant tip speed, the blade bending moment from the aerodynamic force increases with R^3 , and so does the blade sectional moment of resistance, resulting in equal material stress for all sizes. However, as blade mass increases with R^3 , the bending moment from gravity increases with R^4 . This means that gravity plays a relatively increasing role, proportionally to size, R .

6.1. Up-scaling to 1MW.

In order to illustrate and clarify in more detail the potentials for up-scaling, an aeroelastic modelling of a

1MW, 65 m diameter turbine was performed [4] by almost direct up-scaling of the test turbine with a factor of 5 and by increasing the tip speed to 59 m/s. The blade mass distribution was assumed to be almost constant at 100 kg/m, the pre-coning was 10° and aeroelastic simulations were performed at 8, 14 and 24 m/s, respectively, and at 12 % turbulence.

The main dynamic characteristics are reflected in the simulated teeter angle in Figure 5 and the yaw-stability in Figure 6.

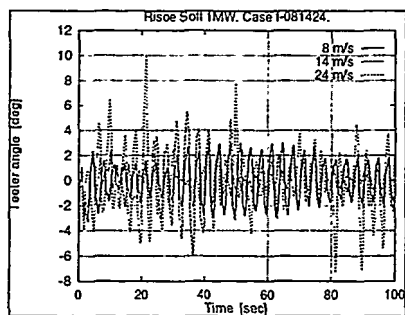


Figure 5 Teeter angle at 3 different wind speeds.

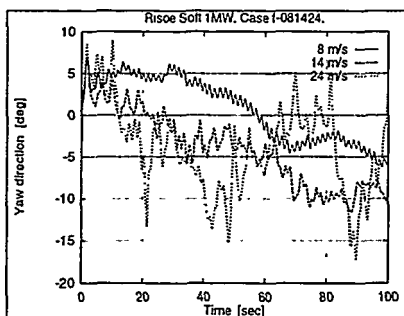


Figure 6 Yaw angle at 3 different wind speeds.

These graphs show that the 1 MW turbine has no stability problems and generally behaves much like the small test turbine. The blade tip deflection is in the range from -1 m to a maximum of +5 m from the unloaded starting point.

For illustrative reasons a comparison has been made to a similar turbine with rigid hub, rigid blade root, fixed yaw and zero pre-coning. The blade root bending moments for the soft and the stiff rotors are presented in Figure 7, which reflects that both mean and fatigue loads are less than half for the soft rotor.

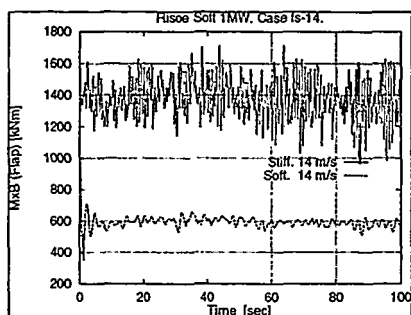


Figure 7 Blade flapwise moments for stiff and soft designs.

Altogether, the preliminary aeroelastic predictions indicate that up-scaling to 1MW could be done fairly straight forward, and reasonable response characteristics could be

obtained without having performed a detailed optimisation with respect to blade aerodynamic shape, mass distribution, tip speed and structural characteristics for the actual turbine size.

6.2. Up-scaling to 5 MW

Wind turbine sizes of 2 MW are now in production, and even larger turbines are in the design phase. It is thus relevant to investigate the possibility for further up-scaling of the 1 MW by a factor of 2 and slightly increased tip speed to 5 MW at a rotor diameter of 130 m. Similarity would require a blade weight of 28 tons (8x3500 kg), which would represent no problem for the blade itself, however, the turbine yaw response characteristics would be unfavourable. This was reflected by aeroelastic simulations on the previous 1MW turbine with gravitation increased by a factor of 2 to 19.6 ms^{-2} . The turbine would be stable in operation, however, the yaw response characteristics would be so far from optimal that a detailed optimisation of both aerodynamic and structural dynamic characteristics should be performed specifically for the 5 MW size. Although the characteristics would differ from the ones of the small turbine, the 5 MW turbine would still be perceived as the same basic concept.

7. CONCLUSION

The work has confirmed that substantial load reductions can be obtained for the presented concept in comparison to stiff ones, and that the applied calculation tools are applicable even for such an extreme configuration.

Altogether, the experience from design of the soft rotor and the investigations on upscaling is that the resulting design represents a frame for a quite universal concept, which contains potentials for future detailed optimisations.

8. ACKNOWLEDGEMENT

The work was supported by the EC under Contract JOR3-CT95-0062 and the Danish Energy Agency under the contract ENS 1363/95-0002. The authors want to thank P. Vølund, P. Leconte, E. Szechenyi, C. Westergaard, L. Jensen, S. Olsen, B. S. Johansen and P. Ellebæk for their contributions to the *Soft Rotor Design* project.

REFERENCES

- [1] P. Leconte, E. Szechenyi. *Aeroelastic Tailoring of Blades: Prospects for Reducing Unsteady Loads and Enhancing Performance*. EUWEC '96, Göteborg.
- [2] C. Bak. *Aerodynamic Optimisation of a Two-Bladed Wind Turbine*. Risø-I-1343(DA), Risø National Laboratory, 1998.
- [3] H. Aa. Madsen and F. Rasmussen. *Flexible Blades, and Coning Change the Efficiency Locally*. Risø-AED-RB-5. Risø National Laboratory, 1998.
- [4] J. T. Petersen. *The Aeroelastic Code HawC – Model and Comparisons*. In "State of the Art of Aeroelastic Codes for Wind Turbine Calculations". 28th Meeting of Experts, IEA, Annex XI. TUD, Lyngby, Denmark. April 1996, pp. 129-135.

OFFSHORE WIND FARM BOCKSTIGEN - INSTALLATION AND OPERATION EXPERIENCE

Bernhard Lange^o, Erik Aagaard, Paul-Erik Andersen, Anders Møller, Staffan Niklasson*, Andreas Wickman*

Wind World af 1997 A/S, Voerbjergvej 40, DK-9400 Nørresundby, Denmark

* Vindkompaniet, Gettlinge 2081, S-380 65 Degerhamn, Sweden

^o now at: RISØ National Laboratory, Wind Energy and Atmospheric Physics Department, P.O.Box 49, DK-4000 Roskilde

ABSTRACT: The first Swedish offshore wind farm Bockstigen is operating since March 1998 near the coast of Gotland. It was built as a demonstration project by the Swedish wind farm developer Vindkompaniet, the Danish wind turbine manufacturer Wind World and the British offshore construction company Seacore and partly funded under the EU-THERMIE program. Bockstigen is the fourth offshore wind farm world-wide. While at previous wind farms the main emphasis laid on the demonstration of the technical feasibility of offshore wind energy utilisation, Bockstigen was aimed at demonstrating its economic viability. A number of innovative concepts have been employed: Drilled monopile foundations were used to save costs. A new construction method has been applied making use of a jack-up barge. A new control system for the turbines and the whole wind farm was developed, which controls the maximum power output, the flicker and the reactive power consumption depending on online measurements of the actual grid state. These new developments have been implemented successfully. A substantial cost reduction compared to previous offshore projects could be achieved.

Keywords: Demonstration Projects, Off-shore, Operating Experience, Bockstigen

1. INTRODUCTION

Offshore wind energy is one of the most important options for the future expansion of wind energy utilisation. In several European countries the available space with favourable wind conditions is getting scarce. Developing the offshore potential means to have ample space available with very favourable wind. The main disadvantages of offshore locations are the higher costs of foundations and sea cables and of the installation and maintenance work. The aim of developing offshore wind energy is therefore to be able to build wind farms at a cost compatible to installations on land. Therefore the additional costs have to be low enough to be outweighed by the additional energy production due to the more favourable wind regime.

2. THE WIND FARM BOCKSTIGEN

2.1 Location

The wind farm is located south-west of the Swedish island Gotland in the Baltic Sea (see figures 1 and 2). Its distance to the coast is about 4 km and the water depth app. 6 m.

The site has the main advantages of:

- low water depth in relative large distance to land
- suitable soil conditions for drilling and monopile foundation
- harbour for installation and maintenance within reasonable distance



Figure 1: Bockstigen wind farm



Figure 2: Site and layout of the wind farm Bockstigen

2.2 Turbines

The wind farm consists of 5 Wind World 550 kW turbines which were especially adapted to offshore conditions. This type was chosen because of its simple and reliable technology and high availability record. The design characteristic of all Wind World turbines is a ridged integrated gearbox with a flange mounted generator. This construction ensures long life time and low service costs. The 3 bladed rotor with a diameter of 37 m is mounted upwind of the tower. The turbine is stall regulated with tip air brakes. The tower is a modified 38 m standard tubular steel tower in two sections. It is flange mounted on a steel monopile of 21 m length. The hub height of the turbine is app. 40 m above normal sea level. For easy access a platform is mounted between tower and monopile. In the design of the whole construction special attention is paid on the resonance frequencies of the turbine with the monopile foundation and the additional loads from current, waves and ice.

Some offshore modifications have been applied to the turbines: Hoist equipment allows replacement even of major components. The compartments in the monopile and the tower are equipped with a closed ventilation system to ensure dry, cool and condense free environment for control system, switchgear and transformer.

2.3 Grid connection

The connection point in Gotland-Valar is a 10 kV net with a short-circuit power of only 16.9 MVA, which means a ratio of almost 15% wind park power per short-circuit power. To operate such amount of stall-regulated turbines without conflict with the IEC standards required a complete new innovative solution: The 'Master Controller' system for a wind farm and the 'Optimal Speed' control system for a turbine have been employed to achieve this. The 'Optimal Speed' control system uses a power converter to perform its two main functions:

1. At low wind speeds (up to app. 20% of rated power output) the converter operates as frequency converter. The turbines generators run with variable speed to increase the power output.
2. At medium and high wind speeds the turbines are directly grid coupled. Here the power converter operates as a precision blind current source. This gives a fast and full dynamic flicker compensation and also enables the cos-phi regulation.

The 'Master Controller' for the whole wind farm is located at the grid connection point on land. Its main function is to guarantee the IEC compatibility of the grid voltage between the connection point (CP) and the next bus-bar (10 kV to 30 kV station). These control tasks are:

- perform a complete 3 phase U/I/P measurement at the CP
- operate the whole wind park at cos-phi = 1 as long as the grid voltage is uncritical and to decrease cos-phi up to a specified value in order to hold down the voltage if it comes close to the limit
- use additionally a set of dumploads (0-500 kW in 20 steps) and to stop and restart one or more turbines to limit the wind park real power output
- control the flicker compensation parameter (psi-K) for all turbines to minimise the flicker along the line from the CP to the bus-bar

The wind farm 'Master Controller' additionally performs the functional control of the wind farm including turbine remote control. Data communication with the turbines is done via an optical fibre grid.

2.4 Foundation

To achieve a low foundation cost at Bockstigen the technology of drilled monopile foundations was used for the first time for wind energy applications. The foundation consist of a 21 m long tubular steel monopile. It is fixed with concrete in a 10 m deep hole drilled in the sea bed rock (see figure 3). The suitability of the rock and the required hole depth have been evaluated by probe drillings. The completed construction has the following advantages compared to previously used solutions:

- The weight is only 43 tons.
- Ice and wave loads are heavily reduced since the waterline is only 2.1m wide.
- The foundation can be towed to the site by a normal tug boat and can be lifted into place by a crane with 35 tons lifting capacity by using the lifting capacity of the water.

3. CONSTRUCTION METHOD

Turbines and monopiles were manufactured at Wind World's factory in Skagen. Monopile foundations are relatively simple and inexpensive to produce compared to concrete gravity foundations. Transport of the components was made by ship directly to the harbour Klintehamn from where the installation took place. Transport on site was performed by Vindkompaniet's own small ferry together with a barge and a small tug boat. For transport the monopiles were sealed watertight and could therefore be floated.

To drill the foundation hole the jack-up barge is used. A hole of 2.4 m diameter and 10 m depths is drilled in the

rock. Drilling can be performed in any kind of rock which is hard enough to be self supporting. When the drilling is finished the tug boat tows out the monopile which is then lifted into the hole. Finally the monopile is grouted into position by filling the gap between the 2.25 m diameter monopile and the rock with special concrete.

After finishing all foundations the jack-up barge was also used as a stable and efficient tool to erect the turbines. They are mounted onto the foundation by means of the platform's crane and the ability of the platform to lift itself up on the supporting legs.

The electrical sea cable and the glass fibre communication cable were laid with help of the ferry and anchored to the seabed. Thereafter they were connected to the turbines and to the land grid.

4. PROJECT ECONOMICS

The total cost of the Bockstigen wind farm was 4 mio. Euro. The projected power output is 8 GWh per year. The cost per estimated yearly power output is 0.50 Euro/kWh/y. This figure can be compared with the cost of previous offshore installations and with that of land based wind farms:

- Vindeby offshore wind farm: app. 0.91 Euro/kWh/y [1],[2].
- Tunø Knob offshore wind farm: The cost per estimated yearly power output is app. 0.76 Euro/kWh/y [2].
- The last land based wind farm (10 MW) built by Vindkompaniet cost 0.41 Euro/kWh/y.

It turns out that a substantial cost reduction compared to the wind farms Vindeby and Tunø Knob could be achieved which were about 80% and 50% more expensive than Bockstigen. A favourable location on land is now only about 15-20% cheaper than the offshore installation at Bockstigen.

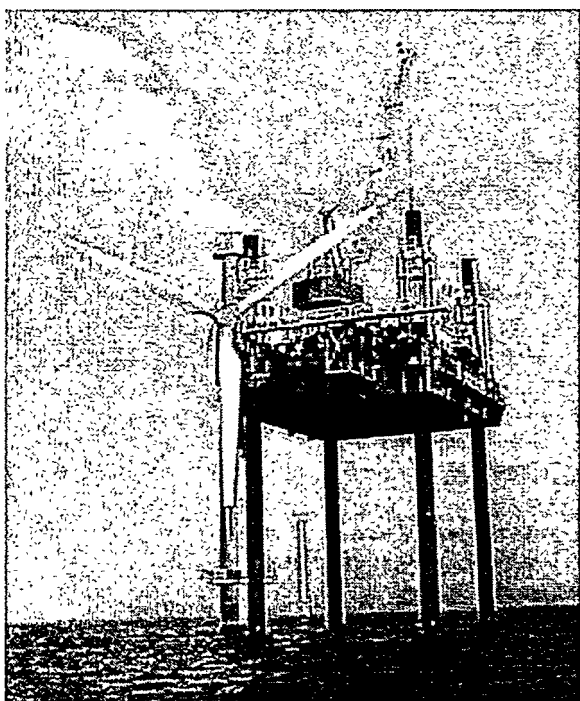


Figure 4: SEACORE jack up barge used for drilling and erection

5. LESSONS LEARNED

A number of new technologies were developed and implemented to make the offshore wind farm Bockstigen technically and economically feasible. Through the whole construction process only one genuine technical problem was encountered, which was the anchoring of the sea cables. The water current was larger than assumed due to an acceleration of the flow over a ridge and the difficulty to anchor the sea-cable to the sea bed was underestimated. Where large areas of the seabed were free from loose layers it proved necessary to anchor parts of the sea-cable with the use of steel hoops. The first attempt was to use concrete sacks as weights. The second attempt was to anchor the cable with hooks made of 12 mm steel. Both failed and first the third attempt employing 25 mm U-shaped hooks anchored in two holes in the sea bed was successful.

On the planning side, the time plan could not be met. This was due to the combination of a number of reasons:

The late arrival of the jack-up barge delayed the start of the construction work. The lifting of the monopiles into the holes turned out to be very sensitive for waves. Also wave heights at the site were higher than assumed due to the building up of waves when they reached lower water depth. This further delayed the work and finally the anchoring problems could not be solved before winter started. Therefore the wind farm was operational first in spring 1998.

Despite these delays the cost plan could almost be kept with only about 10% cost rise over the budgeted cost. The cost rise was mainly due to the problem with anchoring the sea cable.

The main lessons learned during the project are:

- Wind, wave and sea current conditions at the site should be carefully investigated.
- Installation of the sea-cable can be carried out at a lower cost if the right method is chosen from the beginning.
- The installation process of the monopile foundation can be made even less weather sensitive, reducing time and therefore cost.

Throughout the planning, construction and operation a lot of valuable knowledge was gained by all partners involved. Plans are going ahead to build further offshore wind farms in Sweden with the same technology which was successful at Bockstigen. It is believed that due to the experience and knowledge gained from this first demonstration wind farm future projects can be built at even lower costs.

6. POWER OUTPUT MEASUREMENTS

On Gotland several turbines of the same type as used for the offshore wind farm are operating very close to Bockstigen. Measurements are performed to investigate the difference in production between land based and offshore turbines. Meteorological measurements including 1-min. mean values of wind speed and direction at different heights are available from a 145 m high mast at Näsudden. The power output of the Bockstigen turbines is available as 10-min mean values from the wind farm 'Master Controller'. For a number of land based turbines hourly power output measurements are available for comparison.

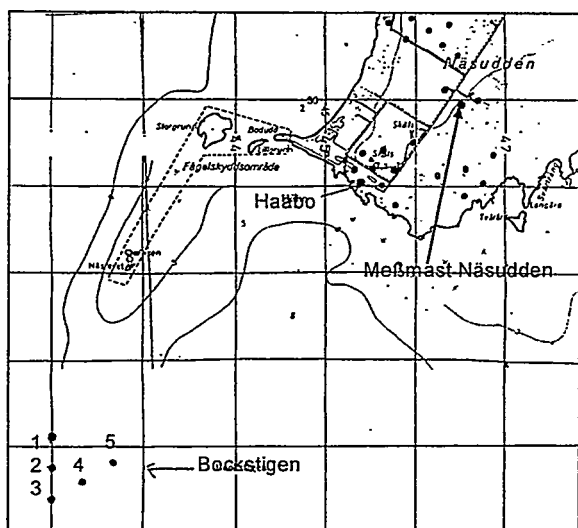


Figure 4: Map of the locations of the measurements

The locations of the different measurements are shown in figure 4. In a first preliminary measurement campaign these values have been collected for a period of two weeks. As it can be seen in figure 4 there is a great number of wind turbines located on the peninsula Näsudden. This limits the wind directions for which the measured turbines are not disturbed by wakes of other turbines. The turbine Håbo on land and the Bockstigen turbine 3 have a common sector of undisturbed wind flow for wind directions between 150° and 290° . For these directions both turbines have sea fetch.

Up till 194° for the land turbine and 186° for the Bockstigen turbine the fetches are influenced by the southern part of Gotland. For all other directions both have the same long fetch across the Baltic Sea to Sweden.

Figure 5 shows a one day long time series of wind speed and direction at 145 m from the Näsudden mast and power output measurements from the turbines Håbo and

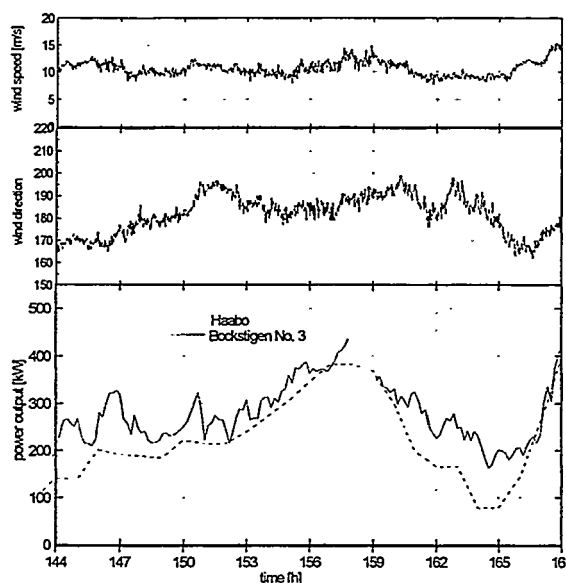


Figure 5: Time series of the 9.9.1998 of wind speed and direction at 145 m height measured at the Näsudden mast and power outputs of the turbines Håbo (hourly means) and Bockstigen 3 (10-min. means)

Bockstigen 3. The wind direction is around 180° , i.e. the fetch is limited by the coast of Gotland. Here the Håbo turbine has a sea fetch of 5 km while the Bockstigen 3 turbine has about 10 km fetch. It can be seen that this fetch difference leads to a significant difference in power output. For the directions with wind speeds from the open sea such a difference can not be found.

However, to quantify this effect a statistical analysis of a much longer measurement period is required.

7. CONCLUSION

The first Swedish offshore wind farm Bockstigen near Gotland has been constructed successfully and is operating since March 1998. The farm consists of 5 Wind World turbines of the type W-3700/550 kW which were especially adapted to offshore conditions. A number of new innovative technological solutions have been developed and implemented successfully which make offshore wind energy technically and economically more attractive.

For the first time rock-socketed monopile foundations were used. Drilling of the holes and erection of the turbines was performed from a mobile jack-up barge. It has been shown that this technology considerably reduces the cost of offshore installations compared to the conventional gravity foundations. The previous Danish offshore wind farms Vindeby and Tunø Knob were about 80% and 50% more expensive than Bockstigen. A favourable location on land is only about 15-20% cheaper. With the experiences from this demonstration project future offshore wind farms will be built at an even lower cost.

The maximum power output of the wind farm is limited by the capacity of the grid at the connection point. This is done by means of the newly developed wind farm 'Master Controller'. It uses online measurements of the grid properties to control the reactive power production of the turbines as well as the maximum total delivered power of the wind farm. This is possible since the wind turbines are equipped with Wind World's Optimal Speed Control. This system delivers a high power quality with low inrush current, full compensation of reactive power and very low flicker.

Measurements are performed at the Bockstigen turbines as well as at turbines of identical type on land. These are used for a direct comparison of the power output between onshore and offshore turbines. Preliminary results indicate a significant difference of power outputs depending on the lengths of the sea fetches involved.

ACKNOWLEDGEMENTS

The Bockstigen wind farm project was supported by the European Commission in the THERMIE program. The meteorological measurements at Näsudden were supplied by Vattenfall AB.

REFERENCES

- [1] Olsen, F.A. and K.Rasmussen: Vindeby offshore wind farm. in: Proceedings of the European Seminar on offshore wind energy in Mediterranean and other European seas. Rome, Italy, 1994

[2] Lemming, Jørgen and Maj Dang Trong: Danish investigations and plan of action for offshore wind power. in: Proceedings of the European Seminar on offshore wind energy in Mediterranean and other European seas. La Maddalena, Italy, 1997

WIND POWER AND A LIBERALISED NORTH EUROPEAN ELECTRICITY EXCHANGE.

Lars Henrik Nielsen¹, Poul Erik Morthorst¹, Klaus Skytte¹, Peter Hjulær Jensen¹,
Peter Jørgensen², Peter Børre Eriksen², Aksel Gruelund Sørensen², Flemming Nissen³,
Bjørn Godske⁴, Hans Ravn⁴, Charlotte Søndergren⁴, Kaj Stærkind⁴, Jan Havsager⁴.
¹Risø National Laboratory, Roskilde. ²Eltra, Fredericia. ³Elsam, Fredericia. ⁴Elkraft, Ballerup.

ABSTRACT: Conditions for wind power on a liberalised North European electrical power market are addressed in the paper. Results are presented from a recently completed study carried out by Risø National Laboratory in collaboration with the Danish electric utilities Eltra, Elsam and Elkraft. A main result from the study is, that the market will be able to provide the necessary power regulation, that will be required year 2005 as a consequence of the expected wind power capacity extension, according to the Danish energy plan, Energy21. The average sales price on the market for the wind-generated electricity is less than the average spot market price, due to provision of power regulation to balance the unpredictability of the wind power. This reduction in the market value of wind power has been calculated to 10-20 DKK/MWh or 1.3-2.7 EUR/MWh.

Keywords: Electricity Market, Power Regulation Costs, Forecasting Methods, Power Generation.

1. INTRODUCTION

System integration of wind power on a liberalised North European electrical power market has been analysed in a study carried out by Risø National Laboratory in collaboration with the Danish electric utilities Eltra, Elsam and Elkraft. The Risø part of the project has been financed by the Danish Energy Agency.

A main objective of this methodical study has been to analyse the value of fluctuating power production, especially wind power, in the context of a liberalised power market. Market prices and power regulation costs on the market are estimated and related to the uncertainty associated with predicting wind power production. Consequences of the prediction accuracy and the market strategy on the market value of wind-generated electricity are addressed.

A second objective of the study has been to analyse consequences of introducing technologies, able to provide power regulation, to improve utilisation of large capacities of wind power in the Danish and North European power system. Potential contributors, electricity suppliers and consumers, able to increase the power regulation capability on the market are mentioned.

The Danish energy plan, Energy21, forms the starting point of the analysis, and main emphasis is put on the system aspects year 2005.

2. BASELINE ELECTRICITY EXCHANGE

An essential part of the work has been to construct a model of a baseline market for sale and purchase of electricity in Northern Europe year 2005 (Fig.1).

The set up baseline electricity market comprises a spot market and a balance market for electricity. The structure chosen for the baseline spot market for year 2005 is close to the structure of the existing Nord Pool electricity market and the structure of the balance or regulatory market is close to the existing Norwegian model.

At the spot market sales and purchase of electricity are traded for the next 24 hours period. Producers and consumers state their offers daily before noon (12 a.m.) concerning

prices and amounts for delivery in the forthcoming period from 0 a.m. to 12 p.m. Thus, offers are given 12-36 hours before the delivery. Based on these offers the spot market prices are determined by demand and supply on an hourly basis for the next 24 hours period.

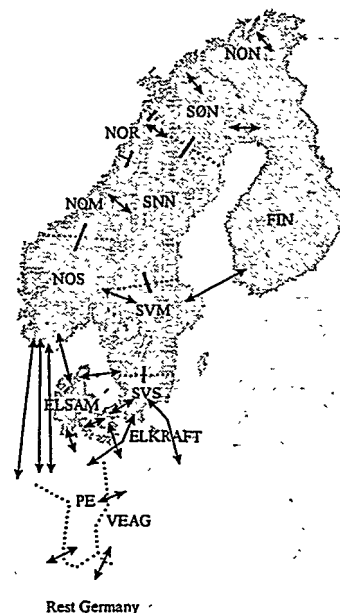


Figure 1: Extent of the electricity market analysed.

Deviations from the planned trade at the electricity exchange spot market relative to the actual delivery and consumption in (and during) a particular hour are handled by the balance market. The electricity balance market must continuously secure the balance between power production and consumption. The balance market determines the price of short notice power regulation in the system and handles the necessary trade of power regulation based on received offers on short notice regulating (up and down) from both producers and consumers in the market.

Detailed model calculations on the North European electricity production system and data from the existing Nord Pool electricity market form the basis for the set up baseline market.

Using the EMPS model (Samkøringsmodellen), calculations have been carried out to determine expected electricity price levels and the power exchange among the North European electricity systems during year 2005. The model operates with a time resolution of weeks, based on inputs concerning e.g. power plants, fuel prices, hydro inflow statistics and power demand.

Conversion of the calculated price levels on a weekly basis to baseline spot market prices on an hourly basis is carried out subsequently. This is done based on a statistical analysis of the observed hourly price variations at the Nord Pool spot market.

Uncertainties due to annual precipitation variations in the Scandinavian hydropower production and consequences of CO₂-taxation are reflected in the analysis. Baseline spot market prices are set up on an hourly basis for cases termed normal, wet and dry years for the precipitation in Scandinavia. In dry years electricity prices tend to increase and the opposite is the case in wet years. Furthermore, these baseline spot market prices are analysed for a situation where a general CO₂-tax of 100DKK/ton CO₂ (13.5EUR/ton CO₂) is imposed on the market considered as a whole.

The corresponding baseline balance market is set up using a relation which is estimated from the balance market prices observed at the Norwegian electricity exchange. An outline of this relation is shown on Figure 2.

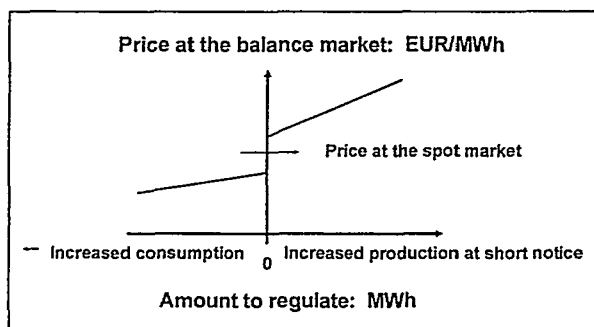


Figure 2: Regulation cost structure assumed at the balance market.

The estimated balance market prices are functions of the spot market price at the hour and the amount (and direction) of the short notice power regulation required at the market.

3. MARKET VALUE OF WIND-GENERATED ELECTRICITY

Wind power plants are treated in line with any other electricity production system in the analysis, and the wind-generated electricity is sold at market terms just as any other electricity produced.

However, the predictability of the wind power influence the market value or the sales price of the wind-generated electricity. If the amount of wind-generated electricity offered by the producer at the spot market

deviates from the later actual delivery then this discrepancy (surplus production or absent production) must be settled on the balance market. This implies a reduced sales price and a reduced income for the producer.

The reduction in the annual average sales price for the wind-generated electricity at the baseline market has been calculated for different assumptions concerning the prediction accuracy of wind power production and the strategy chosen by the producer when offering the electricity production at the baseline power exchange.

For three levels of prediction accuracy the annual average sales prices of wind-generated electricity are calculated. Results are shown on Figure 3. The average sales prices shown are derived by simulating the wind power production interacting with the baseline electricity market during one year on one hour basis using the ES³-model. In Figure 3 it is assumed that throughout the year the producer offers sales at the spot market in amounts, which are equal to the predicted wind power production (12-36 hours in advance). As mentioned before, deviations from this in the later actual wind power production are settled at the balance market, where regulation costs corresponding to the amounts to regulate are settled. Such regulation costs due to the level of unpredictability of the wind-generated electricity are included in the annual average sales prices shown on the figure.

Prices at the baseline balance market reflect prices on power regulation in the Scandinavian electricity system, which is dominated by hydropower.

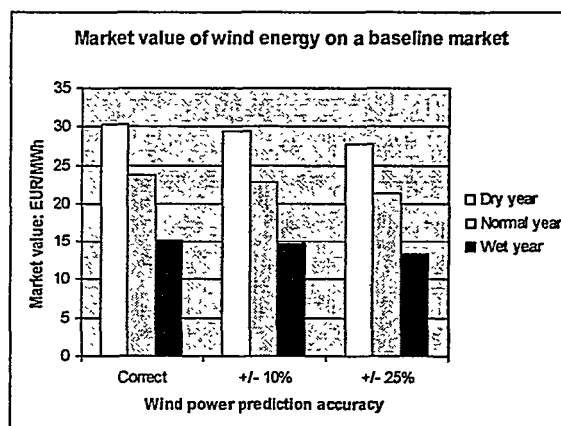


Figure 3: Average sales prices of wind-generated electricity on a North European electricity market depending on the prediction accuracy for wind power.

The prediction accuracy for wind power year 2005 can be expected to be somewhere between +/- 10% and +/- 25% of the electricity produced annually. Forecasts for the annual wind power production in total are relatively more accurate than predictions on a shorter time scale, and therefore it is assumed in calculations that the total annual offer at the spot market equals the actual annual production. A deviation between the predicted and the actual production of +/- 25% here means that a surplus production relative to the predicted production occurs to an extent that equals 25% of the annual production. Furthermore this indicates, that absent production relative to the predicted production occurs to an extent that likewise

equals 25% of the production. Thus in total the balance market settles amounts corresponding to 50% of the annual wind power production in this situation. A deviation termed +/- 10% thus implies that in total only 20% of the production are settled via the balance market.

Results termed 'Correct' on Figure 3 are based on the ideal assumption, that the prediction is correct. Thus no power regulation premium is included, and the average spot market prices achieved are shown in cases of dry, normal and wet years. It is observed that the major part of the variations illustrated in Figure 3 are related to the hydropower. This is in part due to the relatively large variations of the hydro inflow between dry, normal and wet years, and due to the magnitude of hydropower relative to the total production. In the Nordic countries hydropower accounts for around 45 % of the energy, while wind power accounts for around 1.5% year 2005. In Denmark wind power accounts for about 11% year 2005.

If a CO₂ tax of 13.5EUR/ton CO₂ is assumed for the market as a whole, the average sales prices achieved would increase about 12EUR/MWh in normal years for the precipitation in Scandinavia.

In Figure 3 it is assumed that the structure of the balance market is close to the Norwegian model. Had alternatively the structure of the balance market been based on the corresponding Swedish market, the average regulation costs would be slightly higher.

Deviations relative to the forecast in the wind power production from an installed capacity of 1700 MW are of about the same magnitude as the observed magnitude of the balance market. Therefore it is concluded that the market will be able to provide the necessary power regulation, that could be required year 2005 as a consequence of the expected wind power capacity extension, according to the Danish energy plan, Energy21. Year 2005 about 1700MW installed capacity on wind power is expected.

Taking into account uncertainties related to the structure chosen for the balance market it is concluded, that the sales price reduction amounts to 10-20 DKK/MWh or 1.3-2.7 EUR/MWh for wind-generated electricity. This reduction is due to provision of power regulation to balance the unpredictability of the wind power. The reduction includes transmission costs between the production sites for wind power (Denmark) and the production sites (Sweden and Norway) for hydropower that are assumed to deliver the main power regulation.

4. TRANSMISSION AND NETWORK CONSIDERATIONS

Simulations carried out using the SIVAEL and PSS/E models show that the present transmission capacity for Danish import/export in periods may have 'bottlenecks' or insufficient transmission capacity for supporting the power import/export trade and transit assumed at the liberalised market. A large combined wind power production and heat constrained power production (CHP) may cause such situations to occur in the period analysed up to year 2015. Such situations may reduce the regulation strength in the power system and may threaten the stability of the grid. Thus transmission grid expansions may be required.

Furthermore, simulations show that large wind power capacities in the Danish power system may cause

'bottlenecks' within the Danish grid. A strengthening of the internal transmission grid may thus also be required. Such costs are not included in the study.

5. REGULATION TECHNOLOGIES AND THE BALANCE MARKET

The ability of local combined heat and power systems (CHP) to offer active power regulation on the balance market has been analysed for cases, in which heat storage and/or heat pumps are included to increase the CHP-system flexibility. Furthermore load management options offered by electric vehicles have been studied relative to the electricity market.

These situations illustrate regulation options both on the power supply side and on the power demand side of the system.

In short the method applied is the following. If a so-called regulation technology is economically viable at market terms and furthermore is able to gain from locating a part of its electricity trade on the balance market then this technology increases the supply of active power regulation capability on the balance market. Such increased supply of power regulation capability on the market increases the ability of the market to integrate or absorb electricity production that requires power regulation, such as wind power.

5.1 Combined heat and power systems

The relevance of introducing heat pumps and/or heat storage in cases where the existing heat production systems are natural gas based combined cycle CHP-systems is analysed.

The introduction of heat pumps in CHP systems increases the ability of the system to take advantage of the varying electricity prices at the market. Within limits such combined systems can choose to be net electricity producers or net electricity consumers along with the heat production. In a large part of the year the heat pump part of the system may benefit from low electricity prices at the spot and balance markets. Likewise the natural gas based combined cycle CHP part of the system may gain from high electricity market prices in other periods.

Simulation of these systems interacting with the baseline power exchange shows, that such technologies or system modifications can increase the supply of power regulation on the market at prices on a level with the balance market.

Thus, if large quantities of fluctuating electricity production (e.g. wind power) build up a strain on the balance market, such technologies can form backstop prices on this market.

This conclusion applies to situations where new or increased heat production capacity is required in the district heating system.

If a CO₂-tax of 13.5EUR/ton CO₂ is assumed the combined heat pump solution may not be attractive. However, the economic advantage in wet years may still make the heat pump solution an interesting option. The frequency of appearance of normal, wet and dry years has to be taken into account in order to determine this.

5.2 Electric vehicles (EVs)

Electricity-based vehicles form new CO₂ reduction options in the transport sector even with the present fuel mix for power generation. In addition these vehicles increase the flexibility of the overall power system due to the substantial load management potential they offer. In the power sector an increased load flexibility increases the ability of the system to integrate fluctuating electricity production e.g. from renewables such as wind power and photo-voltaic. Thus, concurrent CO₂ reductions in the transport and power sectors can be achieved.

Typically EVs charge batteries during the night, a time when electricity prices are low due to low loads. However, to benefit fully from the varying electricity spot market prices, which customers may have direct access to in the future, domestic electricity metering on an hourly basis is required. This enables EV owners to suspend charging until favourable low electricity prices occur. As future EV battery packs are expected to increasingly prolong the driving range per charge (and thus increase the market for EVs) battery recharge may no longer be required on a daily basis. Full recharge may only be required once or twice a week.

Simulations of EVs interacting with the baseline spot market for electricity show, that the load flexibility of the EV can be used to lower purchasing costs of electricity (excluding tax) about 5% relative to the average spot market price year 2005. Furthermore, calculations show that an increase in battery pack capacity of the EV (to about 200km/charge) may enable owners to purchase a substantial part of the electricity needed from the electricity balance market, and savings of more than 10% may be achieved.

Consequently, development towards increased utilisation of EVs for transport has the potential to increase the supply of active power regulation capability on a future balance market. The capability of the overall electricity system, to integrate fluctuating electricity production that requires power regulation, such as wind power, therefore increases. The power regulation potential from EVs may become substantial, and even a few percent of EVs in the transport vehicle fleet can constitute an important player on the electricity balance market. It must be observed, though, that from the point of view of the individual owner of an EV, the economic incentive is small.

6. CONCLUSIONS

A main result from the study is, that the electricity market will be able to provide the necessary power regulation, that will be required year 2005 as a consequence of the expected wind power capacity extension to 1700MW, according to the Danish energy plan, Energy21.

Due to provision of power regulation to balance the unpredictability of wind power the average sales price for wind-generated electricity on the market is less than the average spot market price. This reduction in the market value of wind power has been calculated as 10-20 DKK/MWh or 1.3-2.7 EUR/MWh.

Improving the prediction accuracy of wind power production therefore increases the market value of wind-generated electricity.

Transmission grid expansion and reinforcements may be required to support the power regulation and trade on the liberalised market.

Technologies such as electric vehicles and heat pumps integrated in combined heat and power (CHP) systems may serve as regulation technologies that can increase the supply of power regulation on the market at prices on a level with the balance market. Thus, if large quantities of fluctuating electricity production (e.g. wind power) build up a strain on the future balance market, such technologies can form backstop prices on this market.

REFERENCES:

- [1] Nielsen, L.H.; Morthorst, P.E. (eds.), *Fluktuerende vedvarende energi i el- og varmeforsyningen – det mellemlange sigt*. (System integration of wind power on liberalised electricity market conditions. Medium term aspects (In Danish)). ISBN 87-550-2396-7. ISSN 0106-2840. Risø-R-1055(DA) (April 1998) 154p.
- [2] The Danish Ministry of Environment and Energy, *Energy 21*, Denmark (1995).
- [3] Nielsen, L.H. (ed.), *Vedvarende energi i stor skala til el- og varmeproduktion. Indpasning i elsystemet af vedvarende energi i stor skala i en usikker fremtid. Hovedrapport*. (Renewable energy for large-scale power and heat production in the future Danish energy system, main report (In Danish)). ISBN 87-550-2029-1, ISBN 87-550-2087-9(KPL). ISSN 0106-2840. Risø-R-784(DA)(1994) 114 p.

Correspondence to:

Senior Scientist Lars Henrik Nielsen, Systems Analysis Department, Risø National Laboratory, P.O. Box 49, DK-4000 Roskilde, Denmark. Phone:+45 4677 5110, Fax:+45 4677 5199, Internet: l.h.nielsen@risoe.dk.

Address/phone/fax/e-mail:

¹⁾ Risø National Laboratory, Systems Analysis Department, P.O. Box 49, DK-4000 Roskilde, Denmark. Phone:+45 4677 5110, Fax:+45 4677 5199, Internet: l.h.nielsen@risoe.dk.

²⁾ Eltra, Fjordvejen 1-11, DK-7000 Fredericia, Denmark, Phone:+45 7556 2500, Fax:+45 7556 4510, Internet: pjq@eltra.dk.

³⁾ Elsam, Overgade 45, DK-7000 Fredericia, Denmark, Phone:+45 7622 2400, Fax:+45 7622 2009, Internet: fn@elsam.com.

⁴⁾ Elkraft, Lautruphøj 5, DK-2750 Ballerup, Denmark, Phone:+45 4466 0022, Fax:+45 3947 3810, Internet: hrv@elkraft.dk.

CLASSIFICATION OF OPERATIONAL CHARACTERISTICS OF COMMERCIAL CUP-ANEMOMETERS

Troels Friis Pedersen, Uwe Schmidt Paulsen
 Risø National Laboratory / Wind Energy and Atmospheric Physics Department
 P.O. Box 49
 DK-4000 Roskilde
 Denmark
 Phone: +45 4677 5042
 Fax.: +45 4677 5083
 Email: troels.friis.pedersen@risoe.dk

ABSTRACT:

The present classification of cup-anemometers is based on a procedure for classification of operational characteristics of cup-anemometers that was proposed at the EWEC '97 conference in Dublin 1997. Three definitions of wind speed are considered. The average longitudinal wind speed (1D), the average horizontal wind speed (2D) and the average vector wind speed (3D). The classification is provided in these terms, and additionally, the turbulence intensities, which are defined from the same wind speed definitions. The commercial cup-anemometers have all been calibrated in wind tunnel for the normal calibrations and angular characteristics. Friction was measured by flywheel testing, where the surrounding temperatures were varied over a wide range. The characteristics of the cup-anemometers have been fitted to the heuristic dynamic model, and the response has been calculated in time domain for prescribed ranges of external operational conditions. The results are presented in ranges of maximum deviations of "measured" average wind speed. For each definition of wind speed and turbulence intensity, the cup-anemometers are ranked according to the most precise instrument. Finally, the most important systematic error sources are commented.

Keywords: cup-anemometer, anemometry, measurements, classification

CLASSIFICATION PROCEDURE

The classification procedure, described in Ref. 1, is taking primary relevant characteristics of cup-anemometers into account. The elements of the classification procedure are shown in Figure 1.

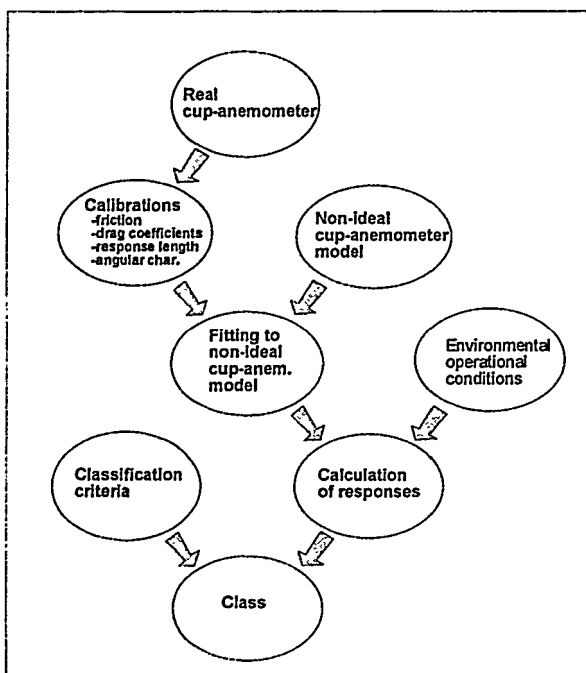


Fig. 1. Elements of the classification of cup-anemometers

The heuristic cup-anemometer model

The model is a heuristic time domain dynamic model, which takes account of dynamics of the rotor, angular characteristics, and friction in rotor bearings. The describing equation of the cup-anemometer is:

$$M = \frac{1}{2} \rho R A ((U - R\omega)^2 C_{DH} - (U + R\omega)^2 C_{DL}) - (B_0 + B_1\omega + B_2\omega^2) \quad (1)$$

where R is the rotor arm to centre of cup

ρ is the air density

A is the projected cup area

U is the wind speed

ω is the angular speed of the anemometer

C_{DH} is the high drag coefficient (concave side)

C_{DL} is the low drag coefficient (convex side)

B_0, B_1, B_2 are friction constants

The assumptions of the model are:

- Uniform wind flow over the cup-anemometer rotor (defined at the centre point)
- Aerodynamic loads are based on integrated (1/3 rotation) quasi-static drag (high and low) on either side of rotor, not dependent on Reynolds number
- Angular characteristics dependent on wind speed is interpolated from table
- Newtonian dynamics of rotor
- Parabolic friction of rotor, dependent on air temperature is interpolated from table

Ranges of operational characteristics

Table 1 summarises the environmental operational conditions used for the evaluations.

Table 1 Environmental operational conditions

Parameter	Range	
	Minimum	Maximum
Wsp (10min)	4m/s	16m/s
Turb. intensity	5%	(113m/s/ $V_{hub}+12$) %
Air temperature	-10°C	40°C
Air density	0.90 kg/m ³	1.35 kg/m ³
Slope of terrain	-10°	10°

An input file of 10 minute, 3D time series of wind data (32Hz, 8m/s average wind speed, and 20% turbulence intensity) is used throughout the calculations for linear scaling to other wind speeds and turbulence intensities.

Classification definition

The class of a cup-anemometer, for a given definition of average wind speed or turbulence intensity, is defined as the maximum calibrated, fitted and calculated systematic absolute or relative deviation from the normal applied linear regression line, when the operational conditions are varied over the defined ranges.

Definition of wind speeds

The definitions of wind speed are shown in Table 2.

Table 2 Definitions of wind parameters

Wind parameter and type of wind speed sensor	Dimension of wind speed
Average longitudinal wind speed "Longitudinal wind speed sensor"	1D (u)
Average horizontal wind speed "Horizontal wind speed sensor"	2D (u,v)
Average vector wind speed "Vector wind speed sensor"	3D (u,v,w)

CUP-ANEMOMETERS

The cup-anemometers covered by this classification analysis are being used in wind energy, except for the Dana cup-anemometer, which is used for wind monitoring on sailing ships. The cup-anemometers are shown in Figure 2, and described in Table 3.

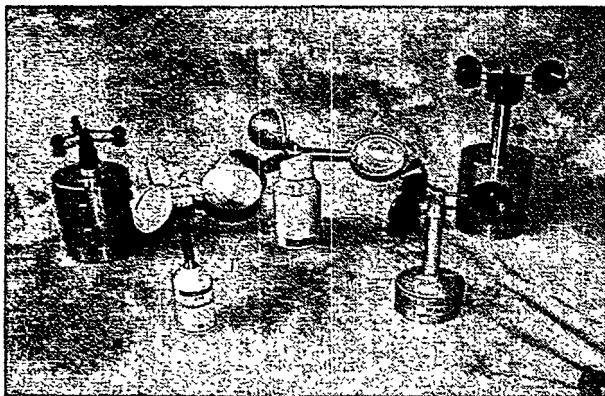


Fig. 2 Cup-anemometers

Table 3 Description of cup-anemometers

Cup-anemometer	Cup shape	Dir. of rotation	Cup diam. [mm]	Rotor diam. [mm]	Total height [mm]	Total weight [g]	Rotor weight ¹⁾ [g]	Pulses per rev.
RISØ P2445b	Conical	CW	70	186	282	420	58	2
NRG Maximum 40	Conical	CCW	50.5	190	75	95	65 ²⁾	2
Dana WSI-0141	Semi-spherical	CCW	24	125	200	108	20	1
Thies 4.3303.22	Semi-spherical	CCW	79	320	228	890	96	44
Vaisala WAA 151	Conical	CCW	54	182	240	552	39	14

1) excluding shaft

2) including shaft and magnet

Calibration and fitting of cup-anemometer data

Calibrations were not necessarily made on the same individual cup-anemometer. Several calibrations were taken from other sources, as mentioned in Table 4. The following list summarises the calibrations made:

1. Calibration of rotor friction at different temperatures to find B_0 , B_1 and B_2
2. Normal wind tunnel calibration 4-16m/s (deriving linear regression line for calibration expression, and fitting to model with known B's to find C_{DH} and C_{DL})
3. Wind tunnel calibration of angular characteristics
4. Calibration of rotor inertia

The angular characteristics were calibrated for some cup-anemometers at three wind speeds, see Table 4. In Fig.3 the angular characteristics are shown for 8m/s.

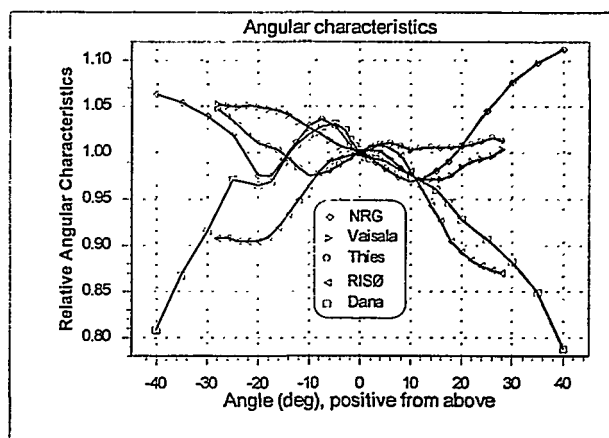


Fig. 3 Angular characteristics at 8 m/s

Rotor friction was calibrated by a flywheel method, described in Ref. 2, using data at rotational speeds, corresponding to 4-16m/s. The friction at 8m/s at different temperatures are shown in Fig. 4 for all cup anemometers.

The rotor inertia (excluding shafts, which can be neglected) were calibrated by a rotor pendulum method, where the rotors were dismantled from the shafts and mounted in three strings and put into oscillations.

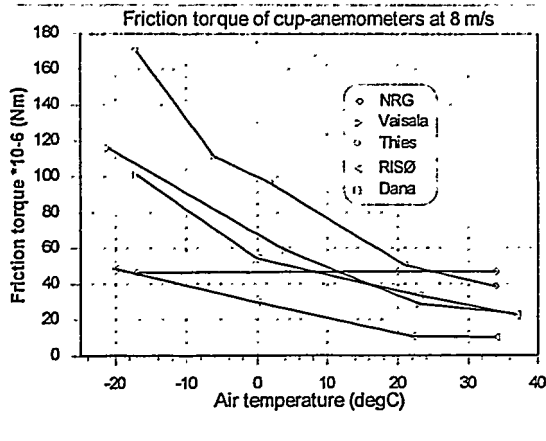


Fig. 4 Rotor friction found by flywheel tests

The inertia was found from the following formula:

$$I = \frac{T^2 M g r^2}{4 \pi^2 l}$$

where:

Table 4 Results of calibrations and fitting of data

Cup-anemometer type	Rotor inertia I $\cdot 10^{-6}$ [kg m ²]	Response length l_0 [m]	Drag coefficients C_{DH} C_{DL}	Drag ratio C_{DL}/C_{DH}	Calibrated Angular responses, wind speeds [m/s]
RISØ	97.4	4.569	1.2214 0.36677	0.30029	5,8,11 ²⁾
NRG	92 ¹⁾	6.704	1.2145 0.38652	0.31825	8.3 ³⁾
Dana	12.3	5.602	1.2871 0.32470	0.25227	8.3 ³⁾
Thies	887	8.158	1.2774 0.30698	0.24032	5,8,11 ²⁾
Vaisala	52	3.334	1.2134 0.37640	0.31020	5,8,11 ²⁾

1) manufacturers information

2) FFA KTH-L2 tunnel (CLASSCUP project)

3) RISØ, DMI-BL tunnel

Table 5 Results of friction and wind tunnel calibrations

Cup-anemometer type	T [°C]	Friction coefficients			Calibration regression line $U=AF+B$ $U=A\omega+B$
		B_0 $\cdot 10^{-5}$ [Nm]	B_1 $\cdot 10^{-7}$ [Nms]	B_2 $\cdot 10^{-9}$ [Nms ²]	
RISØ	-20	2.59	14.7	-6.43	0.6132m/s ² •F[Hz]+0.210m/s ²⁾ =0.1952m/s ² • ω [rad/s]+0.210m/s
	0	0.662	6.52	-1.98	
	22	0.297	1.88	0.0103	
	34	0.452	1.38	0.0678	
NRG	-17	2.84	7.22	-4.78	0.764m/s ² •F[Hz] ¹⁾ 0.7662m/s ² •F[Hz]+0.365m/s ²⁾ =0.2439m/s ² • ω [rad/s]+0.365m/s
	20	3.16	6.26	-4.48	
	34	3.16	6.26	-4.48	
Dana	-17	1.67	18.3	-2.52	0.9305m/s ² •F[Hz]+0.672m/s ²⁾ =0.1481m/s ² • ω [rad/s]+0.672m/s
	0	0.961	9.33	-0.731	
	23	0.738	5.35	-0.220	
	37	0.570	3.60	-0.430	
Thies	-17	2.44	72.9	-36.0	0.05m/s ² •F[Hz] ¹⁾ 0.04791m/s ² •F[Hz]+0.453m/s ⁴⁾ =0.3355m/s ² • ω [rad/s]+0.453m/s
	-6	1.83	44.4	-13.3	
	2	1.92	35.3	-5.05	
	21	1.49	14.8	4.10	
Vaisala	34	1.78	7.50	7.60	
	-21	1.39	32.8	-9.61	0.09853m/s ² •F[Hz]+0.4054m/s ¹⁾ 0.09853m/s ² •F[Hz]+0.347m/s ³⁾ =0.2196m/s ² • ω [rad/s]+0.347m/s
	4	1.29	13.9	-2.06	
	23	1.15	4.75	0.473	
	36	0.793	4.48	0.00832	

1) manufacturers information

2) RISØ, DMI-BL tunnel

3) FFA, Ref. 3

4) RR-calibration EWTS-I

T is average time of one oscillation

M is mass of rotor

r is radius of the three strings

l is the length of the strings

The response length in Table 4 is calculated by the following formula for an air density of 1.23kg/m³:

$$l_0 = \frac{I}{2\rho A R^2 \sqrt{C_{DH} C_{DL}}}$$

CALCULATIONS AND CLASSIFICATION

The calculations of the cup-anemometer “readings” and their deviations to the linear regression line were made on a regular 200MHz PC; each calculation taking about a quarter of an hour.

The results of the calculations and classifications are shown in Fig. 5 to 8. Fig. 5 shows the absolute deviations of average values, called class A. Fig. 6 shows the maximum relative deviations of average values, called class B. Fig. 7 shows

the maximum absolute deviations of turbulence intensities, called class C, and Fig. 8 shows the maximum relative deviations of turbulence intensities, class D.

DISCUSSION

It is obvious from Fig. 5 to Fig. 8, that there are significant deviations from the calibration line for all cup-anemometers within the operational ranges. Maximum absolute deviations of average values, Class A, exceed 1m/s, Fig. 5, and the relative deviations, Class B, exceed 20%, Fig. 6. The maximum absolute deviations of turbulence intensity, Class C, exceed -15%, and the maximum relative deviations of turbulence intensity exceed -35%. Generally, it is so that the maximum absolute deviations occur at the highest wind speeds, and the maximum relative deviations occur at the lowest wind speeds.

The positive deviations shown in Fig. 7 and 8 might be surprising. Normally, the transfer function of a cup-anemometer is regarded as a first order dynamic system, which have no overshooting at all. The cup-anemometer, though, is not a regular first order dynamic system. It has an overspeeding effect on the average values, but also on the standard deviations, and hence the turbulence intensities.

RISØ

The RISØ cup-anemometer is having the highest ranking as a 2D sensor for all classes. The high ranking of the RISØ cup-anemometer as a 2D sensor is not surprising, since it has angular characteristics which resembles somewhat a cosine function, that is the optimum for a 2D sensor. Also, the friction is the lowest measured on all cup-anemometers. As a 3D sensor, it is also ranked the highest for Class B, whereas rank 4, regarding Class A, is more to be expected, since a cup-anemometer is not supposed to be both a good 2D and 3D sensor.

NRG

The relatively cheap NRG cup-anemometer is having a surprisingly good ranking. It is the highest ranked 3D sensor in Class A and number two in Class B, which makes it a good 3D sensor for average wind speed measurements. These qualifications are due to the totally temperature independent friction, and the somewhat constant, but very wavy and unsymmetrical angular characteristics. Flat angular characteristics is the optimum for a 3D sensor. The ranking as a Class C and D sensor is rather low due to the relatively high inertia.

Dana

The cheap Dana cup-anemometer is having the lowest ranking as a class A sensor but is ranked no. two as a 1D sensor and three as a 2D sensor. Regarding class C and D it is ranked no. two, which is due to its low inertia. The friction is very high considering the small size of the rotor. This is the major drawback of the sensor. The cup-anemometer seems to have its best qualifications as a 1D sensor.

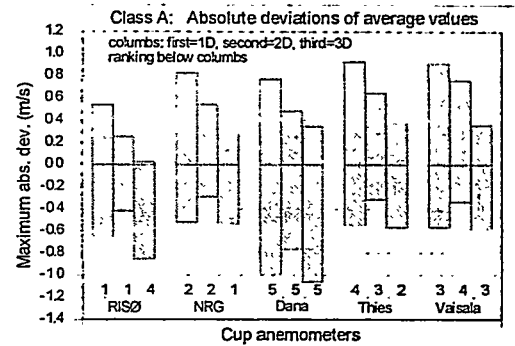


Fig. 5 Max. absolute deviations of average values

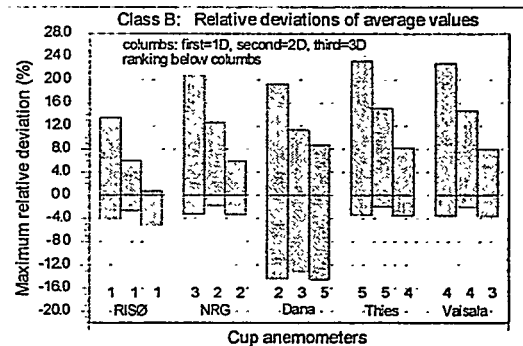


Fig. 6 Max. relative deviations of average values

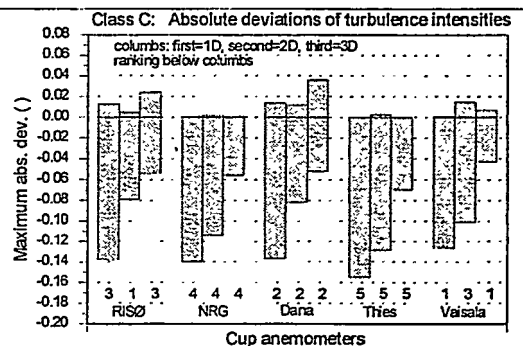


Fig. 7 Max. absolute deviations of turbulence intensities

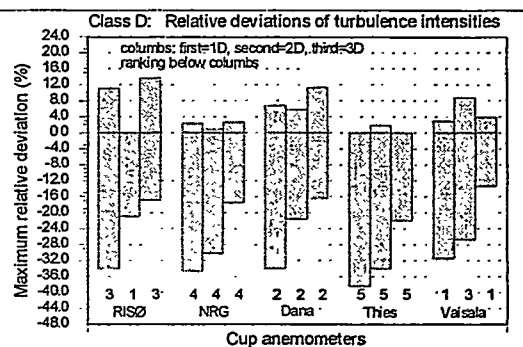


Fig. 8 Max. relative deviations of turbulence intensities

Thies

The Thies cup-anemometer is having its highest ranking, no. two, as a 3D sensor in Class A, whereas the ranking in Class B is the next lowest, and in Class C and D it is the lowest, due to its high inertia. The angular characteristics is relatively flat, which gives it good 3D characteristics, but it is rather unsymmetrical. The friction is the highest measured on the cup-anemometers, and it has the steepest friction gradient at the lowest temperatures. This is somewhat compensated by the large cups, but the high friction is confirmed in the high offset of the calibration line. The cup-anemometer has a possibility for heating the bearings. This was not used in this analysis.

Vaisala

The Vaisala cup-anemometer is ranked no. three as a 3D sensor in both Class A and B, and it is having the highest ranking as a 1D and 3D turbulence sensor. This is due to its low inertia. The angular characteristics is relatively flat, which gives it good 3D characteristics, but it is also rather unsymmetrical. The friction is rather high, giving it characteristics very similar to the Thies cup-anemometer regarding average wind speed measurements. The cup-anemometer has a possibility for heating the bearings. This was not used in this analysis.

CONCLUSIONS

From the assessment, the following conclusions can be made:

- The classification of five cup-anemometers showed that for a prescribed wind climate (comparable to design wind climate for wind turbines) they all have very high maximum deviations from the calibration line, which means that their performance under such "normal" operational conditions is associated with high uncertainties.
- The angular characteristics of the cup-anemometers are far from being optimal for their purpose. Some tend to have flat response, some to have cosine response, but all of them have quite wavy characteristics, and none have an ideal shape.
- The friction showed very high dependencies on temperature, except for the NRG, which is totally independent on temperature. The Thies and Vaisala cup-anemometers are the most sensible at lower temperatures, but they have possibilities of heating bearings, which was not considered in this analysis.
- The NRG, Thies and Vaisala cup-anemometers seem to be better vector wind speed sensors than horizontal wind speed sensors, whereas the opposite is valid for the RISØ and Dana cup-anemometers
- The perspectives for improving cup-anemometers is very high. Having defined which type of sensor to improve (2D or 3D), there is quite a lot that can be done on improving angular characteristics and friction

ACKNOWLEDGEMENTS

The present work is part of the JOULE project CLASSCUP. The classification procedure was developed under the Danish Energy Agency contract, on Basic Test Development Activities.

REFERENCES

- [1] T.F.Pedersen, U.S.Paulsen "A procedure for classification of cup-anemometers", EWEC 97, Dublin
- [2] O.Fabian "Fly-wheel calibration of cup-anemometers", EWEC '95, Thessaloniki
- [3] G.Ronsten, J-Å.Dahlberg, "Calibration of Anemometers in FFA-L2 Wind Tunnel Including Twin Calibration and Tests of Sensitivity to Wind Velocity Gradient and Tilt", FFA TN 1996-51

IS THE NACELLE MOUNTED ANEMOMETER AN ACCEPTABLE OPTION IN PERFORMANCE TESTING ?

Jan-Ake Dahlberg, FFA, The Aeronautical Research Institute of Sweden, P.O. Box 11021, 161 11 Bromma, Sweden
Sten Frandsen, Helge A. Madsen, Ioannis Antoniou and Troels Friis Pedersen, RISØ, Box 49, DK-4000, Roskilde, Denmark
Raymond Hunter, RES, Renewable Energy Systems, 11 Elmbank Street, Glasgow, G2 4FB, Scotland.
Helmut Klug, DEWI, Ebertstrasse 96, 26382 Wilhelmshaven, Germany

ABSTRACT

Although the nacelle anemometer method has been used for power verification purposes for several years, it is only relatively recently that a full understanding of its limitations has emerged. The technique is totally dependent upon the assumption that the nacelle to free wind speed relationship established for a reference turbine in free air can be applied universally to other turbines. Facts emerged from research projects have shown that this assumption is unjustified. In the present paper facts are presented of which some have not been identified nor presented before. E.g. the effect related to wake conditions is novel as a phenomena and the size of the effect can be considerable. The analysis shows that the total error caused by the effects considered in this paper can, in the worst case reach unacceptable high values, 24%, but by taking precautionary measures the errors can be kept at acceptable low levels, 4%. It is found probable that the future use of nacelle anemometry for power performance verification will be subject to strong restrictions.

Keywords: Nacelle Anemometer, Power verification, Power performance

1 INTRODUCTION

For reasons of low costs and convenience the application of an anemometer mounted directly on the wind turbine's nacelle has been seen as an attractive way of acquisition of the reference wind speed. Although the nacelle anemometer method has been used for several years, it is only relatively recently that a full understanding of its limitations has emerged. The technique is totally dependent upon the assumption that the nacelle to free wind speed relationship established for a reference turbine in free air can be applied universally to other turbines of the same make and kind.

2 OUTLINING THE PROBLEM

However, there are several potential problems in the use of nacelle anemometry:

- **Wake conditions:** In wake conditions from other wind turbines, the reading from the nacelle anemometer may not be representative for what the whole rotor experiences. Two sets of independent measurements enlighten this problem.
- **Flow induction:** The flow speed in the rotor plane is aerodynamically linked to the power output. The effect is investigated with data from two different MW-sized wind turbines and with results from a flow model.
- **Flow over nacelle:** the nacelle anemometer is in a position of significant flow disturbance caused by blade passage and flow over the nacelle. If the flow regime change due to topographically induced change in general vertical inclination in the incident flow or due to changed nacelle alignment then the anemometer reading will change, hence invalidating the assumed relationship to free field conditions. This effect has been investigated by means of full-scale tests.

3 NACELLE ANEMOMETRY PROBLEMS

3.1 Wake Operation

Wake Operation In The Alsvik Wind Farm

Data from the Alsvik wind farm (Fig. 1&2) on the isle of Gotland have been used to investigate [1] how the power curve is affected when using the nacelle anemometer under wake conditions.

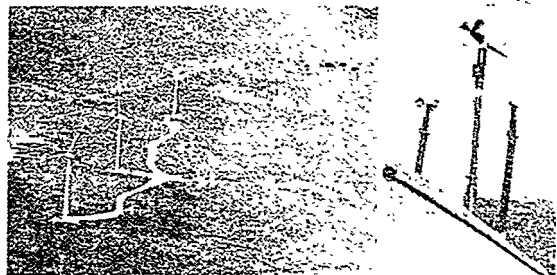


Figure 1&2: The Alsvik wind farm and a close up view of the instruments on the nacelle. The middle propeller anemometer was used for the test.

The rear turbine was exposed to wake flow at a distance to the upstream turbines varying from 5, 7 and 9.5 turbine diameters (D). The average turbulence level was about 7%, measured during 10 minutes. The low turbulence levels at the site gave very clear wake conditions.

A relationship between free wind speed and the wind speed on top of the nacelle was established from open sectors. This relationship was used to determine the power curves in 6° sectors. The figure (Fig. 3) below shows the derived normalised power curves.

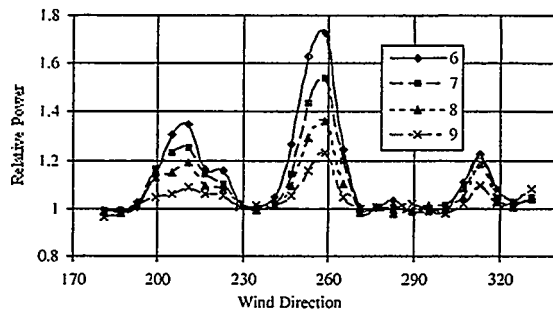


Figure 3: Normalised power curves for different wind speeds.

From the figure it is evident that the power is considerably exaggerated in the centre of the wakes. The power value is for the worst case, $5xD$ and 6 m/s , increased by more than 70%. A possible explanation could be that the nacelle anemometer does not measure a wind speed that is representative for the whole turbine. The anemometer is exposed to the low velocity in the centre of the wake compared to the higher wind speed in the outer region of the wake. This will cause a shift towards lower wind speed for the power curve based on the nacelle anemometer and an apparently higher power output.

A model has been used to quantify the uncertainty in annual mean power (AMP), the use of nacelle anemometer may have, for a turbine embedded in a wind farm (see Table I). The turbine of interest is assumed to be surrounded by turbines in a hexagonal pattern. The first "row" consists of 6 turbines, the second "row" consists of 12 turbines and so on.

The model was fitted to the measured data and takes the fraction of time the turbine is exposed to wake conditions, the effects from wind speed and the effects of distance into account. The integrated apparent % increase in AMP for a range of wind farm sizes and spacing between turbines are presented. The table is calculated for an average, Rayleigh distributed, wind speed of 7 m/s .

Table I: Apparent % increase in AMP for a range of wind farm sizes and spacing

		Turbine Inter Spacing X/D										
No of rows	No of turbines	3	4	5	6	7	8	9	10	11	12	
1	7	14.7	8.7	5.4	3.4	2.2	1.5	1.0	0.7	0.5	0.4	
2	19	21.5	11.7	6.8	4.1	2.6	1.7	1.2	0.8	0.6	0.4	
3	37	24.6	12.8	7.2	4.4	2.8	1.8	1.2	0.8	0.6	0.4	
4	51	26.1	13.2	7.4	4.4	2.8	1.8	1.2	0.8	0.6	0.4	
5	81	26.8	13.5	7.5	4.5	2.8	1.8	1.2	0.8	0.6	0.4	

As seen from the table the use of nacelle anemometer in power performance assessment may have a considerable effect on the derived annual mean power. The over estimation of the AMP is for reasonable inter turbine spacing in the order of 2-5%. Although these values were derived for very smooth conditions and for a relatively low mean wind speed the influence on the power curve is of such a magnitude that the effects has to be taken into account in the uncertainty analysis.

A Small Wind Farm In Semi-Complex Terrain

Data from a small wind farm in semi-complex terrain in the British Isles was analysed in a similar manner as the data from Alsvik. The average turbulence level on this site was higher, approximately 11%. The results are similar (Fig. 4) and confirms the findings from Alsvik. The maximum performance enhancement, is in this case, in the order of 40%. The lower performance enhancement compared to the Alsvik case could be due to the higher turbulence levels.

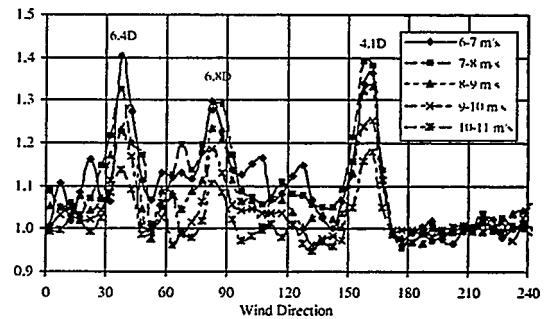


Figure 4: Normalised power curves from a small wind farm in semi-complex terrain.

3.2 Induction Effects

Induction effects on the Näsudden 3 MW turbine

In order to find the optimum pitch settings on the Näsudden 3 MW wind turbine a test was carried out, during 3 month, with the turbine operating at different pitch angles. The pitch angle was set, at fixed values between 0 and 5 degrees, in a repetitive manner.

The database from this test has been made available in order to investigate [1] the applicability of using the nacelle anemometer to determine the changes in power performance due to different pitch angle settings.

Figure 5 shows density corrected power curves from the test. Only data in a free sector and with a yaw misalignment within $\pm 5^\circ$ from the average yaw misalignment were used.

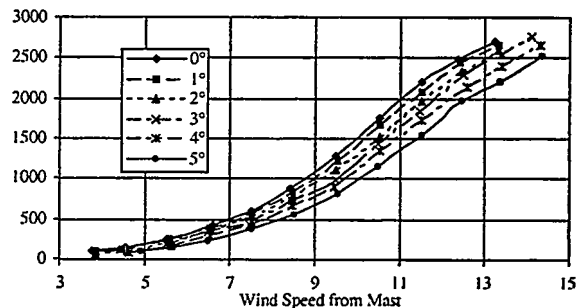


Figure 5: Power curves from "pitch" tests

The relationships between the wind speed measured by the nacelle anemometer and the "free undisturbed wind speed" measured by the mast anemometer, are plotted in the figure below (Fig. 6) for the pitch angles 0° and 5° .

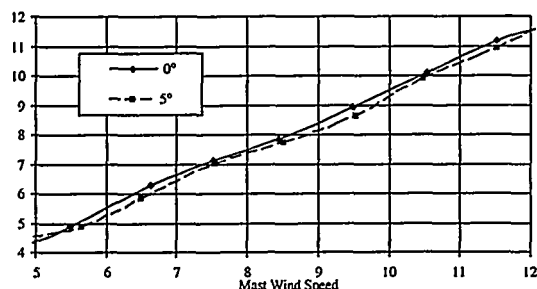


Figure 6: Wind speed Nacelle-Mast relationship for pitch angles 0° and 5°.

It is noticeable that although the power, for increasing pitch settings, is reduced the speed on top of the nacelle is also reduced. The consequence of this is that a reduction in power partly will be covered by the apparent lower wind speed.

The effects on the assessed annual mean power (AMP) have been quantified for an average Rayleigh distributed wind speed of 7 m/s.

The table below (Table II) shows the error introduced by using the nacelle anemometer in this case. The values are integrated values over the whole wind speed range. The % error in each bin in the low wind speed range, are approximately 2-3 times higher than the integrated values.

Table II: Error in annual mean power (AMP) introduced by using the nacelle anemometer

Pitch angle	Based on Mast WS		Based on Nacelle WS		
	AMP [kW]	Actual Reduction %	AMP [kW]	Apparent Reduction %	Error %
0	796	0.0	796	0.0	0.0
1	759	-4.6	768	-3.5	1.1
2	719	-9.7	735	-7.7	2.0
3	679	-14.7	704	-11.6	3.1
4	635	-20.2	668	-16.1	4.1
5	590	-25.9	629	-21.0	4.9

A pitch error in the order of 1° must be considered to be a rather large structural deviation which in this case introduces a moderate error in the order of 1%.

Although the consequences are limited, these results are different from the findings in other projects [2] where they concluded that the dependency of the calibration formula to the wind and wind turbine parameters was expected to be magnified if tested under other conditions.

Induction effects on the ELKRAFT 1 MW turbine

Tests have been carried out with the ELKRAFT 1 MW stall-regulated wind turbine in order to investigate the applicability of nacelle anemometry methods for power verification. Data were collected from three phases of operation according to Table III.

Table III: The three measurement periods

Phase	1	2	3
Pitch setting	+0.5°	+0.5°	-1.0°
Yaw error	12	7	7
Vortex Generators	No	No	Yes

In the following table (Table IV), the normalised annual energy production figures are presented both as function of the mast anemometer and as function of the

corrected nacelle anemometer. The correction applied to the nacelle anemometer is derived from phase 1.

Table IV: The normalised annual energy production calculated both as function of the mast (m) and the corrected nacelle anemometer (n) from phase 1.

WS	Ph1(m)	Unc.	Ph1(n)	Ph2(m)	Ph2(n)	Ph3(m)	Ph3(n)
6	100	9.9	100.1	101.7	90.1	101.5	88.7
7	100	7.8	100.2	101.5	93.2	102.7	92.7
8	100	6.3	100.2	101.3	95.2	103.0	95.1

As seen from the table the method of using the nacelle anemometer fails to detect the changes in power when going from phase 1 to phase 2 & 3. For example going from phase 1 to phase 2 gives an actual increased production of 1.5%. The nacelle method gives a reduction of 6.8%. Changing to phase 3 gives even larger discrepancies. The reason for the discrepancies can be found from the figure below (Fig. 7), which shows how the mast-nacelle anemometer relations change for the three phases. Changing from phase 1 to 2 and from 1 to 3 give rise to slightly higher power output as indicated from the tabulated production figures. However the changes also causes a change in the mast-nacelle anemometer relations which may have a considerably larger influence on the derived power curve.

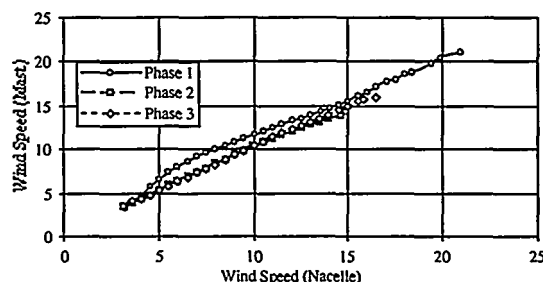


Figure 7: The mast-nacelle anemometer relations for the three phases.

Should, on the other hand, the conditions from phase 2 be taken as the reference conditions then the change to phase 1 would give an apparent considerable increase in production although we know that this change in reality implies a slight decrease in production capability.

This enlightens one serious problem in power performance verification when using the nacelle anemometer namely how to distinguish changes in mast-nacelle anemometer relations from deviations in performance of the machine.

3.3 Flow Over Nacelle

The nacelle anemometer is in a position of significant flow disturbance caused by blade passage or flow over the nacelle. Should the flow regime change due to changed nacelle alignment or due to topographically induced change in general vertical inclination in the incident flow then the anemometer reading may change, hence invalidating the assumed relationship to free field conditions.

The first-mentioned case was demonstrated in section 3.2 where the change in operational conditions from phase 1 to phase 2 was due to changed alignment of the nacelle.

This was shown to have a strong influence on the nacelle wind speed to free field relationship.

The change vertical inclination in the incident flow is demonstrated in figure 8 which show power and C_p curves derived from [3] met-mast-based and nacelle-anemometer-based conditions.

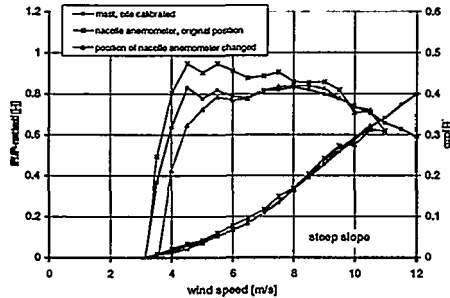


Figure 8: Power curves from sectors with different slopes. The curve denoted "nacelle anemometer, original position", derived from sectors with steep slopes deviates significantly from the curve denoted "mast, site calibrated" derived from sectors with low terrain inclination. This effect was most probably caused by nacelle body flow distortion. In this case the problem was reduced by changing the position of the nacelle anemometer and determining a new nacelle anemometer correction from sectors with low terrain inclination.

4 MEASURES TO MITIGATE THE PROBLEMS

Wake Operation

Data collected when the wind turbine is affected by the wake from another turbine or a nearby obstacle should be rejected. The wake rejection criteria used in IEC [4], could be used as a basis for rejection.

Induction Effects

It is vital to be able to demonstrate whether the use of corrected nacelle anemometry will tend to indicate enhanced, attenuated or reversed performance differences. This knowledge could be gained by carrying out calibration tests on the reference wind turbine at different pitch settings.

Flow Over Nacelle

Nacelle to free wind speed relationships should only be applied to a turbine if its flow regime is similar to that seen by a reference turbine. The key considerations are, that the upwind terrain adjacent to the test turbine is of similar slope to that for the turbine on which the relationship was determined, and that the controlled nacelle alignment behaviour is similar.

During evaluation of the nacelle to free wind speed relationship for a reference turbine in a wind farm, changing wind directions will give rise to changing inclination angles and therefore a possible change in wind speed relationship. The spread of the nacelle to free wind speed data can give an indication of the flow angle sensitivity.

It is also vital to be able to demonstrate whether the use of corrected nacelle anemometry will tend to indicate enhanced, attenuated or reversed performance differences. This knowledge could be gained by carrying out

calibration tests on the reference wind turbine at different nacelle alignments.

Additional Essential Steps

There are a number of additional essential steps which must be taken when using nacelle anemometry, these being:

The nacelle anemometers on the reference turbines should be calibrated to ensure that apparent difference in nacelle to free wind speed relationships between reference turbines are real and not a consequence of differences in anemometer sensitivities.

Ideally the nacelle anemometers from each individual turbine in a wind farm should be calibrated, or at least a representative sample, so an objective assessment can be made of their population scatter.

5 UNCERTAINTIES INHERENT IN THE USE OF NACELLE ANEMOMETRY

In the following type B (bias) uncertainty levels on annual energy production are estimated both for the case when the nacelle anemometer method is used incautiously and for the case when every precaution measures have been taken.

Wake effects

In some special conditions, errors in power performance of up to 70% have been noted. For a typical wind farm the mean error will be of the order of 7%, but this value can easily reach 15%. On the other hand, by suggested mitigation measures this value can be kept low, 2%.

Induction

Worst case uncertainty values can certainly reach 10%, but by adopting best practise this value can be low, say 1%.

Flow over nacelle

Worst case uncertainty values can certainly reach 15%, but by adopting best practise this value can be low, say 3%.

Assume independence:

$$u_T = \sqrt{u_{wake}^2 + u_{Ind}^2 + u_{dist}^2}$$

Table V: Estimated worst and best uncertainty values.

Component	High	Low
Wake effects	15	2
Induction	10	1
Nacelle flow distortion	15	3
Total	24	4

6 CONCLUSIONS

The use of nacelle anemometry is a questionable means for estimating power curves for individual wind turbines in a complex environment.

The technique is not without its shortcomings and can be very misleading if applied without caution.

The analysis shows that the total error caused by the considered effects can, in the worst case reach

unacceptable high values. By taking precaution measures the errors may be kept at fairly low levels.

It is found probable that the future use of nacelle anemometry for power performance verification will be subject to strong restrictions.

7 REFERENCES

- [1] S.Frandsen, et al., POWER PERFORMANCE ASSESSMENT, JOR3-CT96-0114, (to be published 1999)
- [2] EWTS II, Executive Summary
- [3] H.Klug et al., Power Performance Verification, PB9.6, EWEC 1999.
- [4] Wind turbine generator systems - Part 12: Wind turbine power performance testing, IEC-61400-12

HARMONISATION OF WIND TURBINE CERTIFICATION IN EUROPE JOULE PROJECT EWTC

Christian Nath, Germanischer Lloyd, Vorsetzen 32, 20459 Hamburg, Germany,
Phone: +49-40-36 149-480, Fax: +49-40-36 149-1720, E-Mail: na@germanlloyd.org
Christer Eriksson, Det Norske Veritas, Tuborg Parkvej 8, 2900 Hellerup, Denmark,
Phone: +45-39454-800, Fax: +45-39454-801, E-Mail: ccri@dnv.com
Frans van Hulle, Westerduinweg 3, 1755 ZG Petten, The Netherlands,
Phone: +31-224-56-4274, Fax: +31-224-56-3214, E-Mail: vanhulle@ecm.nl
Carsten Skamris, Risø National Laboratory, 4000 Roskilde, Denmark,
Phone: +45-4677-5060, Fax: +45-4677-5960, E-Mail: c.skamris@risoe.dk
Wim Stam, CIWI Holland, Utrechtseweg 310, 6800 ET Arnhem, The Netherlands,
Phone: +31-26-3562806, Fax: +31-26-44536-79, E-Mail: stam@ccn.nl
Pantelis Vionis, CRES; 19th km Marathonos Av., 190 09 Pikermi, Attiki, Greece,
Phone: +30-1-6039-900, Fax: +30-1-6039-904, E-Mail: pvioni@cres.gr

ABSTRACT: Wind turbine certification requirements are currently fairly diverse within Europe. Therefore the leading European certification bodies initiated a JOULE project to harmonise the certification procedure on the basis of the current set of IEC/EN 61400 series standards. The paper presents a review of the state of the art of wind turbine certification in European countries and an outline of the structure of the project. The main steps of the project are (a) the collection of differences in certification practices by round robin certification of three wind turbine types; (b) assessment of the different certification results and (c) the development of a harmonised certification procedure.

Keywords: Certification, Harmonisation, Standards, Wind Turbines

1. GENERAL

The discussion in Working Groups 7 and 9 of the International Electrotechnical Commission (IEC), dealing with IEC 61400-1 [1] and IEC 61400-22 [2], clearly indicated the need for additional information on how to apply the relevant standards in the certification of wind turbines. A JOULE 3 project called European Wind Turbine Certification (CT98-0265) was therefore initiated by the major European certification bodies represented by the authors. The main objective of this project is to arrive at an harmonised wind turbine certification all over Europe. This harmonisation has been anticipated to remove trade barriers, to improve the implementation and to reduce the cost of wind energy by avoiding multiple certifications.

The first task of the project which started in May 1998 is a preparation phase in which an inventory of the current certification systems in European countries is described. Furthermore a questionnaire sent to manufacturers to investigate their opinions on certification of wind turbines will be evaluated. The main project task comprises type certifications of three different wind turbine types at the four participating certification bodies and the subsequent comparative analysis of the different assessment reports. The ultimate aim of the project will be the development of a common, harmonised certification basis and the relevant guidelines.

This paper describes the current status and the work done and will outline the tasks to be carried out in the remaining time of project which is due to reach completion by mid 2000.

2. CERTIFICATION IN EUROPE

2.1 General

The European countries at present apply considerably different wind turbine certification systems the scope of which is ranging from „no specific requirements„ to „full

type certification„, plus assessment of site conditions and foundation design. In the following sections the specific certification schemes and certification agencies will be described. Within the section the term certification will be used as a synonym for examination, evaluations, approvals and certifications. A more detailed description of the certification in the different countries can be found in an intermediate report of the project [3].

2.2 Austria

The erection of wind turbines in Austria requires the property to be transferred from normal use to special use. The second step is the application for a building permit covering all the different aspects described in the following. As building law is state law and not federal law requirements can be somewhat different in the federal states. Notified experts in the relevant field investigate the subjects covered by the building permit.

Each project needs an application for a civil engineering approval of a state authority. In some states this procedure is limited to a notification. The civil engineering approval is in general based on examinations carried out for German type approvals or Danish/Dutch type certificates. Remarks/requirements/obligations from the relevant certification reports are directly copied for the Austrian approval. Where relevant Austrian standards are to be applied. This holds e.g. for materials and steel grades. Suitability of soil is to be assessed by a competent, notified engineer.

The procedure of the electrotechnical approval (changed by a new law in February 1996) covers not only the electric matters but also the problems of neighbourhood, the proof of economic feasibility and the requirement for a trained and checked operator.

Noise and light effects are also assessed by notified experts. There are neither a written basis nor accepted regulations for these assessments. For the assessment of the environmental noise, the background noise has to be meas-

ured as well as the effect of the wind turbine. This has to be done for a wind speed range and not for a deterministic wind speed of 8 m/s at 10 m height as defined in IEC 61400-11 [4].

Conservation of nature is dealt with at the district level. In general notification is sufficient, except for protected areas.

Austria does not have a standards committee for wind energy.

2.3 Belgium

There are at present no specific regulations requiring certification in Belgium. It is expected however, that certification will become mandatory in the future. Generally for most wind turbines certificates and measurements are available and accepted by authorities and financing bodies. Existing rules concerning labour safety and electrical installations are to be applied.

For the erection of wind turbines two permits have to be obtained: a building and an exploitation permit.

In the Flemish Region noise levels have to meet the requirements for industrial noise as no specific requirements for wind turbines exist. For wind farms larger than 10 MW an environmental impact study is to be submitted.

Subsidies for wind turbines range from demonstration funding (for prototypes) to expansion and site assessment subsidies. In addition the electricity payment was raised to 0.08 EUR/kWh in July 1998.

2.4 Denmark

Certification of wind turbines was initiated in Denmark as early as 1979. In the beginning certification was a requirement within the subsidy scheme. Since 1991 certification is a legal requirement if wind turbines are to be connected to the grid. Utilities are not allowed to connect wind turbines to the grid if these are not certified. The local building authorities issue erection permits, the type certificate is accepted as a proof of the safety of the turbine.

The Danish type certification (approval) is carried out on the basis of technical criteria [5] and the Danish standard DS 472 [6]. There are some distinct differences in the Danish certification requirements: a wind turbine can only be certified as a complete unit, i. e. including tower and foundation; the certification includes safety, strength and performance testing; the technical criteria specify static and dynamic blade testing as well as one of the braking systems to be aerodynamic.

(In Denmark there is no direct subsidising any more. However, there are a number of incentives for the promotion of wind energy both as tax credits and as legal requirements for the installation of a certain power per year.

2.5 Finland

At present there are no certification requirements in Finland. Local building authorities issue building permits on a case by case basis. Normally the building permit is based on a type approval issued by foreign certification bodies. Implementation of specific Finnish requirements especially for cold climate are being considered presently.

Subsidies are given as investment subsidies based on an application to Ministry of Trade and Industry. The amount of the subsidy is decided case by case and is ap-

proximately one third of the investment costs. In addition an electricity refund is given.

2.6 Germany

The certification in Germany is governed by state law and not by federal law. There is a common set of regulations („Richtlinie für Windkraftanlagen„, [7]) for loads, towers and foundations. However, rules for safety systems and requirements on machinery and electrics may vary in the different states. A building permit requires among others a single approval or a type approval. A type approval once granted in one of the federal states is valid in every state. The German type approval comprises examination of loads and machinery by an expert organisation and approval of tower and foundation by authorities. Electric systems are not checked by a third party. There is no commonly agreed set of rules and standards on which the examination of the machinery is to be based on, many wind turbine designs are approved with reference to Germanischer Lloyd's Regulations. [8].

Although building law is not federal law there is generally consensus among the states on the requirements for loads and structures. The German Institute for Civil Engineering (DIBt) („Deutsches Institut für Bautechnik„) in Berlin is the responsible institution for the development of new regulations, for the acknowledgement of new standards (without this acknowledgement standards cannot be used in type approvals) and for European Technical Approvals, as specified in the Construction Product Directive [9]. In August 1998 DIBt installed a project group for the development of a new set of regulations on the basis of the recently accepted IEC 61400-1, ed. 2 [1]. The new regulations will address those aspects that are not covered by the IEC- or EN-standards and will specify parameters and/or methods to be used in combination with these standards. It is one of the aims to amend the IEC standards in a way that as little as possible additional regulatory text is necessary.

Within the German certification system the examination of the loads and the machinery shall be carried out by expert organisations. These are for example CIWI/ECN, GL, RISØ/DNV and TÜV.

2.7 Greece

In Greece legal provisions require a certificate of approval for the specific wind turbine type from the Centre for Renewable Energy Sources (CRES). Up to date, CRES issues the certificate based on the certificate of a foreign institute approved by the responsible authorities of the corresponding country and acceptable by CRES.

As part of the National Wind Energy Programme CRES is currently developing the National Certification System and participates in the standardisation work carried out by the Hellenic Organisation for Standardisation (ELOT) in the framework of European (CENELEC BTTF83-2) and international organisations (IEC TC88), regarding Wind Energy matters.

The certification system under development is based on the on-going international and European standardisation work, taking into account the particular wind conditions in the country. More specifically the certification system is developed on the basis of the draft IEC standard 61400-22 for wind turbines designed in accordance with IEC 61400-1.

In Greece two national programmes support the development of wind energy projects:

In the framework of the "Law for the Economical Development" 2601/98, wind energy projects may be subsidised by 40% of the cost and get up to 40% reduced soft loan (up to 20% of the project cost).

In the framework of the so-called „Operational Program for Energy - Renewables“, wind energy projects get a financial support of 40% considering maximum subsidised project cost of approx. EUR 1000/kW.

2.8 Ireland

There is no legal requirement for the certification of wind turbines in Ireland and neither is there a certification body nor a testing laboratory. Ireland does not develop standards in the field of wind energy but applies the available international and European standards.

The Irish utility issued requirements for the connection of wind turbines to the grid [10]. Most of the wind turbines to be installed in the near future are the result of the „Alternative Energy Requirement., (AER), a programme which asks for competitive bids for the price of electricity.

Although there is a system for obtaining planning permission (i.e. permission to build) there is no national system of building inspection and control applicable to wind turbines. A self regulatory system is effectively in place since there are obvious legal and economic consequences of taking inadequate care in design and installation.

2.9 The Netherlands

In the Netherlands certification is not required as a prerequisite for a building permit. However, a type certificate according to the Dutch requirements is accepted by the authorities as a demonstration that the certified wind turbine is sufficiently safe to comply with the relevant Dutch laws for the environment. New Dutch regulations which are expected to come into force in 2000 will require a type certificate for wind turbines to be installed in the Netherlands.

Up to now certification was governed by the Dutch preliminary draft standard NEN 6096/2 [11] which was issued in 1991 and revised in 1994. On the basis of the recently adopted standard IEC 61400-1, ed. 2 [1] the Netherlands developed NVN 11400/0 [12], which came into force in March 1999. In addition to the IEC document the Dutch standard contains requirements on material properties, labour safety, safety systems and the type certification procedure.

The present Type Certification system, as specified in the above-mentioned standards, comprises the following elements.

Design evaluation, including labour safety aspects and manuals;

Evaluation of quality system, quality plans for manufacturing and assembling;

Check on the actual manufacturing and assembling by means of inspection;

Type tests of a specimen of the assessed design. This includes inspection, functional tests of safety and control system;

Evaluation of power performance and acoustic noise production. The Dutch criteria specify minimum require-

ments for wind turbine efficiency and maximum requirements for the acoustic source strength;

The quality system and procedures of the manufacturer are checked after the design assessment. The advantage of this approach is that it allows to verify if critical points in the design are properly implemented in the manufacturing and procurement processes, e.g. quality classes of gears, surface finishes, special welding procedures, material quality grade specifications etc.

There are no subsidies any more for wind turbines. The financial incentives mainly consist of various types of tax reductions.

2.10 Norway

In Norway there are two permits required in order to install wind turbines.

The local authorities issue a building permit under the Plan & Building Act. This act does not require certification or type approval of the wind turbines. The requirements are mainly related to noise emission and visual impact as well as environmental aspects.

The national authorities, NVE, issue an installation permit under the Energy Act. The requirements for the installation permit include electrical aspects for the grid as well as environmental, noise emission and visual aspects.

A wind turbine is regarded as a machine and thus no specific design documentation is required. However, the major wind turbine owners are interested in well-defined type approvals for wind turbines.

Only very limited subsidies are offered in Norway. Subsidies are given as a deduction on the electrical consumption tax and as a deduction on the investment tax.

2.11 Portugal

There is no general requirement for certification in Portugal. Wind turbines need to have a building permit from the General Directorate of Energy (DGE). To obtain a building permit building plans and an environmental study have to be presented to DGE. Details can be found in [13].

2.12 Spain

There are no legal requirements for certification of wind turbines to be erected in Spain. The approval system and the subsidy scheme do not ask for certification either. The building permission for a wind energy project requires the elaboration of a project file under supervision of an Official Mechanical Engineering Professional College. This is to be presented to the relevant Administrative Authority. The approval is based on a number of general standards and regulations; specific wind energy standards have neither been developed nor applied yet.

The Spanish wind turbine manufacturers generally apply the available international regulations in their designs. In the future more and more of them will base their designs on the requirements of IEC 61400-1, ed. 2 [1]. For the issues of labour safety prEN50308 [14] is being used and procurement will follow the guidelines in EN 45510-5-3 [15].

Performance, acoustic noise and load measurements are based on the relevant IEC standards [4], [16], [17] as well as MEASNET [18] and IEA- [19] documents. Most of the recently finalised IEC standards are in the process to become national Spanish (UNE) standards.

2.13 Sweden

There are two methods of type approval of wind turbines in Sweden. One method is based on a complete inspection of all documents relating to the wind turbine. The other method is based on the fact that the unit has already been approved by some well known classification (certification) authority, or similar.

The application for type approval is treated by "The Committee on Type Approval of Wind Power Stations in Sweden". The committee consists of individuals from FFA (The Aeronautical Research Institute of Sweden), SP (The National Authority for Testing, Inspection and Metrology), and SITAC (Swedish Institute for Technical Approval in Construction). The Certificate of Type Approval is issued by SITAC.

The complete inspection comprises a Swedish inspection of all documentation related to the dimensioning, manufacture and erection of the wind turbine. Electrical installations, control and protection systems are also inspected. A system for quality control of the manufacturing process is required. This system shall comply with the requirements of the SS/EN 29000 series (=ISO 9000 series) or similar.

The following documents are required for the Swedish approval:

- a general description of the unit, including a description of the environmental conditions (wind, temperature, etc.) that have been used in the dimensioning;

- a type certificate from a well known classification (certification) authority or an appropriate national/international organisation;

- a report which describes the inspection work done in connection with the type certificate to which is referred;

- a list of all documents which have been the basis for the type certificate by the other certification authority;

- manuals, in Swedish, for operation and maintenance intended for the user/owner of the unit.

Production and installation certificates for each wind power station to be built are required for funding.

2.14 Switzerland

In Switzerland wind turbines are considered mainly as buildings and not as machinery. However, there is no special legislation concerning wind turbines. For the erection of a wind turbine the following permits are to be obtained: a building permit and permits from the Swiss federal inspectorate for high-voltage installations, from the labour safety inspectorate and from the civil aviation department.

Switzerland does not have a standards committee in the field of wind energy. For funding a measured power curve is required. There are subsidy schemes for installation costs and site assessment costs. The Federal Office for Energy is responsible for granting of subsidies.

2.15 United Kingdom

In the UK, adherence to wind turbine standards is not a legal requirement, nor is it likely to be so unless future legislation in support of Directives from the European Union requires it. Nevertheless, the UK is playing a very active role in various international initiatives, particularly those of the International Electrotechnical Commission (IEC). The UK wind turbine industry and market sees advantage in having standards in place which can provide

the basis of voluntary regulation and of contractual agreements.

Standards activity in the UK is organized through the British Standards Institute (BSI), the committee looking after wind turbine standards being called PEL/88. As for other BSI committees, PEL/88 comprises representatives from trade associations (such as in this case the British Wind Energy Association) rather than individual companies. Thus, in addition to mainstream wind turbine opinions, the interests of utility and construction industries amongst others are also represented.

In the UK there are no legal requirements for wind turbines to be certified, nor does the subsidy system require certification. However, in practice manufacturers and developers welcome the availability of independent certification. For instance, local planning authorities can and do insist upon evidence of the safety or acoustic characteristics of wind turbines, and a very effective way of providing such information can be in the form of an independent conformity assessment.

A portion of wind projects in the UK is financed by a mix of equity and debt, with the latter accounting for perhaps 70%, and being in the form of unsecured project finance. Before such finance is made available, the bank(s) will undertake a thorough risk analysis, which will comprise an assessment of the site's potential, the credentials of the developer, the viability of the supplier, and of the technical pedigree of the proposed machinery. The last aspect is normally addressed by the bank commissioning a technical report. The extent of this survey can be reduced greatly if a type conformity assessment report exists. Certification does not routinely address reliability, which is why in its own right it is not sufficient for this particular application. Nevertheless, certification can go a long way towards avoiding the need for the same machine to be scrutinized by different technical assessors for different banks.

Since certification is not a legal requirement in the UK, it follows that those customers wishing to commission conformity assessment reviews can deal with whatever certification agency they wish. The market for conformity assessment is thus quite open.

3. ROUND ROBIN CERTIFICATION

Within IEC Working Group 9 where the Committee Draft of IEC 61400-22 [2] was developed discussions among the participating members showed the necessity of the present harmonisation project EWTC. Even the newly formulated „harmonised„ requirements of that document could be interpreted in different ways. In order to find out these differences in interpretation and application of the standard a „round robin certification exercise„ will be carried out.

Within the round robin certification every project partner (CIWI/ECN; CRES; GL; RISØ/DNV) will be certifying the same set of documents for the same turbine. This procedure will be carried out for three different turbines using IEC 61400-1, ed. 2 for loads, safety and design and IEC 61400-22 for the overall procedure to obtain a Conformity Statement for Design Evaluation or a Type Certificate.

The certification is carried out in several steps following the different modules and elements in IEC 61400-22. The modules are design evaluation, manufacturing

evaluation and type testing. The first step in design evaluation is the evaluation of loads and safety concept being the basis for the design of the turbine. Each step is concluded by each partner with a certification report. The certification reports are to be sufficiently detailed to allow a comparison of the evaluation work of the different partners. The certification reports will be compared and conclusions will be drawn on the necessity of additional regulations as e. g. requirements for materials, and the establishment of an interpretation document for formulations which reveal not to be clear enough. The latter might come up when looking at requirements of IEC 61400-22 as e. g. manufacturing quality evaluation or blade testing or the interpretation of the definition of load cases in IEC 61400-1.

In order to have a sufficient basis for the identification of specific differences in the interpretation of the standards it is anticipated to review three wind turbines with distinct differences in design and technologies applied and preferably turbines from different countries. The certifications of the three wind turbines will be carried out sequentially in order to have a learning effect for the harmonisation process.

The first machine to be evaluated is the new Enercon 600 kW E40 design. The new machine based on the old E40 500 kW type. It is a three bladed variable speed direct drive machine with AC-DC-AC conversion.

Principal data:

Rated power	600 kW
Diameter of rotor (Base Version)	43,7 m
Power control	pitch
Blade pitch	individual
Survival wind speed	IEC Class 2.

4. CONCLUSIONS

It has been clear from previous discussions that there are specific differences in the interpretation of the standards guidelines and Eurocodes. It is therefore very important to draft a common certification procedure and specific interpretation and application documents. The main areas addressed in this task are differences in local codes, material values and design technology. Based on the findings of the comparative analysis of the certification reports the common procedure will be modified and a uniform code for certification will be proposed. In addition guidelines will be drafted for design evaluation, type testing and manufacturing quality evaluation.

The results of the EWTC project will be introduced into standardisation work of IEC and CENELEC through personnel of the participating project partners.

In view of this it is expected that a common European/International certification will be available in the near future and replace the different national certification and technical approval system.

5. REFERENCES

- [1] IEC 61400-1, ed. 2: Safety Requirements, 1999
- [2] IEC 61400-22 (CD): Wind Turbine Certification, 1999
- [3] Hulle, Frans van: Overview of Wind Turbine Certification System in Europe, EWTC, Feb. 1999
- [4] IEC 61400-11: Acoustic Noise Measurements Techniques, Sept. 1998
- [5] Danish Energy Agency: Technical Basis for Type Approval and Certification of Wind Turbines in Denmark, Aug. 1996
- [6] DS 472: Loads and Safety for Wind Turbine Construction, 1992
- [7] Deutsches Institut für Bautechnik: Richtlinie für Windkraftanlagen, Juni 1993
- [8] Germanischer Lloyd, Regulations for the Certification of Wind Energy Conversion Systems, Hamburg, 1998.
- [9] European Commission: Construction Product Directive, 89/106/EEG, Feb. 1989, amended by 93/68/EEG, July 1993
- [10] ESB (Irish Utility): Requirements for Connection of Generators to ESB distribution network (G 10/94), 1994
- [11] NEN 6096/2: Regulations for the Type Certification of Wind Turbines, ECN, Feb. 1994
- [12] NVN 11400/0: Regulations for the Type-Certification of Wind Turbines: Technical Criteria, April 1999
- [13] Direcção - General de Energia: Guia Técnico das Instalações Eléctricas de Produção Independente de Energia Eléctrica, 2nd edition, Lisbon, 1994
- [14] prEN 50308: Wind turbines - Labour Safety, 1998
- [15] EN 45510-5-3: Guidelines for the Procurement of Power Plants - part 5-3: Wind Turbines, Jan. 1998
- [16] IEC 61400-12: Wind Turbine Power Performance Testing, Feb. 1998
- [17] IEC 61400-13 (CD): Mechanical Load Measurements, 1998
- [18] J. P. Molly, et al.: MEASNET: Network of EUREC-Agency recognised measuring institutes, EWTS, Volume No.8, EUREC-Agency, Leuven, Belgium.
- [19] International Energy Agency (IEA): Recommended Practices for Wind Turbine Testing Evaluation, 1. Power Performance Testing, 2. Edition 1990 3. Fatigue Loads, 2. Edition 1990.

European Wind Turbine Standards II (EWTS-II)

J.T.G. Pierik, J.W.M. Dekker, H. Braam, B.H. Bulder, D. Winkelaar
G.C. Larsen [♣], E. Morfiadakis [◇], P. Chaviaropoulos [◇], A. Derrick [♡], J.P. Molly [♠]

ECN - Solar & Wind Energy, P.O. Box 1, 1755 ZG Petten, The Netherlands

[♣]Risø National Laboratory, P.O. Box 49, Roskilde DK-4000, Denmark

[◇]CRES, 19th km Marathonos Av., Pikermi 19009, Greece

[♡]NEL, East Kilbride G75 0QU, UK

[♠]DEWI, Ebertstr. 96, D-26382 Wilhelmshaven, Germany

ABSTRACT: A summary is given of the main results of the European Wind Turbine Standards II project.

Keywords: Standards, fatigue, wind conditions, failure probabilities, blade tests, power performance, site evaluation, measurements.

1. INTRODUCTION

The increase in industrial activity in wind energy in turn generates a demand for generally accepted and standardized methods of design, testing and certification of wind turbines. This demand is partly covered by the activities of standardization bodies (CEN/CEGECLEC, IEC), however a number of bottle-necks in knowledge and technical harmonization still exists. It was the objective of the European Wind Turbine Standards projects I and II to remove some of the constraints and bottle-necks and contribute to the harmonization.

EWTS-II was completed in 1998 [1] and included investigations on:

- 1) wind farms-wind field and turbine loading;
- 2) complex terrain and fatigue loading;
- 3) extreme wind conditions;
- 4) quantification of failure probabilities;
- 5) integration of blade tests in design;
- 6) power performance in complex terrain;
- 7) site evaluation.

In addition to these scientific evaluations, the EWTS-II participants established an organization of qualified measuring institutes in the field of wind energy, the MEASNET organization [2]. MEASNET unifies measurement procedures of the participating institutes and guarantees qualified measurements and mutual acceptance among its members.

2. WIND FARMS-WIND FIELD TURBINE LOADING

When operating under wake conditions, an increase in fatigue consumption of wind turbines has been observed. The changes in the load patterns originate both from modifications in the mean wind field and from modifications in the turbulence field. By means of a parameter study, the significant wind field parameters, in relation to the increased wind turbine fatigue consumption in wakes, are identified. The analysis is based on a large number of aeroelastic simulations for five significantly different wind turbine concepts [5].

The main findings from the investigation are:

- All four investigated parameters representing the wake wind field, viz. wake deficit, wake turbulence intensity, wake turbulence length scale and wake turbulence coherence, were demonstrated to be significant in relation to increased fatigue

life consumption in wakes compared to ambient conditions.

- It is possible to quantify the relevant wake parameters by use of simple models.
- The fatigue contributions, caused by the investigated four parameters, are shown to behave additively. This implies, that a simple approximate method, involving only a very limited number of aeroelastic calculations, can be applied for fatigue estimates taking into account the detailed wind farm topology and the particular wind turbine concept.
- The effect due to increased turbulence intensity is crucial and usually dominates the fatigue effects caused by the other investigated parameters with a factor of 2 to 3.

3. COMPLEX TERRAIN AND FATIGUE LOADING

The aims of this subtask are:

- To investigate the effect of the terrain complexity on the wind field properties that drive the fatigue loading of wind turbines (like wind shear, Reynolds stresses, etc.);
- To investigate and quantify the impact of the above properties on fatigue loading for machines of different size and design philosophy.

Recommendations are made on how to include the present findings into the IEC Standards [7]:

- When a turbine is erected at a site which differs significantly from the design conditions of the IEC standard, the fatigue and the extreme loads have to be recalculated. The estimation of the turbulence parameters at a specific site must be part of the site assessment procedure. If a turbine, designed according to the standard classes, is intended to operate at a site with a Weibull shape factor k lower than 1.8, the fatigue load has to be recalculated using the actual Weibull parameters. The actual extreme wind speed events at the site need to be re-evaluated also.
- It is felt that the 16% to 18% turbulence intensity values used in the IEC 1400-1 standard can cover complex terrain operation with turbulent intensities from 13% up to 15% respectively, without additional design calculations. It was estimated that this 3% extra turbulent intensity value can compensate a 20% increase in fatigue loading due to overall complex terrain effects. When a machine is intended to operate at a complex terrain site with a turbulent intensity larger than 15%, the fatigue loads have to be re-evaluated based on the actual values of the Weibull parameters and

turbulence conditions at the site.

- The wind shear law used in the standards can be maintained, having in mind that a conservative estimation of complex terrain loading is thus achieved.
- Sites with wind inclination more than 20 degrees should be considered within the S(pecial)-class context.
- A site assessment of a complex terrain site must, as a minimum include the following parameters:
 - Weibull scale and shape factors C and k,
 - turbulence intensity,
 - flow tilt (inclination) angle.

Characteristic values of the remaining wind field parameters can be selected on basis of these values.

4. EXTREME WIND CONDITIONS

The objective of this part of the project is to provide the designer with a methodology to derive the probability of the extreme wind events [7], in particular those described by the IEC.

- Probability density functions and distribution functions have been derived for extreme wind speeds, extreme gusts and extreme wind direction changes. With these density functions it is not only possible to assign a probability to certain extreme wind conditions, but it is also possible to construct a standard where the model for extreme winds and the model for 'normal' turbulence and the site classification are logically related, both mathematically and physically.
- The derived distribution functions have been used to compute the magnitude of extreme wind speeds, extreme gusts and extreme wind direction changes with a confidence level of 98%. Comparison with the values given by the IEC 1400-1 standard confirms the observation that the IEC values are generally too benign. It is recommended however to re-evaluate the distribution function for the extreme direction change.
- Finally a rare meteorological phenomenon, called a downburst, is described, which, together with tornadoes, should be included in the extreme climate events of the IEC standard

5. QUANTIFICATION OF FAILURE PROBABILITIES

For a safe design of load carrying components a margin is introduced between the design value of the strength and the characteristic value of the load. Over the years various methods to define safety margins have been used, but nowadays the concept of the partial safety factors is commonly embodied in the structural design codes. The determination of the magnitude of the partial safety factors can be done empirically. However, a probabilistic approach is preferred. To calibrate partial safety factors based on a probabilistic method target values for the structural reliability of load carrying components have to be drawn up. This aspect has been considered in the current subproject by means of a literature study [8]. From this literature study it is concluded that:

- The Scandinavian countries and The Netherlands seem to be leading in the application of structural reliability methods.
- The code which is not local to a country, but shall be applied Europe-wide, is the Eurocode 1.

- It is recommended to apply the safety level of the Eurocode to wind turbines, which would mean a yearly safety index of 4.7, corresponding to a failure probability of 10^{-6} /year.

Guidelines to collect data for quantitative safety and reliability analyses have been formulated, based on a limited benchmark study. The following is recommended:

- The recommendations set out in the LW15/75 and NEWECs-45 studies can be used for design of specific data collection and parameter estimation. Also, the recommendations of the LW 15/75 study on the use of generic data are still valid.
- Preferably, use should be made of standard, proven methods as laid down in reliability handbooks. Preferably, computerised versions of (generic) databases and existing software for reliability data analysis should be used.
- Generic wind turbine data sources can be used if no specific data are available or if there are no time or resources available to collect design specific data.
- Generic wind turbine data sources can be used to provide data on a high level, e.g., an estimate of blade failure frequency to be used in risk studies, or for frequencies of certain initiating events, e.g., grid loss.
- If generic data are used to estimate a particular parameter (e.g., a failure rate), the following should be documented clearly for each parameter estimated:
 - the reference(s) to the source(s) used,
 - a discussion why the source is considered valid or why the source is used,
 - the calculation procedure to arrive at the final estimate if multiple sources are used.
- If engineering judgement is used to provide an estimate, the reason for this should be indicated. Engineering judgement should be used to provide an estimate if design specific or generic sources do not provide an adequate answer.

From a literature study it is concluded that risk criteria related to the risk to the public, applicable for wind turbines are:

- the individual risk and
- the group risk (as defined in the official Dutch premises for risk management).

For the use of the individual risk a risk target level of 10^{-5} /year is recommended. The target value for the group risk is that the likelihood of an accident with 10 deaths occurring should not exceed one in every hundred thousand years (10^{-5} /year).

6. INTEGRATION OF BLADE TESTS IN DESIGN

The objective of this part of the project is to develop a recommended methodology to include full-scale blade tests in the wind turbine design process. Full scale blade tests, as performed nowadays, are executed to demonstrate adequate safety margins and to verify design calculations.

Property tests are intended to check whether properties, like mass, centre of gravity, eigenfrequencies and static strength are (almost) equal to the values assumed in the load spectrum calculations:

- Mass and centre of gravity are the easiest measurements to perform. The values give a very good indication whether the blade has been produced according to the specifications.

- Stiffness is very important, it indicates whether tower clearance is sufficient and together with the mass distribution it provides the input for the calculation of the natural frequencies. The stiffness distribution is not that easy to determine, especially when the lay-up of the laminates across the cross-section is not symmetric and coupling between deformation modes has to be taken into account.
- Natural vibration tests are very important to verify whether the aeroelastic calculations have been performed on an accurate model of the wind turbine (rotor blades). The eigenfrequencies are not that difficult to determine, however the actual mode shape is more difficult to measure. Differences compared with the assumed values should be consistent with the differences between assumed mass and stiffness distribution.

The static test results, usually strain gauge readings on a number of selected spots give a fair indication whether the structural design is accurate enough to predict the strains/stresses. Strain/stress concentrations are difficult to determine due to the fact that only a limited number of strain gauges will or can be monitored.

The fatigue test has limited value for the designer, especially when the designer wants to improve the design from the test results. The main reason is that the test loading differs much from the design loading, due to the fact that a test is made up of only $3 \cdot 10^6$ to 10^7 cycles and the design loading comprises up to $5 \cdot 10^8$ cycles. For coupon fatigue tests the scatter in allowable number of cycles is almost a factor 10. When only 1/3 of that scatter is present at a full scale test, the results of two or even more tests are needed to obtain clear conclusions, except when a failure occurs early in the fatigue test.

7. POWER PERFORMANCE IN COMPLEX TERRAIN

This subproject intends to clarify the status of power performance verification and assessment in complex terrain, putting emphasis on the following items [4]:

- power performance verification for wind turbines operating in complex terrain,
- assessment of developed, applied and verified tools for WECS power performance in complex terrain,
- assessment of the available international and national standards.

The assessment of the nacelle anemometer on running machines was performed for a wide range of wind turbine sizes ranging from 110kW up to 1MW machines. The conclusions are:

- the correct application of the methodology and the transfer of the calibration formula to other wind turbines of the same make and type, presupposes that the wind turbine rotor settings, yaw behaviour, the position on the nacelle anemometer are unchanged as well as that the terrain remains flat.
- the dependency of the calibration formula to wind and wind turbine parameters was found to be limited. On the other hand these effects are expected to be magnified in cases where wind structure and wind turbine response at the calibration site compared with the testing site are quite different.

- lower scatter in the measured power curve as a function of the nacelle wind speed may be obtained.
- the introduction of the nacelle cup calibration formula introduces a statistical error that should be taken into account in the uncertainty estimation.
- The use of nacelle wind speed measurements may decrease the error induced by site calibration significantly in cases where large discrepancies are encountered between the measured and reference wind speed.

A parameter identification of wind turbine power performance investigated the dependency of power characteristics on deterministic and stochastic wind characteristics, especially mean value and standard deviation, for identification of the site related effects. The following issues were clarified by means of this parameter identification procedure:

- identification and quantification of the wind parameters that affect power performance,
- assessment of the sensitivity of power characteristics for wind turbines of different size and control system,
- assessment of the sensitivity of power characteristics for the same wind turbine type when operated in different sites,
- assessment of causal parameters in relation to complex terrain characteristics,
- assessment of a power curve normalising procedure based on parameter identification results.

8. SITE EVALUATION

The site evaluation is at the core of the economic evaluation process but needs to consider more than just energy yield potential if other aspects such as turbine integrity and safety are to be assessed. The intention of this sub-project has been to provide information and methods which will be of practical use to those involved in the application of the IEC wind turbine safety standard (IEC-1400-1).

A comprehensive review of the technical status of modelling and measurement based techniques was carried out [3]. As dictated by the results of the survey, specific emphasis was placed on WASP and MCP with a view to proposing guidelines for use. In the case of WASP the main recommendations for successful implementation are:

- both the reference and predicted sites are subject to the same weather regime,
- neutral atmospheric conditions prevail,
- the surrounding terrain is sufficiently gentle and smooth to ensure mostly attached flows,
- the reference data are reliable,
- the description of the background roughness length must be as accurate as possible.

The MCP technique can be successfully applied where the following conditions can be satisfied,

- validated, long-term and short-term concurrent measured reference wind speed data are available at a reference site within the same climatological zone as the prediction site.
- validated prediction site wind speed measurements are available for a period of at least 8 months and more typically 12 months or more.

Perhaps the major shortcoming in the commercial use of wind flow models (and MCP) is the difficulty in the quantifi-

cation of uncertainties. A philosophy for the assessment of uncertainty is proposed which, although not necessarily easy to apply to wind models, does highlight the components of uncertainty of relevance. Derivation of a specific parameter (Ruggedness Index) for categorising terrain has been summarised from recent literature and is proposed as a useful technique for identifying when the limits of applicability of a model may have been exceeded.

Methods for assessing parameters other than mean wind speed are proposed. In each case, the theoretical background is also presented. The following parameters have been considered:

- reference wind speed;
- characteristic turbulence intensity at 15 m/s;
- annual average wind speed distribution;
- normal wind profile;
- turbulence length scales ;
- coherence ;
- standard deviation ratios ;
- negative gust.

9. IMPLEMENTATION OF MEASNET

More than three years ago the six the European institutes CIEMAT, CRES, DEWI, ECN, NEL, RISØ later joined by WINDTEST, decided to improve their measurement quality jointly in order to avoid any problems of future mutual recognition. Measurements performed by the institutes, even applying the existing IEA, IEC and other standards and recommendations, showed remarkable differences in their results, a situation which is unacceptable in an open international market. The main task of the project team consisted of creating an organisational structure and of establishing rules and requirements which will guarantee that high quality measurements are carried out by the participants. In effect, the objective of this project was to arrive at the situation where the measuring institutes are able to perform measurements of equal quality which are sufficient for the mutual comparison and acceptance.

During the course of the two projects, the members of MEASNET agreed on the following measurement and quality evaluation procedures to be performed under the MEASNET quality criteria [6]:

- anemometer calibration;
- power performance;
- noise ;
- power quality.

Several quality evaluations have been made during the two projects. The most intensive one was for anemometer calibration, because a procedure had to be found, how to judge the quality of the wind tunnel which should be used for the anemometer calibration. Other round robin evaluations were performed for power performance and noise measurements. In both cases a set of measured data were sent around for evaluation by the individual institutes. Differences in the evaluation results were discussed and led to correction measures concerning the established measurement and quality evaluation procedures. All round robin tests showed, that the idea of MEASNET to harmonise the interpretation of standards and the applied measurement methods is of very high importance. Guidelines for evaluation, for example

stated in the existing IEC standards, even when correctly applied led to different interpretations of requirements and consequently to differences in the results.

All agreed measurement procedures except power quality, take into account the final and draft documents of international organisations, e.g. IEC, IEA and in addition requirements derived from results of related projects and measurement experiences. The agreed noise measurement procedure is an example for the necessity of additional MEASNET measurement requirements. The performed round robin evaluation of a measured noise data set led to comparable results because the IEC recommendation concerning the evaluation of tonality was improved.

As a result of their intensive and detailed work, MEASNET members now mutually accept their measurement results and guarantee high quality by regularly performed quality evaluation programmes. The main advantages for the industry when contracting a MEASNET institute for the execution of a measurement campaign are:

- the measurements are accepted in other countries,
- the quality of the measurements is high and comparable,
- an order can be issued on the basis of competitive offers from the member institutes.

ACKNOWLEDGEMENT

The EWTS-I and II projects have been funded by the European Commission as part of the Non-nuclear Energy Programme. Additional funding for this project was supplied by the Governments of the participating countries.

REFERENCES

- [1] J.W.M. Dekker and J.T.G. Pierik (ed.). European Wind Turbine Standards II. Technical report, EC, 1999. to be published.
- [2] J.P. Molly (ed.). Implementation of the network of European Measuring Institutes, MEASNET. Technical report, DEWI, 1998.
- [3] A. Derrick et al. A unified approach to the evaluation of site specific wind characteristics for use in both energy and load modelling of a potential wind turbine development site. In *EWEC97*, Dublin, 1997.
- [4] E. Morfiadakis et al. Assessment of power performance measurement and evaluation in complex terrain. In *EWEC97*, Dublin, 1997.
- [5] G.C. Larsen et al. Fatigue life consumption in wake operation. In *EWEC97*, Dublin, 1997.
- [6] J.P. Molly et al. MEASNET: Network of EUREC Agency recognized measuring institutes. In *EWEC97*, Dublin, 1997.
- [7] S.M. Petersen et al. EWTS-II Load spectra and extreme wind conditions. In *EWEC97*, Dublin, 1997.
- [8] A.J. Seebregts and P. Christensen. EWTS-II benchmark on datacollection and parameter estimation for safety and reliability analysis of wind turbines. In *EWEC97*, Dublin, 1997.

EXPERIMENTAL VERIFICATION OF THE NEW RISØ-A1 AIRFOIL FAMILY FOR WIND TURBINES¹

Kristian S. Dahl, Peter Fuglsang, Ioannis Antoniou
Risø National Laboratory
P.O. Box 49
DK-4000 Roskilde, Denmark
Phone: +45 4677 5071, Fax.: +45 4677 5083
Email: peter.fuglsang@risoe.dk

ABSTRACT: This paper concerns the experimental verification of a new airfoil family for wind turbines. The family consists of airfoils in the relative thickness range from 15% to 30%. Three airfoils, Risø-A1-18, Risø-A1-21, and Risø-A1-24 were tested in a wind tunnel. The verification consisted of both static and dynamic measurements. Here, the static results are presented for a Reynolds number of 1.6×10^6 for the following airfoil configurations: smooth surface (all three airfoils) and Risø-A1-24 mounted with leading edge roughness, vortex generators, and Gurney-flaps, respectively. All three airfoils have constant lift curve slope and almost constant drag coefficient until the maximum lift coefficient of about 1.4 is reached. The experimental results are compared with corresponding computational results from the general purpose flow solver, EllipSys2D, showing good agreement.

Keywords: AIRFOIL SECTION, VORTEX GENERATORS, WIND TUNNELS, WIND TURBINES(HAWT)-ROTORS

1 INTRODUCTION

This paper concerns two-dimensional wind tunnel measurements on the Risø-A1-18, Risø-A1-21, and Risø-A1-24 airfoils with the relative thicknesses of 18%, 21% and 24%, respectively. All three airfoils are members of a new airfoil family for wind turbines, developed at Risø National Laboratory [1].



Figure 1: Risø-A1-18, Risø-A1-21, and Risø-A1-24.

The measurements were carried out in the Velux wind tunnel, Østbirk, Denmark. The wind tunnel is of the closed return type with an open test section. It is not ideal for two-dimensional testing, but Fuglsang *et al.*, [2] validated the testing method on the NACA 63-215 airfoil and showed that by proper application of boundary corrections, the experimental results compare well with 2D-calculations and other measurements from closed test section wind tunnels.

The measurements comprised pressure distribution on the airfoil section and wake rake pressure measurements. For both steady and quasi-steady inflow, mean values of lift, drag, and moment coefficients were obtained. In the steady measurements, the angle of attack was changed in steps of 2° and a 20 second time series was obtained for each angle of attack. Alternatively, in the quasi-steady measurements, the angle of attack was changed continuously at an average rate of about $0.3^\circ/\text{s}$. The presented results are all for quasi-steady angles of attack in the range $-5^\circ < \alpha < 30^\circ$ and Reynolds number, $Re =$

1.6×10^6 . We present results for smooth airfoil surface conditions for all three airfoils and additionally, for Risø-A1-24 results for leading edge roughness (LER), vortex generators (VG), and Gurney-flaps (GF).

2 METHOD

The experimental set-up is briefly described in this section. A more complete description can be found in [2,3]. The Velux wind tunnel has a cross section of $7.5 \times 7.5 \text{ m}$ and a length of 10.5m, Figure 2. The cross section of the jet blowing into the test section is $3.4 \times 3.4 \text{ m}$. The maximum flow velocity is 45m/s and the turbulence intensity at the test section inlet is 1%. The airfoil sections with a span of 1.9m and a chord of 0.6m were mounted in a test stand 1.7m above the tunnel floor and 3.2m from the nozzle outlet with end plates to limit three-dimensional flow effects. Three Pitot tubes measured static and total pressure at different locations in the test section allowing estimation of the free stream reference pressures.

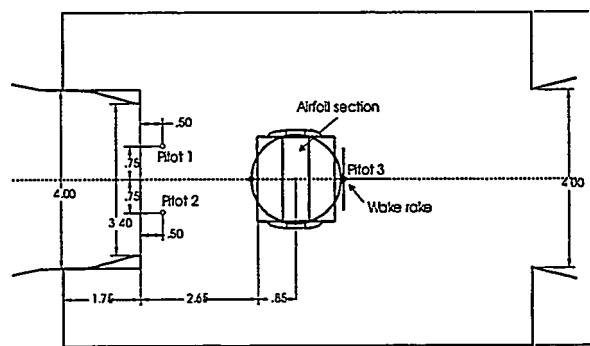


Figure 2: Top view of wind tunnel test section and the test stand. The flow is from left to right. Dimensions are in meter.

¹ Presented at EWEC'99, Nice, France

The vertical span of the wake rake was 0.456m. The distance between the airfoil trailing edge and the wake rake was 0.7 airfoil chords and the centre line of the wake rake was placed at the height of the trailing edge at 0° angle of attack in the middle of the airfoil section. The wake rake was not traversed in the horizontal or the vertical directions.

A total of 134 signals were measured by the data acquisition system during the measurement campaigns, i.e., 64 airfoil surface static pressures, 5 wake rake static pressures, 53 wake rake total pressures, 3 Pitot tube static pressures, 3 Pitot tube total pressures, angle of attack, air temperature, air density, 2 strain gauges for recording shaft bending to be able to derive integrated lift and drag forces for the airfoil section, and finally a signal for reduced frequency.

2.1 Wind tunnel boundary corrections

Wind tunnel corrections were applied for streamline curvature and down-wash. Horizontal buoyancy, solid and wake blockage were neglected because the test section configuration corresponds to an open jet, which is free to expand, [4]. The application of wind tunnel boundary corrections for the Velux wind tunnel was verified in [2]. For the correction of streamline curvature, the method of Brooks and Marcolini, 1984, [5] was used.

The corrected free flow angle of attack, α , is found from

$$\alpha = \alpha_t - \frac{\sqrt{3}\sigma}{\pi} C_L - \frac{2\sigma}{\pi} C_L - \frac{\sigma}{\pi} (4C_M) \text{ [rad]},$$

$$\text{where } \sigma = \frac{\pi^2}{48} \cdot \left(\frac{c}{h} \right)^2.$$

The drag coefficient, C_D , is calculated from

$$C_D = C_{D_t} + \left[-\frac{\sqrt{3}\sigma}{\pi} C_L \right] C_L,$$

and the moment coefficient, $C_M = C_{M_t} - \frac{\sigma}{2} C_L$.

The lift coefficient is denoted C_L , c is airfoil chord and h is the jet height. Subscript t denotes measured, uncorrected data.

2.2 Wake rake total drag

The total drag (skin friction and pressure drag) can be calculated from the balance of the momentum flux entering a control surface in front of the airfoil and the momentum flux exiting the control surface behind the airfoil section. The momentum profile entering is assumed uniform and is calculated from the wind tunnel free stream reference pressures. The momentum profile exiting the control surface is calculated from the pressures measured by the wake rake. Assuming that the flow is two-dimensional, the total wake drag coefficient is calculated according to [4].

3 AIRFOIL SECTIONS

The airfoil sections were equipped with 62 pressure taps of 0.5 mm inner diameter in the centre line region. The taps were placed along the chord at the centre line of the model in a staggered arrangement to minimise disturbances from upstream taps. Additional taps were drilled close to the centre line as a back-up to taps at important positions,

e.g., the leading and trailing edges, and in order to allow measurements away from the centre line.

The distributions of the pressure taps reflected the expected pressure gradients with dense tap spacing at the leading edge and more taps on the suction side than on the pressure side.

3.1 Leading edge roughness

Zigzag tape was mounted on the airfoil section surface to simulate the effects of leading edge roughness from accumulation of dirt and bugs, etc. In all measurements the zigzag tape was mounted in 5% chord on the suction side and in 10% chord on the pressure side. The zigzag tape has an angle of 90°, a chord wise width of 3mm and a height of 0.35mm.

3.2 Vortex generators and Gurney flaps.

Vortex generators (VGs) are most often used at the inner part of wind turbine blades in chord wise positions between 10% to 30% from the leading edge on the blade suction side. VGs increase maximum lift by delaying separation on the airfoil suction side to higher angles of attack, but at the same time, they increase drag. Here, we applied VGs with a height of 6mm and a length of 18mm. The VGs sit in pairs with an angle to the flow of $\pm 19.5^\circ$ with the leading edges 10mm apart and a pair spacing of 25mm.

A Gurney-flap at the trailing edge is another way of modifying the aerodynamic performance of an airfoil. Increasing airfoil camber, GFs increase maximum lift and shift the lift curve toward lower angles of attack. Here, we tested flaps of 1% and 2% of chord.

4 RESULTS AND DISCUSSION

Risø-A1-18 and Risø-A1-21 were designed to operate at $Re = 3.00 \times 10^6$ and Risø-A1-24 were designed to operate at $Re = 2.75 \times 10^6$, [1]. The following results are all for $Re = 1.6 \times 10^6$. Computations show that going from the higher to the lower Reynolds number typically decreases the maximum lift coefficient by 0.1. All computational results are from the general purpose flow solver, EllipSys2D, [6] using the k- ω SST turbulence model, [7] and the Michel transition criterion, [8].

In Figure 3 to Figure 5 the polars for smooth measurements are compared with the computational results of EllipSys2D with both free transition and fully turbulent flow conditions. The measurements show that the lift increases almost linearly until the maximum lift coefficient of about 1.4 is reached at around $\alpha = 10^\circ$ where there is a well defined and distinct stall. The drag coefficient does not change much below stall and has a value of about 0.01, Table I.

Table I: Aerodynamic coefficients smooth measurement.

	C_{Lmax}	C_{Dmin}
Risø-A1-18	1.41 @ 10.8°	0.010 @ 3.9°
Risø-A1-21	1.38 @ 9.7°	0.009 @ -0.8°
Risø-A1-24	1.36 @ 9.9°	0.010 @ 2.9°

Risø-A1-18 has the smoothest stall of the three airfoils. For Risø-A1-21 and Risø-A1-24 the experimental and

computational results, respectively, look very much alike both showing a more abrupt stall.

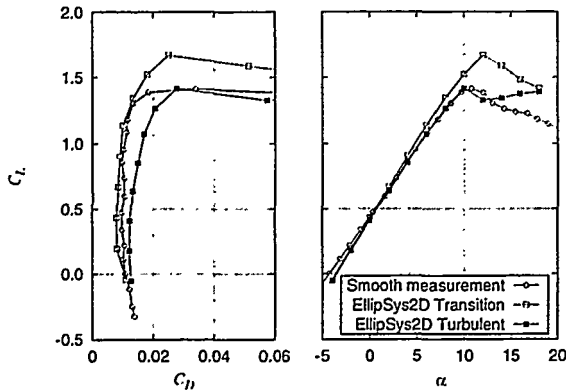


Figure 3: Polar for Risø-A1-18

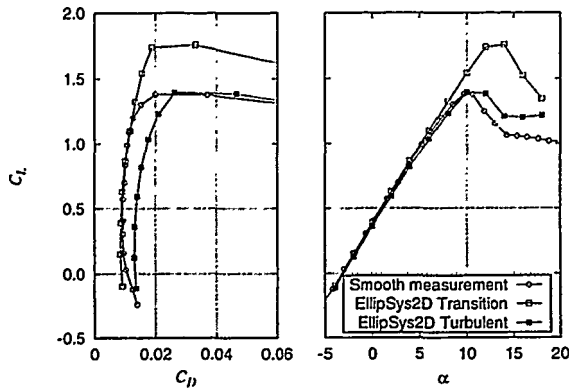


Figure 4: Polar for Risø-A1-21

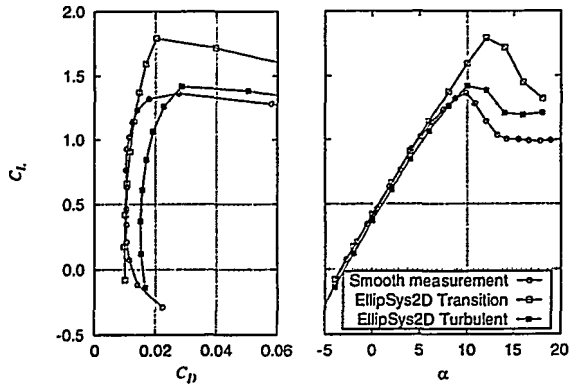


Figure 5: Polar for Risø-A1-24

For all three airfoils the position and value of maximum lift are predicted very well with the assumption of fully turbulent flow whereas the free transition computations overestimate maximum lift significantly showing that the Michel transition criterion used in EllipSys2D does not perform well. The difference between measured maximum lift and the free transition predictions is also due to the relatively high tunnel turbulence.

Drag is more difficult to predict than the lift. Here, the free transition results compare well with measurements for angles of attack below stall whereas the fully turbulent results for drag are in reasonably good agreement with measurements in post stall.

Now having presented smooth measurements for all three airfoils, the remaining part of the paper concentrates exclusively on Risø-A1-24 beginning with measured and computed pressure distributions for $\alpha = 8^\circ$ which is just before maximum lift is obtained, Figure 6. The fully turbulent pressure distribution is in very good agreement with the experimental pressure distribution on the entire airfoil except for the first 5% of the suction side where the free transition computation compares better with measurements.

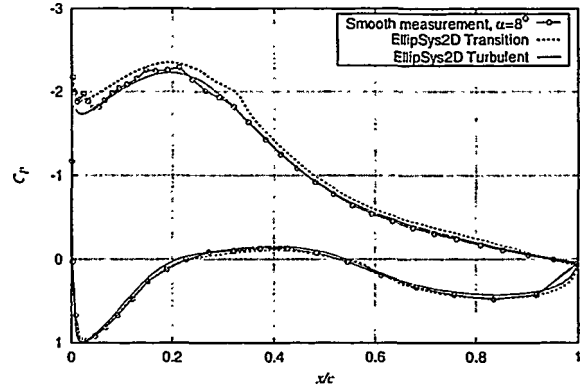


Figure 6: Pressure distribution for Risø-A1-24 at $\alpha = 8^\circ$.

The small suction peak on the leading edge is a result of the design strategy aiming for a roughness insensitive airfoil. The suction peak increases with angles of attack when getting closer to the stall angle. The peak eventually causes transition from laminar to turbulent flow close to the leading edge making the maximum lift insensitive to leading edge roughness. In Figure 7, the experimental results of simulating leading edge roughness with zigzag tape are compared with smooth measurements and fully turbulent computations with EllipSys2D. The lift curve slope is not affected by the presence of zigzag tape but the position and value of the maximum lift coefficient is changed from $\alpha = 9.9^\circ$ to $\alpha = 9.1^\circ$ and from $C_{Lmax}=1.36$ to $C_{Lmax}=1.17$, respectively. Now, the fully turbulent drag predictions are in very good agreement with experimental results for angles of attack below stall.

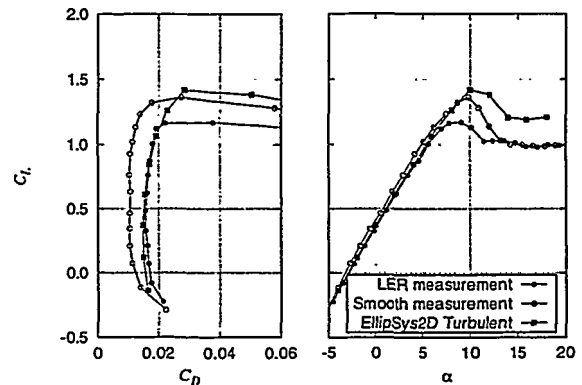


Figure 7: Polar for Risø-A1-24 with leading edge roughness (LER).

The Risø-A1-24 airfoil will typically be used on the inboard sections of the blade and therefore, load and noise issues are of less importance compared to what holds for outboard section airfoils. So, there is room for modification of Risø-A1-24's performance using maximum lift

increasing aerodynamic devices such as vortex generators and Gurney flaps. Unfortunately, they increase drag as well.

Figure 8 and Table II show the experimental results for vortex generators mounted in four different chord wise positions, i.e., 15%, 20%, 25%, and 30%. We see, as expected, that stall is delayed and maximum lift is increased as the VGs move towards the leading edge. For angles below the maximum lift angle of the smooth measurement, the lift curve slope is unchanged for all the VG-positions. Stall is very abrupt in these two-dimensional measurements, but on a rotor rotational effects will soften this. For lower angles of attack the 15% position shows significantly larger drag than the other VG-positions.

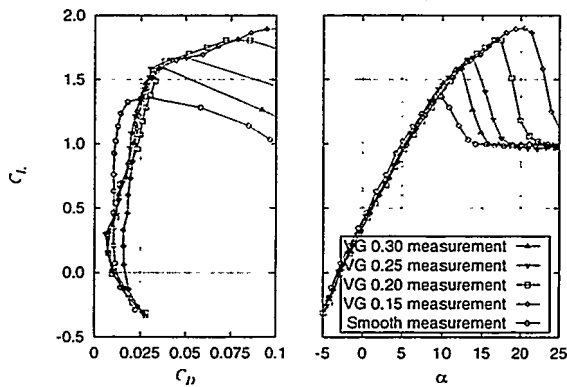


Figure 8: Polar for Risø-A1-24 with vortex generators in different chord wise positions.

In Figure 9 and Table II, two different sizes of Gurney flaps, i.e., 1% and 2% of chord, respectively, are compared with the smooth measurements. There is not much difference between GF 1% and GF 2% as far as the lift curve and maximum lift go, but there is a significant difference in drag below stall.

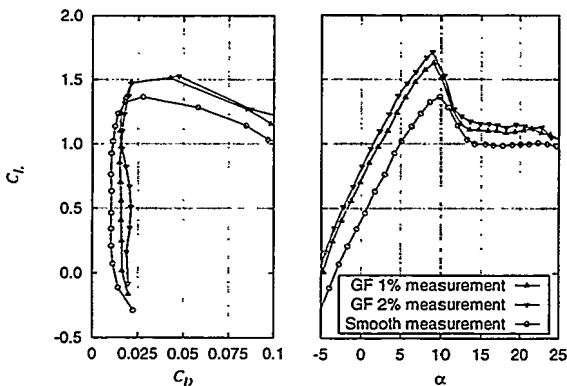


Figure 9: Polar for Risø-A1-24 with Gurney-flaps.

5 CONCLUSIONS

Three new airfoils dedicated for wind turbine application have been tested experimentally in a wind tunnel. The tunnel has relatively high background turbulence making the results more representative for natural conditions than would be the case for a low turbulence wind tunnel. For smooth surface conditions, all three airfoils have the desirable properties of constant lift

curve slope and almost constant drag coefficient until maximum lift is reached. The maximum lift coefficient and the minimum drag coefficient for the airfoils are about 1.4 and 0.01, respectively. Tests on Risø-A1-24 mounted with zigzag tape show that it is reasonably insensitive to leading edge roughness (holds true for Risø-A1-18 and Risø-A1-21, as well). Furthermore, mounting of vortex generators and Gurney flaps show that there is room for modification of the aerodynamic properties of the airfoil by relatively simple means, e.g., vortex generators in 15% chord increased the maximum lift coefficient from 1.36 to 1.90. The smooth experimental results compare well with computational results from the general purpose flow solver, EllipSys2D.

Table II: Aerodynamic coefficients for Risø-A1-24.

	$C_{L,max}$	$C_{D,min}$
Smooth	1.36 @ 9.9°	0.010 @ 2.9°
LER	1.17 @ 9.1°	0.016 @ 1.1°
VG, 15%	1.90 @ 20.5°	0.016 @ -0.2°
VG, 20%	1.81 @ 17.4°	0.007 @ -0.5°
VG, 25%	1.67 @ 13.8°	0.006 @ -0.7°
VG, 30%	1.59 @ 12.4°	0.008 @ -1.5°
GF, 1%	1.63 @ 9.1°	0.015 @ 1.0°
GF, 2%	1.72 @ 9.0°	0.016 @ 1.3°

ACKNOWLEDGEMENTS

The Danish Energy Agency funded the present work in the contracts ENS-1363/95-0001 and ENS-1393/98-0038.

REFERENCES

- [1] Fuglsang, P., Dahl, K. S., 1999, Design of the New Risø-A1 Airfoil Family for Wind Turbines, European Wind Energy Conference and Exhibition, Nice, France, March 1-5, 1999.
- [2] Fuglsang, P., Antoniou, I., Sørensen, N.N., Madsen, H. Aa., 1998, 'Validation of a Wind Tunnel Testing Facility for Blade Surface Pressure Measurements.' Risø-R-981(EN), Risø National Laboratory, Denmark.
- [3] Fuglsang, P., Antoniou, I., Dahl, K.S., Madsen, H.A., 1998, 'Wind Tunnel Tests of the FFA-W3-241, FFA-W3-301 and NACA 63-430 Airfoils.', Risø-R-1041(EN), Risø National Laboratory, Denmark.
- [4] Rae Jr., W.H., Pope, A., 1984, Low-Speed Wind Tunnel Testing, SE, John Wiley & Sons, ISBN 0-471-87402-7.
- [5] Brooks, T.F. and Marcolini, M.A., 1984, Airfoil Trailing Edge Flow Measurements and Comparison with Theory Incorporating Open Wind Tunnel Corrections, AIAA-84-2266, AIAA/NASA 9th Aeroacoustic Conference.
- [6] Sørensen, N.N., 1995, General Purpose Flow Solver Applied to Flow over Hills, Risø-R-827(EN), Risø National Laboratory, Denmark.
- [7] Menter, F.R., 1993, Zonal Two Equation k- ω Turbulence Models for Aerodynamic Flows. AIAA Paper 93-2906.
- [8] Michel, R., 1952, Etude de la transition sur les profils d'aile. ONERA Report 1/1578-A. See White F.M., Viscous fluid flow, p. 442.

DERIVATION OF AIRFOIL CHARACTERISTICS FOR THE LM 19.1 BLADE BASED ON 3D CFD ROTOR CALCULATIONS

Christian Bak, Niels N. Soerensen, Helge A. Madsen
Risoe National Laboratory
P.O. Box 49
DK-4000 Roskilde
Denmark
Phone: +45 4677 5091
Fax: +45 4677 5083
Email: christian.bak@risoe.dk

ABSTRACT: Airfoil characteristics for the LM 19.1 blade are derived from 3D CFD computations on a full-scale 41-m rotor. Based on 3D CFD the force distributions on the blades are determined, from which airfoil characteristics are derived using the momentum theory. The final airfoil characteristics are constructed using both wind tunnel measurements and 3D CFD. Compared to 2D wind tunnel measurements they show a low lift in stall for the airfoil sections at the tip. At the airfoil sections at the inner part of the blade, they show a high lift in stall. At about 60% radius the lift agrees well to 2D wind tunnel measurements. Aeroelastic calculations using the final airfoil characteristics show good agreement to measured power and flap moments. Furthermore, a fatigue load analysis shows a reduction of up to 15 % of the load compared to commonly used data.

Keywords: BLADE AERODYNAMICS, STALL ROTATION EFFECTS, NAVIER-STOKES EQUATIONS

1. INTRODUCTION

Calculations of power and loads for wind turbines are mainly carried out by using the Blade Element Momentum theory (BEM). The input for this model is in addition to operational conditions and blade geometry also the lift and drag coefficients, C_L and C_D , for the airfoils used on the blades.

The airfoil characteristics used in BEM until now are based on 2D wind tunnel measurements on airfoils. However, a direct use of 2D wind tunnel measurements in BEM calculations cannot reproduce the measured power since they are known to underpredict the forces acting on the blades in stalled conditions (Rasmussen et al. [8]). This fact has lead to a correction of the 2D wind tunnel measurements so that the correct power can be reproduced, e.g., . This correction has typically been based on qualified estimations and experiences rather than on a systematic derivation. Furthermore, different sets of airfoil coefficients are often used for the same rotor.

This paper describes the results using a systematic method for derivation of airfoil characteristics. The method is based both on computations of the forces on a full-scale rotor and on wind tunnel measurements. The computations are carried out using Computational Fluid Dynamics (CFD), in which the rotational and 3D effects are taken into account as the full Navier Stokes equations are solved. This means that these effects are included in the airfoil characteristics.

In the following the systematic method is described and is applied to the derivation of airfoil characteristics for the LM 19.1 blade, which is used on 500 kW to 750 kW wind turbines.

2. METHOD

The method contained three steps:

1. Computation of the flow and thereby the forces on the blades using 3D CFD on a full-scale rotor.
2. Derivation of the airfoil characteristics by using inverse BEM calculations. This was possible because the forces were known from the CFD computations.
3. Construction of the final airfoil characteristics in the full incidence interval by supplementing with wind tunnel measurements.

In general, CFD computed power curves and measured power curves are not identical. If a complete correspondence between the two kind of power curves is desired, a correction of the CFD computed forces can be carried out before step 2 in the method. Before introducing the correction, one should be aware of the different causes for deviations as described in Section 2.2.

2.1. CFD computations on the LM 19.1 blade

CFD computations on full-scale rotors have recently shown good results. As the full Navier-Stokes equations are solved the results will reflect the influence of rotational and 3D effects. The computations were carried out using the program EllipSys (Michelsen [5], [6] and Sørensen [9]). The computations determined the forces on the blades, but furthermore, distributions of pressure and velocity, separation patterns, velocity profiles, etc. were determined, which gave an understanding of the flow around the rotor. Computations were carried out on a rotor using LM 19.1 blades with 1.5-m root extenders. Since the computations were very time consuming only computations for six wind speeds

were carried out; 7, 8, 10, 12, 15 and 18 m/s. The input for these computations were the rotor geometry, rotational speed and average wind speed. The computations were carried out for a three-bladed rotor and included the wakes from all the three blades. However, it did not include the influence from the tower and the nacelle. Constant wind and no wind shear were assumed. Radial distributions of axial and tangential forces on the blades were extracted for use in the generation of airfoil characteristics.

2.2. Correction of computed forces

Since the computed and the measured power curve were not identical, a correction of the computed power curve was carried out so that the power curves became identical. This correction was carried out for each computed wind speed by determining a correction factor. The correction factors were multiplied on the corresponding CFD computed blade force distributions. For each wind speed, both the tangential and the axial force distribution were corrected linearly for the entire blade. Thus, it was assumed that the circulation around the blade was corrected.

In Figure 1, a measured power curve for a rotor using LM 19.1 blades are compared to a CFD computed power curve. A binning of the measured power curve was necessary to obtain an unambiguous value for each wind speed. The maximum deviation between the two curves existed at 12 m/s with a correction factor of 0.91.

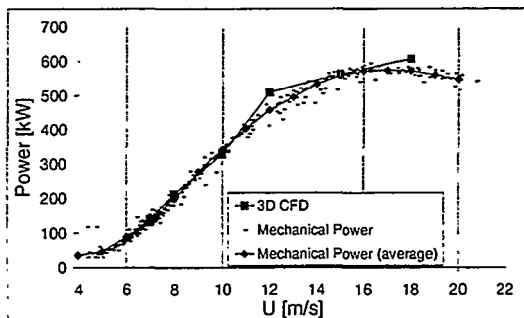


Figure 1 Measured and CFD computed power curve for the Nordtank NTK 500/41 using LM19.1-blades and 1.5 m root extender.

Comparing the measured and CFD computed power curves one should note that the inflow to the rotor in the CFD computations was uniform and had no wind shear. Neither nacelle nor tower was present in the computations and uncertainties were present in the CFD turbulence model. However, also the measurements were influenced by several effects. These were, e.g., turbulence, wind shear, rain, bugs on the blades, different pitch angles ($\pm 0.2^\circ$), temperature differences and data averaging. Paulsen [7] describes details about the measurements.

2.3. Derivation of airfoil coefficients based on CFD

The airfoil coefficients were derived using BEM in an inverse manner since the force distributions were known. The angle of attack, α , and C_L and C_D were computed for different sections on the blade. Given a force at one radial station one set of corresponding values were determined consisting of one C_L value, one C_D value and one α value. This was done for all radial stations and for all wind speeds in the CFD computations. Other methods for deriving the airfoil coefficients are described by Bak et al. [3].

2.4. Deriving the final airfoil coefficients

2D wind tunnel measurements were used in the linear part of the C_L curve since BEM calculations using 2D airfoil coefficients were believed to give more realistic results than using the CFD computed coefficients at this part of the curve. This is shown in the sketch Figure 2. The airfoil coefficients derived from the CFD computations were used in light stall and towards deep stall. Wind tunnel measurements and estimations were used for α beyond the α computed by CFD. Getting the three parts of the curve to fit together required small adjustments to obtain smooth curves. The 2D wind tunnel measurements are carried out by NASA (Abbott and Doenhoff [1]) for the NACA airfoils, which are used on the outer part of the blade. For the FFA airfoils, which are used on the inner part of the blade, the measurements are carried out by Risø (Fuglsang et al. [4]). Airfoil coefficients for high α were partly based on measurements on blades with finite aspect ratio (Bak and Petersen [2]) and partly on estimations.

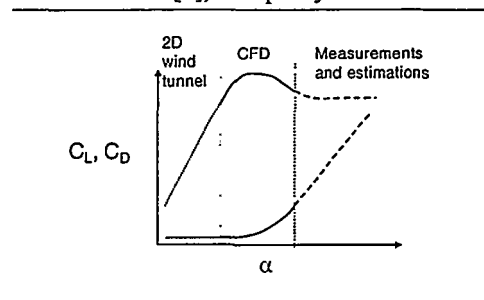


Figure 2 Sketch of how the final airfoil coefficients are constructed based on measurements and CFD.

3. RESULTS

Airfoil characteristics for the LM 19.1 blade were derived using two different assumptions:

- One set based on the force distributions as computed with CFD.
- One set also based on the force distributions as computed with CFD, but with the axial and tangential force corrected to obtain the measured power.

The airfoil characteristics are shown in Figure 3 to Figure 5 for the sections 1.5 m, 8.0 m and 10.5 m

from the tip. The rotor radius was $R=20.5$ m. The dots show the airfoil coefficients derived directly from the CFD computations. The constructed airfoil characteristics based on the uncorrected blade forces are named *Uncorrected Data*. The airfoil characteristics based on the corrected blade forces are named *Corrected Data*. These data corresponded to the measured power curve. The constructed airfoil characteristics are compared to 2D wind tunnel measurements.

For the airfoil section 1.5 m from the tip, C_L was low in stall compared to measurements for both the *Uncorrected* and *Corrected Data*, however, with the *Corrected Data* as the lowest. C_D was in good agreement with the wind tunnel measurements until $\alpha=10^\circ$. The dots, showing the derived data from CFD, were in good agreement with the constructed airfoil characteristics.

For the airfoil section 8.0 m from the tip the airfoil characteristics were in good agreement with measurements, however, the *Uncorrected Data* were slightly higher. The dots reflect an over-prediction of C_L and an under-prediction of C_D for α below 10° . In fact, C_D is negative. This could be due to an under-prediction of the induction in the CFD computations for small α , e.g., due to the finite size of the computational domain.

For the airfoil section 10.5 m from the tip both of the constructed C_L curves were higher in stall compared to measurements. The *Corrected Data* set was in good agreement with measurements at light stall. Towards deep stall C_L , however, deviated. C_L increased until $\alpha=20^\circ$ in contrast to the measurements for which C_L decreased from $\alpha=10^\circ$. C_D were slightly lower than the measurements until $\alpha=20^\circ$, after which it increased. The dots show an over-prediction of C_L and an under-prediction of C_D as for the airfoil section 8.0 m from the tip.

To obtain the correct power curve in aeroelastic calculations the constructed airfoil characteristics were used in five spanwise sections. The distances from the tip were: 1.5 m, 4.0 m, 8.0 m, 10.5 m and 12.5 m. The exact relative thickness was used so that the airfoil characteristics were used in the correct radial stations to resolve the force distribution. With this procedure, flap moments were computed. Compared to measurements they were in good agreement when using the *Corrected Data*, while they were slightly over-predicted when using the *Uncorrected Data*.

Aeroelastic calculations for wind speeds from 6 to 24 m/s resulted in a fatigue analysis with equivalent loads as shown in Table 1 and with turbulence intensity of about 15 %. In Table 1 the loads calculated with the *Corrected Data* are compared to loads calculated with data named *Original Data*, which were a set among several sets used for this

rotor and derived on basis of qualified estimations and experience.

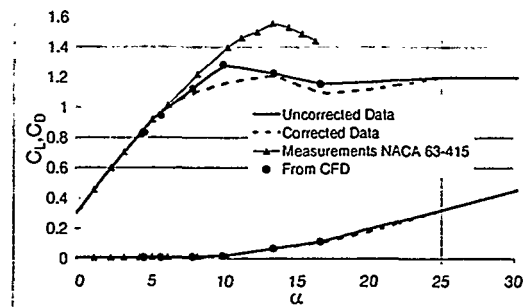


Figure 3 C_L and C_D curve for the NACA airfoil with 15.75% relative thickness corresponding to 1.5 m from the tip, $0.93R$.

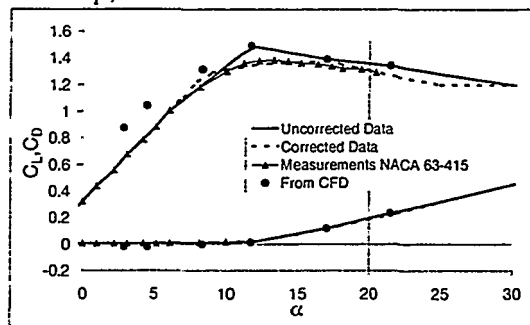


Figure 4 C_L and C_D curve for the NACA airfoil with 18.20% relative thickness corresponding to 8.0 m from the tip, $0.61R$.

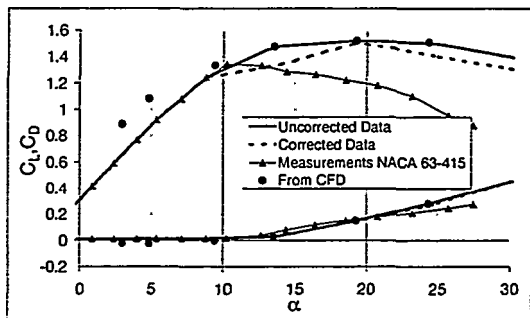


Figure 5 C_L and C_D curve for the FFA airfoil with 24.19% relative thickness corresponding to 10.5 m from the tip, $0.49R$.

Table 1 Comparison of fatigue loads (10^7 cycles) using different airfoil characteristics.

m	Load	Unit	Corr. (1)	Uncorr. (2)	Frac. (2)/(1)	Orig (3)	Frac. (3)/(1)
3	Power	kW	459.92	499.07	1.09	460.18	1.00
12	Root flap moment	kNm	233.61	239.35	1.02	243.70	1.04
12	Root edge moment	kNm	343.99	352.44	1.02	369.74	1.07
5	Tilt moment	kNm	326.23	358.19	1.10	347.37	1.06
5	Yaw moment	kNm	327.54	362.14	1.11	331.96	1.01
3	Tower moment L	kNm	1754.28	1950.18	1.11	1837.22	1.05
3	Tower moment T	kNm	645.86	786.08	1.22	741.52	1.15

The *Original Data* had a high C_L in stall at the tip and a high C_D and a low C_L in stall at the inner part of the rotor compared to the derived airfoil characteristics. It was corrected by fitting the data to a measured power curve.

Compared to the *Corrected Data* the *Uncorrected Data* over-predicted all loads as expected. Comparing the *Original Data* to the *Corrected Data* all loads were over-predicted from 1% to 15% except for the power. The high C_L in stall near the tip caused the over-prediction of all other loads.

4. DISCUSSION

The modifications of 2D airfoil characteristics have so far typically been based on qualified estimations and experiences. In contrast to this, the results described above were based on a systematic method.

No matter which method is used for derivation, the airfoil characteristics are dependent on the geometry of the rotor. Airfoil characteristics for instance for the NACA 63-418 airfoil would thus in general be different for another blade since rotational and 3D effects will differ because of the differences in geometry and rotational speed. The derived data set should thus be used for rotors with approximately the same configuration.

Furthermore, the data set depends on the quality of the CFD computations. The boundary conditions, turbulence modelling and the lack of transition modelling could cause some deviation from measurements. Thus, in 2D CFD computations some under prediction of C_L and C_D on thick airfoils have been observed, while the coefficients on medium thick airfoils agree well with measurements.

In addition, differences in operational conditions between the CFD computed rotor and the rotor, for which measurements were carried out, could influence the quality of the data. These differences could be roughness on the airfoil, no modelling of the nacelle and the tower in the CFD computations, the exact time history of the wind, etc. Although these uncertainties exist, the main 3D flow effects and rotational effects can be fairly predicted and the quality of the rotor flow can be investigated. Including these effects resulted in fatigue loads up to 15 % below loads determined with commonly used data. More aeroelastic calculations should be carried out to estimate the influence of the included effects.

5. CONCLUSION

Airfoil coefficients for the LM 19.1 blade are derived based on 3D CFD computations on a 41-m rotor using the program EllipSys. The following conclusions can be drawn:

- 3D effects and rotational effects are important,
- Calculations with the derived airfoil coefficients agree well with measured flap moments,

- A fatigue analysis show a reduction of the loads of up to 15 % compared to commonly used airfoil characteristics.

Comparing 2D wind tunnel measurements to the constructed airfoil characteristics it is seen that:

- C_L is low in stall at the tip,
- C_L is in good agreement at 0.6R,
- C_L is high in stall at the inner part of the blade,
- C_D is in good agreement at the outer part of the blade,
- C_D is slightly lower on the inner part of the blade until $\alpha=20^\circ$ after which it exceeds the 2D data.

6. ACKNOWLEDGEMENTS

The present work was funded by the Danish Energy Agency under the contract: ENS 1363/98-0005.

7. REFERENCES

- [1] Abbott, I.H., Doenhoff, E.v., 'Theory of Wing Sections', Dover Publ., Inc., New York (1959).
- [2] Bak, C. (ed.), Petersen, H., 'Blade Profile Coefficients C_L and C_D . From the unpublished report: "Benchmark Tests on Power Curve Computations on Wind Turbines - a Compendium" ', Risø-I-1369(EN), Risø National Lab., Denmark (1998).
- [3] Bak, C., Fuglsang, P., Sørensen, N.N., Madsen, H.A., Shen, W.Z., Sørensen, J.N., 'Airfoil Characteristics for Wind Turbines', Risø-R-1065(EN), Risø National Lab., Denmark (1999). (In preparation)
- [4] Fuglsang, P., Antoniou, I., Dahl, K.S. and Madsen, H.A., 'Wind Tunnel Tests of the FFA-W3-241, FFA-W3-301 and NACA 63-430 Airfoils', Risø-R-1041(EN), Risø National Lab., Denmark (1998).
- [5] Michelsen, J.A., 'Basis3D - a Platform for Development of Multiblock PDE Solvers', Technical Report AFM 92-05, Tech. Univ. Denmark (1992).
- [6] Michelsen, J.A., 'Block Structured Multigrid Solution of 2D and 3D Elliptic PDE's', Technical Report AFM 94-06, Tech. Univ. Denmark (1994).
- [7] Paulsen, U.S., 'Investigation of Concept. Nordtank NTK 500/41. Structural loads' (in Danish), Risø-I-936(DA), Risø National Lab., Denmark (1995).
- [8] Rasmussen, F., Petersen, S.M., Larsen, G., Kretz, A., Andersen, P.D., 'Investigations of Aerodynamics, Structural Dynamics and Fatigue on Danwin 180 kW', Risø-M-2727, Risø National Lab., Denmark (1988).
- [9] Sørensen, N.N., 'General Purpose Flow Solver Applied to Flow over Hills', Risø-R-827(EN), Risø National Lab., Denmark (1995).

PRODETO, A COMPUTER CODE FOR PROBABILISTIC FATIGUE DESIGN

H. Braam*, C.J. Christensen**, K.O. Ronold***, M.L. Thøgersen**
*ECN-Solar & Wind Energy, P.O. Box 1, 1755 ZG Petten, The Netherlands
**Risø National Laboratories, P.O. Box 49, DK-4000 Roskilde, Denmark
***Det Norske Veritas, P.O. Box 300, N-1322 Høvik, Norway

ABSTRACT: A computer code for structural reliability analyses of wind turbine rotor blades subjected to fatigue loading is presented. With pre-processors that can transform measured and theoretically predicted load series to load range distributions by rain-flow counting and with a family of generic distribution models for parametric representation of these distributions this computer program is suitable for carrying through probabilistic fatigue analyses of rotor blades.

Keywords: Computer Programs, Reliability, Fatigue, Blades

1. INTRODUCTION

To assess the fatigue damage in wind turbine rotor blades one has to deal with uncertainties in the loading and uncertainties in the fatigue strength. These uncertainties are not only caused by the natural variability of the wind loading and the inherent scatter in the fatigue strength, but are also due to statistical uncertainty, which is an estimation uncertainty caused by a limited amount of data available. The cumulative load spectrum is based on a limited number of measured or simulated 10-minute time series, while only a limited number of coupon tests are performed to determine the $S-N$ curve that gives the number of cycles to failure. The statistical uncertainty gets smaller when the number of observations increases.

To take into account these uncertainties (partial) safety factors are used quite often in design codes. In former days these safety factors were determined empirically, however structural reliability methods form the formal and rational basis for calibration of structural design codes. In practice, this means that structural reliability methods can be used as a basis for calibration of the partial safety factors, which are used in traditional deterministic design. A calibration of partial safety factors implies calculation of the values that the partial safety factors need to have such that they, when used in conventional design, ensure that a required low probability of failure is achieved.

Such a calibration is by no means a trivial task. It requires probabilistic models for representation of load and resistance to be established and combined for use in structural reliability analyses. The results of such reliability analyses come out in terms of estimates of failure probabilities. In a probabilistic design, the reliability analyses are tuned by adjusting the structural design appropriately until a required safety level in terms of a particular prescribed failure probability is met. When the particular structural design that exactly meets the prescribed safety thus is established, the corresponding requirement to the partial safety factors in a deterministic code format can be determined.

The application of probabilistic methods to partial safety factor calibration within the wind turbine community is fairly new. During the work on development of design codes for wind turbines in recent years, the need for probabilistic models of load and resistance has become still more evident. In the past few

years, work has therefore been undertaken to develop such probabilistic models [1-3].

To further introduce structural reliability methods in the design procedures of wind turbines the use of tailor-made computer codes to determine the failure probabilities accurately and efficiently are inevitable. For this reason the JOULE III project PRODETO (Probabilistic Design Tool) has been carried out in the period January 1996 through November 1998 [4-6]. The main objective of this project is the development of a computer code to be used partly as a tool for structural reliability analyses of wind turbine components and partly as a safety factor calibration tool.

A brief overview of the theoretical background and the structure of the computer code is presented in this paper. To provide a better understanding of what partial safety factors represent and how they are derived and calibrated a case study has been carried out, covering analyses of the rotor blades of a prototype wind turbine. Some results of this case study will be presented.

2. COMPUTER CODE

2.1 Theoretical background

Limit state function

In structural design, the reliability of a structure or a structural component is evaluated with respect to one or more limit states. Only one such limit state is assumed in the following. The structure is described by a set of stochastic basic variables grouped into one vector \mathbf{X} , including, e.g. its strength, stiffness, geometry, and loading. For the limit state under consideration, the possible realisations of \mathbf{X} (i.e. the different value sets of X_1, X_2, \dots, X_n) can be separated into two sets; the set for which the structure will be safe, and the set for which the structure will fail. The surface separating the safe set from the failure set in the space of basic variables is denoted the limit state surface which can be described by the limit state function $Z = g(\mathbf{X})$ such that

$$Z = g(\mathbf{X}) \begin{cases} > 0 & \text{for } \mathbf{X} \text{ in safe set} \\ = 0 & \text{for } \mathbf{X} \text{ on limit state surface} \\ < 0 & \text{for } \mathbf{X} \text{ in failure set} \end{cases} \quad (1)$$

The failure probability can be expressed as

$$P_T = P\{Z < 0\} = \int_{g(X) \leq 0} f_X(x) dx \quad (2)$$

where $f_X(x)$ is the probability density function for X .

To determine the structural reliability Eq. (2) has to be solved. To do this a description of the limit state function $Z = g(X)$ is required and the probability density functions of the random variables grouped into the vector X have to be defined.

In the PRODETO software a limit state function to analyse the fatigue damage in a blade due to the flapwise bending moment has been developed based on Miner's rule. According to Miner's rule, fatigue failure in a structural material is defined when the accumulated damage D exceeds 1.0, where D is defined as

$$D = \sum_{k=1}^{N_L} \frac{\Delta n(S_k)}{N(S_k)} \quad (3)$$

where $\Delta n(S_k)$ is the number of load cycles at stress range S_k , $N(S_k)$ is the number of cycles to failure at stress range S_k , and the summation is over an appropriate discretisation of the stress range axis. The limit state can be defined in several manners. In the PRODETO software the following two commonly used definitions are optional:

$$g(X) = 1 - F_M D(X) \quad (4)$$

and

$$g(X) = -\ln(F_M D(X)) \quad (5)$$

where F_M is a random factor to represent model uncertainty.

Lifetime load spectra

The loading of a wind turbine blade is represented by the distribution of the load ranges over the design life of the structure. There are two possible sources for obtaining this distribution. One is an aeroelastic model, which will allow for theoretical predictions of the load range distribution by a simulation technique. The other is a distribution based on full-scale measurements on a specific turbine. Regardless of which approach is chosen, a limited number of 10-minute time-series is collected, and based on these load series rain-flow counted load range distributions are calculated. Only limited data are available, and the load distributions are sorted by

- 10-minute mean wind speed, U_{10}
- 10-minute mean turbulence intensity, I_T

and interpreted with respect to load range distributions conditioned on the wind climate (U_{10} , I_T). Now a distribution fitting technique can be used to characterise the natural variability of the load ranges in the 10-minute time series. For the flapwise bending moment in the blade load amplitudes (or load ranges) in short-term conditions, during which the load process can be assumed stationary, often appear to have a distribution which resembles a Weibull distribution. In the present case, we are dealing with short-term conditions in terms of 10-minute periods of approximately stationary wind climate, i.e., constant mean wind speed U_{10} and turbulence intensity I_T . The load ranges considered are those of the flapwise bending moment at the blade root. By inspection of measured bending moment ranges, conditioned on (U_{10} , I_T), their

distribution is seen to resemble a Weibull distribution. On Weibull paper, the distribution appears as a curve with only minor deviations from the straight line that a pure Weibull distribution would give. It is therefore natural, when a parametric representation of the distribution is sought-after, to start out with a Weibull distribution and subject it to a slightly non-linear transformation to something that fits well with the measured distribution. Such a generalised or distorted Weibull distribution can be generated in many ways. In [2], a third-order polynomial expansion of a parent Weibull-distributed variable was explored, in which the four coefficients of the polynomial were fitted to retain the first four central moments of the measured distribution. Whereas this model provides a good fit to the data, it is prohibitively computer intensive, in particular for applications where multiple distribution fits need to be made during each analysis. An alternative model for representation of short-term bending moment amplitudes X for a given wind climate (U_{10} , I_T) is the so-called quadratic Weibull model [1,2]. Because the coefficients in the quadratic Weibull model have to be solved iteratively the 3-parameter Weibull distribution has been used as an alternative to the quadratic Weibull distribution. The cumulative distribution function of the 3-parameter Weibull distribution reads

$$F_W(x) = 1 - \exp\left[-\left(\frac{x-\varepsilon}{u-\varepsilon}\right)^k\right], \quad x \geq \varepsilon \quad (6)$$

The parameter k is calculated such that the skewness of the 3-parameter Weibull distribution equals the skewness a_3 of the distribution $X|(U_{10}, I_T)$. After k has been calculated the parameters u and ε are calculated such that the mean value and the standard deviation of the 3-parameter Weibull distribution equal respectively the mean, a_1 , and the standard deviation, a_2 , of the distribution $X|(U_{10}, I_T)$. Integration of the conditional load range distributions with respect to the site-specific distribution of the wind climate (U_{10} , I_T) leads to the unconditional long-term distribution of load ranges over a specified design life.

As only a limited number of 10-minute time series is available for determining the first three statistical moments (the mean value a_1 , the standard deviation a_2 and the skewness a_3) a statistical uncertainty will be associated with them. To deal with this uncertainty in the structural reliability analyses the three statistical moments are treated as random variables. The standard deviation of these three moments is derived by means of the jackknife method. In order to generate a firm basis for determining the statistical moments for the load series for every combination of (U_{10} , I_T) the expected values, a_p^E , and the standard deviations, $D[a_p]$, of a_1 , a_2 , and a_3 are represented by 2nd order polynomials over the (U_{10} , I_T) space. Based on the assumption that the central limit theorem holds for the three moments a_1 , a_2 , and a_3 they can be represented as random variables by:

$$a_p(U_{10}, I_T) = a_p^E(U_{10}, I_T) + U_p D[a_p](U_{10}, I_T), \quad p = 1, 2, 3 \quad (7)$$

in which the vector $U = (U_1, U_2, U_3)^T$ is a three dimensional normally distributed variable with zero mean, unit variance and correlation matrix ρ .

Fatigue strength

To assess the fatigue damage in a component, a material model suitable for the material the component is made of should be applied. For steel the $S-N$ curves are generally suitable. In tests of composite materials for use in rotor blades, the strain amplitude ϵ is usually measured rather than the stress range S . Hence for such materials the number of cycles N to failure is expressed through an $\epsilon-N$ curve. Actually this relation gives the expected value of $\log N$ given $\log \epsilon$ and there is a natural variability around the expected value of $\log N$. On a linear scale the $\epsilon-N$ curve generally is expressed by

$$\log N = \log K - m \log \epsilon + e \quad (8)$$

The residual e is a random variable with zero mean, representing local variations from test specimen to test specimen or from one point on the rotor blade to another. The coefficients $(\log K, m)$ describe the expected behaviour of the $\epsilon-N$ curve and can be estimated by a linear regression analysis of the available test data. Due to the limited amount of tests a statistical uncertainty will be associated with the parameters K and m . To deal with this uncertainty these parameters are treated as random variables. With the regression analysis the mean values, the standard deviations and the correlation coefficient for $\log K$ and m as well as the standard deviation of the zero-mean random variable e can be estimated straightforward.

The behaviour of GRP materials exhibits a dependency on the mean value of the strain, which can be dealt with using Goodman diagrams. In fatigue tests this mean strain is characterised by the ratio R of minimum to maximum strain or stress. Application of the Goodman diagram requires a statistical elaboration of the mean strain. This implies that much more measurements are necessary, which in practice probably will not be attainable. To avoid an increase in measurements it is assumed that the R -ratio is constant during the life-time. The fatigue assessment will be performed on the $\epsilon-N$ curve based on the R -ratio relevant for the fatigue loading being considered.

2.2 Structure

The PRODETO software consist of the subroutine *damage.for* and the two pre-processors RAINSTAT and FATSTAT. The subroutine *damage.for* contains the source code for the limit state function and has to be linked to a computer code capable to solve the structural reliability problem. The implementation of the limit state function was done in connection with the commercially available code RELIAB01, marketed by CSRconsult in Denmark. However, the structure is such that it can easily be adjusted for other general purpose structural reliability codes. The current version of the software is mainly focussed at fatigue damage due to the flapwise bending moment in the blade.

As part of the pre-processor RAINSTAT the 10-minute time series are rainflow counted and the expected value and the standard deviation of the mean value, the standard deviation, the skewness and the kurtosis are estimated for each bin. Although the kurtosis is not of

importance for the 3-parameter Weibull distribution it is considered to make distribution fitting based on the first four statistical moments optional. Furthermore the parameters of the 2nd order polynomials representing the expected values and the standard deviations are determined and written to an output file such that they can be transferred to an input file required for the structural reliability analysis. Likewise the deterministic lifetime load spectrum based on the rainflow counted results is produced.

In the pre-processor FATSTAT the statistical material parameters are determined by means of a regression analysis for n pairs (ϵ_i, N_i) of coherent strain (or stress) range ϵ and number of cycles to failure N , available from measurements on n coupon tests.

For the calibration of the partial safety factors for a specific design case of one wind turbine and one specific location, the subroutine *damage.for* is linked to the structural reliability program RELIAB01. The failure probability and the corresponding reliability index β are calculated for a number of values of the section modulus W at the blade root, which is a geometry dependent design parameter, and the value of W that leads to the desired target reliability is determined. For this particular value of W the partial safety factors for load, γ_F , and fatigue strength, γ_M , are determined in accordance with the procedure described in [3]. This procedure is briefly outlined in [4,5] and will not be presented here.

3. RESULTS OF CASE STUDY

To demonstrate the PRODETO software and to spread the knowledge about structural reliability analyses a case study has been performed, covering analyses of the rotor blades of a prototype wind turbine [4]. The prime focus of the analyses has been on design against fatigue failure in flapwise bending, with application of the procedures outlined above. One set of analyses has been carried out based on load measurement obtained at two different locations, one in Denmark and one in the Netherlands. Another set of analyses has been based on predicted load distributions, simulated according to state-of-the-art theory of aero-elasticity. Table 1 gives the

Table 1: Results of Reliability Analysis for Fatigue in Flapwise Bending.

Rotor Blade, $W=0.0018 \text{ m}^3$			
Probability of Failure $P_F=0.39 \cdot 10^{-4}$			
Reliability Index $\beta=3.95$			
Variable	Distribution	Design point x^*	Importance factor α^2
U_1	Normal	1.3025	0.190
U_2	Normal	1.4830	
U_3	Normal	0.8413	
$\log_{10} K$	Normal	-11.855	0.081
m	Normal	7.6534	
e	Normal	-1.3131	0.702
F_M	Normal	0.6614	0.028

results of one of the data sets, but is representative for all four data sets. The results in Table 1 can be interpreted with respect to estimation of the probability of fatigue failure in the design lifetime of the rotor blades, and with respect to identification of the most important uncertainty sources. It is a general finding from all analyses performed that the single most important uncertainty source is the inherent variability in the number of cycles to failure as represented by the ε - N curve.

The analyses have all been carried one step further in the sense that they have been used as a basis for calibration of a site- and turbine-specific set of two partial safety factors, one on load and one on resistance, for use in conventional deterministic fatigue design. For a target reliability of $\beta_1 = 3.54$, the calculated safety factors are given Table 2.

Table 2: *Partial Safety Factors for the Four Cases.*

Load Series	Material Factor, γ_m	Load Factor, γ_T
Measured (NL)	1.08	1.11
Measured (DK)	1.11	1.20
Simulated (NL)	1.08	1.17
Simulated (DK)	1.16	1.08

It should be emphasised that the reliability-based safety factors in Table 2 are site and wind-turbine specific and only applicable to flapwise bending of rotor blades. Different safety factors may result for different sites, different wind turbines, and different blade materials. Similar calibrations can be carried out for such different wind turbines at various sites. A common set of partial safety factors for a class of wind turbines, sites, and materials can then be optimised in dependence of the expected demand for each individual combination of wind turbine, site, and material within the class.

4. CONCLUSIONS

A computer program for structural reliability analyses of wind turbine rotor blades subjected to fatigue loading has been developed. The program is based on the general purpose structural reliability program Reliab01, which is commercially available, and which has been tailor fitted with the necessary subroutines for carrying through probabilistic fatigue analyses of rotor blades. The current version of the software is mainly focused on fatigue damage due to the flapwise bending moment in the blade. For this purpose a number of models are available but the main problem is that they are very computer intensive. As the 3-parameter Weibull distribution provides a good fit to the data and does not cause a high computer load it was chosen for use in the PRODETO software.

Furthermore the procedure for the calibration of the partial safety factors for fatigue loading as outlined in [4] has been applied to determine partial safety factors for a prototype wind turbine.

The partial safety factors found by applying the above procedure are calibrated on a level, where only the statistical uncertainty in the observed loads, model

uncertainty in load predictions, and the statistical uncertainty and inherent variability in the material fatigue properties are considered. The following effects have not been considered but are covered by partial safety factors in existing codes and should therefore be taken into account by appropriately increasing the partial safety factors found herein.

- Wear of materials;
- Variability in fabrication methods;
- Size effects;
- Uncertainty in load measurements;
- Uncertainty in wind climate determination/site parameters;

Although the software developed together with the presented procedure for the calibration of the partial safety factors is not a fully developed design tool yet, it is expected to be of significant benefit for the wind turbine industry and for certifying bodies. For the industry it is a tool to analyse the structural reliability (failure probability), so that different designs can be compared. Furthermore a better understanding of partial safety factors can be obtained. Certifying bodies can use it as a tool to evaluate measurements and to define partial safety factors.

Furthermore, future work should be devoted to extending the site- and turbine-dependent safety factor calibration presented herein to a calibration that covers a family of many turbines and many locations, representative for the future demand of wind turbines. This would represent the ultimate step in a full code calibration for wind turbine design against fatigue, and this would be one step further than the site- and turbine-specific calibration presented herein. Such a code is not to be limited to rotor-blade fatigue in flapwise bending alone, as extensions to other design cases such as rotor-blade fatigue in edgewise bending as well as fatigue of other wind-turbine components are foreseen.

REFERENCES

- [1] K.O. Ronold, J. Wedel-Heinen, and C.J. Christensen, *Reliability-based fatigue design of wind-turbine rotor blades*, accepted for publication in Journal of Engineering Structures, Elsevier, 1999.
- [2] C.H. Lange and S.R. Winterstein, *Fatigue data of wind turbine blades: Load and resistance factors from limited data*, Proc. 15th ASME Wind Energy Symposium, Houston, Texas, 1996.
- [3] European Commission, *European Wind Turbine Standards - Part 2 : Calibration of Safety Factors*, Contract JOU2-CT93-0387, Final Report, EUR 16898 EN, 1996.
- [4] H. Braam, J.J.D. van Dam, C.J. Christensen, M.L. Thøgersen, G.C. Larsen, K.O. Ronold, *Methods for Probabilistic Design of Wind Turbines*, Risø-R-1082(EN), Dec. 1998.
- [5] H. Braam, K.O. Ronold, C.J. Christensen, *PRODETO - Computer Program, Theory and Program Structure*, ECN-C--97-093, May 1998.
- [6] H. Braam, *PRODETO - Computer Program, User's Manual*, ECN--97-096, July 1998.

Acknowledgement

The PRODETO project was funded in part by the European Commission in the framework of the Non Nuclear Energy Programme JOULE III, JOR3-CT95-0026.

EXPERIMENTAL INVESTIGATION OF ULTIMATE LOADS

S.M. Petersen, G.C. Larsen, I. Antoniou, S.O. Lind, M. Courtney
 Risoe National Laboratory, Wind Energy and Atmospheric Physics
 P.O. Box 49
 DK-4000 Roskilde
 Denmark
 Phone: +45 4677 5043
 Fax.: +45 4677 5083

ABSTRACT: Verification of the structural integrity of a wind turbine involves analysis of fatigue loading as well as ultimate loading. With the trend of persistently growing turbines, the ultimate loading seems to become relatively more important. For wind turbines designed according to the wind conditions prescribed in the IEC-61400 code, the ultimate load is often identified as the leading load parameter. Exemplified by the use of an extensive measurement campaign a procedure for evaluation of the extreme flapwise bending moments, occurring during normal operation of a wind turbine, is presented. The structural measurements are made on a NEG Micon 650kW wind turbine erected at a complex high wind site in Oak Creek, California. The turbine is located on the top of a ridge. The prevailing wind direction is perpendicular to the ridge, and the annual mean wind speed is 9.5 m/s. The associated wind field measurement, are taken from two instrumented masts erected less than one rotor diameter in front of the turbine in direction of the prevailing wind direction. Both masts are instrumented at different heights in order to gain insight of the 3D-wind speed structure over the entire rotor plane. Extreme distributions, associated with a recurrence period of 10 minutes, conditioned on the mean wind speed and the turbulence intensity are derived. Combined with the wind climate model proposed in the IEC standard, these distributions are used to predict extreme distributions with recurrence periods equal to one and fifty years, respectively. The synthesis of the conditioned PDF's and the wind climate model is performed by means of Monte Carlo simulation.

Keywords: Ultimate load, extreme distribution, flap bending.

1. INTRODUCTION

The verification of structural integrity of a wind turbine involves analysis of fatigue loading as well as extreme loading. As the turbines increase in size the ultimate loads seem to be relatively more important. The ultimate load situations are associated with different operational conditions for example normal operation or standstill at high wind speeds above the cut-out wind speed. All potential failure modes, together with their probability of occurrence must be considered in the design phase.

Typically the ultimate loads are predicted as the maximum values in time series of limited duration (often 10 minutes) simulated with an aeroelastic code. Due to the stochastic nature of the turbulence wind field, the variation of the maximum value from one realization to another is considerably. As a consequence the simulations must be repeated several times. This procedure is time consuming, and in ref.[3] statistical methods are introduced in order to reduce the number of realizations and still obtain reliable results.

This paper introduces a method to estimate the ultimate flapwise loads during normal operation at specific wind and turbulence conditions. The method is applied on measurements carried out on a 650kW stall regulated wind turbine. Even though the test site is a high wind speed site, the recordings suffer from lack of results at high turbulence in combination with high wind. The suggested procedure is equally well applicable on load predictions originating from simulations. The achievements can be used to verify and improve aeroelastic codes.

2. DESCRIPTION OF THE EXPERIMENT SETUP

The measurements presented here are carried out in Oak Creek, near Tehachapi in California. The wind turbine is a

NEG Micon 650kW stall regulated machine. The hub height and the rotor diameter are 55m and 44m, respectively. The site is very complex. The turbine is erected on a hilltop. The prevailing wind direction is 320° , and thus perpendicular to the ridge. The wind field is measured on two met-masts erected in front of the turbine. The met-masts are instrumented at several heights with both sonic and cup anemometers. The wind turbine and the met-masts are shown in Figure 1. Only the cup wind speed at 65m is used in the present analysis.

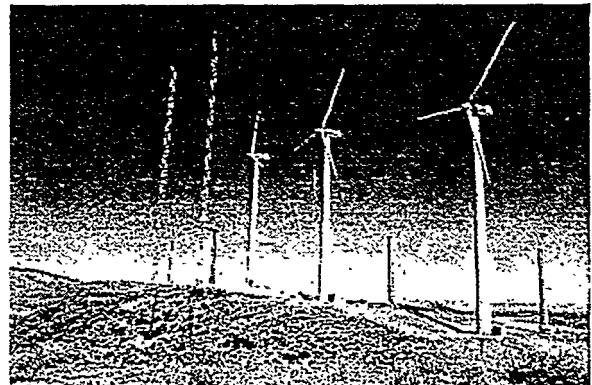


Figure 1 Experimental setup showing the wind turbine and the met-masts.

The power production of the turbine indicates that the mean wind speed at 65m corresponds approximately to the wind speed at hub height. Figure 2 shows the turbulence intensity measured at 65m. Also the high and low turbulence intensities, corresponding to the two turbulence classes prescribed in the IEC-61400 code ref.[1], are shown in Figure 2. Even though the site is complex, the low IEC turbulence class turns out to be more severe. The turbulence prescribed in IEC is defined as the 84% quantile of a normal distribution. The inclination angle of the flow, relative to a horizontal plane at the meteorological mast

position, is calculated from the sonic anemometer measurements. The inclination angle is found to be between 0° and 5°.

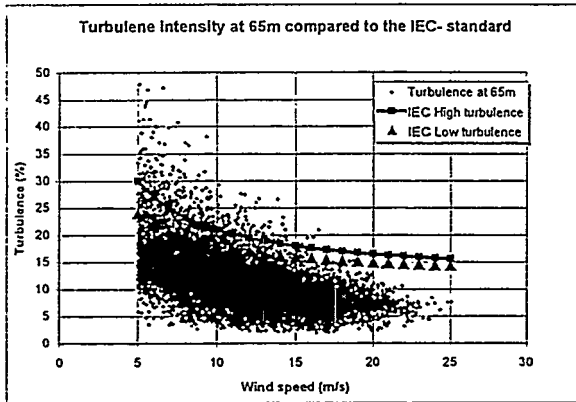


Figure 2 Turbulence intensity versus wind speed.

3. DISTRIBUTION OF THE EXTREME FLAP LOAD

The flapwise bending is measured by strain gauges, which experience some moderate zero drift due to change in the ambient temperature. Therefore the applied mean-value curve is based on measurements performed at stable temperature conditions during nights. In order to eliminate the zero drift in the 10-minute extremes, the 10-minute extreme, x ($x = x_{\max} - x_{\text{mean}}$) is defined as the maximum value subtracted the mean value associated with the particular 10-minute series. Figure 3 shows the mean value and the corresponding maximum value of the flapwise bending moment based on 10-minute time series. The maximum values shown in Figure 3 are defined as x added to the mean-value curve.

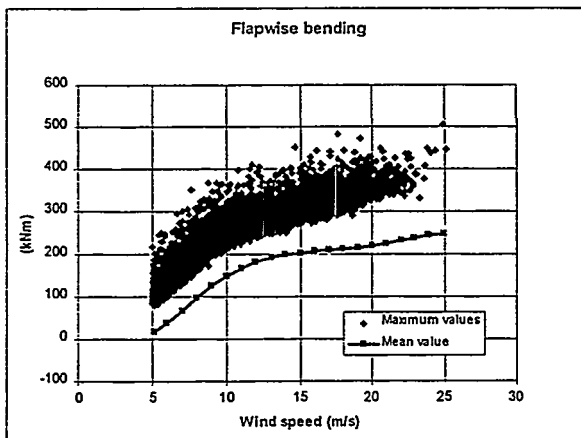


Figure 3 Flapwise bending versus wind speed.

The 10-minutes extremes x conditioned on the mean wind speed and the turbulence standard deviation are assumed to follow an Extreme Value 1 (EV1) distribution ref[2]:

$$F(x; \alpha, \beta) = \exp(-\exp(-\alpha(x - \beta)))$$

The mean and the standard deviation of the EV1 distribution are determined by $\hat{\mu} = \beta + 0.5772$ and $\hat{\sigma} = \pi/(\alpha 6)$, respectively

For practical use the data material are categorized in wind speed and turbulence bins. The width of the mean wind speed bins is selected to 2 m/s, and the width of the turbulence bins, expressed as standard deviation, is selected to 0.4 m/s. Measurements above 21 m/s are only classified according to turbulence due to the limited amount of data. A comparison between the realized distribution from the experimental data material and the EV1 distribution is shown in Figure 4 for $9 < U < 11$ m/s and $0.8 < \sigma_U < 1.2$ m/s. The CDF is transformed in order to (ideally) express a straight line.

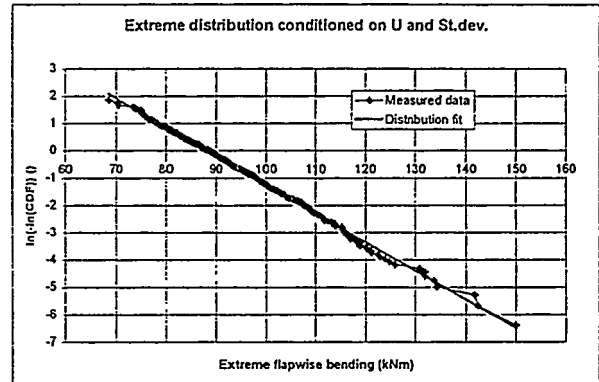


Figure 4 Comparison between measured and fitted distribution for $U=10$ m/s and $\sigma_U=1$ m/s.

The distribution parameters α and β are estimated using linear regression. Both the lower and upper tails are fitted satisfactory, and the residual is insignificant and randomly distributed around zero. This verifies that the recorded extremes follow an EV1 distribution. The measured distribution in Figure 4 consists of 588 samples. In general the estimation of α and β converge when the number of samples exceeds about 20. Figure 5 shows the EV1 for $21 < U < 25$ m/s and $1.6 < \sigma_U < 2.0$ m/s. The fit is based on 93 samples. Both the lower and upper tails are fitted satisfactory as in the previous distribution.

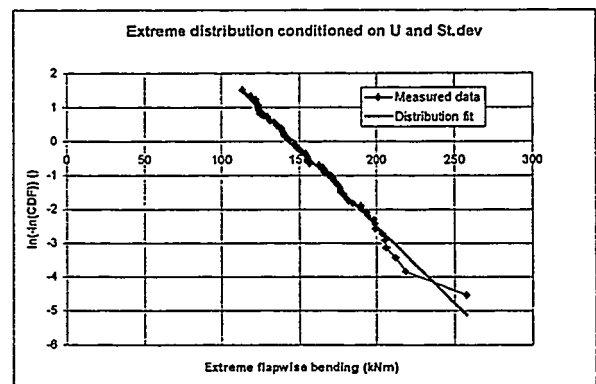


Figure 5 Comparison between measured and fitted distribution for $U=23$ m/s and $\sigma_U=1.8$ m/s

To estimate the load extremes at wind and turbulence conditions, as prescribed in the IEC-61400 code, we need to extrapolate the α and β parameters (if not covered by the experimental database) to these conditions.

Figure 6 shows the estimated mean value of the fitted EV1 distribution as function of the turbulence for $U=10\text{m/s}$ and 23m/s , respectively. The relation between the two parameter is seen to be well approximated by a second order polynomial.

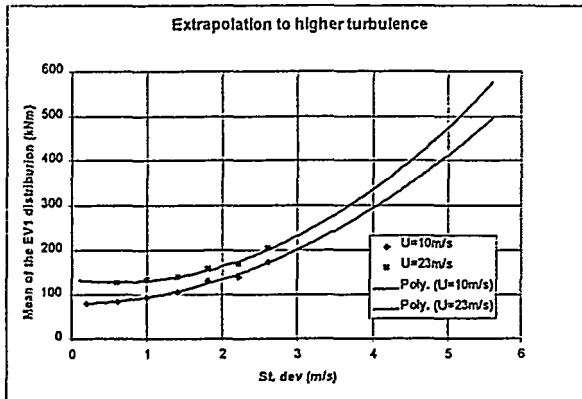


Figure 6 Fit of the mean in the EV1 distribution vs. wind speed standard deviation.

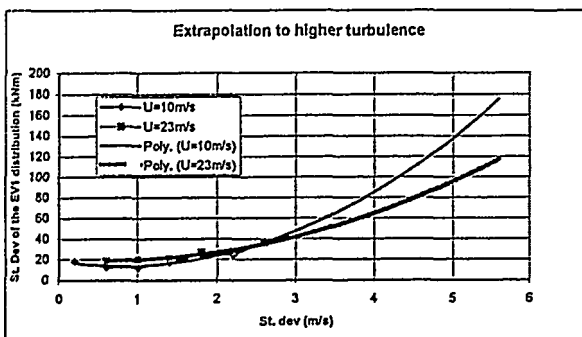


Figure 7 Fit of the standard deviation in the EV1 distribution vs. wind speed standard deviation.

Figure 7 shows the estimated standard variation of the fitted EV1 distributions as function of the turbulence standard deviation for $U=10\text{m/s}$ and 23m/s , respectively. As for the mean value the relation between the two parameters is seen to follow a second order polynomial with a good approximation. The α and β parameters for the EV1 distribution can now be estimated for all turbulence intensities and for all wind speeds. Note, however, that extrapolation beyond the parameter values covered by the available data material is uncertain and should be verified by inclusion of additional data or simulations, as they influence heavily the final extreme load estimate.

4. ONE-YEAR EXSTREME DISTRIBUTION

An extreme distribution, associated with an unconditioned 10-minute observation period, can now be established by a weighted integral of the established extreme distributions conditioned on the mean wind speed as well as on the turbulence intensity. The weight factor is taken as the joint probability of a given mean wind speed and a given turbulence intensity as prescribed in the IEC-64100 code.

Based on this (reference) extreme distribution the extreme distributions with recurrence periods one-year and fifty-years can subsequently be determined by using a Monte

Carlo simulation technique, ref.[4]. In addition to the extreme distribution the Monte Carlo technique also provides information on the wind conditions (in terms of mean wind speed and turbulence intensity) that contribute significantly to the distribution.

With reference to IEC-61400 code, the extremes are calculated based on Rayleigh mean wind distributions with mean wind speeds corresponding to class I, II, III and IV, both for high and low turbulence classes (corresponding to $I_{15}=18\%$ and $I_{15}=16\%$). The turbulence is assumed to be Gaussian distributed as prescribed in the code. The standard deviation of σ_u is equal to 0.32m/s and 0.36m/s for low and high turbulence class, respectively.

The extreme load, within an arbitrary 10-minute period has been demonstrated to follow an EV1 distribution with a very convincing approximation. Assuming the individual extreme loads, associated with different 10-minutes time series, to be statistically independent, the extreme distribution related to a period of arbitrarily length, $N \cdot 10$ minutes, is expressed as the extreme distribution for an arbitrary 10 minutes period raised to the N^{th} power.

Extremes associated with different 10 minutes periods are likely to be well separated in time, and with the usual turbulence time scale important for the wind turbine loading, they will consequently be nearly independent. Therefore the extreme distribution related to a one-year period, is anticipated to follow an EV1 distribution provided that the extreme distribution, related to a 10-minute period, is EV1 distributed. This observation is confirmed by the present Monte Carlo simulation, see Figure 8.

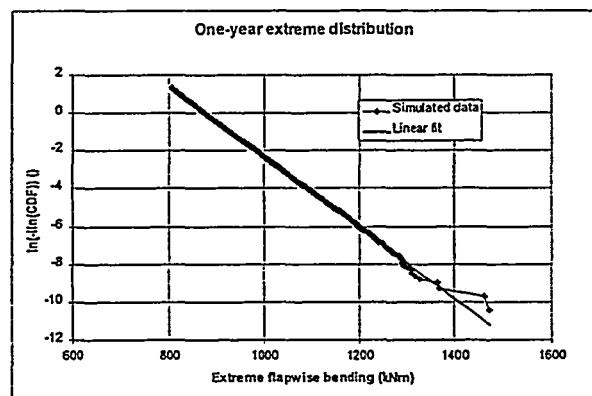


Figure 8. Monte Carlo simulated one-year distribution.

The most likely fifty-year extreme value is defined as the one-year extreme, which in average occur one time in a fifty-year period, corresponding to the 98% quantile in the one-year extreme distribution. The one-year extreme distribution and the corresponding 98% quantile has been predicted based on different number of samples. Figure 9 shows the convergence of the quantile value for 14 simulations ranging from 4 to 2^{15} years. The 98% quantile corresponding to 2^{15} years is selected as reference. The 98% quantile is determined from the fitted EV1 distribution. The deviation is seen to converge at approximately 500 years, but already at 4 years the relative deviation is less than 2.5%. The relative deviation is always less than 3%.

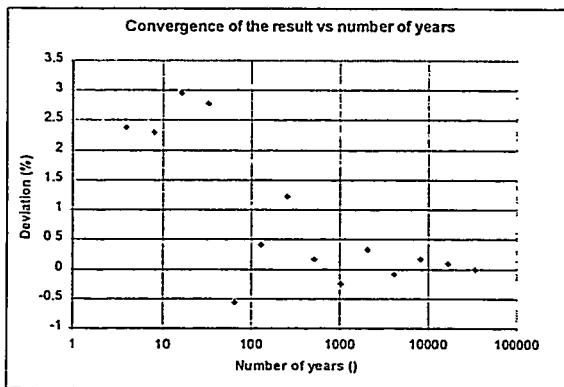


Figure 9. Convergence of the 98% quantile for the one-year extreme for a IEC class I wind distribution.

The following estimations are based on simulations corresponding to 4096 years. The one-year 98% quantile values for the different IEC classes are given in Table 10. The predicted one-year extremes are compared to the one-year extremes predicted for mean wind speeds between 24m/s and 25m/s (class I to III) and for mean wind speeds between 20m/s and 25m/s (class IV, due to the limited duration of high wind speeds for this class). The duration, expressed as the number of 10-minute periods, is given in the last columns in Table 10. The extremes calculated only from the high wind speeds are somewhat lower. The relative decreases are shown in brackets in Table 10. The reduction is between 3 and 11%. Consequently it is needed to take into account the contribution from the lower wind speed ranges, in the calculation of the overall extremes, especially for the high turbulence and the low wind speed classes.

Cl.	$F_{98\%}$ $I_{15}=0.18$ (kNm)	$F_{98\%}$ $I_{15}=0.16$ (kNm)	$F_{98\%}$ $I_{15}=0.18$ (kNm)	$F_{98\%}$ $I_{15}=0.16$ (kNm)	No
I	1083	972	1010(-7%)	935(-4%)	182
II	1014	914	925(-10%)	858(-6%)	41
III	951	854	834(-12%)	775(-9%)	8
IV	815	737	736(-10%)	678(-8%)	8

Table 10 Simulated fifty-year extremes

The simulated value for the high turbulence class I is more than twice the measured extreme value. Table 11 shows the probability to catch the one-year extreme at a given wind speed for class I (high turbulence).

Wind (m/s)	<18	19	20	21	22	23	24	25
%	10	4	4	7	11	13	21	30

Table 11 Occurrence of one-year extremes

The fifty-year extreme distribution has also been calculated using the Monte Carlo model. Theoretically the 36.4% quantile in that distribution should correspond to the fifty-year extreme value calculated as the 98% quantile of the one-year extreme distribution. Figure 12 compares the one- and fifty-year distributions. The 98% and the 36.4% quantile for the two EVI distributions are shown in the figure. The two quantiles are in good agreement as expected.

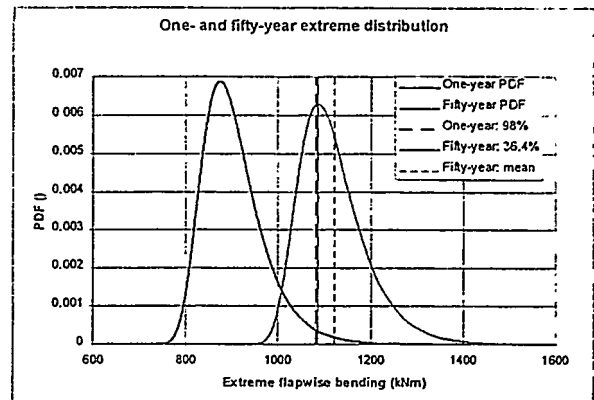


Figure 12 One- and fifty-year extreme distribution

5. CONCLUSIONS AND DISCUSSIONS

A method to estimate the extremes occurring during normal operation at different wind climates has been demonstrated using Monte Carlo simulation. The method is believed to be appropriate for load processes, which are dominated by stochastic wind excitation. As a consequence it is likely that the method can be applied in estimation of the extremes during standstill.

The present result is based only on measurements, but the method can also be combined with aeroelastic simulations in order to improve the accuracy of the result in the wind speed and turbulence ranges where experimental results are missing.

The 10-minute extreme flapwise bending moments conditioned on mean wind speed and turbulence, are seen to be EVI distributed. The most likely fifty-year extreme value during normal operation is influenced also from lower mean wind speed. Even though that 10% of the yearly extremes are estimated to occur at wind speeds below 18 m/s, but their contribution to the fifty-year extreme is moderate.

6. ACKNOWLEDGEMENTS

The support from The Danish Energy Agency to the present work is acknowledged.

REFERENCES

- [1] IEC-61400-1, Wind Turbine Generator Systems -Part 1: Safety Requirements, second edition.1996.
- [2] J. Abild, Application of the Wind Atlas Methods to Extremes of Wind Climatology. Risø R-772(EN), Risø National Laboratory 1994.
- [3] K. Thomsen and P.H. Madsen, Application of statistical methods to extreme loads for wind turbines, Proceedings of EWEC 97, Ireland, October 1997.
- [4] T.H. Wonnacott and R.J. Wonnacott, Regression: A Second Course In Statistics, John Wiley & Sons. 1981.

PREDICTION OF INDUCED VIBRATIONS IN STALL

Jørgen Thirstrup Petersen, Kenneth Thomsen and Helge Aagaard Madsen
Wind Energy and Atmospheric Physics Department
Risø National Laboratory, DK-4000 Roskilde, Denmark

ABSTRACT: The main results from recent research in stall induced vibrations are presented. The focus is on the edgewise blade vibrations, which during the last decade have turned out to be a potential threat against the stable operation of stall regulated wind turbines and a fact, which must be dealt with by the designer. The basic physical explanation for the phenomenon and examples of design precautions, which can be taken, are presented. **Keywords:** Stall Induced Vibrations, Aeroelastic Stability, Blade Aerodynamics.

1 INTRODUCTION

Results from research in an EC Joule-III project and from Danish Energy Agency projects are presented [2][3]. The objectives are improvement of design methods for stall regulated wind turbines, focusing on stall induced vibrations and dynamic stall. The primary concern is the edgewise vibrations in the fundamental blade natural mode shape, which have caused trouble on modern wind turbines.

A theoretical study, based on quasi-steady aerodynamics, confirms that the basic source driving the vibrations is energy supplied from the aerodynamic forces to the vibration during stalled operation. The phenomenon can be described as negative aerodynamic damping. The theoretical approach identifies the main parameters controlling the phenomenon. They are related to the static and the dynamic airfoil characteristics, the overall aerodynamic layout of the blade, e.g. chord length and twist, the structural properties of the blade, e.g. structural damping and properties controlling the resulting vibration direction.

Furthermore, full aeroelastic calculations and comparison with measurements show that the properties of the supporting structure, i.e. the nacelle and the tower, are important, as the vibrating blade might exchange energy with the support. In this exchange the location of the blade natural frequency relative to the frequencies of the coupled rotor tilt-yaw mode shapes plays an important role. The work confirms that qualified aeroelastic calculations can be used for determining the influence of changing the primary design parameters.

Prediction and design recommendations therefore build on both the simple quasi-steady models, which can be used for the preliminary choice of the design variables mentioned above, and full aeroelastic calculations. The full aeroelastic calculations refine the design basis and should be used for choosing the final design variables and for final verification of the design. Through this design procedure it is possible to assess the required safety margin against stall induced vibrations. The findings have been formulated into a set of design guidelines, which are presented in [2].

Below the basics of aerodynamic damping and the involved parameters are explained. Examples of predictions in relation to aerodynamic and structural modifications are presented.

2 AERODYNAMIC DAMPING

The aerodynamic conditions, which might lead to exchange of energy between the air stream and a vibrating blade, is most easily illustrated by looking at the quasi steady aerodynamic force at a blade cross section, e.g. the grayed section in Fig. 1. Expressing this force as a linearized function of the blade deformation velocity – by expanding the force in a truncated Taylor series – forcing terms proportional to the blade velocity arise. These forcing terms are interpreted as aerodynamic damping. The damping might be negative, and in this situation the blade is potentially self-exciting, as a once initiated vibration develops a force in the same direction as the vibration. The resulting force per unit blade length in matrix-vector notation yields

$$\begin{Bmatrix} F_x^R \\ F_y^R \end{Bmatrix} \simeq \begin{Bmatrix} F_{x0}^R \\ F_{y0}^R \end{Bmatrix} - \begin{bmatrix} c_{xx}^R & c_{xy}^R \\ c_{yx}^R & c_{yy}^R \end{bmatrix} \begin{Bmatrix} \dot{x}_R \\ \dot{y}_R \end{Bmatrix}, \quad (1)$$

where the vectors are referenced to the (x_R, y_R) -coordinate system in Fig. 1, and e.g. \dot{x}_R is the blade deformation velocity in the rotor plane. The vector with lower index 0 expresses the mean force, and the 2×2 matrix is the aerodynamic damping matrix with terms

$$c_{xx}^R(r, V) = \frac{1}{2} c_g \frac{r\Omega}{W} \left[\left(\frac{2r^2\Omega^2 + V^2}{r\Omega} \right) C_D - V \frac{\partial C_D}{\partial \alpha} - VC_L + \frac{V^2}{r\Omega} \frac{\partial C_L}{\partial \alpha} \right]. \quad (2)$$

$$c_{xy}^R(r, V) = \frac{1}{2} c_g \frac{r\Omega}{W} \left[-VC_D - r\Omega \frac{\partial C_D}{\partial \alpha} + \left(\frac{2V^2 + r^2\Omega^2}{r\Omega} \right) C_L + V \frac{\partial C_L}{\partial \alpha} \right]. \quad (3)$$

$$c_{yx}^R(r, V) = \frac{1}{2} c_g \frac{r\Omega}{W} \left[-VC_D + \frac{V^2}{r\Omega} \frac{\partial C_D}{\partial \alpha} - \left(\frac{2r^2\Omega^2 + V^2}{r\Omega} \right) C_L + V \frac{\partial C_L}{\partial \alpha} \right]. \quad (4)$$

$$c_{yy}^R(r, V) = \frac{1}{2} c_g \frac{r\Omega}{W} \left[\left(\frac{2V^2 + r^2\Omega^2}{r\Omega} \right) C_D + V \frac{\partial C_D}{\partial \alpha} + VC_L + r\Omega \frac{\partial C_L}{\partial \alpha} \right]. \quad (5)$$

Here r is the actual blade radius, V the free stream wind speed, Ω the rotor angular velocity, W is the resulting wind speed – i.e. the size of the vectorially added free wind V and the rotation speed Ωr . C_L and C_D are the airfoil lift and drag coefficients, respectively, α the angle of attack, c the profile chord and ρ the air density. $\partial/\partial\alpha$ expresses partial derivation with respect to angle of attack, geometrically interpreted as the slope of the airfoil data plotted against the angle of attack.

From Eqs. (2)-(5) it is observed that the airfoil data – both the actual values and their derivatives with respect to angle of attack – are important for the local damping. This is further illustrated by examples in Sec. 3.1.

To facilitate the derivation of damping for a given mode shape, say mode number n , Eq. (1) is transformed to a coordinate system following the local vibration direction, identified in Fig. 1 by the angle θ_{RB} . This results in the damping in direction of the x_B -axis

$$\begin{aligned} c_{xx}^{Bn}(r) = & \cos^2(\theta_{RB})c_{xx}^R \\ & + \cos(\theta_{RB})\sin(\theta_{RB})(c_{xy}^R + c_{yx}^R) \\ & + \sin^2(\theta_{RB})c_{yy}^R. \end{aligned} \quad (6)$$

Now, expressing the mode shape by its polar coordinates, $\varphi_n(\theta_{RB}, r)$ gives the deformation in direction of x_B , and the modal damping expressed as logarithmic decrement is obtained by integration along the blade

$$\delta_n = \frac{C_n}{2f_n M_n} = \frac{\int_0^R c_{xx}^{Bn}(r) \varphi_n^2(\theta_{RB}, r) dr}{2f_n \int_0^R m(r) \varphi_n^2(\theta_{RB}, r) dr}, \quad (7)$$

where R is the tip-radius, f_n the natural frequency and $m(r)$ is the mass per unit length of the blade. Eqs. (6) and (7) show the importance of the local vibration direction, which is further treated in Sec. 3.2.

In Eq. (7) it is also important to note that the local damping properties are weighted with the mode shape amplitude squared, a fact that has to be considered, when local properties are optimized to give the integrated blade properties, e.g. damping and power performance, which – as shown next – are inherently related.

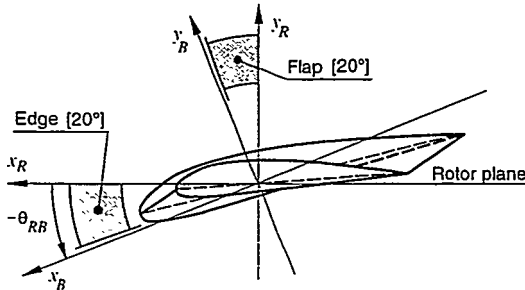


Figure 1. Coordinate systems and typical ranges for direction of modal blade vibration.

2.1 Damping – Power and Axial Force

It is interesting to observe and useful in a design situation to apply that the damping terms in Eqs. (2)-(5) can be expressed by the power and the axial force per unit length, $P_u(r)$ and $F_u(r)$. The power originates from the in plane force per unit length, $F_x^R(r)$, $P_u = r\Omega F_x^R$, and the axial force is $F_u = F_y^R$, both with reference to the R -coordinates.

The equivalent terms in the damping matrix – listing only the diagonal – yield:

$$c_{xx}^R(r, V) = -\frac{2}{r^2 \Omega^2} P_u(r, V) + \frac{V}{r^2 \Omega^2} \frac{\partial P_u(r, V)}{\partial V}. \quad (8)$$

$$c_{yy}^R(r, V) = \frac{\partial F_u(r, V)}{\partial V}. \quad (9)$$

These equations show that there is a close connection between the design with respect to power performance, thrust and aerodynamic damping, and these properties have to be considered simultaneously in the design phase.

Eq. (8) might erroneously lead to the conclusion that a turbine, which delivers power in stall, $P_u > 0$, would always have a negatively damped edgewise mode shape, as $\partial P_u / \partial V$ is ideally zero during stall. This conclusion is wrong for a couple of reasons. First of all, the edgewise mode shape will have an out of plane component due to blade twist, and further the weighting by the mode shape, when integrated properties are determined, differs for the power and the damping case.

3 PREDICTION EXAMPLES

Two fundamental prediction examples are presented. In Section 3.1 we give a summary of a method used in practice for improvement of damping properties [3]. This method is based on modification of the airfoil characteristics. In Section 3.2 we show how structural properties – specifically the blade twist – might influence the mode shape vibration direction and through that the aerodynamic damping.

3.1 Modified Airfoil Characteristics

As shown in Section 2 the airfoil characteristics, C_L and C_D , are important for the damping properties. Usually the characteristics are determined from the basic choice of airfoil and built into the blade through the production equipment, e.g. a mold. It is well known that the basic properties can be modified by use of aerodynamic devices, e.g. stall strips and vortex generators. We demonstrate how stall strips can be used to improve the damping properties. In addition vortex generators are applied to compensate for the reduction in power, caused by the stall strip modification.

The influence from stall strips mounted on a NACA 63-215 airfoil has been investigated experimentally in wind tunnel [1]. The result is shown in Fig. 2. Based on the wind tunnel measurements a set of airfoil data has been generated for an airfoil (14–18%) with stall strip. This set of data is applied in an aeroelastic cal-

culation on a 19 m blade on a 41 m diameter rotor. The stall strip covers 2 m from radius 16.5 m and outwards.

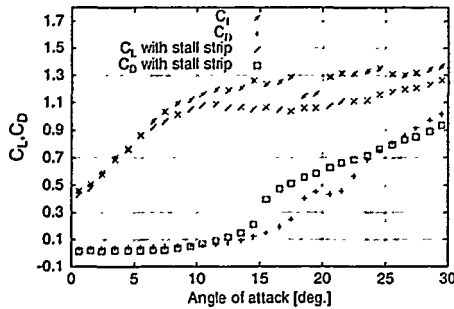


Figure 2. Measured characteristics for a NACA 63-215 airfoil with and without stall strip.

Due to the changed airfoil characteristics the rotor power curve is changed as well, as reflected in Eq. (8) and shown in Fig. 3. The example compensates for this by changing airfoil characteristics along the inner part of the blade by applying vortex generators ($r = 3-14$ m). The pitch setting is changed simultaneously. The final power curve is shown in Fig. 3.

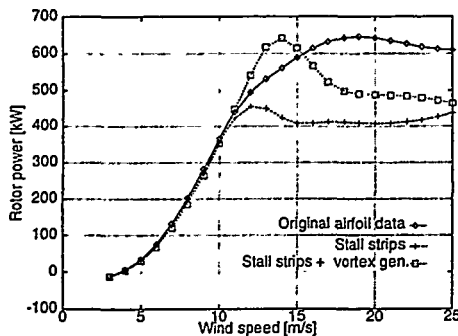


Figure 3. Calculated rotor power curves corresponding to original and modified airfoil characteristics, respectively.

The presented changes of the airfoil characteristics have significant influence on the aerodynamic damping. In Fig. 4 the aerodynamic damping in the edgewise mode shape is shown with the original data and the modified airfoil data, respectively.

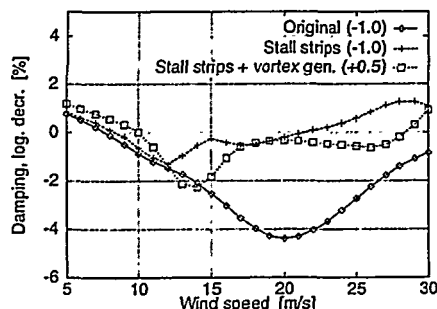


Figure 4. Calculated aerodynamic damping in edgewise mode shape as function of free wind speed. The numbers in parentheses are the tip pitch settings.

Fig. 4 shows how the total damping is changed from a minimum value of approximately -4% to a value of approximately -2% . At the same time the critical

operational wind speed is changed from 20 m/s to 14 m/s. This shift is caused primarily by the influence from the vortex generators.

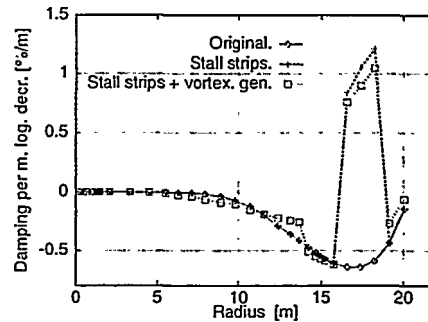


Figure 5. Calculated aerodynamic damping per unit length at 20 m/s.

From Fig. 5 it is observed that the damping is negative along the whole blade for the original configuration at 20 m/s wind speed. For the configurations with stall strips the influence from these is a local increase of the damping in the area with stall strips of approximately 1.5-2.0%/m. The example shows that the choice of the radial position, where the aerodynamic devices are applied, is important, due to the weighting by the mode shape.

3.2 Modified Vibration Direction

As illustrated by Eq. (6) in Section 2, the local vibration direction (θ_{RB}) of an airfoil section determines the resulting damping coefficient as function of the four coefficients given in Eqs. (2)-(5), and the vibration direction thus turns out to be an important design parameter, which should be taken into consideration in the design phase. That this is possible, is demonstrated by the example below.

In Fig. 6, the resulting damping coefficient for the angular range $[-90^\circ; +90^\circ]$ is illustrated for a section located at 75% radius of a 19 m blade, and the intervals usually covering the edgewise and the flapwise directions are indicated.

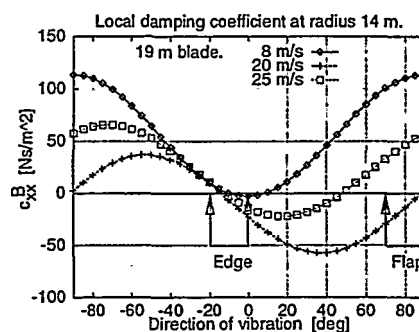


Figure 6. Damping coefficient as function of vibration direction, θ_{RB} .

It is observed that no principal vibration directions can be found, where the damping is positive in both edgewise and flapwise directions. If the direction of vibration is changed towards increased edgewise damping, the damping in the flapwise direction decreases, since the two directions are approximately perpendicular to each other. However, since these results are

based on a quasi-steady calculation, the damping for a real blade will be different. In particular, the damping in the flapwise direction will be modified (increased) by the dynamic airfoil characteristics. A certain optimal direction of vibration can be determined and aimed at, when designing a blade with a minimal risk of experiencing stall induced vibrations.

In order to determine realistic vibration directions at different radial stations of a blade, a finite element model of a 19 m blade has been established [4]. The model is based on four node shell elements with isotropic material properties. Two different blades are considered: 1) The original 19 m blade and 2) A 19 m blade with a different twist distribution. For the latter, the twist increment – compared to the original blade – is 5° at the blade root and 0° at the tip. The twist increment is linear with radius. The reason for considering a blade with modified twist distribution is that it is a realistic and simple way to change the local vibration direction. Increased twist – θ_{RB} in Fig. 1 becomes more negative – will increase the damping in the edge-wise mode shape. The resulting vibration directions for the two blades are illustrated in Fig. 7.

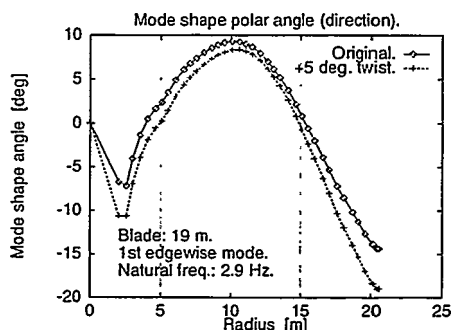


Figure 7. Vibration direction – angle θ_{RB} in Fig. 1 – of 1st edgewise mode shape.

The general characteristics of the vibration direction is a negative direction at the root and tip and a positive direction at the middle of the blade. The blade with increased twist has – as expected – a more negative vibration direction than the original blade. At the tip the difference is 5° and due to the influence of the mode shape amplitude, Eq.(7), this is the most important region. The difference in total damping for the two blades are significant, as shown in Fig 8.

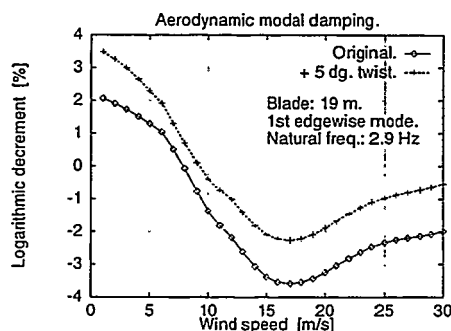


Figure 8. Aerodynamic damping as logarithmic decrement of 1st edgewise mode shape.

For the blade with increased twist, the resulting total damping is increased by approximately 1.5% at all

wind speeds, and the lowest damping is 2.2% at a wind speed of 17 m/s. The distribution of damping along the blade at this wind speed is shown in Fig. 9, showing that additional damping improvements should be concentrated around radius 16 m.

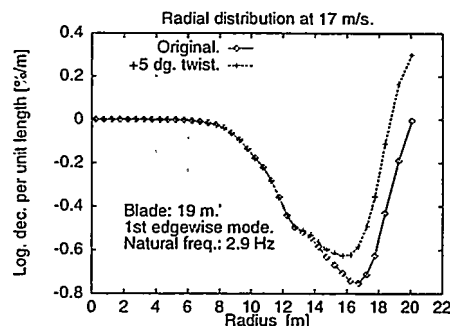


Figure 9. Aerodynamic damping per unit length at 17 m/s in the 1st edgewise mode shape.

4 CONCLUSION

Main results from stall induced vibration research are presented, showing the fundamental characteristics of the phenomenon and highlighting the areas, which can support design work aiming at reducing the risk for stall induced vibrations. The presentation is based primarily on the quasi-steady theory, but it should be stressed that the dynamic conditions – both aerodynamic and structural – play a very important role, and they must be considered in an actual design situation. The reader is referred to the extensive reporting of the research results in [2].

5 ACKNOWLEDGEMENT

The work was supported by the EC under Contract JOR3-CT95-0047 (STALLVIB) and the Danish Energy Agency under the contracts ENS 1363/96-0001 (Kantsvingninger i Stall) and ENS 1363/97-0002 (Aeroelastisk Program). The authors want to thank the participants in these projects for their contribution to the work.

REFERENCES

- [1] I. Antoniou, H. Aa. Madsen and F. Rasmussen. *Wind Tunnel Measurements on a LM 8.2 m Blade*. Risø-I-800(EN), Risø National Laboratory, 1995.
- [2] J. T. Petersen, H. Aa. Madsen, A. Björck, P. Enevoldsen, S. Øye, H. Ganander and D. Winke-laar. *Prediction of Dynamic Loads and Induced Vibrations in Stall*. Risø-R-1145(EN), Risø National Laboratory, 1998.
- [3] J. T. Petersen, K. Thomsen and H. Aa. Madsen. *Stall Strips can Control Edgewise Vibrations*. Risø-RB-6(EN), Risø National Laboratory, 1998.
- [4] M. Thøgersen. *Internal note on blade structural modelling*. Risø National Laboratory, 1998.

TURBULENCE IN COMPLEX TERRAIN

Jakob Mann

Risø National Laboratory

Wind Energy and Atmospheric Physics Department

P.O. Box 49, DK-4000 Roskilde, Denmark

ph. +45 4677 5019, fax +45 4677 5970, email jakob.mann@risoe.dk

ABSTRACT: The purpose of this work is to develop a model of the spectral velocity-tensor in neutral flow over complex terrain. The resulting equations are implemented in a computer code using the mean flow generated by a linear mean flow model as input. It estimates turbulence structure over hills (except on the lee side if recirculation is present) in the so-called outer layer and also models the changes in turbulence statistics in the vicinity roughness changes. The generated turbulence fields are suitable as input for dynamic load calculations on wind turbines and other tall structures and is under implementation in the collection of programs called WASP Engineering.

Keywords: Terrain, Turbulence, WASP Engineering.

1 INTRODUCTION

The modeling of the turbulence structure is divided into two parts: Roughness variations and orography. For the second rapid distortion theory (RDT) is used. Effects of both on the turbulence are treated as perturbations to a homogeneous terrain turbulence model [10, 11]. The model is restricted to neutral atmospheric stratification.

The modeling of the change of turbulence due to orography is limited to the so-called outer layer. For a simple isolated hill Jensen [8] estimates the height of the inner layer by

$$\frac{\ell}{L} \ln^2 \left(\frac{\ell}{z_0} \right) = 2\kappa^2, \quad (1)$$

where z_0 is the roughness length, L the upwind distance where the elevation is half the hill height and $\kappa \approx 0.4$ the von Kármán constant. At heights lower than ℓ there is approximately local equilibrium between production and dissipation of turbulent kinetic energy, and above ℓ the perturbations caused by the hill are approximately inviscid. The inner layer height is also approximately equal to the height above which the travel time over the hill is shorter than the Lagrangian time scale or the eddy 'turn-over' time scale.

Inner scales derived from (1) are typically much less than the height of wind turbines.

The modeling of turbulence changes due to roughness variations does not have this limitation, and should apply all the way down to the roughness sub-layer which is very close to the ground. The flow disturbances produced by roughness changes are by nature viscous and thus much "slower" than RDT. We use and modify the idea that eddies respond to roughness changes on the order of "the eddy turn-over time scale" [12, 6]. A consequence of this is that the low frequency end of the spectrum responds very slowly to roughness changes while small eddies quickly become in equilibrium with the underlying surface.

This paper may be viewed as an extension of the work of Frank [4], which considers spectra over a single hill with constant roughness.

1.1 Model input

The model needs two types of input: The spectral velocity tensor for homogeneous terrain, and the mean flow perturbations produced by the roughness variations and the orography.

We use the spectral tensor by Mann [11] which can be adjusted to resemble either the spectra of Kaimal (which are used in micro-meteorology [9]), of Simiu and Scanlan [13] mainly used in wind engineering, or of ESDU [3].

The mean flow perturbations are calculated by the linear flow model LINCOM [1, 5].

2 NOMENCLATURE

The instantaneous wind speed as a function of space and time $\tilde{U} = \tilde{U}(x, t)$ is decomposed into the ensemble mean and fluctuations:

$$\tilde{U} = U + u, \quad (2)$$

$U \equiv |U|$. The unperturbed stationary velocity field is denoted by U^0 and is only dependent on the height above the surface z . The unperturbed fluctuations are denoted by u^0 .

The correlation and spectral tensors $R_{ij}(r)$ and $\Phi_{ij}(k)$ are defined in the usual way using homogeneity, eg. $R_{ij}(r) = \langle u_i(x)u_j(x+r) \rangle$. However, it should be noted that the turbulence is not homogeneous, not even in the horizontal directions, so the tensors are meant as approximations to the real inhomogeneous correlation structure. The corresponding unperturbed tensors which equal those for flat terrain have a superscript 0.

Since the flow model LINCOM is linear the perturbation to the mean flow can be written as a sum of two terms

$$U - U^0 = U^r + U^t, \quad (3)$$

where U^r refers to flow perturbations due to roughness variation and U^t due to variations in the height of the terrain.

3 VARIABLE ROUGHNESS

Højstrup's [6] model concerning the adjustment of velocity spectra downstream of an abrupt change of roughness is the starting point of a more general model for the spectral tensor downstream of any slowly varying or abrupt change of roughness.

3.1 Outline of the model by Højstrup

In the special case of neutral stability, which is the only concern here, Højstrup [6] assumes that the height z^{top} separat-

ing air which has or has not felt the abrupt change of roughness is governed by the differential equation:

$$\frac{dz_{\text{top}}}{dx} = D \frac{\sigma_w}{U} = D \frac{\kappa 1.22}{\log(z_{\text{top}}/z_0)}, \quad (4)$$

where z_0 refers to the downstream value of the roughness and D is a constant of the order of one.

When an eddy hits the upper edge of this internal boundary layer its energy is supposed to change according to

$$\frac{dE_e(k_1)}{dt} = \frac{E_{e2}(k_1) - E_e(k_1)}{\tau(k_1)}, \quad (5)$$

where $E_e(k_1)$ the energy of the eddy with wavenumber k_1 and $E_{e2}(k_1)$ is the energy the eddy would have had being above a homogeneous surface having the downstream roughness.

In the equation for the change of energy (5) above we use the suggestion by [10] for the 'eddy time scale' τ , which is a function of $k = |k|$ and in the inertial subrange it is

$$\tau(k) = C \varepsilon^{-1/3} k^{-2/3} \quad (6)$$

with $C = 1.5 - 1.8$. At smaller wavenumbers outside the inertial subrange τ behave asymptotically as $\propto k^{-1}$.

3.2 Spectral tensor model: Roughness

As a generalization of (5) we propose that the three-dimensional spectral energy density (or the spectral tensor) approaches some equilibrium spectral tensor Φ_{ij}^{eq} according to the equation

$$\frac{d}{dt} \Phi_{ij}(k) = \frac{\Phi_{ij}^{\text{eq}}(k) - \Phi_{ij}(k)}{\tau(k)}, \quad (7)$$

where $\frac{d}{dt}$ is a Lagrangian derivative. The time scale τ is the "the eddy turn-over time scale" as defined by eq. 6 or in [10]. To simplify things we suppose k , and all parameters describing the tensor, except the energy dissipation ε , are constants as the turbulence is advected over varying roughness and that the equilibrium energy dissipation is given by

$$\varepsilon_{\text{eq}} = \kappa^2 z^2 \left(\frac{dU^r}{dz} \right)^3, \quad (8)$$

where κ is the von Kármán constant (the superscript r on the mean velocity U refers to the part of the mean velocity perturbation that is due to roughness changes). Then (7) can be written as

$$\frac{d}{dt} \varepsilon^{2/3} = \frac{\varepsilon_{\text{eq}}^{2/3} - \varepsilon^{2/3}}{\tau(k)}, \quad (9)$$

where ε is no longer the instantaneous energy dissipation, but merely a spectral multiplier dependent on k .

This equation is derived in the same spirit as [6] but uses the calculated flow field U^r as given by LINCOM and does not require explicit calculations of the positions of internal boundary layers. This formulation should be advantageous when dealing with a terrain with an arbitrarily complex roughness distribution, and not just simple changes along lines in the terrain.

Assuming $t \approx -x/U^0$ (where U^0 is the unperturbed mean wind speed) the solution of (9) is

$$\varepsilon^{2/3} = \frac{1}{U^0 \tau} \int_{-\infty}^0 \exp\left(\frac{x}{U^0 \tau}\right) \kappa^{4/3} z^{-4/3} \left(\frac{\partial U^r}{\partial z} \right)^2 dx. \quad (10)$$

Once LINCOM has calculated $\frac{\partial U^r}{\partial z}$, spectra, cross-spectra and simulated Gaussian wind fields can be calculated from this equation together with a suitable form of the spectral tensor (see sec. 1.1).

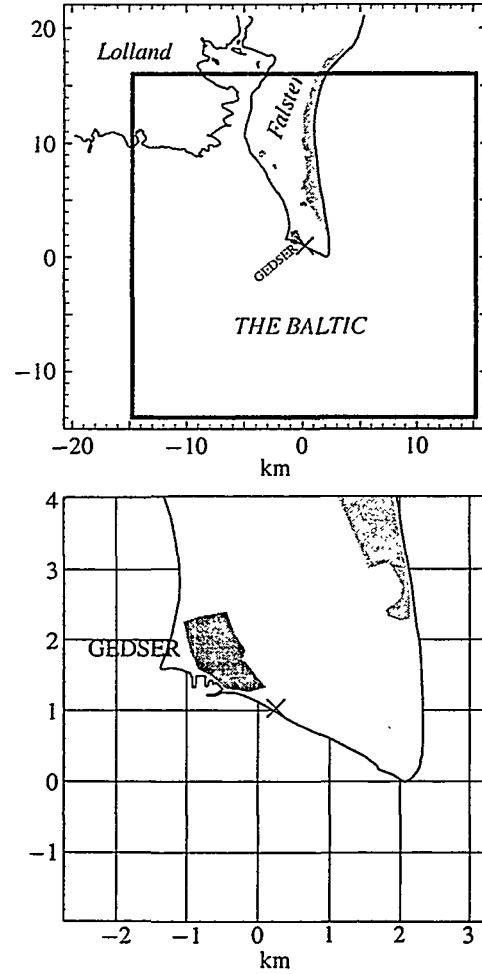


Figure 1: The Gedser land mast (cross). On the upper plot the computational domain used in LINCOM is marked. The lower plot shows the situation of the town Gedser, which has been assigned a roughness length of $z_0 = 1.0$ m (dark area). Other smaller towns and the forest/summer house area on the east coast have $z_0 = 0.5$ m (gray) while the country side has 0.05 m (light gray).

3.3 Example: The Gedser land mast

For offshore wind energy resource estimation one land mast and two offshore masts have been erected in the vicinity of Gedser on the southern tip of Falster, which is an island south of Zealand [2]. The land mast is ideal for testing the roughness model for turbulence, because it is situated in a very flat terrain with drastically varying roughness (see figure 1). The mast is instrumented with cup anemometers at 10, 30 and 45 m, wind vanes, various temperature sensors and a sonic anemometer at 42 m, suitable for turbulence measurements.

We use an almost contiguous record of data from August 1996 to June 1998 in this analysis. All half hour average turbulence intensities measured at 42 m with an average wind speed of more than 12 m/s are plotted in figure 2. Intensities with a positive heat flux (measured with a sonic anemometer) indicating unstable stratification are shown as diamonds, while negative heat flux (stable atmospheric stratification) corresponds to crosses. As it may be seen, there is a systematic difference between the two, showing that atmospheric stability plays a significant role, even at $U > 12$ m/s.

As input for the turbulence calculation we used the LIN-

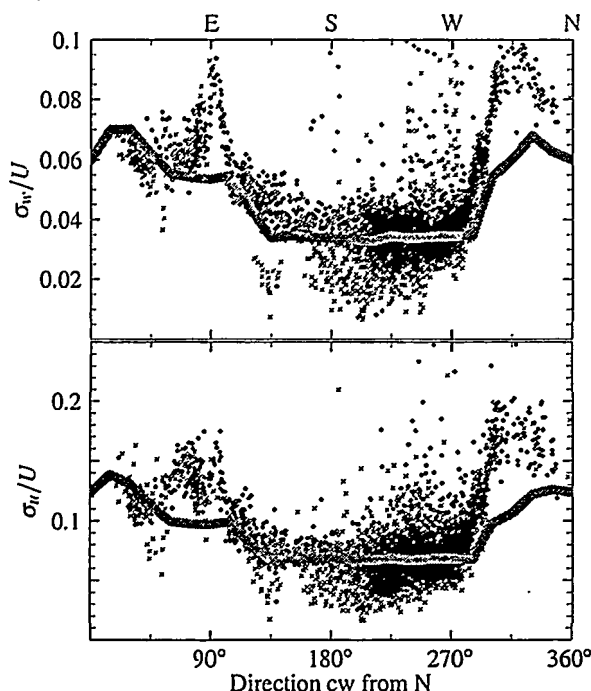


Figure 2: Turbulence intensities from the Gedser land mast. See the text.

COM mean flow generated from the maps shown in figure 1 together with a unperturbed spectral tensor resembling Kaimal's spectra. The predicted turbulence intensities are shown as broad gray curves.

Three things immediately catch the attention:

- The large scatter of measured intensities, which, as shown, is at least partly due to atmospheric stability variations.
- The excess intensity around 90° most noticeable in w . This is due to the instruments being in the wake of the mast, which is not modeled.
- The excess intensity around 315°, which might be due to large obstacles at the harbour of Gedser, a kilometer upstream in that direction.

4 OROGRAPHY

Rapid distortion theory was originally developed to model turbulence in wind tunnel contractions, but has later been applied to a variety of atmospheric turbulence problems. In many applications both the "rapid" condition and the condition of homogeneity have been treated rather loosely but often with good results.

The rapid distortion equations describe the response of turbulence to a uniform gradient of the mean velocity $\partial U_i / \partial x_j$ over times which are small compared to the time scales of the eddies. In complex terrain the mean velocity gradients are far from constant and small eddies typically have short life times compared to the advection time over features in the terrain. Rapid distortion theory (RDT) should thus be applicable for eddies smaller than the scale of variations in the mean flow gradients but larger than the eddies with a too small life time.

At low wavenumbers the distortion will typically not be homogeneous over the entire extent of the eddy, which is

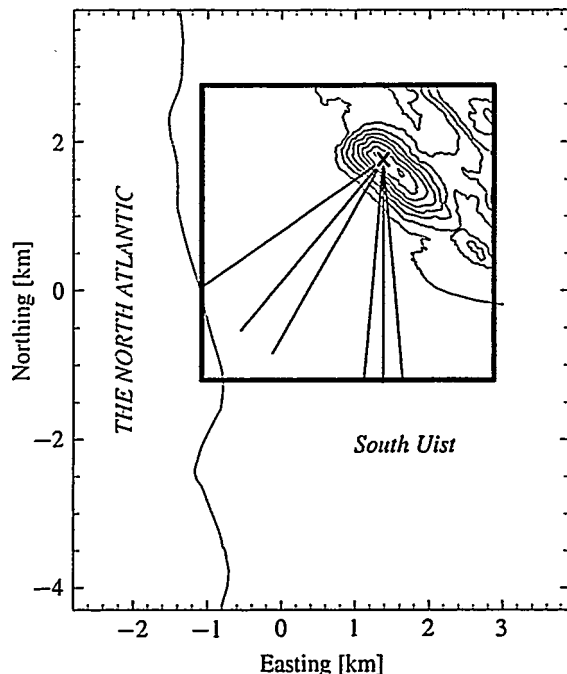


Figure 3: The Askervein hill. The position of the 46 m mast is indicated by a cross and the straight lines indicate the estimated mean directions for the analysed runs. The box is the computational domain used by LINCOM. Gray corresponds to $z_0 = 0.03$ m and white to 5×10^{-4} m.

one the basic assumptions in RDT. There has been attempts to generalize RDT to inhomogeneous mean flows, but they did not result in closed-form solutions and would require excessive computing time [7].

We have implemented some simplified solutions to take into account these deficiencies of RDT. However, the calculated spectra do not compare better to the few measurements in complex orography we have analysed, so, until more experimental evidence is present, we assume no lower wavenumber limit of the validity of RDT.

Usually, the effect of irrotational distortion along the coordinate axes is estimated by RDT through the *total strain ratios* e_i [14]

$$\ln(e_i) = \int_{-\infty}^0 \frac{\alpha_i(x)}{U(x)} dx, \quad (11)$$

where the integration is done over the entire upstream track (negative x) and where $\alpha_i \equiv \partial U_i / \partial x_i$ (no summation).

We modify this to take into account finite lifetime:

$$\ln(e_i) = \int_{-\infty}^0 \exp\left(\frac{x}{U(x)\tau(k)}\right) \frac{\alpha_i(x)}{U(x)} dx, \quad (12)$$

where $\tau(k)$ is the eddy time scale (see discussed leading to eq. 6), i.e. small, short-lived eddies hardly experience any distortion at all. This guarantees the $\frac{2}{3}$ -ratio between transversal (v and w) and longitudinal spectra (u) at high frequencies. These modified strain ratios are subsequently used in the RDT calculations.

4.1 Example: The Askervein Hill

The Askervein Hill Field Experiment took place in September/October 1982 and September/October 1983. The purpose was to study boundary-layer flow over a low hill [15].

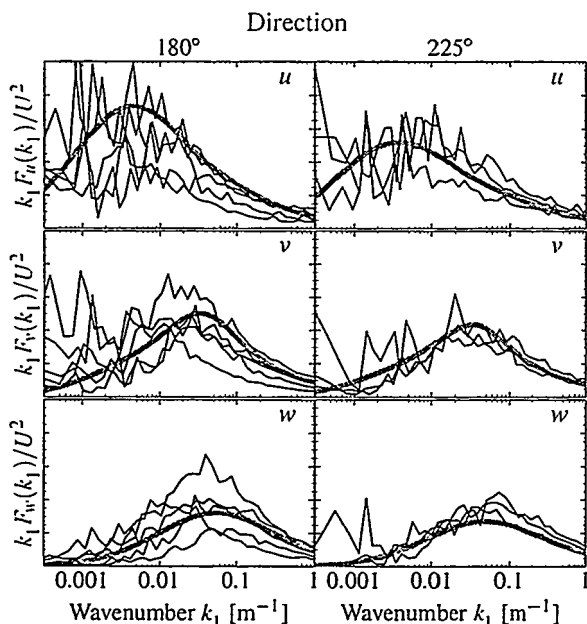


Figure 4: Measured and modeled spectra at $z = 47$ m at the top of the Askervein Hill. The broad, gray curves are the model calculations and the black curves are measurements. All plots have the same scaling on the axes.

Askervein is a 116 m high hill (126 m above sea level) on the west coast of South Uist of the Outer Hebrides, Scotland. As seen from figure 3 it has an essentially elliptical base.

Spectra from the sonic anemometer at $z = 47$ m on the mast at the hill top are calculated and runs with mean wind directions around 180° and 225° are shown in figure 4. Most runs are longer than one hour and they have all wind speeds larger than 13 m/s. Superimposed in the same figure are calculated model spectra for the two directions. The hill top spectra have considerably different distribution of turbulent energy among the three component spectra compared to what is found over flat terrain. The u -spectrum is considerably attenuated while the w -spectrum is enhanced. The modeled spectra agrees reasonably well with the measured, however, the experimental spectra have considerable scatter, probably caused by variation in the atmospheric stability.

5 CONCLUSION

A model of the spectral velocity-tensor in neutral flow over complex terrain is developed. It estimates turbulence structure over hills in the so-called outer layer and also models the changes in turbulence statistics in the vicinity roughness changes.

It compares well with the atmospheric experiments analysed so far, however, the measured turbulence quantities have considerable scatter, mainly caused by variations in the atmospheric stability.

It is essential to analyse more experiments in order to gain confidence in the model. Because of the lack of stability effects in wind tunnels, it might also be very useful to analyse turbulence data from terrain models in boundary layer wind tunnels.

The experience with the Gedser data indicate that it might be necessary to model obstacle generated turbulence apart from the roughness and orography generated.

The Danish Energy Agency is acknowledged for support for the preparation of this manuscript through the project WASP Engineering (EPF-97, 1363/97-0004). Also the support from the EU project MOWIE ("Improved tool to predict wind energy production in mountain" JOR3-CT98-0254) is appreciated.

REFERENCES

- [1] P. Astrup, T. Mikkelsen, and N. O. Jensen. A fast model for mean and turbulent wind characteristics over terrain with mixed surface roughness. *Radiation Protection Dosimetry*, 73(1-4):257-260, 1997.
- [2] R. J. Barthelmie, M. S. Courtney, B. Lange, M. Nielsen, A. M. Sempreviva, J. Svenson, and T. Christensen. Offshore wind resources at danish measurement sites. Technical Report RISØ-I-1339(EN), Risø National Lab., November 1998.
- [3] ESDU International. *Characteristics of atmospheric turbulence near the ground. Part III: variations in space and time for strong winds (neutral atmosphere)*. ESDU International, London, 1986.
- [4] H. P. Frank. A simple spectral model for the modification of turbulence in flow over gentle hills. *Boundary-Layer Meteorol.*, 79(4):345-373, June 1996.
- [5] C. B. Hasager and N. O. Nielsen. Surface flux aggregation in heterogeneous terrain. *Q. J. R. Meteorol. Soc.*, 1999. In the press.
- [6] J. Højstrup. A simple model for the adjustment of velocity spectra in unstable conditions downstream of an abrupt change in roughness and heat. *Boundary-Layer Meteorol.*, 21:341-356, 1981.
- [7] J. C. R. Hunt. A theory of turbulent flow round two-dimensional bluff bodies. *J. Fluid Mech.*, 61:625-706, 1973.
- [8] N. O. Jensen, E. L. Petersen, and I. Troen. Extrapolation of mean wind statistics with special regard to wind energy applications. Technical Report WCP-86, World Meteorol. Organ., Geneva, 1984.
- [9] J. C. Kaimal and J. J. Finnigan. *Atmospheric Boundary Layer Flows, Their Structure and Measurement*. Oxford University Press, New York, 1994.
- [10] J. Mann. The spatial structure of neutral atmospheric surface-layer turbulence. *J. Fluid Mech.*, 273:141-168, 1994.
- [11] J. Mann. Wind field simulation. *Prob. Engng. Mech.*, 13(4):269-282, 1998.
- [12] H. A. Panofsky, D. Larko, R. Lipschutz, G. Stone, E. F. Bradley, A. J. Bowen, and J. Højstrup. Spectra of velocity components over complex terrain. *Q. J. R. Meteorol. Soc.*, 108:215-230, 1982.
- [13] E. Simiu and R. H. Scanlan. *Wind Effects on Structures*, 3. ed. John Wiley & Sons, 1996.
- [14] A. A. Townsend. *The Structure of Turbulent Shear Flow*. Cambridge University Press, 2nd edition, 1976.
- [15] J. L. Walmsley and P. A. Taylor. Boundary-layer flow over topography: Impacts of the Askervein study. *Boundary-Layer Meteorol.*, 78:291-320, 1996.

MODELLING OF EXTREME GUSTS FOR DESIGN CALCULATIONS (*NewGust*)

Wim Bierbooms¹, Po-Wen Cheng¹
Gunner Larsen²
Bo Juul Pedersen³
Kurt Hansen⁴

¹ Institute for Wind Energy, Delft University of Technology
Stevinweg 1, 2628 CN Delft, The Netherlands
tel. +31 15 278 20 97, fax +31 15 278 53 47, e-mail: w.bierbooms@ct.tudelft.nl
² Risø National Laboratory, Roskilde, Denmark
³ Vestas Wind Systems A/S, Lem, Denmark
⁴ Technical University of Denmark, Denmark

ABSTRACT

The main objective of the *NewGust* project is to come to a realistic and verified description of extreme gusts based on the stochastic properties of wind. In this paper the first results of the project are presented. Theoretical considerations indicate that the shape of extreme gusts is very sharp. Based on simulated wind time series, mean gust shapes (for several amplitudes and mean wind speeds) are determined and compared with the theoretical curves. The resemblance turned out to be very good. Furthermore, the influence of the sampling rate and the dynamics of a cup anemometer on the empirical mean gust shape are examined. The promising results are confirmed by a (preliminary) verification based on measured wind time series, available from the database on wind characteristics. The mean shape of gusts, of certain amplitude, together with their probability of occurrence can be used to obtain the distribution of the extreme response of wind turbines to gust loading.

Keywords: Gust Models, Extreme Wind Conditions, Turbulence, Wind Field Simulation

1. INTRODUCTION

For design load calculations of wind turbines it is necessary to determine the fatigue loads as well as the extreme loads. Up to now simple deterministic and coherent gusts (e.g. a cosine gust) have been used to determine the extreme response. The shape, amplitude and duration specified for these discrete events remain rather arbitrary and largely unvalidated. This is in contrast to the fatigue analysis, which conventionally rely on a synthetic stochastic wind field reflecting the stochastic properties of natural turbulence.

The main objective of the here presented *NewGust* project is to achieve a realistic and verified description of extreme gusts based on the (stochastic) properties of wind. The basic ideas of this advanced method are given in [1]. From theoretical considerations it has been demonstrated that the shape of extreme gusts is (very) sharp, which is in contrast with the gust shapes given in present standards. A preliminary verification of the predicted mean gust shape can be found in [2] and [3]. This paper focus on the first results of the *NewGust* project.

Only the longitudinal turbulence component will be considered, and consequently no account is given on wind direction changes.

2. THE NEWGUST PROJECT

In this section a global overview of the *NewGust* project is presented. The project is a cooperation between Delft University of Technology (coordinator), Risø and Vestas.

2.1 Technical approach

In essence the new method to be developed in the project, describes a way to combine a stochastic turbulence field (as used for fatigue analysis) and a well defined deterministic gust shape (which can be theoretically derived) in such a way that a realistic extreme gust is obtained.

The project approach can be divided into the following steps:

1. Experimental verification of the shape of extreme gusts.
From theory it follows that the gust shape resembles the autocorrelation function of turbulence. This will be verified by comparing with shapes extracted from an existing database of wind measurements.
2. Determination of the probability distribution function of extreme gusts from a database of wind measurements and/or from theory (in case wind measurements are not available for a long enough period).
3. Development of an advanced method to determine the dynamic response of a wind turbine to extreme gusts. The advanced method will generate wind time series which can not, in a statistical sense, be distinguished from natural extreme wind gusts.
4. Implementation of the advanced method in a number of existing design packages.
5. Experimental verification of the predicted loading and response of a wind turbine to extreme gusts.

2.2 Expected achievements

The project will result in an advanced and verified method to determine the extreme response to gusts. The method will be worked out in a way that enables it to be implemented in state-of-the-art design packages for wind turbine design as

used by the industry.

The more accurate description of the extreme loading will enable wind turbine manufacturers to build more reliable and optimised wind turbines.

3. ANALYSIS METHOD FOR THE VERIFICATION

For the determination of a mean gust shape, the primary task to address is the definition of gusts occurring in wind time series. One possibility is to consider a gust as the part of the signal between a positive and a successive negative zero crossing. However, usually several (local) extremes may occur between the two zero crossings, for a broad banded signal as it is the case for turbulence. Furthermore, it is difficult to attach a corresponding gust amplitude.

Therefore a different method has been applied. A gust is interpreted as the time period, say 20 s, around a (local) extreme in the time series (mean subtracted) with a certain amplitude (e.g. between 2.7 and 3.3 times the standard deviation). The mean gust shape, with a given amplitude, follows by straightforward averaging of the pieces of the wind time series around all found extremes. In this method a (local) maximum is counted as +1 and a (local) minimum as -1. In such way a gust with a small dip has about the same effect as a gust without the dip, see Figure 1. Furthermore, a small disturbance, around a certain magnitude, in a flank of some higher peak will have a minor influence only on the mean gust shape of that specific magnitude.

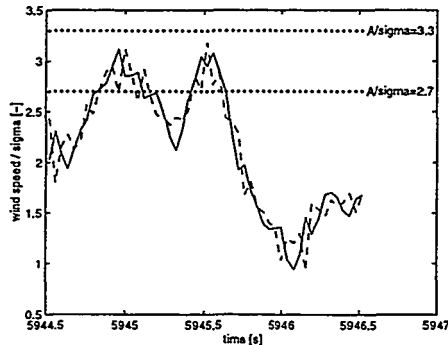


Figure 1: Original wind signal (solid line) with 2 maxima and 1 minimum around $t=5945.5$ s and the corresponding mean gust shape (dashed line) according to the applied analysis method.

Surprisingly, it turned out to be possible to derive an analytical expression for the mean gust shape $\bar{u}_{gust}(\tau)$ (with amplitude between A and $A+dA$), based on the stochastic properties of turbulence:

$$\frac{\bar{u}_{gust}(\tau)}{\sigma} = \frac{A}{\sigma} r(\tau) - \frac{\sigma}{A} \left[r(\tau) - \frac{\ddot{r}(\tau)}{\ddot{r}(0)} \right] \quad (1)$$

where r denotes the normalized autocorrelation function and σ is the standard deviation.

A full treatment of the analytical derivation of this expression is given in [2]. In the same article a preliminary verification can be found.

There are of course alternative ways to define a gust. In section 5 a gust is regarded as a suitable large wind speed excursion from a (local) minimum inside a certain time

interval (of say 5 s).

4. VERIFICATION OF THE MEAN GUST SHAPE WITH SIMULATED WIND

For evaluation of the analytical expression for the mean gust shape, the autocorrelation function (ACF) should be known. This implies that a comparison between the determined mean gust shape as obtained from measurements and the theoretical prediction may be affected by uncertainty in the ACF. In order to avoid this problem a preliminary verification is conducted based on a simulated wind field where the ACF is known priori, as input of the wind field simulation. Furthermore, possible influences on the determined mean gust shape originating from the measurement can easily be studied by computer simulations.

4.1 Comparison gust shape predicted from theory and determined from simulated wind

With the aid of the wind field simulation package SWING4 [4], time series are generated for two mean wind speeds (10 m/s and 20 m/s), for a height of 40 m. For each mean wind speed 10 wind field realisations have been generated, each of a duration of more than 10 minutes (16384 time steps of 0.04 s).

In Figure 2 the mean gust shapes are given according to the theoretical expression (1) and compared with the mean shapes determined from the simulated wind time series. As it can be seen the resemblance is very good.

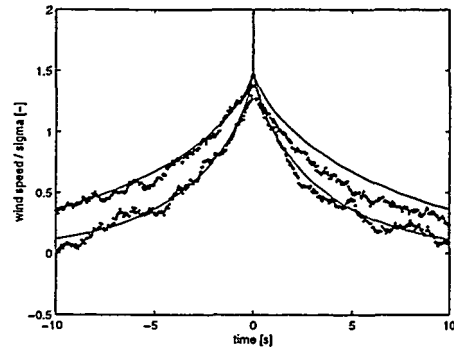


Figure 2: The comparison of the mean gust shapes (amplitude 2σ) according to theory (solid lines) and from simulated wind (dotted lines) for 2 wind speeds: 10 m/s (upper curves) and 20 m/s (lower curves).

4.2 Influence of the sample frequency

This subsection deals with the influence of the sample frequency of the wind on the determined mean gust shape. The theoretical expression (1) has a (very) sharp peak, which can not be resolved in case the sampling rate is too small. This effect can easily be examined by first sampling the generated wind time series and afterwards determining the mean gust shape. The results are shown in Figure 3 for two different sampling rates, 0.1 s and 1 s. As seen, the influence on the shape originating from the sampling rate may be substantial.

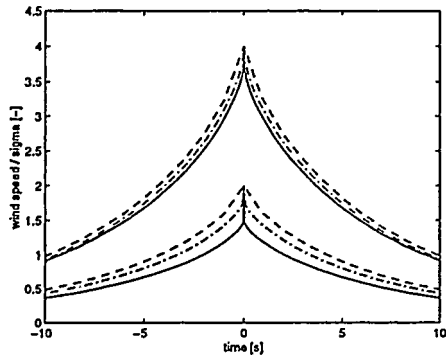


Figure 3: The mean gust shapes (upper curves: amplitude 4σ ; lower curves: 2σ) for two sampling rates: 1 s (dashed lines) and 0.1 s (dash-dot lines) compared to the theoretical ones (solid lines).

4.3 Influence of the dynamics of a cup anemometer

The dynamics of a cup anemometer will also have an effect on the empirical mean gust shape. In order to investigate that, a simple model for the cup anemometer has been applied: a first order system with a 'time constant' which depends on the momentary wind speed. The generated wind field is used as input to this dynamic model of a cup anemometer. The results are shown in Figure 4 for two different distance constants of the cup anemometer, i.e. 2 m and 15 m. The effects are somewhat similar to the smoothing effect caused by sampling. In addition an asymmetry is introduced, which is very modest for realistic distance constants of the cup anemometer.

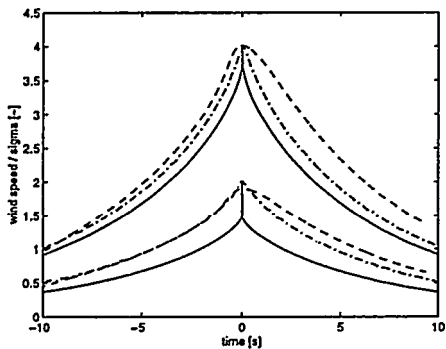


Figure 4: The mean gust shapes (upper curves: amplitude 4σ ; lower curves: 2σ) for two distance parameters: 15 m (dashed lines) and 2 m (dash-dot lines) compared to the theoretical ones (solid lines).

5. VERIFICATION OF THE MEAN GUST SHAPE WITH MEASURED WIND

5.1 Background

The present section deals with a preliminary experimental verification of the theoretical expression for the gust shape at a particular spatial point as presented in section 3. Assuming Taylor's frozen turbulence hypothesis to be valid, the (frozen) turbulence is presumed to convect in the mean wind direction with the mean wind speed. Thus, the hypothesis enables us to convert temporal measurements at a given point in space to spatial patterns in space. The implication for the autocorrelation function is that it must depend on the mean

wind speed. Denoting the autocorrelation in space and in time by R_s and R_t , respectively, the following relation holds

$$R_s(U\tau) = R_t(\tau) \quad (2)$$

where U denotes the advection speed

The left hand side of relation (2) is directly determined from the frozen turbulence structure. The autocorrelation in time is thus obtained from the spatial autocorrelation by an affinity of the independent variable. The theoretical expression for the gust shape depends on the autocorrelation coefficient in time and consequently on the mean wind speed. Two possible methods to compare experimental and theoretical gust shapes thus emerges. One is to apply a suitable detailed binning in the mean wind speed for the experimental data and base the theoretical determination on an averaged autocorrelation coefficient associated with one particular bin which is thus subsequently compared with bin-averaged gust shapes. A second, and more consistent method, is to derive the spatial autocorrelation coefficients from each measuring series applying the scaling relation (2) and subsequently evaluate an average autocorrelation coefficient. Application of the averaged normalised autocorrelation coefficient in the theoretical expression should enable a comparison with a mean of the identified experimental gusts, each with the physical time axis multiplied by the associated mean wind speed.

The theoretical gust shape is based on an assumption of stationary "parent" stochastic processes. In order to obtain a consistent comparison with experimental time series, it is necessary to remove possible (linear) trends in these.

5.2 Application

A number of high wind situations (mean wind speeds between 13 m/s and 17 m/s) from the Cabauw site, extracted from "Database on Wind Characteristics" [5], has been selected. The measuring height was 40 m and the length of each run were converted to 600 s with a sampling rate of 2 Hz. The total available data material consisted of 129 runs, of which 66 were associated with mean wind speeds between 13 m/s and 15 m/s and the remaining 63 related to mean wind speeds between 15 m/s and 17 m/s.

The experimentally determined gusts were classified into 4 groups depending on the ratio between the gust amplitude and the (de-trended) standard deviation associated with the particular time series. The ratio intervals defining the classes were 1.75-2.25, 2.25-2.75, 2.75-3.25 and 3.25-3.75. The gust amplitude in this respect was defined as the difference between the maximum recorded wind speed and the minimum recorded wind speed within a centred time interval of 20 s length around the gust maximum. It should be noted that this procedure deviates from the analysis method as described in section 3.

Two types of comparisons have been performed. In the first place the investigated mean wind speed interval has been subdivided into two mean wind speed bins of equal size (13 m/s - 15 m/s and 15 m/s - 17 m/s). For each of these bin intervals the classification according to gust size is performed, and within each resulting class the experimentally identified gusts are averaged and compared with the theoretical expression (1) based on the related averaged autocorrelation coefficients and the mean standard deviation associated with each class. Autocorrelation coefficients and standard deviations are evaluated from the total time series, per class, in which gusts were identified. The results are

presented in Figure 5 and 6.

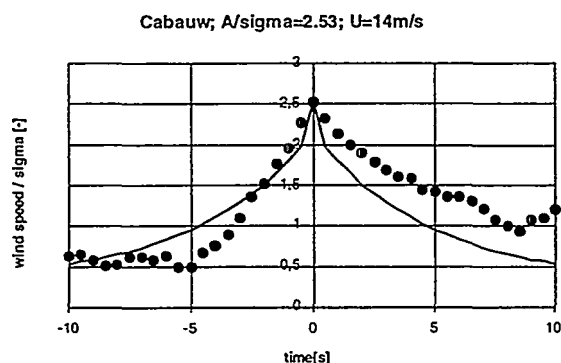


Figure 5: Comparison between theory (line) and mean experimental (dots) gust shape for the mean wind speed ranging between 13 m/s and 15 m/s.

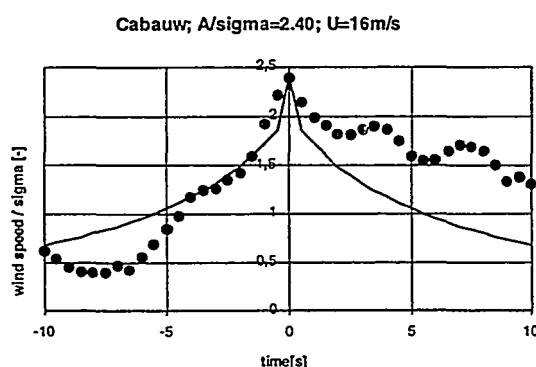


Figure 6: Comparison between theory (line) and mean experimental (dots) gust shape for the mean wind speed ranging between 15 m/s and 17 m/s.

In the second place the mean wind speed binning is omitted. Instead, a spatial normalised "time" axis, obtained from the physical time axis by multiplying with the mean wind speed, is applied within each gust class. The resulting gusts are averaged within each class and subsequently compared with the theoretical expression based on a mean of the related autocorrelation coefficients with time axes transformed in the same way as for the gust shape. The average standard deviation associated with each gust class are applied as standard deviation in the theoretical determination of the gust shape. Figure 7 shows the results of the above described comparison for one of the gust classes (representing in total 45 gusts).

The shape of the gusts are predicted well by the theoretical curves, although the measured wind speeds are not strictly Gaussian. The asymmetry in Figures 5-7 may be due to the dynamics of the cup anemometer as explained in subsection 4.3.

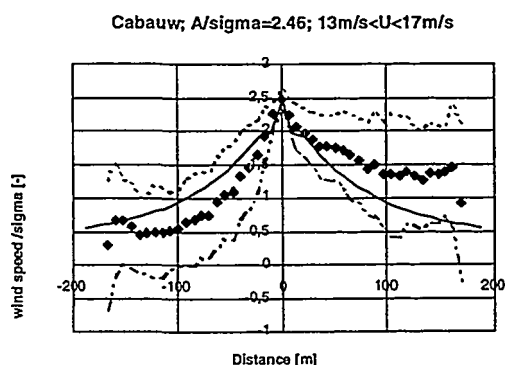


Figure 7: Comparison between theory (line) and mean experimental (dots) gust shape in spatial representation; including the confidence intervals, $\pm \sigma$ (dashed lines).

6. CONCLUSIONS AND OUTLOOK

According to presented theory a gust has a sharp peak in contradiction to standards. The predicted mean gust shape has been verified by comparison with simulated as well as measured wind data. These promising results demonstrates the viability of a new method to determine the extreme loading of wind turbines (*NewGust* project).

Further work, in the scope of this project, constitutes the determination of the probability density function of gusts for a given mean wind speed. Combining the constrained simulation for wind turbine response [1] and the occurrence probability of extreme gusts, the distribution of extreme response can be obtained. By applying the reliability method, the failure probability due to gust loads can be determined.

7. ACKNOWLEDGEMENT

The work is partially financed by the Commission of the European Union under the DG XII Non-Nuclear Energy Programme, contract JOR3-CT98-0239.

8. REFERENCES

- [1] J.B. Dragt, W. Bierbooms, Modelling of extreme gusts for design calculations, EUWEC '96 (p. 842).
- [2] Wim Bierbooms, Jan B. Dragt, Hans Cleijne, Verification of the mean shape of extreme gusts (submitted to Wind Energy).
- [3] W. Bierbooms, J.W. Cleijne, P. Cheng, Uitbreiding en verificatie van methode voor extreme windbelastingen [in Dutch; to be published], 1999.
- [4] Wim Bierbooms, SWING4 (Stochastic WIND Generator) - User Guide, DUT, 1998.
- [5] K. Hansen and M. Courtney, Data Base on Wind Characteristics, Final Report (to be published).

THE ECONOMIC VALUE OF ACCURATE WIND POWER FORECASTING TO UTILITIES

S J Watson¹, G Giebel² and A Joensen²

¹Building R63, Rutherford Appleton Laboratory, Chilton, Didcot, Oxfordshire, OX11 0QX, UK, Tel: +44 1235 445559, Fax: +44 1235 446863, E-mail: sjwatson@casynet.co.uk

²Dept of Wind Energy and Atmospheric Physics, Risø National Laboratory, DK-4000 Roskilde, Denmark, Tel: +45 46 77 5095, Fax: +45 77 5970, E-mail: Gregor.Giebel@risoe.dk, Alfred.Joensen@risoe.dk

ABSTRACT

With increasing penetrations of wind power, the need for accurate forecasting is becoming ever more important. Wind power is by its very nature intermittent. For utility schedulers this presents its own problems particularly when the penetration of wind power capacity in a grid reaches a significant level (>20%). However, using accurate forecasts of wind power at wind farm sites, schedulers are able to plan the operation of conventional power capacity to accommodate the fluctuating demands of consumers and wind farm output.

The results of a study to assess the value of forecasting at several potential wind farm sites in the UK and in the US state of Iowa using the Reading University/Rutherford Appleton Laboratory National Grid Model (NGM) are presented. The results are assessed for different types of wind power forecasting, namely: persistence, optimised numerical weather prediction or perfect forecasting. In particular, it will be shown how the NGM has been used to assess the value of numerical weather prediction forecasts from the Danish Meteorological Institute model, HIRLAM, and the US Nested Grid Model, which have been 'site tailored' by the use of the linearised flow model WAP and by various Model Output Statistics (MOS) and autoregressive techniques.

Keywords: Computer Programs, Forecasting Methods, Integration, Fossil Fuel Power Generation

1. INTRODUCTION

When the penetration of wind power in a national electricity grid reaches a given level (>20%) the fluctuating nature of wind farm output starts to become important [1]. In certain areas of Denmark and Northern Germany, penetration levels are exceeding this figure and interest in the accurate forecasting of wind power is becoming more widespread. If it is possible to accurately forecast up to a day ahead the expected output from wind farms connected to a network, it is then possible to schedule and dispatch the conventional power plant more efficiently.

This paper shows a study of how numerical weather prediction (NWP) forecasting of wind power can aid central power unit dispatch and result in overall fossil fuel savings. The two study cases of the England and Wales national grid and the grid of the US State of Iowa are presented.

2. THE NATIONAL GRID MODEL

2.1 Outline

The Reading University/Rutherford Appleton Laboratory National Grid Model (NGM) [1] has been developed over a number of years to simulate the scheduling and dispatch of conventional power plant connected to a national electricity grid system and can also simulate the integration of renewable energy sources, namely wind and photovoltaic power plant. The NGM has been used to assess the value of forecasting at UK Meteorological Office sites [2]. In this paper, the model is used to assess the value of forecasting at real or potential wind farm sites.

The model works by tracking hour-by-hour the status of each power unit. At each hour, the start-up and shutdown of plant is planned up to a day ahead in order to meet the predicted hourly demand. This planning of start-up and shutdown of plant is dependent on the prediction of load and wind power (if wind power is integrated into the network) for each hour ahead.

2.2 Power Plant

The model can simulate the operation of several different types of conventional plant namely:

- Nuclear – assumed to operate as inflexible base load
- Hydro – assumed to operate partly as base load and partly as fast response.
- Combined cycle gas turbine (CCGT) – modelled as having a three-hour start-up time from cold (idle for >120 hours), two hour start-up time if idle for >8 hours but <120 hours and a one hour start-up time if idle for less than eight hours.
- Coal/oil-fired steam turbine – modelled as having an eight-hour start-up from cold, but can be on a given number of hours warm standby if required in less than eight hours.
- Pump-storage – assumed to be available 'instantaneously' within the hourly time resolution of the model.
- Open cycle gas turbine (OCGT) – also assumed to be available 'instantaneously'.

Plants are scheduled in a merit order, which depends on plant type and overall fuel efficiency. Nuclear plant is used first in the merit order followed by CCGT, oil/coal thermal, pump-storage and OCGT. Hydro plant is used both as base load and peaking plant in a similar manner to pump-storage.

2.3 Wind Power

If wind power is present in the system then it is accepted after nuclear plant in the merit order. This is subject to whether all the thermal plant is minimum part-loaded. If the supply is greater than the demand for any given hour even if all the thermal plant is at minimum part-loading (50%) then excess wind power is discarded until this is no longer the case. This has to be done as the thermal plant cannot be switched off instantaneously, it has to be done within the one-hour time resolution of the model.

2.4 Spinning reserve

In general, for a national power system, there is only a limited amount of fast response plant available (generally pump-storage, hydro or OCGT). In the case of the England and Wales grid, this is mainly in the form of OCGTs, which are expensive to run. Fast response plant is therefore only used as a last resort at times of peak demand or when there is an unexpected surge in demand. Alternatively, 'spinning reserve' can be scheduled in advance. The term spinning reserve corresponds to thermal power plant at part-load whose loading can be quickly increased to meet a surge in demand or, if there is a significant amount of wind power integrated into the system, an unexpected fall in generated wind power. The NGM therefore plans at each hour the amount of spinning reserve that is required up to a day ahead. This spinning reserve is planned as a fixed fraction of the predicted load (called SR1) and a fixed fraction of the predicted wind power, if any wind energy is integrated into the system (called SR2). An extension to the spinning reserve algorithm can be used, whereby SR2 can also be specified as a fraction of the expected standard deviation of the forecast error divided by the predicted wind power. The expected standard deviation is assessed statistically off-line beforehand using historic data classified by key parameters such as time-of-day, season, direction, forecast lead-time, etc.

When the NGM is run it carries out a simulation for the period of interest, usually one year, with fixed values of SR1 and SR2. The model repeats each yearly run, optimising the values of SR1 and SR2 until the total fossil fuel cost is minimised subject to there being no loss-of-load events (power cuts) during the period of simulation. The load is much more predictable than the wind power and so SR1 is generally far smaller than SR2.

2.5 Load data and load prediction

Load data is accepted by the model as an hourly or half-hourly time series. It is assumed that the standard deviation accuracy of load prediction is 1.5% for all hours up to a day ahead. The model is run such that the *actual* load is used as the forecast and the real load at dispatch, as far as the model is concerned, is the actual load multiplied by a gaussian uncertainty factor with mean 1 and standard deviation 0.015.

2.6 Wind power data and wind power prediction

Wind power data is accepted as one dataset of hourly wind power values. These values are a combination of the power output from whatever sites are being used as input to the grid. The wind power data can be real or 'simulated'

(where wind speed at a site is converted to wind power using a suitable wind turbine power curve).

The NGM can accept wind power predictions in several formats:

- **Persistence** - The wind power at time x hours ahead ($t+x$) is predicted to be same as it is at the present time, t .
- **Numerical weather prediction model hybrid** - Forecasts of the wind power are accepted from whatever hybrid forecast is available whether it be statistical, enhanced numerical weather prediction or a hybrid of the two. A forecast can be accepted either hourly or 12-hourly.
- **Perfect** - Wind power is assumed to be forecasted perfectly.

The term 'numerical weather prediction model' refers to a computer model used typically by a national meteorological bureau to predict meteorological parameters. Such models output values on a regular grid. In this case, values from a regular grid are interpolated to the wind farm site and 'tailored' to the site using Model Output Statistics (MOS) [3], a wind flow model such as WA⁵P [4], a time series autoregressive model [5], or a hybrid of these, depending the data available.

3. THE GRIDS STUDIED

3.1 England and Wales

The England and Wales 1994 plant mix is summarised in Table 1. There are interconnections with Scotland (2200MW) and France (1988MW). These are treated by the NGM as output from coal units. This is an approximation but allows the source of the power transmitted by the interconnections to be treated as plant in the merit order with a given start-up time. It can be seen that the grid is dominated by thermal plant with only a small fraction of fast response plant (pump-storage and OCGT).

3.2 Iowa

The US State of Iowa 1996 plant mix is also summarised in Table 1. There are interconnections to neighbouring states which are neglected by NGM. This is to simulate the situation where the Iowa grid is self-sufficient in terms of electricity. The Iowa grid is also dominated by thermal plant but there is a larger proportion of fast response plant (OCGT) than for the England and Wales grid.

Table 1: England & Wales (1994) [6] and Iowa (1996) plant mix [7].

Plant	Capacity (MW)	
	England and Wales	Iowa
Nuclear	10642	475
Coal	31370	2286
Oil	5934	3102
CCGT	8915	107
OCGT	1559	1443
Pump-storage	2088	-
TOTAL	60508	7413

4. WIND FARM SITES

4.1 United Kingdom

Wind speed data from eleven sites monitored as potential wind farm sites were used as supplied by the UK wind farm developer Renewable Energy Systems Ltd. The data from these sites, which were used for this study, covered the calendar year 1994.

Wind speed forecast data were interpolated from the nearest grid points of the Danish Meteorological Institute's HIRLAM model [8] to the potential wind farm sites. HIRLAM forecasts are made at 00Z and 12Z up to $t+36$ hours with a temporal resolution of 3 hours. The high-level geostrophic wind speed from HIRLAM was then transformed to the ground using the WA⁵P model. Orography data, from UK Ordnance Survey 50m Panorama grid point files, and roughness data, from UK Ordnance survey 1:25000 Pathfinder maps, for each site were used as input to the WA⁵P model. In addition, the HIRLAM forecasts were combined with historic observed values using an autoregressive time series model, called the Wind Power Prediction Tool (WPPT) [5] to produce hourly forecasts. It was found that the WPPT forecasts gave more accurate predictions than the HIRLAM/WA⁵P forecasts and it is the results using these forecasts, which are reported here. These forecasts are henceforth referred to as the WPPT forecasts.

Wind speed was transformed to potential wind power using the power curve of the largest commercial wind turbine on the market at the time when this project was started, namely the Vestas V66 1650kW wind turbine.

4.2 The US State of Iowa

Wind speed data for two potential wind farm sites in the State of Iowa were made available by Wectec. Data for the calendar year 1996 were used in the NGM analysis.

In this case, wind speed forecast data were interpolated from the nearest grid points of the US National Weather Service Nested Grid Model to the two potential wind farm sites. The Nested Grid Model forecasts are made at 00Z and 12Z up to $t+48$ with a temporal resolution of 6 hours. As no orography and roughness data were available, interpolated geostrophic wind speed values were 'tailored' to the two sites using historic data and Model Output Statistics (MOS) as a function of direction and time-of-day. These forecasts are referred to as the NWS/MOS forecasts.

Wind speed was transformed to potential wind power using the power curve of the Vestas V66 1650kW turbine once again.

5. RESULTS

5.1 Overview

For both the England and Wales grid and the grid covering the US State of Iowa, fossil fuel savings for a one-year simulation period were calculated for different penetrations of wind power and different forecasting methods. Fossil fuel savings are defined as the difference between the fossil fuel cost with no wind power and the fossil fuel cost for a given penetration of wind power. The wind power penetration is adjusted by multiplying the Vestas V66 wind turbine output as calculated in Section 4

by an appropriate number of installed turbines at each site. For simplicity, the same number of turbines was assumed to be installed at each site.

5.2 England and Wales

Figure 1 shows the fossil fuel savings resulting from different penetrations of wind power for the England and Wales grid for 1994. The x-axis displays the total rated energy output as a fraction of the total energy demand for the year (273TWh), assuming that the wind turbines would be operating at maximum output throughout the entire year. The y-axis displays the fossil fuel saving relative to the total fossil fuel cost when no wind power is integrated into the grid. What is noticeable from Figure 1 is:

- The value of forecasting becomes significant when the rated output as a fraction of total demand reaches around 0.6, which corresponds to a penetration level of 25%.
- It is beneficial to use the standard deviation of the historic forecast errors in planning the spinning reserve (see Section 2.4). This can also be seen when using persistence forecasting at high penetration, where the rated output as a fraction of total demand reaches 1.3 (penetration level of 40%).

When the rated output as a fraction of total demand reaches 1.3 (penetration level of 40%), the fossil fuel savings using the WPPT forecasts and the standard deviation of the historic forecast errors to plan the spinning reserve are 26% higher than persistence. However, it should be noted that if persistence forecasting is used in conjunction with the standard deviation of the historic persistence forecast errors to plan the spinning reserve, the savings are still 13% better than persistence alone. NB Penetration is defined as the installed wind power capacity as a fraction of the total conventional and wind power plant.

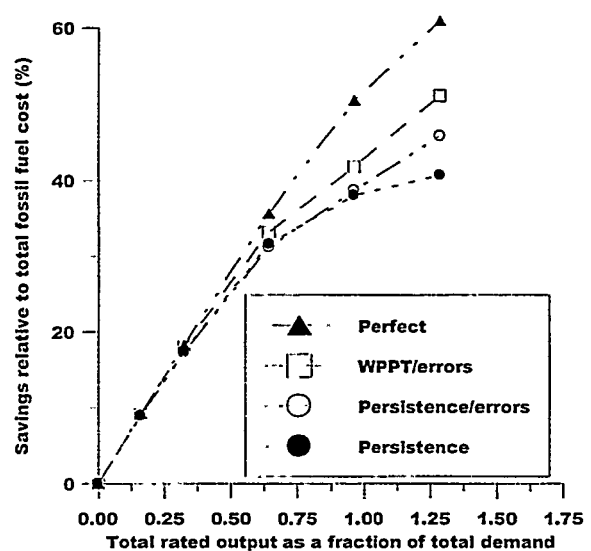


Figure 1: Fossil fuel savings for different forecasting methods for the England and Wales grid (1994).

5.3 Iowa

Figure 2 shows the equivalent fossil fuel savings for the Iowa grid comparing perfect, persistence and NWS/MOS forecasts. The total demand here was 28TWh. It can be seen that:

- Perfect forecasting performs increasingly better than persistence as the penetration level increases.
- The NWS/MOS forecasts perform significantly worse than persistence at all penetrations.

The first point indicates that 'intelligent' forecasting is beneficial from the point of plant scheduling. However, the second point shows that the NWP forecasts produced every 12 hours at lead-times in increments of six hours are not good enough in comparison with persistence.

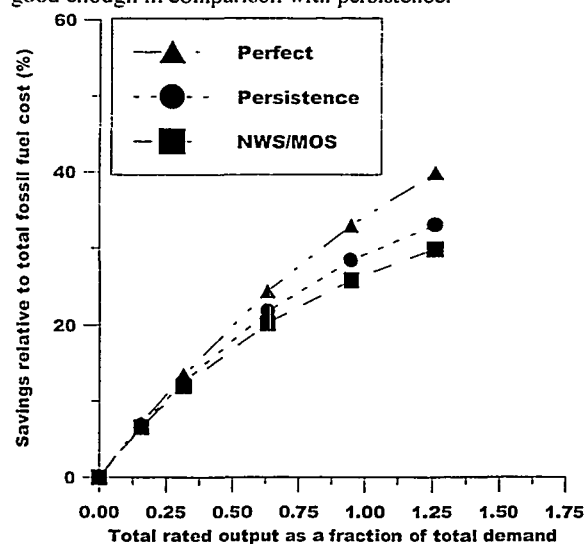


Figure 2: Fossil fuel savings for different forecasting methods for the Iowa grid (1996).

6. DISCUSSION

The WPPT forecasts give greater fossil fuel savings than persistence in the case of the England and Wales grid. In the case of Iowa, the NWS/MOS forecasts perform worse than persistence. However, if one compares the forecasts with persistence as a function of forecast lead-time for the individual sites then it is found that the forecasts outperform persistence at lead-times of 3-4 hours and this is approximately the same for the sites in England and Wales and those in Iowa.

Although the NGM results for Iowa seem disappointing, it should be noted that the WPPT forecasts are optimised as far as possible for the UK sites giving hourly forecasts which are based on three-hourly HIRLAM forecasts, whereas the NWS/MOS are only available every six hours. This means that much of the time, quite 'old' forecasts are being used by the NGM in the case of the Iowa grid to plan plant scheduling and spinning reserve.

7. CONCLUSIONS

It has been shown that enhanced numerical weather prediction forecasts of wind power at potential wind farm sites can improve the efficiency of plant scheduling resulting in fossil fuel savings when compared with persistence. Indeed, for the England and Wales grid WPPT forecasts can result in a saving of up to 26% compared to persistence at a wind power penetration level of 40%. However, it has also been shown that the quality of the forecasts is quite critical. If thermal plant has a start-up time of eight hours then six-hourly forecasts updated every 12 hours do not show an improvement over persistence. The next step would be to optimise the NWS/MOS forecasts using a site 'tailored' WPPT model.

8. ACKNOWLEDGEMENTS

The authors would like to acknowledge the support of the Directorate General XII of the European Commission who are providing part funding for this project under the JOULE programme, contract JOR3-CT95-0008, 'Implementing Short-Term Prediction at Utilities' and also the Marie-Curie-Fellowship, JOR3-CT97-5004, 'European Wind Energy Capacity Effects'.

9. REFERENCES

- [1] E A Bossanyi (1983) 'Use of a grid simulation model for longer-term analysis of wind energy integration', *Wind Eng.* 7 pp 233-246.
- [2] S J Watson, L Landberg, J A Halliday (1994) 'Application of wind speed forecasting to the integration of wind energy into a large scale power system'. *IEE Proc. C* 141 pp 357-362.
- [3] H R Glahn and D A Lowry (1972), 'The use of model output statistics (MOS) in objective weather forecasting', *J. Appl. Met.*, 11 pp 1203-1211.
- [4] N G Mortensen, L Landberg, I Troen and E L Petersen (1993) 'Wind Atlas Analysis and Application Program (WAAP) Vol 1: Getting Started'. Risø National Laboratory user guide: Risø-I-666(EN)(v.1).
- [5] ELSAM (Ed.) (1995), 'Wind power prediction tool in central dispatch centres'. Final report to the EC for contract J0U2-CT92-0083.
- [6] National Grid Company plc (1996), '1996 Seven Year Statement'. Published by the National Grid Company plc, UK.
- [7] Mid-Continent Area Power Pool (1997), '1996 Coordinated bulk power supply program/load and capability report'. Published by the Mid-Continent Area Power Pool, USA.
- [8] B Machenauer (Ed.) (1989), 'The HIRLAM final report'. HIRLAM Technocal Report 5. Danish Meteorological Institute, Denmark.

THE IRISH WIND ATLAS

Rick Watson
University College Dublin
Department of Electronic and Electrical Engineering
Dublin 4, Ireland
rwatson@ollamh.ucd.ie

Lars Landberg
Risø National Laboratory
Meteorology and Wind Energy Department
DK-4000 Roskilde, Denmark
lars.landberg@risoe.dk

ABSTRACT:

The development work on the Irish Wind Atlas is nearing completion. The Irish Wind Atlas is an updated improved version of the Irish section of the European Wind Atlas. A map of the Irish wind resource based on a WASP analysis of the measured data and station descriptions of 27 measuring stations is presented. The results of previously presented WASP/KAMM runs show good agreement with these results.

Keywords: Wind resource assessment, windatlas, WASP.

1 Introduction

The European Wind Atlas was published in 1989 [1]. In the section which covers Ireland wind data covering ten year periods at a selection of Met Eireann synoptic stations were analysed using the windatlas/WASP methodology [2].

The Irish Wind Atlas is an updated and expanded version of the Irish section of the European Wind Atlas. The basic windatlas/WASP methodology remains the same but the number of stations has been increased and the station descriptions used have been improved. The initial work was reported previously in [3] and further progress elaborated in [4].

Three elements make up the Irish Wind Atlas:

- A WASP analysis of wind data collected at the Met Eireann synoptic stations over typically 10 to 20 year periods but in some cases (due to availability of suitable data) over shorter periods all between the years 1974 and 1998.
- A WASP analysis of wind data collected at a network of wind measuring stations which were setup especially for wind energy purposes typically over 2-3 year periods all between 1992 and 1998.
- Results generated by the meso-scale model KAMM (Karlsruhe Atmospheric Mesoscale Model) modelling the flow over the island.

2 MEASURED WIND DATA USED

Two sets of measured wind data are made use of in the Irish Wind Atlas. The first is the wind data set measured at the Met Eireann network of synoptic stations. The second set of measured wind data is that collected by a number of organisations especially for wind energy purposes. The organisations involved were UCD, ESBI, Arigna Fuels Ltd and the Irish Electricity Company. All of the data has been quality controlled and

analysed by UCD and will be referred to henceforth as UCD data.

The full list of 27 measuring stations used is shown in Table I. 14 of the stations are at inland locations while 13 are coastal (coastal being defined as within 10 km of the coastline). The elevation of the stations above sea level is also shown. There is a good spread between coastal and inland stations and over the range of elevations.

Table I: The full list of measuring stations used in the Irish Wind Atlas.

	code	met/ ucd	inland/ coastal	alt. [m] a.s.l
Annestown	ANN	ucd	coastal	60
Belmullet	BLT	met	coastal	10
Birr	BIR	met	inland	73
Cahermurphy	CMY	ucd	inland	175
Carnsore Pt	CSP	ucd	coastal	7
Casement Aero.	CSA	met	inland	90
Clady	CDY	ucd	coastal	60
Claremorris	CMS	met	inland	61
Clones	CNS	met	inland	90
Cork Airport	CKA	met	inland	140
Corrie Mt.	CEM	ucd	inland	420
Dublin Airport	DNA	met	inland	63
Finner Camp	FNC	met	coastal	31
Kilkenny	KKY	met	inland	66
Kilronan Mt.	KLM	ucd	inland	320
Knock Airport	KKA	met	inland	197
Knockanore	KAN	ucd	coastal	264
Knocknagarhoon	KAG	ucd	coastal	122
Malin Head	MLD	met	coastal	27
Mount Eagle	MEG	ucd	inland	394
Mullingar	MNG	met	inland	104
Rath Hill	RHL	ucd	coastal	63
Roches Point	RHP	met	coastal	40
Rosslare Harbour	RSH	met	coastal	12
Rostonstown	ROS	ucd	coastal	5
Shannon Airport	SHA	met	inland	4
Valentia Obs.	VLO	met	coastal	21

2.1 Met Eireann measured wind data

The location of the Met Eireann stations is shown in Figure 1. The duration of measurements used for data analysis the type and the height of anemometer used for all the Met Eireann stations are listed in Table II.

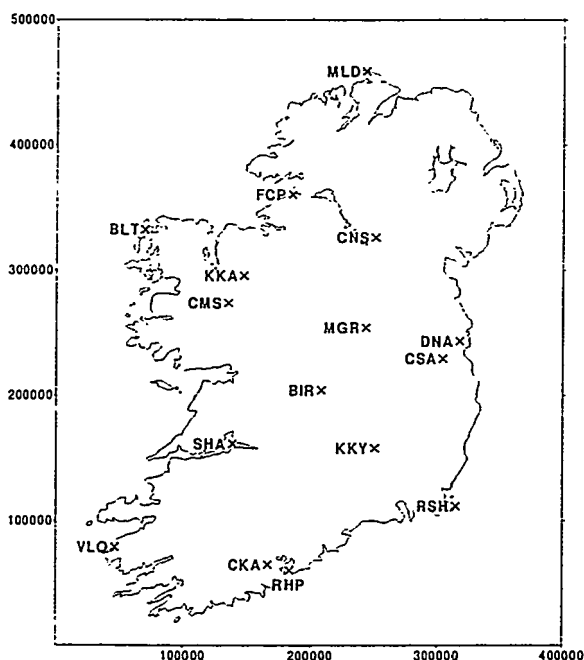


Figure 1: Location of Met Eireann wind measuring stations.

Table II: Duration of measurement, type and height of anemometer at the Met Eireann wind measuring stations.

	duration of measurement	anemo type	anemo height a.g.l [m]
Belmullet	010174-311293	dines	12
Birr	010174-311293	dines	12
Casement Aero.	010174-311293	dines	12
Claremorris	010174-311293	dines	12
Clones	010174-311293	dines	12
Cork Airport	011195-311098	cup	10
Dublin Airport	010189-311298	cup	10
Finner Camp	010397-311298	cup	10
Kilkenny	010174-311293	dines	12
Knock Airport	010896-311298	cup	10
Malin Head	010174-311293	dines	12
Mullingar	010174-311293	dines	12
Roches Point	010293-311298	cup	12
Rosslare Harbour	010174-311293	dines	12
Shannon Airport	090490-311298	cup	10
Valentia Obs.	010174-311293	dines	12

The locations of the Met Eireann stations were not chosen initially for wind energy purposes. At many of the stations local building developments have had a negative effect on the exposure of the measuring instruments to the winds. In particular at the airport measuring stations developments have made it necessary to relocate the wind measuring instruments to more exposed locations on the airfields.

The wind measuring instruments used are typically Dines pressure anemometers and windvanes while at the airport stations Vaisala cup anemometers

and windvanes are used. The wind measurements used in this study are hourly means at an effective height of 10 m a.g.l.

Despite the reservations referred to, the Met Eireann data set represents an unequalled source of good quality long term wind data. The station description data input to WAsP for each of the Met Eireann stations has been thoroughly checked and revised from that used in the European Wind Atlas. In particular the digitised contour and roughness data for many stations has been updated and improved using the improved resolution O.S. 1:50000 Discovery Series maps which have become available in recent years and which are a great improvement on the O.S. 1:126720 maps which were used in the European Wind Atlas.

2.2 UCD data

The locations used in the Irish Wind Atlas are shown in Figure 2. The duration of measurements, type and height of anemometer for all the UCD stations are listed in Table III.

These measurements were carried out for wind energy purposes mostly at potential windfarm sites with good exposure to the winds. In most cases these measurements are ten minute means made using cup anemometers and windvanes at 30 m a.g.l. The wind measuring campaigns are described more fully in [5, 6].

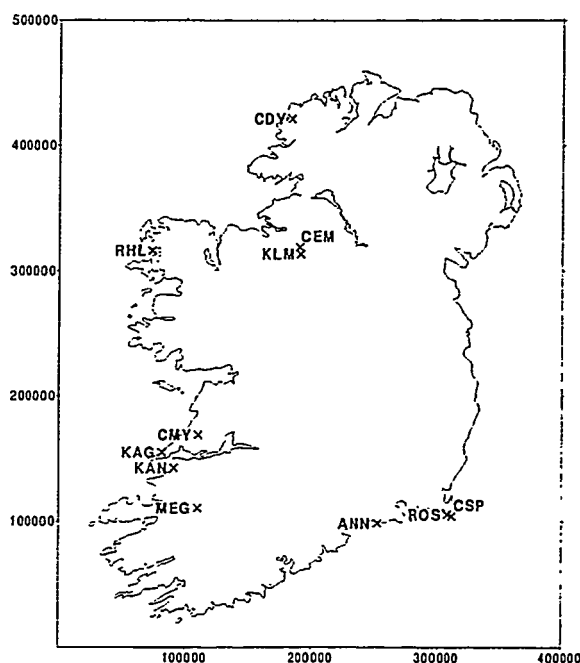


Figure 2: Location of UCD wind measuring stations.

3 LAYOUT OF THE IRISH WINDATLAS

The Irish Wind Atlas is made up of:

- a full description and WAsP analysis for each of the measuring stations.
- worked examples on the use of the Irish Wind Atlas in estimating the resource at potential windfarm locations.

Table III: Duration of measurement, type and height of anemometer at the UCD wind measuring stations.

	duration of measurement	anemo type	anemo height a.g.l [m]
Annestown	020794-300696	cup	40
Cahermurphy	220192-241194	cup	10
Carnsore Pt	010293-151195	cup	30
Clady	010192-101294	cup	30
Corrie Mt.	010192-111194	cup	30
Kilronan Mt.	181191-180594	cup	30
Knockanore	010192-310894	cup	30
Knocknagarhoon	010192-300994	cup	30
Mount Eagle	010192-080994	cup	30
Rath Hill	010692-300994	cup	10
Rostonstown	010694-300696	cup	30

- wind resource maps obtained from the WASP analysis in the Irish Wind Atlas and runs of the mesoscale model KAMM combined with WASP.

For each of the 27 measuring stations the detailed WASP analysis and station description includes:

- The name and the exact location of the station in Irish National Grid (ING) and Lat/Lon coordinates and the height above ground level at which the measurements were made.
- A detailed description of the station surroundings and any relevant comments on factors affecting the measurements.
- A map of the terrain contours and the different roughness areas.
- A table showing the contributions from each of the three physical models (orography, roughness and obstacle effects) to the corrections of the sector-wise Weibull parameters.
- A summary table of the measured data.
- A joint distribution of windspeed and direction and a Weibull fit and histogram of the measured data.
- A table showing the diurnal and seasonal variations of the measured data.
- A fingerprint graph (identical in format to that used in the European Wind Atlas).
- A table showing the monthly means of the measured data over the period of the measurements.
- The contents of a WASP .LIB-file which represents the generalised windatology calculated for the measured wind data and corrected for the three physical effects modelled, listed in tabular form. It shows the sectorwise and total A and k parameters for each of 5 standard heights above ground level (10m, 25m, 50m, 100m and 200m) for each of 4 roughness classes corresponding to roughness lengths 0.0002m, 0.03m, 0.1m and 0.4m. The mean windspeeds in [m/s] and power fluxes in [W/m^2] are also tabulated for the 5 standard heights and the 4 roughness classes.

A full station description and WASP analysis result was presented previously in [4].

4 WIND RESOURCE MAP

An Irish wind resource map is shown in Figure 3. This shows the power flux [W/m^2] at a height of 50m a.g.l.

for uniform roughness of 3 cm and flat terrain. The values of power flux are shown for each of the 27 stations as calculated by the WASP analysis. The contours are an interpolation between these data points.

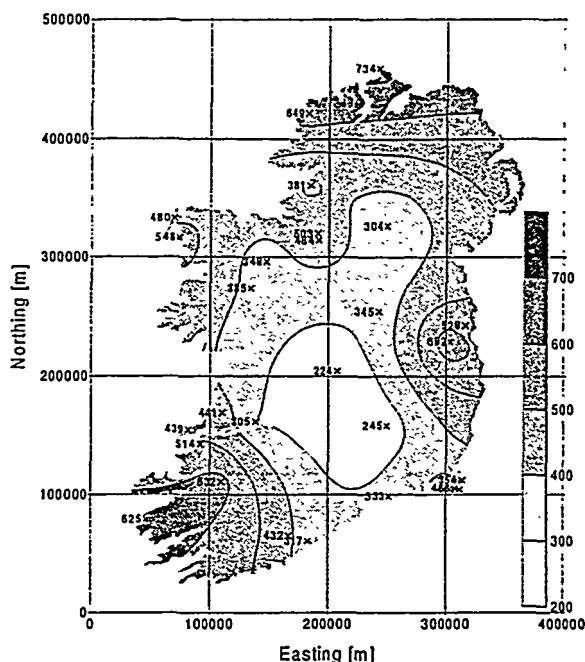


Figure 3: The Irish Wind Resource Map showing power flux [W/m^2] at 50m a.g.l. over flat terrain of roughness 3cm.

5 KAMM

WASP is normally used for sites separated by 10s of km however it cannot take account of effects on the meso-scale such as the channeling effects produced by mountain ranges. Neither can WASP take account of thermally induced circulations like sea breezes. These meso-scale effects and thermal effects can be calculated using a full atmospheric model like KAMM [7]. KAMM cannot however account for local influences on scales below its grid size. The concept where both models are combined has been developed at Risø National Laboratory [8].

KAMM is a meso-scale model and has been run for Ireland for grid sizes down to 10 km \times 10 km. KAMM runs are quite onerous in terms of computation time.

KAMM requires three inputs:

- A geostrophic wind climatology used to force the flow over the model domain which has been determined from geostrophic wind data obtained from European Centre for Medium-range Weather Forecasts (ECMWF).
- Orographic information which has been obtained by digitising the O.S. 1:625000 map of Ireland with height contour resolution of 91m.
- Roughness data which was generated from the CORINE land-use database where each land-use category has been assigned a roughness value.

The output of KAMM is used by WASP to generate wind atlas files for each grid point.

The results of a KAMM/WASP run for a height of 50m above the surface and a roughness length of 3cm as previously presented in [8] are in good agreement with the Irish Wind Atlas results as presented in Figure 3.

6 CONCLUSIONS AND FURTHER WORK

The major part of the work on the Irish Wind Atlas (i.e. the detailed WASP analysis of the 27 stations) is now complete. Detailed cross checking and fine tuning are now required before the final document can be published. It is anticipated that the Irish Wind Atlas will be completed and published in summer 1999. It is hoped that it will prove to be a valuable tool for wind resource assessment in Ireland.

ACKNOWLEDGEMENTS

The cooperation of Met Eireann, ESBI, Arigna Fuels Ltd and the Irish Electricity Company for allowing access to their wind data is acknowledged. Helmut Frank of Risø National Laboratory is gratefully acknowledged for running the KAMM model. University of Karlsruhe is acknowledged for allowing Risø National Laboratory to use the KAMM model. The financial support of the European Commission under a Joule contract to UCD to carry out its wind measuring campaign is gratefully acknowledged.

REFERENCES

- [1] Troen, I and EL Petersen, 1989: *The European Wind Atlas*. Published for the CEC by Risø National Laboratory, Roskilde, Denmark. 656 pp.
- [2] Mortensen, N.G., L Landberg, I Troen and EL Petersen, 1993: *Wind Atlas Analysis and Application Program (WASP), User's Guide*. Risø-I-666-(EN)(v.2), Risø National Laboratory, Roskilde, Denmark. 133 pp.
- [3] Landberg L. and Watson R., 1994: *The New Irish Wind Resource Atlas*, Proceedings of the European Wind Energy Association Conference, Thessaloniki, Greece.
- [4] Watson R. and Landberg L., 1997: *The Irish Wind Atlas*, Proceedings of the European Wind Energy Association Conference, Dublin, Ireland.
- [5] Watson R. 1993: *Wind measurements and Modelling in Ireland*, Proceedings of the European Community Wind Energy Conference, Travemünde, Germany.
- [6] Watson R. 1994: *Wind Measurements and Modelling in the Republic of Ireland*, Proceedings of the European Wind Energy Association Conference, Thessaloniki, Greece.
- [7] Adrian G. and Fiedler F., 1991: *Simulation of Unstationary Wind and Temperature Fields over Complex Terrain and Comparison with Observations*. Beitr.Phys.Atmosph., 64, 27-48.
- [8] Frank H., and Landberg L., 1997: *Modelling the wind climate of Ireland*, Boundary Layer Meteorology, 85, 359-378.

OFFSHORE WIND RESOURCES AT DANISH MEASUREMENT SITES

R.J. Barthelmie, M.S. Courtney, B. Lange, M. Nielsen, A.M. Sempreviva¹
J. Svenson, F. Olsen²
T. Christensen³

¹Department of Wind Energy and Atmospheric Physics, Risø National Laboratory, 4000 Roskilde, Denmark, Tel: +45 46 77 50 20, Fax: +45 46 77 56 90, Email: R.Barthelmie@risoe.dk

²ELKRAFT v/SEAS, Haslev, Denmark

³Elsamprojekt, Denmark

ABSTRACT: In order to characterise wind and turbulence characteristics at prospective offshore wind energy sites, meteorological observations from a number of purpose-built offshore monitoring sites have been analyzed and compared with long wind speed time series. New analyses have been conducted on the data sets focussing on meteorology, turbulence, extreme winds and wind and wave interactions. Relationships between wind speed, turbulence and fetch are highly complex. Minimum turbulence intensity offshore is associated with wind speeds of about 12 m/s. At lower wind speeds, stability effects are important while at higher winds speeds wind and wave interactions appear to dominate. On average, turbulence intensity offshore at 48 m height is approximately 0.08 if no coastal effects are present. However, the effect of the coastal discontinuity persists in wind speed and turbulence characteristics for considerable distances offshore. The majority of the adjustment of appears to occur within 20 km of the coast.

1. INTRODUCTION

Following the successful installation and power generation at two offshore wind farms, Danish energy policy now includes the vigorous pursuit of offshore wind energy. As part of this program, a monitoring program has been established to investigate the characteristics of wind and turbulence at a number of prospective wind energy sites in the coastal waters around Denmark.

The main characteristics of offshore wind climates are higher wind speeds and lower turbulence than are generally found on land. Wind energy estimates made using the Wind Analysis and Applications Program (WAAP) [1] are typically in good agreement with measurements where these exist. However, it remains a problem to confidently predict wind energy resources at offshore sites which are influenced by the coast. The effects of land on the climate are most important within 0-15 km of the coastline but can still be detected at 40 km and are especially important under stable conditions offshore when the internal boundary grows very slowly [2]. As the prevailing wind direction in Denmark is south-westerly, wind farms off the east coast can be expected to be most influenced by land-sea interactions and those off the west coast least influenced. A further complicating factor is the effect of the wind speed itself since higher wind speeds are associated with the prevailing wind directions and these can be expected to drive conditions towards neutral but also to increase roughness lengths. To reduce uncertainties regarding offshore wind climates a strategy of making long-term measurements of wind speed profiles, turbulence and temperature structures offshore has been adopted. Unfortunately making offshore measurements is not a simple task and requires considerable investment. This paper describes the measurements and how they are used to characterise offshore wind climates to reduce uncertainties in wind farm planning. This analysis is still in progress.

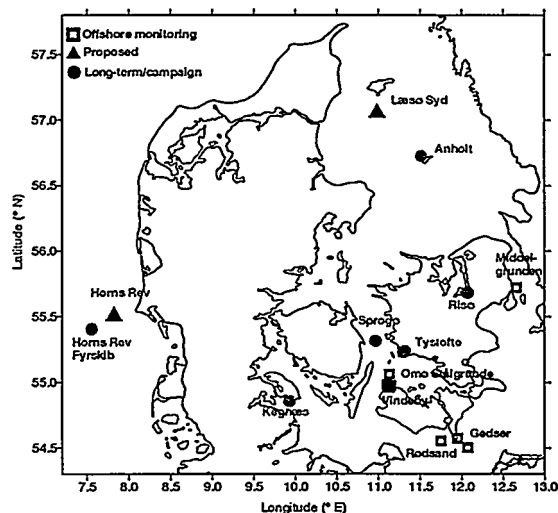
Vindeby, monitoring of the wind climate has been given priority. To date, eight purpose-built masts have been installed (including the three masts at Vindeby). Two of the masts are coastal masts and the remaining six are offshore. Sites used in this analysis (as shown in Figure 1) are divided into three types:

- measurement sites which were established as part of the offshore wind resource assessment projects (this group also includes prospective wind farm sites Læsø Syd and Horns Rev which will be established as measurement sites during 1999).
- climatological sites which are used to provide longer term meteorological records.
- campaign measurements e.g. Anholt

2.2 Data availability and quality control

Problems experienced during data collection at the offshore masts can be broadly divided into three categories:

Figure 1. Location of monitoring and reference sites



2. DESCRIPTION OF SITES AND DATA

2.1 Sites and data

From establishment of the first offshore wind farm at

- Access
- Power supply
- Communications

Data availability varies for the masts according to their position and the power supply. Data collection at Vindeby and the land mast at Gedser is good since these sites have access to mains power and are relatively easy to access. Poorest data collection has been at the sites at Omø and Gedser Rev which are the farthest from land and are 'stand-alone' in terms of power supply. All data have been subject to quality control as described in [3].

3. OVERVIEW OF WIND SPEEDS AND TURBULENCE

3.1 Temporal and directional variability

As expected and in accord with synoptic information highest wind speeds occur in the southwest/west sectors. Seasonal variations at offshore sites follow the same general patterns as are found on land with highest wind speeds in winter and lowest wind speeds in summer. However, if the site is close enough to land for the wind climatology to be influenced by the surface type the pattern becomes more complicated than from solely synoptic influences as the direction of the wind (and therefore the fetch changes) become important. Diurnal cycles of wind speed at offshore sites are typically thought to be small since, away from land, the sea surface temperature does not vary substantially on a diurnal basis. Previous research has suggested that close to land diurnal cycles may be inverted compared to land sites [4] i.e. wind speeds at night are higher than those during the day. The cause of this is the difference in temperature between air advected from land and the sea surface temperature. It is also likely to be complicated by advection of higher wind speeds from land during the day and sea breeze effects. At Vindeby and Rødsand, wind speed from different sectors exhibit a mean diurnal range which is of the order of 0.8-1.2 m/s. This varies according to the season.

3.2 Wind speed profiles

Wind speed profiles offshore should conform to logarithmic profiles and hence be easy to predict. The fact that they do not always do so can be ascribed to four factors:

1. flow distortion in the measurements caused by the mast structure
2. the presence of internal boundary layers
3. non-neutral stability conditions
4. effects of wind/wave/roughness on the wind speed profile.

It is worth noting that changes in the state of the sea surface should not lead to distortions of the profile away from logarithmic predictions but to changes in roughness which cannot be predicted using the Charnock equation relating roughness to friction velocity [5]. At all the offshore sites, the observed wind speeds at 48 m are higher than those predicted using 10 m wind speeds and the logarithmic profile. Using a higher roughness length gives better predictions but does not capture the shape of the profile. This could be due to atmospheric conditions being slightly stable offshore – however further analysis is required to clarify this point. Since offshore wind speed profiles are affected by both stability and roughness it

appears that a model which takes account of both effects is required for their accurate prediction.

3.3 Turbulence intensity

Turbulence intensity is calculated here as the ratio between the standard deviation of wind speed and the wind speed. In offshore regions, turbulence intensity is high at low wind speeds then decreases as wind speeds increase to about 12 m/s and then begins to increase in response to increasing wave height. Figure 2 shows the relationship between turbulence intensity and wind speed at Vindeby Sea Mast West (SMW). For wind speeds lower than 20 m/s the relationship between wind speed and turbulence intensity offshore can be modelled using an empirical fit to the 48 m data as a 6th degree polynomial.

Figure 2. Variation of turbulence intensity with wind speed at Vindeby SMW

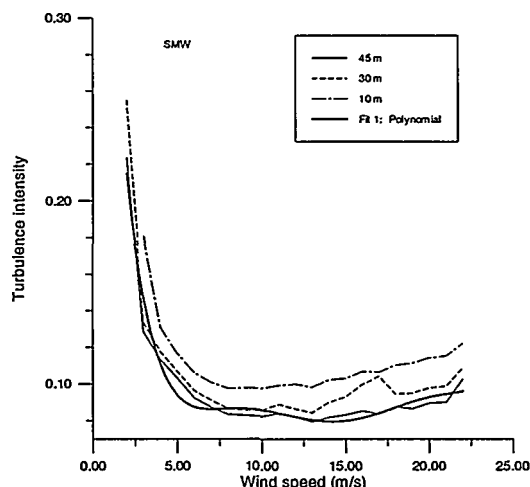
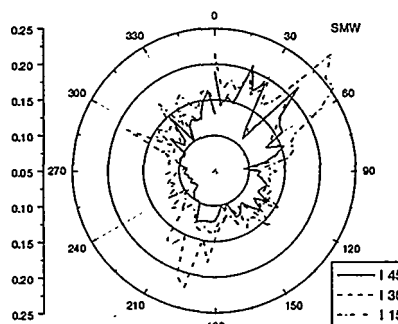


Figure 3 shows the mean turbulence intensity by direction for Vindeby SMW. At SMW turbulence intensity is influenced by the wind farm in the north east sectors. It is also apparent that surface characteristics influence the mean turbulence intensity for considerable distances. At SMW increased turbulence intensity presumably relating to the presence of land in the fetch is evident in the south west sectors. Mean turbulence intensity at Gedser Rev, Omø Stålgunde and Gedser Land (sea sectors) is 0.10, 0.09 and 0.08 at 10, 30 and 45 m heights, respectively. This profile, shown in Figure 4, suggests that turbulence intensity decreases linearly with height.

Figure 3. Mean turbulence intensity by direction at SMW



Turbulence intensity is expected to decrease with increasing distance from the coast. Figure 5 shows sector mean turbulence intensity from SMW and Rødsand plotted by mean sector fetch distance (sectors containing the wind farm at SMW and mast influences are excluded). There is considerable scatter in the diagram but a log-linear fit suggests that after 20 km or so fetch turbulence intensity reaches a level (around 0.08 at 45 m height) beyond which it will not decrease substantially with increasing fetch. Further analysis is required to assess these relationships.

Further analysis of extreme winds and spectra are given in [3], analysis of stability offshore in [6] and [7]. Analysis of wind/wave relationships are detailed in [8].

Figure 4. Vertical profile of turbulence intensity offshore

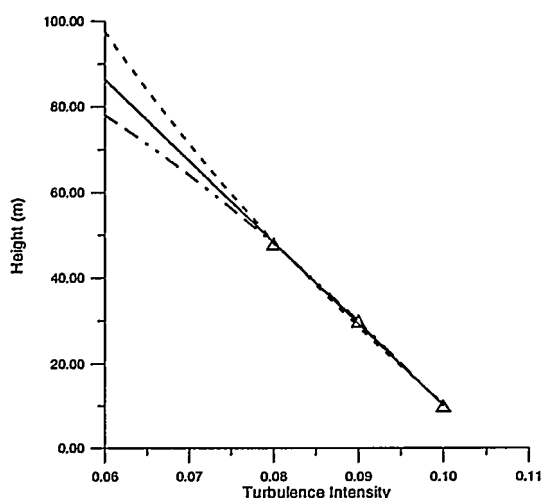
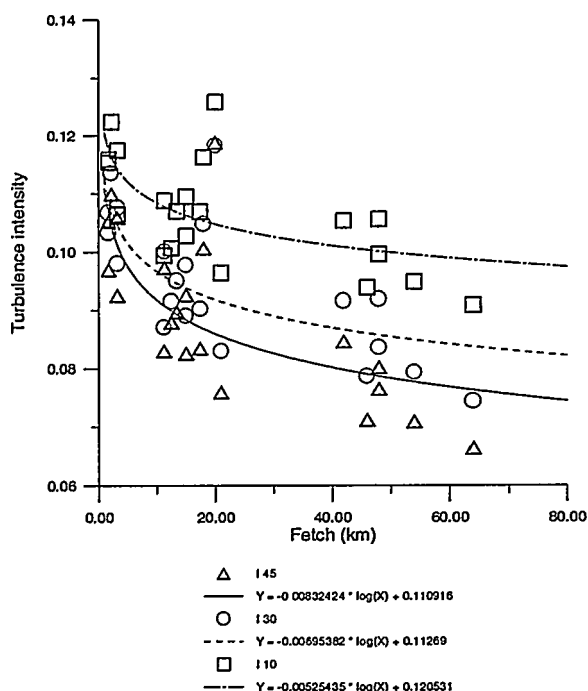


Figure 5. Relationship between turbulence intensity and fetch



4. OFFSHORE WIND RESOURCE ANALYSIS

It is well-known that short-term measurements do not capture the full-range of variability of wind speeds at a site. The aim of this analysis is to use different methods to assess the wind resource at the offshore measurement sites based on longer-term (climatological) data sets. The purpose of using different methods is that each methodology has different strengths and weaknesses and by comparing the results an estimate of the uncertainty in the analysis can be made. Wind speed measurements from 48 m height at the offshore sites are compared with a long-term time series from the 39 m level at Tystofte during the period 1984-1997. Data from this reference and various offshore sites observed during individual overlap periods ending on July 15 1998 were used in this analysis. Potential power output is based on the characteristics of the Offs1500 turbine (given in WA^{SP}). A more detailed description of the methodology can be found in [9].

4.1 Weibull correction method

The first method for assessment of the long-term energy potential by the relatively short observation periods is to establish a relationship between the wind speed distributions observed at the offshore site and that of a longer observation period at a nearby reference station by comparing the Weibull parameters in each directional sector. The uncertainty of these estimates is assessed by the 'bootstrap' method described in [10]. This statistical method evaluates the spread of the predictions of a family of synthetic data sets generated by random selection from the observed one. The statistical uncertainty depends on the data coverage, i.e. it is best at the Vindeby sites and worst at Omø Stålgrunde and Gedser Rev because these sites have shorter data records.

4.2 WA^{SP} analysis

Predictions of the wind resource of specific sites from measured wind data and standard wind climatologies were performed with the 'Wind Atlas Analysis and Application Program' (WA^{SP}) [1] of the European Wind Atlas [11]. This program contains models for the vertical extrapolation of wind data taking into account sheltering of obstacles, surface roughness changes and terrain height variations. For the sites with onsite measurements WA^{SP} was used to develop offshore wind climatologies. Additionally, nearby coastal measurements were utilised wherever available. These climatologies were subsequently used for the estimation of the wind resource and power production at the sites under investigation. For the description of a wind climatology a continuous long term measurement of high quality should ideally be used (since short data sets can give poor Weibull fits). Since the available measurement periods of the offshore and coastal measurements are too short to be representative of a long term average, these were corrected for the deviations of the wind regime of the measurement period from the long term average.

4.3 Correlation method

This method is based on the well-known measure-correlate-predict technique. The methodology involves calculating regression equations for each sector between wind speeds as the reference site and the test site. The regression constants are then used with the whole record at the reference site to generate a longer wind speed time series for the test site. From this an average is calculated and the time series is input to the WA^{SP} model to generate energy density, potential power production for a given

wind turbine and Weibull shape and scale parameters. For the sites examined, the correlations are significant at greater than 95% confidence levels. The level of variance explained by the regression constants is much greater if the intercept is set to 0 and this is also physically reasonable.

Table 1 is a comparison of results for Vindeby (48 m height). All three methods give similar predictions of the long-term wind speed at Vindeby and hence give similar energy and potential power predictions. Using different methods to establish the relationship between the measured time series offshore and a reliable long-term time series helps to reduce the uncertainties in the wind resource prediction at the offshore sites. The Weibull correction method relies on correct fits of the Weibull distribution to the observed wind speed data in each sector. Where WA^{SP} is used with on-site data this also applies. However, WA^{SP} has also been applied using longer time series from nearby sites to reduce this uncertainty. The MCP method typically predicts lower wind speeds than the other two methods; this is most likely due to linear regression of wind speeds. As the distance between the measurement and prediction sites increases the probability of introducing errors into the correlation also increases.

Table 1. Results for 48 m height at Vindeby SMW

Prediction method	Mean wind speed (m/s)	Weibull scale parameter (m/s)	Weibull shape parameter	Mean energy density (W/m ²)	Annual power production (GWh/y)
Weibull	7.9	8.9	2.1	540	4.6
WA ^{SP}	8.1	9.2	2.4	550	4.8
Correlation	7.9	8.9	2.2	540	4.8
Observed	8.1	9.1	2.3	-	-

5. SUMMARY

Meteorological observations from a number of offshore and coastal measurement sites have been carried out to determine wind and turbulence characteristics which will be experienced at planned offshore wind farms in Danish coastal waters. Different methods have been used for this process and the values given are the best estimates based on all results but taking into account the different strengths and weaknesses of each method. Uncertainties associated with the energy predictions range from $\pm 4\%$ at Vindeby, which has the longest and most reliable data record, to $\pm 15\%$ at Omø Stålgunde and Gedser Rev. On-site measurements are not yet available for Horns Rev and Læsø Syd which meant that not all methods could be applied. Wind resources estimates at these sites were made using WA^{SP}.

In addition to the wind resource predictions, new analyses have been conducted on the data sets focussing on meteorology, turbulence, extreme winds and wind and wave interactions. Relationships between wind speed, turbulence and fetch are highly complex. Minimum turbulence intensity offshore is associated with wind speeds of about 12 m/s. At lower wind speeds, stability effects are important while at higher winds speeds wind and wave interactions appear to dominate. On average, turbulence intensity offshore at 48 m height is approximately 0.08 if no coastal effects are present.

However, the effect of the coastal discontinuity persists in wind speed and turbulence characteristics for considerable distances offshore. This distance is estimated here as approximately 40 km although the majority of the adjustment of turbulence appears to occur within 20 km of the coast.

ACKNOWLEDGEMENTS

This research was conducted as part of the European Union Joule Program project 'Cost optimisation of large wind turbines' (contract no. JOR3-CT95-0089) and under the 'Offshore wind resources' project (contract no: UVE J.nr. 51171/96-0040) funded by the Danish Energistyrelsen Udviklings-programmet for Vedvarende Energi. This project was initiated by Jørgen Højstrup at Risø (present affiliation NEG Micon).

We would also like to acknowledge the large contribution to the project by the engineering and technical support staff of the Wind Energy and Atmospheric Physics Department and the Engineering and Mechanics Department at Risø.

REFERENCES

1. Mortensen, N.G., L. Landberg, I. Troen and E.L. Petersen, *Wind Analysis and Application Program (WASP)*, 1993, Risø National Laboratory: Roskilde, Denmark.
2. Garratt, J.R., *The stably stratified internal boundary layer for steady and diurnally varying offshore flow*. Boundary-Layer Meteorology, 1987. 38(4): 369-394.
3. Barthelmie, R.J., M. Courtney, B. Lange, M. Nielsen, A.M. Sempreviva, J. Svenson, F. Olsen and T. Christensen, *Offshore wind resources at Danish measurement sites*, 1998, Risø National Laboratory: Roskilde, Denmark.
4. Barthelmie, R.J., B. Grisogono and S.C. Pryor, *Observations and simulations of diurnal cycles of near-surface wind speeds over land and sea*. Journal of Geophysical Research (Atmospheres), 1996. 101(D16): 21,327-21,337.
5. Charnock, H., *Wind stress on a water surface*. Quarterly Journal of the Royal Meteorological Society, 1955. 81: 639.
6. Barthelmie, R.J., *The effects of atmospheric stability on coastal wind climates*. Meteorological Applications (in press), 1999.
7. Pryor, S.C. and R.J. Barthelmie, *Analysis of the effect of the coastal discontinuity on near-surface flow*. Annales Geophysicae, 1998. 16: 882-888.
8. Lange, B. and J. Højstrup. *The influence of waves on the offshore wind resource*. in 1999 European Wind Energy Conference and Exhibition. 1999. Nice.
9. Højstrup, J., B. Lange, R.J. Barthelmie, A.M.J. Pedersen, F.A. Olsen and J. Svenson, *Offshore wind resources at selected Danish sites*, 1997, Risø National Laboratory: Roskilde, Denmark.
10. Press, W.H., B.P. Flannery, S.A. Teukolsky and W.T. Vetterling, *Numerical Recipes in FORTRAN - The art of scientific computing*. Second ed. 1989: Cambridge University Press. 963pp.
11. Troen, I. and E.L. Petersen, *European Wind Atlas*. 1989, Denmark: Risø National Laboratory. 656pp.

A METHODOLOGY FOR THE PREDICTION OF OFFSHORE WIND ENERGY RESOURCES

S J Watson¹, G M Watson¹, J P Palutikof², T Holt², R J Barthelmie³, J P Coelingh⁴, E J van Zuylen⁴ and J W Cleijne⁵

¹Building R63, Rutherford Appleton Laboratory, Chilton, Didcot, Oxfordshire, OX11 0QX, UK, Tel: +44 1235 446455, Fax: +44 1235 446863, E-mail: sjwatson@casyncl.co.uk, Gillian.Watson@rl.ac.uk

²Climatic Research Unit, University of East Anglia, Norwich, NR4 7TJ, UK, Tel: +44 1603 593647, Fax: +44 1603 507784, E-mail: J.Palutikof@uea.ac.uk, T.Holt@uea.ac.uk

³Dept of Wind Energy and Atmospheric Physics, Risø National Laboratory, DK-4000 Roskilde, Denmark, Tel: +45 46 77 5020, Fax: +45 77 5970, E-mail: R.Barthelmie@risoe.dk

⁴Ecofys Energy and Environment, PO Box 8408, NL-3503 RK Utrecht, The Netherlands, Tel: +31 30 2808 395/396, Fax: +31 30 2808 301, E-mail: J.Coelingh@ecofys.nl, E.vanZuylen@ecofys.nl

⁵Kema Sustainable, Utrechtseweg 310, PO Box 9035, NL-6800 ET Arnhem, The Netherlands, Tel: +31 26 356 6393, Fax: +31 26 445 8279, E-mail: J.W.Cleijne@kema.nl

ABSTRACT

There are increasing constraints on the development of wind power on land. Recently, there has been a move to develop wind power offshore, though the amount of measured wind speed data at potential offshore wind farm sites is sparse. We present a novel methodology for the prediction of offshore wind power resources which is being applied to European Union waters. The first stage is to calculate the geostrophic wind from long-term pressure fields over the sea area of interest. Secondly, the geostrophic wind is transformed to the sea level using WASP, taking account of near shore topography. Finally, these values are corrected for land/sea climatology (stability) effects using an analytical Coastal Discontinuity Model (CDM). These values are further refined using high resolution offshore data at selected sites. The final values are validated against existing offshore datasets. Preliminary results are presented of the geostrophic wind speed validation in European Union waters.

Keywords: Off-shore, Models (Physical), Resources, Boundary Layer

1. INTRODUCTION

For the economic siting of an offshore or onshore wind farm, there needs to be an accurate estimate made beforehand of the average wind speed at the proposed site. In the case of an offshore site, wind speed data are spatially and temporally quite sparse and of variable quality. A methodology has been developed which can produce long term and spatially detailed estimates of the wind speed at offshore sites covering a wide area. The case of European Union offshore areas is taken as an example of the implementation of this methodology. These estimates can then be used to pinpoint areas which are favourable for the siting of a wind farm. At this stage more detailed monitoring can be undertaken to improve the initial estimate.

2. THE METHODOLOGY

2.1 Outline

The methodology for the prediction of offshore wind speeds is based on three basic steps:

1. Interpolate the pressure gradient from a gridded pressure dataset and use this to calculate the geostrophic wind.
2. Apply the linearised flow model WASP to transform the geostrophic wind to the sea surface layer.
3. Apply an analytical Coastal Discontinuity Model to the surface layer values to take account of land/sea climatology.

The final values are 'fine-tuned' using sea surface roughness data inferred from a hindcast wind/wave archive. In addition, the Coastal Discontinuity Model is fine-tuned using both existing offshore mast data and coastal SODAR data.

2.2 Geostrophic wind speed values

Two different datasets have been used to illustrate the implementation of this methodology:

- The six-hourly NCEP 2.50°×2.50° dataset covering the period 1975-present.
- The daily mean sea level pressure (12-hourly from 1962) 50° latitude × 50° longitude dataset for the Northern Hemisphere covering the period 1899-present obtained from the US National Center for Atmospheric Research (NCAR).

The southerly and westerly components of the pressure gradient are interpolated for the two datasets onto a 0.50°×0.50° grid using a bi-cubic polynomial interpolation. These values are then converted to the components of the geostrophic wind thus:

$$U_g = -\frac{1}{f_c \rho} \frac{\partial p}{\partial y} \quad (1)$$

$$V_g = +\frac{1}{f_c \rho} \frac{\partial p}{\partial x} \quad (2)$$

where f_c is the local Coriolis parameter at latitude ϕ given by:

$$f_c = 2\Omega \sin \phi \quad (3)$$

U_g and V_g are the westerly and southerly components of the geostrophic wind speed, respectively, Ω is the Earth's angular velocity ($7.29 \times 10^{-5} \text{ rad s}^{-1}$), ρ is the density of air, $\partial p / \partial x$ is the component of the pressure gradient from south to north and $\partial p / \partial y$ is the pressure gradient from west to east.

2.3 WASP transformation

The linearised flow model WASP [1] is used to transform the geostrophic wind speed values to the surface layer using the geostrophic drag law, the standard stability conditions over sea, and roughness values appropriate to the sea (and land, where the grid point is sufficiently close to the coast).

2.4 Coastal Discontinuity Model (CDM)

For the WASP transformed values in the coastal areas, the Coastal Discontinuity Model (CDM) is applied. This uses analytical equations for the development of the Internal Boundary Layer (IBL) and is dependent on roughness and stability changes as the wind blows from land to sea or *vice versa*. The CDM is based on two models: the Monin-Obukhov Length anaLYsis (MOLLY) model (which uses routines from [2]) and a three layer IBL model. MOLLY estimates the Monin-Obukhov (MO) length from routine meteorological measurements. Temperature values from the NCEP dataset are also used to initialise this model. Average MO lengths for different coastal regions can be inferred from the existing offshore datasets. MOLLY and the three layer IBL model are combined to correct the WASP transformed wind speed values at grid points in the near-shore areas. The three layer IBL is an extension of a two layer IBL [3].

3. APPLICATION OF METHODOLOGY TO EUROPEAN WATERS

3.1 Introduction

To illustrate the application of the methodology described above, it is being tested as part of an EU-funded study over the sea areas surrounding the coast of Europe. This paper shows some preliminary results illustrating the accuracy of calculating the geostrophic wind using the long-term pressure fields. Validations have been made against radiosonde data. The refinement and 'fine-tuning' of the methodology are also described below.

3.2 The studied European sea area

Figure 1 shows a map of the sea area where the methodology is being applied. The area stretches from 15°W to 30°E and 30°N to 70°N . This covers the major sea areas bordering the European Union countries, namely the North Sea, the Baltic, the Mediterranean and the eastern North Atlantic.

3.3 Validation of the geostrophic wind speed values

Figure 1 also shows isobars plotted for a typical 12-hourly record from the $5^\circ \times 5^\circ$ Northern Hemisphere

NCAR sea level pressure dataset. The pressure gradient for each record in this and the NCEP dataset was interpolated onto a $0.5^\circ \times 0.5^\circ$ grid covering the sea area shown for the period 1985-1997. The geostrophic wind speed for both datasets was calculated using Eqs. 1 and 2.

One possible way of validating the accuracy of these interpolated values is to compare them with radiosonde data. Therefore, in order to assess the accuracy of these values, the $5^\circ \times 5^\circ$ Northern Hemisphere dataset was interpolated to the site of seven radiosonde stations covering the sea areas of interest. The locations of these sites are shown in Figure 2. It should be noted that there are few radiosonde stations actually within the sea areas of interest and the stations chosen are located on islands within these areas, with the exception of Ekofisk which is on an oil platform.

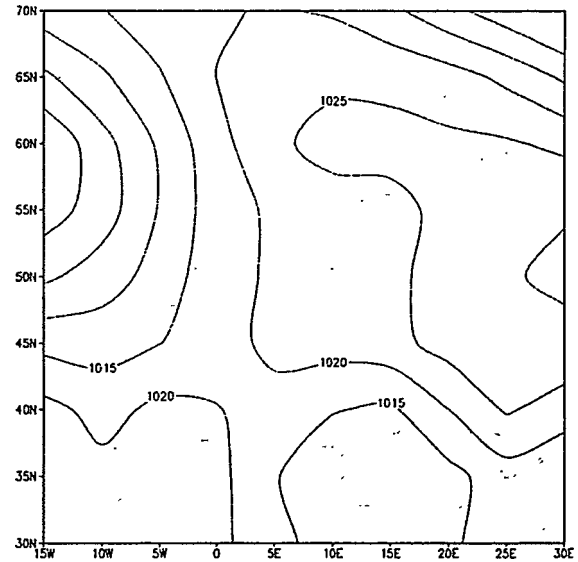


Figure 1: Map showing the European sea area where the methodology is applied.

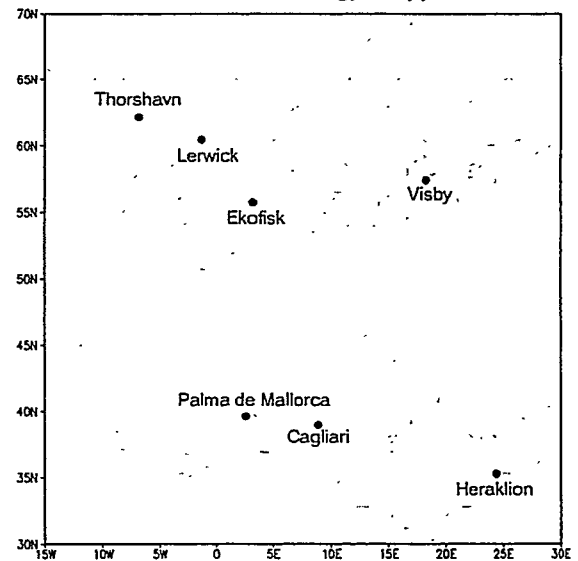


Figure 2: Locations of the seven radiosonde stations used in the geostrophic wind speed validation.

The mean geostrophic wind speed at the seven sites was inferred by averaging the data from each radiosonde ascent between 800mb and 900mb. Data for the seven radiosonde stations were available between 1990 and 1999, though for some of the sites the data are patchy. Ascents are made normally twice a day, though this varies from station to station. Table 1 shows the results of the validation. In this table, the mean geostrophic wind speed inferred from the radiosonde data and the percentage difference between this value and that calculated using the NCAR sea level pressure dataset are shown. The validation is made only for those concurrent data which are present in both datasets.

It can be seen that the methodology gives a good estimate of the inferred geostrophic wind speed for the stations in the North Atlantic, the North Sea and the Baltic Sea, but a relatively poor estimate for the stations in the Mediterranean. It is likely that surface temperature effects are going to be more important for the Mediterranean stations than for those in the Northern European sea-areas. What the results seem to show is that temperature effects in the Mediterranean are persisting even at the 800mb-900mb height and the inferred wind speed at this height cannot simply be modelled using Eqs. 1 and 2.

Table 1: Validation of the estimated geostrophic wind speed against data from seven radiosonde stations.

Data source		Radiosonde	NCAR slp
Station	No. obs.	Mean geostrophic wind speed (ms^{-1})	Percentage difference
<i>North Atlantic/North Sea/Baltic Sea Stations</i>			
Thorshavn	5508	12.5	-1%
Lerwick	5707	12.5	-1%
Ekofisk	2516	11.1	-2%
Visby	3439	10.6	-4%
<i>Mediterranean stations</i>			
Palma de Mallorca	5304	7.1	-17%
Cagliari	5323	8.6	-27%
Heraklion	1940	7.3	+12%

Table 2: Validation of the estimated geostrophic wind speed by season at Visby and Palma de Mallorca.

Data source		Radiosonde	NCAR slp
Season		Mean geostrophic wind speed (ms^{-1})	Percentage difference
<i>Visby</i>			
Winter		13.3	-1%
Spring		10.0	-4%
Summer		8.4	-15%
Autumn		10.3	-1%
<i>Palma de Mallorca</i>			
Winter		8.2	-4%
Spring		7.1	-16%
Summer		5.6	-25%
Autumn		7.7	-24%

The effect of temperature is also confirmed by the results in Table 2. This shows a comparison of the geostrophic wind speed inferred from the radiosonde data with that calculated using the NCAR sea level pressure data for the sites of Visby and Palma de Mallorca broken down by season, where Winter is December, January and February, Spring is March, April and May, Summer is June, July and August and Autumn is September, October and November. It can be seen that the best estimate is during the winter months for both stations whereas the worst estimate is during the summer months.

These findings are preliminary and further research will need to be done to investigate how surface temperature affects the coupling of the geostrophic wind speed to the ground level particularly if accurate estimates of the long term offshore wind speed are to be made in Mediterranean areas.

3.4 Application of WASP

The WASP model is being used to transform the geostrophic wind speed values to the surface layer at several heights above mean sea level between 10m and 150m in order to cover the expected hub height of wind turbines which are likely to be sited offshore within the coming years. For each grid point, a WASP map of size 20km×20km is created centred on the grid-point. Where the grid point is situated far offshore (>10km), a constant roughness value of 0.0001m is assumed. Where the grid-point is <10km then a value of 0.0001m is assumed over the sea area and 0.03m over land. The coastline is defined using the Digital Chart of the World with a scale of 1:1,000,000.

3.5 Application of the CDM

The CDM is being refined in the northern European coastal areas. This is being done using existing coastal/offshore data from the Danish sites of Horns Fyrskib, Anholt, Risø, Sprogø, Kegnæs, Rødsand, Omo, Tystofte and Gedser. In addition, data are to be collected using a SODAR device off the coast of East Anglia, UK and off the Dutch coast for model development.

3.6 Refinement/validation of the final values

The final step in the methodology as applied to the European coastal waters is data refinement and validation. There exist certain datasets of offshore data with varying degrees of quality. These include ship-borne data, hindcast model archives, offshore platform data, SODAR data and radiosonde data. These datasets are being evaluated for use in model refinement/validation. As discussed above, the radiosonde data has been used to validate the geostrophic wind speed values. The hindcast model data (available from the UK Meteorological Office) provides gridded data of wind speed and wave height. The wave height data is used to infer surface roughness variability which is then used to modify the WASP estimate. Data from several offshore masts that have been installed for the purposes of assessing wind power potential are also being used for validation.

4. VARIABILITY OF THE RESOURCE

4.1 Long-term variability

The application of the methodology is primarily to produce an estimate of the wind speed at each grid point averaged over the period 1985-1997.

However, an important aspect of the methodology as applied to European Union waters relates to how the average wind speed at each grid point is expected to vary over several decades. The fact that the 50°50' Northern Hemisphere sea level pressure dataset extends back to 1899 gives an ideal opportunity to assess the long-term variability. This dataset is used to calculate the expected uncertainty on the values at each grid point due to long term variability. Use of this dataset has been made for the assessment of long term variability on land [4.5].

4.2 Short-term variability

An understanding of the variation in the wind speed on a diurnal basis is important for the effective integration of wind power into the mainland grid.

The existing offshore mast data, hindcast data and SODAR data are used to assess the diurnal variability of offshore wind speed at several locations. These data are used to give average diurnal variations in wind speed and stability climate for different European sea-areas. In addition, this high temporal resolution data of wind speed and wave height is used to assess the joint potential wind and wave loading on an offshore structure. This information can then be used to highlight areas where siting might be hazardous from a structural viewpoint.

5. CASE STUDIES

As part of the application of the methodology for EU sea areas a case study of two Danish offshore sites and a Dutch offshore site is being undertaken. The refined wind speed values are to be compared with measurements made at masts at Horns Rev and the Kattegat in Danish waters and as part of the proposed Dutch 100MW offshore wind farm. The results of this validation will be presented in a future paper.

6. CONCLUSIONS

This paper has presented an outline of a methodology to assess the wind power resource in offshore waters. The methodology can be used to pinpoint promising sites for wind farms after which more detailed monitoring can be undertaken.

Some preliminary results have been described concerning the implementation of the methodology in European Union sea-areas. Specifically, a validation of the geostrophic wind speed calculations has been made using observed radiosonde data. This validation has shown that temperature effects can still be quite important at the 800mb-900mb level. This effect is seen in the Mediterranean data and also during the summer months in the Northern sea-area data. Account will need to be taken

of this effect in order to produce accurate surface level wind speed values particularly in the Mediterranean areas.

A future paper will present case studies validating the final refined grid point estimates of wind speed at potential wind farm sites.

It is intended that once the implementation has been completed, the grid point values will be packaged as a database with a Geographical Information System (GIS) interface for easy retrieval of the data by potential offshore wind farm developers.

7. ACKNOWLEDGEMENTS

The authors would like to acknowledge the support of the Directorate General XII of the European Commission who are providing part funding for this project under the JOULE programme, contract JOR3-CT98-0286, project POWER (Predicting Offshore Wind Energy Resources).

8. REFERENCES

- [1] N G Mortensen, L Landberg, I Troen and E L Petersen (1993) 'Wind Atlas Analysis and Application Program (WASP) Vol 1: Getting Started'. Riso National Laboratory user guide: Riso-I-666(EN)(v.1).
- [2] A C M Beljaars, A A M Holtslag and R M van Westrhenen (1989) 'Description of a software library for the calculation of surface fluxes'. KNMI, De Bilt, Netherlands.
- [3] H Bergstrom, P-E Johansson and A-S Smedman (1988) 'A study of wind speed modification and internal boundary-layer height in a coastal region', *Boundary-Layer Meteorology* 42 (4), 313-335.
- [4] J P Palutikof, X Guo and J A Halliday (1992) 'Climate Variability on the UK Wind Resource', *J. Wind Eng. Ind. Aerodyn.* 39, 243-249.
- [5] J C Woods and S J Watson (1996) 'Improving techniques for statistical and physical modelling of wind resource in complex terrain'. Annex II of the final report to the European Commission for project JOU2-CT93-0370.

MODELIZATION OF A LARGE WIND FARM, CONSIDERING THE MODIFICATION OF THE ATMOSPHERIC BOUNDARY LAYER.

A. Crespo, S. Frandsen*, R. Gómez-Elvira, S. E. Larsen*
Mecánica de Fluidos, E.T.S.I. Industriales, Universidad Politécnica de Madrid (UPM)
José Gutiérrez Abascal, 2 -28006 Madrid, Spain.
Tel.3491 3363152 , Fax 34913363006, crespo@enerflu.upm.es
*Riso National Laboratory
DK 4000 Roskilde Denmark

ABSTRACT: A method is presented to adapt existing models of wind farms to very large ones that may affect the whole planetary boundary layer. An internal boundary layer is considered that starts developing at the leading edge of the farm until it reaches, sufficiently far downstream, the top of the planetary boundary layer, and a new equilibrium region is reached. The wind farm is simulated by an artificial roughness that is function of the turbine spacing, drag and height. From this model the flow conditions are calculated at a certain reference height and then are used as boundary conditions for a numerical code used to model a wind farm. Three-dimensional effects are considered by applying appropriate conditions at the sides of the farm. Calculations are carried out to estimate the energy production in large wind farms, and it is found that additional losses due to modification of the planetary boundary layer may be of importance for wind farms of size larger than about 100 km.

Keywords: Wind Farms, Boundary Layer, Wakes, Resources, Off-shore.

1. INTRODUCTION.

Large wind farms, may affect significantly the whole planetary boundary layer. It is the purpose of this work to take into account this large perturbation and adapt existing wind farm models, in particular the UPMPARK code, to this new situation. UPMPARK is described in Crespo et al. [1] and [2]. It solves the Navier Stokes equations for the complete park assuming that the equations are parabolic in the unperturbed wind direction, and uses the k-ε method for turbulence closure. The basic atmospheric flow in which the wakes diffuse is described by means of the friction velocity, the surface roughness of the ground, and the Monin-Obukhov length associated to the atmospheric stability. For off-shore wind farms the roughness is not an independent datum, and it has to be estimated from the wind characteristics by means of Chamock's relation, or a similar one. In this work we integrate the variations of the ambient conditions, as given by an internal boundary layer model, in UPMPARK. This integration is facilitated by the possibility of UPMPARK of considering moderate changes in orography, that, in our case, will correspond to changes in surface roughness and turbulent friction velocity.

UPMPARK uses boundary conditions imposed by an ambient flow that, in a real situation, has been perturbed by the wind farm itself, and consequently these conditions are not known a priori. The correct answer to this mathematical problem would be to locate the boundaries in a region far enough so that the flow will not be affected by the park, this may be above the planetary boundary layer. This procedure will create a very large domain in which the computing requirements would be very large. An alternative method is proposed in this work.

Emeis and Frandsen [3], show that the effect of a wind farm at a certain height about hub height, can be simulated by a terrain whose artificial roughness is calculated analytically as a function of real terrain roughness, hub height, turbine spacing and drag coefficient of the machines.

It is assumed that, at the leading part of the wind farm, an internal boundary layer starts, which separates the two regions with different roughness, and grows downstream

until it reaches the height of the planetary boundary layer corresponding to the upstream roughness. Then, there is a transition region where the internal boundary layer grows until it reaches the height of the planetary boundary layer corresponding to the artificial roughness created by the turbines, see figure 1.

The characteristics of this internal boundary layer are calculated, and, in particular, the wind conditions at a certain reference height, which are used as boundary conditions for UPMPARK, are obtained. Then, UPMPARK gives the flow characteristics inside the farm and the output of the wind turbines.

The perturbation created by the wind-park also grows horizontally on its sides. This three dimensional effect has also to be taken into account. However, this lateral growth is much slower than the vertical one, and can be handled more easily by displacing laterally the boundaries. Corrections due to the three-dimensionality of the park have also to be introduced in the wind characteristics calculated at the reference height.

2. EQUIVALENT SURFACE ROUGHNESS OF THE WIND PARK.

Frandsen [4] and Emeis and Frandsen [3] propose that in the terrain occupied by an infinitely large wind farm, the flow corresponding to an equilibrium planetary boundary layer is established, in which there is an artificial surface roughness given by

$$z_{02} = h \cdot \exp \left(\frac{\kappa}{\sqrt{c_t + \kappa^2 I_{01}^2}} \right) \quad (1)$$

where h is the turbine height, $\kappa=0.4$, c_t is the drag coefficient per unit area of the ground, and I_{01} the ambient turbulence intensity. Subscript 1 means upstream conditions, in the region not perturbed by the internal boundary layer, subscript

2 means conditions inside the internal boundary layer. For c_i the following expression is given:

$$c_i = \left(\frac{C_T}{8s^2} \right) \quad (2)$$

where C_T is the thrust coefficient of the turbine, and s is the non-dimensional separation of wind turbines, defined as:

$$s = \sqrt{\frac{A}{D^2}} \quad (3)$$

where A is the area occupied by each machine (total area divided by the number of machines), and D the turbine diameter. For I_0 the following expression based on equilibrium neutral flow is given:

$$I_0 = \frac{1}{\log(h/z_{01})} \quad (4)$$

where z_{01} is the real roughness of the ground.

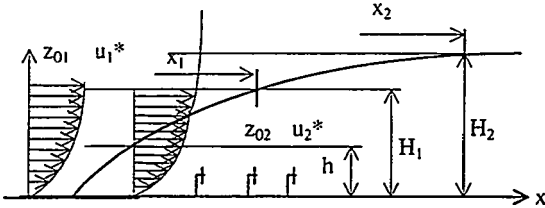


Figure 1. Schematic showing the growth of the internal boundary layer created by the wind farm.

3. EVOLUTION OF THE BIDIMENSIONAL INTERNAL BOUNDARY LAYER.

In figure 1 is shown schematically the form of the internal boundary layer (IBL). The model to be used has been proposed by Sempreviva et al. [5]. The height of the internal boundary layer is h ; for $z < h$ there is a flow corresponding to the artificial surface roughness z_{02} , and for $z > h$ the flow corresponds to the actual surface roughness, z_{01} . The velocity is given by:

$$u = 2.5 u_{0i}^* \left(\log \left(\frac{z}{z_{0i}} \right) - 2 \frac{z}{H_i} \right), \text{ where } i=1,2 \quad (5)$$

where subscript zero means ground conditions, subscripts $i=1,2$ correspond to conditions outside and inside the IBL respectively. u_{0i}^* is the turbulent friction velocity, z the height above ground and H_i the scale height of the planetary boundary layer (PBL), given by:

$$H_i = \frac{u_{0i}^*}{f} \quad (6)$$

and f is the Coriolis parameter. The standard deviation of the vertical wind speed is given by:

$$\sigma_w = \sigma_{w0} \left(1 - \frac{z}{H_i} \right)^2 \quad (7)$$

The height of the internal boundary layer is given by:

$$\frac{dh}{dx} = A \frac{\sigma_{w2}(h)}{u(h)} \quad (8)$$

where A is a constant. Integrating equation (8), with the condition $h=0$ for $x=0$, and from equations (5) to (7), it is obtained that:

$$c \frac{x}{z_{02}} = \frac{h}{1 - \frac{h}{H_2}} \left(\log \left(\frac{h}{z_{02}} \right) - 1 \right) - y \left(\frac{h}{H_2} \right) \quad (9)$$

where $c = A \sigma_{w0} / (2.5 u_{01}^*)$ is a constant supposed to be equal to 0.9 and $y(h/H_2)$ is a function that can be approximated by h/H_2 .

The values of u_{01}^* and z_{01} are data known from the upstream flow. The value of z_{02} is given by equation (1). If the IBL has not reached the height of the PBL, $h < H_1$, the value of u_{02}^* is obtained from equating the velocities at $z=h$, and we get:

$$u_{02}^* = u_{01}^* \frac{\log \frac{h}{z_{01}} - 2 \frac{h}{H_1}}{\log \frac{h}{z_{02}} - 2 \frac{h}{H_2}}, \text{ for } h < H_1, \quad (10)$$

where H_2 also depends on u_{02}^* as indicated in equation (6). According to this, equation (9), obtained assuming that H_2 is constant, is not correct, however, this is a small error, because H_2 varies very slowly.

In the transition region, $H_1 < h < H_2$, it has to be considered that the surface wind has turned to approach the drag law. Under equilibrium conditions, the surface wind turns an angle α to reach geostrophic wind conditions as $z \rightarrow H$, which are given by the following expressions:

$$U_G = 2.5 u_{01}^* \left(\log \left(\frac{H}{z_{01}} \right) - 2 \right) \quad (11)$$

$$V_G = -1/2 u_{01}^* \quad (12)$$

$$G = \sqrt{U_G^2 + V_G^2} \quad (13)$$

$$\sin \alpha = -\frac{V_G}{G} \quad (14)$$

Sempreviva et al. (1990) assume that in the transition region the value of G calculated with conditions in region 2 is constant, and give for u_{02}^*

$$u^*_{02} = u^*_{01} \frac{\cos \alpha}{\cos \alpha_1} \frac{\log \frac{H_1}{z_{01}} - 2}{\log \frac{h}{z_{02}} - 2 \frac{h}{H_2}}, \text{ for } H_2 > h > H_1$$

Where

$$\sin \alpha_1 = -12 H_1 \frac{f}{G},$$

$$\sin \alpha = -12 h \frac{f}{G}, \text{ for } H_2 > h > H_1$$

It should be noted that in the previous calculations H_2 decreases with x , and tends to a constant value, obtained from equations (6) and (11) to (13), with G equal to its upstream value.

In the following application, the upstream roughness is $z_{01}=0,001$ m, the incident velocity 10 m/s at hub height, $h_1=55$ m; and $f=0,00012$ 1/s. Then, $u^*_{01}=0,366$ m/s, the geostrophic wind is $G=12,6$ m/s, the PBL scale height $H_1=3054$ m, and the turning angle $\alpha=20^\circ$. For a thrust coefficient $C_T=0,7$, and a non-dimensional spacing of $s=6$, the equivalent roughness is $z_{02}=1,501$ m, the turbulent friction velocity will tend to $u^*_{02}=0,65$ m/s, the PBL scale height to $H_2=5381$ m, and the turning angle to $\alpha_2=38^\circ$. The downstream distance for which $h=H_1$ is $x_1=42$ km, and $h=0,95H_2$ for $x_2=74$ km. For distances larger than 74 km, the flow over the wind farm would be in equilibrium, u^*_{02} will be uniform, and the velocity at hub height will be $2.5u^*_{02}\log(h/z_{02})=5.84$ m/s, very small compared to the 10 m/s upstream.

4. APPLICATION TO THE MODELIZATION OF A LARGE WIND FARM.

The Rodsand large wind farm, described in detail in Crespo et al. [6], has been considered for application of this model. It has 384 turbines of 1.5 Mw rated power each. The design speed of the machine is 14 m/s and its cut in velocity is 5 m/s. The maximum thrust coefficient is 0,9 for 5 m/s and decreases non-linearly to 0,3 for 20 m/s. Length and width of the wind farm are 13 km and 6 km, respectively. The maximum length of the park is smaller than that required to make $h=H_1$. Typical characteristics of the incident wind have been indicated previously. Using the model of the previous section, the velocity has been calculated at a certain reference height, $h_{ref}=400$ m, appropriate to apply the boundary conditions of UPMPARK. This velocity as function of downstream distance is represented in figure 2. The three dimensional character of the problem is taken into account by imposing appropriate boundary conditions on the sides, where it is assumed that the flow has not been perturbed by the wind park, and the flow corresponds to the unperturbed one upstream of the wind park.

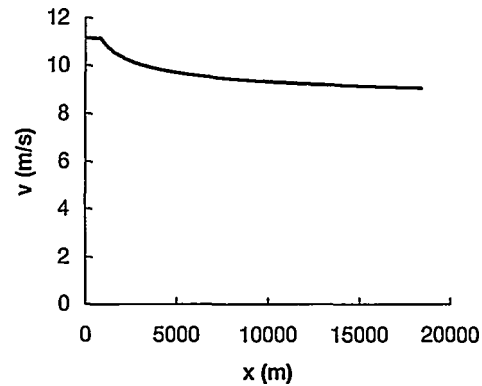


Figure 2. Velocity at reference height, to use as boundary condition for UPMPARK; as function of downstream distance.

In figure 3 is presented the power produced by the wind farm, for a fixed wind direction and different velocities. It is compared with the result obtained assuming that the flow has not been perturbed by the wind farm at $h_{ref}=400$ m, and with the power produced without interference effects at all (which will also be the power curve of the turbine multiplied by the number of turbines, 384). It can be observed that there is a decrease of 15% of the power produced assuming constant conditions at the reference height, and an additional 5% when the IBL effect is considered.

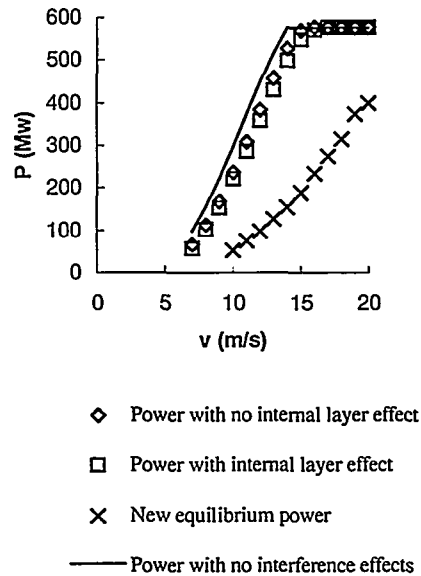


Figure 3 Power produced by a large wind farm for different wind velocities, and fixed wind direction. Comparison with power produced without interference, with calculations carried out assuming that the wind at the reference height has not been perturbed, and with the production if the modelled farm were a section of an infinitely large wind farm immersed in an equilibrium region

In figure 3, is also presented the production of a section of the size of Rodsand of an infinitely large wind farm

immersed in an equilibrium region, it can be observed that the power production is then drastically reduced.

The boundary condition at $h_{ref}=400\text{m}$ is only for the velocity, and the turbulence field is expected to be obtained from the UPMPARK calculations. In figure 4 is presented the evolution of the local turbulence intensity at hub height, $\sigma_u(h_t)/u(h_t)$, as the fetch increases and it is compared with the prediction by Frandsen [4]:

$$I = \sqrt{I_0^2 + 2.5^2 c_1} \quad (15)$$

It can be seen that in spite of the small downstream distances, so that conditions are far from equilibrium, there is a tendency for the two values to become equal.

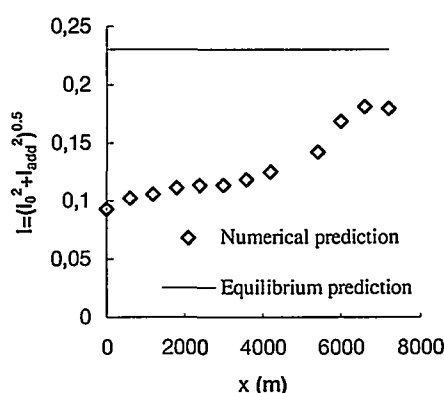


Figure 4 Local turbulence intensity at hub height, as function of the distance from the leading edge of the wind farm. Comparison with analytical prediction for equilibrium conditions in an infinitely large wind farm.

CONCLUSIONS

A method to calculate the performance of very large wind farms, such that they can change the planetary boundary layer is presented. This method has been applied to offshore wind farms of 10 to 15 km length, and whereas with the classical approach the interference effects will reduce the power produced by an order of 15 %, this new approach will introduce an additional reduction of the order of 5 %, or less. However, for very large wind farms (with lengths of the order of 100 km), that may perturb the whole planetary boundary layer, more drastic reductions, of the order of 50 %, may appear, particularly in the downstream rows.

The simple expression (16), proposed by Frandsen [4], can be used to calculate local turbulence intensity for locations deeply immersed in a large wind farm, even for conditions far from equilibrium.

ACKNOWLEDGMENTS

This work has been supported by the EU through contract JOR3-CT95-0089 of the JOULE III programme.

REFERENCES

- [1] Crespo, A., Chacón, L., Hernández, J., Manuel, F. and Grau, J. C. "UPMPARK a parabolic 3D code to model wind farms". Proceedings of EWEC' 94 pp. 454-459 (1994).
- [2] Crespo, A., Chacón, L., Hernández, J., Manuel, F., and Gómez-Elvira, R. "Modelization of Offshore Wind Farms. Effect of the Surface Roughness of the Sea". Proceedings of EUWEC' 96. pp. 644, 647 (1996).
- [3] Emeis, S. and Frandsen, S. "Reduction of horizontal wind speed in a boundary layer with obstacles" Boundary Layer Meteor., 64, 297-305, 1992.
- [4] Frandsen, S. "On the wind speed reduction in the center of large clusters of wind turbines" Journal of Wind Engineering and Industrial Aerodynamics, 39, 251-265. 1992.
- [5] Sempreviva, A. M.; Larsen, S.E.; Mortensen, N.G. and Troen, I. "Roughness change effects for small and large fetches". Risø report m-2749, October, 1988.
- [6] Crespo, A., Hernández, J., and Frandsen, S. "Survey of modelling methods for wind-turbine wakes and wind farms" accepted for publication in Wind Engineering, 1999.

STANDARDS FOR MEASUREMENTS AND TESTING OF WIND TURBINE POWER QUALITY

Poul Sørensen, Risø National Laboratory, P.O.Box 49, DK-4000 Roskilde, Denmark.
 Gert Gerdes, Rainer Klosse and Fritz Santjer, DEWI, Ebertstrasse 96, D-26382 Wilhelmshaven, Germany.
 Niel Robertson and Willie Davy, NEL, East Kilbride, UK-Glasgow G75 0QU, United Kingdom.
 Maria Koulouvari and Evangelis Morfiadakis, CRES, 19th km Marathonos Ave., GR-19009 Pikermi, Greece.
 Åke Larsson, Chalmers University of Technology, S-412 96 Göteborg, Sweden.

ABSTRACT: The present paper describes the work done in power quality subtask of the project "European Wind Turbine Testing Procedure Developments" funded by the EU SMT program. The objective of the power quality subtask has been to make analyses and new recommendation(s) for the standardisation of measurement and verification of wind turbine power quality. The work has been organised in three major activities.

The first activity has been to propose measurement procedures and to verify existing and new measurement procedures. This activity has also involved a comparison of the measurements and data processing of the participating partners.

The second activity has been to investigate the influence of terrain, grid properties and wind farm summation on the power quality of wind turbines with constant rotor speed.

The third activity has been to investigate the influence of terrain, grid properties and wind farm summation on the power quality of wind turbines with variable rotor speed.

Keywords: Power Quality, Standards, Electrical System, Wind Farm.

1 INTRODUCTION

The increased size of standard grid connected wind turbines and the utilisation of wind turbines in larger scales has caused an increasing influence of wind turbines on voltage quality of the power system.

Methods to measure and quantify the power quality of wind turbines were early developed on national level, but the need for common reference across the borders has initiated international standardisation work in the field.

The EU project "European Wind Turbine Standards" (EWTS) [1] funded by the Joule II Programme defined an "Electrical Power Quality Measurement Procedure" in February 1996, based mainly on the German standard. The EWTS procedure formed the basis for the Measnet measurement procedure on "Power Quality of Wind Turbines"[2].

IEC initiated the standardisation on power quality for wind turbines in 1995 as a part of the wind turbine standardisation in TC88, and ultimo 1998 IEC issued a draft IEC-61400-21 standard for "Power Quality Requirements for Grid Connected Wind Turbines"[3].

2 MEASUREMENT PROCEDURES

To verify the measurement procedures, all partners have measured power quality characteristics simultaneously on a 600 kW Bonus wind turbine in Hagshaw Hill wind farm in Scotland 13 - 17 October.

The power quality characteristics that were measured were reactive power, power variations, flicker, transients and harmonics. Both Measnet and IEC definitions have been applied.

2.1 Reactive power

The measured reactive power is shown vs. active power in Figure 1. Only data from a single hour is included, to avoid the influence of different voltage levels on the reactive power.

The figure reveals that Risø measures slightly lower values of consumed reactive power than DEWI and CRES. Analysis of the differences showed that the measurements were within the 2 % required in the Measnet procedure, and the requirements of the draft IEC61400-21.

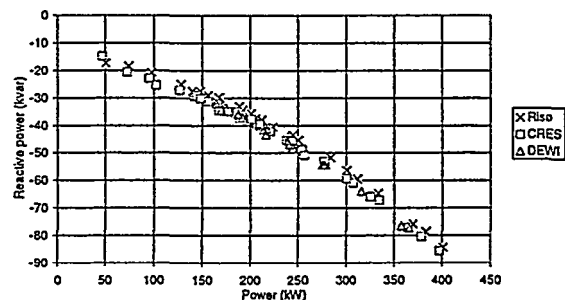


Figure 1. One minute mean values of reactive power vs. active power measured in the same period by Risø, DEWI and CRES.

2.2 Power variations

IEC and Measnet prescribes measurement of maximum instantaneous values of power as a characteristic for the power variations. Besides, a power variability is defined in the Measnet procedure as the relative standard deviation of the power.

The measured standard deviations of the power have shown to be very close. The maximum values show more deviations in the results. One reason for this has been the sampling rate. In Hagshaw Hill, CRES measured power with 20-25 samples per minute, which showed to be too little to measure the power peaks, because some of the power fluctuations are much faster.

2.3 Flicker simulation procedure

Flicker is defined in IEC 868 [4] and [5] to quantify the annoyance in the illumination from lamps. This

annoyance depends on the voltage fluctuations at the consumers.

The voltage fluctuations at the consumers depend on fluctuating loads as well as fluctuating production in the power system. The power from wind turbines is fluctuating, and therefore the wind turbines contribute to the voltage fluctuations on the grid.

IEC 61000-3-7 [6] states a method to plan the voltage flicker level in the MV and HV level of a power system, based on the emission level of the individual loads on the system. The emission level of a fluctuating load is defined as the flicker level, which would be produced in the power system if no other fluctuating loads were present.

Measurements of power quality are done on real grids with other fluctuating loads. To eliminate the influence of the fluctuations of the other loads, a method has been developed to simulate the voltage, which would be on a power system with no other fluctuating loads.

The voltage is simulated as $u_{fic}(t)$ on the fictitious reference grid seen in Figure 2.

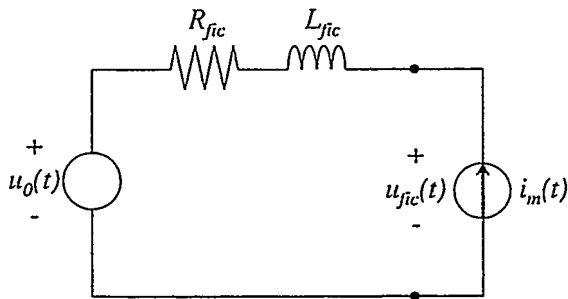


Figure 2. Simulation of voltage which would be on a power system with no other fluctuating loads.

The fictitious grid is represented by an ideal phase to neutral voltage source $u_0(t)$ and a grid impedance given as a resistance R_{fic} in series with an inductance L_{fic} . The wind turbine is represented by the current generator $i_m(t)$, which is the measured instantaneous value of the phase current.

With this simple model, the fluctuating voltage $u_{fic}(t)$ in the power system is given as

$$u_{fic}(t) = u_0(t) + R_{fic} \cdot i_m(t) + L_{fic} \cdot \frac{di_m(t)}{dt}$$

$u_{fic}(t)$ is then used as input to a voltage flicker algorithm as described in IEC 868.

2.4 Flicker during continuous operation

Table 1 shows measurements of flicker short term values with continuous operation of the Bonus 600 kW wind turbine in Hagshaw Hill. The measurements were synchronised manually, i.e. within 1-2 seconds.

Table 1. Simultaneously measured flicker Pst with short circuit ratio 20, grid impedance angles Ψ_k

Me. #	Ψ_k	CRES	DEWI	NEL	Risø
1	30	0.185	0.184	0.169	0.191
2	50	0.121	0.129	0.116	0.138
3	70	-	0.042	-	0.053
	85	-	0.025	-	0.041
4	70	0.074	0.060	0.074	-

Risø used active and reactive power measurements to predict the flicker level with a power based method described in [7], CRES and NEL used a Voltech power analyser with built in current flicker software, and DEWI used own software to simulate the flicker.

This and other results show that flickermeters have a minimum Pst value due to the binning of the instantaneous flicker level in classes. The Voltech power analyser have a minimum Pst value of 0.074, even though it uses a more detailed binning than required in IEC 868.

Consequently, a weak reference grid (i.e. low short circuit power) shall be selected for the reference calculations. If a too strong grid is selected then the calculated flicker value will be the minimum value of the instrument. Using this Pst value to estimate Pst on weaker grids will only give a scaled minimum value.

2.5 Transients during switching

Wind turbines typically generate transient currents during cut-in and cut-out and switching between generators.

In the EWTS procedure, the transients were characterised by current spike factors, i.e. the ratio between the maximum RMS value of the current and the rated current.

In the Measnet procedure, the current spike factor was supplemented with a grid dependent switching factor, which can be used to predict the maximum voltage variation, taking into account the grid impedance angle.

The definitions in the draft IEC 61400-21 aim to specify characteristics, which can be used to assess the voltage fluctuations according to IEC 61000-3-7 [6]. Consequently, the IEC draft has omitted the current spike factor, but defines a voltage change factor almost similar to Measnets grid dependent switching factor. Moreover, the draft IEC 61400-21 defines a flicker step factor which can be used to predict the flicker influence of the switching operation.

A set of reference measurements logged by DEWI in Hagshaw Hill have been used to compare the calculation routines for flicker. The results of the calculated flicker step factors for the cut-in operation are shown in Figure 3.

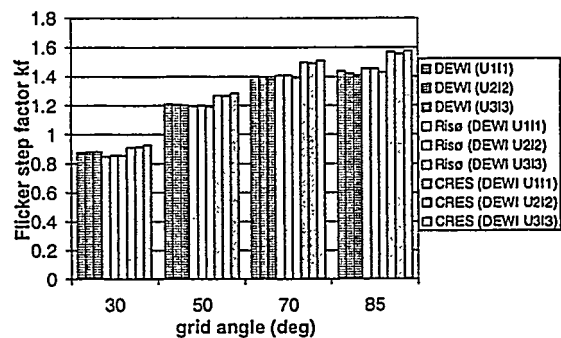


Figure 3. Comparison of calculated flicker step factors k_f during cut-in.

2.6 Harmonics

The harmonic measurements in Hagshaw Hill have also been compared. Generally, the harmonic emission was very low, because the wind turbines are not equipped with power electronics for power conversion. However,

the comparisons have shown that the measurements and calculation software of the partners predict harmonics within the 0.1 pct. of rated current which is required in the draft IEC 61400-21.

3 CONSTANT SPEED WIND TURBINES.

The power quality measurements in Hagshaw Hill have been compared to measurements on the same type of 600 kW Bonus wind turbine in Gudum in Denmark. The wind turbine is stall regulated with one rotor speed.

The main difference between the two sites is the terrain. The Hagshaw Hill wind farm is sited in complex terrain, whereas the Gudum wind turbines are sited in a more flat terrain. Another difference appeared to be that the voltage level in Hagshaw Hill is higher than in Gudum.

3.1 Reactive power

Figure 4 shows 10 min mean values of the reactive power vs active power measured by Risø with the same power transducers in Hagshaw Hill and Gudum.

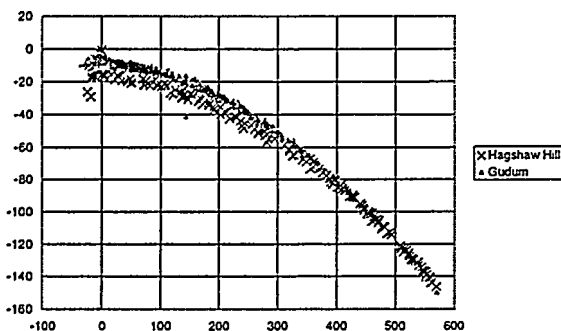


Figure 4. The reactive power consumption of the Bonus 600 kW wind turbine in Hagshaw Hill (Scotland) and Gudum (Denmark)

The analysis showed that the deviations in reactive power are due to a combination of different effects. First, the difference in reactive power consumption at low power levels is most likely due to deviations in the capacities in the capacitor banks. Secondly, the reactive power consumption increases more with power in Gudum than in Hagshaw Hill, which is implied by the higher voltage level in Hagshaw Hill. The lower voltage in Gudum gives higher currents, which again implies higher reactive power consumption in the leak inductance of the induction generator.

3.2 Flicker during continuous operation

The flicker level is effected by the terrain as illustrated in Figure 5. Generally, the Pst values are higher in Hagshaw Hill than in Gudum. This is as expected because of the complex terrain in Hagshaw Hill. But it is also seen that the flicker values increase faster with power in Gudum than in Hagshaw Hill. This is a very important point, because the requirements on flicker emission are based on 99% percentile values. Figure 5 indicates that even though the flicker level is 100% higher in Hagshaw Hill in the medium power range, the 99 % percentiles will

only be approximately 20 % higher in Hagshaw Hill than in Gudum.

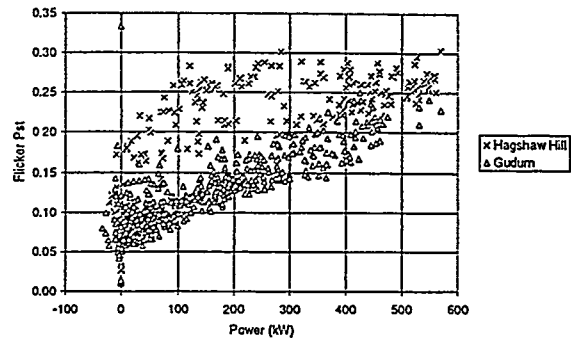


Figure 5. Flicker Pst values vs. power of Bonus 600 kW wind turbines in Hagshaw Hill (complex terrain) and Gudum (flat terrain) for grid angle 30 deg.

3.3 Transients during switching

The higher voltage level in Hagshaw Hill also effects the flicker emission during cut-ins of the wind turbine, and consequently the flicker step factor. The higher voltage level implies more reactive power to magnetise the induction generator at cut-in. This transient reactive power for magnetising has a decisive influence on the flicker emission during cut-in.

3.4 Summation of flicker

According to IEC 61000-3-7, the combined flicker emission P_{st} from various loads can be found as

$$P_{st} = \sqrt[m]{\sum_i P_{st,i}^m}$$

where $P_{st,i}$ is the flicker emission from the i^{th} load, and m is an exponent depending on the type of the loads. Analyses have shown that for continuous operation of wind turbines, $m=2$ gives excellent results. For switching operations, $m=3.2$ is recommended because this value fits when the switching operations do not coincide.

3.5 Harmonics

The harmonic measurements in Hagshaw Hill have also been compared. Generally, the harmonic emission was very low, because the wind turbines are not equipped with power electronics for power conversion. However, the comparisons have shown that the measurements and calculation software of the partners predict harmonics within the 0.1 pct. of rated current which is required in the draft IEC 61400-21.

4 VARIABLE SPEED WIND TURBINES.

The analyses of power quality of variable speed wind turbines are based on measurements on Enercon E-40 wind turbines with power converters based on forced-commutated semiconductors.

4.1 Reactive power

The use of forced-commutated semiconductors makes it possible to control the power factor. Figure 6 shows the measured reactive power as a function of the active power

from two different sites. The averaging time in the measurements are in both cases 1 minute. At Gotland the power factor is approximately 0,98 and at Skåne 0,99.

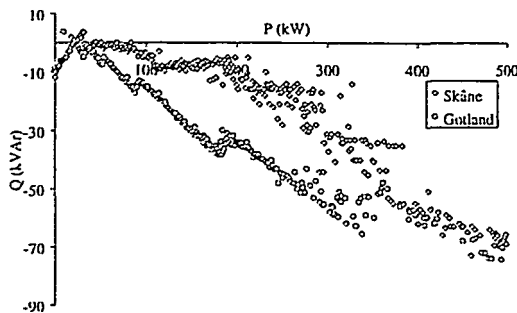


Figure 6. Reactive power as a function of active power from two different sites, Gotland and Skåne.

4.2 Transients during switching

With a combined variable speed control and pitch control of the Enercon wind turbine, the cut-ins and cut-outs can be controlled to a very low level of flicker emission.

4.3 Harmonics and interharmonics

The use of power converters implies a higher emission of harmonics and interharmonics on the grid. The traditional self-commutated semiconductors, i.e. thyristors, mainly emit harmonics at low orders. Modern power converters based on forced-commutated semiconductors like IGBTs can be controlled to switch at much higher frequencies. Besides, the emission is not concentrated on harmonics of the fundamental grid frequency, but distributed between the harmonics as interharmonics.

IEC has initiated a revision of 61000-4-7[8] in order to improve the measurement methods for interharmonics. The draft IEC 61400-21 keeps measurements of interharmonic under consideration, awaiting this revision. Meanwhile, Measnet will specify a method based on a CD of the revision [9].

5 CONCLUSIONS

The results from comparisons of simultaneous measurements in Hagshaw Hill show good agreement between the measurements of Risø, DEWI, NEL and CRES. Moreover, the comparison of calculation results based on a set of reference measurements showed very good agreement between the analysis software of Risø, DEWI and CRES.

Measnet and IEC define methods to measure power quality characteristics, which aim at being independent on the grid where the measurements are done. The measured power quality characteristics can then be applied to calculate the influence on the voltage quality on another grid, characterised by a short circuit power and an impedance angle.

The present work has illustrated that the grid properties still have an influence on the specified power quality characteristics.

Another factor, which influences the results, is the terrain. The comparison between measurements in complex terrain and in relatively flat terrain showed significant difference between the measurements of power variability and flicker at low and medium wind speed, but the designing 99% percentiles were less sensitive to the terrain.

All these effects could be taken into account by advanced methods, but such methods would depend strongly on the technology. The strength of the existing methods is their simplicity combined with a high degree of independence of technology. Even the specified methods do have limits concerning the technology. For instance, the specified method to measure flicker emission is not relevant to characterise a wind turbine with a voltage controlling power converter.

REFERENCES

- [1] European Wind Turbine Standards. Volume 7. Electrical Power Quality Measurement Procedure. Final Draft February 1996.
- [2] Measnet Measurement Procedure. Power Quality of Wind Turbines. Draft 27.11.96.
- [3] International Electrotechnical Commission. Draft IEC 61400-21: Power Quality Requirements for Grid Connected Wind Turbines. Committee Draft (CD) 1998-12-11.
- [4] International Electrotechnical Commission. IEC Report. Publication 60868. Flickermeter. Functional and design specifications. First edition 1986.
- [5] International Electrotechnical Commission. Amendment 1 to Publication 60868 (1986). Flickermeter. Functional and design specifications. 1990-07.
- [6] International Electrotechnical Commission. Technical Report 61000-3-7. Electromagnetic compatibility (EMC) – Part 3: Limits – Section 7: Assessment of emission limits for fluctuating loads on MV and HV power systems – Basic EMC publication. First edition 1996.
- [7] P. Sørensen. Methods for calculation of the flicker contributions from wind turbines. Risø-I-939(EN). December 1995.
- [8] International Electrotechnical Commission. IEC 61000-4-7. Electromagnetic compatibility (EMC) – Part 4: Testing and measurement techniques – Section 7: General guide on harmonics and interharmonics measurements and instrumentation, for power supply systems and equipment connected thereto. First Edition 1991-07.
- [9] International Electrotechnical Commission. Revision of 61000-4-7. Electromagnetic compatibility (EMC) – Part 4: Testing and measurement techniques – Section 7: General guide on harmonics and interharmonics measurements and instrumentation, for power supply systems and equipment connected thereto. Committee draft 1997-12-15.

POSSIBILITIES FOR WIND ENERGY ON THE KOLA PENINSULA

J. Wolff¹⁾, O. Rathmann²⁾, P. Lundsager³⁾, G. Gerdes⁴⁾, P. Zorlos⁵⁾, P. Ladakakos⁵⁾, P. Ahm⁶⁾, B. Tammelin⁷⁾, A. Tiilikainen⁸⁾, V. Minin⁹⁾, G. Dmitriev⁹⁾, S. Islander¹⁰⁾

¹⁾ VTT Energy, P.O.Box 1606, FIN-02044 VTT, Finland

²⁾ Risø National Laboratory, P.O.Box 49, DK-4000 Roskilde, Denmark

³⁾ Darup Associates, P.O.Box 30, DK-4000 Roskilde, Denmark

⁴⁾ DEWI, Ebertstraße 96, D-26382 Wilhelmshaven, Germany

⁵⁾ CRES, 19 km Marathonos Ave., GR-19009 Pikermi, Greece

⁶⁾ PA-Energy, Snovdrupvej 16, DK-8340 Malling, Denmark

⁷⁾ Finnish Meteorological Institute, P.O.Box 503, FIN-00101 Helsinki, Finland

⁸⁾ University of Lapland, Kirkkopuistokatu 9, FIN-94600 Kemi, Finland

⁹⁾ Kola Science Centre, 14 Fersman Str, Apatity, Murmansk Region, 184200 Russia

¹⁰⁾ SI-Credit, Koivikkotie 30 F, FIN-00630 Helsinki, Finland

ABSTRACT: This paper presents an extensive feasibility study regarding the introduction of wind energy in the energy supply of the Kola peninsula in north-western Russia that was carried out during 1996–97. The study covers as well grid connected wind turbines as autonomous systems and a wind atlas was prepared. Special emphasis is put on non-technical activities and objectives like financing models, international funding and a sound politic support. The wind resources on the Kola peninsula are excellent and there are still no reasons to why wind energy installations couldn't be carried out successfully. Recommendations for starting this development are presented.

Keywords: Feasibility studies, Resources, Integration, Policies

1 OBJECTIVES

The overall objective was to assess the possibilities for substantial integration of wind energy in the energy supply system of the Kola peninsula in the Murmansk region of Russia. A broad multi-disciplinary feasibility study took both social, technical and economical problems into account and the following issues were studied:

- the wind potential,
- autonomous wind power supply systems,
- large-scale grid-integration of wind energy,
- the economic potential,
- the potential of local industry and other business and
- the political and regional interest in wind energy.

2 THE KOLA PENINSULA

The Kola peninsula is located in the most north-western part of Russia between the 66–70° latitude and 28°30'–41°30' longitude, bordering on Finland and Norway. The peninsula is facing the Barents Sea in the north and the White Sea in the south. The climate is harsh and snow covers the ground for most of the year. The Gulf stream, however, keeps the Barents Sea cost ice-free throughout winter and prevents permafrost. The average temperature varies between –13 °C in January and +14 °C in July. Most of the terrain is taiga or forest-tundra and inland are mountainous areas, with the highest peaks (1200 m a.s.l.) in the Khibiny massive.

The peninsula constitutes the administrative unit Murmansk region within the Russian Federation. The highest administrative power is executed by the regional governor and the local government. The region has an area of 145 000 km² and has a population of 1,1 million.

The total energy consumption on the Kola peninsula has during the 90's been 13–20 TWh/year and in 1995 consumption rose for the first time since 1989. The total

generating capacity is 3,66 GW, of which 1,6 GW is hydro and 1,8 GW nuclear power. The public power company AO Kolenergo owns the network, handles all sales and distribution and all production, except for the nuclear power plant from which Kolenergo buys the production. 68 % of power and 33 % of heat production is used by the industry and respectively 11 and 52 % by domestic users. Energy prices have, as in Russia in general, been rising steadily for the past years but are still remarkably low, compared to other industrialised countries.

3 METEOROLOGY

3.1 Wind resources

The wind energy potential on the Kola peninsula is known to be extremely good, comparable to the best regions in Europe [1]. The wind atlas method from the European Wind Atlas incorporated in the well-known WASP program, was used to make a wind atlas of the area based on 12 meteorological stations shown in Figure 1.

The map in was prepared giving the estimated variation of the wind resource over the peninsula. The wind atlas indicates good wind resources along the north coast, the south coast and in the valley region between Murmansk and the White Sea.

3.2 Icing

Icing on the Kola peninsula was studied on the basis of statistical data either from the database of the Finnish Meteorological Institute or from European Centre for Medium-Range Weather Forecasts databases. The number of icing days at weather stations was calculated from the temperature and humidity observations. Icing is expected when the air temperature T_a is lower than the dew point temperature T_d : $T_a < T_d$, if $T_d < 0^\circ \text{C}$.

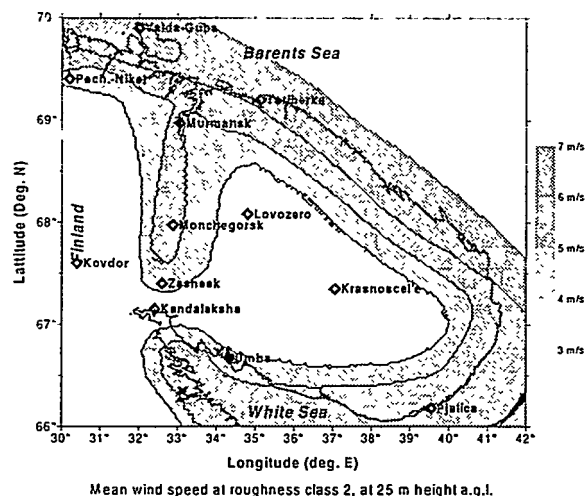


Figure 1. Estimated wind resource variation over the Kola Peninsula. Mean velocities refer to roughness class 2, 25 m a.g.l.

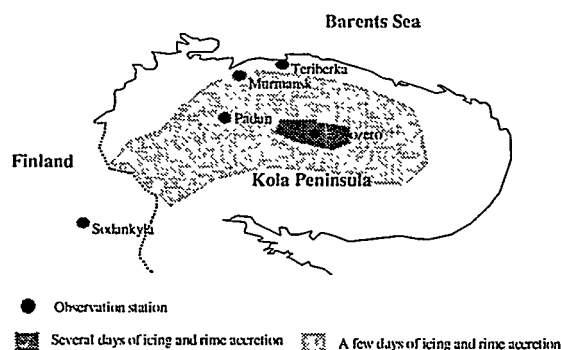


Figure 2. Icing map of the Kola peninsula.

The results indicate the variation in icing and rime accretion is very large, as can be seen from Figure 2. At coastal sites there is no icing but moderate icing occurs inland already quite close to the coastline. From these results it may be noted that icing is not a problem at coastal sites. At inland sites the effect of icing depends strongly on the geographical location and on altitude. Even at sites with moderate icing, wind power production is significantly decreased. At sites with heavy icing, ice-preventing systems have to be used. Anyway, icing on the Kola Peninsula is not as severe as at typical sites in northern Finland where wind turbines with ice-preventing systems are operated.

4 INTEGRATION OF WIND ENERGY

4.1 Autonomous and small scale wind energy

In Russia 20 million people are either not connected to a common electricity distribution networks, or they are connected to the end of long feeder lines. These areas are very sparsely populated, but a considerable proportion of vital activities in Russia takes place there, which gives widespread implications to the present study [2].

There are at least more than 40 such locations on the Kola peninsula, some of them with their own autonomous power supply while others are connected to the periphery of the public grid. Several types of autonomous and local consumers have been identified and prospective wind energy

system opportunities can be summarised into three main groups.

The first group consists of technical installations like lighthouses, frontier posts and meteorological stations under administration of the Russian North Fleet. They are small (1–50 kW) or medium (50–100 kW) sized high reliability systems.

The second group consists of installations serving mainly the heating supply of communities or public and military installations which have their heating needs served by oil fired boiler houses. They are stand alone turbines for heat and/or electricity supply or electricity producing turbines connected to existing power supply with electrical heaters as base load, 150 kW and upwards.

The third group consists of installations in remote settlements, fishing villages and kolkhozes. They are autonomous village power type systems, 50–500 kW or more, or on-d-of-line systems, 300–500 kW or more.

Table I gives a summary of the specific sites for further study. The location of the sites is shown in Figure 3.

Table I. Possible demonstration sites for autonomous technology. Mean annual wind speed is given for a hub height of 30 m.

Name, mean wind	Type	Summary
Tsyp-Navolok 8,2 m/s	Navy: Lighthouse, Frontier Post, Met. Station	3 semi-independent diesel power plants. Medium size high reliability wind diesel system. Permission to visit was not given. Thus the location is possible only on a later stage.
Beloka-menka 6,8 m/s	Civil: Fishing village	Grid connected power supply 300–500 kW standard WTG connected to the grid in "weak grid" fashion.
Chapoma 5,9 m/s	Civil: Fishing village	Autonomous diesel power supply. 150–300 kW standard WTG connected to the diesel plant in "simple, robust & reliable" wind diesel fashion.
Chavanga 6,2 m/s	Civil: Fishing village	Autonomous diesel power supply. 150–300 kW standard WTG connected to the diesel plant in "simple, robust & reliable" wind diesel fashion.

4.2 Case studies for autonomous supply

Two fishing villages, Chapoma and Chavanga, organised as cooperatives (kolkhozes) were chosen for further analysis. Both exhibit a strong local commitment to wind energy and are apparently in control of the factors of infrastructure necessary for implementing wind energy.

The diesel power plants have multiple diesels manufactured in Russia or Czechoslovakia, of differentiated sizes in order to match a load pattern with clear seasonal peaks demands, according to the main local activities. The diesel plants are manned during operation, implying around the clock supervision during peak seasons. Parallel operation seems to be the exception, and shifts between diesels are handled manually.

The staff of the diesel plants seem competent and able to perform operation & maintenance of all kinds. They appear to be able to operate standard wind turbines in wind diesel

system configurations, in particular if simple and robust architectures are implemented.

One village (Chapoma) presented a cost of energy (COE) breakdown, where the fuel cost amounts to some 60 % of the total COE including investment. O&M amounts to some 20 %, split between maintenance costs and salaries. This breakdown is believed to be fairly representative for the fishing villages. Fuel costs may be very high, and therefore wind could be competitive with present COE.

Wind energy may also be economically viable in connection with autonomous power supply but with uncertainties in the economical parameters, in particular real fuel costs and marginal value of additional energy supply.

Based on this, conclusions and recommendations were made with respect to system demonstrations with international financing contribution.

4.3 Grid integration of wind energy

The area east of Murmansk, in close vicinity to the four hydro-power stations at Teriberka and at Serebranskaja, was suggested as a target area for the analysis on grid connected wind turbines. Network calculations were carried out to investigate the possible capacity of wind energy that could be installed in the existing grid. Five sites, close to hydro-power stations and along the 350 kV line from Murmansk to Serebrjanskaja, were selected for possible installations of wind farms

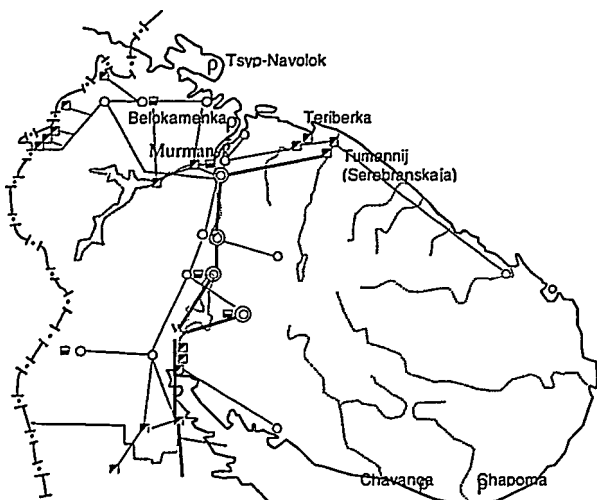


Figure 3. The public grid on the Kola Peninsula and an illustration of the sites for which case studies are made and demonstrations considered.

An initial analysis was done for a couple of pre-selected sites, representative for the area and "visibly" the most natural sites. The complete high voltage network was taken into the network model "DigSILENT". Network nodes, that are close to the wind farm installation areas or close to the consumers, were included in the model.

Five nodes were chosen to give a representative monitoring of the grid situation. The voltage changes due to fluctuating operation or cut-off of the wind farms is assumed not to exceed a level of 5 %, to guarantee a sufficient voltage quality for the consumers. To investigate the influence of different types of installation, network calculations with a wind energy installation of 500 kW, five wind farms of 100 kW each, in Tumannij, Serebrjanskaja and three sites

along the line were performed. A maximum deviation of -4 % occurs, which is within the acceptable limits.

Table II. Change in voltage levels compared to the situation without wind farm installations, for two load situations: maximum / minimum loading of the network.

Voltage changes (in % of nominal voltage)		
Kolskaja 300	Kolskaja 700	Serebrjanskije 215
-3/0	-3/0	-4/+1
Tumannyy 216	Murmansk 653	Zapoljamyj 721
-3/+1	-3/+1	-3/+1

The calculations were separated into five categories each consisting of an number of different wind farm configurations. The maximum power possible to be installed are listed in Table III. The results show that the capacity depends very much on the reactive power generated by the turbines.

Table III. Maximum installable wind farm capacity for 5 different categories.

Category	possible capacity
a) Wind farms with inductive reactive power of -25 Mvar at an active power of 100 MW each	300 MW
b) Wind farms without reactive power generation; 3 sites with 200 MW each	700 MW
c) Wind farms with capacitive reactive power of +25 Mvar at an active power of 100 MW each	300 MW
d) Wind farms with inductive reactive power in changed grid constellation of -25 Mvar at an active power of 100 MW each	400 MW
e) Wind farms without reactive power in improved grid constellation; 3 sites with 200 MW each	800 MW

All in all it can be stated that the high-voltage grid connecting the hydro-power stations to the national network is fairly strong and up to 800 MW of wind power, with an annual production of 2 TWh, can be connected, in this one line, without grid reinforcement.

4.4 Case studies for grid connected turbines

Based on the initial study two sites were chosen for detailed analysis. The hills close to the village of Tumannij seems to be a good location for a large wind park. Largely, the same conditions apply for most hills along the road and the power to Murmansk. However, Tumannij was chosen as it is representative for the area and as it was easy to make the wind estimate for the site.

On the other hand, there is no reason to bring the first demonstration with only one or a few turbines away from Murmansk, where service is best organised, the demonstration is close and visible and there are hill sites with good wind resources. However, there might be some land-use restrictions which are not probable further away.

No pay-back tariff for wind energy production is decided upon and it is therefore difficult to present detailed economic calculations. However, provided a relatively moderate cost escalation of 4 %/a wind energy is on the bring of being feasible, with an IRR of 5.25 % in Murmansk and 7 % in Tumannij.

From the gathered information it is evident that large amounts of wind energy can be produced in the region, provided that the developers find the incentive to start the process. The concept of using wind turbines for heating, requires still some technical and conceptual development. Wind power has to be compared to other measures, that might prove more advantageous, e.g. an renovation of the district heat distribution system or promoting energy efficiency. In a straightforward comparison wind energy for heat seems to be as feasible as wind energy for power production.

5 FINANCING WIND ENERGY INSTALLATIONS

The energy sector of Russia is now in a transitional phase leaving the strict state control and moving more and more towards a self-sustainable position. One immediate consequence is rapidly increasing costs of energy and this has hit the northern regions of Russia hard, due to high distribution cost. Energy prices are expected to rise further as general world market price levels are to be reached by the year 2000, according to a presidential decree regarding all natural monopolies, including the energy sector [3].

For the first wind energy installations, it seems necessary to involve international financing organisations or development funds. The prevailing economic situation in Russia makes national finance extremely difficult. Both federal and regional administrative budgets are stretched far beyond any reasonable limits, and available funds are allocated very carefully. Russian banks are for the moment not able to give long-term loans. The electric utilities have a certain degree of freedom to invest, but given current priorities, conservative attitudes and lack of information, one can not expect substantial financial commitment.

Although donor money may be identified for some demonstration projects and the associated activities such as dissemination, training etc., sustainable deployment of wind energy technology can not happen without financial viability. There are several bilateral and international development schemes and models that can be applied. However these have often quite strict rules for project studies and requirements.

The local demand, however, is in small village communities organised as cooperatives or small companies. Their energy supply is organised by the communities themselves or by small service companies. The economic possibilities for these are changing rapidly and they are for the moment not able to take long-term liabilities.

6 RECOMMENDATIONS

6.1 Autonomous wind energy systems

There is presently a recognised need for generating capacity and fuel replacement in communities with autonomous power supply. Although wind energy may be economically viable in connection with autonomous power supply, given the present real cost of energy, the kolkhozes are not, however, bankable at present, seen with the eyes of western banks and other financial sources.

Thus it is recommended that a task should be formed to establish the organisational and financial framework necessary to make the kolkhozes bankable.

6.2 Grid connected wind energy systems

With the present surplus capacity there is no short term need for additional generating capacity in the Kolenergo grid. This may change within the next decade, as electricity rates and tariffs approach market levels and existing generating capacity is phased out. With the wind resource identified by the study, the cost of energy from modern wind turbines is competitive. Wind energy has a lead time of the order 10 years and a 20 year economic life-time.

Thus it is recommended that efforts should be made to familiarise Kolenergo (and the administration) with the issues related to integrating wind energy into the power supply system. Co-operation between Kolenergo and western utilities with experience in wind energy integration would be a useful.

6.3 Conclusions

Demonstration projects should be implemented with international funding and financing with the aim to carry on towards large scale implementation as recommended in federal programmes.

A body that can provide guarantees for financing investments in remote kolkhozes is needed. This is acknowledged by the regional administration, which has initiated the work to establish such a body.

Once bankability is established, national and international funding can be applied for to demonstrating wind energy technology.

7 ACKNOWLEDGEMENTS

The work was carried out with support from the European Union's Programmes Non-nuclear Energy (JOR3-CT95-0036) and International Cooperation (INCOP-DISS-2004-96).

The authors are thankful for the support and hospitality shown during site and technical visits in Chapoma, Chavanga and by A/O Kolenergo, the Murmansk administration and above all Dr Pavel Bezroukikh in the Russian Ministry of Fuel and Energy.

8 REFERENCES

- [1] Minin, V. A. et al. Perspectives of Industrial Use of Wind Energy on the Kola Peninsula. In: Stepanov I.R. Murmansk Region Energy Problems-Collected Volume of Scientific Works. Kola Science Centre. Apatity, Russia. 1992. pp. 60-73.
- [2] Bezroukikh, Pavel. The Role of Wind Energy in the Programme of Power Supply for Northern Russian Territories. In: Vihriälä (Ed.). Proceedings of the EWEA Special Topic Conference '95: The Economics of Wind Energy, 5-7 September, 1995. Finnish Wind Power Association. Helsinki, Finland. Pp. 132-135.
- [3] Presidential Decree No 426/28.4.1997 published in the Rossiskaja Gazeta.

Effects of distributing wind energy generation over Europe

Gregor Giebel

Wind Energy and Atmospheric Physics Department,
Risø National Laboratory, DK-4000 Roskilde,
Phone: +45 4677 5095, Fax: +45 4677 5970,
Email: Gregor.Giebel@Risoe.dk

ABSTRACT:

Using data from 60 meteorological stations distributed all over Europe in conjunction with the National Grid Model (NGM) from the Rutherford Appleton Laboratory, the effects of the large-scale distribution of wind energy generation are studied. In some regions of Europe, wind energy already covers a significant proportion of the electricity demand. But the intermittence of the wind resource is always a limiting factor when penetration levels are high. Studies for single countries have shown that distributing the generation over a large area reduces the variability of the output and hence makes wind energy more appealing to utilities, since the stability requirements of the network are easier to fulfil.

The data are analysed in terms of absolute highs and lows, temporal and spatial correlations. To assess the financial benefits, the NGM is used to evaluate the match of electricity demand and generation as well as the possible savings of fossil fuel in an electricity grid incorporating various capacities of wind energy generation. To assess the value of wind energy on a trans-national scale, the European plant mix is modelled, and the NGM is used to simulate the scheduling of these plants in the presence of different penetrations of wind energy.

KEYWORDS: Cost of Energy, Dispersed Turbine Systems, Integration, National/International, Utility-Integration

1 Introduction

Wind energy is currently the energy source with the highest growth rate in Europe. But even considering the millions of euros spent on wind turbines in the last few years, and the tens of thousands of jobs created, wind energy only accounts for a very low percentage of the total electricity demand in the EU. The latest white paper of the EU on renewable energy proposed an indicative objective of 12% for the contribution by renewable sources of energy to the European Union's gross inland energy consumption by 2010 [1]. The growth of wind energy will ultimately be limited by the intermittence of the resource - the wind is just not blowing at all places all the time. Good sites for wind turbines have about 3000+ hours at full rated capacity or 'Full Load Hours' (FLH), and only a few exceptional sites have 4000+ hours. Even though the offshore resource is less variable, the load factor will most likely remain below 40%. But if we consider more than just one turbine, the effects of distributing them over a large area also lessen the variability. Hence it is informative to look in detail on the resource when spread out all over Europe. This work uses wind time series from all over Europe, and analyses them in terms of wind energy generation.

2 The National Grid Model

The assessment of the economic value of forecasting is routinely done at the Rutherford Appleton Laboratory using the National Grid Model (NGM) [2,3], which models the scheduling and dispatch of power plant to meet the demand on a large scale electricity grid. Inputs to the model are the actual power plants available for dispatch, and the prices for fossil fuel. Additionally, three time series are needed in the resolution of the time step, which typically is one hour: demand on the whole grid, wind power measurements and wind power forecasts. This tool has been used and improved continually over more than ten years.

The model runs in hourly time steps. At every step, the number of plants needed in the near future to cover the predicted demand is scheduled ahead. The predicted wind power is treated as negative load. To account for the uncertainty of the demand, the actual demand is multiplied by a Gaussian distributed random number with a distribution mean of 1 and a standard deviation of 0.015. This number is consistent with the published deviations for load prediction algorithms [4]. An assumption is made for each type of plant regarding its start-up time: a maximum of eight hours is assigned to coal- and oil-fired plant, while gas turbines are considered to start up immediately within the time frame of the model. Other plant types have start-up times in between. The eight-hour maximum also limits the time frame for looking ahead - there is no need to look beyond the maximum start-up time. Any shortfalls in load not covered by the scheduled power plant are met by either fast response plant (pumped hydro or gas turbines) or through the spinning reserve. This is thermal plant, which is not being run at full output, but at, say, 95%. The remaining 5% can be activated very fast if need be. Thermal power plants cannot be operated at less than 50% load factor, hence this is set as the minimum load factor. The spinning reserve is planned as a fraction of the predicted load (SR1) as well as a fraction of currently available wind power (SR2). Both these fractions remain fixed for a model run (typically one year), but are optimised to yield a minimum fuel cost under the condition that no loss-of-load-events (LOLE) occur. The condition that no LOLE may occur can lead to a rather high SR2 and hence a high overall spinning reserve requirement. Since power plants can only be dropped from service from one time step to the next in the model, not all of the wind power production can be accepted into the grid when all running steam plants are already at the minimum load. This means that high values of SR2 at high penetrations of wind energy can also lead to significant wind power production being discarded.

3 Input preparation

In order to simulate the European grid, the details of every power station in Europe, the fuel prices, a full demand time series of the selected countries and the corresponding wind speed/power time series would be needed. Unfortunately, not all of this was available. The installed capacity in the selected countries (Austria, Belgium, Denmark, France, Germany, Greece, Ireland, Italy, The Netherlands, Portugal, Spain, Switzerland, and the United Kingdom) was available [5], broken down by plant type. Additionally, the full individual power unit details for England/Wales, Ireland and Portugal were known, as were the details of all European nuclear power stations [6]. In order to estimate the distribution of the individual power units for the remaining countries, the known power units were divided into 8 categories. For each category, the number of units was scaled up to the appropriate total capacity for the European countries selected. The overall capacity for all categories is 461.42 GW [5].

The wind data came from 60 meteorological stations in the selected countries and is detailed elsewhere [7,8]. The simulation period was December 1990 to December 1991. In order to calculate the total European wind power generation from these sites, a European average wind turbine distribution was used. The distribution can be found in Table 1. Since the time series is only three-hourly, the wind was linearly interpolated at every station before applying the power curve. The wind was scaled to a height of 50m above ground level. The total power curve incorporating all the turbines in Table 1 corresponds to a 6.1 MW unit and is a superposition of the power curves of:

1	Vestas V66	1650 kW
1	Avedøre test turbine	1000 kW
2	Micon	750 kW
1	Wind World W-3700	500 kW
1	Windane 34	400 kW
2	Vestas V27	225 kW
2	Danwin 27	225 kW
1	Nordtank	150 kW

Table 1: Overview of wind turbines used to model the European wind turbine distribution.

The sum is 6100 kW, the average is 554.5 kW. This is adequate since the average among newly installed turbines in Germany up until October 1998 was 764 kW, while the installed base rated capacity was 444 kW/unit [9]. Extrapolating these trends, this turbine distribution should be representative for late 1999. Using the superposed power curve for each site, the power output time series was aggregated over Europe. A data point was only used if at least 25 sites had a non-missing wind speed value - otherwise, linear interpolation of the resulting time series was used. This was necessary in 76 cases. This time series is referred to as 'EU-Averaged'. In order to measure the effects of time series with higher load factors, but also higher variability, two additional series were created: the one called 'Selection' is averaged over the 25 farms with more than 2000 FLH, while the series called 'Malin Head' is the single site time series with the most FLH, which came from Malin Head in the Republic of Ireland, with 3865 FLH.

The demand time series were available from France, the UK and Portugal. These were scaled in order to fit the

overall European load, which was 1603 TWh. Every time series had a weight of 1/3, as determined by the cumulative load in that period.

4 Results

4.1 Wind Time Series Properties

Here are some properties of the European average wind profile: Maximum power generated was 4085.6 kW on December 26 1990 at 1100 hours, minimum was 93.8 kW on October 22, 0100 hours. (In fact, maximum generation was 4414.7 kW at 1200 hours on December 19, 1991, but since the NGM only takes one year as an input, the last December was omitted.) It is also worth noting that neither the full rated capacity nor zero rated output occur during the year in question. The mean generation is 1346.9 kW, while the standard deviation is 772.7 kW. This corresponds to 1934 FLH, which reflects the fact that the data come from all over Europe, including a large number of inland sites. The smoothness of the wind power generation is important for large-scale integration. Therefore, the distance dependency of the wind time series was analysed in terms of cross- and autocorrelations of the combined time series.

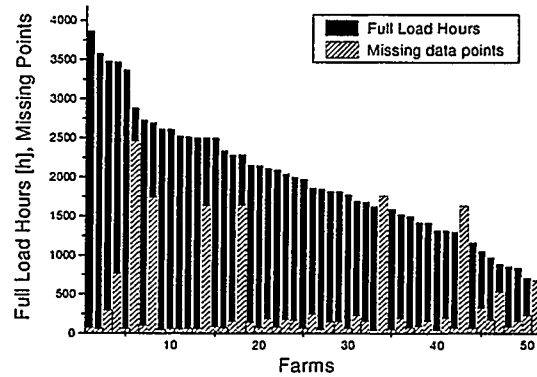


Figure 1: Number of full load hours in the single station time series. Here many stations are inland and in practice would only see development where local topographical effects enhance the resource.

The first test was to investigate the cross correlation between two stations. The correlation function of two time series p_t and q_t is as follows [10]:

$$a_k = \frac{1}{N} \sum_{t=1}^{N-k} \hat{p}_t \hat{q}_{t+k} / \sigma_p \sigma_q$$

with

$$\hat{p}_t = p_t - \mu_p \text{ and } \hat{q}_t = q_t - \mu_q.$$

μ_{pq} is the mean of the corresponding time series, σ_{pq} is their standard deviation. k refers to the time lag between the two series.

A value of 1 means that the time series are completely correlated, while a value of 0 means that the data is completely uncorrelated.

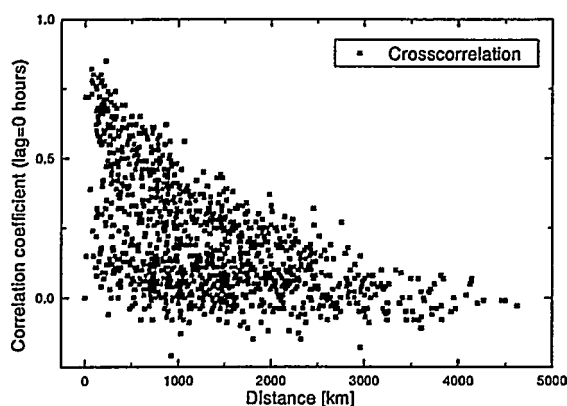


Figure 2: Correlation coefficient for every pair of stations at lag=0 hours.

Figure 2 shows the correlations for all pairs of farms with their respective distances. While short distances give the highest correlations, a short distance does not necessarily mean that the time series are correlated. Local effects can actually lead to a significant decoupling of the time series[11]. For longer distances the result is as expected: the correlation is very small. Interestingly, in some cases the time series are even somewhat anticorrelated, meaning that a wind speed increase at one station often coincides with a wind speed decrease at the other station. (The two pairs with the most negative correlation are Roches Point/IE-Lisboa/PT with -0.21 and Zaragoza/ES-Naxos/GR with -0.18.) It is also easy to see that the average correlation decreases with distance. Hence spreading out the wind power generators should give a less variable resource.

4.2 Averaged Time Series Properties

But this is for two farms only. How does this behave if one combines the time series of all farms within a certain radius and calculates the standard deviation of this resultant time series? The answer is to be found in figure 3.

At every station, an averaged time series was calculated, which included the time series of every other station within a circle with radius R . The radius R was then varied in steps of 100 km around the station. Care was taken to only include unique combinations of stations for the final plot. For every unique combination, if there was the possibility to reach the same combination from various stations, the smallest radius R was chosen as the radius for inclusion in the plot. Note that at the outside borders of the domain, less farms are included in the same circle, since the circles were centered around each station.

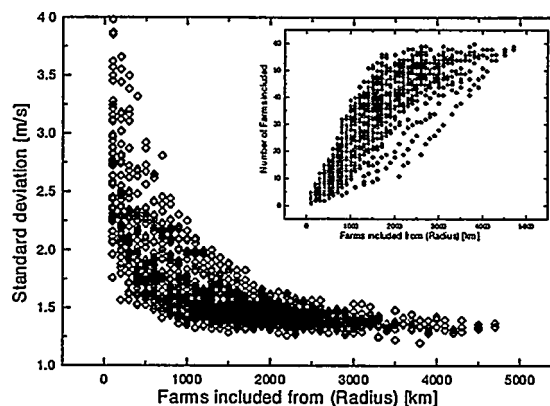


Figure 3: Standard deviation of the time series resulting from combining all available stations within a circle of radius R around any one station, and number of included farms for a given radius.

This also shows that the time series resulting from combining many farms in a large area is considerably smoother than a single time series. Another explanation for this behaviour could be that the higher the radius chosen, the more time series were averaged. Naturally, for a larger radius more of the met stations are within the circle, hence the averaging is done including more stations, as can be seen in the inset in Figure 3. To cover for this effect, in Figure 4 only averaged time series from a combination of between 15 and 20 stations was taken into account. Here, no real trends are noticeable, hence the reduction of standard deviation in Figure 3 must be an effect of the distance.

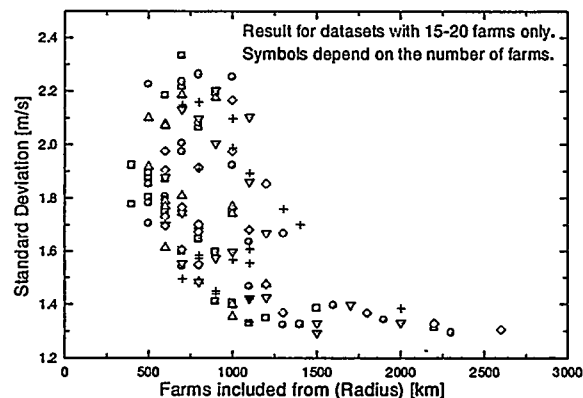


Figure 4: Standard Deviation as in Figure 33, but this time only for data sets containing between 15 and 20 stations. Different symbols refer to different numbers of stations included for the averaging.

5 Financial assessment

Below is a table with the main parameters for the three wind power data sets used:

Units: [kW]	Mean	SDev
Average:	1347	773
Selection:	1850	1055
Malin Head:	2646	2202

Note here that Malin Head has by far the highest standard deviation, but also the highest mean.

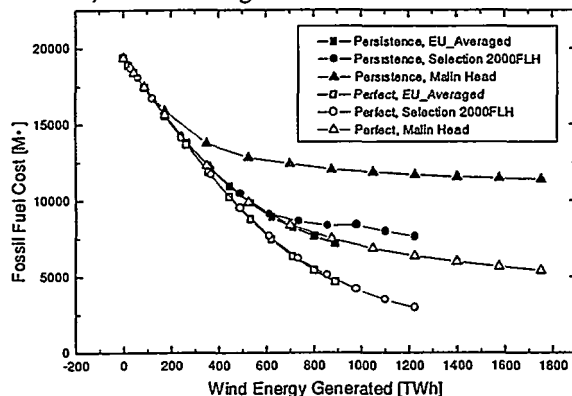


Figure 5: Fossil fuel cost for different wind energy production. The x-axis denotes wind energy produced by the simulated turbines. For comparison note that the European overall demand was 1603 TWh that year.

In figure 5 we see that for small penetrations the possible savings correlate with the amount of wind energy which is fed into the network. The shape of the graphs in figure 5 are determined by the ability of the grid to accommodate all of the produced wind energy without compromising the stability of the supply. This can be seen from figure 6, where the fraction of the produced wind energy that is accepted into the grid is shown as a function of the produced wind energy. Actually, at high penetrations the fuel savings correlate with low variability of the time series and high forecast accuracy - the highest savings for very high penetrations are attainable with a medium of perfect forecasting and high wind energy generation. All the data points of the different graphs are equidistant in installed wind capacity. The saturation effects for high variability of the input, coupled with bad forecasting, are clearly visible, even though in no case it reaches full saturation. Note that the spread between the forecasting methods is bigger for more variable wind time series.

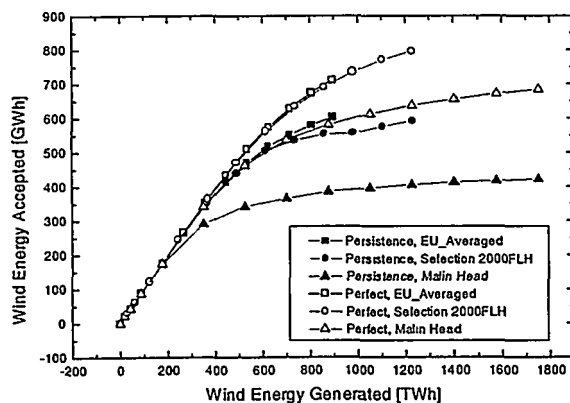


Figure 6: Accepted wind energy production. This figure shows, how much wind energy is accepted into the grid, for how much energy generated.

Figure 6 tells us that good forecasting combined with a low variance wind production leads to a better integrable resource, while high variability and bad forecasting leads to

much wasted wind energy, since the grid cannot accept all the wind energy due to security of supply reasons.

6 Conclusions

Spreading out the wind energy production over all of Europe leads to a significantly less variable resource. This is both an effect of the inclusion of many turbines in the generation and of the geographical spread of the generation. This is also beneficial in a financial analysis, where it could be shown that a low variability in the generated wind production coupled with good forecasting can lead to higher fossil fuel savings for the grid than without, especially for high penetrations of wind energy.

7 Acknowledgements

This work was funded by the JOULE contract JOR3-CT97-5004. A great thanks to Simon Watson, who showed me around the NGM a lot and made my stay in England so pleasurable.

8 References

- 1 http://www.europa.eu.int/en/comm/dg17/599fi_en.htm
- 2 Bossanyi, E.A. (1983): Use of a grid simulation model for longer-term analysis of wind energy integration, *Wind Eng.* 7, 223-246.
- 3 Bossanyi, E.A. and Halliday, J.A. (1983): Recent developments and results of the Reading/RAL grid simulation model, *Proc. 5th BWEA Conf.*, Reading (Cambridge University Press, Cambridge, 1983), 62-74.
- 4 See fx. Input Variable Selection for ANN-based Short-Term Load Forecasting, I Drezga, S Rahman, *IEEE Trans on Pow syst.*, Vol 13, no4, Nov 98, 1238-1244. Neural Network with fuzzy set-based classification for short-term load forecasting, MDaneshdoost, MLoftalian, GBumroongit, JPNgoy, *ibid.*, 1386-1391. ANNSTLF - Artificial Neural Network Short-Term Load Forecaster - Generation Three, Alireza Khotanzad, Reza Afkhami-Rohani, Dominic Maratukulam, *ibid.*, 1413-1422.
- 5 IEA Electricity Information 96, OECD Publications, Paris 1996,, ISBN 92-64-15585-6
- 6 *Nuclear Engineering Int*, vol 43, no 532, p 36-39, Nov 1998
- 7 Landberg, L., S.J. Watson, J. Halliday, J.U. Jørgensen and A. Hilden, 1993: *Short-term prediction of local wind conditions*, Report to the Commission of the European communities, JOULE programme, JOUR-0091-C(MB), March 1994
- 8 Landberg, L., The Availability and Variability of the European Wind Resource, *Int J Solar Energy* 18, 1997, p 313-320.
- 9 Taken from REISI, http://www.iset.uni-kassel.de:888/reisi_dw.html.
- 10 Madsen, H, Tidsrækkeanalyse, 2. Udgave, IMM-DTU, Lyngby 1995
- 11 Joensen, A., L. Landberg, and H. Madsen, A new measure-correlate-predict approach for resource assessment, poster on the EUWEC99, 1st-5th March, Nice

WIND TURBINES - FACTS FROM 20 YEARS OF TECHNOLOGICAL PROGRESS

Lars Henrik Hansen and Per Dannemand Andersen
 Risø National Laboratory
 DK-4000 Roskilde
 Denmark.

Phone: +45 4677 4677 and Fax.: +45 4677 5083

Emails: lars.henrik.hansen@risoe.dk and per.dannemand@risoe.dk

ABSTRACT: The first Danish commercial wind turbines were installed in the late 1970s. Over the last 20 year the Danish wind turbine market has been relatively stable concerning annual installations, and the wind turbine technology has been able to develop continuously. This gives a unique time track for technology analysts. The aim of this paper is to extract reliable information on this time track from existing archives and statistics. Seven generations of wind turbine technology have been identified mainly based on "characteristic" rotor diameters. The technological development of each generation is described using indicators such as: market share in Denmark, generator size, rotor diameter, hub height, electricity production and productivity. Economical indicators comprise: costs of turbine and standard foundation.

KEYWORDS: Commercial Wind Turbines, Cost of Energy, Economics, Technological Development.

1. INTRODUCTION

During the last decade a number of surveys and analyses on the technological development of wind turbines have been carried out in a number of international contexts. Reliable empirical input to these surveys is vital. In this sense Danish wind turbine technology is of interest. First, the technology has a 20-year track record. Second, the technology has developed along a certain technological trajectory without major discontinuities and changes big enough to exclude comparisons. Third, the Danish wind turbine manufacturers have provided more than 50% of the accumulated world market for wind turbines. Finally, technological and economical data can be made available and comparable with a limited effort.

The aim of this paper is to extract reliable information on this time track from existing archives and statistics. It is not the aim of the paper to discuss the findings in a context of innovation theory or the like. A more profound presentation is provided in [1]. Evaluation of the development of cost of energy is reported in another paper on this conference [2].

2. SOURCES OF DATA

This survey is based on three sources of data.

First, the firm E&M Data in Aalborg, Denmark has established a database of all Danish wind turbines, based on manufacturers voluntary reports to the database. This database contains information of technical matters (type, make, actual site, etc) but no information on installation costs.

Second, in the period 1979–84, prices and technical data for all approved wind turbines on the Danish market were published in the monthly magazine *Naturlig Energi*, based on information from Risø's programme for *Type-Approvals & Certification*. The data includes: nominal generator power (kW), rotor diameter (m), hub height (m), and list price of the wind turbine (kDKK). The list price of a wind turbine includes transport, installation and running-in time. For some of the wind turbines, the annual energy production in roughness

class 1 and 2 are also presented. In case of turbines without production data, this information has been constructed from other sources (from approval archives at Risø or from E&M Data).

Third, from 1984 and until today the Danish Energy Agency has sponsored the quarterly *Vindmølleoversigten*, with technical data on approved turbines on the Danish market and list prices. This data includes the data mentioned above plus production data, in MWh/year, for roughness classes 0, 1, 2, and 3 and list prices of standard foundations (in kDKK).

3. METHOD AND REDUCTION OF DATA

Technical data and prices for all turbines available on the Danish market 1979–1997 from *Naturlig Energi* and *Vindmølleoversigten* constitute the base material.

Step 1: Data was reduced to cover only manufactures with a significant marked share over several years: *Bonus*, *Micon*, *Nordtank* and *Vestas*. For the late 70's and early 80's the manufacturers *Kongsted* and *Wind Matic* are included as they had a considerable market share. The included machines represent in average over the years 56% of all sold turbines and ca. 80% of turbines sold in the 1990's.

Step 2: Vintages 1979 and 1980 were omitted due to high uncertainty on prices and technical data. Furthermore, a portion of common sense and experience is added to exclude other data and examples that are irrelevant.

Step 3: Most manufacturers have several versions of each type of turbines – with, for example, different hub heights. The one with the best cost/performance value for roughness class 1 has been selected.

Step 4: By 1991 the definition of roughness classes was changed from referring to [2] to [3] using Beldringe wind data. A simple formula for transferring the old data to the new definition was developed. In case of roughness class 1, the scaling factor (to be multiplied on the annual production) as function of the hub height z is calculated as:

$$factor_{class\ 1} = 0.0023z + 0.8059,$$

while roughness class 2 is recalculated as:

$$\text{factor}_{\text{class } 2} = 0.0019z + 0.8428.$$

Step 5: Seven generations of turbine technology were defined, as described in the following section. Even though over the years, blade length has been determining for the major specifications for the wind turbine generations, the generator size in kW has been chosen as a reference through the paper. That is to facilitate comparisons with other electricity producing technologies.

Step 6: For each set of data (generation of turbine and vintage) a weighted average for each indicator (generator capacity, hub height, price, etc.) was calculated. Weighting was made by using the actual market share of each manufacture and type of turbine (based on the database from E&M Data).

Step 7: Prices were deflated to a 1996 price level.

Validity of the resulting costs has been checked by analyzing an available questionnaire survey made by E&M Data on 17 500 kW and 33 600 kW turbines. A larger statistical basis would be preferable, but this is not available. Comparisons concluded, that for the 500 kW turbines actual prices and list prices are almost identical (>1/2% difference). For the 600 kW turbines the actual prices are 2 1/2% lower than the list prices.

4. SIX GENERATIONS OF WIND TURBINE TECHNOLOGY

The Danish wind turbine industry has developed its technology within a certain technological concept or technological paradigm: the upwind, three bladed, stall regulated, grid connected, and horizontal axle concept. Nevertheless, in the mid-seventies several other concepts were tried – first of all the other classic concepts such as the multi-bladed wind rose, the two bladed concept, the Darrieus concept, and the gyro concept were in commercial production.

Up-scaling within such a technological paradigm is a key word for the technological development of Danish wind turbines. Each generation is larger than the preceding generation measured in rated capacity, swept rotor area, etc. But also within each generation incremental up-scaling has taken place. Typically, a new generation of turbines has been designed conservatively with some extra safety margins on critical details. When the first experiences of the turbines were collected extra safety margins could be narrowed in. Typically, the gained experiences have not been used to produce the same design cheaper but to increase the electricity output from the design by means of slightly larger rotor diameter, changed pitch angle, etc.

The first generation of industrially produced turbines was based on a 5 meter blade as for example the blade produced by the company "Økær Vind-Energi". The turbines had rotor diameters of 10 to 11 meters and they were equipped with a 22 kW or a 30 kW generator. This generation was primarily sold from 1978 to 1981.

The second generation started as the very popular 55 kW machine with a 15 meter rotor and was up-scaled to a 75 kW machine with a 17 meter rotor. This generation of turbines was developed in the late 1970's. The first versions were designed with a 45 kW generator, but very few of these early 45 kW versions were actually sold. The second generation of turbines was based on a 7.5 meter blade from the company Altermeg, and it dominated the

Danish and the international wind turbine market in the first half of the 1980's. Vestas started producing its own blades from 7.5 meter generation.

Third generation was turbines based on the 9 meter blade with generators in the range of 90 to 100 kW. Rotor diameter was between 18 to 20 meter. From this generation LM Glasfiber A/S has been the dominating blade manufacturer supplying all Danish wind turbine manufacturers except Vestas. Vestas has developed its own blade manufacturing capability. For private wind turbine owners a maximum allowed machine size was limited to less than 100 kW in the late 1980s. That is why several manufacturers sold 95 kW and 99 kW turbines during these years. The sales to this generation peaked in 1987.

Fourth generation of Danish wind turbines covers turbines between 150 to 250 kW and were based on 11 and 12 meter blades. This size range dominated the market between late 1980's to early 1990's. The 150 kW turbines (23–25 meter rotor diameter) and the 200–250 kW turbines (25–29 meter rotor diameter) have been among the best selling turbines over the years.

An intermediate fifth generation of turbines covers the range 300 kW and 400 kW with a rotor diameter of 30–31 meter based on 13 and 14 meter blades.

The sixth generation started with the early Bonus 450 kW turbines with a rotor diameter of 35 meter in the late 1980's. This generation took pace with the 500 kW turbines based on 37 meter to 39 meter diameters in the early 1990's. During the mid 1990's this generation has been up-scaled to 600 kW with rotor diameters of 43 and 44 meter.

Based on the sixth generation an intermediate size range (a seventh generation of technology) has been developed between the 500/600 kW and the MW size turbines. These are turbines of 600 kW, 660 kW, 750 kW and 800 kW generators and 47 to 50 meter rotor diameter.

This paper focuses on the first six generations, and the market share in numbers of each generation is indicated in Figure 1. Only very few turbines fall outside these six generations defined by generator rating. See "sum" line in Figure 1. Turbines not included in this survey are typically turbines from small manufacturers, and for the period 1978 to early 1980s, turbines of other concepts than the Danish concept. The technological development over the years is illustrated in Table 1 based on a number of representative turbines.

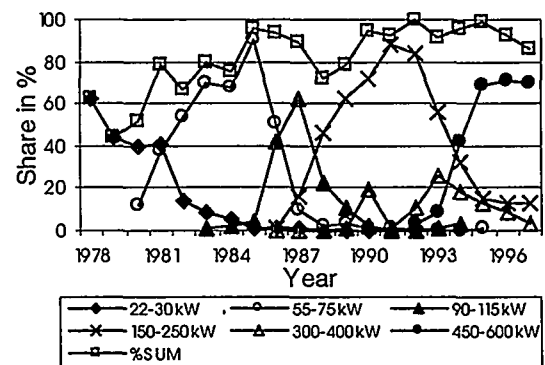


Figure 1: Market shares of each generation of turbines, i.e. share of total annual no. of installed wind turbines in Denmark. Source: E&M Data, Aalborg.

Table 1: Nine typical wind turbines representing the technological development 1981 to 1997. Turbine cost is in a 1996 price level.

Year	1981	1983	1985	1987	1989	1991	1993	1995	1997
Power [kW]	30	55	75	95	150	225	300	500	600
Diameter [m]	10.4	15.5	17.0	19.4	23.5	27.0	31.0	39.6	45.3
Hub height [m]	18.1	21.3	18.0	24.4	30.3	30.0	30.1	40.7	44.3
Production in R.c.1 [kWh/m ²]	498	530	598	692	837	891	872	935	960
Production in R.c.2 [kWh/m ²]	373	413	452	551	689	722	697	760	792
Turbine cost (kDKK/kW)	11.1	9.59	7.43	8.08	7.04	7.39	5.94	5.92	5.83

Table 2 presents the extracted data on the six generations. The first two columns in the table contains the no. of turbines with known list prices (*Wind Turbines*) and the total no. of installed turbines in Denmark (*Total Turbines*), while the columns (*Nominal Gen. size*) through (*Production R.class 2*) are weighted averages (i.e. using the actual market share). Moreover, the presented prices are current prices.

5. TECHNO-ECONOMIC INDICATORS

A comprehensive tradition of research is established in the area of technological trajectories and technological paradigms [4,5].

The data in Table 2 are now used to illustrate the technological and economical development of the six generations.

Figure 2 and Figure 3 show the evolution in hub height and rotor area, respectively. The increasing trends of each generation are mainly due to upscale effects.

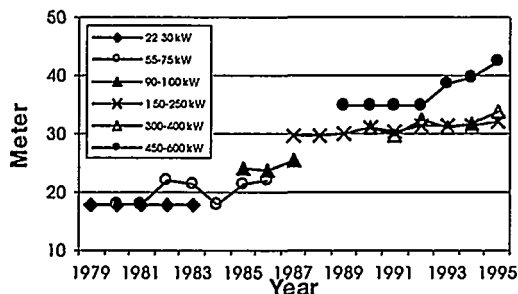


Figure 2: Evolution of hub height.

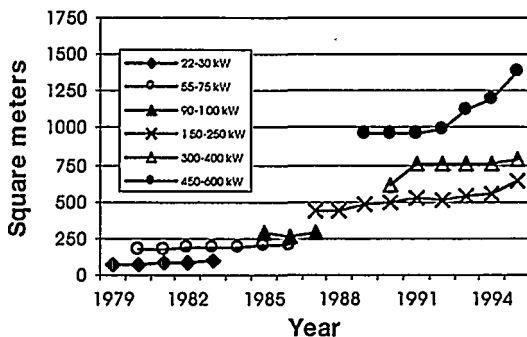


Figure 3: Evolution of rotor area.

The technical performance of wind turbines can be accessed in a number of ways. Figure 4 and Figure 5 illustrate the rotor area per nominal generator size and the annual energy production (in roughness class 1) per rotor area, respectively.

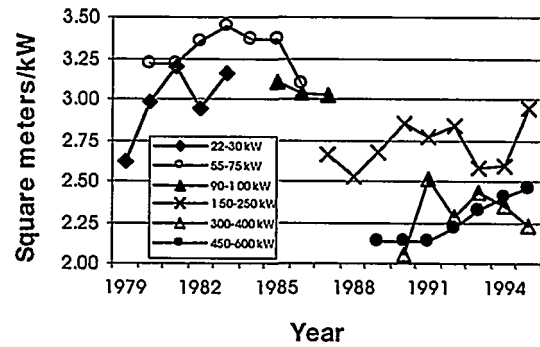


Figure 4: Rotor area per nominal generator size.

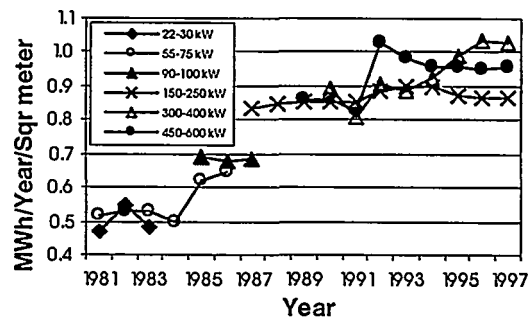


Figure 5: Annual energy production in roughness class 1 per rotor area.

Analogous, the economical performance of wind turbines can be accessed in a number of ways. Usually, the price of the wind turbines per nominal generator size and specific investment are evaluated as in Figure 4 and Figure 5, respectively.

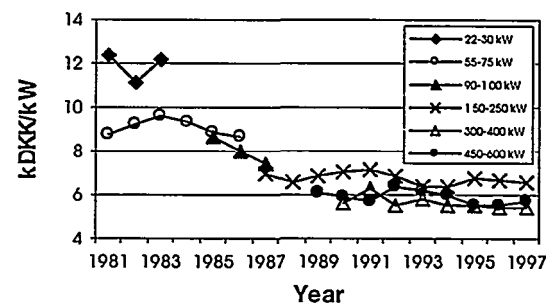


Figure 6: Price of wind turbines per nominal generator size (in 1996 values).

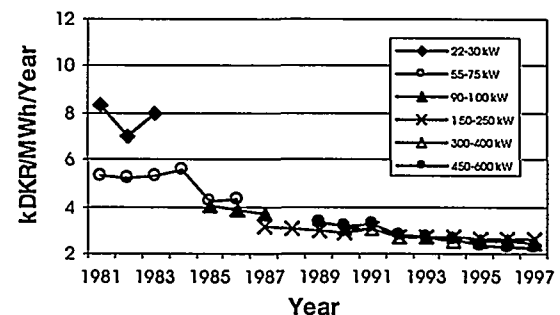


Figure 7: Specific investment as the price of wind turbines per annual energy production in roughness class 1 (in 1996 values).

6. CONCLUSION

As the wind power technology has increased its market share and market volume, professional technology analysts and students of technology and business require reliable historical data on this technology's technological development. In this paper such data are provided in the most reliable and valid manner possible without use of large questionnaire surveys. A more detailed discussion of cost structures have been made in another paper on this conference [6].

REFERENCES

- [1] P.D. Andersen and L.H. Hansen, Technical and Economical Development of Danish Wind Turbines 1979-1997. Risø-R-1083(EN), 1999. Risø National Laboratory, Roskilde, Denmark.
- [2] E.L. Petersen, I. Troen, S. Frandsen, and K. Hedegaard. *Wind Atlas for Denmark*, Risø National Laboratory, Roskilde, Denmark, 1980.
- [3] I. Troen and E.L. Petersen. *European Wind Atlas*, Risø National Laboratory, Roskilde, Denmark, 1989.
- [4] N. Rosenberg. *Inside the Black Box: Technology and Economics*, Cambridge University Press, Cambridge, 1982.
- [5] G. Dosi, Sources, Procedures, and Microeconomic Effects of Innovation. *Journal of Economical Literature*, vol. XXVI, pp. 1120-1171, 1988.
- [6] J. Lemming, P.H. Jensen, L.H. Hansen, P.E. Morthorst, and P.D. Andersen, O&M Costs and Economical Life-Time of Wind Turbines. No. 314, 1999. 1999 European Wind Energy Conference and Exhibition.

Table 2: Background data on the six Wind Turbine generations. Wind Turbines is the no. of turbines with known list prices, while Total Turbines is the total no. of installed turbines in Denmark. Nominal Generator size through Production R.class 2 are weighted averages (using the actual market share of each manufacture and type of turbine). Prices are current prices.

Generation	Year	Wind Turbines	Total Turbines	Nominal Gen. Size	Hub Height	Rotor diameter	Prices of Turbines	Prices of Foundations	Production R.Class 1	Production R.Class 2
		No.	No.	kW	Meter	Meter	kDKK	kDKK	MWh	MWh
22-30 kW	1979	1	7	30.0	18.0	10.0	—	—	37.3	27.2
	1980	13	43	26.9	18.0	10.0	—	—	35.6	26.7
	1981	28	39	26.9	18.0	10.4	183	—	40.0	30.4
	1982	6	14	30.0	18.0	10.6	209	—	48.0	37.0
	1983	2	10	30.0	18.0	11.0	246	—	46.0	35.0
55-75 kW	1980	11	13	55.0	18.0	15.0	—	—	91.0	68.0
	1981	14	36	55.0	18.0	15.0	270	—	91.0	68.0
	1982	37	55	55.0	22.0	15.3	317	—	98.0	74.5
	1983	54	77	55.0	21.3	15.5	355	—	99.9	77.9
	1984	49	105	55.0	18.0	15.4	365	—	92.4	69.3
	1985	94	308	62.7	21.5	16.3	404	33.1	130	101
	1986	4	163	65.0	22.0	16.0	430	35.0	129	103
90-100 kW	1985	8	14	95.0	24.0	19.4	610	40.0	205	163
	1986	109	135	94.7	23.8	19.2	583	40.8	197	158
	1987	130	182	94.3	25.6	19.1	560	38.3	196	159
150-250 kW	1987	30	48	167	29.6	23.7	925	60.0	367	299
	1988	130	193	180	29.7	23.8	947	60.8	376	305
	1989	172	273	183	30.0	24.7	1065	58.8	413	335
	1990	163	256	179	30.9	25.2	1105	62.9	428	350
	1991	253	344	193	30.2	25.8	1242	59.5	447	364
	1992	147	201	183	31.3	25.4	1166	61.4	451	364
	1993	85	102	215	31.3	26.3	1288	58.8	492	394
	1994	40	47	216	31.4	26.6	1340	59.9	502	403
	1995	27	30	218	31.9	28.5	1446	58.9	555	451
	1996	41	51	218	31.7	28.6	1456	59.0	556	452
300-400 kW	1997	61	66	225	31.5	29.0	1500	60.0	571	464
	1990	42	69	300	31.0	28.0	1500	80.0	550	429
	1991	4	5	300	29.5	31.0	1720	90.0	612	490
	1992	27	27	337	32.3	31.0	1744	75.9	684	545
	1993	22	47	314	30.9	31.0	1716	77.5	668	533
	1994	26	26	327	31.7	31.0	1733	76.3	697	558
	1995	25	25	364	33.9	31.7	1954	73.2	774	621
	1996	37	37	376	36.2	31.4	1999	72.0	799	644
450-600 kW	1997	20	20	370	36.3	31.5	2000	72.5	797	644
	1989	2	2	450	35.0	35.0	2350	140	828	669
	1990	4	4	450	35.0	35.0	2350	125	828	669
	1991	15	16	450	35.0	35.0	2350	125	798	650
	1992	4	8	450	35.0	35.6	2700	125	1022	825
	1993	15	15	483	38.7	37.9	2833	135	1107	899
	1994	48	61	496	39.6	38.9	2877	145	1141	929
	1995	117	134	566	42.4	42.1	3086	117	1334	1086
	1996	255	290	585	43.4	44.0	3252	159	1450	1193
	1997	354	373	598	44.2	45.2	3474	164	1538	1270

European Wind Turbine Testing Procedure Development

Blade test methods and techniques

B.H. Bulder†, J.J.D. van Dam†, D.R.V. van Delft‡, E.R. Jørgensen**, V. Kolovos*,
S. Larwood¶, W. Musial¶, A. Verheul‡, P. Vionis*, M. Winther-Jensen**

† Netherlands Energy Research Foundation ECN P.O. Box 1, 1755 ZG Petten, The Netherlands. E-mail: bulder@ecn.nl

‡ Technical University Delft, Stevin Laboratories Stevinweg 1, 2628 CN Delft, The Netherlands. E-mail: D.R.V.vanDelft@ct.tudelft.nl

** Risø National Laboratories P.O. Box 49, DK 4000 Roskilde Denmark. E-mail: martin.winther@risoe.dk

* Centre for Renewable Energy Sources 19km Marathon Ave, Pikermi, Athens, Greece E-mail: pvioni@cres.gr

¶ National Renewable Energy Laboratory 18200 State Highway 128 Golden, Colorado 80403 USA E-mail: walter_musial@nrel.gov

Abstract:

In this paper the preliminary results obtained by performing the second task of the "European Wind Turbine Testing Procedure Development" project are presented. This project is performed within and with financial support of the Standards, Measurements and Testing programme of the European Commission.

Keywords: Testing, Rotor blades, Procedures, Standardisation

1 INTRODUCTION

The objective of the European Wind Turbine Testing Procedure Development (EWTPD) project is to develop and improve instrumentation and measurements methods for wind turbines and to provide reference data required for this development. The second task of this project concerns: *Blade Test Methods and Techniques*. The main objectives of this part of the project are:

- to compare the different test methods used in different test laboratories and to check whether the test results are comparable and unambiguous
- to make a reference database for different test methods, test techniques and test results of static and dynamic tests of wind turbine rotor blades.

This task of the project is carried out, by the laboratories of CRES (Gr), ECN (NL), RISØ (DK), TUD (NL), who receive a 50% funding of the European Commission DG XII, and in close co-operation with NREL (USA) (without EC funding).

The work, performed by the partners is based on, full scale tests on 7 equal rotor blades of approximately 12 m length by all partners. CRES and NREL will test two rotor blades. The two tests at CRES will be identical and the two tests at NREL differ. Each laboratory will perform the tests in "their usual manner".

The work to be done in the project is:

- defining a test plan;
- a blade property test resulting in accurate values of the blade mass, stiffness, eigenfrequencies, at least the first flapwise, lead/lag-wise and torsional, and damping;
- a blade strength tests resulting in strain distributions and deflection;
a blade fatigue test(s) resulting in an indication whether the blade will suffer any fatigue problems;

- if the blade didn't fail during the fatigue test the blade will be destroyed during a residual strength test;
- a post mortem test resulting in data on fibre volume ratio's and fibre directions in some specific areas where failures or damage occurred during one of the tests, to verify whether production variations are the cause of these.

When the tests are performed a comparison will be made between the test results and the used test methods. The differences can be due to a number of reasons:

- differences in test methods;
- differences in blades, due to the manufacturing process;
- statistical variations in material properties;
- etc.

The aim of this project is to identify differences in the test results due to testing methods. However due to the limited number of test blades per test laboratory, 2 test laboratories test two blades and 3 test laboratories a single blade, will it be very difficult to identify differences due to the test procedure.

The tests are performed in the second half of 1998 and the first 6 month of 1999. The preliminary results of this project will be presented in this paper.

2 DESCRIPTION OF THE WORK PERFORMED

To start the work, first a suitable test specimen had to be chosen. An important condition is that all design analyses of this rotor blade had to be made public to the project participants. All partners will have to use the same data to make up a test plan. Another condition was that the chosen design should have been produced in series for at least two years and would hopefully still be on the market for a number of years. This condition was given to make sure that the blade

chosen is designed and manufactured in a way still common for presently designed and manufactured rotor blades.

The blade chosen is the NEDWIND 25, a 12.5 m GFRP rotor blade with a steel flange. At the time of obtaining the blade it was no longer in production which made it easier for the manufacturer, ROTORLINE, and NEDWIND to make all design data public. However the original design analyses had been performed in 1992 which are not as sophisticated as the design analyses are today.

The blade data consisted of a

- drawings of the design, including airfoil coordinates;
- laminate lay-up and properties;
- material fatigue properties;
- used material and load factors;
- 100 load cases with the loading at 10 equally spaced spanwise positions. Each load case consisted of a mean and range of the, flap & lead-lag bending moments and of the centrifugal force.

The second main activity is to prepare test and measurement plans which define in detail the blade property, static strength and fatigue strength tests. The following tests with associated results are foreseen:

TASK	RESULT
• Blade Property tests	– mass distribution; – stiffness distribution; – eigenfrequencies, damping;
• Static Strength test	– strain/stress - load relations at a number of positions; – deflection at load introduction and at the tip;
• Fatigue Strength test	– indication of fatigue failures; – stiffness degradation; – strain distribution at the end of the fatigue test
• Postmortem test	– fibre volume fraction; – fibre alignment; – laminate thickness;

For the measurement plan it was decided that at 10–12 points on the blade all partners would attach strain gauges which could easily be compared. To be sure that the position of all strain gauges is equal one partner made indications on all blades before they were shipped to the individual laboratories.

The third task is to:

- performing the tests according to the test plans;
- report the test, findings and conclusions;

The fourth task is to compare the test and make a final report. The comparisons and reporting will consist of the reference database of results and a description of the difference between the test methods.

3 PRELIMINARY RESULTS

At the time of writing this paper most fatigue tests are still running. The blade property tests and the static tests have been performed. The measured data of the blade property tests are reported in table I. The sensitivity of the common strain gauges, i.e. strain gauges which are monitored by all partners, see figure 1, are shown in figure 2. In table II the standard deviation divided by the mean value of the sensitivity is shown. The test methods for the blade property tests are different at each laboratory but the results are reasonably well comparable. The test methods used for the static and fatigue strength tests however differ much more. At RISØ the blade was loaded with cables, see figure 4, for the strength test, and with an eccentric mass for the fatigue test, while the other laboratories used hydraulic actuators for loading the blade, see figures 3–5. This also implies that RISØ performed a separate fatigue test in flap and edgewise direction, while at the other laboratories 2 axis loading could be performed with two actuators. NREL performed one test with a single actuator, loading the blade combined in flap and lead-lag and one test was performed with two actuators loading the blade in flap and lead-lag with a less correlation between both loads. Most laboratories have performed or are all most ready with one fatigue test. During the fatigue tests all blades have shown some damage, a crack, at the trailing edge near the largest chord. This crack grows quite rapidly at the beginning of the test and slows down after 10^6 cycles.

4 ACKNOWLEDGEMENT

This project is performed within and partly funded by Standards, Methodologies and Testing programme of the European Commission, DG XII.

Tabel II: $\frac{\text{standard deviation}}{\text{mean}}$ of the sensitivity of the common strain gauges.

Sensor	standard deviation/mean	
	Edge	Flap
400E1	0.036	0.520
400F1	-6.866	0.134
400E2	-0.028	1.361
400F2	0.228	-0.058
1500P1	0.174	0.081
1500P0	0.082	0.109
1500P90	-1.821	0.436
1500P45	0.831	0.187
1500S1	-0.351	-0.052
1500S0	0.160	-0.128
1500S90	-1.680	-1.066
1500S45	8.255	-0.138
2500P1	0.802	0.230
2500P0	0.117	0.085
2500P90	-0.744	-0.285
2500P45	1.731	0.145
2500S1	-0.194	-0.506
2500S0	0.273	-0.104
2500S90	-0.695	0.894
2500S45	-0.694	-0.648

Table I: The preliminary results of the blade property tests

		DESIGN	CRES1	CRES2	ECN	NREL1	NREL2	RISØ	TUD
MASS	[kg]	799.	769.	768.	765.	N.A.	N.A.	N.A.	762.
Center of Gravity	[m]	3.48	3.06	3.06	2.96	N.A.	N.A.	N.A.	3.06
Eigenfrequencies									
1 st flapwise	[Hz]	2.52	2.53	2.53	2.59	2.50	2.50	N.A.	2.34
2 nd flapwise	[Hz]	7.80	8.27	8.07	8.30	8.25	7.88	N.A.	7.57
1 st leadwise	[Hz]	4.00	4.92	4.92	4.93	5.00	4.88	N.A.	4.69
2 nd leadwise	[Hz]	26.1	19.55	19.69	19.92	20.00	19.37	N.A.	18.46
1 st torsional	[Hz]	37.5	25.29	26.18	25.3	25.88	25.25	N.A.	29.69

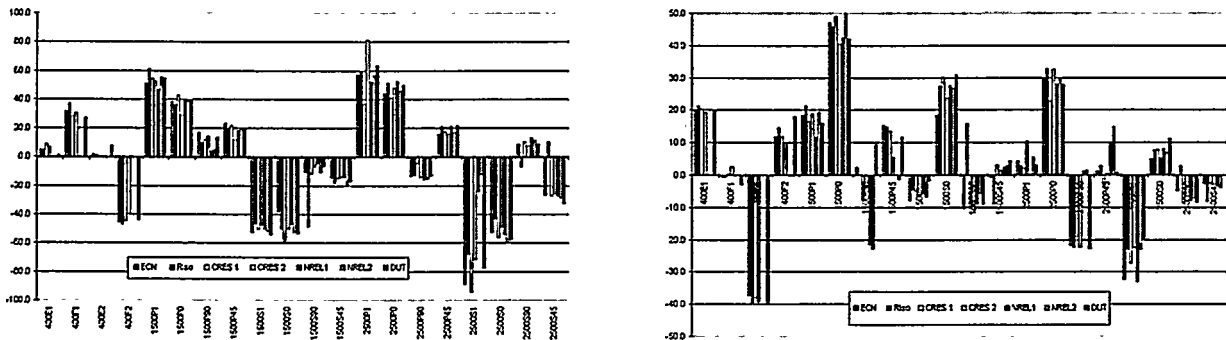


Figure 2: The sensitivity of the common strain gauges in flap (a) and lead-lag (b) direction.

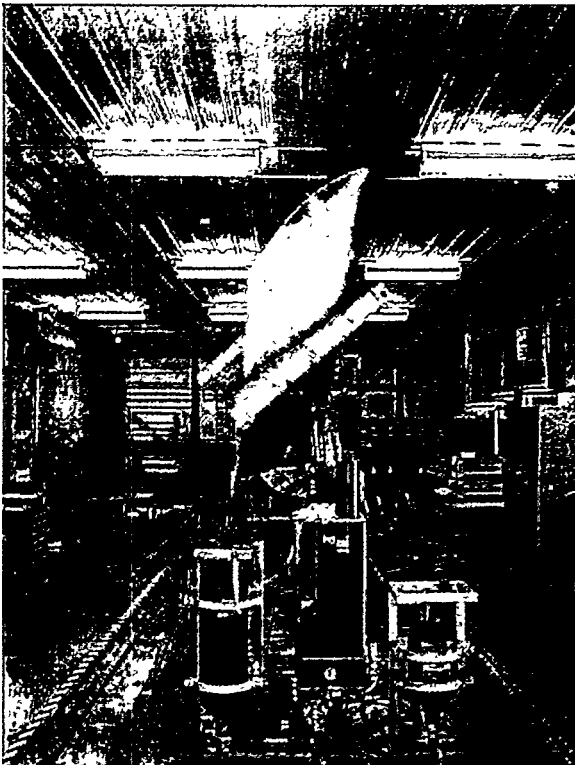


Figure 3: The test setup at NREL (USA).

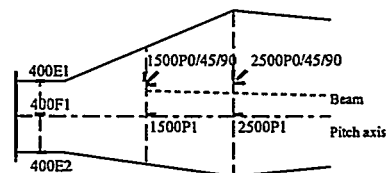


Figure 1: The position of the common strain gauges.



Figure 4: The test setup for the static test at RISØ (Denmark).

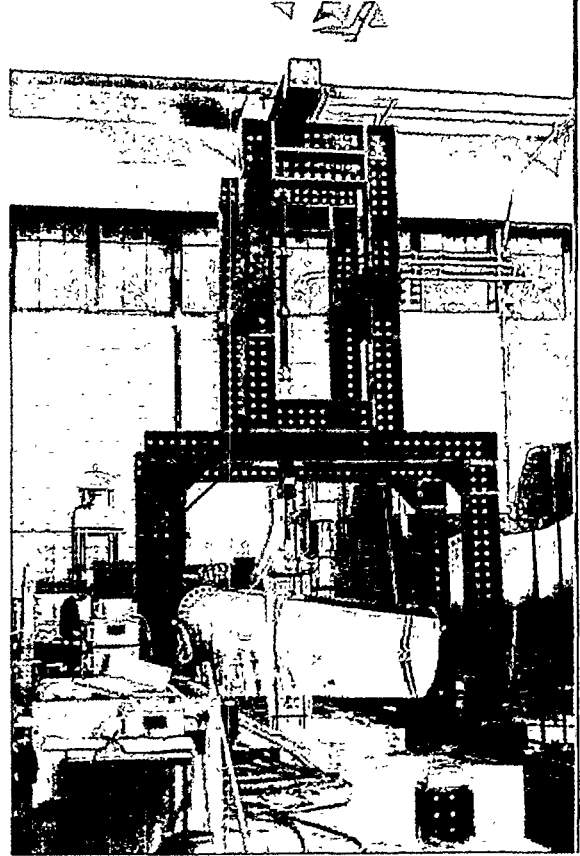
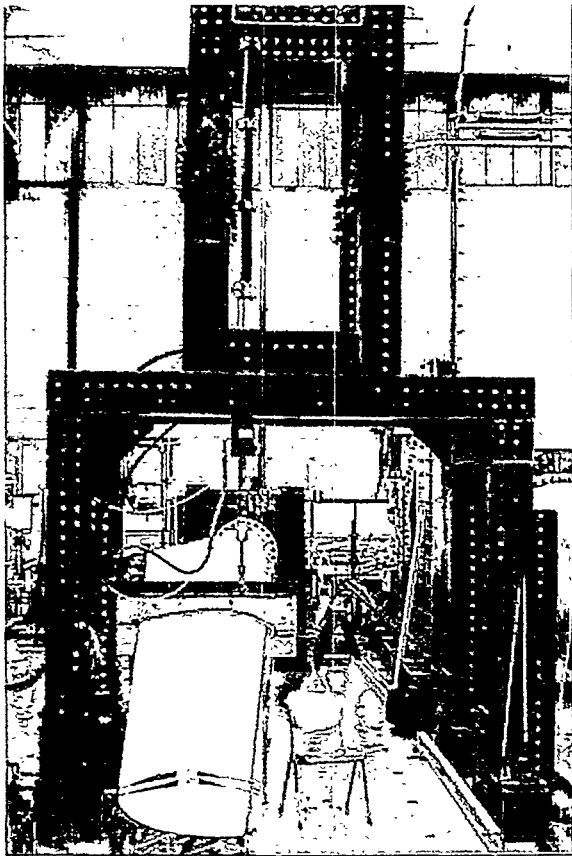


Figure 5: Test setup at Delft University of Technology (Netherlands).

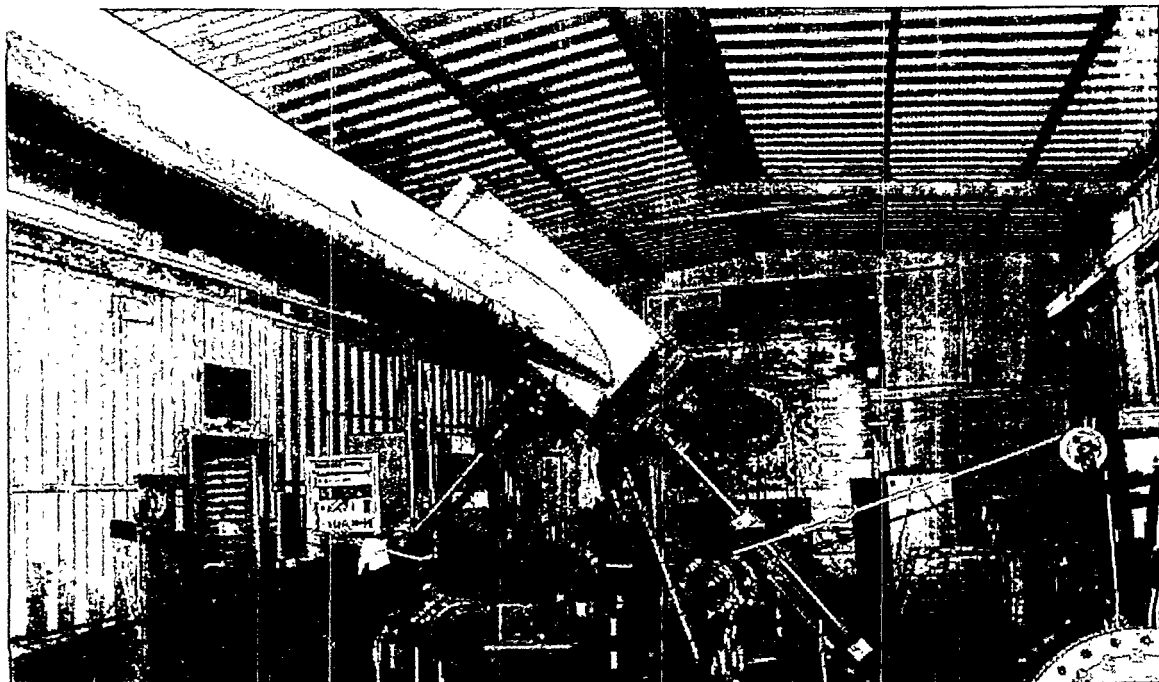


Figure 6: The test setup at CRES (GREECE).

WIND TURBINE CERTIFICATION - THE COMMITTEE DRAFT BY IEC-TC88-WG9

Peter Hauge Madsen
 Risoe National Laboratory / Wind Energy and Atmospheric Physics Department
 P.O. Box 49, DK-4000 Roskilde, Denmark
 and
 William E. Holley
 Consultant to
 National Renewable Energy Laboratory
 Golden, 80303 Colorado, USA

ABSTRACT: In 1995 the Technical Committee TC88 of the International Electrotechnical Commission decided to start a new work item, namely to prepare a standard for the certification procedures for wind turbines with respect to safety, performance, interaction with the public grid, environmental requirements and the documentation requested by the certification bodies. The purpose was to provide a common basis for certification of wind turbines, including a basis for accreditation of certification bodies and mutual recognition of certificates. A working group (WG9) was created to prepare a committee draft. WG9 submitted the result late in 1998 to TC88. This paper presents the committee draft Standard, which defines a certification system for Wind Turbine Generator Systems. Key issues in the evaluation of conformity with these standards and identified needs for other technical criteria and procedures are presented.

Keywords: Certification, Standards, Wind Turbines

1. INTRODUCTION

Traditionally, most countries with active wind energy programmes have had their individual arrangements for approval and certification of wind turbines. These national arrangements are sufficiently different that a manufacturer who wants to market his wind turbine in many countries, typically must comply with several different standards and secure certification or type approval with different authorities and according to different procedures. The development of wind turbines has been characterised by lively international trade. National certification arrangements and standards have provided difficulties or barriers for such trade.

This is indeed the reason that IEC, the International Electrotechnical Commission, in 1988 established the Technical Committee TC88 with the objective to prepare standards for wind turbine generator systems. A number of working groups were created to prepare standards, initially with basic safety and design requirements followed by standards for test procedures, these standards to be found in the IEC 61400 series.

Having developed or started the development of the basic normative documents for wind turbine certification, i.e. the basic design and test standards, the Technical Committee TC88 of the International Electrotechnical Commission decided to start a new work item in 1995. The task was to prepare a standard for the certification procedures for wind turbines with respect to safety, performance, interaction with the public grid, environmental requirements and the documentation requested by the certification bodies. The committee draft, see Figure 1, was completed by late 1998 and submitted for discussions in TC88.

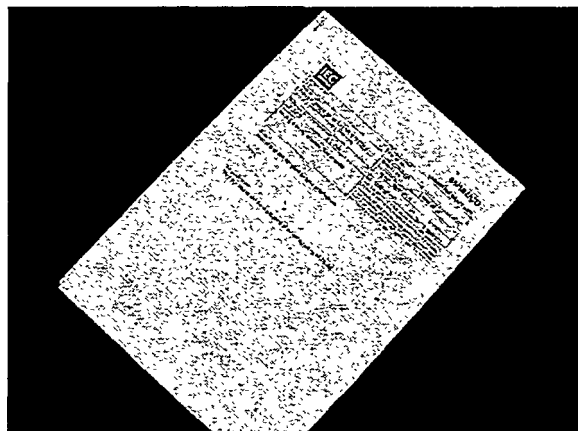


Figure 1: The Committee Draft 88/102/CD

2. IEC TC88 WORKING GROUP 9

A working group WG9 was set up to draft the standard, and the first meeting was held in late 1995. Five wind turbine certification bodies were represented in the working group, which have had members from Denmark, Germany, Greece, Italy, Japan, the Netherlands, UK and USA. Initially, Dr J. Maguire convened the working group. At the third meeting Peter Hauge Madsen took over the convenorship. Alan Johnston and William E Holley have acted as secretary for the working group. The following have participated in the work on a regular basis:

- Mr. Sandy BUTTERFIELD
- Mr. Christer ERIKSSON
- Dr. William E. HOLLEY
- Mr. Alan G. JOHNSTON

- Dr. Peter Hauge MADSEN
- Mr. Fumio MINO
- Dipl.-Ing. Christian NATH
- Dr. Diego PRISCHICH
- Dr. Bob SHERWIN
- Mr. Carsten SKAMRIS
- Mr. Wim J. STAM
- Dr. Christof STORK
- Mr. Pantelis VIONIS

After eleven working group meetings the working group in September 1998 submitted a draft [1] to IEC TC88.

3. SCOPE OF THE DOCUMENT

The standard specifies rules and management procedures for carrying out conformity assessment of wind turbines, with respect to specific standards and other technical requirements, relating to safety, reliability, performance, testing and interaction with the electrical power network. The standard thus primarily affects the Certification Bodies.

Its purpose is to provide a common basis for certification of wind turbines, including a basis for accreditation of certification bodies and mutual recognition of certificates. The goal is that the standard will help to harmonise the national certification arrangements, and in the future together with the other IEC 61400 series standards, replace or harmonise the various certification procedures and requirements, illustrated in Figure 2.

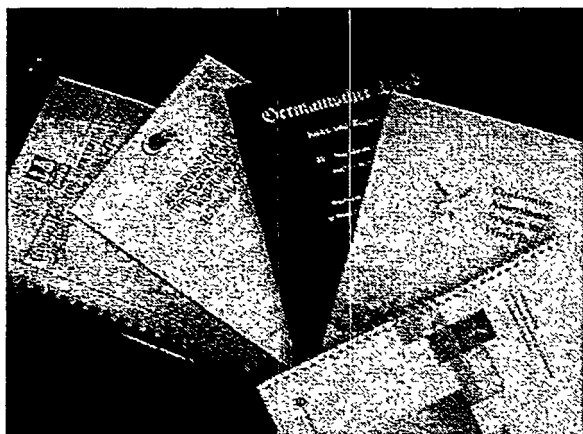


Figure 2: Procedures and Criteria in different Certification Arrangements

The draft standard provides:

- definitions of the elements in a wind turbine certification process;
- procedures for the conformity assessment in a wind turbine certification system;
- procedures for conformity surveillance;
- rules for the documentation to be supplied by the Applicant for the conformity assessment; and
- requirements for certification and inspection bodies and testing laboratories;

The draft standard is not limited to wind turbines of any particular size or type. Some elements of certification, primarily associated with safety, are mandatory, whilst provision is specifically made for others to be optional.

4. CONTENTS OF THE DOCUMENT

4.1 Background

The certification system specified in the draft standard is based on relevant IEC/ISO Guides, in particular IEC/ISO Guide 65 [2]. This guide provides the general requirement for the management and operation for the certification body. In general, the specified certification system is assumed to be operated by accredited bodies, which in the case of testing laboratories and inspection bodies shall comply with IEC/ISO Guides 25 [3] and 39 [4].

The draft standard describes procedures for all stages of wind turbine use: design, manufacturing, erection and installation as well as operation and maintenance. The procedures deal with the assessment of loads and safety, tests, performance, noise, power quality and manuals as well as surveillance of manufacturing, installation, project implementation and operation.

The certification system applies the other technical standards and reports in the IEC 61400 series as the primary normative documents.

The certification procedures constitute a complete third party conformity evaluation of a wind turbine type, a major component type or one or more wind turbines at a specific location. They may result in two fundamentally different certificates:

- Type Certificate
- Wind Turbine Certificate

In addition, the draft standard offers the possibility of a component certificate. The purpose is to confirm that a major component of a specific type is designed, documented and manufactured in conformity with design assumptions, specific standards and other technical requirements. Component certification is a subset of type certification.

4.2 Type Certification

The purpose of type certification is to confirm that the wind turbine type is designed, documented and manufactured in conformity with design assumptions, specific standards and other technical requirements. It shall also be demonstrated that it is possible to install, operate and maintain the turbines in accordance with the design documentation at a site appropriate for the type. Type certification applies to a series of wind turbines of common design and manufacture.

The primary purpose is to demonstrate conformity with the safety requirement in IEC 61400-1 [5] or IEC 61400-2 [6].

The mandatory and optional modules are illustrated in Figure 3. The certificate documents conformity for the mandatory modules and may document conformity with the optional modules. Satisfactory evaluation of a module is concluded with a conformity statement.

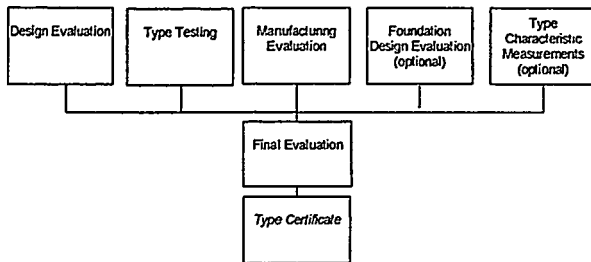


Figure 3: Modules of Type certification

During *Design Evaluation*, the Certification Body shall evaluate whether the particular wind turbine type is designed and documented in conformity with design assumption, standards and other agreed normative documents

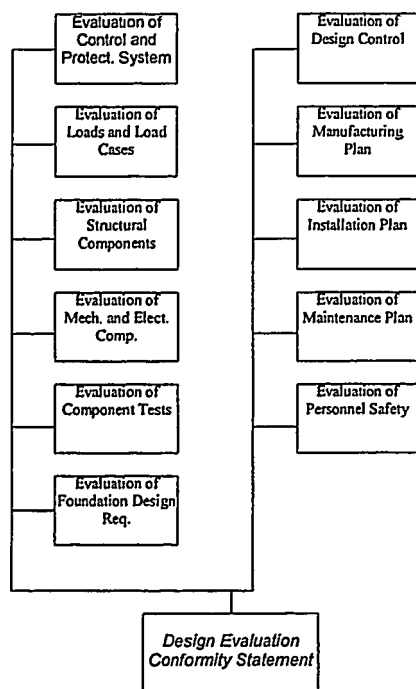


Figure 4: Elements of Design Evaluation

Normally the design evaluation comprises the elements shown in Figure 4, but for small wind turbines designed according to [5] the following elements shall as a minimum be evaluated:

- control and protection system;
- loads and load cases;
- structural components; and
- mechanical and electrical components.

The Design Evaluation does not require a specimen of the wind turbine type to be manufactured and tested, and the documentation only consists of drawings, analysis, descriptions, specifications and schematics. The process, however, includes evaluation of a manufacturing, an installation and a maintenance plan. The Certification Body shall evaluate the plans to verify that the requirements for manufacture, installation, commissioning and maintenance are in accordance with the quality requirements in the design documentation.

The purpose of *type testing* is to provide data needed to verify aspects, which are vital to safety and need additional experimental verification, and aspects that cannot be reliably evaluated by analysis. Type testing comprises the elements shown in Figure 5.

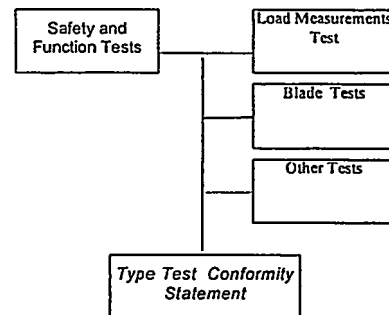


Figure 5: Type testing elements

Testing shall be carried out on a turbine or component of a turbine representative of the type to be certified. Note that the tests of the control and protection system functions, load measurements and blade tests (in general both static and fatigue tests) are proposed as mandatory.

The optional *type characteristics tests* include

- power performance tests;
- power quality tests; and
- acoustic noise measurements

according to the relevant IEC 61400 series standards [7], [8] and [9].

The *manufacturing evaluation* comprises an evaluation of the quality management system and a surveillance/inspection of the manufacturing. The quality management system is not necessarily a certified ISO 9000 system, but shall include the most important elements.

4.3 Wind Turbine Certification

The purpose of wind turbine certification is to evaluate whether type-certified wind turbines and particular foundation designs are in conformity with the external conditions, applicable local codes and other requirements relevant to a specific site.

The certificate documents conformity for the mandatory modules and may document conformity with the optional modules. The certificate and conformity statements arising from the modules in Figure 6, will only be issued for wind turbines that are type-certified.

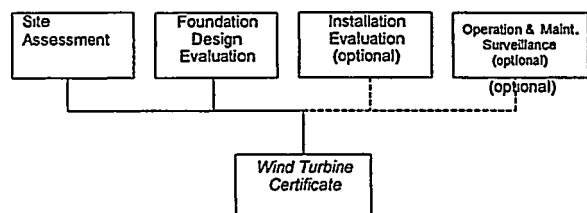


Figure 6: Modules in wind turbine certification

The purpose of site assessment is to examine whether the environmental, electrical and soil properties at the site conform to the parameter values defined in the design documentation.

The site conditions are evaluated on the basis of measurements and/or applicable standards valid for the installation site. The following external conditions shall be evaluated:

- wind conditions;
- other environmental conditions;
- electrical network conditions; and
- soil conditions.

The purpose of *foundation design evaluation* is to examine whether the foundation design is in conformity with specific standards and other technical requirements.

Normative design codes and other criteria shall include all requirements of the local jurisdiction applicable to the installation site and shall be IEC or ISO codes where applicable.

The purpose of *installation evaluation* is to evaluate if one or more wind turbines have been installed and commissioned in conformity with specific standards and other technical requirements. It comprises an evaluation of the installation quality system and surveillance/audits. The party responsible for installation may operate a quality system that meets the requirements specified in ISO 9001 or 9002. Alternatively, systematic surveillance by the Certification Body will be required.

The Certification Body shall witness commissioning of at least one wind turbine at the site.

The purpose of *operation and maintenance surveillance* is to establish that all the wind turbines at a specific site are operated and maintained in conformity with the relevant manuals included in the wind turbine type design documentation.

This surveillance requires examination of operation and maintenance records and random inspection of turbines.

5. COMPARISON WITH CERTIFICATION PROCEDURES IN DENMARK

The certification system presented in the Committee Draft is naturally influenced by the existing national certification arrangements. Adoption of the Committee Draft is expected to cause some, primarily minor changes for all existing certification arrangements. As an example, the elements of the proposed design evaluation and type certification have been compared to the elements of the different Danish type approvals in Table 1.

6. CONCLUDING REMARKS

The Committee draft is presently circulated with the National Committees for comments. The deadline for comments is 31 March 1999. The Draft and the national comments will be discussed at the next IEC TC 88 meeting in May 1999.

If the document is accepted by TC88 the voting steps follow, first as a Committee Draft for Voting and then as a Draft International Standard before the document can be issued as an International Standard.

The hope is that this document as an International Standard can be instrumental in the harmonisation of certification. The present differences between European certification arrangements and the first steps in obtaining common interpretation of the requirements in this document and other IEC 61400 series standards are described in [10].

	IEC		Denmark		
	Design evaluation	Type certificate	A-type approval	B-type approval	C-type approval
Control and protection system	x	x	x	x	x
Loads and load cases	x	x	x	x	x
Structural components	x	x	x	x	x
Mechanical components	x	x	x	x	x
Electrical components	x	x	x	x	x
Component tests					
Foundation design requirements	x	x			
Foundation			x	x	x
Design control	x	x			
Manufacturing plan	x	x			
Installation plan	x	x			
Maintenance plan	x	x			
Personal safety	x	x	x	x	x
Safety and function test		x	x	x	
Load measurements		x	x	x	
Blade test		x	x	x	x
User manuals		x	x	x	
Installation manuals		x	x	x	
Power performance			x	x	
Power Quality			x	x	
Acoustic noise			x	x	
Quality management system		x			
Manufacturing surveillance		x			
ISO 9001 certificate			x		
ISO 9002 certificate			x		

Table 1: Comparison with Danish type approval elements

REFERENCES

- [1] IEC/TC88 88/102/CD (1998), Draft IEC 61400-22: Wind Turbine Certification.
- [2] ISO/IEC Guide 65: 1996, General requirements for bodies operating product certification systems.
- [3] IEC/ISO Guide 25: 1990, General Requirements For The Competence Of Calib.And Testing Laboratories.
- [4] IEC/ISO Guide 39: (1988), General Requirements For The Acceptance Of Inspection Bodies
- [5] IEC 61400-1: 1994, WTGS. Safety requirements.
- [6] IEC 61400-2: 1996, WTGS. Safety of small wind turbines.
- [7] IEC 61400-11: 1998, WTGS. Acoustic Noise Measurement Techniques.
- [8] IEC 61400-12: 1998-02, WTGS. Wind turbine power performance testing.
- [9] IEC 61400-21: WTGS. Power quality requirements for Grid Connected Wind Turbines.
- [10] C. Nath et al, Harmonisation of Certification in Europe, JOULE Project EWTC, paper presented at European Wind Energy Conference and Exhibition, Nice, France, 1999.

Kurt S. Hansen[‡] and Michael S. Courtney[†]

[‡]*Department of Energy Engineering, Technical University of Denmark,
DK-2800 Lyngby, Denmark
fax +45 4588 2421 / telephone +45 4525 4318 / E-mail ksh@et.dtu.dk*

[†]*Wind Energy and Atmospheric Physics Department, Risø National Laboratory
DK-4000 Roskilde, Denmark
fax +45 4677 5970 / telephone +45 4677 4677 / E-mail Michael.Courtney@risoe.dk*

ABSTRACT

This paper describes the "Database on Wind Characteristics", a world wide web hosted database of wind time series suitable for wind turbine designers. The paper marks the conclusion of the initialising Joule project and presents the database as a functioning and useful tool for the wind turbine community. An overview of the current contents of the database is given. The browser based search system is described and examples of potentially damaging wind time series found using the search system are presented. The paper concludes by placing the database in context, briefly mentioning associated projects and describing how the database will continue to function as an IEA annex.

Keywords: wind flow measurements; data bases; turbulence, extreme wind conditions

1. INTRODUCTION

This paper marks the successful conclusion of the EC funded project "Database on Wind Characteristics", a web hosted database of wind time series suitable for wind turbine designers. The intention of this paper is to highlight the features and diversity of the database, hopefully enticing members of the wind energy community to explore the web site, <http://www.winddata.com/>.

As part of the Joule III programme, the project had participants from many EC member countries with major contributions from Sweden, The Netherlands, Greece and Denmark. The project has been coordinated by Risø National Laboratory, Denmark and The Technical University of Denmark. These two institutions, in cooperation, have engineered the time series database and its web interface. A more detailed description of the project's institutional organisation can be found in [1].

Time series data are accessible both via ftp and directly from a web browser. From the web browser, background information may be viewed and statistics and indexing parameters used to search for data with specific characteristics. A logical and carefully considered data structure is an essential prerequisite for building a database of this size and complexity. The main features of the data structure are described in [2] together with details of how the data are quality checked and indexed.

2. STATUS

At the end of February 1999, the database contains over 40000 hours of wind speed measurements from 22 different sites. Data have been chosen selectively with a deliberate over-representation of high wind and complex terrain cases. This makes the database ideal for wind turbine design needs but completely unsuitable for resource studies. Diversity has also been an important aim and this is realised with data from

a large range of terrain types; everything from offshore to mountain, from Norway to Greece. Table 1 shows a summary of the current database contents and figure 1 shows all 10 minute turbulence intensities (representing all sites) versus mean wind speed. Because of this large amount of observations (>1.000.000) the confidence levels are plotted.

3. FINDING AND DOWNLOADING DATA.

Physically, the time series data reside on cd-roms loaded in a so-called "jukebox". This is a storage system comprising 4 cd-rom drives, racks for 150 cd-roms and a robot system for automatically loading and changing cd-roms. The jukebox data is accessible via the ftp server at address 130.225.71.50 (nt50.afm.dtu.dk). This is the first and most direct method of access to the data. All the time series data files are visible but none of the background information, statistics or indexing parameters. For a user requiring data from a specific site at a specific time this is the fastest and most effective access method.

With such vast amounts of data available, it is essential to have a search system that can guide a user to the time series relevant for a particular purpose. This is the role of the web-server which is the second and principal gateway to the time series data. Here all the background information can be viewed and the statistics and indexing parameters used to search for data with specific characteristics. Having found interesting data, time series can be downloaded simply by clicking on the file name.

If a user requires many time series or has only a slow internet connection, a third, less exotic possibility exists. On request (and for a handling charge), copies of cd-roms can be made and sent by conventional post. Here the web-server can still be used to choose the relevant data since the search and browse systems perform well even over dial-in internet connections.

4. THE WEB BROWSER SEARCH SYSTEM

The principal gateway to the time series data is through a web browser from which the user can access the wind database web-server at address <http://www.winddata.com/>. Here the user can view background information and search for data. In the following sections a brief description of the search system is given. We encourage readers to follow the description whilst seated at a web browser.

The most central link on the home page is to the search system. Clicking this link opens the login form which presents two possibilities; login as unregistered or as registered user. Unregistered entry requires only an e-mail address (no password) and gives access to the "Simple" query system described below.

For access to the more sophisticated "Advanced" query system the user must first register (by filling out and submitting the registration form) and subsequently receives a password. At the present time registration is free but this login system gives the possibility of implementing registration tariffs at a later date.

4.1 Searching using the simple query system

The simple query has been designed as a straightforward and fast tool for finding time series. It contains only the most fundamental parameters (speed, turbulence intensity, direction, terrain and orography type) and uses only the "nominal" run statistics (one speed, one direction and one turbulence intensity value per time series). Despite the simplicity, it is anticipated that the simple query will be able to satisfy a large majority of user requests.

In order to prevent unnecessarily large network traffic, the user is not permitted to view results from a query until the number of resulting time series is less than 500. To enforce this discipline, only the "count" button is visible until the parameters selected result in a number of time series under this limit. In other words, no other operations will be available until the "count" button has been pressed and the number of resulting time series is under 500.

Having entered selection parameters resulting in under 500 time series, the user is presented with a further 3 operations; "view", "files" and "plot":

Pressing "view" results in a list of matching runs together with site name and "nominal" statistics as shown in Figure 2. On this page, site names and run names appear as hyperlinks. Clicking a site name enters the background information viewing system at the appropriate site. Clicking a run name results in a report giving an overview of the run including the run statistics for each channel and the names of the data files, as shown in Figure 3. By clicking on the file names, the time series can be directly downloaded.

Pressing "files" from the query form results in a list of data files fulfilling the search criteria. Here time series can be downloaded by clicking on the individual data file names. Alternatively the file list can be saved locally and all the data files downloaded as a background task using the *dbwind.exe* utility. Offline signal plots can be made by *danap.exe*.

Pressing "plot" from the query form calls a Java based plotting routine which is supplied with the mean speeds, direc-

tions and turbulence intensities of the time series satisfying the search criteria. Data can be viewed in various parameter combinations by selecting from the menu in the plot. Right clicking on a point in the plot displays an overview of the run (Figure 4) from which time series may be downloaded by clicking the file name.

4.2 Searching using advanced queries.

For searching using 10 minute statistics and indexing parameters, the advanced query is used. Here the volume of statistics is many times greater since we are concerned with 10 minute statistics (as opposed to run statistics) and each channel is represented individually. Combining several parameters can result in a time consuming query. The combined search conditions are defined on three separate forms; basic ten-minute statistics, transient events (gusts and direction change) and wind shear parameters.

Advanced queries operate in much the same way as simple queries - the user must find a combination of selection parameters resulting in under 500 ten minute periods before any further viewing functions are available. Much the same viewing facilities are available as for the simple query, but broadened to allow viewing of ten minute statistics and indexing parameters.

5. RESULTS

As an illustration of the data that can be found using the advanced search system, we have chosen two examples.

The first example Figure 5 shows a very large gust (17 m/s) occurring in a period with a mean speed of over 30 m/s. Here we used the following search criteria; minimum speed 30 m/s, minimum gust 17 m/s and a gust period of 10 seconds. Two 10 minute periods satisfy these criteria, the series shown in Figure 5 being from the Skipheia site on the Norwegian coast, measured at a height of 11 metres.

The second example, Figure 6 shows a simultaneous gust and direction change (a severe loading condition for a wind turbine) found using the "gust directional index" (gdi) indexing parameter. The idea here is to define a parameter that quantifies the contemporarity of the maximum gust and the largest direction change in a given 10 minute period. For maximum gust and maximum direction change occurring simultaneously, gdi has a value of 2.0. If there is no correlation between these two events, gdi has a value of 1.0. The data shown in Figure 6 was found by specifying a minimum value of 2.0 for gdi and wind speed in the range 10 to 12 m/s.

6. CONCLUSION

At the conclusion of the project the database contains over 40000 hours of data from over 20 sites, resulting in over 1 million individual ten minute periods of wind speed. This vast database of time series would be useless without adequate experimental documentation, effective quality control and indexing together with a flexible search system. We believe that all these criteria are amply fulfilled by the system in its current state. By basing the database around a web interface, the potential audience is maximised both geographically and in terms of computer technology.

The Database on Wind Characteristics now exists and is a valuable and useable tool for the wind turbine industry. The task lying ahead is to capitalise on this achievement, getting the database employed to the degree it deserves. As a step in this direction, the database will now be operated as Annex XVII of the International Energy Agency's Wind Research and Development programme. Annex XVII aims to bring the database to a level where it can be financially self-supporting. This will be achieved by increasing the geographical coverage of the database and by disseminating knowledge of the database, particularly to the wind turbine industry.

As an indication of the applicability of the database, we can refer to two projects that are already benefiting from this rich resource. The Joule "New Gust" project, coordinated by The Delft University of Technology, uses wind data from the database to verify and calibrate theoretical models for gust shape [4]. A Danish project [5] uses database wind time series to examine the precise form of the high speed tails of the wind speed distribution and determine how much these deviate from a Gaussian form. This has particular relevance to fatigue loading of wind turbines.

In conclusion, it should be remembered that the database coordinators welcome offers of new data. We consider the Database on Wind Characteristics to be the natural repository for many of the numerous existing and future wind datasets.

7. REFERENCES

- [1] Hansen, K.S. et al "Database on Wind Characteristics". 1996 European Union Wind Energy Conference proceeding held 20-24 May in Göteborg, p. 1063-1066
- [2] Hansen, K.S. et al "Winddata on the World Wide Web". 1997 European Wind Energy Conference proceeding held October in Dublin; page 397-401
- [3] Hansen, K.S. and Courtney, M.S. Online documentation of database structure, guidelines, contents and user instructions. <http://www.winddata.com/>
- [4] Biernbooms, W. et al "Modelling of Extreme gusts for Design Calculations (NewGust)" 1999 European Wind Energy Conference held 1-5 March in Nice; to be published.
- [5] Højstrup, J. et al "Non-Gaussian Turbulence" 1999 European Wind Energy Conference held 1-5 March in Nice; to be published.

8. ACKNOWLEDGEMENTS

The project is being supported by the European Union, DG XII, contract no. JOR3-CT95-0061.

Table 1: Available sites represented in the database

Site	Terrain Orography	Speeds	Dirs	Sonics	Hours
Alsvik	coastal/flat	16	16	0	17500
Andros	pastoral/mountain	6	6	0	625
A. Spruzza	pastoral/mountain	3	1	0	543
Cabauw	pastoral/flat	4	4	0	49
La Clape	scrub/hill	1	1	1	242
ECN/Petten	coastal/flat	9	3	0	49
Emden	coastal/flat	2	1	0	780
Jade	rural/flat	3	1	0	4
K.W.Koog	coastal/flat	20	18	0	344
Lammefjord	pastoral/flat	9	9	1	663
Lavrio	pastoral/mountain	4	4	2	730
Lyse	coastal/mountain	12	12	0	3355
S. Jorge	coastal/mountain	2	1	1	5
Skipheia	coastal/hill	17	1	2	>6200
Sletringen	coastal/flat	5	1	0	3355
Tarifa	pastoral/mountain	5	2	3	280
Tjareborg	pastoral/flat	12	6	0	64
Toplou	pastoral/mountain	1	1	1	172
Vindeby	offshore/flat	21	6	6	2060
Vallersund	coastal/hill	4	1	0	3756
Zeebrugge	coastal/flat	2	1	0	?
Windy		4	1	1	>400
Total	> 40.000 hours				

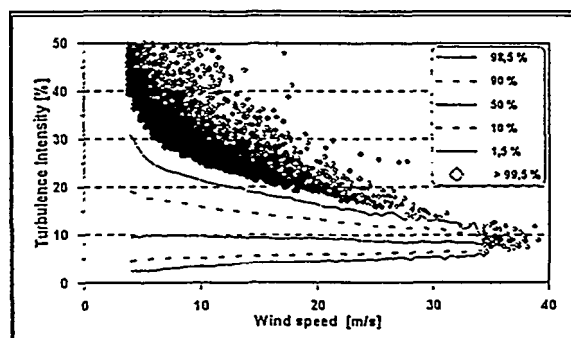


Figure 1: Turbulence intensity for wind speeds above 4 m/s, based on 10 minute values.

Matching runs

page 1 of 13

Run	Site	Speed	Dir	T.I.%	Duration
199510071250	lavrio	18.0	17	13	600
199510071430	lavrio	18.5	17	12	600
199510071440	lavrio	18.7	17	13	600
199510071450	lavrio	18.3	17	11	600
199510071510	lavrio	18.9	17	11	600
199510071530	lavrio	18.0	17	13	600
199510071540	lavrio	18.1	17	11	600
199510071630	lavrio	18.7	14	12	600
199510071750	lavrio	18.6	8	13	600
199510071830	lavrio	18.2	4	14	600
199510071840	lavrio	18.2	8	14	600
199510072210	lavrio	19.0	17	15	600
199510072220	lavrio	19.3	19	13	600
199510072230	lavrio	21.0	18	13	600
199510072240	lavrio	21.0	14	12	600
199510072250	lavrio	20.6	16	13	600
199510072300	lavrio	20.6	15	13	600
199510072310	lavrio	20.9	13	15	600
199510072320	lavrio	22.4	17	11	600
199510072330	lavrio	21.2	16	12	600
199510072340	lavrio	19.9	15	14	600
199510072350	lavrio	21.4	15	15	600
199510070550	lavrio	13.1	6	13	600
199510070910	lavrio	13.4	13	14	600
199510070920	lavrio	18.5	15	14	600

Next 25 matches

Figure 2: List of matching runs

Database of wind time series

Site <u>lavrio</u>		Run: 199510160930						
Start: 16-10-95 09:20:00		Duration: 600.00						
File	Frequency	Packed size						
<u>lavrio/1995/10/16/0930_010.m</u>	1.00	11792						
<u>lavrio/1995/10/16/0930_010.m</u>	8.00	129012						
Channel	Type	Freq	Height	Mean	Stdv	Min	Max	Turb
u10z	u	1.0	16	22.26	3.26	11.4	32.1	
u10z	u	1.0	16	22.11	3.16	10.7	29.0	
u10z	u	1.0	32	22.96	2.97	12.7	29.5	
u10z	u	1.0	32	22.69	2.90	12.2	28.3	
u10z	d	1.0	16	15.50	7.40	0.0	59.9	
u10z	d	1.0	16	20.60	7.60	1.0	49.0	
u10z	d	1.0	32	15.30	6.20	0.0	41.0	
u10z	d	1.0	32	16.70	6.30	0.0	47.0	
u10z	u1z	1.0	5	16.08	0.19	17.5	19.4	
u10z	u1z	2.0	22	16.75	2.35	4.4	28.4	
u10z	u1z	2.0	22	12.68	2.46	3.5	21.2	
u10z	u1z	2.0	22	1.47	1.59	-0.0	9.6	
u10z	u1z	2.0	22	-12.43	2.45	-22.1	-2.0	
u10z	u1z	2.0	22	15.33	2.76	7.7	24.4	
u10z	u1z	2.0	22	1.52	1.58	-4.3	8.1	
u10z	u1z	2.0	22	21.68	3.00	10.6	27.5	

Figure 3: Run statistics.

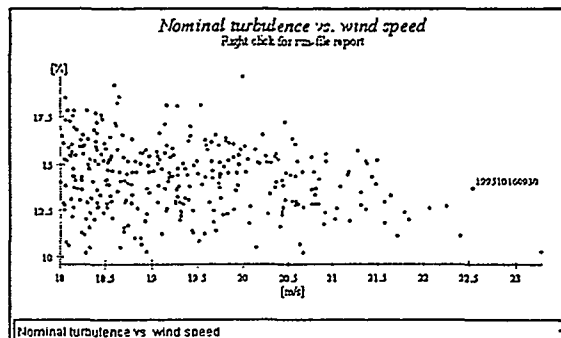


Figure 4: Plot of nominals (turbulence intensity versus wind speed).

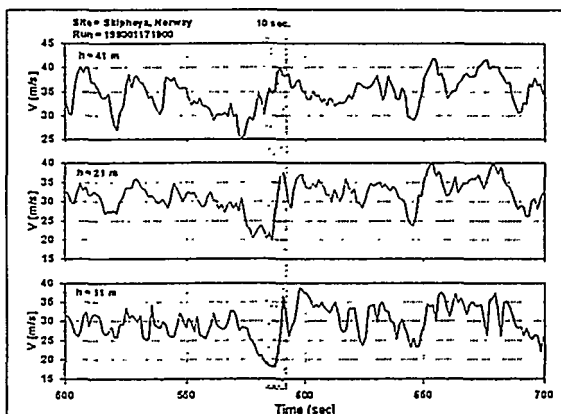


Figure 5: Very large gust, $V_g = 17$ m/s; period = 10 sec.

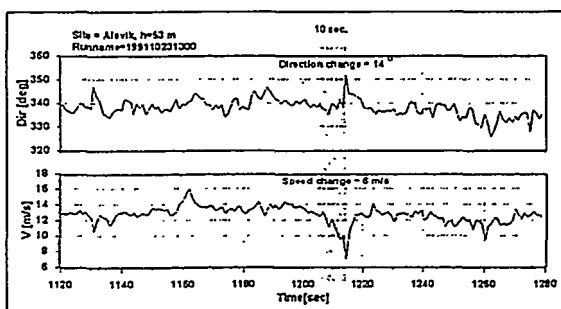


Figure 6: Simultaneous gust and direction change, period=10 sec.

DESIGN OFF-SHORE WIND CLIMATE

Gunner C. Larsen and Hans E. Jørgensen
Wind Energy and Atmospheric Physics Department
Risø National Laboratory
DK-4000 Roskilde, DENMARK
phone: +45-46775056
e-mail: gunner.larsen@risoe.dk

ABSTRACT: Specific recommendations on off-shore turbulence intensities, applicable for design purposes, are lacking in the present IEC-code. The present off-shore wind climate analysis presents the distribution of the turbulence standard deviation around the mean turbulence standard deviation, conditioned on the mean wind speed. Measured distributions, based on a huge amount of measuring data from two shallow water off-shore sites, are parameterized by fitting to a three parameter Weibull distribution. Combining a simple heuristic load model with the parameterized probability density functions of the turbulence standard deviations, an empirical off-shore design turbulence intensity is evaluated that in average yields the same fatigue damage as the distributed turbulence intensity. The proposed off-shore design turbulence intensity is, within the IEC code framework, applicable for extreme as well as for fatigue load determination.

Keywords: Fatigue, Off-shore, Turbulence

1. INTRODUCTION

An increasing part of wind turbines will be erected at off-shore sites in the future due to environmental requirements and the limited number of on-shore sites with favourable wind potential. The wind load conditions are the primary external load concern for the structural integrity of a wind turbine. Consequently, the off-shore design wind climate becomes of increasing importance.

According to the IEC-61400 design code proposal, the *on-shore* design wind climate may be classified into a limited number of wind categories reflecting differences in wind potentials as well as in variability of the turbulence components. The *off-shore* design wind climate, however, is to be specified entirely based on information provided by the manufacturer. One of the issues, that is of particular importance in that respect, is the turbulence intensity as function of the mean wind speed.

At off-shore sites, the roughness length will depend on the mean wind speed, which in turn means that the description of the turbulence intensity, as function of mean wind speed, becomes qualitatively different from the on-shore load situation. However, where on-shore sites display large differences in terrain topology, the off-shore sites are far more homogeneous as the majority of off-shore sites are likely to be associated with shallow water areas. This in turn opens for a simple and relative general description of the variability of an off-shore design turbulence intensity as function of the mean wind speed. The present paper presents such a model.

Based on a huge amount of 10-minute shallow water off-shore wind statistics, originating from the Vindeby and the Gedser experiments, the variability of the standard deviation of the horizontal wind speed is quantified in terms of a set of probabilistic models conditioned on the mean wind speed.

Due to the strongly non-linear relationship between wind loading and the fatigue life time consumption in a wind turbine structure, the design turbulence intensity can not be taken as the mean of estimated probability densities. Instead the mean fatigue life time consumption is estimated by combining the probability density distributions of the turbulence intensities with a (simple heuristic) general load model. The particular turbulence intensity resulting in the mean fatigue life time consumption, as determined from the conditioned probability distributions, is defined as the *design turbulence intensity*.

2. METHOD

At a given site and in a given height above the ground (or water surface), the standard deviation, σ_u , of the arbitrary wind speed, conditioned on the mean wind speed, will follow some probability distribution in the long term. This reflects a natural variability over time owing to, e.g., varying atmospheric stability conditions, varying wind directions (and thus varying roughness conditions) etc.. It is appropriate to consider the standard deviation, $\sigma_{u,T}$, of the arbitrary wind speed in the short term - i.e. over some limited time span T. The mean wind speed associated with this the time span T is denoted U_T .

The variability of the turbulence standard deviation, $\sigma_{u,T}$, is approached empirically in the present analysis. Based on a huge data material, a suitable binning-matrix in the mean wind speed and in the standard deviation can provide an estimate of the probability density function (PDF) of the standard deviation, $\sigma_{u,T}$, conditioned on the mean wind speed as expressed by

$$\varphi_{\sigma}(x|U_T) = \frac{P(x \leq \sigma_{u,T} \leq x + dx | U_T)}{dx} \quad (1)$$

where P denotes probability.

The binning procedure results in PDF-estimates represented as histograms. Provided that the number of bins in the standard deviation is large, the resolution of the estimated PDF's are good. The selection of bin interval sizes is a compromise between sufficient resolution and a reasonable number of data within each bin - in the present analysis the mean wind speed has been binned using a bin interval equal to 2 m/s. As for the binning in the standard deviation, a total of 20 bin intervals have been selected which is somewhat more than the number of bin intervals proposed in (Conradsen, 1976).

Having established estimates of the conditional probability density functions of the turbulence standard deviation, $\sigma_{u,T}$, in terms of histograms, the results are parameterized by fitting a three parameter Weibull PDF to these experimentally based estimates. The three parameter Weibull PDF, which is known to be a very "flexible" distribution type, is expressed as

$$f(x; k, \alpha, \beta) = \frac{k}{\beta} \left(\frac{x - \alpha}{\beta} \right)^{k-1} \exp \left[- \left(\frac{x - \alpha}{\beta} \right)^k \right]; x \geq \alpha \quad (2)$$

where k is a shape parameter, α a position parameter and β a scaling parameter (k and β are required positive). Subsequent numerical testing has shown that it is suitable for representation of the body of the distribution, however, it has a tendency of underestimating the upper tail.

The basic presumption, in the succeeding determination of a design turbulence intensity, is that the fatigue load spectrum, in a first order approximation, is proportional to the standard deviation of the horizontal wind fluctuations. The physics behind the assumption is the following: for a given mean wind speed (expansion point) the dynamic wind loading of a turbine can be approximated by a "gradient" multiplied by the (horizontal) turbulence fluctuations. It is here further assumed that this "gradient" is independent of the size of the fluctuations.

For a given mean wind speed, U_T , the *mean fatigue loading*, $L_f(U_T)$, of the turbine is then symbolically determined from the expression

$$L_f(U_T) = C \int_0^{\infty} \varphi_{\sigma}(\sigma_{u,T}|U_T) \sigma_{u,T}^m d\sigma_{u,T} \quad (3)$$

where C is a characteristic constant for the particular load on the particular wind turbine, and m is the Wöhler exponent for the particular material. In the above formulation it is implicitly assumed that the fatigue loading is caused exclusively by the stochastic part of the wind field.

Defining the *design standard deviation* as the standard deviation, $\sigma_{d,T}(U_T)$, giving rise to the above mean fatigue loading we find

$$L_f(U_T) = C \sigma_{d,T}(U_T)^m \quad (4)$$

$$= C \int_0^{\infty} \varphi_{\sigma}(\sigma_{u,T}|U_T) \sigma_{u,T}^m d\sigma_{u,T}$$

whereby the design standard deviation is expressed only in terms of the conditional distributions of the standard deviation of the horizontal turbulence component as

$$\sigma_{d,T}(U_T) = \sqrt[m]{\int_0^{\infty} \varphi_{\sigma}(\sigma_{u,T}|U_T) \sigma_{u,T}^m d\sigma_{u,T}} \quad (5)$$

In case the fatigue loading, in addition to the turbulence contribution, originates from a periodic deterministic load component, it can be shown that the design standard deviation defined according to equation (5) will be conservative. Due to the non-linear weighting of the standard deviation performed in equation (5), the design standard deviations do not correspond to 50% quantiles (or mean values) in the associated empirical distributions conditioned on the mean wind speed. The quantile level will depend on the value of the Wöhler exponent.

3. RESULTS

The analysis is based on a huge amount of wind speed statistics originating from measuring campaigns conducted at 2 different shallow water off-shore sites in Denmark - Gedser and Vindeby. All the available statistics on the data material have been transformed to 10-minute statistics.

At the Vindeby site the investigated wind data originate from a meteorological mast erected very close to the coast line. The data are recorded at level 37.5m and, depending on the wind direction, a sea fetch, a land fetch and a mixed fetch are represented at this site. In the present investigation only the pure sea fetch is considered. The sea fetch is characterised by having more than 15 km of sea upstream (Barthelmie, 1994). The data, within the sea fetch, are selected in order to avoid mast- and boom effects. With the defined selection criteria, the available data material constitutes 5566 10-minute time series with an overall mean wind speed equal to 7.92m/s.

The meteorological mast at the Gedser site is also erected close to the coast line providing the possibility of analysing both land- and sea fetches. The present investigation relates to (sea fetch) wind observations recorded at level 30.0m. Based on the available 21622 10-minute time series, the overall mean wind speed, associated with the sea fetch, is estimated to 7.87m/s.

3.1 Vindeby

The Vindeby data material covers 10-minute mean wind speeds ranging from 2m/s to approximately 20m/s. The distribution of the wind speed standard deviation is evaluated for each mean wind speed bin as described in section 2. As an example the result, associated with the mean wind speed bin ranging from 8m/s to 10m/s, is illustrated in Figure 1. The dotted line in the figure

represents the three parameter Weibull fit, whereas the full line is the estimated distribution determined directly from the measurements. Note, that the abscissa values relate to the shifted standard deviation as determined by the Weibull parameterization.

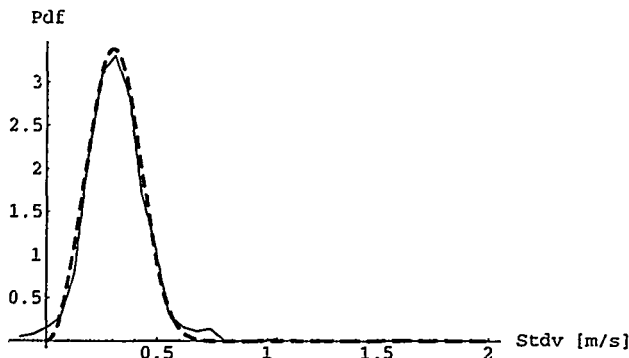


Figure 1: Measured and fitted PDF's representing the mean wind speed bin 8m/s-10m/s.

The design turbulence intensity, as defined in section 2, is subsequently determined by numerical integration of equation (5) applying the fitted PDF's. Two different Wöhler exponents - 4 corresponding to loading on a steel component, and 12 corresponding to the loading of a GRP component - were applied. As expected, the design turbulence intensity increases with increasing Wöhler exponent. However, the increase is moderate as shown in Figure 2.

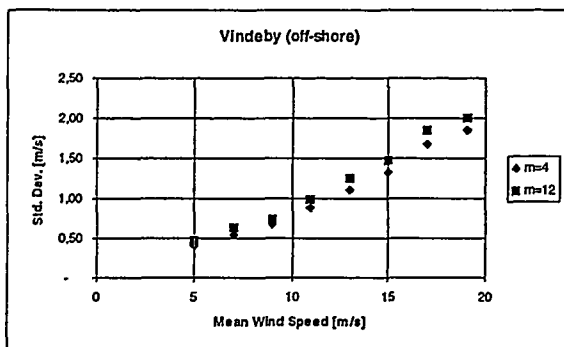


Figure 2: Design turbulence intensities as computed based on $m=4$ and $m=12$, respectively.

From a design point of view it is not practical to deal with design turbulence intensities that depend on the material properties. The off-shore design turbulence proposal will therefore (conservatively) be based only on the part of the analysis related to the largest Wöhler exponent ($m=12$).

As a consequence the Vindeby analysis finally results in the following empirical relationship between design turbulence intensity and the mean wind speed

$$TI_V = 0.0031 U_{10} + 0.0409 + \frac{0.1790}{U_{10}} \quad (6)$$

where index V indicates that the result is based on Vindeby data. U_{10} denotes a mean wind speed based on a 10-minute averaging period. The result is obtained by applying a second order polynomial fit to the dependence of the

estimated design standard deviation with the mean wind speed as illustrated in Figure 3.

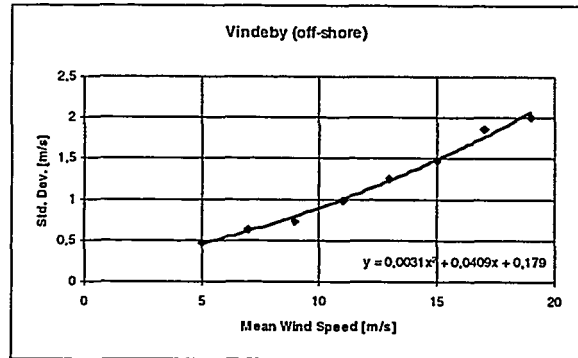


Figure 3: Polynomial least square fit of ($m=12$) design standard deviation as function of the mean wind speed.

3.2 Gedser

The data material covers 10-minute mean wind speeds ranging from 2m/s to approximately 22m/s. In analogy with the investigation of the Vindeby data, the conditioned PDF's of the 10-minute standard deviation are established for all mean wind speed bin intervals. The result for the mean wind speed bin ranging from 8m/s to 10m/s is illustrated in Figure 4.

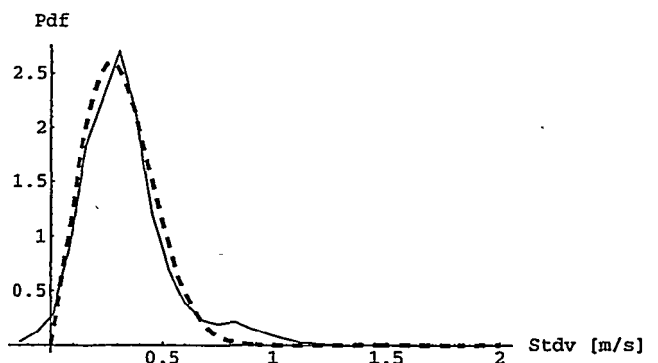


Figure 4: Measured and fitted PDF's representing the mean wind speed bin 8m/s-10m/s.

Proceeding along the lines described in section 3.1, the result presented in Figure 5 for the design turbulence standard deviation, as based on Gedser data, is obtained.

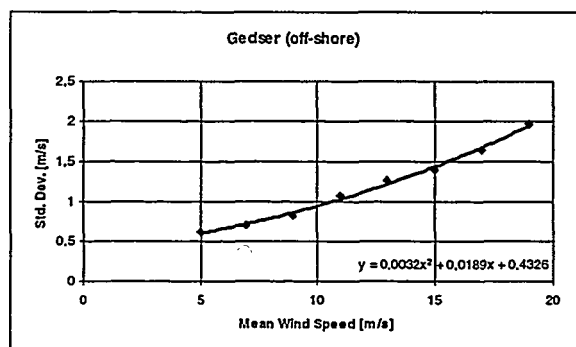


Figure 5: Polynomial least square fit of ($m=12$) design standard deviation as function of the mean wind speed.

The derived design turbulence intensity is thus expressed as

$$TI_G = 0.0032 U_{10} + 0.0189 + \frac{0.4326}{U_{10}} \quad (7)$$

where index G refers to Gedser data.

3.3 Synthesis

The results obtained from the two independent analyses are in good agreement, as shown in Figure 6.

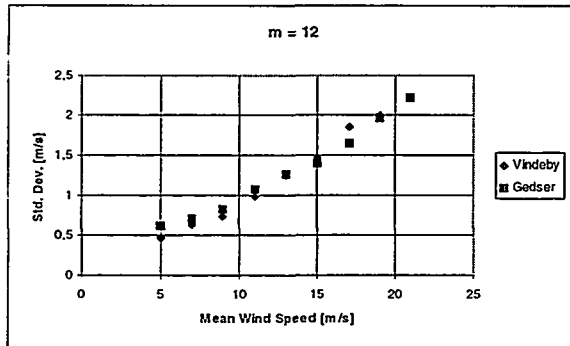


Figure 6: Design standard deviations based on Vindeby- and Gedser data, respectively

The close agreement is interpreted as a confirmation of the conjecture that off-shore sites generally are relatively homogeneous. As a consequence, based on the available data material, it makes perfectly sense to determine a "general" expression for the design turbulence intensity applicable for shallow water off-shore site conditions.

The resulting proposal for an off-shore design turbulence intensity, TI_D , is based on a weighted mean of the results obtained from the two investigated sites. The weighting factor is selected as the relative number of the total number of available data series associated with each site (5566/27188 for the Vindeby experiment and 21622/27188 for the Gedser experiment). The final expression for the design turbulence intensity is

$$TI_D = 0.0032 U_{10} + 0.0234 + \frac{0.3807}{U_{10}} \quad (8)$$

The above expression applies to extreme load design as well as to fatigue design provided that the guidelines in IEC 61400 are adopted.

Note, however, that the present investigation only includes mean wind speed values up to approximately 22m/s, and that the above specification of design turbulence intensity consequently should be used with care in wind regimes outside this range. However, compared to the conventional practice where off-shore conditions, according to the IEC 61400 standard must be considered as a "S" class type situation (where the required parameters must be entirely supplied (and documented) by the designer), the present proposal gives considerable guidance.

4. CONCLUSION

Specific recommendations on off-shore design turbulence intensities are lacking in the present IEC-code. A simple expression for a design turbulence intensity, applicable for shallow water off-shore siting of wind turbines, has been proposed. The proposal is based on extensive analyses of a huge data material originating from two Danish off-shore sites situated in shallow water regions.

The analysis embraces quantification of the distribution of the horizontal turbulence standard deviation conditioned on the mean wind speed and subsequent application of a simple heuristic load model.

The application of the proposal will, until further analyses of other categories of water regions are available, be limited to *shallow water regions*. However, at present most off-shore turbines are erected at such sites.

5. ACKNOWLEDGEMENT

The present work is partially financed by the Commission of the European Union under the DG XII Non-Nuclear Energy Programme, contract JOR3-CT95-0026, which is gratefully acknowledged.

6. REFERENCES

- [1] Larsen, G.C. and Jørgensen, H.E. (1999). Variability of Wind Speeds. Risø-R-1078(EN).
- [2] Draft IEC 61400-1, Ed. 2 (1998). Wind Turbine generator Systems - Part 1: Safety requirements. International Electrotechnical Commission (unpublished).
- [3] Barthelmie, R.J. et. al. (1994). The Vindeby Project: A Description. Risø-R-741, Risø National Laboratory, Denmark.
- [4] Conradsen, K. (1976). An Introduction to Statistics (in Danish). IMSOR, DTU.

NON-GAUSSIAN TURBULENCE

J. Højstrup, NEG Micon Project Development A/S, Alsvej 21, DK8900 Randers, Denmark, jho@neg-micon.dk
 K.S.Hansen, Dept. of Energy Engineering, DTU bld.404, DK2800 Lyngby, Denmark, ksh@et.dtu.dk
 B.J.Pedersen, VESTAS Wind Systems A/S, Smed Hansens Vej 27, DK6940 Lem, Denmark, bjp@vestas.dk
 M.Nielsen, Wind Energy and Atmospheric Physics, Risø National Laboratory, n.m.nielsen@risoe.dk

ABSTRACT: The pdf's of atmospheric turbulence have somewhat wider tails than a Gaussian, especially regarding accelerations, whereas velocities are close to Gaussian. This behaviour is being investigated using data from a large WEB-database in order to quantify the amount of non-Gaussianity. Models for non-Gaussian turbulence have been developed, by which artificial turbulence can be generated with specified distributions, spectra and cross-correlations. The artificial time series will then be used in load models and the resulting loads in the Gaussian and the non-Gaussian cases will be compared.

Keywords: Turbulence, loads, non-Gaussian, wind timeseries.

1 INTRODUCTION

It has long been common knowledge that turbulence is the result of a non-Gaussian process. This has been confirmed both by windtunnel and field measurements that typically show wind speeds following a Gaussian distribution, but accelerations and higher order derivatives can be strongly non-Gaussian in the sense that their distributions show a higher probability for large events than that expected from a Gaussian process, or in other words, the distributions have longer 'tails'. Calculations of loads on wind turbines and other structures have traditionally utilised the Gaussian approximation, which must be assumed to potentially underestimate the large loads. Systematic investigations into the effects of non-Gaussianity of atmospheric turbulence have hitherto been hindered by the fact that very large amounts of data are needed in order to obtain statistically reliable estimates of the quantitative effects since the largest deviations occur with low probabilities.

Recently a very large database of fast sampled wind data has become available to the engineering community, and this database has been used to quantify the amount of non-Gaussianity. These investigations confirm that atmospheric turbulence measured in conditions such as those interesting for windturbine research in general is non-Gaussian. The amount of non-Gaussianity is related to differences in terrain types and atmospheric conditions. Models for the non-Gaussian distributions have been developed, by which timeseries can be generated with specified characteristics regarding distributions, spectra and cross-correlations. These models will be used to demonstrate the effects of non-Gaussianity on simple load cases.

2 NON-GAUSSIAN DATA

Fig.1 shows pdf's of the three components of the velocity vector and the corresponding accelerations. It is quite obvious that in this case velocities are close to being Gaussian and accelerations are non-Gaussian with significantly longer 'tails' in the distribution. This can also be illustrated by calculating the higher order normalized moments of the distributions. For a Gaussian all even order moments are zero, and fourth (kurtosis) and sixth order moments 3 and 15 respectively. Using data from the WEB database, it is easy to look at a large number of time series and see whether this type of behaviour is a general one.

The next figure shows the fourth order moments for a large number of time series (15000 hours), and it is quite obvious again, that the velocities (fig.2) are near-Gaussian with

kurtosis values near three, and the accelerations show non-Gaussian behaviour with significantly larger kurtosis.

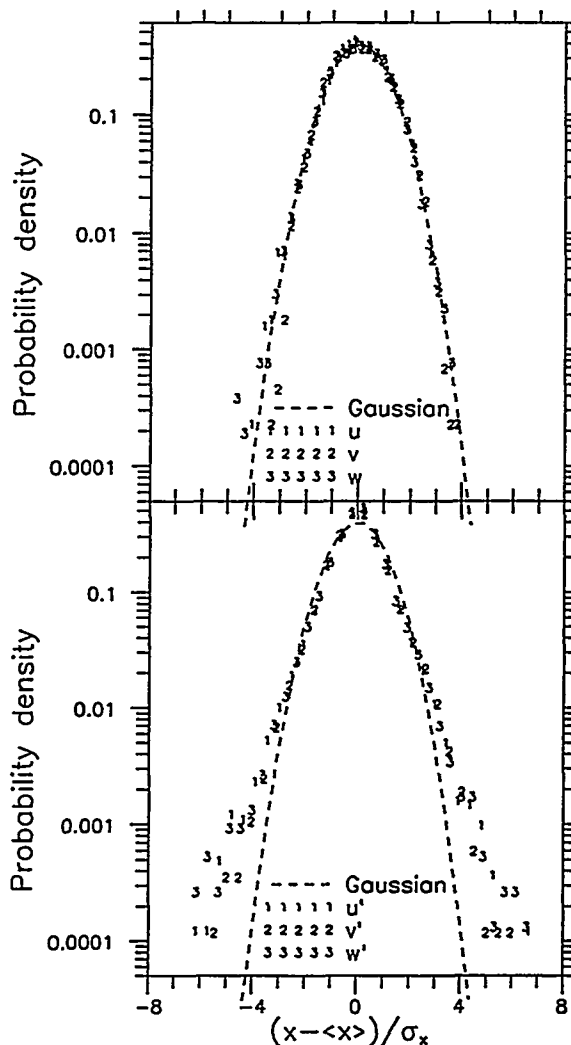


Figure 1 Top frame shows pdf of velocities (sonic anemometer), bottom frame shows the corresponding accelerations. Note that velocities are near-Gaussian, whereas accelerations show larger 'tails' in the distributions.

One of the objectives of this project is to try to parameterize this non-Gaussian effect in terms of terrain type, turbulence intensity, height ... This part of the project is still ongoing, so far no clear correlations have been established.

ARTIFICIAL TURBULENCE

In order to apply our knowledge of non-Gaussian behaviour to actual load calculations, it is necessary to be able to generate wind timeseries of specified characteristics. It is obviously easy to filter a Gaussian time series through a non linear filter, renormalize and thus obtain a new timeseries with the specified non-Gaussian distribution. The difficult part is to be able to control also the power spectra, cospectra and cross correlations for different velocity components and in different positions in space.

The standard technique for modeling the correct spectral distribution is 1) to estimate amplitudes of the Fourier representation of the synthetic time series by square roots of components in the power spectrum, 2) select random phases, and 3) simulate a time series by inverse Fourier transformation. The random phases imply that the pdf becomes close to Gaussian. Many investigators have proposed [1,2,3,4] methods for non-Gaussian time series. These methods often operate with subtle transformations between the process of interest and auxiliary Gaussian process with a modified spectrum. See [5] for a good discussion of these techniques. One of the successful techniques developed in this project is based on a combination of the methods applied by [5] and [2].

CONCLUSIONS

The ultimate goal of the project is to be able to state whether the loads in a given type of environment is well described by the normally applied Gaussian methods, or whether more sophisticated methods should be used. The status for this process is presently:

1. Quantification of the non-Gaussianity as function of a number of parameters, terrain, stability, turb. Int. Status: Ongoing, no clear correlations so far.
2. Generation of artificial turbulence with specified distribution, spectra and correlations between velocity components. Status: Successfully concluded.
3. Application of artificial turbulence (Gaussian and non-Gaussian) to simple load cases and look for differences. Status: Ongoing.

ACKNOWLEDGEMENTS

This project is being supported by the Danish Ministry of Energy (J.Nr.1663/97-0032)

REFERENCES

- [1] Shinozuka, M. & C.-M. Jan, 1972: Digital simulation of random processes and its applications, JSV, 25, 111-128
- [2] Yamazaki, F. & M.Shinozuka, 1988: Digital generation of non-Gaussian stochastic fields, J. Engng. Mech. ASSC. 114, 1183-1197
- [3] Johnson, G.E., 1994: Construction of particular random processes, Proc. IEEE, 82, 270-285
- [4] Gurley, K.R., A.Kareem, M.A.Tognarelli, 1996: Simulation of a class of non-normal random processes, Int. J. Non-Lin. Mech, 31, 601-617

- [5] Seong, S.H. & J.A. Peterka, 1997: Computer simulation of non-Gaussian multiple wind pressure time series. J. Wind Eng. Aerodyn, 72, 95-105

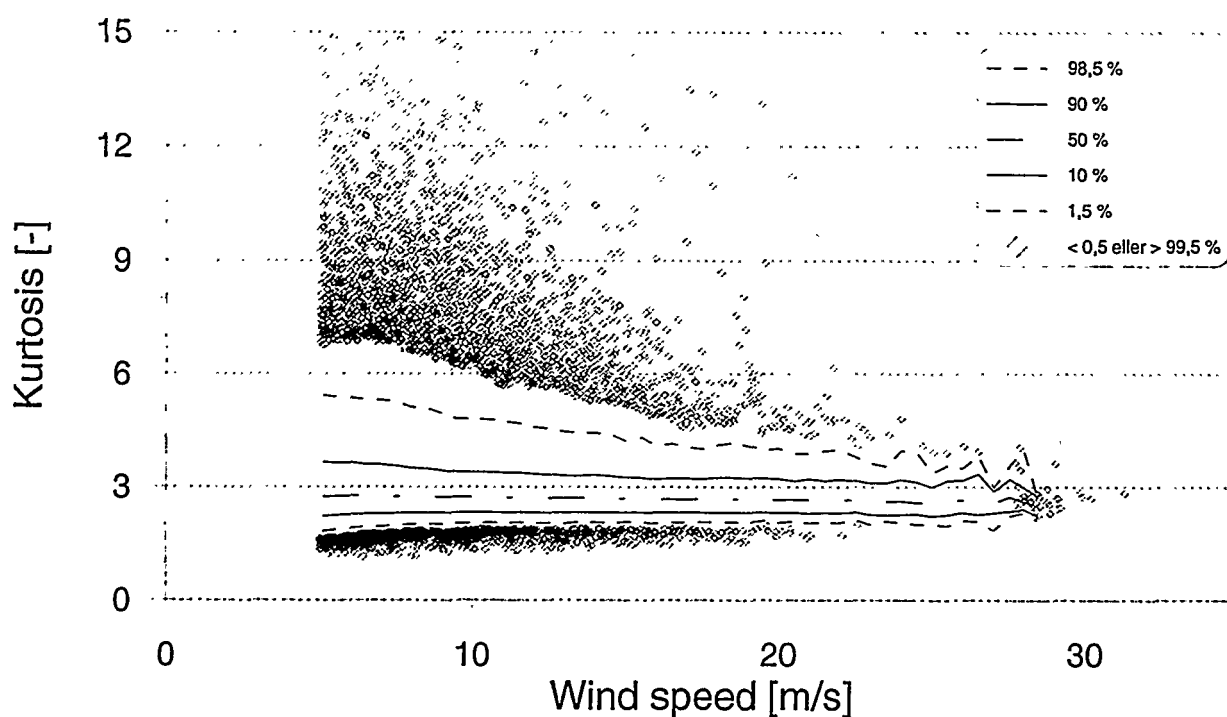


Figure 3 Summarized kurtosis values from about 15000 hours of wind time series. We see that the median of the data is close to three (slightly less), independently of wind speed. At lower wind speeds we note a very large spread of the data due for the most part to stability effects.

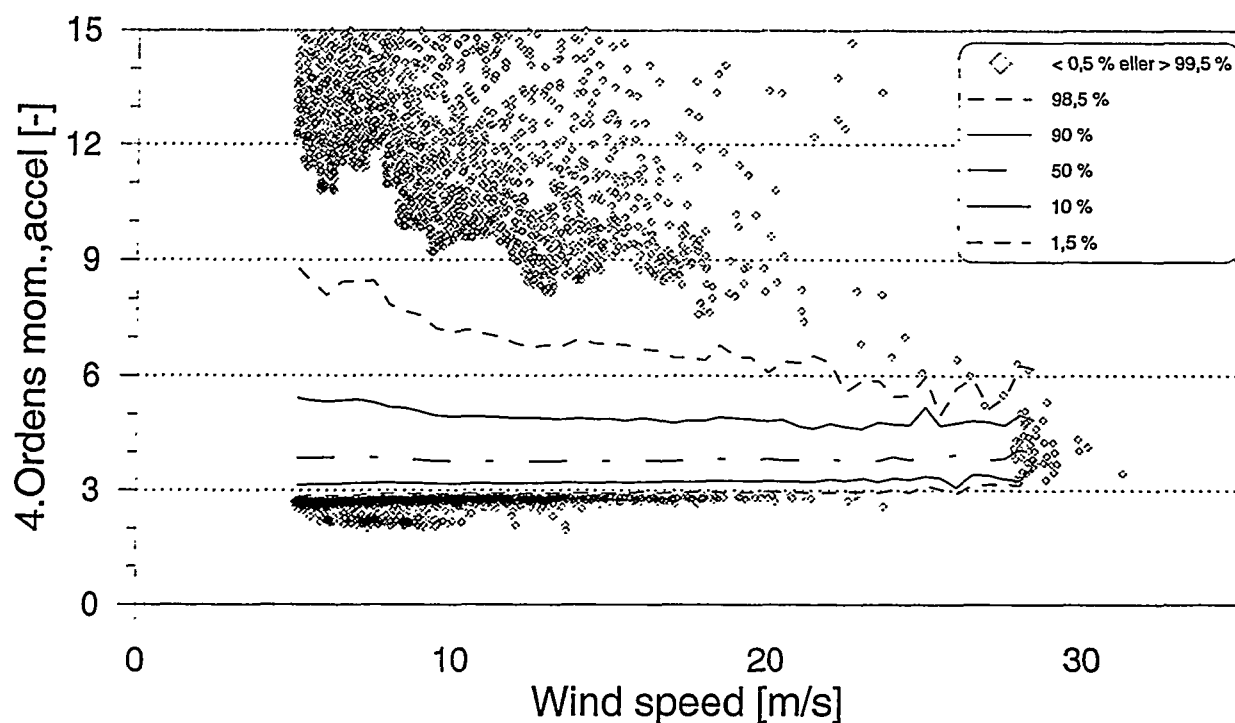


Figure 2 Summarized kurtosis values for the accelerations corresponding to the velocities above. Note that the values are generally larger and that the median value is significantly larger (close to four) than the Gaussian value of three.

DANISH EXTREME WIND ATLAS: BACKGROUND AND METHODS FOR A WAsP ENGINEERING OPTION

Ole Rathmann¹, Leif Kristensen¹, Jakob Mann¹ and
Svend Ole Hansen²

¹Wind Energy and Atmospheric Physics Department, Risø National Laboratory,
P.O.Box 49, DK-4000 Roskilde, Denmark

e-mail: ole.rathmann@risoe.dk., Tel: +45 4677 5003, Fax: +45 4677 5970

²Svend Ole Hansen ApS,
Skt. Jørgens Allé 5, DK-1615 Copenhagen V, Denmark

ABSTRACT: Extreme wind statistics is necessary design information when establishing wind farms and erecting bridges, buildings and other structures in the open air. Normal mean wind statistics in terms of directional and speed distribution may be estimated by wind atlas methods and are used to estimate e.g. annual energy output for wind turbines. It is the purpose of the present work to extend the wind atlas method to also include the local extreme wind statistics so that an extreme value as e.g. the *50-year wind* can be estimated at locations of interest. Together with turbulence estimates such information is important regarding the necessary strength of wind turbines or structures to withstand high wind loads. In the "WAsP Engineering" computer program a flow model, which includes a model for the dynamic roughness of water surfaces, is used to realise such an extended wind atlas method. With basis in an extended wind atlas, also containing extreme wind statistics, this allows the program to estimate extreme winds in addition to mean winds and turbulence intensities at specified positions and heights.

Keywords: Extreme winds, Wind statistics, Flow model, Water roughness, WAsP.

1. INTRODUCTION

For more than 10 years the *wind atlas method* [1] has been used to estimate wind climate for several purposes of which prediction of power production from wind turbines is the most important. The wind atlas method is represented by a number of software programs of which WAsP [2] is the most prominent.

The basic concept is the *wind atlas*, a collection of regional Weibull (or similar) wind statistics for a number of standard heights and homogeneous roughnesses of plane surfaces. The statistics contain directional information using a number of sectors, normally 12. The term regional indicates that the wind atlas applies to a region that is subject to the same basic wind climate, i.e. the same geostrophic wind, and of an extension of typically 50 km. By means of a wind flow model, including a digital representation of terrain topography, and supplemented with the geostrophic drag law, the wind atlas is transformed to wind climatological statistics for a specified site and height above terrain by introducing local terrain curvature, roughness inhomogeneities and sheltering obstacles. Using the same flow model, but in a reverse process, a wind atlas may be constructed on basis of wind observations from a meteorological mast by cleaning the data for the same kind of topography effects.

The mean wind distribution obtainable from the classical wind atlas method, however, is insufficient to predict wind load for design purposes of wind turbines as well as for buildings and bridges and other open-air structures, not the least for off-shore installations: here also extreme winds, gusts, profiles and turbulence distribution are important parameters. The WAsP Engineering project was initiated with the aim of developing methods to supply such wind predictions and, in turn, implement them in a software product.

This paper focuses on the treatment of extreme wind prediction and the extreme wind part of the extended wind atlas in WAsP Engineering.

2. FLOW MODEL

WAsP Engineering uses a flow model called LINCOM [3], an acronym for linearised computation. Contrary to the classical WAsP, which uses a polar grid focusing on the point of interest, LINCOM uses a rectangular grid which allows an entire field of velocities to be obtained in a single calculation. This has certain calculational advantages in connection with widely extended wind farms, but is also a necessary pre-requisite for the turbulence estimation [4] used in WAsP Engineering.

LINCOM is based on the family of Fourier transformed linearized flow models developed by Jackson & Hunt [5] and Troen & de Baas [6]. Basic assumptions for the flow model are:

- moderately complex terrain
- neutrally stable atmospheric boundary-layer

2.1 Spectral Flow Perturbations

The flow is modelled as a sum of a basic equilibrium wind flow field U_0 with a vertical logarithmic profile; and a Fourier sum of perturbations originating from variations in terrain and roughness:

$$U_0(z) = U_* / \kappa \ln(z / z_{0,a}) \quad (1a)$$

$$U(x, z) = U_0(z) + \sum_k [u'_k \exp(-z/L_k) + u''_k \exp(-z\alpha_k)] \exp(x \cdot k) \quad (1b)$$

where standard notation is used together with $z_{0,a}$ as the log-average roughness over the calculation domain and u'_k and u''_k as the (complex) velocity amplitudes of the Fourier components with wave number vector k , of the outer (inertial) and inner (viscously dominated) parts of the flow field, respectively.

A central concept is the use of the spectral length scales L_k (outer) and l_k (inner), related by the Navier-Stokes equations through the wavenumber to effective advection velocities U^* and eddy viscosities K^* (h = horizontal, z = vertical)

$$L_k = 1/|k|, \quad (2a) \quad l_k = 1/|\alpha_k|, \quad (2b)$$

$$\alpha_k = \sqrt{\left(K_h^2 |k|^2 + i k \cdot U^a \right) / K_z^2} \quad (2c)$$

It should be noted that α_k is complex, and the principal root should be chosen.

The advection velocity U^a and the eddy viscosity K^a are spectrally modelled to be related to the basic flow field by means of the inner length scale l_k as

$$U^a = U_0(l_k c_1) \quad (3a) \quad K_h^a = K_z^a = \kappa U_* l_k c_2 \quad (3b)$$

where c_1 and c_2 are empirically determined model constants of order unity.

The height-variation part of the perturbations is defined by a boundary condition requiring the flow to be parallel to the surface. This condition is implemented spectrally, by requiring the vertical velocity components of the outer perturbation terms to match terrain slope and basic flow field in height $L_k c_1$.

The roughness-variation part of the perturbations is determined from the hypothesis that the flow is in equilibrium with the local surface roughness below a certain height z_r . The corresponding spectral boundary condition requires this stress-velocity equilibrium to be fulfilled in an empirically determined height z_r , which is also spectral:

$$z_r = 0.3 z^{0.33} L_d^{0.67}, \quad L_d = U_0 / |U_0 \cdot k| \quad (4)$$

L_d is upwards limited to the extension of the calculational domain divided by 2π .

2.2 Water Roughness Model

For off-shore wind farms and other installations it is important that the equivalent roughness of the water surface is not constant, but depends on the wind flow itself as the waves normally grow with the wind speed. The Charnock correlation [7] is used as basis

$$z_0 = A_c U_*^2 / g \quad (5)$$

but where Charnock assumes A_c to be constant (0.011) we follow a number of investigators [8,9,10] who found A_c to have a power dependence on friction velocity normalised by the wave velocity c :

$$A_c = \text{const.} (U_* / c)^p \quad (6)$$

Depending on the order of magnitude of U_*/c , different correlations are relevant, and three such correlations have been combined [11]. The wave speed is found to be dependent on the water fetch X , and we have used Hasselman's expression [12]:

$$(U_*/c) = 3.5 / (2\pi) (U_{10m}^2 / (X g))^{0.33} \quad (7)$$

3. EXTREME WIND ANALYSIS

For the establishment of a Danish extreme-wind atlas, data from four meteorological stations have been analysed (the positions are indicated on Fig. 1.) [13].

Kegnæs	Jan 91	-	Dec 97
Skjern	Mar 82	-	Dec 97
Sprogø	Sep 77	-	Dec 97
Tystofte	May 82	-	Dec 97

The 10-min timeseries of wind data were as a first step quality-checked and unreliable data were removed. Next, the data were cleaned for the effects of local terrain, roughness variations and sheltering obstacles using the wind atlas method, based on digital maps of the surroundings of the met-stations; and the cleaned data were then transformed to a surface shear stress

$$q = 1/2 \rho (U_*)^2 \quad (8)$$

at a roughness equal to 5 cm using the geostrophic drag law.

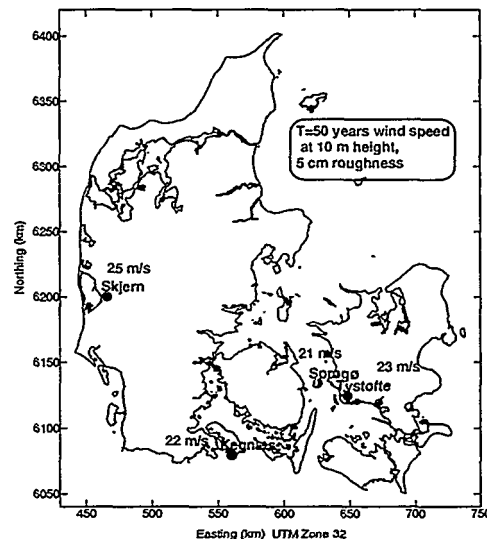


Figure 1. Meteorological stations used for Extreme Wind Analysis.

The q -timeseries were then analysed using a ranking procedure, where each of the timeseries were subdivided into M smaller sub-series of identical duration T_0 , and where the maximum- q values were subsequently ranked in ascending order, $q[m]$, $m=1..M$. This ranking procedure was performed for each of the twelve 30°- sectors as well as for the omnidirectional (i.e. irrespective of direction) maximum values.

The analysis was based on the recommendation by Gumbel [14] that the accumulated probability distribution of the extreme events be assumed double exponential, i.e.

$$P(T_0, q) = \exp(-\exp(-(q-Q)/\alpha)) \quad (9)$$

Here $Q = Q(T_0)$ is the most probable value of q and also the value of q , which, on average, is exceeded once in the period T_0 as pointed out by Kristensen et al. [15]. Furthermore, following the arguments in ref.[13], when the extreme events can be assumed to be independent, the parameter α may also be used to relate the values for different sub-series durations:

$$Q(T_2) = Q(T_1) + \alpha \ln(T_2/T_1) \quad (10)$$

From the above arguments the value of q for a standard return period T_1 , e.g. 50-year, can be found by plotting the ranked values of q versus $-\ln(-\ln(m/(M+1)))$, fitting a straight line through the plot and determine the zero-offset Q and the slope α . The value $Q(T_1)$ can then be determined from α , using eq.(10), and the corresponding wind speed (for the return time T_1) can in turn be found by transforming Q to the wind speed in standard height (here 10 m) using equations (8) and (1a).

This ranking procedure is illustrated for the omnidirectional extreme wind of the Sprogø met-station in Fig.(2). Within uncertainty the two subdivisions result in the same value of α , and the two Q -values relate to each other as expected from eq.(10).

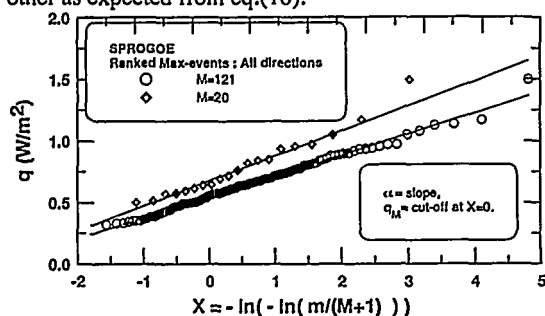


Figure 2. Ranking procedure for extreme winds at Sprogø, irrespective of direction. Two different subdivisions are shown: $M=20$ corresponding to a return time $T_0 = 1$ year, and $M=121$, corresponding to $T_0 = 61$ days.

Table 1. Obtained 50-year extreme wind speeds for Sprogø at standard conditions (10 m a.g.l., 5 cm roughness) derived from two subdivisions of 20-years timeseries.

	$T_0 = 61$ days		$T_0 = 1$ year	
D	U_{50} (m/s)	α	U_{50} (m/s)	α
0-360°	20.7 ± 0.6	0.170 ± 0.02	20.4 ± 1.3	0.203 ± 0.05

The resulting 50-year wind speeds and the α -value are given in Table 1.

For the Tystofte met-station the procedure is illustrated for a selected number of directional sectors in Fig.(3), and the resulting values are given in Table 2.

Table 2. Resulting 50-years extreme wind speeds for Tystofte, for 12 sectors and omnidirectionally derived from analysis of 61-days sub-timeseries.

D	U_{50} (m/s)	α
0	18.0	0.1554
30	16.0	0.1242
60	19.1	0.1729
90	19.3	0.1649
120	15.8	0.1048
150	17.7	0.1473
180	19.2	0.1653
210	19.5	0.1630
240	21.1	0.1988
270	21.4	0.2035
300	20.8	0.1920
330	18.8	0.1634
0-360	22.6	0.2053

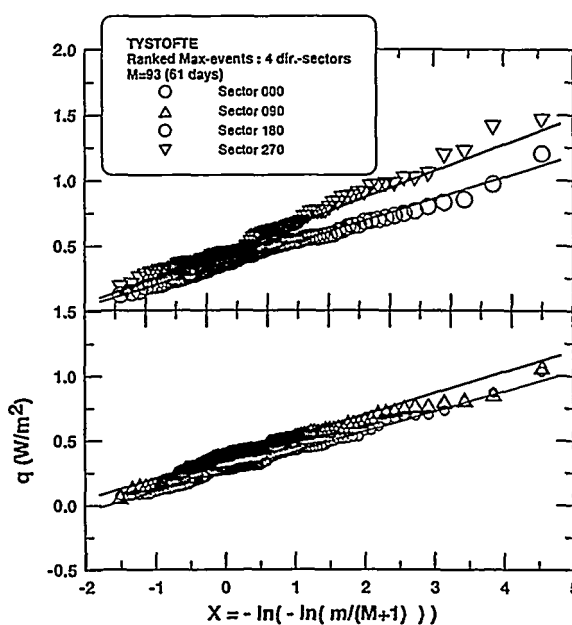


Figure 3. Ranking procedure for extreme winds at Tystofte for 4 selected sectors.

The analysis of all 4 stations resulted in tables of sectorwise and omnidirectional values of Q_{50} , U_{50} (wind speed) and α (for a return period of 50 years), from which the following main results, referring to a height of 10 m a.g.l. and 5 cm roughness, are extracted:

Station	Sprogø (m/s)	Tystofte (m/s)	Kegnes (m/s)	Skjern (m/s)
0-360°	21 ± 1	23 ± 1	22 ± 1	25 ± 1

4. EXTENDED WIND ATLAS

With the classical wind atlas data (e.g. as used by WASP) supplemented with extreme wind statistics as described above, the extended wind atlas in WASP Engineering will have a format as indicated below:

Table 3. Extended wind atlas format. Subscripts "wb" indicates Weibull parameters.

Sector	000	030	060	090	... 300	330
A_{wb}	4.4	4.4	4.3	4.8	5.2	4.6
k_{wb}	1.58	1.63	1.71	1.88	1.77	1.58
q_{50y}	0.791	0.718	0.822	0.976	1.251	0.902
α	0.1016	0.0977	0.1100	0.1186	0.1549	0.1125

Using position and height specifications together with the digital map, WASP Engineering then uses the extended wind atlas to drive the LINCOM flow model with a number of basic wind speeds and directions, thus building up the wind statistics at the specified site(s):

- Normal (mean) wind statistics, in terms of Weibull distributions;
- Extreme wind statistics;

- Furthermore, from the flow fields corresponding to the mean statistics, an estimate of the turbulence at specified site(s) is calculated.

5. CONCLUSION

With extreme wind estimation included, it is believed that WAsP Engineering will be an important step towards more realistic wind-load design for wind turbines and other open-air structures by including - besides regional wind norms - also local terrain effects.

6. ACKNOWLEDGMENT

This work was supported by the Danish Energy Agency through its Energy Research Programme (EFP), contract no. ENS-1363/97-0004.

REFERENCES

- [1] Troen, I. and Petersen, E.L., European Wind Atlas. Risø National Laboratory, Denmark, 1989.
- [2] Mortensen, N.G. et al. Wind Atlas Analysis and Application Program (WAsP), User's Guide. Risø National Laboratory, Denmark, 1993.
- [3] Astrup, P., Jensen, N.O. and Mikkelsen, T. Surface Roughness Model for LINCOM. Risø-R-900(EN). Risø National Laboratory, Denmark (1996).
- [4] Mann, J. Modelling of the Spectral Velocity Tensor in Complex Terrain. To be presented in the Proceedings of the 10th International Conference on Wind Engineering, June 21-24 1999, Copenhagen, Denmark.
- [5] Jackson, P.S. and Hunt, J.C.R. Turbulent wind flow over a low hill. Quarterly Journal of the Royal Meteorological Society 101, pp929-955 (1975).
- [6] Troen, Ib and de Bass, Anne. A Spectral Diagnostic Model for Wind Flow Simulation in Complex Terrain. In: Proceedings of the European Wind Energy Association Conference & Exhibition, Rome 1986, pp 37-41.
- [7] Charnock, H. Wind Stress over a Water Surface. Quarterly Journal of the Royal Meteorological Society 81, pp 639-640 (1955).
- [8] Johnson, H.K., Højstrup, J., Vedsted, H.J. and Larsen, S.E. On the Dependence of Sea Surface Roughness on Wind Waves. J. Phys. Oceanography, accepted for publication (1998).
- [9] Hansen, C. and Larsen, S.E. Further Work on the Kitaigorodskii Roughness Length Model: A New Derivation using Lettau's Expression on Steep Waves. Geophysica, 33(2), pp 29-44 (1997).
- [10] Toba, Y., Iida, N., Kawamura, H. Ebuchi, N. and Jones, I.S.F. Wave Dependence of Sea-Surface Wind Stress. J. Phys. Oceanography 20, pp 705-721 (1990).
- [11] Astrup, P., Larsen, S.E. Rathmann, O. and Madsen, P.H. WAsP Engineering -Wind Flow Modelling over Land and Sea. To be presented in the Proceedings of the 10th International Conference on Wind Engineering, June 21-24 1999, Copenhagen, Denmark.
- [12] Hasselman, K. et al. Measurements of Wind-Wave Growth and Swell Decay During the *Joint North Sea Wave Project (JONSWAP)*. Deutsche Hydrographische Zeitschrift, Reihe A (8°) no. 12, Hamburg (1973).
- [13] Kristensen, L., Rathmann, O. and Hansen, S.O. Extreme Winds in Denmark. Risø-R-1068(EN), Risø National Laboratory, Denmark (1999).
- [14] Gumbel, E.J. Statistics of Extremes, Columbia University Press, New York and London (1958)
- [15] Kristensen, L., Casanova, M., Coutney, M.S. and Troen, I. In Search of a Gust Definition. Boundary-Layer Meteorol. 55, pp 91-107 (1991).

Relative Performance of different Numerical Weather Prediction Models for Short Term Prediction of Wind Energy

Gregor Giebel, Lars Landberg, Kai Mönnich*, Hans-Peter Waldl*

Wind Energy and Atmospheric Physics Department, Risø National Laboratory, DK-4000 Roskilde,
Phone: +45 4677 5095, Fax: +45 4677 5970, Email: Gregor.Giebel@Risoe.dk, Lars.Landberg@Risoe.dk

*Dept. of Energy and Semiconductor Research EHF, Faculty of Physics,
Carl von Ossietzky Universität 26111 Oldenburg, Germany

ABSTRACT

In several approaches presented in other papers in this conference, short term forecasting of wind power for a time horizon covering the next two days is done on the basis of Numerical Weather Prediction (NWP) models. This paper explores the relative merits of HIRLAM, which is the model used by the Danish Meteorological Institute, the Deutschlandmodell from the German Weather Service and the Nested Grid Model used in the US. The performance comparison will be mainly done for a site in Germany which is in the forecasting area of both the Deutschlandmodell and HIRLAM. In addition, a comparison of measured data with the forecasts made for one site in Iowa will be included, which allows conclusions on the merits of all three models.

Differences in the relative performances could be due to a better tailoring of one model to its country, or to a tighter grid, or could be a function of the distance between the grid points and the measuring site. Also the amount, in which the performance can be enhanced by the use of model output statistics (topic of other papers in this conference) could give insights into the performance of the models.

1. Introduction

High penetrations of wind energy in an electrical supply grid require special precautions to ensure the reliability of the supply. Furthermore, knowing the wind energy output for a day or two ahead not only enables safe network conditions, but also strengthens the position of an utility or power broker on the market for electricity. At the moment, several approaches for short term prediction based on Numerical Weather Prediction (NWP) models are under investigation. Various other papers in this conference analyse various methods to ease the use of prediction, improve the accuracy or show the economic value. However, the weak (or strong) link in all these is the NWP. Hence, here it will be tried to have a comparison of three weather prediction models: the HIRLAM model of the Danish Meteorological Institute, the Deutschlandmodell of the Deutscher Wetterdienst, and the Nested Grid Model (NGM) of the US National Weather Service. The methodology will be as described in [1] and [2]. Any prediction method involving NWP can only be as good as its weakest link, which in previous works has been shown to be the NWP. Hence, looking for the best possible numerical model can improve the accuracy of the forecasts.

2. NWP description

2.1 HIRLAM

For this study, the Danish contender is actually a team effort of the Nordic countries, the Netherlands, Ireland and Spain. The High Resolution Limited Area Model HIRLAM consists of four submodels, consisting of the identical mathematical core, each covering a part of the total domain in various resolutions[3]. The furthest out is HIRLAM-G, which covers an area with cornerpoints in Siberia, California, the Caribbean and Egypt, hence a good share of the Northern Hemisphere. This model is the coarsest, with a horizontal resolution of 48 km and a time step of 240 s. The boundary conditions for this model stem from the global ECMWF model [4], which is run twice a day and gives boundary conditions with a 6 hour time step. This model, like the HIRLAM models, has 31 vertical levels. The HIRLAM-G hands over the boundary conditions to two models with a 16km horizontal resolution and 90s time step, one (N) covering Greenland, the other (E) covering Europe. HIRLAM-E is then used to provide the boundary conditions to the model used here, HIRLAM-D, which covers Denmark and parts of northern Germany, western Sweden and southern Norway with a resolution of 5.5 km, with a 30 s time step. The DMI provided us every 12 hours with forecasts in three-hourly time steps for up to 36 hours ahead, which were interpolated from the nearest grid points of the HIRLAM-D to the locations of the farms.

2.2 Deutschlandmodell

The Deutschlandmodell (DM) is the finest of a cascade of models operated by the German Weather Service DWD. It is nested inside the so called Europamodell EM, which itself is driven by a DWD own global model. The horizontal resolution of the DM is $14 \times 14 \text{ km}^2$. The predictions are provided by two model runs each day (0 UTC and 12 UTC). The forecast horizon of the DM is 48 hours.

2.3 Nested Grid Model

The National Weather Service NWS in the United States provides the Nested Grid Model NGM, which is run twice daily at the National Center for Environmental Protection NCEP. These were provided by the National Center for Atmospheric Research NCAR. Among the many models available, the NGM was chosen despite its relatively coarse resolution, since it was the only data set complete enough for the purpose of the overall task.

The NGM uses a sigma vertical coordinate system. It has 16 vertical levels up to the 25 mb level, with resolution comparable to the global spectral model.

The original version of the NGM included a three-grid configuration. The innermost grid (Grid C) had the highest horizontal resolution (84 km at 45 fti N). The largest grid (Grid A) covered the entire Northern Hemisphere and had the lowest horizontal resolution (336 km). The original three-nested grid configuration was changed to a two-grid configuration in 1991. Grid C was expanded in all directions to completely encompass the domain of the original Grid B and extend beyond the North Pole. Grid B was expanded to cover the remainder of the hemispheric domain, rendering Grid A unnecessary. The grid spacing, that is, the distance between points, is quite large, ranging from 137 kilometers (km) at 20 degrees latitude to 204 km at 90 degrees latitude. At 40 degrees latitude, the distance is 153 km. Forecasts from the 0000 and 1200 UTC cycles are available in gridded form in 6-hour intervals out to 48 hours.

The NGM model will be dropped from the NCEP production suite when the AVN MOS is developed in 1999. The model may be used as a possible component of the short-range ensemble forecasting system.

NGM Model Data Application of the Risø Model to the wind speed and power data bases which were available required access to historical numerical weather prediction data. The data period for the meteorological data from Iowa was June 1994 to April 1997. The NGM data for a 9×18 grid encompassing an area from the North Central US to Southern Texas included U- and V-component of the wind at 950, 850, and 700mb, as well as the U- and V-component at 10 meters above ground level. The period of record was January 1, 1994 to March 31, 1996.

3. Reference Data

3.1 Hoheging

The measurement data for the German site Hoheging are gained in the framework of the WMEP, a measuring program

accompanying the German wind energy promotion program "250 MW Wind" (managed by ISET Kassel). The site is situated inland in Northern Germany. The surroundings are flat with a moderate surface roughness. The wind turbine is a Südwind type SW20/110 with 31 m hub height. Measurements were available from January 1, 1998 to December 31, 1998.

3.2 Iowa

In an aggressive program to map out the wind resource in the state, the State of Iowa set up a large monitoring program comprising, amongst other things, of a dozen 50 meter wind monitoring masts throughout the state. The data of one of these, from Alta in the north west corner of the state, not far from the better known Buffalo Ridge site, was used in this comparison. The data reached from January, 1994 to March, 1996.

4. Methodology

4.1 Forecasting

The setup of the modeling is used routinely to forecast wind power output from farms in Denmark. The data provided by the NWP for the wind speed at 10 m a.g.l. is scaled by the logarithmic profile to the hub height of the turbine. A local flow model like WASP [5] is then used to correct the output for local effects like roughness and orography. The power output of the turbine(s) is simulated using a power curve, either as provided by the manufacturer or from the analysis of historical data of that farm/turbine. If the forecast is for more than one turbine at a time, the wind directional dependent efficiency of the wind farm is assessed off-line, e.g. by PARK [6]. To account for effects not accessible to the physical models, some kind of Model Output Statistics (MOS) is usually performed. In this case, the MOS was done with the model $Pred = Pow(a * w + b)$. a and b are statistical parameters here, $Pow()$ refers to the power curve, and $Pred$ is the corrected prediction.

For the Iowa case, no power production data was available, and therefore the analysis was done on the basis of wind speed only. Also, the topography was not available, and hence no WASP analysis could be performed. The HIRLAM output was used with WASP as local flow model. The same manufacturer supplied power curve as for the Deutschlandmodell was used. For the calculations on base of the Deutschlandmodell, no MOS was applied yet.

4.2 Statistical comparison

To evaluate the predictions from different sources, the multiple correlation coefficient ρ given by

$$\rho = \frac{VAR(w_{t+k}) - MSE_k}{VAR(w_{t+k})} \quad (1)$$

is used. Since no absolute values are present in this skill score, it can be used to compare different sites and predictions. VAR is the variance of the (centered) time series of the observations and MSE_k is the mean square error of the

predictions k hours ahead. The interpretation of this coefficient is that it measures how much of the total variation in the observations is explained by the predictions, i.e. 1 means that the predictions are perfect and zero means that predictions are useless.

This coefficient is actually identical with the Skill Score, usually expressed as [7]

$$S = \frac{MSE_{ref} - MSE_{model}}{MSE_{ref}} \quad (2)$$

MSE refers to the Mean Square Error of the reference model (the one to compete against) and the model to evaluate. Since the variance is defined as

$$VAR = \overline{(w_i - \mu_w)^2} = \overline{w^2} - \overline{w}^2 \quad (3)$$

With $\mu \equiv \overline{w}$ follows, that the multiple correlation coefficient is nothing else than the Skill Score against the easiest possible model, which is to predict the mean of the timeseries for all times ahead.

5. Results

5.1 Hoheging – HIRLAM

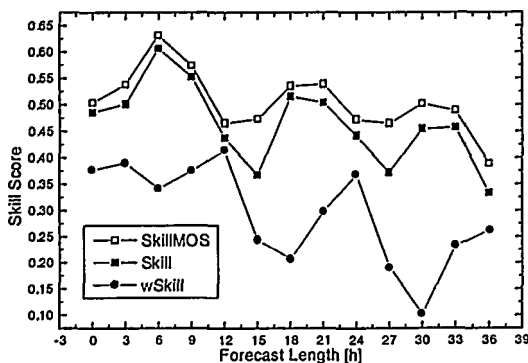


Figure 1: Skill scores for the HIRLAM/WAsP/MOS combination.

This picture shows the result for the multiple correlation coefficient, denoted skill score, for the power (denoted Skill, squares) as well as for the wind (denoted wSkill, circles). Note that this is the pure predictions, no MOS'ing has been performed for these two curves. Using MOS leads us to the graph denoted SkillMOS. We see that the statistical model does not ameliorate the prediction by a lot, even though it tends to smooth out the skill curve.

Interesting here is that obviously in this case the power can be better predicted than the wind – but this might be an artefact of the relative variance (which is the variance normalized with the mean of the time series): this can be seen in Table 1.

	Mean	Variance	rel. Variance
Power [kW]	16.6	22.5	1.3
Wind [m/s]	3.9	2.3	0.56

Hence, the power is much more variable, and a relatively good performance of the forecast will lead to a higher skill score.

5.2 Hoheging – Deutschlandmodell

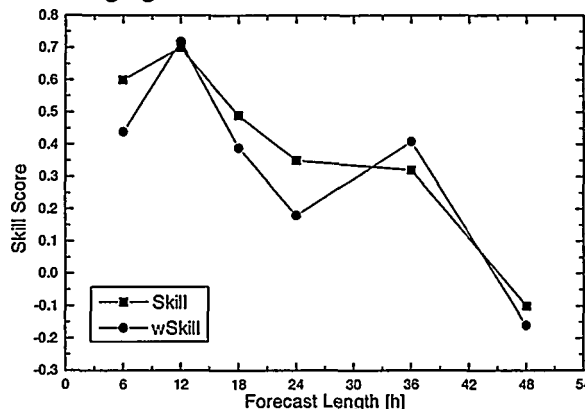


Figure 2: Skill Score for the Deutschlandmodell at Hoheging.

In this model, the tendency for the model to deteriorate with forecast length is rather strong – the 48-hour forecast is having a skill score of below zero. Then again, the forecasts up to 36 hours ahead are about as good as or better than the ones for HIRLAM. Here the difference in performance between the wind and the power forecast is not so distinctive as in the case of HIRLAM. This different behaviour may be due to the fact that this model still lacks an MOS procedure which may compensate a poor (theoretical, not measured) power curve.

5.3 Iowa – NGM

Looking at figure WHATEVER, not to have local topography effects included is apparently a real loss, since the model itself is not able to predict the site wind climate correctly. Then again, using fairly simple MOS the result for the Alta site can be improved dramatically – this is very clear in the skill score. The three lines refer to

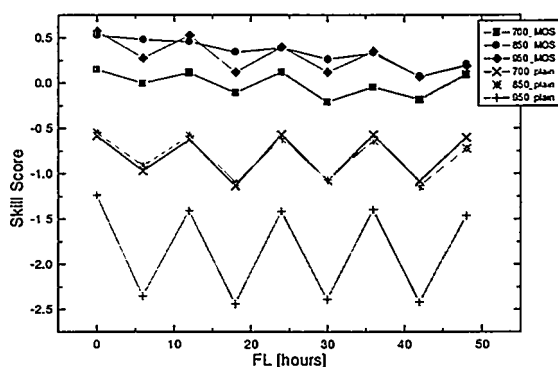


Figure 3: Skill Score with and without MOS for the NGM in Alta, Iowa.

Since the power curve in this case is not used, the MOS in this case is a simple linear regression.

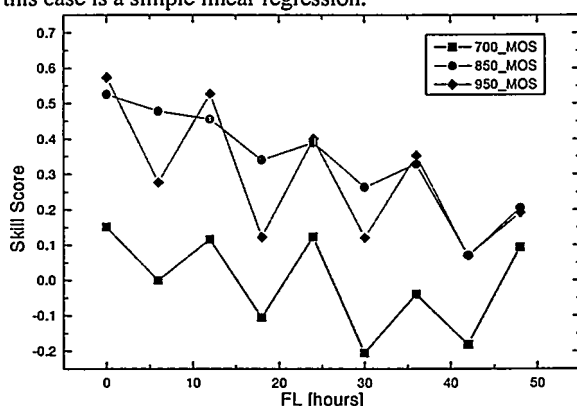


Figure 4: Detail of Figure 3: Skill Score with MOS for the NGM in Alta, Iowa.

The difference in performance of the three different levels is obvious. Level 850 is best, the 950 mbar level is not much behind, and the 700 mbar level is hardly usable.

Note that the 10 m a.g.l. forecasts of the NGM were evaluated, but in comparison to the higher atmosphere levels performed even more poorly. This is not surprising considering the horizontal resolution of the NGM of about 170 km, the distance of Alta from the next grid point (between 89 and 169 km) and the fact that we did not have the opportunity to account for local effects by means of a WASP analysis.

6. Conclusions

The performance of the pure NWP model is highly depending on the model and its resolution, but even a bad performance of the pure model can often be remedied by using a simple statistical analysis. The HIRLAM and the Deutschlandmodell show quite similar behaviour. For prediction horizons longer than 36 hours, the performance of both is not satisfying yet.

In any case, it can be shown clearly that applying a MOS procedure increases the prediction performance distinctively.

7. Acknowledgements

This study is financed partly by EU project JOR3-CT95-0008 and JOR3-CT98-0272. GG was financed by the Marie-Curie-Fellowship JOR3-CT97-5004. KM is financed by the Hans-Böckler foundation.

8. References

- [1] L. Landberg, Short-term Prediction of Local Wind Conditions, *Boundary-Layer Meteorology*, 70, 171.
- [2] Hans Georg Beyer, Detlev Heinemann, Harald Mellinghoff, Kai Mönnich, Hans-Peter Waldl: *Forecast of Regional Power Output of Wind Turbines*. This conference.
- [3] B. Machenhauer (Ed), 1988, *HIRLAM final report*, HIRLAM Technical Report 5, Danish Meteorological Institute, Copenhagen, Denmark. For an introduction, see also <http://www.dmi.dk/englf+ul>.
- [4] <http://www.ecmwf.int/>
- [5] N. G. Mortensen, L. Landberg, I. Troen and E. L. Petersen, Wind Atlas Analysis and Application Program (WASP), User's Guide, Risø-I-666(EN) (v.2), Risø National Laboratory, Roskilde, Denmark (1993).
- [6] P. Sanderhoff, PARK – User's Guide. A PC-program for calculation of wind turbine park performance, Risø-I-668(EN), Risø National Laboratory, Roskilde, Denmark (1993).
- [7] T. S. Nielsen, A. Joensen, H. Madsen, L. Landberg and G. Giebel 'A New Reference for Predicting Wind Power', *Wind Energy* 1, p29-34 (1998).

OPERATIONAL RESULTS FROM A PHYSICAL POWER PREDICTION MODEL

Lars Landberg
Risø National Laboratory
Meteorology and Wind Energy Department
DK-4000 Roskilde, Denmark
lars.landberg@risoe.dk

ABSTRACT: This paper will describe a prediction system which predicts the expected power output of a number of wind farms. The system is automatic and operates on-line. The paper will quantify the accuracy of the predictions and will also give examples of the performance for specific storm events. An actual implementation of the system will be described and the robustness demonstrated.

Keywords: Short-term prediction, wind farm power output, HIRLAM, WASP, MOS

1 WHY?

In many places around the world, but in Europe in particular, the electricity production from wind farms is now so high that these wind farms have (sometimes critical) effect on the running and control of the overall electrical grid.

To fully benefit from these large amounts of wind energy (in some areas up to 20%) it is necessary to have some kind of idea of the expected production over the next few days. This will enable the electrical utilities to control the conventionally fueled plants in such a way that fossil fuels will be saved.

A prediction model has been developed to this end and this paper will describe the model in some detail, but the main focus will be on the performance and operational aspects of the implemented model. The on-line implementation was carried out in an EU JOULE-funded project.

2 HOW?

This section will describe the model: the idea behind it and the equations used. Furthermore, an actual on-line implementation will be described.

2.1 The model

The method for predicting the output of a wind farm is outlined in Figure 1. The idea is to use physical models as 'far' as possible, this is done such that the large-scale flow is modeled by a NWP (Numerical Weather Prediction) model, here HIRLAM [6] of the Danish Meteorological Institute (DMI); the wind is transformed to the surface using the geostrophic drag law and the logarithmic profile. As we zoom in on the site more and more detail is required, this detail is provided by the Risø WASP program [7]. WASP takes local effects (lee from obstacles, effect of roughness and roughness changes and speed-up/down of hills/valleys) into account. To take the shadowing effects of turbines in a wind farm into account the PARK program [9] of Risø is used. Finally, to take any effects not modeled by the physical model and general errors of the method into account two model output statistics (MOS) modules are used. The model is described and analysed in great detail in [4, 5, 2].

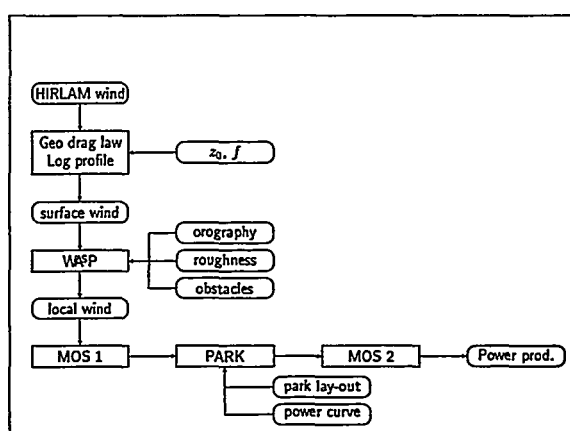


Figure 1: Flow chart describing the idea behind the model. The prediction from HIRLAM enters at the top and is transformed to the local wind moving down the figure, the production (including shadowing effects from the wind farm) is calculated moving along the bottom line. From [4].

2.2 The implementation

To demonstrate that it is possible, not only to obtain accurate predictions of the wind farm production, but also to use these predictions in an on-line environment, the model was implemented at Risø. The implementation is outlined in Figure 2. The principle is that as soon as the over-all meteorological situation has been predicted by DMI's operational HIRLAM model the forecasts are transmitted via Internet e-mail to Risø. Here a UNIX computer, dedicated to the task, registers the arrival and executes the Risø prediction model, the calculation module then sends the predictions to the output module which generates pages containing the predictions in graphical as well as textual form written in HTML (Hyper Text Mark-up Language). These pages are uploaded to a Web-server accessible via any Web browser (as eg Netscape and Internet Explorer). The address is not public and the site has no links pointing to it, so only utilities with permission can view the predictions. If the information contained on the pages at some point will be considered requiring a higher level of security, it is very simple to change the site to be password protected.

Predictions are made for the 47 wind farms shown in Figure 3 and the model is run twice a day generating predictions 36 hours ahead each time.

The model is implemented in such a way that a new wind farm can be added in a matter of a few minutes, HIRLAM predictions for the new site are typically available within 24 hours.

Each wind farm can also be changed to represent a region instead of just itself, this is done by scaling the power output with a factor, determined by the total installed capacity of the wind farms in the region.

The on-line predictions are available to the two Danish utilities, and since the focus of the Risø model is on the Elkraft area, the Elkraft utility is the one which has used the predictions in their daily planning and dispatch. This has been going on for seven months now (Feb 99).

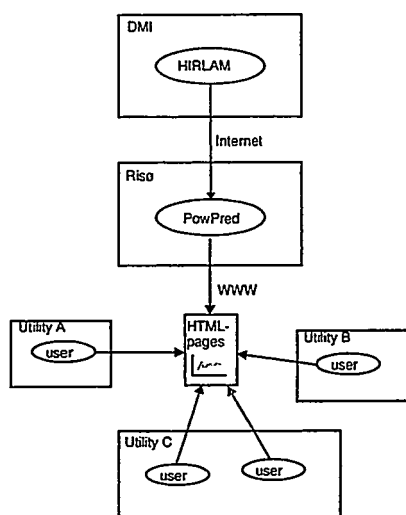


Figure 2: The on-line implementation. See text for details.

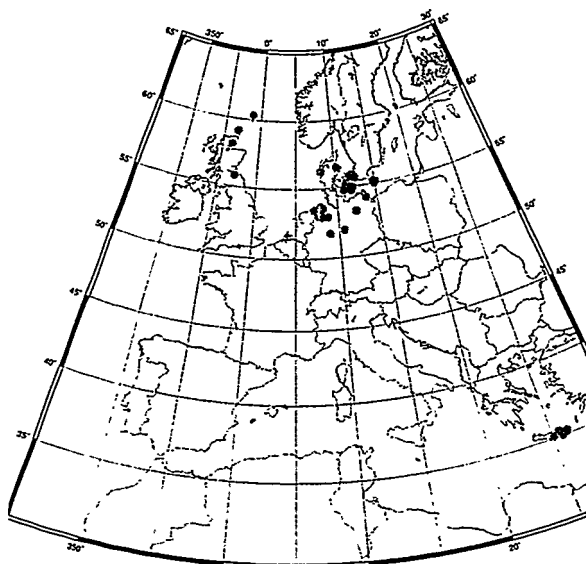


Figure 3: The location of the 47 wind farms. The wind farms are located in Denmark, United Kingdom, Greece and Germany.

3 HOW WELL?

In this section the quality of the model will be assessed in two ways: the standard way of comparing actual productions to predicted, but also by trying to see how successful the on-line implementation has been. At the end of the section another way of assessing the accuracy and usefulness will be described briefly.

3.1 Accuracy

The model has now run for two entire years and it is possible to draw some firm conclusions as to its performance. For independence of the evaluation, the model is evaluated on one year's worth of data taken from the Elkraft SCADA system. The wind farm observations are recorded every hour.

To get an estimate of the skill of the model the predictions are compared to those of the *persistence* model, which is a very simple model stating that

$$P(t + \ell) = P(t) \quad (1)$$

where $P(t)$ is the production at time t and ℓ is the look-ahead time. This model could popularly be called the 'what-you-see-is-what-you-get' (WYSI-WYG) model! Despite its seeming simplicity, this model describes the flow in the atmosphere rather well, due to the characteristic time scales of weather systems; it is often experienced that the weather in the afternoon is the same as it was in the morning, so for some typical weather situations it is a rather difficult model to beat.

The results of the comparison between the two models for the Nøjsomhedsodde Wind Farm are shown in Figure 4 where the the mean error and the absolute mean error ($=|\text{predicted} - \text{observed}|$, a measure of the scatter, giving less weight to outliers than the standard deviation) of the prediction model are compared to those of the persistence model. The following can be seen:

- The prediction model outperforms the persistence model after six hours.
- The mean absolute error of the prediction model is around 15% of the installed capacity.
- The decay of the performance of the prediction model is very gentle, over the 36 hour time-span the error is only increased by less than 10%.
- The mean error of the persistence model is very small. This follows from the definition of the persistence model.

These predictions are not the best and not the worst examples of the performance, a well-predicted wind farm has a scatter as low as 10% of the installed capacity and a not-so-well-predicted up to 20%.

One very important feature which can not be seen from this figure is how well the model predicts storms. Here the persistence model has no chance, since it assumes status present. In a previous study [3] all storms in 1997 and 1998 in the period 1 Jan 97 to 1 Aug 98 were identified for the Avedøre Wind Farm and the performance of the prediction model was evaluated in qualitative terms. The result can be found in Table I.

The definition of 'storm' is here taken to mean an event where the production rose from a very low value (ie close to 0 kW) to around 3000 kW (approx. 80% of the total installed capacity) and then down again to a low value over a period of a few days. Using this

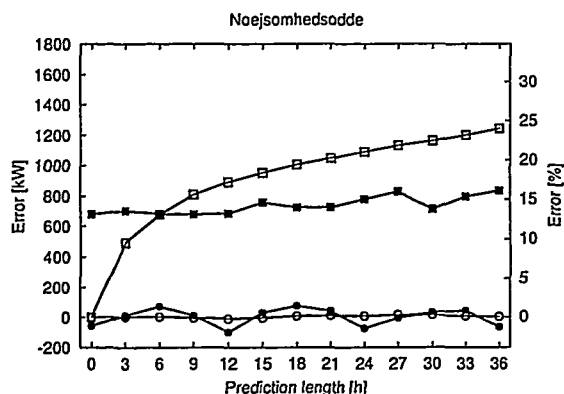


Figure 4: The mean error (circles) and the mean absolute error (squares) for the prediction of the power output of the Nøjsomhedsodde Wind Farm for the prediction model (filled symbols) and the persistence model (open symbols). The left-hand y -axis shows the absolute numbers (in kW) and the right-hand axis the numbers relative to the total installed capacity (in %). One year's worth of data has been used in the comparison. The farm is rated at 5.2 MW.

selection criteria 7 storms were found in 1997 and 9 in the first seven months of 1998.

Studying the data in detail reveals that of the seven storms in 97 two were predicted very well and one was predicted satisfactorily. In 98 five were predicted very well and three satisfactorily. This is very much in line with the results found for the wind speed at the Risø mast: in the first half of 1997 the HIRLAM model had problems, which then seem to have been fixed.

The results shown here differ slightly from the results in [3], in that the cases where cut-out (ie the wind is so high that the turbine must stop in order to avoid structural damage) was originally predicted are now removed, since the model has been changed to reflect the fact that cut-out very seldomly is seen in the observations. It is critical to get this right, of course, since missing a cut-out situation will make an enormous difference for the dispatch, by either predicting 100% production (no cut-out) or 0% prediction (cut-out).

3.2 Track record/reliability

This section will focus on some operational aspects of the implementation.

The results from the HIRLAM model are typically available after 2 hours, the transit time between DMI and Risø is typically less than a minute and the prediction model runs in less than two minutes for the predictions to be calculated and another two minutes for the web-pages to be generated, the upload is instant. So, typically around two hours after the measurements have been taken at a large number of places around the Northern Hemisphere the predictions are available to the utility.

The system has run operationally for more than two years, with no break-downs. One planned shutdown took place, when the operating system was upgraded. The only problems have occurred when the DMI forecasts have been delayed for some reason. It is of course not possible to do anything about this from

the utility side, so the times different from two hours are an indication of how often this occurs.

Figure 5 shows the distribution of the delay time, as can be seen, most of the time the delay is around two hours and after four hours 90% of the predictions have arrived. There are some outliers, and as mentioned earlier all of them are due to the fact that the HIRLAM predictions were delayed.

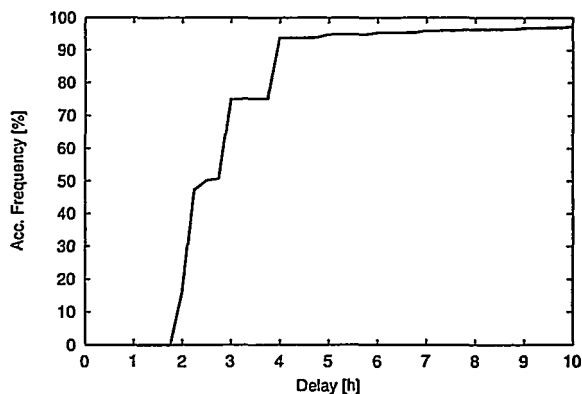


Figure 5: Accumulated distribution of the delay time of the predictions from the E (previously called DKV) version of the HIRLAM model.

3.3 Savings in fossil fuel

Another very important way of accessing the accuracy from a utility point of view is to see how much conventional fuel and thereby money is saved because of the predictions, other papers are dedicated to this, see [10, 11]. The main conclusion is that significant savings are indeed found, the higher the penetration the higher the savings. Typical results are that the use of predictions becomes significant at 25% penetration (note that many areas today have a penetration of more than 20%) and that the savings are more than 25% higher than just using persistence.

4 WHAT'S NEXT?

At present the model is used as-is in a JOULE project, predicting the power for 13 wind farms in Germany (location of the wind farms is shown in Figure 3).

For the very near future two model refinements are planned, the first one is a direct improvement of the existing model (described in the following) and the second is a completely new model, where the Risø model described here is combined with the IMM model [8], this development will be carried out in a project funded by the Danish Energy Agency, with the goal of implementing this model at all the Danish electrical utilities.

It is also hoped that other utilities will be interested, EPRI in the US has already shown interest.

4.1 Using the 10 m wind as input

Due to the decrease in grid size and the improvement of the boundary-layer parameterisation of HIRLAM, the level from which the wind has to be taken has changed from when the model was first developed and implemented (see [1] for further details). In the original model the wind found in model level 5 (approx.

Table I: The storms identified in the period 1 Jan 97 to 1 Aug 98. In the column marked 'Quality' the predictions are graded according to the following: - bad, = OK, + good.

1997				1998			
Start	End	Quality	Notes	Start	End	Quality	Notes
7/1	9/1	-	level missed	14/1	18/1	+	
12/1	15/1	-	start-up missed	26/1	29/1	+	
18/3	20/3	=	end missed	15/2	18/2	=	
21/4	24/4	-	missed completely	25/2	2/3	+	
10/5	12/5	-	missed completely	6/3	8/3	=	
17/11	22/11	+		10/3	13/3	-	level missed
25/12	27/12	+		19/3	20/3	=	
				15/6	19/6	+	
				14/7	16/7	+	

550 m agl) should be used as the best approximation of the geostrophic wind, now, however, the wind from the lowest level has the smallest scatter when compared to the observed wind at the wind farm site. This means that since the original model had to transform the wind from a geostrophic wind via the geostrophic drag law to the surface the model must be changed, since this transformation has already been done by the HIRLAM model. Referring to Figure 1 the box labeled 'Geo. drag law, Log profile' must therefore be removed. Calculating the mean error and std. dev. of the original model and the model proposed here applied to the Risø mast, the same qualitative picture is found as in Figure 4, however, the predictions using the 10 m wind show a reduction in the standard deviation of typically 20% on the prediction of the wind speed.

5 SUMMARY

This paper has described an automatic on-line prediction system for wind farm production output. The model was described and analysed and the performance of it was shown to be good. The on-line implementation was also described and it was shown that the model had been operational for two years with very few interruptions. The predictions have been used by the Danish utility Elkraft for seven months. Lastly, new applications of the model were described.

ACKNOWLEDGEMENTS

The on-line implementation of the model has been funded by the Commission of the European Communities under the JOULE programme, contract JOR3-CT95-0008. The on-going project in Germany is also funded by the JOULE programme, contract JOR3-CT98-0272. The development of the original model was as funded by the EFP-programme under the Danish Ministry of Energy and the Environment, contract 1363/94-0005 and the JOULE programme, contract JOUR-0091-MB(C). G Giebel, Risø, is thanked for calculating the delay time of the HIRLAM predictions.

REFERENCES

- [1] Joensen, A, G Giebel, L Landberg, H Madsen, 1999: *Model Output Statistics Applied to Wind Power Prediction*. Proceedings from EWEC99, Nice (FR).
- [2] Landberg, L, 1998: *A mathematical look at physical power prediction model*. Wind Energy, 1, 23-28.
- [3] Landberg, L and A Joensen, 1998: *A model to predict the power output from wind farms - an update*. In proceedings from BWEA 20, Cardiff(UK), 127-132.
- [4] Landberg, L, 1999: *Short-term prediction of the power production from wind farms*. J. Wind Eng. Ind. Aerodyn., 80, 207-220.
- [5] Landberg, L and SJ Watson, 1994: *Short-term prediction of local wind conditions*. Boundary-Layer Meteorol., 70, 171-195.
- [6] Machenhauer, B (ed), 1988: *HIRLAM final report*. HIRLAM Technical Report 5, Danish Meteorological Institute, Copenhagen, Denmark.
- [7] Mortensen, NG, L Landberg, I Troen and EL Petersen, 1993: *Wind Atlas Analysis and Application Program (WASP), User's Guide*. Risø-I-666-(EN)(v.2), Risø National Laboratory, Roskilde, Denmark. 133 pp.
- [8] Nielsen, TS and H Madsen, 1999: *Experiences with Statistical Methods for Predicting Wind Power*. In proceedings from EWEC99, Nice(FR).
- [9] Sanderhoff, P, 1993: *PARK - User's Guide. A PC-program for calculation of wind turbine park performance*. Risø-I-668(EN), Risø National Laboratory, Roskilde, Denmark. 8 pp.
- [10] Watson, SJ, L Landberg, and JA Halliday, 1994: *Application of wind speed forecasting to the integration of wind energy into a large power system*. IEE Proc.-Gener. Transm. Distrib., 141, No. 4, 357-362.
- [11] Watson, SJ, G Giebel and A Joensen, 1999: *The Economic Value of Accurate Wind Power Forecasting to Utilities*. Proceedings from EWEC99 Nice (FR).

A NEW MEASURE-CORRELATE-PREDICT APPROACH FOR RESOURCE ASSESSMENT

A Joensen^{1,2}, L Landberg¹ and H Madsen²

¹Dept of Wind Energy and Atmospheric Physics, Risø National Laboratory, DK-4000 Roskilde, Denmark, Tel: +45 4677 5095, Fax: +45 4677 5970, E-mail: Alfred.Joensen@risoe.dk, Lars.Landberg@risoe.dk

²Dept of Mathematical Modelling, The Technical University of Denmark, DK-2800 Lyngby, Denmark, Tel. +45 4525 3418, Fax: +45 4588 1397, E-mail: hm@imm.dtu.dk

ABSTRACT: In order to find reasonable candidate sites for wind farms, it is of great importance to be able to calculate the wind resource at potential sites. One way to solve this problem is to measure wind speed and direction at the site, and use these measurements to predict the resource. If the measurements at the potential site cover less than e.g. one year, which most likely will be the case, it is not possible to get a reliable estimate of the long-term resource, using this approach.

If long-term measurements from e.g. some nearby meteorological station are available, however, then statistical methods can be used to find a relation between the measurements at the site and at the meteorological station. This relation can then be used to transform the long-term measurements to the potential site, and the resource can be calculated using the transformed measurements. Here, a varying-coefficient model, estimated using local regression, is applied in order to establish a relation between the measurements.

The approach is evaluated using measurements from two sites, located approximately two kilometres apart, and the results show that the resource in this case can be predicted accurately, although this approach has serious shortcomings.

KEYWORDS: Wind Energy, Statistics, Resource Assessment, Siting

1 INTRODUCTION

The idea behind the Measure, Correlate and Predict (MCP) methodology [1,3] is to establish a relation between concurrent measurements of wind speed (ω_p) and direction (θ_p) at a potential wind farm site and wind speed (ω_r) and direction (θ_r) at a reference site, e.g. a meteorological station where wind speed and direction have been measured for a long period, e.g. tens of years. Subscript p refers to the potential wind farm site, and r to the reference site.

Considering the flow in the atmosphere the relation, which is found using measurements only at the two sites, will only be approximate, e.g. no advection dependency is included, which implies that the found relation is not the true relation between concurrent wind measurements at the two sites. As will be shown in this paper this is a serious shortcoming of the MCP methodology.

Note also that if the measurements at the potential site are only from one mast and one height, the layout of the potential wind farm and the local topography should be taken into account before the long term resource is estimated, i.e. by using the transformed wind speed and direction time series as input to e.g. WA⁵P [4] and PARK [5].

2 DATA

The data which has been used in this study is from two sites in Denmark, the Risø mast at Risø National Laboratory which is used as the reference site, and the RIMI (Risø's Integrated Environmental Project) mast approximately two kilometres to the east of the Risø mast, which is used as the potential site.

Both sites are located in relatively homogeneous and flat terrain and considering the relatively short distance

between the two sites, this should be considered as a perfect case for the MCP method.

As we will see later it is of importance to consider the measurement heights. At the RIMI mast only measurements from 10 m a.g.l. were available while at the Risø mast measurements from 44, 76 and 125 m a.g.l. were available. Preferably the measurements should be from the same heights, to ensure that the measurements are on the same point of the height profile. The closest we can come to this is to use the 10 and 44 m heights, respectively.

When the resource is estimated it is usually the wind speed distribution which is used [4], and the goal of the MCP method is thus to find the distribution of the wind speed at the potential site, using information about the wind speed at the reference site. From Figure 1, where the kernel smoothed distributions [5] at the two sites are shown, it is clearly seen that this is no easy task, as the distributions are very different.

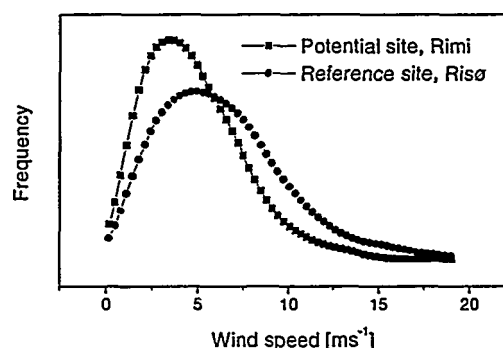


Figure 1: Smoothed wind speed distributions

3 PROPOSED MODELS

The relations or models which are proposed are based on physical knowledge about how flow is distorted by topography, i.e. we expect the relation between the wind speeds to be given by

$$\omega_p = a(\theta_r)\omega_r + b(\theta_r) + \varepsilon \quad (1)$$

and between the wind directions

$$|\theta_p - \theta_r|_c = b(\theta_r) + \varepsilon \quad (2)$$

where ε is assumed to be white noise, and $||_c$ is the shortest distance between two points on the circle defined by the wind direction. Except for the wind direction dependent offset, $b()$, in (1) this is equivalent to the relations which are found by the WAsP application when wind speed measurements at the same heights above some reference level are considered. From a physical point of view it is not reasonable to include the offset, because this implies that wind speed at the potential site will not be zero when the wind speed at the reference site is zero. But in terms of mean square error the performance is increased by including the offset, since the model is only approximate.

The reason for also considering a model for the wind direction is, that for a physical analysis of the estimated production of a potential wind farm, the wind direction is needed to take the shadowing effects between the turbines and the effect of the topography into account.

If the measurements at the two sites are not from the same heights, which is the case in this study, then model (1) is no longer reasonable. In this case the atmospheric stability should be taken into account. Here we propose two alternative ways

$$\omega_p = a_1(\theta_r)\omega_r + a_2(\theta_r)\omega_r^2 + b(\theta_r) + \varepsilon \quad (3)$$

which only should be used if no measure of the turbulence intensity is available, and

$$\omega_p = a(\theta_r)\omega_r + b(\theta_r) + c(\theta_r)\omega_r \Delta T_r + \varepsilon \quad (4)$$

if a temperature gradient or difference ΔT_r between two heights at the reference site is available.

The rationale behind these models is partly physical and partly based on the data that has been studied. Model (3) is based on the knowledge that for high wind speeds the atmosphere will be in a neutral condition, while for lower wind speeds the state of the atmosphere is determined by the sensible and latent heat fluxes. If this is compared with the stability dependent height profile there will be a parabolic dependency on the wind speed. Model (4) is based on the similarity relations for the stability dependent height profile, which suggest that there is a product interaction between the wind speed and temperature gradient. Neither of the models (3) and (4) are completely physically sound, but the models are based on what data most likely will be available, and for the data used in this study these models seemed to be reasonable. Note, furthermore, that in (4) the offset has to be included.

For the wind direction, only model (4) has been considered, as this model seemed to be adequate. Furthermore only small variations in the wind direction between the two sites were found.

4 ESTIMATION

To estimate the coefficient functions, i.e. $a()$, $b()$ and $c()$ of the models proposed in the previous section, local regression has been used [2]. This approach works by estimating a polynomial approximation of the coefficient functions in a grid spanning the wind direction. For a particular direction θ , only observations in the neighbourhood of θ are used, and weights are assigned to each observation depending on the distance from θ to the observed wind direction. The value of the coefficient function for a particular direction θ is then given by the value of the polynomial.

To take the circular nature of the wind direction into account, the wind directions in the data set are centred around θ . If the neighbourhood is local, i.e. limited to or less than the range of the wind direction, this ensures that the estimated coefficient functions are continuous on the circle.

Various parameters need to be determined when this approach is used, i.e. the size of the neighbourhood and the order of the polynomial approximation, depending on the curvature of the coefficient functions. In principle this can be formulated as an optimisation problem, but in practical applications this is not preferable, and in this study it was found that the estimation was not very sensitive to how these parameters were chosen. Therefore a second order wind direction polynomial approximation, and a neighbourhood containing 40% of the observations was used.

As mentioned in the Introduction the models we are proposing are only approximate, which implies that the estimates will be biased. This can partly be corrected for by rotating the space spanned by the reference wind speed and potential site wind speed in which the fit is performed, i.e.

$$\begin{aligned} \omega'_p &= \cos(\alpha)\omega_p - \sin(\alpha)\omega_r \\ \omega'_r &= \sin(\alpha)\omega_p + \cos(\alpha)\omega_r \end{aligned}$$

where ω'_p and ω'_r are the variables in the rotated space.

The inclusion of the offset in the model implies that the centre of the rotation is unimportant. The rotation angle α can be found by maximising

$$\rho = \frac{VAR(\omega'_p) - MSE}{VAR(\omega'_p)} \quad (5)$$

where MSE is the mean square error of the predictions, and VAR is the estimated variance of the potential site wind speed, both in the rotated space. This quotient measures the amount of variance in the observations described by the predictions, and this approach thus corresponds roughly to fitting in a space of maximum correlation.

Figure 2 shows the value of ρ for different angles, using model (4). There is a clear maximum at about 2.8° ,

and in the next section it is shown that the distribution is predicted almost perfectly using this rotation angle.

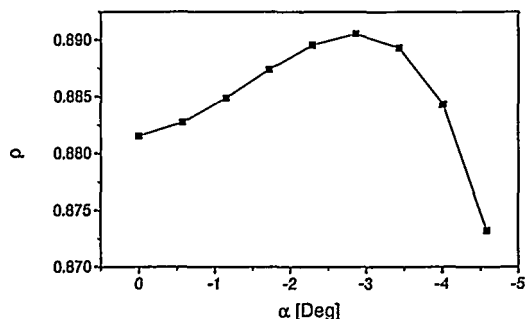


Figure 2: Criteria for determination of rotation angle α

5 EVALUATION

To evaluate the performance of the proposed models data from 1997 has been used for estimation and data from 1996 for validation. The prediction from the wind direction model is compared to no model, i.e.

$$|\theta_p - \theta_r|_c = \varepsilon \quad (6)$$

The root mean square error (RMS) calculated using (6) was 22.68° , while the RMS for model (2) was 3.62° , i.e. a clear reduction. Figure 3 shows the estimated coefficient function $b(\cdot)$ of model (2), and there seems to be a general bias, i.e. $b(\cdot)$ is negative for almost all values of the reference site direction. This could suggest, considering the short distance between the two sites, that the measuring equipment is not correctly aligned.

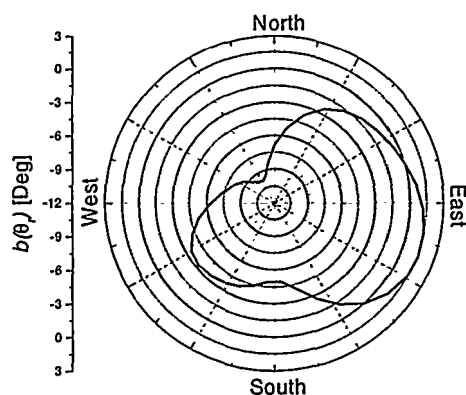


Figure 3: Estimated direction difference $b(\cdot)$.

To evaluate the wind speed models the predicted distributions are compared to the observed distribution in 1996. Figure 4 shows the kernel smoothed distributions of the wind speed predictions calculated by model (3) with and without rotation. Clearly the rotation improves the distribution, but in Figure 5 the distributions for the '97 and '96 observations are shown, and if this figure is compared to Figure 4, it is seen that the deviation between the predicted and observed distribution in '96 is just as

large as the deviation between the observed distributions for '96 and '97. Which means that the observed distribution in '97 could just as well be used to estimate the long-term resource as the predicted distribution using model (3).

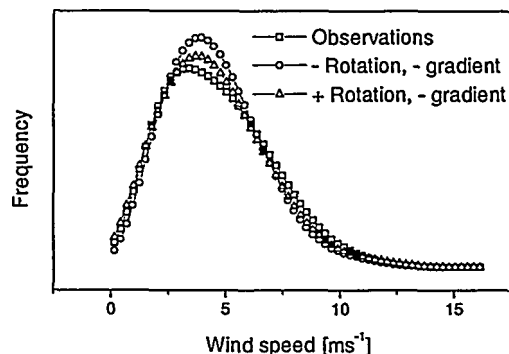


Figure 4: Smoothed observed and predicted distributions with and without rotation using model (3).

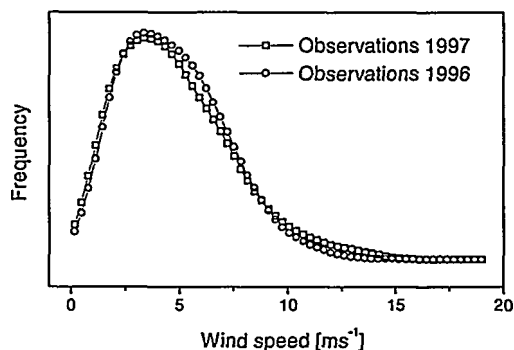


Figure 5: Smoothed observed distributions for 1996 and 1997.

Figure 6 shows the observed and predicted distribution using model (4) and rotation, and in this case it is seen that the distribution is predicted almost perfectly.

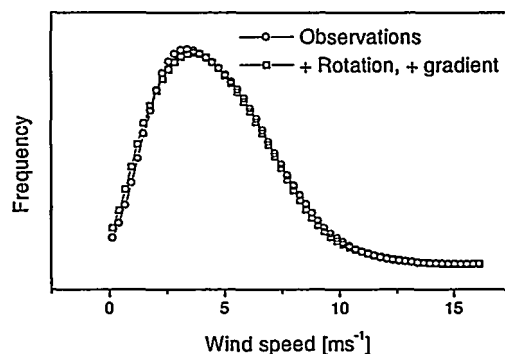


Figure 6: Smoothed observed and predicted distributions using model (4) and rotation.

The predicted distribution will in general be concentrated around the mean of the wind speed at the potential site for the estimation period, when the model deviates from the true model of the flow, i.e. the frequency

of high and low wind speeds will be underestimated, while the frequency of wind speeds around the mean wind speed will be overestimated. This follows from how the models are formulated. The rotation compensated partly for this effect, but it is important that the model is as accurate as possible.

It would be very complicated to derive a general measure of the uncertainty of the resource estimate using the MCP method, as it is not clear how to transform the uncertainty of a model for wind speed predictions to uncertainty in the predicted distribution. This is further complicated by the non-linear shape of a typical wind turbine power curve. However, as a rule of thumb, the estimated distribution can be compared to the observed distribution, using the data set that has been used for the estimation of the model. Only if these distributions are almost identical should the MCP method be used.

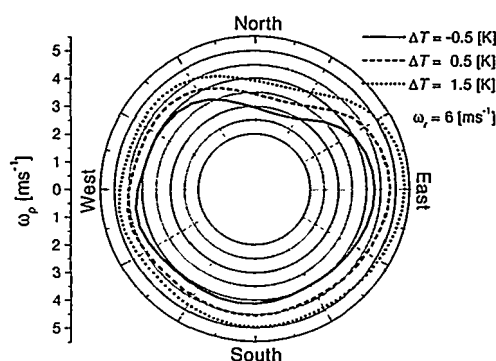


Figure 7: Wind speed dependency on reference site wind direction and temperature gradient

Figure 7 illustrates how the potential site wind speed is affected by the reference site wind direction and temperature gradient ($\Delta T = T_{44m} - T_{118m}$). The figure shows the predicted wind speed at the potential site as a function of the wind direction for fixed reference site temperature gradient (\approx mean gradient ± 1 K) and fixed reference site wind speed (\approx mean wind speed). It is seen that there is a clear dependency on the wind direction, as the variation is in the range 1-2 ms^{-1} . Furthermore, as expected, the difference between the wind speeds increases as ΔT decreases, i.e. as the boundary layer becomes more stable.

6 SUMMARY

In this paper it has been demonstrated how a statistical relation between the wind at a reference site and a potential wind farm site can be used to estimate the long-term resource at the potential wind farm site. Furthermore, the shortcomings of this approach are evaluated, and it is shown that it is critical that the statistical relation is as accurate as possible.

ACKNOWLEDGEMENTS

The work presented in this paper is partly funded by the European Commission under JOULE (JOR3-CT98-0295). A. Joensen is partly funded by the Danish Research Academy.

A special thanks to Risø's Integrated Environmental Project (RIMI) for providing the data which served as potential site data in this study.

REFERENCES

- [1] A. Derrick, Development of the Measure-Relate-Predict Strategy for Site Assessment, Proceedings from ECWEC93, Ed Garrad, Palz and Scheller (1993) 681.
- [2] T. Hastie and R. Tibshirane, Varying-coefficients Models, Journal of the Royal Statistical Society, Series B 55 (1993) 757.
- [3] L. Landberg, N. G. Mortensen, A Comparison of Physical and Statistical Methods for Estimating the Wind Resource at a Site, Proceedings from BWEA 15, Ed K. F. Pitcher (1993) 119.
- [4] N. G. Mortensen, L. Landberg, I. Troen and E. L. Mortensen, Wind Atlas Analysis and Application Program (WAAP), User's Guide, Risø-I-666(EN) (v.2), Risø National Laboratory, Roskilde, Denmark (1993).
- [5] P. Sanderhoff, PARK – User's Guide. A PC-program for calculation of wind turbine park performance, Risø-I-668(EN), Risø National Laboratory, Roskilde, Denmark (1993).
- [6] B. W. Silverman, Density Estimation for Statistics and Data Analysis, Chapman and Hall, London (1986).

A DETAILED AND VERIFIED WIND RESOURCE ATLAS FOR DENMARK

N.G. Mortensen, P. Nielsen*, L. Landberg, O. Rathmann and M.N. Nielsen

Risø National Laboratory, DK-4000 Roskilde, Denmark

T +45 46 77 50 97, F +45 46 77 59 70, E vea@risoe.dk

*Energy and Environmental Data, DK-9220 Aalborg Ø, Denmark

T +45 96 35 44 44, F +45 96 35 44 46, E emd@emd.dk

ABSTRACT: A detailed and reliable wind resource atlas covering the entire land area of Denmark has been established. Key words of the methodology are wind atlas analysis, interpolation of wind atlas data sets, automated generation of digital terrain descriptions and modelling of local wind climates. The atlas contains wind speed and direction distributions, as well as mean energy densities of the wind, for 12 sectors and four heights above ground level: 25, 45, 70 and 100 m. The spatial resolution is 200 meters in the horizontal. The atlas has been verified by comparison with actual wind turbine power productions from over 1200 turbines. More than 80% of these turbines were predicted to within 10%. The atlas will become available on CD-ROM and on the Internet.

Keywords: Wind Atlas, Terrain, Resource Mapping.

1. INTRODUCTION

Information on the actual wind resources of a region or an entire country is a prerequisite for the optimal utilisation of wind energy on a large scale. In the past, this information was often given as the wind resource potential, e.g. in the form of a 'wind atlas'. The wind atlas, however, does not provide directly the detailed information required for planning purposes and siting of large wind farms; it only forms the necessary basis for more detailed resource assessments. The purpose of the present work has been to establish a methodology whereby a detailed and reliable 'wind resource atlas' can be constructed for a not-too-complex terrain, and the approach is illustrated and verified by a new wind resource atlas for Denmark.

The methodology can be described briefly as follows: Wind data from existing meteorological stations are first analysed using the wind atlas methodology, in order to determine the regional or site-independent wind climate at each station. The regional wind climate over Denmark can then be described and stations to be included in the analysis selected. Based on these stations, the regional wind climate (wind potential) can be mapped. An interpolation procedure for points between stations is also developed. The wind potential map is verified using measured power production figures from a large number of wind turbines. The actual wind climate and wind resources all over Denmark can now be modelled using the verified wind potential data as well as digital terrain descriptions of the entire country. Finally, these results are used to map the wind resources of Denmark.

2. DANISH WIND-MONITORING STATIONS

The meteorological basis for the wind resource atlas for Denmark is wind atlas data sets for about 24 stations, carefully chosen to represent all regions of Denmark, Fig. 1.

From each station, continuous wind speed and direction measurements in the period 1987–96 have been analysed. The observation intervals range from 10 minutes to 3 hours, but the averaging period for wind speed is 10 min. for all the stations. Wind directions are instantaneous readings or averaged over 10 min. The wind measurements describe the local or site-specific wind climate at each

station – where wind climate is taken here to mean the frequency distributions of wind speed in a number of sectors (here 12) and the frequency distribution of wind direction in the same sectors (the wind rose). The wind atlas data sets, on the other hand, contain the regional or site-independent wind climate estimates, derived from the measurements using the wind atlas methodology.

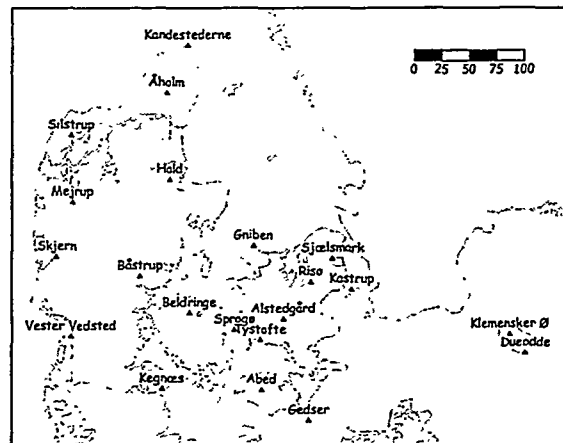


Figure 1. The Danish meteorological stations chosen for the wind atlas analysis. The stations are run by the Danish Meteorological Institute and Risø National Laboratory.

3. WIND ATLAS ANALYSES

The wind atlas methodology has been applied for the analysis of the wind measurements from the meteorological stations. This comprehensive set of models for the horizontal and vertical extrapolation of meteorological data and the estimation of wind resources was developed for the analysis presented in the European Wind Atlas [8, 5]. The actual implementation of the models is the Wind Atlas Analysis and Application Program (WAsP). The models take into account the effect of different surface conditions, sheltering effects due to buildings and other obstacles, and the modification of the wind imposed by the specific variations of the height of ground around the meteorological station in question. The analyses result in regional (site-

independent) wind climates for the met. stations. The application part of the methodology is a procedure in which a regional wind climatology is used as input to the same models to produce site-specific wind climatologies and, given the power curve of a wind turbine, production estimates [8].

Accurate descriptions of each meteorological station and its surroundings were collected from maps and during field trips. The descriptions include details of the terrain roughness (water areas, forests etc.), of nearby sheltering obstacles (such as buildings) and of the terrain altitude variations (orography). Regional wind climatologies were subsequently calculated for the 24 wind atlas stations [4].

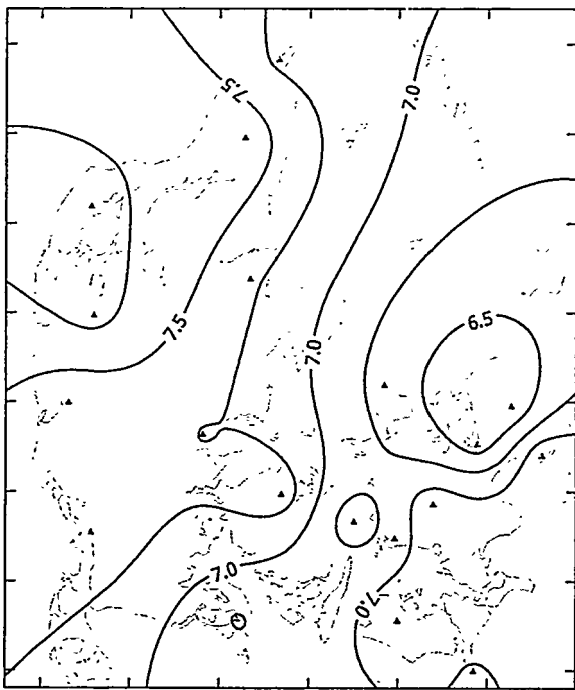


Figure 2. Mean wind speed 50 m a.g.l. in ms^{-1} over a flat, uniform surface with $z_0 = 0.03$ m. The wind speed contour interval is 0.25 ms^{-1} . Distance between tick marks is 50 km.

4. REGIONAL WIND CLIMATE OF DENMARK

The collection of wind atlas data sets is a representation of the regional wind climate over Denmark. As an example, Fig. 2 shows the variation of the mean wind speed 50 meters above ground level over a flat, uniform surface with a roughness length z_0 of 0.03 m.

One meteorological station only, Bønsvig Strand in Fig. 1, was excluded from further analysis because the wind atlas data sets did not compare well with those of the neighbouring stations. Predictions based on data from this station also turned out to be very low when compared to power production data from near-by wind turbines.

The mean wind speed shown in Fig. 2 vary from about 8 ms^{-1} in the NW part of Denmark to 6 ms^{-1} in NE Zealand. It thus decreases from NW towards SE to a minimum around the Great Belt region and north Zealand, where after it increases towards the Baltic Sea. This picture of the magnitude and variation of the regional wind climate over Denmark is largely supported by similar data from Sweden [2] and Germany [7].

In order to be able to calculate the regional wind climate (not just the mean wind speed) for any place in Denmark, a continuous 'wind atlas surface' must be derived by spatial interpolation procedures for both the wind speed and direction distributions.

5. INTERPOLATION OF WIND ATLAS DATA

The starting point of any WASP prediction is the Wind Atlas file describing the regional wind climate. Mapping the wind resource over a country will involve several regions and in order to avoid discontinuities we have to develop an interpolation routine. Setting up an interpolation scheme involves arbitrary choices, so perhaps it is worthwhile to review the objectives. We decide that:

- the interpolation must match the statistics of the measuring stations exactly
- the interpolation must be local, i.e. with emphasis on data from nearby stations
- the interpolation must work with an irregular mesh of data
- the interpolation must be as smooth as possible

The interpolation method implicitly assumes that the available data are of high quality and obtained in compatible sample periods, i.e. it does not intend to smooth extreme values or identify global trends in the data set. Corrections of the reference Wind Atlas files are best done from within the WASP program, i.e. by improved description of the surface roughness and obstacle configuration around the measuring sites.

Wind Atlas files contain wind roses and probability distributions for wind speeds in each sector. The wind speed distributions are approximated by Weibull distributions, and the moments of the wind-speed distributions $\langle u \rangle$ and $\langle u^3 \rangle$ may be found from the Weibull parameters A and k and vice versa. These transformations allow us to interpolate directional distributions and the moments in the total wind-speed distribution independently.

The measuring stations are organised in a grid of triangles with local co-ordinate systems. The first step in the interpolation scheme is to identify the local triangle where the directional distributions and direction-independent $\langle u \rangle$ and $\langle u^3 \rangle$ statistics are known at the corners. The interpolation of $\langle u \rangle$ and $\langle u^3 \rangle$ is based on third-order Bézier polynomials which also require gradients at the measuring points in the corners the triangles. The common gradients ensure continuity between neighbouring Bézier patches and these gradients are settled by an algorithm which minimise the curvature of the interpolation surface. Directional interpolation is made by linear interpolation of Fourier transformations of the three reference distributions relative to a 'typical' wind rose orientation. This orientation is determined as the maximum of the Fourier spline rather than the maximum of the original wind-rose which has a crude directional resolution. Both shape and orientation are smoothly interpolated by this method.

The measuring stations were placed at inland locations and the interpolation grid does not cover all coastal areas. Straightforward extrapolation by the third-order Bézier patches produce large excursions so an alternative method have to be developed. The extrapolation method operates with values and gradients at two reference stations only.

The two reference stations and the interpolation point fix a second-order Bézier curve. This curve is formally interpreted as a third-order Bézier curve, with along-curve nodal gradients determined by projection. The parameters predicted by the extrapolation routine is a smooth extension of the interpolation surfaces and far-field extrapolation becomes more linear. The Bézier patches are defined only once whereas a new extrapolation has to be defined for every extrapolation point. Therefore extrapolation is computationally less efficient than interpolation.

The interpolation procedures have been implemented in a program which makes it possible to predict the wind atlas data sets for any site in Denmark. For the purpose of calculating the wind resource map, a number of stations in Germany and Sweden, where similar data exist, were included in the final analysis.

6. MODELLING OF LOCAL WIND CLIMATES

The site-specific wind climate of any place in Denmark can now be estimated using the application part of the WASP program. The regional wind climate for a given site can be found using the interpolation procedures described above or the simpler one described below in Section 6.1. To account for the influences of local topography we further need digital terrain descriptions of the surrounding terrain. For an area of 43,000 km², it is not feasible to establish these 'by hand' – as was done in the analyses of the 24 meteorological stations – so an alternative approach had to be developed.

For the flow modelling, we have used a vector map of Denmark prepared by the National Survey and Cadastre. This map database contains height contour lines with 5-m vertical contour intervals for the entire country. The map has been established by hand digitisation as well as vectorisation of scanned contour map sheets. This database was reformatted into WASP map files for direct application with the WASP orographic flow model.

To account for the effects of the terrain roughness and roughness changes, a digital roughness map have been established from the land-use classification apparent in standard topographical maps. Map sheets with a scale of 1:50,000 were scanned and six layers of land use extracted: water areas, forests, cities and towns, tree groups, shelter belts and single houses. These layers were subsequently transformed into vector maps and analysed with respect to surface roughness.

Large water bodies, forests and cities are described as polygons and were simply assigned a roughness length. Small towns and forests, as well as tree groups, shelter belts and single houses were recorded and counted in sub-areas of 1 by 1 km². This registration was then used to assign 'background' roughness lengths for each of the sub-areas.

The polygons and background roughnesses were finally merged into several digital roughness maps in WASP map format covering the entire country. Since the digital maps do not contain information on the size and height of single objects, modelling of the shelter effects from houses and shelter belts had to be abandoned. This is a minor problem, since most of the wind turbines are sited in the open landscape. The sheltering obstacles are therefore only treated as roughness elements in the analyses.

6.1 Modelling considerations

In the modelling of site-specific wind climates, two approaches have been tried. One is to employ the wind atlas data sets from one station located centrally in Denmark (here Beldringe on the island of Funen) together with a site-specific correction based on previously measured power productions from a large number (~200) of wind turbines. This approach is feasible in Denmark, because of the large number of turbine installations. The second, and presumably more correct approach, is the one outlined above, where the 'local' regional wind climate is determined from the three nearest met. stations. However, since we verify the methodology against actual wind turbine productions and we further aim at establishing a wind resource map suitable for production estimations, it is not obvious which approach will provide the most accurate results. The experience obtained so far suggests that accurate results may be obtained using the former, simple approach; whereas the second approach seems to be very sensitive to especially the measured wind roses at the reference stations. The results reported below are based on the former, simple approach.

7. VERIFICATION OF THE METHODOLOGY

In order to verify the regional wind climate interpolations, the digital terrain maps and the methodology in general, we have compared predictions of wind turbine power productions with actually measured productions. For this purpose, more than 1200 wind turbines all over Denmark were selected. The selection criteria included availability and quality of production data, minimum size of wind turbine (75 kW) and documentation of turbine history and performance. The power curves for the different turbine types were extensively checked and production data were further referenced to a normal wind year. For turbines in wind farms a simplified park efficiency correction was applied, based on the actual efficiencies of a number of wind farms.

Since there are several more or less 'unknowns' in the final modelling and verification process, this was done by iteration. In this process, errors in the different input data files were identified and corrected and the interpretation and transformation of land-use data to roughness maps were calibrated and made consistent. The main results of the verification are shown in the table below.

Table 1. Distribution of verification wind turbines according to prediction error, expressed here as P_e/P_m in [%].

$P_e/P_m \times 100$ [%]	Number of WT	[%]
90 – 110	979	81
> 110	93	8
< 90	137	11
Total	1209	100

The estimated power productions, P_e , from more than 80% of the 1200+ control turbines thus fall within $\pm 10\%$ of the measured productions, P_m . For about 25 turbines, the difference between predicted and measured production is larger than 20%. These 'out-liers', which are located randomly all over Denmark, can in most cases be explained by severe local shelter effects not accounted for in the modelling, by errors in the digital terrain height map or by errors in the production data.

8. WIND RESOURCE MAP OF DENMARK

The wind resources over the land area of Denmark can now be estimated in the following way: the actual wind resource in grid points with a regular spacing of 200 m are calculated by the WAsP program for several heights above the ground surface: 25, 45, 70 and 100 m. Inputs are the wind atlas climatology from Beldringe and the WAsP terrain descriptions derived from existing databases of terrain orography and land-use. For each calculation point, the program uses terrain height information to at least 5 km from the site and a roughness map covering an area with a radius of at least 20 km. The wind climate and power production estimates are corrected as described above (6.1). The wind resource atlas (database) contains information on the wind speed and direction distributions in 12 sectors, as well as the mean energy density. As an example, Fig. 3 shows an energy density map of the southern part of the municipality of Aalborg in Jutland.

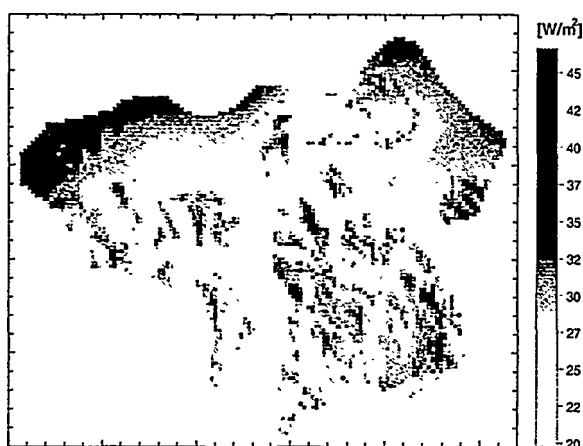


Figure 3. Mean wind energy density in Wm^{-2} 45 m a.g.l. over the southern part of the municipality of Aalborg, Jutland, see Fig. 1. Results are shown with a horizontal resolution of 200 m. Distance between tick marks is 1 km.

Given a specific power curve, it is also possible to display directly the estimated power production for an area, an example of this is given in Fig. 4.

The wind resource atlas for Denmark is not published (yet) as a paper map. The results will be stored and distributed on a CD-ROM, together with software for retrieval, display, printing and export of the data to several common file formats. In addition, the CD-ROM contains a number of actual or generalised wind turbine power curves, in order for the user to be able to estimate actual power productions. An Internet version of the resource map is also in the making and will be made available at www.emd.dk.

9. CONCLUSIONS

The wind resource atlas for Denmark provides a detailed, reliable and coherent database of the variation and magnitude of the wind resource over Denmark. It can be used by planners on all levels of society to ensure a systematic and efficient planning process, whereby the available sites are used efficiently to optimise the power production. The export facility makes it straightforward to e.g. establish layers in common GIS-systems for certain heights and

turbine types. However, given the detail and flexibility of the outputs, also private persons, organisations and wind turbine manufacturers may use the atlas for preliminary siting and power production estimation. Final siting, layout considerations and project feasibility, however, should not be based solely on the wind resource atlas.

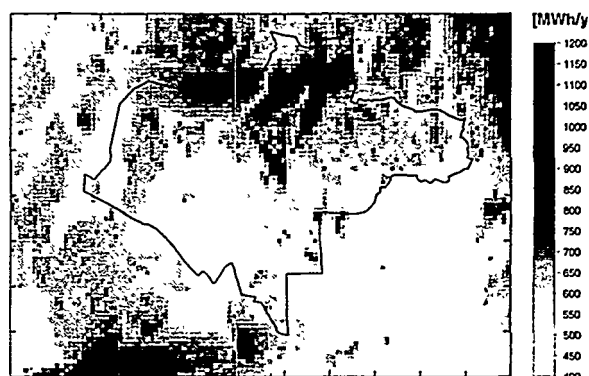


Figure 4. Expected mean power production from a 600-kW wind turbine with a hub height of 40.5 m in the municipality (full line) of Birkørød, Zealand, see Fig. 1. Results are shown with a resolution of 100 m.

The methodology can be used to establish similar wind resource atlases for other regions where reliable wind climatologies and topographical databases exist, and where the terrain in general is not too complex. In mountainous regions, or regions with a more complex wind climatology, the regional wind climate should be determined using meso-scale models [1, 6].

ACKNOWLEDGEMENTS

The wind resource map for Denmark is funded by the Danish Energy Agency under the Ministry of Environment and Energy. Gunnar Jensen, Risø National Laboratory, provided the calibrated and quality-controlled data from the Risø meteorological stations, as well as many observations which proved helpful in the analyses of these stations.

REFERENCES

- [1] Frank, H.P. and L. Landberg (1997). Modelling the wind climate of Ireland. *Boundary-Layer Meteorol.* **85**, 359–378.
- [2] Krieg, R. (1992). Vindatlas för Sverige. Projekt 506 269-2 på uppdrag av NUTEK. SMHI, Norrköping. 26 pp.
- [3] Mortensen, N.G., L. Landberg, I. Troen and E.L. Petersen (1993). Wind Atlas Analysis and Application Program (WAsP). Vol. 2: User's Guide. Risø-I-666(EN). 133 p.
- [4] Mortensen, N.G., L. Landberg, O. Rathmann, G. Jensen and E.L. Petersen (1999). Wind Atlas Analysis of 24 Danish Stations (1987-96). Risø-R-1092(EN).
- [5] Petersen, E.L., N.G. Mortensen, L. Landberg, J. Højstrup and H.P. Frank (1998a). Wind Power Meteorology. Part I: Climate and turbulence. *Wind Energy* **1**, 2–22.
- [6] Petersen, E.L., N.G. Mortensen, L. Landberg, J. Højstrup and H.P. Frank (1998b). Wind Power Meteorology. Part II: Siting and Models. *Wind Energy* **1**, 55–72.
- [7] Traup, S. and B. Kruse (1996). *Wind und Wind-energiepotentiale in Deutschland – Winddaten für Windenergienutzer*. Deutscher Wetterdienst, Offenbach am Main. 445 pp.
- [8] Troen, I. and E.L. Petersen (1989). *European Wind Atlas*. Risø National Laboratory, Roskilde. 656 pp.

WASP FOR OFFSHORE SITES IN CONFINED COASTAL WATERS - THE INFLUENCE OF THE SEA FETCH

Bernhard Lange, Jørgen Højstrup*

Risø National Laboratory, P.O.Box 49, DK-4000 Roskilde, Denmark, phone: +45 4677 5014,
fax: +45 4677 5970, e-mail: bernhard.lange@risoc.dk

* NEG Micon, Alsvej 21, DK8900 Randers, Denmark, phone: +45 8710 5262,
fax: +45 8710 5001, email: jho@neg-micon.dk

The increasing interest in harvesting wind energy offshore requires reliable tools for the wind resource estimation at these sites. Most commonly used for wind resource predictions on land as well as offshore is the WASP program. This program has been validated extensively for sites on land and at the coast. However, due to the lack of suitable measurements there is still a need for further validation for offshore sites. New data from ongoing measurements in the Danish Baltic Sea region are available now. The wind resources estimated from these measurements are compared to WASP-predictions. They are found to agree well. The only deviation found is for two sites with comparable distance to the coast but with a different distribution of land. Here the measurements show slightly different wind resources which are not predicted by WASP. Wind speed ratios of several pairs of stations are modelled with WASP for 12 directional sectors and compared with the measurements. Deviations in the directional wind speed predictions were found to be dependent on the corresponding sea fetches: For smaller sea fetches WASP seems to slightly overpredict the wind speed, while for long fetches of more than 30 km an underprediction is found.

Keywords: Wind resource assessment, Off-shore, WASP, Coastal sea areas

1. INTRODUCTION

Suitable sites for wind farms on land are scarce in some regions in Europe, while the potential areas for offshore installations are huge. Additionally, the wind resource offshore is much better than on land. Therefore the interest in developing offshore sites for wind energy utilisation has been growing in recent years. It is expected that an important part of the future expansion of wind energy utilisation at least in Europe will come from offshore sites. However, compared to land sites the economic viability of offshore wind farms depends on the compensation of the additional installation cost by a higher energy production. A reliable prediction of the wind resource at offshore sites is therefore crucial for project planning and siting.

The wind resource prediction model WASP [1] is the standard method for wind resource predictions on land as well as offshore. It has been validated extensively for land conditions. A validation study for coastal stations was performed by intercomparisons of wind measurements at different heights from high meteorological masts close to the sea [2]. No significant deviation was found. Only very few measurements are available for a validation of WASP for offshore sites. Some comparisons with offshore measurements from measurement platforms have been made and also showed a good agreement [2]. A comparison with Vindeby data showed reasonable agreement with a slight overprediction of the wind speed at Vindeby [3].

In Denmark plans are going ahead to install 4000 MW offshore wind turbines until the year 2030. In the current planing phase offshore wind measurements are being made at three prospective wind farm sites. The measurements are located in the confined Danish waters of the Baltic Sea near the islands of Lolland and Falster at distances of about 10 km from the coast. The data presently available from these measurements are analysed together with data from

the Vindeby offshore wind farm which is located about 2 km from the coast.

2. OFFSHORE WIND CONDITIONS

Modelling wind resources over coastal waters is different to land conditions due to a combination of several effects:

The favourable wind resource offshore is mainly caused by the low surface roughness of the sea. Contrary to land conditions, the sea surface roughness is not constant but depends on the waves present. These are in turn governed by the momentum exchange process between wind and waves which depends on wind speed, water depths and distance from the shore.

The atmospheric stability is the second parameter which differs greatly between land and water areas. This is caused by the different heat fluxes and heat flux variances between land and water. It might also depend on the length of the sea fetch in a transition zone when the wind blows from land to water. The wind speed is influenced by atmospheric stability in two ways:

The vertical wind speed profile is directly dependent on the atmospheric stability.

The internal boundary layer (IBL) which develops at the coastal discontinuity influences the wind speed offshore for wind from land. The growth of this IBL depends on the atmospheric stability.

3. WASP FOR OFFSHORE WIND CONDITIONS

The above mentioned effects influencing the wind speed in coastal waters are treated by WASP with simplified empirical models:

- The atmospheric stability is treated as a perturbation of the logarithmic vertical wind speed profile. It is calculated with an empirical formula taking into account the mean and the variability of the heat flux from the surface to the air. Land and water surfaces are distinguished by different values for these quantities.

An interpolation between land and sea areas is used in a transition zone on both sides of the coastal discontinuity.

- Roughness changes are treated with an empirical formula using an internal boundary layer (IBL) approach. The IBL model does not depend on the atmospheric stability.
- WAsP assumes a constant value of 0.2 mm for the sea surface roughness. No dependency on wind speed or fetch is taken into account.

4. MEASUREMENT SITES

Measurements are being performed at several meteorological masts on and around the islands of Lolland and Falster in Denmark. The locations of the stations used here are shown in figure 1. The measurements at Vindeby sea mast west (SMW), Omø and Rødsand are measurements from offshore meteorological masts. The measurement at Vindeby Land Mast (LM) is an accompanying coastal measurement.

The Vindeby SMW is situated 300 m west of the Vindeby farm 1.6 km from the coast. The Vindeby LM is erected at the coast close to the wind farm. Measurements started in November 1993 and almost 60000 records of half hourly averages are available. For a detailed description of the measurements see [3].

Wind speed measurements at the Sea Mast West are disturbed for some wind direction sectors (330°-120°) by wakes from the wind turbines. This influence has been corrected for by an estimation of the wake effects with the wind farm modelling program FCalc [4].

The sites Omø and Rødsand are offshore sites located in the south-eastern part of Denmark near the island of Lolland. Both sites have a distance of about 10 km to the nearest land. Omø is located to the north of Lolland near the Vindeby site, while Rødsand is situated south-east of Lolland (see Figure 1).

Half hourly averages of wind speeds and directions in different heights, temperatures and temperature differences are collected. Measurements started in August 1996 and

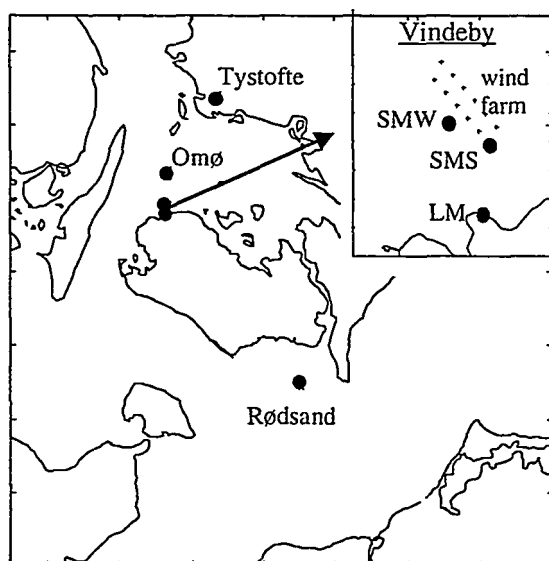


Figure 1: Locations of the measurement sites in the Baltic Sea in the southern part of Denmark; the enlargement shows the Vindeby wind farm area

currently 6200 records are available at the station Omø and 13200 at Rødsand.

5. WIND RESOURCES

The wind resources, i.e. the long term mean wind speed, is estimated from the onsite measurements and compared to WAsP-predictions. Deviations between the wind resource during the measurement period and the long term average were corrected by using a 14 year time series from the station Tystofte. This station is a land measurement located in the southern part of Sealand, about 5 km from the coast. WAsP predictions were calculated using two different measurement stations as input: The Vindeby land mast and the Tystofte meteorological station.

Figure 2 shows the mean wind speeds of the sites at 48 m height (46 m at Vindeby LM) versus their distances to the coast, i.e. their minimum sea fetch. The points connected with lines are WAsP predictions, the squares are the estimations from the onsite measurements.

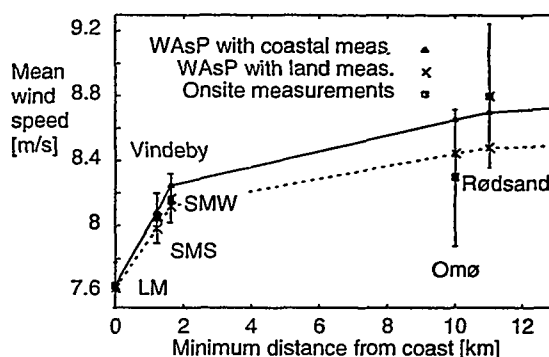


Figure 2: Long term mean wind speeds for a coastal and four offshore sites estimated from onsite measurements (with estimated maximum uncertainties) and predicted by WAsP on the basis of coastal and land measurements

As expected, the mean wind speed rises with increasing distance to the coast. The increase in wind speed with distance is large for the first kilometres but decreases quickly thereafter. Deviations of the WAsP predictions are generally small, up to 5%, and are in the same range as the uncertainties in the wind speed estimations based on the onsite data.

For the WAsP predictions an additional point is shown which gives the results for the open sea. It can be seen that the two sites Rødsand and Omø almost reach that limit. WAsP assumes only a very small influence of the land for distances larger than about 10 km.

Contrary to this prediction the estimations for Omø and Rødsand on the basis of the onsite measurements indicate a difference in the mean wind speed. A possible reason for this is the difference in the fetch situations. Omø is surrounded by land at about 10 km distance in the south, west and north-east directions, while Rødsand has land in this distance only in the northern and north-eastern directions, where the wind speed probability is low. It also has long sea fetches in the most frequent westerly wind directions (see fig. 1).

6. FETCH INFLUENCE ON THE WIND RESOURCE

6.1 Methodology

The measured and WASP predicted wind speed ratios between a number of sites are compared for 12 wind direction sectors. Since the sea fetch for the sectors differ greatly, a possible dependency can be investigated.

The WASP method uses measurements from one site (predictor) to estimate the wind resource at the predicted site. Within the model the measured directional wind speed distributions are described by Weibull functions. For short time series this procedure introduces an error due to deviations of the measured distribution from Weibull curves. To compensate for this error the comparison is made for wind speed ratios rather than wind speeds.

First a common time series of wind speeds and directions is compiled for both stations. The measured data of one site are taken as input to WASP to derive a wind climatology. This is used to predict the sectorwise mean wind speeds for both sites.

Subsequently the predictor and predicted station are exchanged and a new ratio calculated. The average ratio is used for comparison with the measurement.

The ratios of the measured data are derived from the same time series as used for the WASP predictions. The wind speeds of both stations are bin averaged in 30° bins with respect to the wind speed of one station. This is repeated with the wind direction of the other station and the average ratio is used for comparison. Wind direction sectors where the measurement is disturbed by mast interference are omitted. Uncertainties of the measured ratios are estimated as the average standard deviation of the means plus half of the difference of the two ratios calculated.

6.2 Direction dependent wind speed ratios

Examples for measured and WASP estimated direction

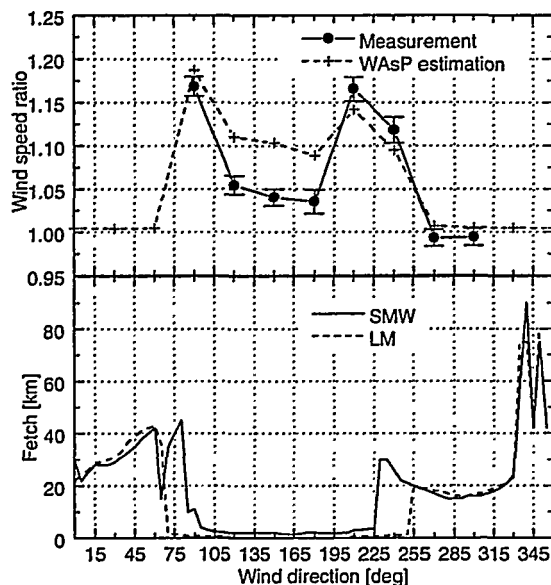


Figure 3: Vindeby SMW / Vindeby LM: Measured and WASP-predicted wind speed ratios (top) and sea fetches (bottom) versus wind direction

dependent wind speed ratios are shown in figures 3 and 4 along with the lengths of the sea fetches of the respective stations. The solid lines show the measured ratios and the dashed lines are WASP predictions. Measured data with possible mast interference have been omitted.

Figure 3 shows the ratios of Vindeby SMW and LM. Vindeby SMW is located 1.6 km off the north coast of Lolland (see figure 1). Here the behaviour of WASP for small fetches can be investigated.

The measurements show two distinct maxima of the ratio which are roughly in the direction of the coastline. This situation leads to a large fetch difference since the SMW has long sea fetches while the LM has mainly land fetch. In between these maxima (sectors 120°-180°) SMW has a short sea fetch of 1.6 to 3 km only. For the other directions both stations have similar long sea fetches and the ratio is close to one.

The WASP-predictions show generally the same directional pattern as the measurements. In most cases the deviations between measurements and WASP-predictions are small and the general behaviour of the directional wind speed difference between two stations is modelled well. Significant deviations are found only for the case with land fetch for LM and short sea fetch for SMW where WASP seems to overpredict the difference between the wind speeds on land and at sea.

In figure 4 the ratios of the two offshore stations Omø and Rødsand are shown. Rødsand is located 11 km off the south coast of Lolland and the two sites are about 60 km apart from each other (see figure 1). A comparison of these sites gives the opportunity to study the measured and predicted differences for two offshore stations with different fetches situations.

The measurements show a minimum in the ratios at wind direction sectors 270° and 300° and a maximum at 330°. This corresponds closely to the very large sea fetches at Rødsand in directions 260° to 290° and at Omø at 330° to 350°. For the other directions the ratio does not deviate much from one.

The WASP-predictions show only very small deviations

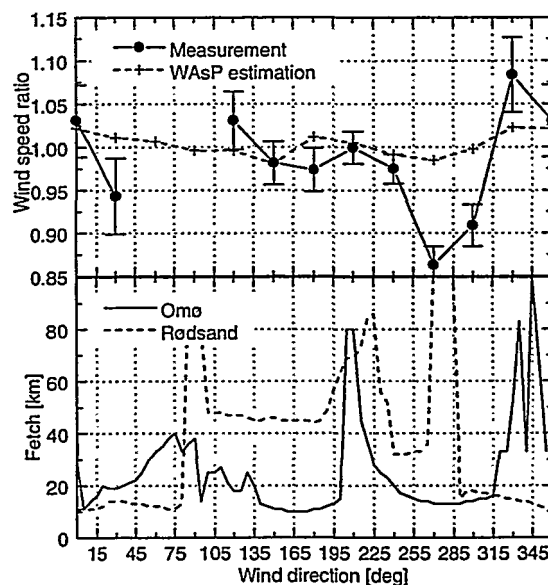


Figure 4: Omø / Rødsand: Measured and WASP-predicted wind speed ratios (top) and sea fetches (bottom) versus wind direction

from unity. This leads to significant deviations of 6-12% from the measurements for the two cases mentioned. For the 30° sector a smaller deviation is visible which can not be assigned to a fetch difference. For all other wind directions the deviations are in the order of the measurement uncertainty.

This result explains the measured differences between wind resources at Omø and Rødsand. The very long fetches at Rødsand which also occur in the prevailing wind directions lead to higher wind speeds compared to Omø. Since WAsP does not take these long fetches into account it underpredicts the wind resource at Rødsand.

7. CONCLUSION

The data presently available from ongoing measurements in the Danish Baltic Sea have been analysed and compared with predictions made with the wind resource estimation program WAsP. Measurements of a coastal and an inland station have been used for the predictions. It was found that the predictions of the long term average wind resource are in good agreement with measurements. However, the measurements indicate a small difference in wind resources between the stations Rødsand and Omø, which is not predicted by WAsP.

The investigation of the direction dependent wind speed also shows a generally good agreement between WAsP-predictions and measurements. Only for some wind directions significant deviations were found. These deviations show a correlation with the length of the upwind sea fetch. WAsP tends to overpredict the wind speed for situations with short sea fetches and underpredict it for long fetches. This effect explains the measured differences between the Omø and Rødsand sites since at Rødsand the wind comes more frequently from directions with long fetches.

A detailed model is needed to find an explanation for these findings. It might have to include several effects like the dependency of the sea surface roughness on wind speed and fetch (see e.g. [5]) as well as the influence of the atmospheric stability on the height profile of the wind speed and on internal boundary layers (see e.g.[3]).

ACKNOWLEDGEMENTS

The offshore measurements were funded by ELKRAFT in the project 'Kortlægning af Offshore Vindressourcer' and by the European Commission in the JOULE-programs. The work of one of the authors (B. Lange) is funded by the European Commission through a Marie Curie Research Training Grant.

REFERENCES

- [1] Mortensen, N.G., L.Landberg, I.Troen and E.L.Petersen: Wind Atlas Analysis and Application Program (WAsP). Version 4.1. Risø National Laboratory, Roskilde, Denmark. 1998
- [2] Petersen, E.L.: Wind Resources Part I, The European Wind Climatology, in: Proceedings of the European Wind Energy Conference, Luebeck-Travemuende; 1993; pp. 663-668
- [3] Barthelmie, R.J., M.S. Courtney, J. Højstrup and S.E. Larsen: Meteorological aspects of offshore wind energy: Observations from the Vindeby wind farm. in: Journal of Wind Engineering and Industrial Aerodynamics Vol. 62 (1996); pp. 191-211
- [4] FCalc: Farm Calculation program. University of Oldenburg, Germany. 1996
- [5] Johnson, H.K., H.J. Vested, J. Højstrup, S.E. Larsen and H. Hersbach: On the Dependence of Sea Surface Roughness on Wind Waves. in: Journal of Physical Oceanography. Vol.28, pp.1702-1716; 1998

MODEL OUTPUT STATISTICS APPLIED TO WIND POWER PREDICTION

A Joensen^{1,2}, G Giebel¹, L Landberg¹, H Madsen² and H Aa Nielsen²

¹Dept of Wind Energy and Atmospheric Physics, Risø National Laboratory, DK-4000 Roskilde, Denmark, Tel: +45 4677 5095, Fax: +45 4677 5970, E-mail: Alfred.Joensen@risoe.dk, Gregor.Giebel@risoe.dk, Lars.Landberg@risoe.dk

²Dept of Mathematical Modelling, The Technical University of Denmark, DK-2800 Lyngby, Denmark, Tel. +45 4525 3418, Fax: +45 4588 1397, E-mail: hm@imm.dtu.dk, han@imm.dtu.dk

ABSTRACT: Being able to predict the output of a wind farm online for a day or two in advance has significant advantages for utilities, such as better possibility to schedule fossil fuelled power plants and a better position on electricity spot markets.

In this paper prediction methods based on Numerical Weather Prediction (NWP) models are considered. The spatial resolution used in NWP models implies that these predictions are not valid locally at a specific wind farm. Furthermore, due to the non-stationary nature and complexity of the processes in the atmosphere, and occasional changes of NWP models, the deviation between the predicted and the measured wind will be time dependent. If observational data is available, and if the deviation between the predictions and the observations exhibits systematic behaviour, this should be corrected for; if statistical methods are used, this approach is usually referred to as MOS (Model Output Statistics).

The influence of atmospheric turbulence intensity, topography, prediction horizon length and auto-correlation of wind speed and power is considered, and to take the time-variations into account, adaptive estimation methods are applied. Three estimation techniques are considered and compared, Extended Kalman Filtering, recursive least squares and a new modified recursive least squares algorithm.

KEYWORDS: Forecasting Methods, Wind Energy, Statistical Analysis, Performance

1 INTRODUCTION

Several models for predicting the output from wind farms have already been developed, some based on observations from the wind farms [7], others based on numerical weather predictions [4], and again others on combination of both [2].

This paper describes how statistical methods, usually referred to as Model Output Statistics (MOS), can be used in models that combine observations and Numerical Weather Prediction (NWP) model predictions, and the approach taken here is slightly different from the approach in [2]. The NWP model, HIRLAM [6], is run by the Danish Meteorological Institute (DMI). The observations, wind speed (w_t) and power (p_t), are from four sites in Denmark: The Risø mast at Risø National Laboratory, and the Avedøre, Kappel and Østermarie wind farms.

The NWP model predicts several meteorological variables, such as temperature, surface fluxes and pressure, wind speed (ω_t) and direction (θ_t) at 31 levels/heights, see [6] for definition of the levels, and at the surface, i.e. 10 m a.g.l. The NWP model is run four times at day, at 00:00, 06:00, 12:00 and 18:00 UTC, and the predictions are given in 3 hourly steps 36 hours ahead.

2 FINDING THE RIGHT NWP MODEL LEVEL

In [4] it was found that the NWP predicted wind from level 27 gave the best results when used as input to the neutral geostrophic drag law to determine u^* , and the neutral logarithmic profile was used to calculate the wind at hub height. It was concluded that the reason why the stability dependant relations did not improve the results

was that the heat fluxes were not predicted accurately enough. Since HIRLAM has been updated several times since the investigation in [4], it is reasonable to re-evaluate these results.

Based on the results in [4] the neutral relations are used to transform the NWP wind down to the surface, and the prediction performance is compared to the performance of the surface wind calculated by the NWP model. HIRLAM takes the stability into account when the surface wind is calculated, and this comparison will therefore show if it is advantageous to include the stability. Furthermore, in order to make a fair comparison, the predictions should be corrected for any bias and offset, i.e. the simple MOS model

$$w_{t+k} = a_k \omega_{t+k} + b_k + \varepsilon_{t+k} \quad (1)$$

where ε_{t+k} is assumed to be white noise and k is the prediction horizon, is fitted to the observations using the least squares method.

Observations from 44, 76 and 125 m above the surface from the Risø mast are used in the comparison, because the wind which should be used might not be the same depending on which height above the surface it is compared to.

To evaluate the performance of the predictions

$$\rho = \frac{VAR(w_{t+k}) - MSE_k}{VAR(w_{t+k})} \quad (2)$$

is used, where VAR is the estimated variance of the observations and MSE_k is the mean square error of the predictions k hours ahead. The interpretation of ρ is that it

measures how much of the total variation in the observations is explained by the predictions, i.e. a value of 1 means that the predictions are perfect and 0 means that predictions are useless.

Figure 1 shows the results for each model height and each prediction horizon compared to the 44 m observations at the Risø mast. It is clearly seen that for all prediction horizons the best result is obtained using the surface wind, and the corresponding figures for the 76 and 125 m show the same results. The conclusion is therefore that it is advantageous to take the stability into account, and hence the surface wind calculated by the NWP model should be used.

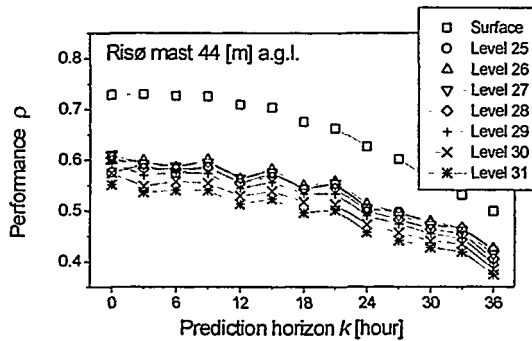


Figure 1: Performance for various NWP model levels.

3 WIND DIRECTION DEPENDENCY

Due to the spatial resolution of any NWP model it should be expected that some kind of wind direction dependant fine-tuning to a specific site should be possible. One way to do this fine-tuning is to apply a MOS model

$$w_{t+k} = a_k(\theta_{t+k})w_{t+k} + b_k(\theta_{t+k}) + \varepsilon_{t+k} \quad (3)$$

From a physical point of view the adjustment due to the topography should be a wind direction dependant factor, but this model also includes a wind direction dependant offset. The reason for this is purely statistical, e.g. if the prediction accuracy of the NWP model is not the same for all directions the inclusion of the offset will increase the performance.

Local regression [1] has been used to estimate the coefficient functions in (3). When using this method it has been assumed that for a given wind direction sector the coefficient functions are well approximated by second order polynomials. Using the terminology of local regression, the nearest neighbour bandwidth was chosen to include 40% of the observations at each fitting point.

A physical way to take the topography into account is to perform a high-resolution analysis of the site and the surroundings, and use this analysis to correct the NWP wind for local topography effects, which obviously are not included by the NWP model resolution. To see if this is advantageous the NWP surface wind has been corrected by matrixes calculated by WASP [8].

Again Risø mast data from the last half of '97 and first half of '98 has been used for the estimation, while

validation was performed with data from the last half of '98. In order to make a fair comparison, the MOS model (1) has been applied after the WASP correction, and the performance has also been calculated for the MOS model applied to the raw NWP surface predictions.

Surprisingly, Figure 2 shows that the performance of the WASP corrected forecast is worse than without, although the difference is only minor. The reason is most likely that the physical assumptions behind WASP are not satisfied when WASP is used for predictions of wind speed and direction that contain errors. Nevertheless, it seems as if there is some dependency on the topography, because the statistical correction (3) improves the performance, but this is not the only reason. This follows from the fact that the wind speed distribution depends on the wind direction, i.e. the wind speed in Denmark is usually higher when coming from west compared to e.g. north or east. This is a feature of the overall flow, and can not be prescribed to the local topography. Because the wind speed is not perfectly predicted by the NWP model this is incorporated by the wind direction dependent offset in (3).

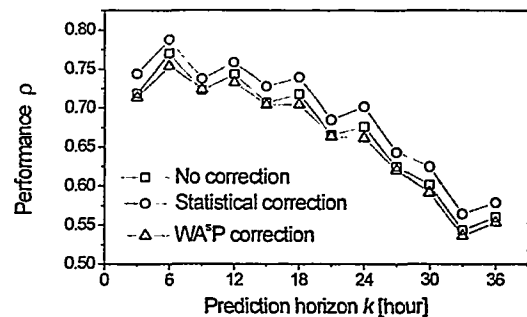


Figure 2: Performance for direction dependent models.

4 DIURNAL VARIATION

Surprisingly, as seen in Figure 2, it seems easier to predict e.g. 6 hours ahead than 3 hours ahead. The reason is that the prediction horizon k aliases with the time of day, and therefore, as shown in Figure 3, with the diurnal variation in the wind speed/atmospheric stability. This is because the NWP model is updated 4 times a day, hence odd prediction horizons correspond to the following times of day: 03:00, 09:00, 15:00 and 21:00, and even horizons correspond to: 00:00, 06:00, 12:00 and 18:00.

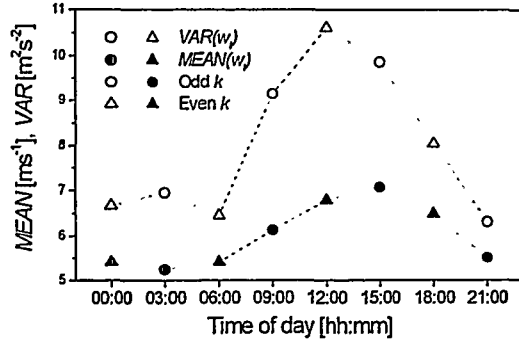


Figure 3: Diurnal variation.

Furthermore, Figure 3 is only based on measurements from the '98 summer period, for latitudes like those of Denmark, there is also an annual variation in the diurnal variation [10]. When the data used for the estimation is not from the same seasons of the year as the data used for the validation, which is the case in Section 3, the parameters of (3) become biased towards the diurnal variation in that specific period. This is the main reason for the effect seen in Figure 2.

5 ADAPTIVE ESTIMATION

In the previous sections only wind speed models have been considered, we now turn to wind power models that are slightly more complicated due to the non-linear relation between the wind speed and the power.

Furthermore, due to the non-stationary nature of the atmosphere, it must be expected that the parameters of a MOS model will be time-varying. Hence adaptive estimation methods are considered. Two widely used methods for this purpose are Kalman filtering and recursive least squares, see [5] and the references cited therein. The key idea behind these methods is the same, which is to discard old information as new one becomes available, or to be more specific, the methods slide a time-window of a specific width over the observations, where only the newest observations are seen. This approach has its drawbacks and advantages. If the true system is non-stationary and if this non-stationarity is not described by the model, the approach implies that the model adapts to the current state of the underlying system. But, on the other hand, because less observations are used to determine the parameters of the model, the parameters might become poorly determined, resulting in large parameter and prediction variance. The optimal model choice is therefore a model that balances simplicity and flexibility.

5.1 Extended Kalman Filter

One way to simplify the model for predicting the power is, to in some way, include a known relation between wind speed and direction and power, i.e. the power curve, in the model that is to be estimated adaptively. One solution is to apply the model

$$p_{l+k} = a_k \text{pow}(b_k \omega_{l+k} + c_k) + d_k p_l + e_k + \varepsilon_{l+k} \quad (4)$$

where $\text{pow}()$ is the wind farm power curve derived by the PARK application [11]. See [3] for a similar analysis.

The reason for the scaling of the NWP wind speed inside the power curve comes from the observation that the ratio between the measured wind speed and the NWP wind speed is different from one and time dependent. The constant inside the power curve lets the estimation determine the cut-in and cut-out wind speeds. The observed power at time t is included because for short prediction horizon the power observations are auto-correlated [10], this is also the reason for including the scaling of the power curve, because for short horizons more emphasis will be on the auto-correlation, i.e. p_t , and for larger horizons more weight will be put on the NWP and hence the power curve. Because this model is not linear in the parameters, the Extended Kalman Filter has been used for the estimation in this model.

5.2 Recursive Least Squares

A way to avoid the non-linearity is to use a polynomial approximation of the power curve, i.e.

$$p_{l+k} = a_k \omega_{l+k} + b_k \omega_{l+k}^2 + c_k \omega_{l+k}^3 + d_k p_l + m_k + \varepsilon_{l+k} \quad (5)$$

This model has the same number of parameters as model (4), but it does not incorporate any knowledge about the wind farm power curve, apart from the fact that most power curves are well approximated by a third order polynomial in the wind speed. The parameters of this model have been estimated using the standard recursive least squares algorithm.

5.3 Recursive Local Regression

So far we have not mentioned how the parameters in the MOS models depend on the prediction horizon. Actually we have just estimated one set of parameters for each prediction horizon. Addressing the variance problem of the Kalman Filter and the usual recursive least squares algorithm, it might be advantageous to make assumptions about how the parameters depend on k . Furthermore, in Section 3 and 4 it was shown that the NWP wind direction improved the performance for the wind speed predictions, and that there was an aliasing effect with the time of day/atmospheric stability, caused by the update frequency of the NWP model. To take all these findings into account the following model is proposed

$$p_{l+k} = a(k, \theta_{l+k}, t_{day}) \omega_{l+k} + b(k, \theta_{l+k}, t_{day}) \omega_{l+k}^2 + c(k, \theta_{l+k}, t_{day}) \omega_{l+k}^3 + d(k, \theta_{l+k}, t_{day}) p_l + m(k, \theta_{l+k}, t_{day}) + \varepsilon_{l+k} \quad (6)$$

This model is similar in structure to (5) except that the parameters/coefficient now are assumed to be functions of the prediction horizon, the wind direction and the time of day.

To take the stability into account it was found sufficient to estimate two sets of coefficient functions, one set for the following times of day: 00:00, 03:00, 06:00, and 21:00, i.e. mainly neutral/stable conditions, and one set for

the times: 09:00, 12:00, 15:00, 18:00, i.e. mainly unstable conditions. For the wind direction and the prediction horizon, the approach described in [9] has been used for the estimation of the coefficient functions. This approach is best described as recursive local regression, and it is an extension of the usual recursive least squares algorithm, where the functional shape is found by estimating the parameters locally over a grid spanning the variables, e.g. for a given wind direction θ in the grid, only observations close to this direction are used when the value of the coefficient function for this particular value of θ is estimated.

In the actual estimation the coefficient functions were estimated in a fine grid spanning the NWP wind direction, using a fixed bandwidth of 100° , and for the prediction horizon an increasing bandwidth was used, i.e. for the 3 hour prediction a bandwidth spanning only the 3 hour prediction was used, increasing to a bandwidth spanning the 12 hour up to the 36 hour prediction for the 36 hour prediction, this choice reflects the fact the variation of the parameters with the prediction horizon was found to be small for large prediction horizons.

When only one set of coefficient functions were estimated for all times of day, the assumption about the variation of the coefficient functions with k failed, because in this case a 6 hourly variation is introduced in the coefficient functions with k .

Because some wind directions are rare it was found important to use a different degree of time adaptation depending on the wind direction [9]. For frequent wind directions the optimal time window was found to be about 2-3 months, while for rare wind direction it was not to use any adaptation at all. This indicates that the variation of the coefficient functions with the wind direction is larger than the time-variation.

6 RESULTS

Figure 4 shows the performance for the three adaptive approaches that have been described in the previous sections. It clearly seen that model (6) gives the best results, the non-linear model (4) and the linear model (5) are close in performance, neither model performs best on all prediction horizons, but overall the linear model seems to perform best. This suggests that the polynomial approximation of the power curve is adequate.

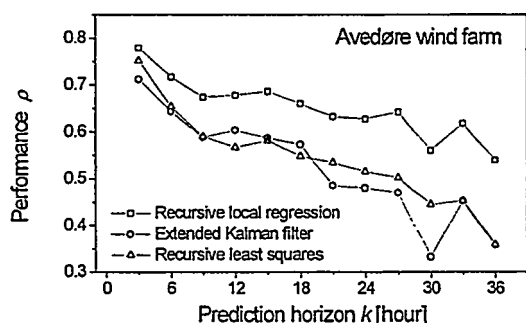


Figure 4: Performance of adaptive approaches.

Figure 5 shows the prediction performance of model (6) for the three wind farms, and it is seen that there is a pronounced variation in the performance for the individual wind farms, which can be due to many factors, e.g. the NWP model accuracy depends on the specific location, or another factor that might be of importance in this study is that the quality of the observations from the wind farms was rather poor, about 30 % of the observations were missing.

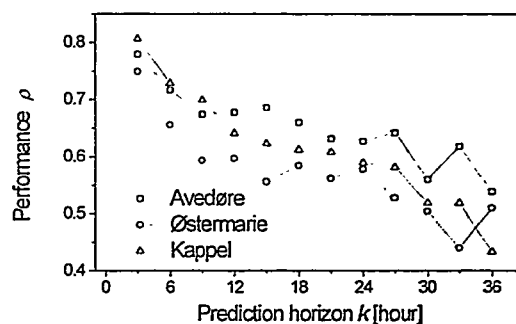


Figure 5: Performance for various wind farms.

7 SUMMARY

In this paper various MOS approaches have been proposed for wind power prediction models, which are based on NWP and observations. Three estimation methods have been considered: Extended Kalman filtering, recursive least squares and a new modified recursive least squares algorithm. The results indicate that the best MOS approach, is one which takes the wind direction, the time of day, the prediction horizon, and auto-correlation of the observations into account when using a wind speed polynomial approximation of the power curve to predict the future power from a wind farm. Furthermore it was found that the surface wind from the NWP model, which in this case is HIRLAM [6], should be used.

ACKNOWLEDGEMENTS

This work is partially funded by the European Commission (EC) under JOULE (JOR3-CT95-0008). A. Joensen is partly funded by the Danish Research Academy. G. Giebel is funded by the EC under JOULE/TMR (JOR3-CT97-5004).

REFERENCES

- [1] T. Hastie and R. Tibshirane, Varying-coefficients Models, *Journal of the Royal Statistical Society, Series B* 55 (1993) 757.
- [2] A. Joensen, H. Madsen and T. S. Nielsen, Non-parametric Statistical Methods for Wind Power Prediction, *Proceedings of the EWEC97, Ireland* (1997) 788.
- [3] L. Landberg, A Mathematical Look at a Physical Power Prediction Model, *Wind Energy* 1 (1998) 23.
- [4] L. Landberg, Short-term Prediction of Local Wind Conditions, *Boundary-Layer Meteorology*, 70, 171.

- [5] L. Ljung and T. Söderström, Theory and Practice of Recursive Identification, MIT Press, Cambridge, Massachusetts (1983).
- [6] B. Machenhauer (Ed), HIRLAM Final Report, Danish Meteorological Institute, Denmark (1988).
- [7] H. Madsen (Ed), Models and Methods for Predicting Wind Power, Dept of Mathematical Modelling, Technical University of Denmark, Denmark (1996).
- [8] N. G. Mortensen, L. Landberg, I. Troen and E. L. Petersen, Wind Atlas Analysis and Application Program (WASP), User's Guide, Risø-I-666(EN) (v.2), Risø National Laboratory, Roskilde, Denmark (1993).
- [9] H. Aa. Nielsen, T. S. Nielsen, A. Joensen and H. Madsen, Tracking Time-varying Coefficient Functions, in preparation.
- [10] T. S. Nielsen, A. Joensen, H. Madsen, L. Landberg and G. Giebel, A New Reference for Predicting Wind Power, Wind Energy 1 (1999) 29.
- [11] P. Sanderhoff, PARK – User's Guide. A PC-program for calculation of wind turbine park performance, Risø-I-668(EN), Risø National Laboratory, Roskilde, Denmark (1993).

WIND RESOURCE MODELLING FOR MICRO-SITING - VALIDATION AT A 60-MW WIND FARM SITE

Jens Carsten Hansen and Niels Gylling Mortensen
Wind Energy and Atmospheric Physics Department
Risø National Laboratory
P.O. Box 49, DK-4000 Roskilde, Denmark

Usama Said Said
New and Renewable Energy Authority
Nasr City, Cairo, Egypt

ABSTRACT: This paper investigates and validates the applicability of the WAsP-model for layout optimization and micro-siting of wind turbines at a given site for a 60-MW wind farm at Zafarana at the Gulf of Suez in Egypt.

Previous investigations show large gradients in the wind climate within the area. For the design and optimization of the wind farm it was found necessary to verify the WAsP extrapolation of wind atlas results from 2 existing meteorological masts located 5 and 10 km, respectively, from the wind farm site. On-site measurements at the 3.5 x 3.5 km² wind farm site in combination with 7 years of near-site wind atlas measurements offer significant amounts of data for verification of wind conditions for micro-siting. Wind speeds, wind directions, turbulence intensities and gusts in 47.5 m a.g.l. have been measured at 9 locations across the site. Additionally, one of the site masts is equipped as a reference mast, measuring both vertical profiles of wind speed and temperature as well as air pressure and temperature. The exercise is further facilitated by the fact that winds are highly uni-directional; the north direction accounting for 80-90% of the wind resource.

The paper presents comparisons of 5 months of on-site measurements and modeled predictions from 2 existing meteorological masts located at distances of 5 and 10 km, respectively, from the wind farm site. Predictions based on terrain descriptions of the Wind Atlas for the Gulf of Suez 1991-95 showed over-predictions of wind speeds of 4 -10%. With calibrated terrain descriptions, made based on measured data and a re-visit to critical parts of the terrain, the average prediction error of wind speeds was reduced to about 1%. These deviations are smaller than generally expected for such wind resource modeling, clearly documenting the validity of using WAsP modeling for micro-siting and layout optimization of the wind farm.

The present work has been funded by the Danish Ministry of Foreign Affairs (Danida) and the New and Renewable Energy Authority (NREA), Egypt.

Keywords: wind resource assessment, wind measurements, site calibration, wind flow modeling, uncertainties, micro-siting, wind farms

1 INTRODUCTION

Micro-siting of wind turbines for determination of the optimal wind farm layout in terms of energy production is essential for the wind farm design. This paper investigates and validates the applicability of the WAsP-model for this purpose, at a given site for a 60-MW wind farm at Zafarana at the Gulf of Suez in Egypt.

The assessments and recommendations of this paper are based on available information and data from the Wind Atlas for the Gulf of Suez 1991-95 (Mortensen and Said [1]) and from the "Zafarana Wind Farm Site Calibration" project. Both projects were funded and executed in cooperation between the New and Renewable Energy Authority (NREA), Egypt, and the Danish Ministry of Foreign Affairs (Danida) with Risø National Laboratory as consultant.

Previous investigations show large gradients in the wind climate within the Gulf of Suez area in Egypt. For the design and optimization of the 60-MW Zafarana Wind Farm it was therefore found necessary to verify the WAsP extrapolation of wind atlas results from the 2 existing meteorological masts located up to 10 km from the selected

wind farm site at Abu Darag to the north and Zafarana to the south. The procedure chosen was

- Perform new on-site measurements with 9 masts
- Compare new measurements and predictions from the 2 original wind atlas masts
- Calibrate terrain descriptions and model parameters
- Determine the resulting revised wind atlas for the site

The paper will present results based on the extended measurements including an analysis of uncertainty for the site. Furthermore, it will make recommendations for micro-siting.

2 THE SITE

The digitized terrain contours of the Zafarana-Abu Darag area used in the wind atlas analyses are shown in Figures 1 and 2. The relative location of the wind farm site appears from the map as the area with high density of contour lines - every 1 m as opposed to every 10 m for the remaining part of the area. The Abu Darag mast is located approximately 10 km north of the site - marked Dar - and the Zafarana mast is approximately 5 km south of the site - marked Zaf.

Figure 1 Location of the Zafarana Wind Farm site in the Zafarana – Abu Darag area with indication of met masts Abu Darag (Dar) and Zafarana (Zaf)

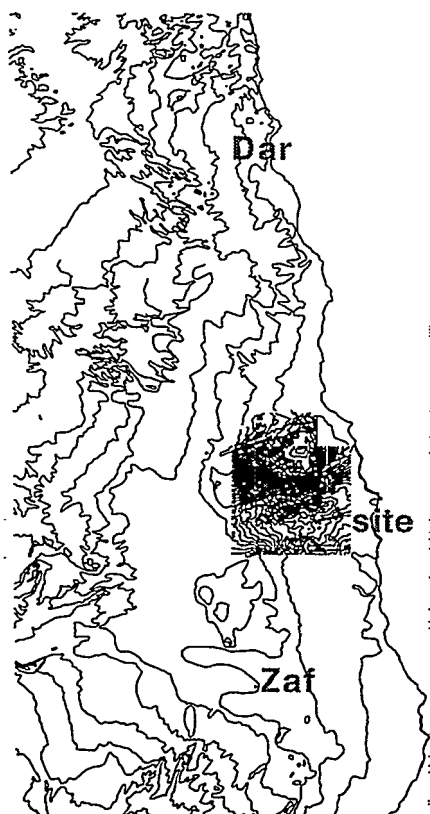
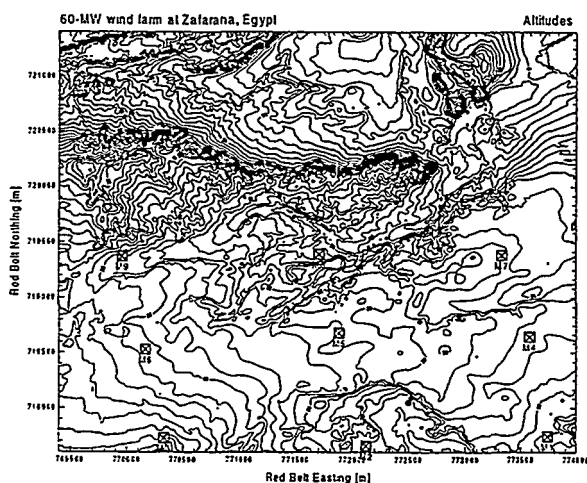


Figure 2 shows height contours of the Zafarana Wind Farm site with the locations of the 9 measuring masts - M1, M2,..., M9.

Figure 2 Map of the Zafarana Wind Farm site indicating locations of the "Site Calibration" masts (M1 – M9)



3 MEASUREMENTS

On-site measurements at the 3.5 x 3.5 km² wind farm site in combination with 7 years of near-site wind atlas measurements offer significant amounts of data for verification of wind conditions for micro-siting.

The wind data used in this paper are simultaneous recordings in the period 09 March – 14 August 1998 at

- 9 "Site Calibration" stations, M1 – M9, with a measuring height of 47.5 m a.g.l.
- 2 Wind Atlas stations at Abu Darag and Zafarana, with a measuring height of 24.5 m a.g.l.

The instrumentations of the 11 masts in this analysis are similar, using

- Battery powered Aanderaa 12-channel data loggers and storage units
- Risø cup-counter anemometers calibrated in the wind tunnel of the Danish Maritime Institute, equipped with electronics to determine averages, standard deviation, gust and lull every 10 minutes based on 1 Hz sampling
- Aanderaa wind-vanes, temperature and pressure sensors

Additionally, one of the site masts (M7) is equipped as a reference mast, measuring both vertical profiles of wind speed and temperature as well as air pressure and absolute temperature in 2 m a.g.l.

The Abu Darag and Zafarana stations do not record wind speed standard deviation, gust and lull, and it should be noted that the calibration of those anemometers was made in 1991. A re-calibration of a sample from that batch of anemometers installed in Egypt in 1991 was made in 1996. This re-calibration showed no significant de-gradation of the anemometer or change of calibration values.

The total number of 10-minute periods available for the analysis amounts to 22760, corresponding to 3793 hours.

4 WASP PREDICTIONS AND CALIBRATION OF SITE PARAMETERS

The main results required are a wind atlas and a corresponding terrain description, enabling accurate wind resource assessment at any location across the entire wind farm site area. First estimates of the wind resource are available from Abu Darag and Zafarana data – Mortensen and Said [1]. However, as it appears from [1], there may be rather large gradients in the wind climate within the Gulf of Suez area, and the level of detail of site descriptions at the selected wind farm site seems inadequate for a large wind farm project.

The procedure for calibration of site parameters for arriving at the resulting calibrated wind resource model and terrain descriptions for the wind farm site is briefly

- to perform new on-site measurements (M1-M9) for a sufficiently long period for obtaining statistical significance and record simultaneously data from Abu Darag and Zafarana
- to compare new measurements and predictions based on data from Abu Darag and Zafarana

- to calibrate terrain descriptions and model parameters (modification of WASP-input descriptions if justified by field observations)
- to determine the resulting modified wind resource model for the site

With new on-site measurements at M1-M9 performed, the quality and applicability of using the Abu Darag and/or the Zafarana wind atlases as a basis for modeling of wind resources across the wind farm site is tested by means of a wind atlas analysis.

Prediction before calibration of site parameters

The wind atlas analysis tests the ability of one reference measurement station to predict the other 10 stations. Initially two analyses were made, using two different reference stations – Abu Darag (measuring height, H=24.5 m a.g.l.) and Zafarana (H=24.5 m a.g.l.). The results are shown in Table 1.

Table 1 Comparison of measured (Um) and predicted (Up) values of wind speeds based on wind atlas modeling using Abu Darag and Zafarana data for 09Mar-02May98

09Mar-02May98 H (m)	M1	M2	M3	M4	M5	M6	M7	M8	M9	Dar	Zaf
Um	9.2	8.7	8.5	9.1	8.7	8.5	9.1	8.6	8.4	8.3	8.1
Up (Dar)	9.6	9.3	9.2	9.7	9.4	9.1	9.7	9.2	8.9	8.1	7.8
Um/Up	0.96	0.94	0.92	0.94	0.93	0.93	0.94	0.93	0.94	1.02	1.04
Up (Zaf)	9.8	9.4	9.4	9.9	9.5	9.3	9.9	9.3	9.1	8.4	8
Um/Up	0.94	0.93	0.90	0.92	0.92	0.91	0.92	0.92	0.92	0.99	1.01

The results of Table 1 show that both Abu Darag (Dar) and Zafarana (Zaf) over-predict the wind speeds at the wind farm site by 4-10%, whereas they predict each other somewhat more accurately. Such over-prediction of wind speed will lead to considerable over-prediction of wind energy production, and it may influence wind farm layout optimization significantly.

Calibration of site parameters

The calibration of site parameters compared to the "Wind Atlas for the Gulf of Suez, 1991-95" [1] was basically

- a modification of the terrain surface roughness description
- inclusion of a detailed map of height contours of the site – approximately 3.5 x 5 km²

The terrain surface roughness description was modified based on

- scrutiny of stereoscopic aerial photos
- a detailed site survey
- "measured" z_0 values at the site - z_0 values found using the vertical profile of wind speeds measured at heights of 10 m, 24.5 m and 47.5 m a.g.l. at M7

Prediction after calibration of site parameters

Table 2 lists wind speed predictions made as wind atlas extrapolations of data from Abu Darag (Dar), Zafarana (Zaf) and from the site reference mast (M7) as well as the actually measured average wind speeds. Measurements and predictions are 10 minutes values during the period 9 March – 14 August 1998 for all wind directions and

climatological phenomena during that period with the weighting that has naturally occurred.

Comparisons of measurements and predictions show accurate predictions of wind speeds at the wind farm site by the Abu Darag mast with resulting average prediction errors less than 1%. The calibration of parameters and terrain description has, however, resulted in the Zafarana mast grossly over-predicting wind speeds at the wind farm site. The average over-prediction by the Zafarana mast is 7.5%.

Table 2 Comparison of measured (Um) and predicted (Up) values of wind speeds based on wind atlas modeling using Abu Darag, Zafarana and M7 data for 09Mar-14Aug98

09Mar-14Aug98 H (m)	M1	M2	M3	M4	M5	M6	M7	M8	M9	Dar	Zaf
Um	10.0	9.6	9.5	9.9	9.7	9.5	9.9	9.5	9.4	8.9	9.2
Up (Dar)	10.0	9.6	9.6	10.1	9.8	9.5	10.2	9.6	9.4	8.9	8.4
Um/Up	1.00	1.00	0.99	0.98	0.99	1.00	0.97	0.99	1.00	1.00	1.10
Up (Zaf)	10.7	10.3	10.3	10.8	10.4	10.2	10.9	10.3	10.1	9.7	9.1
Um/Up	0.94	0.93	0.92	0.92	0.93	0.93	0.91	0.92	0.93	0.92	1.01
Up (M7)	9.6	9.3	9.2	9.8	9.4	9.2	9.8	9.2	9.1	8.6	8.0
Um/Up	1.04	1.03	1.03	1.01	1.03	1.03	1.01	1.03	1.03	1.04	1.15

5 UNCERTAINTIES

The uncertainties of primary interest in this paper are those associated with modeling wind resources at given locations in a wind farm site based on data from a nearby measurement station – in this case by a wind atlas analysis using data from 5-10 km distance.

The purpose of the "site calibration" exercise is to eliminate to the degree possible effects of some of the main sources of uncertainty, particularly

- wind climate gradients within the Abu Darag – Zafarana area (meso-scale effects)
- terrain description, especially surface roughness assessments and quality of height contour specification
- measurement errors, e.g. caused by malfunction or significant degradation or uncertainties of calibrations of anemometers
- WASP models and parameters

The comparisons of modeled and measured values of wind speeds are performed at 9 locations across the wind farm site. The uncertainty of this exercise may be illustrated by the average and the standard deviation of the ratio of measured and predicted wind speed values as shown in Table 3.

Table 3 Averages and standard deviations of the ratios of measured and predicted wind speed values (Um/Up) for the 9 measurement locations – M1-M9

	Average of Um/Up	Standard deviation
modeled from Abu Darag	0.991	0.0103
modeled from Zafarana	0.926	0.0090

Table 3 shows that predictions from Abu Darag with a 68% probability will be within 0 - +2% of the measured wind speed values at M1-M9. However, the measured values are not necessarily true values. The analysis of the statistical

significance of the measured data in Table 4 shows that the duration of the measurement period influenced the statistical uncertainties of the estimated average wind speed for each of the 12 wind direction sectors. The statistical uncertainty of the estimate of the average may be expressed by the relation σ/\sqrt{N} , where σ is the standard deviation of the 10 minute values recorded and N is the number of 10 minute values recorded. The uncertainties in percent of U_m - sectorwise and total - are shown. This analysis has been performed for mast M1.

Table 4 Statistical measurement uncertainty of average wind speeds measured at M1 - wind direction sector by wind direction sector

Wind direction	0	30	60	90	120	150	180	210	240	270	300	330	total
occurrence (%)	62.1	2.9	1.4	1.3	1.8	2.7	0.8	0.7	4.1	2.7	1.1	18.4	100
σ/\sqrt{N} [m/s]	0.03	0.14	0.20	0.20	0.17	0.14	0.26	0.28	0.11	0.14	0.22	0.05	0.02
Uncertainty (% of Umean)	0.27	2.6	5.3	5.9	3.8	1.6	6.4	4.3	1.2	2.2	5.2	0.50	0.23

The number of values recorded differ considerably from sector to sector, and the uncertainty estimates range from 0.023 m/s to 0.276 m/s. The uncertainty analysis shows that the measurement period has been long enough to ensure that these statistical uncertainties are below 0.5% for the predominant wind directions with highest occurrence and highest wind speed and thus most importance. This analysis has been performed for mast M1, but the result would be similar if performed for any of the other 10 masts. All in all, statistical measurement uncertainty levels of this analysis are acceptable, but they surely do account for a significant part of the standard deviation of U_m/U_p shown in Table 3.

6 DISCUSSION AND CONCLUSIONS

The much better predictions of wind farm site wind speeds by the Abu Darag mast than by the Zafarana mast may be explained by the Zafarana mast being more affected by meso-scale effects of the topography at Zafarana, which are not modeled by WAsP. For winds from the west, the Zafarana mast may still be more representative for wind conditions at the wind farm site, but these wind directions occur only 7-8% of the measurement period, and even less on an annual basis. The meso-scale effects are presently being studied as part of "Wind Atlas for Egypt" project, which aims at extending the geographical coverage of the Wind Atlas for the Gulf of Suez, both in the Gulf area and to the rest of Egypt.

It is furthermore seen from Table 2 that wind atlas modeling based on data from mast M4 and M7 under-predict wind speeds at the other site locations (M1-M9) by 2-3%. The reason seems to be related to effects of distance to the sea. The adequacy of the modeling of water surfaces applied should be studied further.

It should be highlighted that

- wind atlas modeling deviations from measurements before calibration of site parameters were about 7% with range of 4 - 10%
- wind atlas modeling deviations from measurements after calibration of site parameters on average are about 1%, when using the Abu Darag mast data

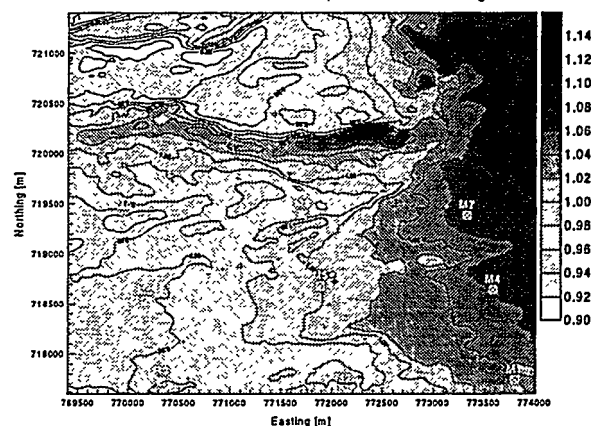
- standard deviation of wind atlas modeling deviations from measurements after calibration of site parameters are about 1%
- effects of distance to the sea seems to introduce uncertainties not yet fully accounted for
- the Abu Darag mast (10 km from site) predicts the site significantly better than the Zafarana mast (5 km from site), probably due to meso-scale effects of near-site topography

In conclusion, 5 months of measurements clearly document the validity of using WAsP modeling for micro-siting and layout optimization of the wind farm, when applying calibrated site parameters and Abu Darag data. At Abu Darag, 8 years of data have been recorded. This is a significant climatological database, which ensures the statistical significance and that predictions are representing long-term averages. Uncertainties may be estimated based on the findings of this paper.

The resulting wind resource map of the wind farm site is shown in Figure 3. The micro-siting and layout optimization can begin.

Figure 3 Wind resource map of the wind farm site, showing relative annual energy production for a 600 kW wind turbine with 45 m hub height

Contours and color scale of relative production at 45 m a.g.l.



REFERENCES

- [1] N.G. Mortensen and U.S. Said. Wind Atlas for the Gulf of Suez, 1991-95. Risø National Laboratory. ISBN 87-550-2143-3 (1996)

A LINEAR MODEL FOR FLOW OVER COMPLEX TERRAIN

Helmut P. Frank

Risø National Laboratory

Wind Energy and Atmospheric Physics Department

P. O. Box 49, DK-4000 Roskilde, Denmark

phone: +45 46 77 50 13, fax +45 46 77 59 70, e-mail: helmut.frank@risoe.dk

ABSTRACT: A linear flow model similar to WASP or LINCOM has been developed. Major differences are an isentropic temperature equation which allows internal gravity waves, and vertical advection of the shear of the mean flow. The importance of these effects are illustrated by examples. Resource maps are calculated from a distribution of geostrophic winds and stratification for Pyhäntunturi Fell in northern Finland and Acqua Spruzza in Italy. Stratification becomes important if the inverse Froude number formulated with the width of the hill becomes of order one or greater.

Keywords: Models (Mathematical); Mountains/High Terrain; Stratification; Resources

1 INTRODUCTION

The Wind Atlas Analysis and Application Program WASP [10, 15] has been designed for use in relatively flat or gentle, hilly terrain. Increasingly wind turbines are placed in mountainous areas with steeper and higher terrain. Lacking other simple models, WASP is still used outside its proper performance envelope. Errors can be expected going from a relatively smooth valley to a rugged mountain or reverse. However, predictions work well if the measurement site and the prediction site have approximately the same ruggedness index [3, 11].

Therefore, a model has been developed to improve some aspects of WASP in these complex situations. Advection of the mean shear by the vertical velocity is accounted for which partly compensates for the neglected advection by the horizontal perturbation velocity in a linear model.

Also, stratification becomes important for greater hills. Therefore, a simple temperature equation allows the simulation of stratified flows. Then, the speed-up does not decrease monotonically at the summit of a hill. The maximum speed may occur downwind of the summit.

The model is similar to other models for flow over hill [7, 6, 2, 9]. It follows the ideas of Troen and de Baas [14]. Jensen's roughness change model [1,] is incorporated to simulate flow over variable surface roughness.

2 DESCRIPTION OF THE MODEL

Equations have been derived which approximate the true velocity profile by a linear shear profile below a height which is proportional to the wave length of the Fourier mode. Then, a solution for the perturbation pressure can easily be obtained. From this pressure solution and the correct mean speed profile equations for the perturbation velocities are obtained.

The approximation of a linear shear profile is better for stably stratified flow than for neutrally stratified flow because then the similarity wind profile in the surface layer consists of a logarithmic plus a linear profile.

The fastest way to solve the equations is to use Fast Fourier Transforms. All velocity components are represented in Fourier space like

$$w(x, y, z) = \iint \hat{w}(k, l, z) e^{i(kx + ly)} dk dl / 4\pi^2, \quad (1)$$

Assuming $\hat{w} \sim \exp(m_2 z)$, the dispersion relation for m_2 in frictionless flow with weak linear shear is

$$m_2^2 = k_h^2 (1 - N^2 / (k_\gamma U_2)^2) \quad (2)$$

where k_h is the magnitude of the horizontal wave number ($k_h^2 = k^2 + l^2$), $k_\gamma = k_h \cos \gamma$, and γ is the angle between the direction of the horizontal wave number vector and the mean wind U . The buoyancy frequency is $N = \sqrt{(g/\theta) \partial \theta / \partial z}$, and $U_2 = U(z_2)$ where $z_2 = 1/|m_2|$. This equation is solved using Newton-Raphson iteration.

The pressure solution ($\psi = p/\rho$) is

$$\hat{\psi} = m_2 (k_\gamma / k_h)^2 U_0 (U_l(z) - U_l' / m_2) \hat{h} e^{m_2 z} \quad (3)$$

which is correct for a linear shear profile with weak shear. $U_l = U_2 + (z - z_2) U_l'$, $U_0 = U_l(0)$.

If the vertical velocity \hat{w} is known, the horizontal velocity components can be calculated directly from the horizontal momentum equations. An approximate solution for the vertical velocity is

$$\hat{w} \approx i k_\gamma U_0 \frac{U(z)}{U_l(z)} \hat{h} e^{m_2 z} \quad (4)$$

which comes from the vertical momentum equation and the isentropic temperature equation.

With the pressure solution (3) and the vertical velocity from (4), the horizontal velocities are

$$\hat{u} = -\frac{k \hat{\psi}}{k_\gamma U} - \frac{U_0}{U_l} U_l' \hat{h} e^{m_2 z} \quad (5)$$

$$\hat{v} = -\frac{l \hat{\psi}}{k_\gamma U} - \frac{U_0}{U_l} V_l' \hat{h} e^{m_2 z} \quad (6)$$

where the shear U' , V' is replaced by the constant shear U_l' , V_l' below z_2 .

The shear has two effects on the horizontal velocity perturbations. First, the scale of the surface pressure perturbation is reduced. For neutrally stratified flow the surface pressure scales with $U_2^2 (1 - z_2 U_2' / U_2)$ and not with U_2^2 . A similar scaling is also used by Hunt and his co-workers [6]. Second, the vertical advection of slower mean flow momentum upstream of a hill decreases the horizontal speeds. This means that the predicted horizontal velocities at the summit of a hill are too big if the shear of the mean flow is neglected. Also, the v -component would be always zero for 2-dimensional flow ($l = 0$). The approximate solution (6)

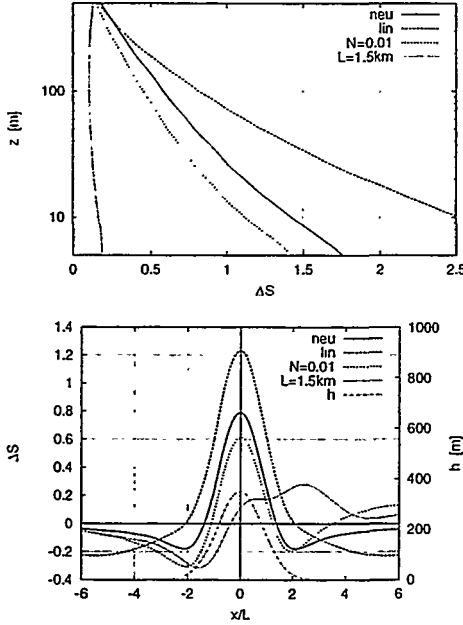


Figure 1: Fractional speed-up ratio $\Delta S = \Delta u/U$ over 2-dimensional gaussian ridges. for different stratification and mean wind profile. See text for explanation.

yields a weak transverse component $\hat{v} = -V_2' \hat{h}$ at the surface. In addition to the acceleration of the u -component, the v -component turns the wind to a direction more perpendicular to a ridge.

2.1 Examples

The fractional speed-up ratio $\Delta S = \Delta u/U$ over 2- and 3-dimensional gaussian mountains are shown in Figs. 1 and 2. The height of the mountains is 350 m. The half-height-at-half-width is $L = 500$ m, except for the case denoted $L=1.5\text{km}$, where it is $L = 1500$ m. The height of the boundary layer is 1000 m, and the wind speed in the free atmosphere is 10 m s^{-1} , perpendicular to the 2-dimensional ridge.

The full lines (neu), show flow in a neutrally stratified atmosphere with a logarithmic profile of the mean surface wind. The dashed lines (lin) shows flow with a log-linear surface wind profile with Monin-Obukhov-length 165 m in a neutrally stratified atmosphere. $N=0.01$ (dotted) shows the flow in a stably stratified atmosphere with buoyancy frequency $N = 0.01 \text{ s}^{-1}$ with a logarithmic surface wind profile. $L=1.5\text{km}$ (dash-dotted lines) is the same flow over a three times wider hill with half-width 1500 m.

The speed-up near the surface is greater for the log-linear mean wind profile. However, it decreases more rapidly with height. Therefore, for the 3-dimensional hill above 30 m a.g.l. it is less than with a logarithmic mean wind profile.

The speed-up at the summit in a stably stratified atmosphere is less than in a neutrally stratified atmosphere. More important is the shift of the position of the greatest speed-up downwind of the summit (see also [7]). This effect is not visible for the smaller hill at 50 m a.g.l.. For the wider hill two maxima appear downwind of the summit. The greater one occurring near the base of the mountain.

2.2 Different stratification in the free atmosphere

If the stratification in the free atmosphere and the boundary layer are different, partial reflection of waves can occur at

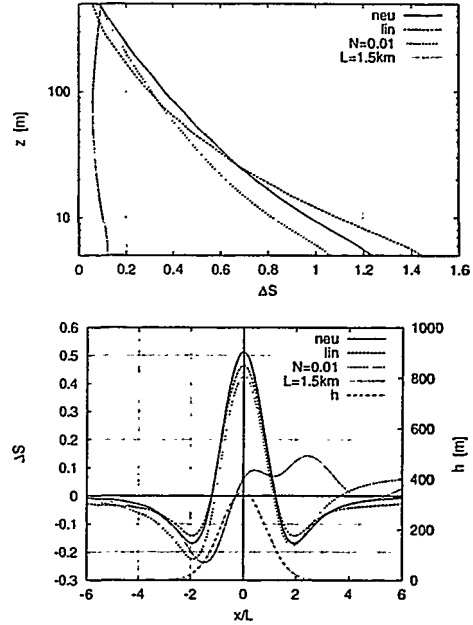


Figure 2: Fractional speed-up ratio $\Delta S = \Delta u/U$ over 3-dimensional gaussian hills. Like Fig. 1.

the top of the boundary layer. The pressure and the vertical velocities have to be continuous across the interface. Then, the horizontal velocities will also be continuous. The temperature perturbation can jump, owing to different values of N in the boundary layer and the free atmosphere.

The most complicated case is a stably stratified boundary layer below a less stably stratified free atmosphere. Then, some waves can exist in the boundary layer, but not in the free atmosphere. The boundary layer forms a wave guide for these waves. They will appear only downwind of hills, but not upwind of them. The flow field can no longer be calculated taking only FFTs of the Fourier modes, because the solution has poles in the complex domain. FFTs assume a periodic domain, where the wave would appear also on the inflow boundary.

The poles must be subtracted out of the total solution as e.g. in [13, 16]. At present this cannot be handled in general. Fig. 3 shows the velocity perturbations over a gaussian hill in a shear-free atmosphere with a fixed lid at height $3L$ for different stratification (similar to [7]). Weak stratification introduces a slight asymmetry upwind and downwind of the hill. The speed-up at the summit is reduced somewhat. Above the critical Froude number $F_r = N\delta/U = \pi/\delta$, where $\delta = 3L$ is the height of the boundary layer, waves appear downwind of the hill, and the wind on the downslope increases strongly. In the example shown in Fig. 3 the maximum perturbation velocity doubles.

3 CALCULATION OF RESOURCE MAPS

3.1 Method

The model was used to calculate wind resource maps for two areas in Italy and Finland. The same method as in [4] is employed. Representative geostrophic winds in 8 sectors were determined from 10 years (1987-96) data of the re-analysis of NCEP/NCAR [8]. Each sector contained 4 to 6 speeds. Using the geostrophic drag law (e.g. [15]) and the

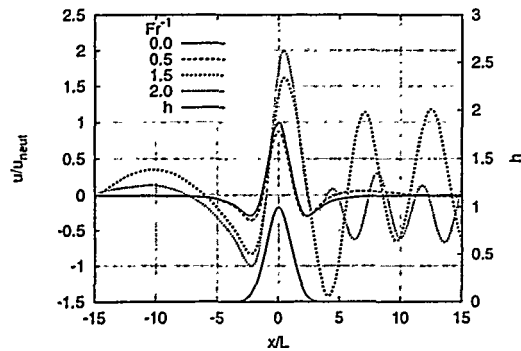


Figure 3: Velocity perturbation in stably stratified atmospheres with Froude numbers Fr below a fixed lid at $3L$ relative to the perturbation in a neutrally stratified atmosphere.

Table I: Extreme wind speeds U [m s^{-1}], and power densities E [W m^{-2}] for the different cases shown in Figs. 5 and 4.

	U_{min}	U_{max}	E_{min}	E_{max}
Pyhäntunturi Fell (61 m a.g.l.)				
neutral	6.2	9.3	483	1605
neut.,stab.	6.3	9.4	517	1624
stable	5.7	8.5	424	1299
Acqua Spruzza (15 m a.g.l.)				
neutral	1.7	7.0	13	959
neut.,stab.	1.5	7.7	11	1213
stable	1.7	6.5	21	848

average roughness of the area, it was rotated to the direction of the surface wind. The mean stratification was also determined from the geopotential heights. The surface wind field was calculated with the model. The average wind speed and power density were calculated weighting each result with the frequency of the particular geostrophic wind.

Three calculations were made for each case. The first uses a neutrally stratified atmosphere. The second assumes a neutrally stratified boundary layer below a stably stratified free atmosphere. The last case takes a uniformly stably stratified atmosphere. A logarithmic profile of the surface wind was used for all simulations.

Results for Pyhäntunturi Fell in Finland are shown in Fig. 4. The mean geostrophic wind is 9.1 m s^{-1} from 267° . A boundary layer thickness of 800 m was used. Fig. 5 shows results for Acqua Spruzza in Italy, where the mean geostrophic wind is 6.2 m s^{-1} from 270° . A boundary layer thickness of 1000 m was used. Extreme values of wind speed and power density in the areas are listed in Table I.

At Pyhäntunturi Fell a neutral or stable free atmosphere above a neutrally stratified boundary makes almost no difference because the mountain is narrow, and only moderate stratifications were used. For this site very strong inversion just above the height of the mountain are very important for the wind climate [12, 5].

The mountain of Acqua Spruzza is greater. Therefore, the stratification of the free atmosphere yields important differences for the best sites.

4 SUMMARY

A linear flow model similar to WASP or LINCOM has been developed. Major differences are an isentropic temperature

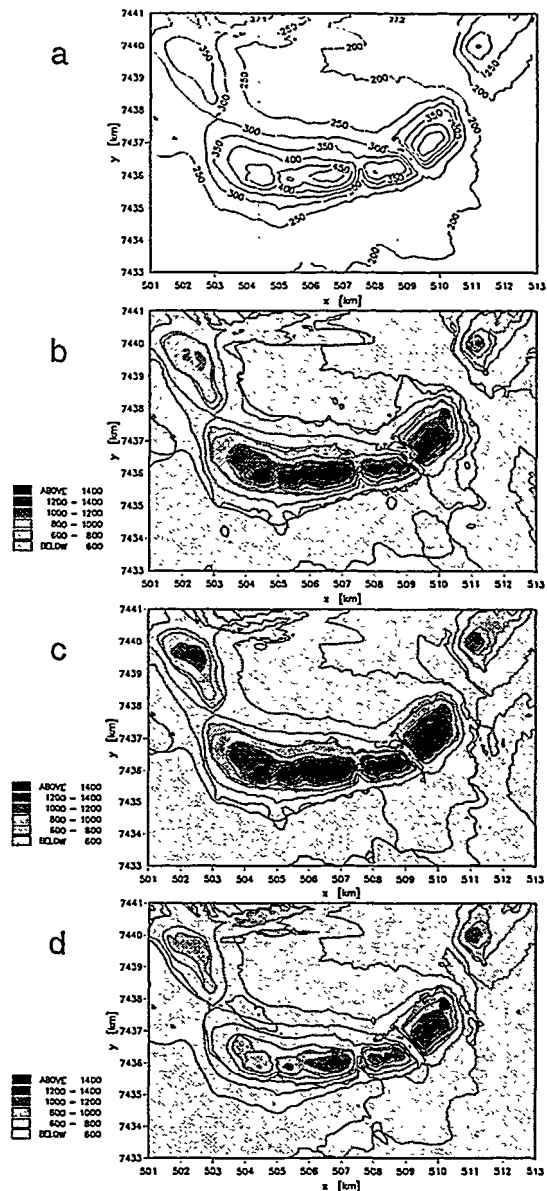


Figure 4: Resource maps of wind power density E at 61 m a.g.l. in W m^{-2} around Pyhäntunturi Fell: a) orography, b) neutral stratification, c) neutral boundary layer below stably stratified free atmosphere, d) stable stratification.

equation which allows internal gravity waves, and vertical advection of the shear of the mean flow. The importance of stratification is measured by the inverse Froude number $Fr = NL/U$, where L is the characteristic width of the mountain. For small mountains it is unimportant.

This is illustrated by resource maps calculated for for Pyhäntunturi Fell in Finland and Acqua Spruzza in Italy. The first is a narrow mountain where the stratification of the free atmosphere above a neutral boundary layer is relatively unimportant. The later mountain is wider. Therefore, greater differences occur.

REFERENCES

- [1] P. Astrup, N. O. Jensen, and T. Mikkelsen. Surface roughness model for LINCOM. Report Risø-R-

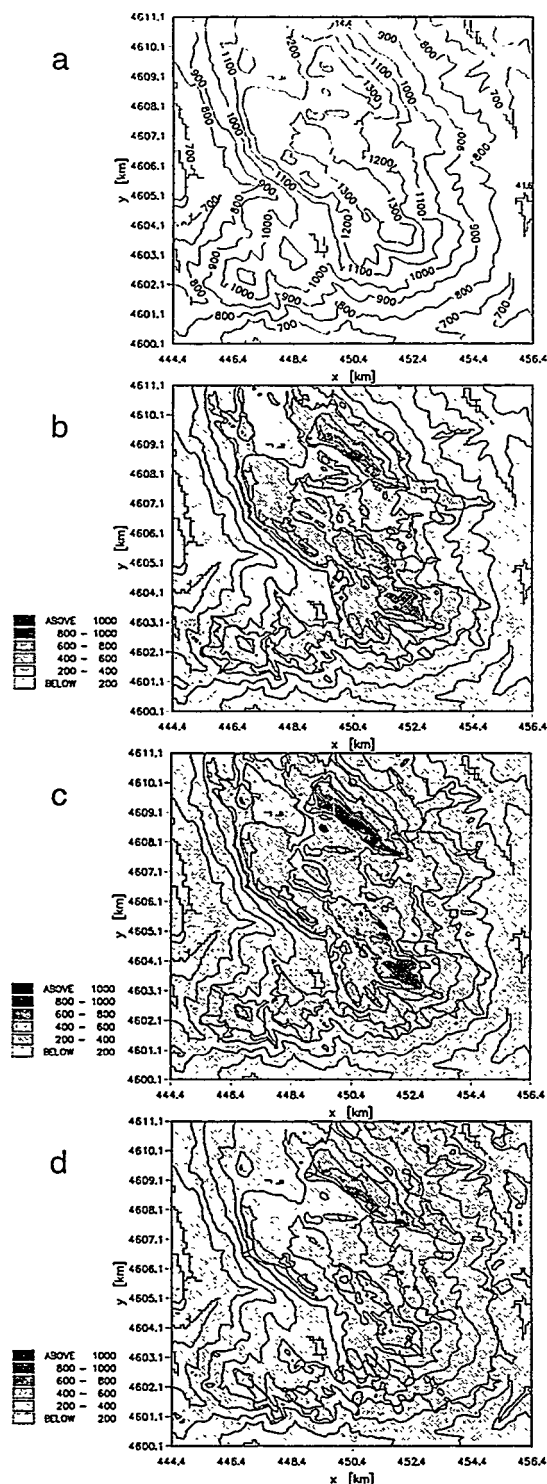


Figure 5: Resource maps of wind power density E at 15 m a.g.l. in W m^{-2} at Acqua Spruzza: a) orography, b) neutral stratification, c) neutral boundary layer below stably stratified free atmosphere, d) stable stratification.

900(EN), Risø National Laboratory, June 1996.

- [2] A. C. M. Beljaars, J. L. Walmsley, and P. A. Taylor. A mixed spectral finite-difference model for neutrally stratified boundary-layer flow over roughness changes and topography. *Boundary-Layer Meteorol.*, 38:273–

303, 1987.

- [3] A. J. Bowen and N. G. Mortensen. Exploring the limits of WAP: The Wind Atlas Analysis and Application Program. In A. Zervos, H. Ehmann, and P. Helm, editors, *Proc. EUWEC'96, Göteborg 1996*, pages 584–587. H. S. Stephens & Associates, 1996.
- [4] H. P. Frank and L. Landberg. Modelling the wind climate of Ireland. *Boundary-Layer Meteorol.*, 85:359–378, 1997.
- [5] H. P. Frank, E. L. Petersen, R. Hyvönen, and B. Tammelin. Calculations on the wind climate in northern Finland. Submitted to *Wind Energy*, 1999.
- [6] J. C. R. Hunt, S. Leibovich, and K. J. Richards. Turbulent shear flow over low hills. *Q. J. R. Meteorol. Soc.*, 114:1435–1470, 1988.
- [7] J. C. R. Hunt, K. J. Richards, and P. W. M. Brighton. Stably stratified shear flow over low hills. *Q. J. R. Meteorol. Soc.*, 114:859–886, 1988.
- [8] E. Kalnay, M. Kanamitsu, R. Kistler, W. Collins, D. Deaven, L. Gandin, M. Iredell, S. Saha, G. White, J. Woollen, Y. Zhu, A. Leetmaa, R. Reynolds, M. Chelliah, W. Ebisuzaki, W. Higgins, J. Janowiak, K. C. Mo, C. Ropelewski, J. Wang, R. Jenne, and D. Joseph. The NCEP/NCAR 40-year reanalysis project. *Bull. Amer. Meteor. Soc.*, 77:437–471, 1996.
- [9] P. J. Mason and J. C. King. Measurements and predictions of flow and turbulence over an isolated hill of moderate slope. *Q. J. R. Meteorol. Soc.*, 111:617–640, 1985.
- [10] N. G. Mortensen, L. Landberg, I. Troen, and E. L. Petersen. *Wind Atlas Analysis and Application Program (WAP) Vol. 2: User's Guide*. Risø National Laboratory, Roskilde, Jan 1993. Risø-I-666(v.2)(EN).
- [11] N. G. Mortensen and E. L. Petersen. Influence of topographical input data on the accuracy of wind flow modelling in complex terrain. In R. Watson, editor, *Proc. EWEC'97, Dublin 1997*, pages 317–320. Irish Wind Energy Association, 1998. ISBN 0-9533922-0-1.
- [12] E. L. Petersen, B. Tammelin, and R. Hyvonen. Wind resources assessment in complex terrain in the far north. In B. Tammelin, K. Säänti, E. Peltola, and H. Neuvonen, editors, *BOREAS - NORTH WIND - POHJATUULI, Hetta 10.-13.2.1992 An International Experts' Meeting on Wind Power in Icing Conditions*, pages 73–87. Finnish Meteorological Institute, 1992.
- [13] J. S. Sawyer. Numerical calculation of the displacements of a stratified airstream crossing a ridge of small height. *Q. J. R. Meteorol. Soc.*, 86:326–345, 1960.
- [14] I. Troen and A. de Baas. A spectral diagnostic model for wind flow simulation in complex terrain. In W. Palz and E. Sesto, editors, *Proc. EWEC'86, Rome, 7-9 October 1986*, volume 1, pages 243–250. Raguzzi, Rome, 1986.
- [15] I. Troen and E. L. Petersen. *European Wind Atlas*. Risø National Laboratory for the Commission of the European Communities, Roskilde, Denmark, 1989. ISBN 87-550-1482-8.
- [16] S. B. Vosper. *Observations and Modelling of Orographic Internal Gravity Waves*. Phd thesis, University of Leeds, 1985.

This work is part of the EU JOULE project MOWIE – “Improved tools to predict wind energy production in mountains”, contract no. JOR3-CT98-0254.

THE INFLUENCE OF WAVES ON THE OFFSHORE WIND RESOURCE

Bernhard Lange, Jørgen Højstrup*

Risø National Laboratory, P.O.Box 49, DK-4000 Roskilde, Denmark, phone: +45 4677 5014,
fax: +45 4677 5970, e-mail: bernhard.lange@risoe.dk

* NEG Micon, Alsvej 21, DK8900 Randers, Denmark, phone: +45 8710 5262,
fax: +45 8710 5001, email: JHO@NEG-MICON.DK

ABSTRACT: With the growing interest in offshore wind resources, it has become increasingly important to establish and refine models for the interaction between wind and waves in order to obtain accurate models for the sea surface roughness. The simple Charnock relation that has been applied for open sea conditions does not work well in the shallow water near-coastal areas that are important for offshore wind energy. A model for the surface roughness of the sea has been developed based on this concept, using an expression for the Charnock constant as a function of wave age [1], and then relating the wave 'age' to the distance to the nearest upwind coastline. The data used in developing these models originated partly from analysis of data from the Vindeby site, partly from previously published results. The scatter in the data material was considerable and consequently there is a need to test these models further by analysing data from sites exhibiting varying distances to the coast. Results from such analysis of recent data are presented for sites with distances to the coast varying from 10km to several hundreds of km. The model shows a good agreement also with this data.

Keywords: Wind resource, Off-shore, Meteorology, Waves

1. INTRODUCTION

The favourable wind resource at offshore sites is caused by the very low surface roughness of water areas. The development of models describing the sea surface roughness is therefore of major importance for offshore wind power utilisation. Widely used is the model by Charnock [2]. It works well for open ocean sites, but is problematic in coastal areas since it does not take into account fetch influences. The traditional way of fixing this problem has been to use increasing values of the constant in the Charnock relation when approaching the coast. The physical explanation for the increased roughness of near coastal waters is based on the fact that wind driven waves are most efficient in taking energy out of the mean flow when they are 'young', i.e. in the phase when they are growing rapidly.

The model by Johnson et al [1] is based on this concept and gives an explicit description of the sea surface roughness depending on wave age. Using an equation by Hasselmann et al [3] relating wave age to fetch, this model can be utilised to predict the sea surface roughness depending on wind speed and fetch only. It has been developed using data from the Vindeby site and from literature. Here it is tested further by analysing data from the two sites Rødsand and Østergarnsholm in the Baltic Sea. Fetches at these sites are in the range of 10 to 200 km. Published results from two other stations are included for comparison. The results are compared with the Charnock model and the model by Johnson et al.

2. MODELING THE SEA SURFACE ROUGHNESS

The surface roughness is used to describe the influence of the surface on the logarithmic vertical wind speed profile. For neutral atmospheric stability it can be written as:

$$u(z) = \frac{u_*}{\kappa} \ln \left(\frac{z}{z_0} \right) \quad (1)$$

where $u(z)$ is the mean wind speed at height z , u_* the wind friction velocity, κ the von Karman constant and z_0 the surface roughness length.

The surface roughness length for land surfaces is typically in the order of centimetres to meters. For sea surfaces the value is typically below one millimetre. Also, for land surfaces the surface roughness length usually is taken as a constant depending only on the surface, i.e. independent of the wind flow. For water surfaces the roughness length depends on the wave field present, which in turn is dependent on the wind speed and other parameters like fetch, current, water depth, etc.

Describing the sea surface roughness for wind resource studies has the aim to find a simple empirical description for this complex dependency. Furthermore, the description should only depend on parameters usually available in wind resource studies, i.e. preferably not on parameters of the wave field.

Widely used is the description by Charnock [2], relating the sea surface roughness to the friction velocity by means of a single empirical constant:

$$z_0 = A_C \frac{u_*^2}{g} \quad (2)$$

where g is the gravitational acceleration and A_C the so-called Charnock constant. Experimental studies determined the Charnock constant to approximately 0.011 for the open sea with fully developed waves. However, the 'constant' has been found to be somewhat higher for coastal waters with a value of 0.018 (or more) usually assumed here.

The uncertainty in the Charnock constant for coastal waters is unsatisfactory from the point of view of offshore wind power utilisation since this is the area most interesting for wind farm development. Johnson et al [1] showed that the Charnock constant can be described as a function of the 'wave age':

$$A_r = 1.89 \left(\frac{c_p}{u_*} \right)^{-1.59} \quad (3)$$

where c_p is the phase velocity of the dominant wave component. The term c_p/u_* is called wave age. Since the wave age or c_p usually are not available for wind power studies, a relation between wave age and fetch is needed. Hasselmann et al [3] found the following relation from the JONSWAP data:

$$\frac{u_*}{c_p} = \frac{3.5}{2\pi} \left(\frac{xg}{u_{10}^2} \right)^{-1/3} \quad (4)$$

where x is the fetch in metres and u_{10} the wind speed at 10 m height. We approximate equation (3) by:

$$A_r = 1.54 \left(\frac{c_p}{u_*} \right)^{-3/2} \quad (5)$$

and combine equations (2), (4) and (5) to:

$$z_0 = 0.64 \frac{u_*^2 u_{10}}{x^{1/2} g^{3/2}} \quad (6)$$

using equation (1) to eliminate u_{10} yields:

$$z_0 = 0.64 \frac{u_*^3}{x^{1/2} g^{3/2} K} \ln \left(\frac{10}{z_0} \right) \quad (7)$$

This implicit equation can be used to determine the sea surface roughness solely from u_* and the fetch.

3. SEA SURFACE ROUGHNESS DETERMINED FROM MEASUREMENTS

3.1 Determination of the sea surface roughness

The surface roughness length is defined as the intercept of the turbulent wind speed profile with the height axis. This is a mathematical concept and z_0 does not have a physical existence. Therefore it can not be measured directly, but has to be derived from atmospheric measurements by theoretical considerations. Different approaches are possible here. The most direct determination is from the measured wind profile, i.e. wind speeds at different heights. The problem of this method for determining very small roughnesses is its sensitivity for errors in the wind speed measurements. Even very small errors lead to a large deviations in the resulting values for z_0 . Another possibility is the use of a measured friction velocity. Equation (1) can be rewritten as:

$$z_0 = \frac{z}{\exp \left(\frac{u(z)K}{u_*} \right)} \quad (8)$$

The difficulty is the large uncertainty usually involved in the measurement of the friction velocity. Here a third method is employed: It is assumed that the standard deviation of the wind speed σ_u is proportional to the friction velocity u_* :

$$u_* = C \sigma_u \quad (9)$$

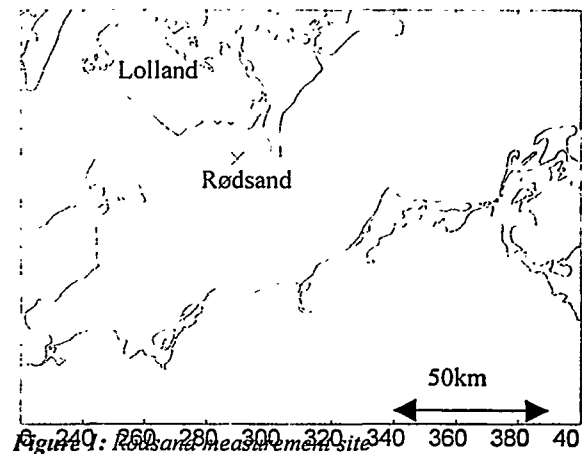
The constant C is usually taken as 2.5. Taking 0.4 for the von Karman constant while substituting u_* in (8) by (9) yields:

$$z_0 = \frac{z}{\exp \left(\frac{u(z)}{\sigma_u} \right)} \quad (10)$$

This is in the following used for a determination of z_0 . This approach is of course restricted to neutral (or near neutral) atmospheric stability.

3.2 Rødsand measurement

Wind and atmospheric measurements are performed at the offshore mast Rødsand south of the Danish island Lolland (see figure 1) since October 1996. The measurement is a part of a Danish study of wind conditions for proposed offshore wind farms (see[4]). Wind speed measurements are performed at heights 10, 30 and 48m by cup anemometers and at 43 m height by a sonic anemometer. Wave and current data are also collected as well as several atmospheric parameters. Data are collected as half hourly averages. They have been quality checked and records with possible mast shading have been excluded. About 10000 records are available for the analysis.



A data subset has been selected containing only near neutral data. Richardson numbers have been used to determine the near neutral cases. Data with $-0.3 < Ri < 0.02$ have been selected. This leaves about 2500 records for the analysis. Wind direction sectors corresponding to different fetches have been selected. For each sector the data were bin-averaged according to wind speeds. The sea surface roughness was calculated from the averaged wind speeds and standard deviations at 10 m height according to equation (10).

3.3 Östergarnsholm measurement

Wind and atmospheric measurements at the measurement station Östergarnsholm were performed by the Department of Meteorology, Uppsala, in the BALTEX (Baltic sea Experiment) experiment [5]. Measurements took place on the island Östergarnsholm, which is located west of the bigger Swedish island Gotland in the Baltic Sea. (see figure 2). Wind measurements were performed at a mast situated on the southernmost tip of the flat island. For a more detailed description of the measurement see [5]. For this study data from two campaign measurements were available. The first took place from 19th to 25th September 1996, the second from 29th April to 10th May 1997. Among other measurements wind speeds were measured at 5 heights from 6.7 to 28.6m. Data are collected as 10 minute averages.

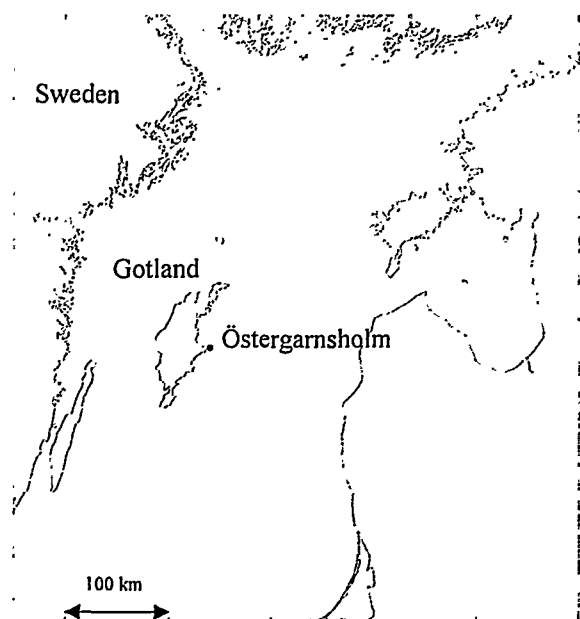


Figure 2: Östergarnsholm measurement site

Richardson numbers have been calculated to select near neutral data. As for Rødsand, data with $-0.3 < Ri < 0.02$ have been allowed. The Östergarnsholm measurement contains mainly unstable data for the first measurement period and mainly stable or very stable data during the second period (see also [2]). Therefore only 340 records were left for the analysis. One wind direction sector with undisturbed sea fetch of more than 150 km has been used for the analysis. Analysis was done as for Rødsand, but for a wind speed measurement at 6.7 m height. Figure 3 shows the result.

3.4 Comparison with Nibe and Vindeby measurements

The sea surface roughnesses found from the Rødsand and Östergarnsholm measurements are compared with earlier published results from the Nibe and Vindeby measurements [6], [7]. The sea surface roughness was calculated with the same method as described above for near neutral data. Wind directions with upstream fetches over water of 7-15 km were used in both cases. Figure 3 shows the results of all four measurements. Two wind direction sectors with different fetches were used for the Rødsand measurement.

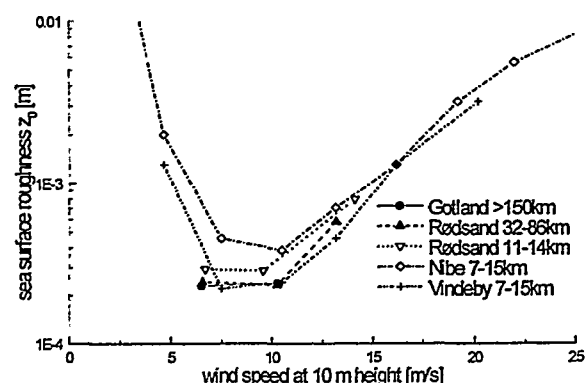


Figure 3: Sea surface roughness versus wind speed for different fetches at the sites Rødsand, Östergarnsholm, Nibe and Vindeby for different fetches

The measured values for the sea surface roughness are very close to each other with the exception of Nibe which gives slightly higher results. For low wind speeds < 10 m/s the z_0 values determined from the measured standard deviations are very large. This is probably due to instationary situations with fluctuating wind speeds and does not reflect the surface roughness.

4. COMPARISON WITH MODELS

A comparison of the measured and modelled sea surface roughness over wind speed is shown in figures 4 and 5. The measured data from figure 3 is plotted together with values calculated with the Charnock model (eq. 2) and the model based on Johnson et al (eq. 7).

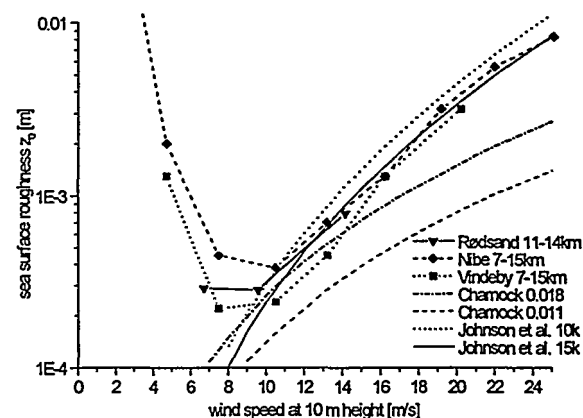


Figure 4: Measured and modelled sea surface roughness versus wind speed for medium fetches

Figure 4 shows the results for medium fetches of 10-20 km. Both models are close to each other in the range of wind speeds where new measurements are available and agree well with the measurements. The Charnock model (with $A_c=0.018$) (eq.2) compares slightly better to the new data, while the model by Johnson et al (eq. 7) performs clearly better for the Nibe and Vindeby data.

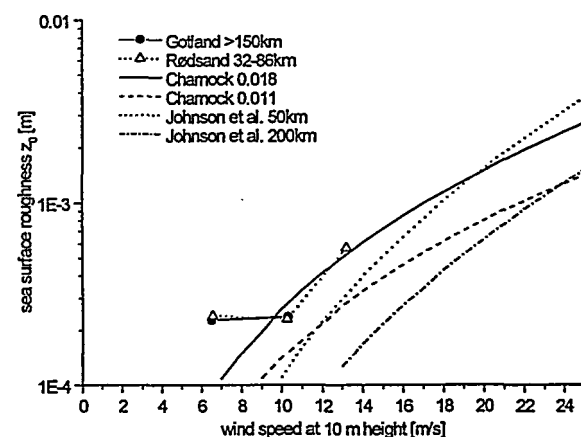


Figure 5: Measured and modelled sea surface roughness versus wind speed for long fetches

Figure 5 shows the results for long fetches of more than 30 km. Unfortunately only very few measured data are available for this situation.

Despite the difference in fetch are the data from Gotland with fetch exceeding 150 km and those from Rødsand with fetches of 32-86 km very close to each other.

Both models fit well to the three data points available for higher wind speeds. The slope of the measurements is fitted slightly better by the Johnson et al model. For the Charnock model the coastal value (0.018) fits best. However, more data points are needed to compare the models for these fetch situations.

5. CONCLUSION

The sea surface roughness has been determined from measurements from the sites Rødsand (south of Lolland, DK) and Östergarnsholm (west of Gotland, Sweden). The values found compare well with the published results from the Nibe and Vindeby sites.

The sea surface roughness has been determined from the measured standard deviation of the wind speed. This method gives rise to high values for the sea surface roughness at low wind speeds, which probably stem from instationarities and stability effects and do not reflect the surface roughness.

Results of the Charnock and the Johnson et al models are compared to the measurements. For medium fetches the model by Johnson et al. is in good agreement with the measurements from Nibe and Vindeby for higher wind speeds, while the few data available from the new measurement at Rødsand fit slightly better to the Charnock model (with constant 0.018). Only few measured data are available for long fetches. The two data sets from Östergarnsholm and Rødsand are very close to each other despite their different fetches. The Charnock model with a constant between 0.011 (open sea value) and 0.018 (coastal water value) as well as the Johnson et al. model for 50 km fetch agree well with the data.

ACKNOWLEDGEMENTS

We would like to thank Ann-Sofi Smedman and Hans Bergström from Uppsala University for providing data from the Östergarnsholm measurement. The Rødsand measurement was funded by the Danish Energistyrelsens Udviklings-programmet for Vedvarende Energi in the 'Offshore wind resources' project (contract no: UVE J.nr. 51171/96-0040). The work of one of the authors (B. Lange) is funded by the European Commission through a Marie Curie Research Training Grant.

REFERENCES

- [1] Johnson, H.K. Højstrup, H.J.Vested, S.E.Larsen: On the dependence of sea surface roughness on wind waves. in: *Journal of Physical Oceanography*, Vol.28, pp.1702-1716; 1998
- [2] Charock, H.: Wind stress over a water surface. in: *Quarterly Journal of the Royal Meteorological Society*, Vol. 81, pp.639-640, 1955
- [3] Hasselmann, K., T. P. Barnett, E. Bouws, H. Carlson, D. E. Cartwright, K. Enke, J. A. Ewing, H. Gienapp, D. E. Hasselmann, P. Kruseman, A. Meerburg, P. Müller, D. J. Olbers, K. Richter, W. Sell and H. Walden: Measurements of Wind-Wave Growth and Swell Decay during the Joint North Sea Wave Project (JONSWAP). in: *Deutsche Hydrogr. Zeits., Reihe A*, Vol. 12, No.8; 1973

- [4] Barthelmie, R.J., M.S. Courtney, B. Lange, M. Nielsen, A.M. Sempreviva, J. Svenson, F. Olsen and T. Christensen: Offshore wind resources at danish measurement sites. in: *1999 European Wind Energy Conference and Exhibition*. 1999. Nice
- [5] Smedman, A.-S., U. Högström and H. Bergström: The turbulence regime of a very stable marine airflow with quasi-frictional decoupling. in: *Journal of Geophysical Research*, Vol. 102, No. C9, pp. 21049ff; 1997
- [6] Petersen, E.L., N.G. Mortensen, L. Landberg, J. Højstrup and Helmut P. Frank: Wind power meteorology. Part II: Siting and models. in *Wind Energy*. 1999
- [7] Højstrup, J., R.J. Barthelmie, M.S. Courtney, P. Sanderhoff: Wind and turbulence in the near-coastal offshore environment. in: *Proceedings of the European Wind Energy Conference, Thessaloniki*, pp.193-197; 1994

OPTIMAL PARAMETERS FOR THE FFA-BEDDOES DYNAMIC STALL MODEL

Anders Björck*, Murat Mert* and Helge A. Madsen**

*FFA, The Aeronautical Research Institute of Sweden, P.O. Box 11021, S-161 11 Bromma, Sweden, bka@ffa.se

**Risø, DK-4000, Roskilde, Denmark, helge.aagaard.madsen@risoe.dk

ABSTRACT: Unsteady aerodynamic effects, like dynamic stall, must be considered in calculation of dynamic forces for wind turbines. Models incorporated in aero-elastic programs are of semi-empirical nature. Resulting aerodynamic forces therefore depend on values used for the semi-empirical parameters. In this paper a study of finding appropriate parameters to use with the Beddoes-Leishman model is discussed. Minimisation of the "tracking error" between results from 2D wind tunnel tests and simulation with the model is used to find optimum values for the parameters. The resulting optimum parameters show a large variation from case to case. Using these different sets of optimum parameters in the calculation of blade vibrations, give rise to quite different predictions of aerodynamic damping which is discussed.

Keywords: Aerodynamics, Aeroelastic Stability, Blade Aerodynamics, Dynamic stall, Models, Optimization, Unsteady effects

1 INTRODUCTION

Unsteady aerodynamic effects, like dynamic stall, must be considered in the calculation of dynamic forces for wind turbines. Models for dynamic stall is therefore commonly incorporated in aero-elastic programs. These models are of semi-empirical nature due to their computing time effectiveness and the results depend on values used for the semi-empirical parameters.

In this paper a study of finding appropriate parameters to use with the Beddoes-Leishman model is discussed

2 THE DYNAMIC STALL MODEL

The dynamic stall model used is an implementation of the Beddoes-Leishman model, see e.g. [1]. The FFA-implementation has previously been described in [2]. The Beddoes-Leishman model can shortly be described as an indicial response model for attached flow extended with models for separated flow effects and vortex lift. The model use static $C_l(\alpha)$ and $C_d(\alpha)$ data as input for the specific airfoil for which the dynamic forces shall be calculated.

In the FFA-implementation, the forces are calculated in the wind reference system (C_l and C_d).

The steps included to calculate the lift are:

- Step 1) Compute impulsive loads
- Step 2) Compute shed wake effects.
- Step 3) Compute a shift in angle of attack due to the lag in leading edge pressure response.
- Step 4) Compute a lag in the separation point position. $\Rightarrow C_{l,f}$
- Step 5) Compute vortex lift.
- Step 6) Add components of lift: Impulsive lift, vortex lift and $C_{l,f}$ to obtain the final value of C_l .

The steps are calculated as described in [2]. The function relating lift to the separation point is, however, now changed to the "Kirchoff flow model",

$$C_{l,f}(\alpha) = C_{l,\alpha} \cdot 0.25(1 + \sqrt{f(\alpha)})^2 \cdot (\alpha - \alpha_0) \quad (1)$$

in favour of the expression previously used by FFA,

$$C_{l,f}(\alpha) = f(\alpha) \cdot C_{l,inv}(\alpha) + (1 - f(\alpha)) \cdot C_{l,sep}(\alpha) \quad (2)$$

This change has been introduced to avoid the arbitrariness in the creation of $C_{l,sep}(\alpha)$ -curves. By using equation (1) the function relating lift to the separation-point is more well-defined.

Much of the dynamic effect on lift is obtained by the introduction of a time lag in the movement of the separation point. The separation point tends to its static value, but lags according to a first order filter with a time constant T_f .

$$\frac{df}{ds} = \frac{f_{static} - f}{T_f} \quad (3)$$

The model for vortex lift is the same as described in [1]. The "feed" of vortex lift is proportional to the difference between the "inviscid" value of circulatory lift and the lift obtained through the Kirchoff flow model. The accumulated vortex lift decays exponentially with time but is also updated with new incremental feed. The time constant for vortex decay, T_v , is one of the semi-empirical parameters in the model. In the currently used model, no criteria for the start of "vortex travelling" is used, and vortex feed is allowed as long as the angle of attack is increasing

The vortex lift is assumed act only normal to the airfoil chord and hence will give a component in the drag direction

The drag is obtained as the static drag plus components of induced drag due to shed wake effects, vortex drag and separation drag, $C_{d,sep}$

The latter is a model of the drag being larger than its static value if the separation point is upstream of its static value and vice versa.

$$C_{d,sep} = a_{cd}(C_{l,stat} - C_{l,f}) \quad (4)$$

s in equation (3) is the non-dimensional time, $s = 2 \cdot V \cdot t / c$. The time constant, T_p , used to determine the α -shift of step 3 has been set to 0.8 in the current study.

3 OPTIMISATION

3.1 Cases and type of object function

The resulting lift and drag for unsteady cases will depend on the semi-empirical parameters T_f , T_v and acd .

What values should be given to these parameters? One way of finding appropriate values is to use an optimiser to minimise some definition of the discrepancy between experimental results and dynamic stall model results.

The definition of a relevant object function is, however, by no way obvious.

A good agreement between experiments and simulations could be good agreement in maximum lift.

The average lift curve slope is very important for aerodynamic damping as pointed out in e.g. [6], and an object function that considers the agreement in "mean lift curve slope" is also imaginable.

In the current study an object function based on minimising the "tracking error" between experiments and simulations has been used:

$$F = \sum_i \eta [(C_{n,sim}(t_i) - C_{n,exp}(t_i))^2 + (1 - \eta)(C_{n,sim}(t_i) - C_{n,exp}(t_i))^2] \quad (5)$$

By using different values of η , different weighting of normal and tangential force can be obtained.

Optimisation has been made using wind tunnel experiments from three sources and also results from Navier Stokes calculation carried out at Risø. The different cases and also the resulting values for optimised parameters are shown in Table 1. The optimisation in Table 1 is made with $\eta = 0.1$.

Table 1. Cases for optimisation and resulting optimal semi-empirical parameters.

Airfoil and cases	α mean	α amplitude	Reduced frequency	Optimised T_v	Optimised T_f	Optimised acd
Ohio State University. Wind tunnel pitching motion. Ref [3]						
NACA 4415	14.2	10.8	0.023	3.1	3.5	0.00
	14.2	10.8	0.046	2.7	3.9	0.01
	14.2	10.8	0.069	3.6	3.6	0.04
LS(1) 0421 MOD	13.2	10.5	0.022	0.0	6.1	0.00
	13.2	10.5	0.045	0.9	7.0	0.00
	13.2	10.5	0.066	0.8	6.5	0.02
SERI 809	12.9	10.6	0.02	0.0	10.9	0.08
	12.9	10.6	0.041	1.6	5.3	0.11
	12.9	10.6	0.061	3.3	4.0	0.16
Optimisation for 9 Ohio state university cases				1.9	5.0	0.04
Glasgow University. Wind tunnel pitching motion. Ref [4]						
NACA 0015	11.	8.0	0.026	2.1	12.3	0.06
	11	7.9	0.051	6.4	8.2	0.14
	11	7.6	0.102	6.3	7.4	0.17
	11	7.0	0.155	6.7	14.6	0.16
	20	7.6	0.025	2.4	9.6	0.27
	20	7.4	0.102	9.2	3.6	0.43
	20	6.8	0.154	9.3	4.1	0.20
Optimisation for all 8 NACA 0015 cases				8.5	5.2	0.17
NACA 0021	11	7.9	0.024	1.0	13.6	0.00
	11	7.8	0.049	2.2	10.9	0.03
	11	7.8	0.097	3.7	8.7	0.14
	11	7.7	0.142	7.1	10.0	0.17
	20	7.9	0.024	0.9	9.4	0.00
	20	7.9	0.049	1.6	5.8	0.08
	20	7.9	0.097	3.4	6.4	0.09
Optimisation for all 8 NACA 0021 cases				3.8	6.7	0.01
Optimisation for all 8 GU cases at mean- $\alpha=11$				5.4	9.1	0.14
Optimisation for all 7 GU cases at mean- $\alpha=20$				7.2	4.5	0.18
Riose- airfoil. Wind tunnel pitching motion. Ref [5]						
No shift	11.8	1.6	0.11	6.2	0.8	0.02
Shift of C_l and C_d	11.8	1.6	0.11	1.2	4.2	0.00
Riose-1 airfoil CFD calculations						
Plunging	11.8	1.6	0.11	0.0	8.7	0.00
Pitching	11.8	1.6	0.11	1.3	1.6	0.10

3.2 Wind tunnel tests from Risø and comments on the effect of small errors in the test-data

Figure 1 show the dynamic loops for four different mean angles of attack for the measurements of Risø [5] and simulations. The static data in figure 1 is input to the dynamic stall model. At the mean angle of attack of 11.8° optimum parameters become $T_v=6.2$ and $T_f=0.8$. Such a low value of T_f can not be found in the optimisation for other airfoils and the value is too low considering the interpretation of the physics of the delay in separation point. Expectations also suggest that the dynamic curve lie rather high compared to the static data. A second optimisation was therefore made with the dynamic wind tunnel data shifted in the C_l direction. A shift of $\Delta C_l = -0.02$ was applied to the dynamic wind tunnel data before optimisation. This resulted in optimised values of $T_v=1.2$ and $T_f=4.2$. Thus quite a difference.

This shows that possible errors in the experiments have a large influence on resulting optimum values of T_f and T_v .

Figure 1 shows that using $T_v=1$ and $T_v=4$ gives a rather good agreement for the higher angles of attack even though the loops are shifted relative to the uncorrected dynamic data of [5].

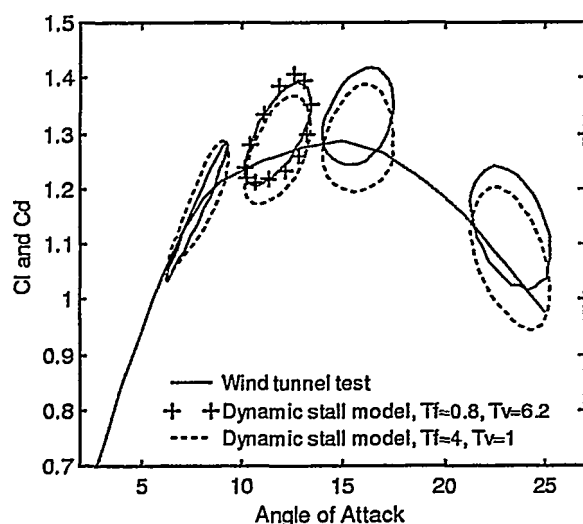


Figure 1. Results from pitching wind tunnel test by Risø compared to dynamic stall simulations.

3.3 Discussion on optimised parameters

Table 1 shows a rather large variation in optimised values for T_v , T_f and acd . Optimised T_v and T_f is larger for the Glasgow University cases than for other cases. For the Ohio State University cases, an optimum average fit was obtained with $T_v=1.9$, $T_f=5$ and $acd=0.04$.

Looking at pitching moment results from the Glasgow cases it can be seen that the dynamic stall process includes the formation of a vortex with associated vortex shedding for these cases. Such a marked vortex shedding process cannot be found in the small amplitude oscillation cases of Risø and only for the SERI airfoil and to a small extent for the NACA airfoil of the Ohio State

University cases. As a general remark it seems as if optimised T_v and T_f become larger for cases where a dynamic stall vortex is developed.

Figure 2 shows results for the NACA 0021 airfoil. The figure shows results for simulations with the optimised values $T_v=3.7$, $T_f=8.7$ and $acd=0.14$ and also for simulations with the values for a good average fit for all Ohio State University cases ($T_v=2$, $T_f=5$ and $acd=0.04$).

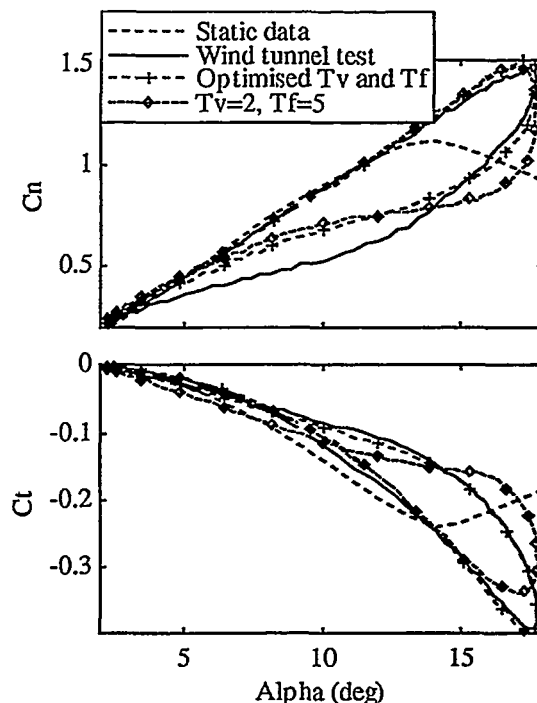


Figure 2. Comparison of wind tunnel test data and simulations with two parameter sets. NACA 0021 airfoil at a reduced frequency of 0.1 and a mean α of 11° .

It can be seen that the agreement is good for the optimised values except from a deviation for decreasing angle of attack below $\alpha=15^\circ$. With non-optimum values of $T_v=2$, $T_f=5$ and $acd=0.04$ the agreement for the reattachment part (decreasing angle of attack) and the agreement of minimum tangential force, C_t , becomes worse. Still, the maximum normal-force, is well predicted.

The figure gives an idea of the change in predicted forces when other than optimum values are used.

3.4 T_f as a function of the separation point

Optimisation was also made with a version of the dynamic stall model where T_f is a function of the separation point. T_f was linearly varying between breakpoints with different T_f -values for increasing and decreasing angle of attack. Four values of T_f at $f=0$, $f=0.33$, $f=0.66$ and $f=1$ were used for both increasing and decreasing angle of attack. An improvement in the tracking error (object function) could be obtained for each case. However, no "pattern" in the $T_f(f)$ variation could be seen and hence no $T_f(f)$ -variation that could be used to represent a good standard variation for a "general airfoil" was found.

3.5 Results from CFD

Navier-Stokes calculations with the Riosse Ellipsys code with a $k-\omega$ SST turbulence model were done for the Risø-1 airfoil. These calculations were carried out at the same reduced frequency and α -amplitude as the wind tunnel test with mean- α of 11° . The calculations were done with the airfoil in pitching motion with an amplitude of 1.6° and also with the airfoil in plunging motion. For plunging motion the plunging amplitude was set to $h/c=0.127$ corresponding to the same α -amplitude as for the pitching case.

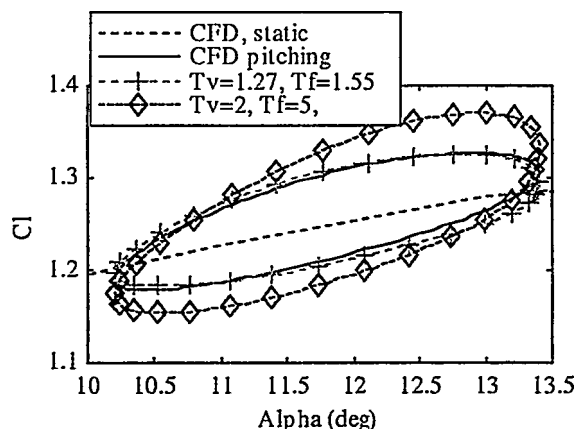


Figure 3. Results from CFD pitching airfoil calculations compared to dynamic stall simulations.

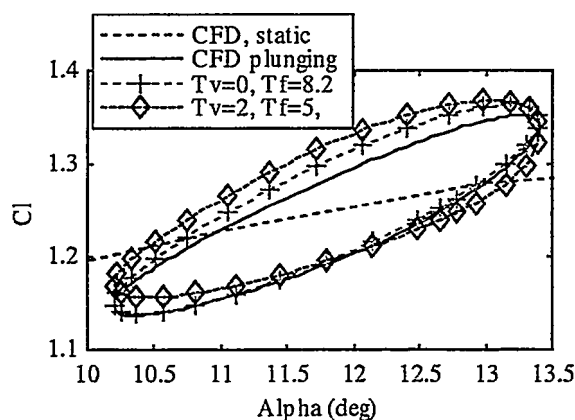


Figure 4. Results from CFD plunging airfoil calculations compared to dynamic stall simulations.

Comparing the results for pitching and plunging motion it can be seen that the mean lift curve slope is larger for the plunging case. Interesting to note is that this is opposite to what is found from analysis of pitching and plunging motion of wind turbine blade in the wind tunnel tests analysed in [6].

Comparing the wind tunnel pitching motion results and CFD pitching calculations, it can be seen that the CFD results show a much smaller mean lift curve slope and that the width of the loop is smaller. This is also reflected in the resulting optimised value of T_f , which is very small for the CFD-case.

By using values for T_v and T_f optimised for the different specific cases, the dynamic stall model can mimic the wind tunnel and CFD results quite well (figures 2, 3 and 4). The variation in optimised T_v and T_f , however varies and it would be difficult to select one set of values that were to be representative for the airfoil without having an idea of which case to trust the most.

The optimum parameters that have to be used to obtain good agreement between the CFD-calculations and dynamic stall simulations differ for the plunging and pitching case. To find out if this is a general effect or not would be valuable to investigate.

4 AERODYNAMIC DAMPING AS FUNCTION OF SEMI-EMPRICAL PARAMETERS.

Aerodynamic damping has a major influence on the blade vibration levels and possible stall induced instabilities. It is therefore of great importance that the damping is correctly calculated.

A measure of the aerodynamic damping can be obtained by looking at the aerodynamic cycle work for sinusoidal oscillations. Figure 5 and 6 shows this aerodynamic work for small amplitude plunging and lead-lag oscillations at different mean angles of attack. The work has in both cases been normalised with the work that would have been obtained with quasi-steady profile aerodynamics for attached flow and plunging motion with the same oscillation amplitude. The calculations are based on the static data profile in figure 2. Figures 5 and 6 show the calculated damping without the dynamic stall model applied (quasi-steady curve) and with the model applied with two different sets of T_v and T_f . The plunging motion cases are calculated for a reduced frequency $k=0.1$ and lead-lag motion cases are calculated for $k=0.2$, both fairly representative for reduced frequencies for the outer part of a wind turbine blade for "normal" blade eigen-frequencies.

The result with crosses are calculated with optimum values of T_v and T_f for the Glasgow University cases at a mean α of 11° . The other curve with $T_v=2$ and $T_f=5$ is close to the optimum values for the Ohio State University cases. The latter set of values also result in relatively good agreement for the CFD plunging case. (The normalised damping work of the plunging motion of figure 4 is 0.53 for the CFD calculations, 0.6 for $T_f=0.82$ and $T_v=0$ and 0.51 for $T_v=2$ and $T_f=5$.)

It is seen that the damping calculated with the two different sets is quite different. If the real damping would be close to the damping calculated with $T_v=2$ and $T_f=5$, then the damping calculated with $T_v=5$ and $T_f=9$ would be far too large and estimations of margins to stall-induced vibrations would be non-conservative with respect to dynamic stall.

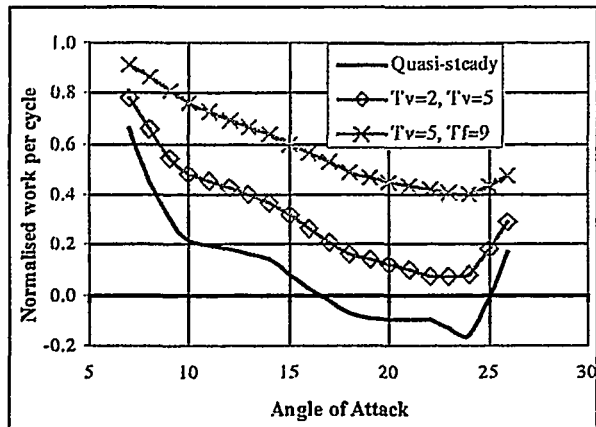


Figure 5. Aerodynamic damping for plunging motion

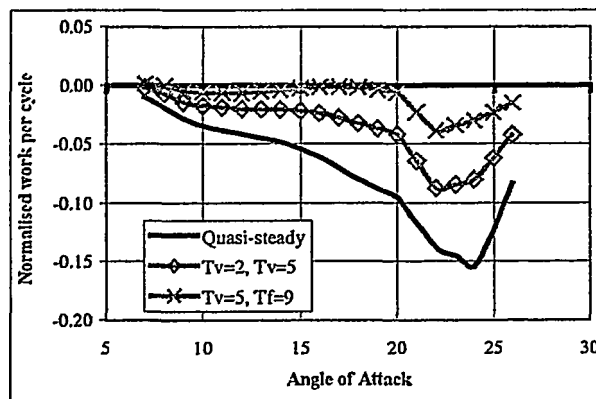


Figure 6. Aerodynamic damping for lead-lag motion

5 CONCLUSIONS AND DISCUSSION

Optimum values for semi-empirical parameters in the Beddoes-Leishman dynamic stall model have been found by use of numerical optimisation such that good agreement between simulations and measured aerodynamic forces are obtained.

Except from the high mean- α , large amplitude, deep dynamic stall cases (Glasgow cases with α -mean $\approx 20^\circ$) the dynamic stall model is capable of representing the dynamic stall data quite accurately with optimised parameters. The optimisation, however, resulted in a large span of the values for the optimised parameters. The small amplitude oscillation cases of Risø result in smaller optimised values of the semi-empirical parameters T_v and T_f than the optimisation for the large amplitude "in and out of stall" cases of Glasgow university cases (cases with α -mean $\approx 11^\circ$).

The use of different sets of optimised parameters in the calculation of aerodynamic damping shows that the calculated damping varies significantly using different parameter sets. Using optimised values of T_v and T_f for the wind tunnel cases of Glasgow with a mean- α of 11° would e.g. highly over-predict the damping for the plunging motion case calculated with Navier-Stokes calculations.

In order to better validate the dynamic stall model for the capability of accurately calculating aerodynamic damping in stall, experiments with plunging and lead-lag motion (or a combination of these cases) is largely wanted.

Future work of tuning parameters of the dynamic stall model could also include optimisation that minimises differences between measured and calculated wind turbine blade loads. The result of such an optimisation will, however, be very much influenced by the static airfoil data that are used and should best be accompanied by a thorough validation of what static that should be used.

With $T_v=2$ and $T_f=5$ a reasonable agreement is obtained for a large number of cases.

ACKNOWLEDGEMENTS

Niels N. Sørensen at Risø has carried out the Navier Stokes calculations.

REFERENCES

- [1] Leishman, J.G. and Beddoes, T.S. "A Generalised Model for Airfoil Unsteady Aerodynamic Behaviour and Dynamic Stall Using the Indic Method", Presented at the 42nd Annual Forum of the American Helicopter Society, Washington D.C. June 1986
- [2] Björck, A. "The FFA Dynamic Stall Model. The Beddoes-Leishman Dynamic Stall Model Modified for Lead-Lag Oscillations". IEA 10th Symposium on Aerodynamics of Wind Turbines i Edingburgh, 16-17 December 1996. Editor Maribo Pedersen, DTU Denmark
- [3] Hoffmann, M. J. et al "Unsteady Aerodynamic Performance of Wind Turbine Airfoil" Presented at American Wind Energy Association Wind Power 94 conference, Minneapolis, Minnesota, May 9-13, 1994
- [4] Galbraith, R.A.M et al, "Summary of Pressure Data for Thirteen Aerofoils on the University of Glasgow's Aerfoil Database", G.U. Report 9221, June 1992
- [5] Fuglesang, P, Antoniou, I, Bak, C and Madsen, H.A., "Wind Tunnel Test of the RISØ-1 Airfoil", Risø-R-999(EN), May 1998
- [6] Rasmussen, F, Petersen, J.T., and Madsen, H.A. "Dynamic Stall and Aerodynamic damping", Paper AIAA-98-0024, presented at the 36th Aerospace sciences meeting & exhibition, Reno, USA, January 12-15, 1998

AEROELASTIC STABILITY OF AIRFOIL FLOW USING 2-D CFD

J. Johansen

Risø National Laboratory, Denmark
P.O. Box 49, DK-4000 Roskilde, Denmark
jeppe.johansen@risoe.dk

ABSTRACT: A three degrees-of-freedom structural dynamics model has been coupled to a two-dimensional incompressible CFD code. The numerical investigation considers aeroelastic stability for two different airfoils; the NACA0012 and the LM 2 18 % airfoils. Stable and unstable configurations and limit cycle oscillations are predicted in accordance with literature for the first airfoil. An attempt to predict stall induced edge-wise vibrations on a wind turbine airfoil fails using this two-dimensional approach.

Keywords: Aeroelastic stability, Airfoil sections, Stall induced vibrations.

1. INTRODUCTION

During certain operational conditions an undesirable instability phenomenon referred to as *stall induced edge-wise vibrations* can occur on wind turbines. During stall the aerodynamic forces can supply the wind turbine blades with energy when they vibrate in a natural mode.

The vibration is governed by the aerodynamic damping and when this is negative a self-excitation of the structure can occur unless dampened through structural damping. Stall induced edge-wise vibrations are known to occur during operational conditions, where light stall is observed on the blade, and where the quasi-steady lift curve for the corresponding airfoil section has a negative slope, i.e. where non-linear aerodynamic effects are present.

Factors which are known to influence on these vibrations are e.g. static and dynamic airfoil characteristics, the overall aerodynamic layout of the blade, i.e. chord length distribution and twist, the structural properties of the blade, i.e. structural damping, and properties controlling the direction of vibration, i.e. the principal bending axes, called the structural pitch. Furthermore the properties of the supporting structure, i.e. the nacelle and the tower has shown to influence the vibrations as they may either resist or support the vibrations.

2. METHODS

The present paper describes a numerical method of predicting aeroelastic stability of two-dimensional (2-D) airfoil flow. The method consists of a coupling of a simple three degrees-of-freedom (DOF) structural dynamics model to a 2-D incompressible computational fluid dynamics (CFD) code. The degrees of freedom are respectively pitch, flap-wise, and edge-wise deflections.

The aerodynamic forces are computed using the incompressible Navier-Stokes code EllipSys2D [3], [4] and [5].

Figure 1 shows the 3 DOF airfoil. The generalized coordinates are (y, x, α) in normal, stream-wise and torsional direction, respectively, positive as indicated in figure 1.

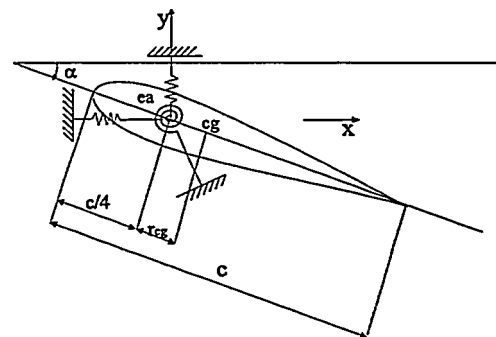


Figure 1: 3 DOF airfoil section. *ea* is the elastic axis and *cg* is the center of gravity.

By using Lagrange equations the following linear equations of motion are obtained

$$[M]\{\ddot{D}\}_n + [C]\{\dot{D}\}_n + [K]\{D\}_n = \{R^{ext}\}_n,$$

where M , C , and K are the mass matrix, damping matrix, and stiffness matrix, respectively. D is the generalized coordinate vector and R^{ext} is the external forces vector. The equations of motion for the non-linear unsteady computations are solved using the trapezoidal rule (or the Crank-Nicolson method) This is an unconditionally stable implicit one-step method, which is second order accurate in time.

3. RESULTS

3.1. NACA0012 airfoil

The first test case chosen in the present study is a NACA0012 airfoil subjected to a flow and the structural dynamics model is a 2 DOF system free to rotate in the $x-y$ plane and free to translate up and down. i.e. bending/torsion deflection. This test case has been chosen for validation purposes. A comparative study is presented in ref. [2] which investigates the flow configuration using a compressible CFD code. The flow parameters used are: $Re = 4.0 \times 10^6$, $M = 0.3$. The structural parameters used are: mass ratio $\mu = m/\pi \rho b^2 = 100$, elastic axis in quarter-chord, non-dimensional static unbalance = 0.25, non-dimensional radius of gyration = 0.5, $\omega_y/\omega_\alpha = 0.2$, and no structural damping. Defining $V^* = U_\infty/(b\omega_\alpha)$ being a non-dimensional velocity, this parameter is a key parameter for flutter investigations. Two values of V^* was investigated, namely $V^* = 4$ and 8, and one initial angle of attack, $\alpha_o = 5^\circ$. A steady state solution is obtained at the initial angle of attack, α_o , after which the airfoil is released from its fixed position. The structural equilibrium position is $\alpha = 0^\circ$. Dependent on V^* and α_o the motion will either stabilize or diverge.

Figure 2 show the computations for initial angle of attack, $\alpha = 5.0^\circ$

The results compare well with results in ref [2]. Note that the plunge motion has a smaller dominant frequency than the pitch motion, which is due to the natural frequency ratio, $\frac{\omega_y}{\omega_\alpha} = 0.2$. Limit cycle behavior was observed at $V^* = 6.0$ as shown in figure 3.

After a short period of time the motion became periodic in angle of attack, α , while the vertical displacement still showed some chaotic behavior.

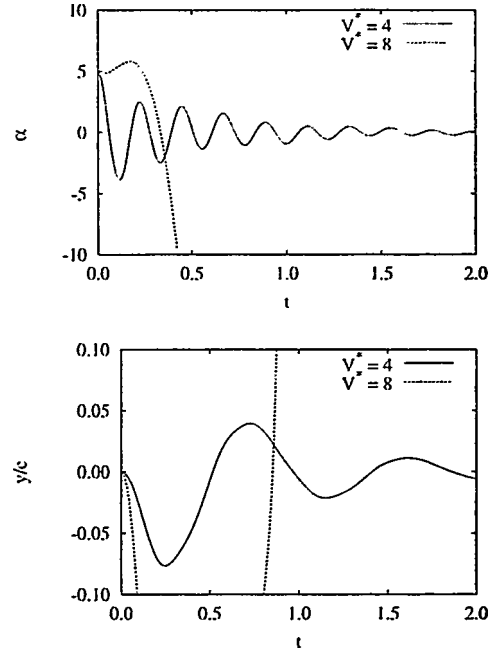


Figure 2: Computations using EllipSys2D , Naca0012, $Re = 4 \times 10^6$, $\alpha_0 = 5^\circ = 0.087rad$

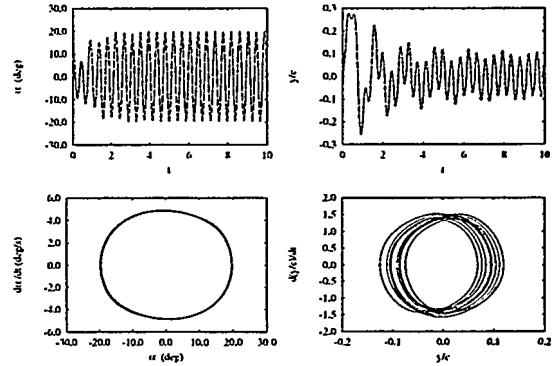


Figure 3: Limit cycle behavior in the phase plane. $V^* = 6.0$. Computations using EllipSys2D , Naca0012, $Re = 4 \times 10^6$, $\alpha_0 = 15^\circ = 0.263rad$

The two phase-plane plots in figure 3 are plotted after ≈ 2.5 sec. In reference [2] the flutter speed was determined to $V^* = 4.75$. The small difference between the two values can be caused by compressibility effects, different grid topology, and time step, difference in implementation, etc.

3.2 LM 2 18 % airfoil

The second airfoil is the LM 2 18 % thick airfoil which is an airfoil developed strictly for wind turbine application. An example taken from [6] is chosen as test case. In that reference the aerody-

namics is based on quasi-steady 2-D aerodynamics, where the influence of lift, drag, lift curve slope, and drag curve slope are investigated. The results show that edge-wise vibrations can occur in the wind speed range 8-25 m/s depending on the structural pitch, θ . The structural pitch is caused by the twist of the blade and the structural properties in general. This effect is modeled by rotating the direction of deflection with respect to the elastic axis.

The main data for the present flow configuration are: Mass = 57.0 kg/m , moment of inertia = 2.25 $kg \cdot m$, elastic axes at quarter-chord, structural pitch angle, $\theta = 0^\circ$, flap-wise natural frequency $\omega_y = 1.79Hz$, edge-wise natural frequency $\omega_x = 2.87Hz$, torsional natural frequency $\omega_\alpha = 20.0Hz$, and no structural damping.

Two wind speeds are concerned in the present study; one corresponding to an angle of attack in the attached flow region and one corresponding to the separated flow region. They are

- Wind speed = 10 m/s , resulting in $Re = 3.29 \times 10^6$ and $\alpha = 11.2^\circ$.
- Wind speed = 20 m/s , resulting in $Re = 3.54 \times 10^6$ and $\alpha = 23.2^\circ$.

Figure 4 shows time series using EllipSys2D with initial angle of attack, $\alpha_o = 11.2^\circ$, structural equilibrium position $\alpha = 11.2^\circ$, and structural pitch, $\theta = 0^\circ$.

The pitch and flap-wise motion are both damped while the edge-wise motion is periodic.

Figure 5 shows time series with initial angle of attack, $\alpha_o = 23.2^\circ$, structural equilibrium position $\alpha = 23.2^\circ$, and structural pitch, $\theta = 0^\circ$.

Finally figure 6 show lift hysteresis curves for initial angle of attack, $\alpha_o = 11.2^\circ$ and $\alpha_o = 23.2^\circ$, respectively, together with a computed static lift curve. Structural pitch $\theta = 0^\circ$. As seen from figure 6 the slope of the main axis of the hysteresis is strongly positive indicating that the aerodynamic damping is negative for both initial angles of attack. This leads to damped motions for both test cases, even though unstable behaviour was expected for the large angle of attack. Purely aerodynamic computations at this frequency also predict positive slope of the lift hysteresis. This is caused by the vortex pattern shed at this high frequency. The frequency of vibration is around 12 Hz for the pitching motion, which is different from the natural frequency, $\omega_\alpha = 20Hz$.

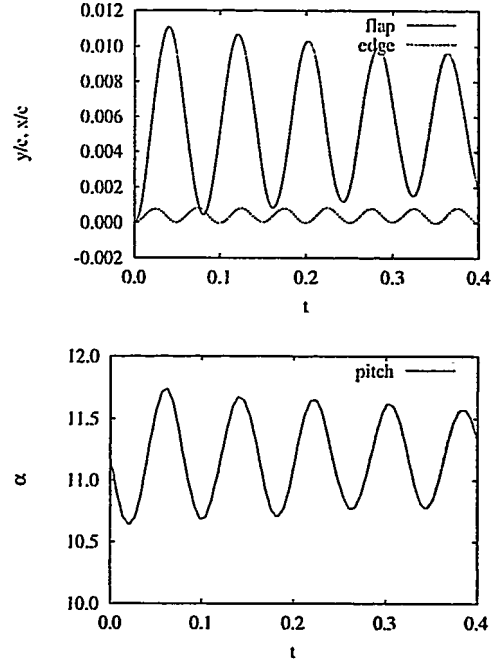


Figure 4: Time series for LM 2 18 % airfoil, $Re = 3.29 \times 10^6$, $\alpha_o = 11.2^\circ$, Structural pitch $\theta = 0^\circ$.

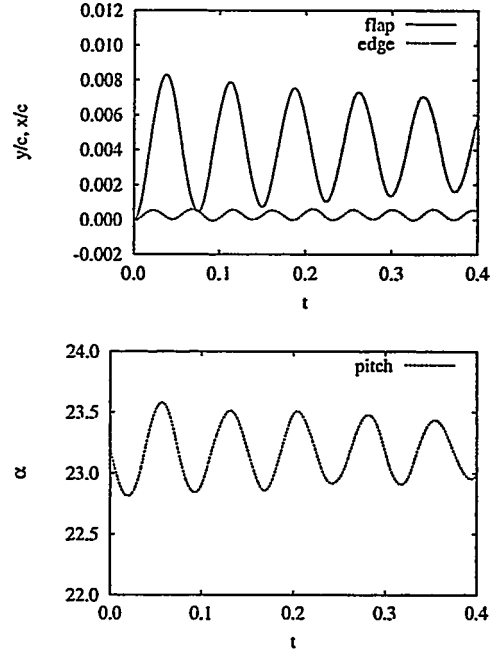


Figure 5: Time series for LM 2 18 % airfoil, $Re = 3.54 \times 10^6$, $\alpha_o = 23.2^\circ$, Structural pitch $\theta = 0^\circ$.

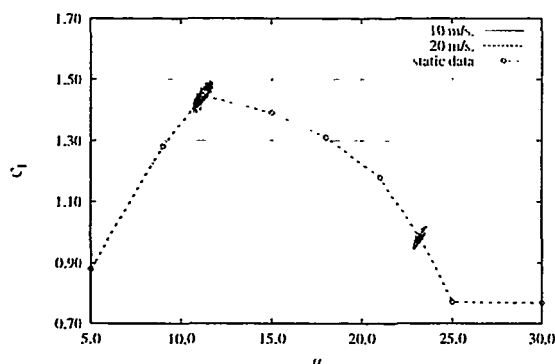


Figure 6: Lift hysteresis curves for LM 2 18 % airfoil, $\alpha_o = 11.2^\circ$ and $\alpha_o = 23.2^\circ$, respectively. Structural pitch $\theta = 0^\circ$, compared with static computed data.

4. CONCLUSIONS

A 3 DOF structural dynamics model has been coupled to a 2-D CFD code in order to study aeroelastic stability on airfoil flow. The method has been validated against published literature using a 2 DOF NACA0012 airfoil, and applied on a 3 DOF wind turbine airfoil section. Stable solutions are predicted for initial angles of attack in both the attached and the separated region. This is interpreted as, the frequency of the pitching motion has a large influence on the aerodynamic damping. Also three dimensional effects such as blade rotation, blade twist, etc. omitted here are important for predicting stall induced edge-wise vibrations.

The present work will be described in depth in ref. [1].

REFERENCES

- [1] J. Johansen. *Numerical Investigation of Unsteady Airfoil Flows with application to Aeroelastic Stability*. PhD thesis, Risø National Laboratory and Technical University of Denmark, 1999. To be published.
- [2] A. J. Mahajan, K. R. V. Kaza, and E. H. Dowell. Semi-Empirical Model for Prediction of Unsteady Forces on an Airfoil with application to Flutter. *J. of Fluids and Structures*, 7:87–103, 1993.
- [3] J. A. Michelsen. Basis3D - a Platform for Development of Multiblock PDE Solvers. Technical report, Technical University of Denmark, 1992. AFM 92-05.
- [4] J. A. Michelsen. Block structured Multigrid solution of 2D and 3D elliptic PDE's. Technical report, Technical University of Denmark, 1994. AFM 94-06.
- [5] N. N. Sørensen. General Purpose Flow Solver Applied to Flow over Hills. Technical report, Risø National Laboratory, Roskilde, Denmark, June 1995. Ph.D. Thesis, Risø-R-827(EN).
- [6] J. T. Thirstrup, H. A. Madsen, A. Björk, P. Enevoldsen, S. Øye, H. Ganander, and D. Winkelaar. Prediction of Dynamic Loads and Induced Vibrations in Stall. Technical report, Risø National Laboratory, Roskilde, Denmark, May 1998.

DESIGN OF THE NEW RISØ-A1 AIRFOIL FAMILY FOR WIND TURBINES¹

Peter Fuglsang and Kristian.S. Dahl
Wind Energy and Atmospheric Physics Department
Risø National Laboratory
P.O. Box 49, DK-4000 Roskilde
Phone: +45 46775071, Fax: +45 46775083,
E-mail: peter.fuglsang@risoe.dk

ABSTRACT: A new airfoil family for wind turbines was developed by use of a design method using numerical optimization and the flow solver, XFOIL. The results were evaluated with the Navier-Stokes solver EllipSys2D. The airfoil family constitutes 6 airfoils ranging in thickness from 15% to 30%. The airfoils were designed to have a maximum lift coefficient around 1.5 in natural conditions and high lift-drag ratios below maximum lift. Insensitivity to leading edge roughness was obtained by securing that transition from laminar to turbulent flow on the suction side occurred close to the leading edge just before stall. The airfoil family was designed for a 600 kW wind turbine and provides a basis for further enhancing the characteristics of airfoils for wind turbines and to tailor airfoils for specific rotor sizes and power regulation principles.
Keywords: Aerodynamics; Airfoil Sections; Optimization; Wind Turbines(HAWT)-Rotors

1 INTRODUCTION

Design of tailored airfoils for rotor blades is important for the continuing development of wind turbines. Wind turbine airfoils should differ from traditional aviation airfoils in choice of design point, off-design characteristics and structural properties. The development of wind turbine airfoils has been ongoing since the mid 1980's and a large effort has been done by Tangler and Somers [1] who have developed several airfoil families. Other airfoil designs for wind turbines can be found in [2]-[6]. Most of these airfoil designs were developed by use of traditional inverse design methods.

Numerous methods for airfoil design are available and a survey of such methods and available references can be found in [7] and [8]. In traditional inverse design, the airfoil surface flow is prescribed at specified operational conditions and a shape is found that will generate these surface conditions. Methods that include a boundary layer formulation like the Eppler [9] and the XFOIL codes [10] represent state of the art.

Traditional inverse design methods in general have limited capabilities for off-design, since there is only a single target pressure distribution at a single design point. The designer must take care of these matters manually in a cut-and-try process. Direct design methods based on numerical optimization provide basically a multipoint and interdisciplinary design procedure where several design parameters can be involved simultaneously. The purpose of the present work was to automate the airfoil design process by using an optimization method for airfoil design [11]. The flow solver, XFOIL, was used with a numerical optimization algorithm. Attention was paid to design from scratch and off-design. A strategy for tailoring of wind turbine airfoils was developed and an airfoil family was designed for a 600 kW rotor.

2 WIND TURBINE AIRFOIL CHARACTERISTICS

The characteristics of an ideal wind turbine airfoil depend in principle on the specific target rotor. Still, some properties can be labeled as desirable for most wind turbine airfoils.

The lift-drag ratio should be high for all angles of attack below maximum lift for maximum power production and for good off-design characteristics.

The design angle of attack should be close to maximum lift for airfoils used on the outer part of the blades to reduce blade area.

Maximum lift should be high for thick airfoils used on the inboard part of the blades to reduce the blade area. These airfoils should be well suited for aerodynamic devices such as vortex generators and Gurney flaps.

Maximum lift should be insensitive to leading edge roughness, which in natural conditions is caused by bugs and dirt soiling the blades.

For stall regulation, the flow at maximum lift should separate from the trailing edge to have smooth behavior in stall. The transition from the linear part of the lift curve to the post stall area should be well defined and the airfoil should be insensitive to double stall.

On the inboard blade section, the airfoils should have high cross section stiffness, to limit blade weight and tip deflection, obtained by increasing the maximum thickness.

The desirable airfoil characteristics constitute both aerodynamic and structural properties and multiple conflicting characteristics are involved. For example high lift-drag ratio is in contrast to high airfoil thickness and high maximum lift is in contrast to insensitivity to leading edge roughness.

¹ Presented at EWEC'99, Nice, France

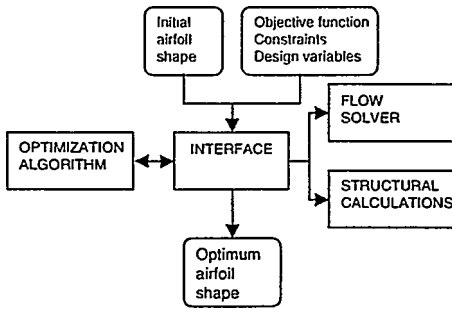


Figure 1: Flow chart of the design method.

3 DESIGN METHOD

The design method is based on numerical optimization. The general formulation of an optimization problem is: Minimize: $F(x)$ Subject to: $G_j(x) < 0, j = 0, m$; where $m+1$ is the number of constraints. The objective function, $F(x)$, is minimized by changing the design variables that compose the design vector, x . Here, the design variables are the control points that describe the airfoil shape. The inequality constraints, $G_j(x)$, are side values for the design variables and bounds on response parameters from flow and structural calculations.

3.1 Design algorithm

The combination of numerical optimization and different tools for flow and structural calculations are shown in Figure 1.

An airfoil shape is input together with the objective function, the design variables and the constraints. The optimization process is iterative involving many calculations of flow and structural properties where the design is improved gradually. The flow and structural calculations are used to estimate the value of the objective function and the constraints. Multiple angles of attack are calculated to allow off-design optimizations. The combination of flow and structural responses allows interdisciplinary optimization and when available, other calculation tools can easily be incorporated, for example calculation of aerodynamic self noise. A simplex optimizer was used with a traditional finite difference sensitivity analysis.

3.2 Geometry description

A smooth airfoil shape is important for the optimization results. The shape description should have as much geometric flexibility as possible with as few design variables as possible to secure an effective and representative search of the design space with acceptable computational costs. In principle, any physically realistic shape should be possible to allow design from scratch. The airfoil shape was represented by a single B-spline curve defined from the trailing edge around the airfoil contour by a set of control points [12]:

$$p(u) = \sum_{i=0}^n P_i N_{i,k}(u), \quad (1)$$

where $0 < u < n-k+2$, k is the order of continuity, $P_i(\eta, \xi)$ are the coordinate points, $n+1$ is the number of coordinate points, $N_{i,k}(u)$ are influence functions. The B-spline curve is continuous of the k th order. Figure 2 shows an example with $n+1 = 12, k = 5$.

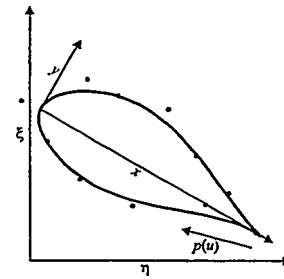


Figure 2: B-spline representing the airfoil shape, $n+1 = 12, k = 5$. the dots are the control points/design variables.

3.3 Flow analysis

The XFOIL code by Drela [10] was used for the flow calculations during the optimizations. XFOIL is developed for transonic and low Reynolds number flows and is well suited for optimization because of the fast and robust viscous/inviscid interaction scheme. For given angle of attack, α , Reynolds number and Mach number, XFOIL provides the pressure distribution, C_p , lift coefficient, C_L , and drag coefficient, C_D . In addition, numerous boundary layer parameters are calculated. In XFOIL, transition was modeled by the e^n method with $n = 9$ as default value. Separation was estimated for a boundary layer shape factor, $H > 2.8$, defined as displacement thickness divided by momentum thickness. Prescribing transition to 1% after the leading edge on the suction side and 10% at the pressure side simulated leading edge roughness.

XFOIL is known to overestimate the maximum lift coefficient, C_{Lmax} , and to underestimate the minimum drag coefficient, C_{Dmin} . Therefore, the Navier-Stokes code Ellipsys2D [13] with the $k-\omega$ turbulence model [14] was used in the evaluation of the final optimized airfoils. Transition was modeled with the Michel criterion [15]. Leading edge roughness was simulated with turbulent flow on the entire airfoil.

4 DESIGN STRATEGY

The Reynolds number based on chord, the Mach number and the trailing edge thickness defined the overall operational conditions. They were chosen for the different airfoils as representative for a 600 kW rotor.

A total of 12 design variables were chosen among the 13 control points of the B-spline describing the airfoil shape. The control points at the trailing edge were fixed in both the x and y directions to provide the desired trailing edge thickness. For most of the remaining control points only the y -coordinate was a design variable to limit the number of design variables and to ensure a uniform spacing between the control points.

The objective function was defined as a linear combination of n objectives:

$$F = \sum_{i=1}^n a_i f_i, \quad (2)$$

where a_i are weight factors and f_i are the different objectives.

The weighting of the different objectives is the responsibility of the designer and this has obviously great influence on the final design. Objectives were the lift-drag ratio, C_L/C_D at five angles of attack on the linear part of the $C_L(\alpha)$ curve with the design angle of attack, α_b , around 9° .

α_i should be chosen 1-2 degrees below C_{Lmax} to ensure a linear $C_L(\alpha)$ and low C_D at angles until C_{Lmax} . All objectives had equal weight factors.

To obtain the desired C_{Lmax} and post stall behavior upper and lower limit constraints were put on C_L at α_i and at the angles of attack during post stall. Constraints were also added to the suction side separation point, $S_{sep}(\alpha)$ to ensure attached flow just until C_{Lmax} . S_{sep} should be at the trailing edge at α_i and then move towards the leading edge just before C_{Lmax} . To ensure a well defined stall, there should be a significant movement in S_{sep} at C_{Lmax} .

Insensitivity to leading edge roughness was obtained by constraining the location of the transition point on the suction side, $S_{tr}(\alpha)$, before and after C_{Lmax} . To increase C_L/C_D at the objective angles of attack, S_{tr} should in general be as far downstream as possible below stall. However, at C_{Lmax} , S_{tr} should be close to the leading edge. The flow on most of the suction side would then be turbulent because of the early transition and the flow would be nearly equal for both smooth and rough leading edges securing minimal difference in C_{Lmax} and the $C_L(\alpha)$ slope. The remaining effect from leading edge roughness is of course an increase in C_D , which is inevitable. The flow constraints are shown for Risø-A1-21 in Table I.

Table I: Flow constraints for the Risø-A1-21 airfoil.

α	9.5	10	10.5	11	12	13
min (C_L)	1.53	-	1.64	1.64	1.60	1.56
max (C_L)	1.55	-	1.65	1.65	1.65	1.65
min (S_{sep})	0.99	0.99	0.99	-	-	-
max (S_{tr})	-	-	-	0.08	0.08	0.08

Structural constraints were added to the airfoil relative thickness, t/c , to give the desired maximum thickness. Other geometric constraints were added to the airfoil shape to ensure compatibility between the different airfoils in the family, such as the pressure side location of the maximum thickness and the curvature on certain parts of the airfoil contour. Overall design parameters are shown in Table II.

Side constraints were added to the design variables to ensure that they moved within reasonable limits. During the optimization, the flow solver calculated the flow for all angles of attack where objectives and constraints were defined. For a reliable optimization process, convergence problems in the flow predictions were avoided by proper convergence criteria.

Table II: Overall design parameters for the Risø-A1 airfoils.

Airfoil	max (t/c)	x/c at max (t/c)	y/c at T.E.	$Re \times 10^6$
Risø-A1-15	15	0.325	0.25	3.00
Risø-A1-18	18	0.336	0.25	3.00
Risø-A1-21	21	0.298	0.5	3.00
Risø-A1-24	24	0.302	1.0	2.75
Risø-A1-27	27	0.303	1.0	2.75
Risø-A1-30	30	0.300	1.0	2.50

5 RESULTS AND DISCUSSION

Figure 3 shows the optimized Risø-A1 airfoil shapes. The transition between neighbor airfoils is smooth as intended. The suction sides are rather similar because of the

constraints on S_{sep} and C_{Lmax} and the shape of the pressure sides are mainly to achieve the maximum thickness. To maintain high C_{Lmax} and low C_{Dmin} for the thick airfoils, the trailing edge angle is at an angle compared to horizontal. This gives increased camber and reduces the zero lift angle of attack, α_0 .

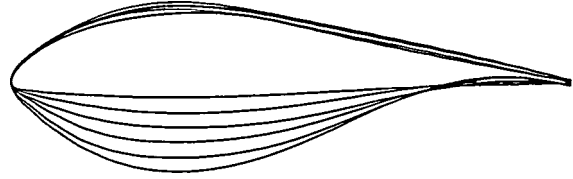


Figure 3: The contours of the Risø-A1 airfoil family.

Figure 4 shows C_p at different angles of attack for the Risø-A1-21 airfoil. For low angles of attack ($\alpha=4^\circ$) the flow around the airfoil nose is smooth and the acceleration on the suction side is very modest. C_p at 8° near α_i is rooftop like with a large area of suction on the front part of the airfoil and only a small amount of after loading. Close to α_i , S_{tr} is located at 0.35 and most of the pressure side flow is laminar.

Insensitivity to leading edge roughness for C_{Lmax} is related to the shape of the leading edge, Figure 4. The small radius of curvature at the leading part of the pressure side causes a narrow suction peak to appear in C_p around α_i because the stagnation point moves downstream on the pressure side, forcing the suction side flow to pass the leading edge. S_{tr} moves to the leading edge before C_{Lmax} and at $\alpha = 12^\circ$ the suction side peak is clearly seen in C_p . The suction peak provokes transition but does not destroy the flow on the suction side in post stall retaining suction on the front part of the airfoil until deep stall.

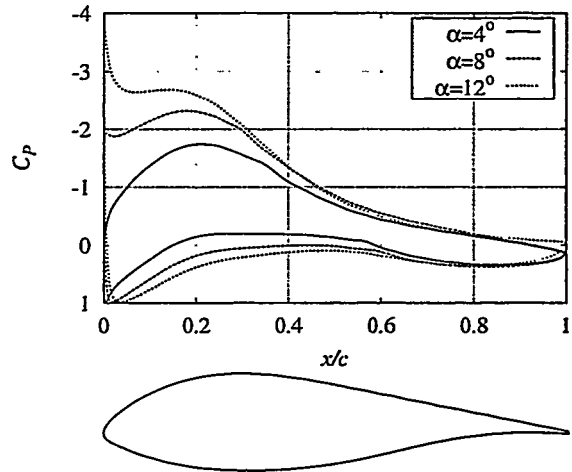


Figure 4: C_p distribution at 4° , 8° and 12° for the Risø-A1-21 airfoil (EllipSys2D free transition).

Figure 5 shows C_L and C_D for the Risø-A1-21 airfoil. C_D for smooth flow remains low and nearly constant below maximum lift, which gives a high C_L/C_D ratio until α_i . C_D for turbulent flow is increased because of the higher skin friction from a turbulent boundary layer. The result of the roughness insensitivity can be seen on the slope of $C_L(\alpha)$ since this is nearly the same for smooth and turbulent flow.

Table III shows the flow characteristics for the Risø-A1 airfoils calculated with EllipSys2D. All airfoils have a C_{Lmax} around 1.5 for turbulent flow and a relative low C_{Dmin} for smooth flow. C_L/C_D at α_{ti} is 135 and 90 for Risø-A1-15 and Risø-A1-30, respectively. XFOIL predicts $C_{Lmax} = 1.65$ for all airfoils which was the design C_{Lmax} and even higher C_L/C_D . However, this is not expected in natural conditions due to turbulence and roughness effects.

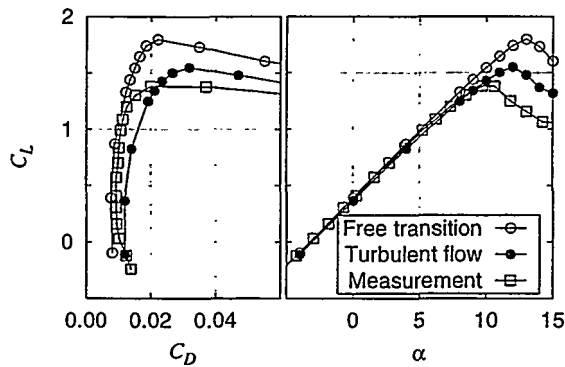


Figure 5: C_L - C_D curve for the Risø-A1-21 airfoil (EllipSys2D).

Table III: Main characteristics of the Risø-A1 airfoils (EllipSys2D).

	α_0 (°)	C_{Lmax} Turb flow	C_{Dmin} Free trans	C_{Dmin} Turb flow
Risø-A1-15	-4.0	1.50	0.067	0.106
Risø-A1-18	-3.6	1.50	0.067	0.108
Risø-A1-21	-3.3	1.53	0.076	0.118
Risø-A1-24	-3.4	1.53	0.087	0.136
Risø-A1-27	-3.2	1.53	0.113	0.172
Risø-A1-30	-2.7	1.46	0.116	0.209

The Risø-A1-18, Risø-A1-21 and Risø-A1-24 airfoils were recently tested in a wind tunnel. Smooth flow as well as leading edge roughness flow was tested at a Reynolds number of 1.6×10^6 . Risø-A1-24 was furthermore tested with vortex generators and Gurney flaps. The results agreed well with the predicted characteristics [16]. The measured C_L and C_D are shown in Figure 5. Minimum C_D and the $C_L(\alpha)$ slope agree well with the EllipSys2D predictions. The difference in C_{Lmax} between the measurement and the predictions is due to the difference in Reynolds number.

6 CONCLUSION

The Risø-A1 airfoil family designed for a 600 kW rotor provides a good basis for further enhancing the characteristics of airfoils for wind turbines and for tailoring airfoils to specific rotor sizes and power regulation principles.

The following characteristics were obtained:

- Insensitivity to leading edge roughness for maximum lift.
- Maximum lift coefficient around 1.5 in natural conditions for all airfoils.

- High lift-drag ratio also at high angles of attack below stall.
- Trailing edge stall, smooth post stall behavior and no double stall.

ACKNOWLEDGEMENTS

The Danish Energy Agency funded the present work under the contracts ENS 1363/95-0001, 1393/98-0038.

REFERENCES

- [1] Tangler, J. L., Somers, D. M. Status of the Special-Purpose Airfoil Families. In WINDPOWER'87, San Francisco (1987).
- [2] Björk, A. Airfoil design for variable RPM horizontal axis wind turbines. In EWEC'89 (Glasgow, Scotland, 1989).
- [3] Timmer, W.A., van Rooy, R. Thick airfoils for HAWTs. Journal of Wind Engineering and Industrial Aerodynamics 39 (1992).
- [4] Timmer, W.A., van Rooy, R. The performance of new wind turbine blade tip and root airfoils up to high angles-of-attack. In EWEC'97 (Dublin, Ireland, 1997).
- [5] Hill, D. M., Garrad, A. D. Design of Aerofoils for Wind Turbine Use. In IEA Symposium on Aerodynamics of Wind Turbines (Lyngby, Denmark, 1988).
- [6] Chaviaropoulos, P., Bouras, B., Leoutsakos, G., and Papailiou, K. D. Design of Optimized Profiles for Stall Regulated HAWTs Part 1: Design Concepts and Method Formulation. Wind Engineering 17, 6 (1993), 275-287.
- [7] Henne, P. A. E. Applied Computational Aerodynamics. American Institute of Aeronautics and Astronautics, Inc., 1989.
- [8] Dulikravich, G. S. Aerodynamic Shape Design and Optimization: Status and Trends. J. of Aircraft 29, 6 (Nov-Dec 1992), 1020-1026.
- [9] Eppler, R., Somers, D. M. A Computer Program for the Design and Analysis of Low-Speed Airfoils. Tech. rep., NASA TM 80210, 1980.
- [10] Drela, M. XFOIL: An Analysis and Design system for Low Reynolds Number Airfoils. In Low Reynolds Number Aerodynamics (1989), vol. 54 of Springer-Verlag Lec. Notes in Eng.
- [11] Fuglsang, P., Dahl, K.S. Multipoint optimization of thick high lift airfoil for wind turbines. In EWEC'97 (Dublin, Ireland, 1997).
- [12] de Boor, C. A Practical Guide to Splines. Springer-Verlag, New York, 1978.
- [13] Sørensen, N. N. General Purpose Flow Solver Applied to flow over Hill. Risø-R-827(EN), Risø National Laboratory, Denmark, 1995.
- [14] Menter, F. R. Zonal Two Equation k-w Turbulence models for Aerodynamic Flows. AIAA Paper 93-2906 (1993).
- [15] Michel, R. Etude de la transition sur les profils d'aile. Tech. Rep. 1/1578-A, ONERA, 1952. See White F.M., Viscous fluid flow, p. 442.
- [16] Dahl, K.S., Antoniou, I.A., Fuglsang, P., Experimental Verification of the new Risø-A1 airfoil family for wind turbines. In EWEC'99 (Nice, France, 1999).

THE INFLUENCE ON ENERGY CONVERSION AND INDUCTION FROM LARGE BLADE DEFLECTIONS

Helge Aagaard Madsen and Flemming Rasmussen
Risoe National Laboratory
P.O. Box 49
DK-4000 Roskilde
Denmark
Phone: +45 46775047
Fax.: +45 4677 5083
Email: helge.aagaard.madsen@risoe.dk

ABSTRACT: Flexible blades or coning means that the swept area is no longer a plane disc as assumed in the blade element momentum (BEM) theory. How is the induced flow field of the rotor influenced by such changes and what does this mean for the loading and energy conversion?

This has been investigated by studying the flow through four different rotor geometries on basis of a numerical, axis-symmetric actuator disc model. Volume forces perpendicular to the local blade surface were applied and the converted power is the work performed by these forces. To simplify the comparisons, only a constant load distribution was used.

The numerical results show that the shape of the rotor disc has considerable influence on the induction or axial velocity. The axial velocities vary with radial position in the case of constant loading where BEM theory gives constant velocities. There is considerable variation of the local power coefficient $C_{p,loc}$ even for constant loading. Locally, $C_{p,loc}$ can exceed the Betz limit. However, integrating $C_{p,loc}$ over the rotor plane, the total power coefficient for the different rotors are exactly the same.

Keywords: Aerodynamics, Actuator Disc Model, Blade Aerodynamics

1 INTRODUCTION

The continuous development and optimisation of wind turbine blades has led to more flexible and lighter designs resulting in large blade deflections during operation. Also new rotors with considerable coning in some operational conditions are presently being studied. The question is now in which way such changes influence the induced flow field of the rotor and what this means for the loading and energy conversion of the rotor. An interesting aspect is to investigate if the energy conversion can be increased by an optimal bending of the blades.

The standard blade element momentum (BEM) model, as implemented in most aeroelastic codes, neglects the influence from out of plane rotor shape or bending of the blades. In contrast to this, an axis-symmetric actuator disc model of the rotor is used in the present study. For simplification the investigation is restricted to application of a prescribed constant load distribution on the rotor where only the integrated loading expressed through the rotor thrust coefficient is varied.

2 MODELLING

When the blades bend out of the plane perpendicular to the free stream velocity, the starting position of the shed vorticity is changed. As the induction is the

integrated influence of the induced velocities from the shed vorticity, it will depend on the actual shape of the rotor surface, swept by the blades.

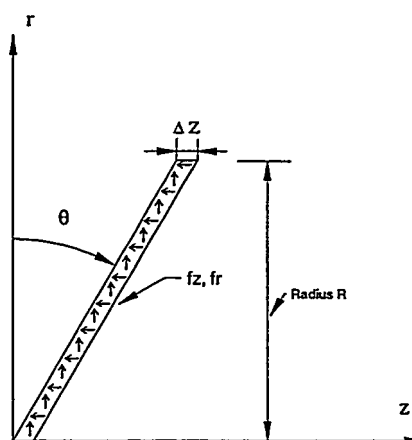


Figure 1. An actuator disc in an angle to the inflow. The resultant volume forces are directed perpendicular to the surface.

Different models can be used to compute the flow through a rotor disc, ranging from simple lifting line models to full 3D CFD models. However, the standard BEM theory cannot be used as the flow in one stream tube is computed without influence from the other neighbouring stream tubes.

2.1 The actuator disc model

The actuator disc concept has been used in the present case. The basic idea [1], [2] is to apply volume forces to the flow at the rotor disc, which are the reaction of the blade forces. However, to simplify the investigation the loading is in the present case directly applied without caring about how the forces are created. It is further assumed that the loading is constant over the rotor disc and the resultant volume force in any point on the surface is perpendicular to the tangent to the surface.

The actuator disc has a final, small axial dimension Δz Figure 1 so that the intensity of the volume forces become final. A value of $0.05R$ where R is the rotor radius is used in the present case and numerical tests have shown that the flow field is only slightly influenced by the value of this parameter.

The loading is applied as axial and radial volume forces f_z , f_r Figure 1, in the following ratio so that the resultant force is perpendicular to the surface:

$$f_r = f_z \tan(\theta) \quad (1)$$

The volume force f_n normal to the surface can then be derived as:

$$f_n = (f_z^2 + f_r^2)^{1/2} = (f_z^2 + f_z^2 \tan^2(\theta))^{1/2} = \frac{f_z}{\cos(\theta)} \quad (2)$$

The energy conversion P is the work of the volume forces:

$$P = 2\pi \int_0^L \int_0^{\Delta z \cos(\theta)} r f_n v_n dl dn \quad (3)$$

where L is the length of the bend or coned blade and v_n is the flow velocity normal to the surface.

The power coefficient can then be worked out as:

$$C_p = \frac{P}{\frac{1}{2} \rho V_0^3 \pi R^2} \quad (4)$$

A local power coefficient $C_{p,loc}$ is defined as:

$$C_{p,loc} = \frac{P_l}{\frac{1}{2} \rho V_0^3 2\pi r \Delta r} = \frac{f_n v_n \Delta z \cos(\theta) \Delta l 2\pi r}{\frac{1}{2} \rho V_0^3 2\pi r \Delta r} \Rightarrow$$

$$C_{p,loc} = \frac{f_n v_n \Delta z}{\frac{1}{2} \rho V_0^3} \quad (5)$$

Finally, the rotor thrust coefficient CT can be derived as:

$$CT = \frac{T}{\frac{1}{2} \rho V_0^2 A} = \frac{2\pi \int_0^R \int_0^{\Delta z} f_z r dr dz}{\frac{1}{2} \rho V_0^2 \pi R^2} \quad (6)$$

and for constant loading f_z the integrations can be worked out yielding:

$$CT = \frac{2 f_z \Delta z}{\rho V_0^2} \quad (7)$$

2.2 The numerical solution

The describing equations for the flow through the actuator disc are the Navier Stokes equations which are solved with the general purpose CFD code FIDAP. A mesh stretching 6R upstream, 40R downstream and 5R in radial direction has been used and the flow is solved as an axis-symmetric problem. Finally, turbulent flow is assumed using a k- ϵ model.

3 NUMERICAL RESULTS

Three different blade deflections have been studied; a rotor coned 20 deg.; a rotor with flexible blades and considerable blade deflection on the outer part of the blade; and a rotor with winglets, Figure 2. A rotor with in-plane straight blades is used as a reference case.

A constant loading perpendicular to the surface has been used in all the computations and the loading is varied by the rotor thrust coefficient CT , equation 6.

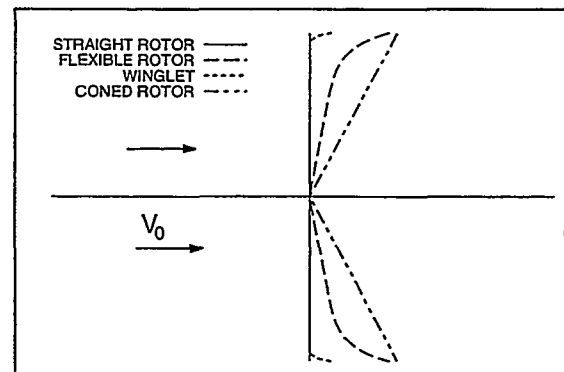


Figure 2. The different investigated rotor configurations.

3.1 The velocities at the disc

Considerable influence on the induced velocities from the rotor geometry is found, Figure 3, where the induction at a rotor thrust coefficient of 0.89 is shown. For the three rotors with out of plane blade bending (coned, flexible and winglet) the axial velocity v_z on the inner part of the rotor surface is higher when compared with v_z for the straight rotor. The difference is up to 12%. For comparison is also shown the induction as computed with the BEM theory at the same loading.

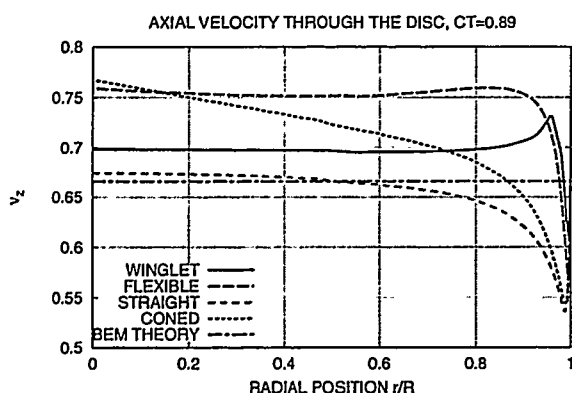


Figure 3. The axial velocity in the rotor plane for the different rotor geometries.

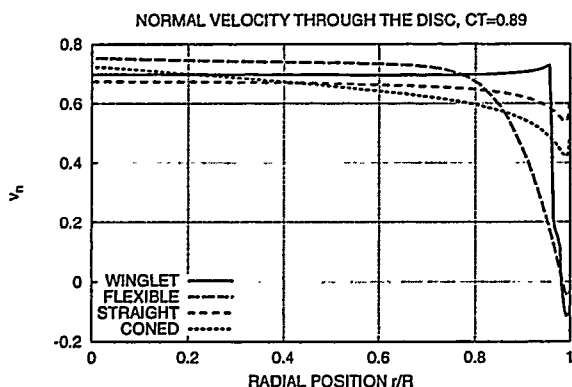


Figure 4. The velocity normal to the blade surface for the different rotor geometries.

For the energy conversion it is the velocity component v_n normal to the surface which is important, Figure 4. The tendencies for v_n are the same as for v_z but due to the geometrical differences between the rotors v_n decreases more rapidly towards the blade tip for the rotors with out of plane blade bending. In fact v_n is negative close to the tip for the flexible rotor and the rotor with a winglet.

Finally, the difference between the radial velocity profiles v_r is in general small, Figure 5. Only in the blade tip region some differences are found.

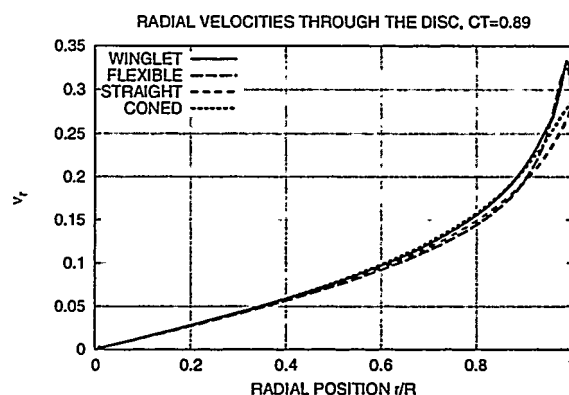


Figure 5 The radial velocity in the rotor plane for the different rotor geometries.

3.2 The energy conversion

The local power coefficient $C_{p,loc}$ as defined by eq. (5) is shown in Figure 6 in comparison with the Betz limit for $CT = 0.89$. On a considerable part of the radius $C_{p,loc}$ for the three rotors with bend blades exceeds $C_{p,loc}$ of the straight rotor but also the Betz limit. Close to the rotor centre $C_{p,loc}$ approaches 0.7 which is considerably above the Betz limit

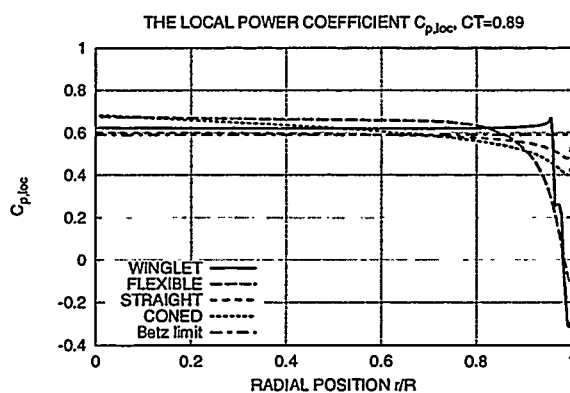


Figure 6 The local power coefficient $C_{p,loc}$ for the different rotor geometries.

$CT \setminus C_p$	STRAIGHT	FLEXIBLE	CONED	WINGLET
0.70	0.528	0.527	0.528	0.528
0.80	0.562	0.560	0.561	0.562
0.89	0.573	0.570	0.571	0.573
0.95	0.559	0.559	0.559	0.562

Table I The power coefficient C_p as function of the rotor thrust coefficient CT for the different rotors.

However, as for v_n $C_{p,loc}$ decreases rapidly towards the tip of the blade and is even slightly negative for the flexible rotor and the rotor with winglets.

The interesting question is now what the integral value of $C_{p,loc}$ for the whole rotor is. This result is shown in Table I for rotor loadings from 0.70 to 0.95. Almost identical total rotor power coefficients C_p are found for the different rotors and the small deviations on the third decimal are ascribed to the uncertainties of the numerical computations. Thus, although there are considerable deviations between the local energy conversion for the different rotors, the integral value is the same.

For the simplified constant loading used in the present case this result can be explained by the fact that the trailing vortices are only shed at the blade tips. If we therefor compare the induced velocities from a plane through the blade tips of the different rotors and downstream, the induction is expected to be identical as the shed vortex system is identical for

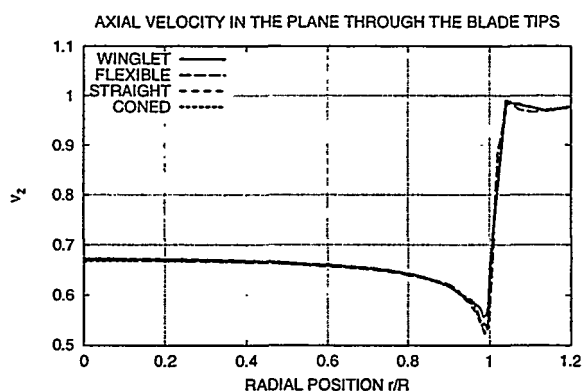


Figure 7 The velocity profiles v_z in a plane through the blade tip for the different rotor geometry's

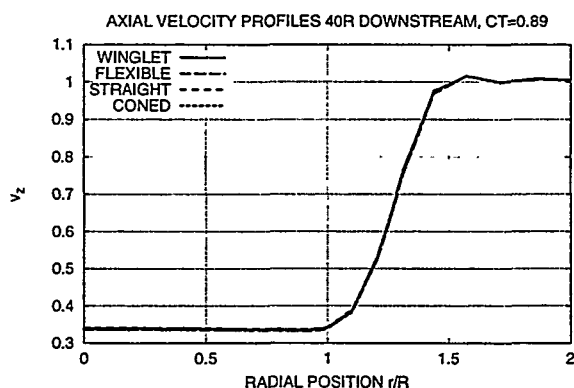


Figure 8 The velocity profiles v_z in the wake 40R downstream the rotors.

the different rotors. This is also confirmed by the numerical results. For example the v_z profiles in the plane through the blade tips of the different rotors compared in Figure 7 are almost identical and the

same holds for the profiles further downstream Figure 8.

4 CONCLUSIONS

A considerable influence on induction from the out of plane bending of blades due to e.g. coning or blade flexibility has been found. The results are based on numerical investigations using the actuator disc concept. Specific results are:

- less axial induction on the inboard part of rotors with blades bend in the downstream direction, and opposite tendency in the blade tip region
- locally the ideal energy conversion can exceed the Betz limit
- the integrated power coefficient for the rotor (ideal energy conversion) is independent of the out of plane blade bending for constant loading
- the influence on induction from the out of plane bending is so big that it should be considered in performance and aeroelastic computations on rotors with big coning or very flexible blades
- the standard BEM theory cannot be used to compute the influence on induction from the out of plane blade bending

5 ACKNOWLEDGEMENT

The work has been funded by the Danish Ministry of Energy, contract ENS 1363/98-0005.

REFERENCES

- [1] H.A. Madsen, Application of Actuator Surface Theory on Wind Turbines. Proceedings of the 2nd IEA Symposium on Aerodynamics of Wind Turbines held at Lyngby 21-22, November 1988.
- [2] H.A. Madsen, A CFD Analysis of the Actuator Disc Flow compared with Momentum Theory Results. Proceedings of the 10th Symposium on Aerodynamics of Wind Turbines, Edinburgh, December 16-17, 1996.

STUDY OF BLADE-TOWER INTERACTION USING A 2D NAVIER-STOKES SOLVER

Franck Bertagnolio

Wind Energy and Atmospheric Physics Department

Risø National Laboratory

P.O. Box 49, DK-4000 Roskilde, Denmark

Phone: (45) 46-77-50-88 – Fax: (45) 46-77-50-83

E-mail: franck.bertagnolio@risoe.dk

ABSTRACT: The aim of this work is to model and study the dynamic interaction of the fluid flow with the structure which occurs when the blades of a wind turbine are passing in front of (or possibly behind) the tower. In order to capture the whole complexity of this phenomenon, the full unsteady Navier-Stokes equations for an incompressible fluid are used as a model. A new computational technique is described. For the sake of simplicity, we restrict ourselves to two-dimensional cases. The present methodology is illustrated by the computation of a wind turbine-like configuration in a periodic domain.

Keywords: NAVIER-STOKES EQUATIONS, AERODYNAMICS, WIND FIELD SIMULATION, UNSTEADY EFFECTS

1. INTRODUCTION

The dynamic interaction of the blades of a wind turbine with its tower is a complex phenomenon. Indeed, the flow is basically unsteady since the blades pass periodically in front of the tower. The vortex shedding from the blades or the tower may participate to the interaction as well. Thus, viscous effects could not be negligible. Moreover, typical Reynolds numbers of wind turbine applications are high, involving turbulent motions in the flow field.

As a consequence, a realistic model for this phenomenon requires the solution of the full unsteady Navier-Stokes equations. However, the inherent geometrical complexity of the flow domain yields several computational difficulties. Firstly, the presence of several bodies (blades and tower) makes the generation of computational meshes uneasy. Secondly, the motion of the airfoil relatively to the tower must be taken into account in the numerical model.

A new solution algorithm has been developed for dealing with these problems. In order to allow an easy mesh generation for any geometrical configuration, a non-overlapping multidomain strategy has been implemented. The solution method is designed such that the grids in the different subdomains do not need to match at the interfaces. Without loss of generality, they remain individually structured.

The second difficulty, namely the relative motion of the blades, requires that two adjacent subdomains, say one attached to the airfoil and the other to the tower, may be able to slide relatively

to each other. This feature has also been incorporated in the numerical model.

The paper is organised as follows. In the next section, the basics of the numerical method are presented. The third section is devoted to the multidomain and sliding meshes implementation. In the fourth section, a simplified numerical test-case illustrates the capabilities of the present methodology. Conclusions are drawn in the last section.

2. NUMERICAL MODEL

In this section, the equations of motion for an incompressible fluid are reminded. The discretisation is then introduced, and the temporal and numerical scheme are presented.

2.1 Basic Equations

Let us consider the unsteady Navier-Stokes equations for an incompressible fluid in a domain Ω :

$$\frac{\partial \mathbf{v}}{\partial t} + \nabla \cdot (\mathbf{v} \otimes \mathbf{v}) = -\nabla p + \frac{1}{Re} \nabla \cdot \mathcal{T}, \quad (1)$$

$$\nabla \cdot \mathbf{v} = 0, \quad (2)$$

where Re is the Reynolds number, \mathbf{v} is the velocity vector, p is the pressure scalar field, and \mathcal{T} holds for the viscous tensor which is deduced from the Newtonian-fluid assumption, that is: $\mathcal{T} = \frac{1}{2}(\nabla \mathbf{v} + \nabla \mathbf{v}^T)$. These equations are supplemented by boundary conditions (BCs) which usually reduces to the Dirichlet conditions for the velocity at the boundary $\delta\Omega$, that is:

$$\mathbf{v} \cdot \mathbf{n} = \mathbf{b} \cdot \mathbf{n}, \quad (3)$$

$$\mathbf{v} \cdot \mathbf{t} = \mathbf{b} \cdot \mathbf{t}, \quad (4)$$

where \mathbf{n} and \mathbf{t} denote the unit vector normal and tangential to the boundary, respectively, and \mathbf{b} is some prescribed boundary velocity field. However, enforcement of the normal flux of the viscous tensor is also permissible. For the sake of generality, and for later use, the following BCs:

$$\mathbf{v} \cdot \mathbf{n} + \alpha (\mathcal{T} \cdot \mathbf{n}) \cdot \mathbf{n} = g_n, \quad (5)$$

$$\mathbf{v} \cdot \mathbf{t} + \beta (\mathcal{T} \cdot \mathbf{n}) \cdot \mathbf{t} = g_t, \quad (6)$$

are assumed on $\delta\Omega$, where g_n and g_t are prescribed source terms. Usual Dirichlet BCs for the velocity can be recovered by cancellation of the coefficients α and/or β .

2.2 Discretisation

In order to deal with curvilinear coordinates systems on non-orthogonal meshes, several projection basis (cartesian or curvilinear) and grid arrangements (staggered or non-staggered) for the vector or scalar quantities are possible. In our case, a discretisation technique which consists in projecting the momentum equation (1) onto the covariant basis is used (see [1,2] for further details). A basis transformation operator expressing the flux components across the cell faces as a function of the covariant components allows an easy handling of the continuity equation (2) and of the pressure-velocity coupling (see below).

The time derivative in the momentum equation (1) is discretised with respect to a second order accurate in time approximation:

$$\frac{\partial \mathbf{v}}{\partial t} = \frac{3 \mathbf{v}^n - 4 \mathbf{v}^{n-1} + \mathbf{v}^{n-2}}{2 \Delta t},$$

where Δt is the time step, and n denotes the time level of the time-stepping iterations. The viscous term is treated implicitly, whereas the convective term are advanced in time by making use of an Adams-Bathforth extrapolation, preserving the second order temporal accuracy.

2.3 Solution Method

In order to solve the velocity-pressure coupling which arises in the set of equations (1-2), the fractional step method by Chorin [3] has been applied. The discrete problem to be solved at each time step reduces to a sequence of two steps:

- A prediction step which amounts to solve a Helmholtz-type vector equation derived from the momentum equation for the predicted velocity \mathbf{v}^* :

$$-\sigma \mathbf{v}^* + \nabla \cdot \mathcal{T}^* = \mathbf{s},$$

where $\sigma = 3 Re / (2 \Delta t)$, and the source term \mathbf{s} gathers all the explicit terms of equation (1), but the pressure gradient.

- A projection step adding the pressure gradient to the predicted velocity:

$$\mathbf{v}^n = \mathbf{v}^* + (2 \Delta t / 3) \nabla p,$$

such that \mathbf{v}^n satisfies the continuity equation (2). Hence, the pressure is deduced from the following Poisson equation:

$$\nabla^2 p = -\frac{3}{2 \Delta t} \nabla \cdot \mathbf{v}^*.$$

Let us now focus on the BCs at walls. As for the first step, Dirichlet BCs for tangential and normal velocity components are enforced. Concerning the projection step, the Poisson equation is supplemented by Neumann BCs which are deduced from the Dirichlet BC for the velocity projected onto the normal to the boundary (Eq. (3)).

3. MULTIDOMAIN IMPLEMENTATION

The case of several subdomains, possibly moving relatively to each other, is now described. The implementation of the BCs at the interface between two subdomains is first considered. Some details about sliding meshes are then given.

3.1 Interface Boundaries

Let us consider two subdomains, numbered 1 and 2 respectively, separated by an interface.

In the first step of the solution method, it can be shown [4] that the continuity of both the velocity vector field and the viscous tensor flux must be enforced across the interface. One solution would be to enforce the former condition on one face of the interface, and the latter on the opposite face. The programmer would then run into troubles when dealing with several meshes sliding one relatively to the others, since the BCs would have to be renewed during the sliding motion. Moreover, it would be difficult to guarantee that every interface has one type of BC on one of its faces, and the other on the other face.

Instead, it has been chosen here to enforce a linear combination of these two conditions as prescribed in equations (5) and (6). The source terms of these equations are then computed by evaluating the left-hand side, that is the velocity and the viscous tensor flux, from the neighbouring subdomain. As a consequence, the value of this linear combination is continuous across the interface. By assigning a similar expression on the other side of the interface, and provided that the coefficients α and β are different from one side to the other (they are actually taken of opposite sign), then it is easy to show that both the velocity and the tensor flux components are continuous.

However, the velocity and the viscous tensor are not known in advance, since they are part of the unknowns of the problem. Therefore, these conditions are incorporated into an iterative Schwarz-type technique. In the end, the interface BCs for the prediction step in subdomain 1 reads:

$$(v \cdot n)^{1,k} + \alpha (\mathcal{T} \cdot n)^{1,k} \cdot n = (v \cdot n)^{2,k-1} + \alpha (\mathcal{T} \cdot n)^{2,k-1} \cdot n, \quad (7)$$

$$(v \cdot t)^{1,k} + \beta (\mathcal{T} \cdot n)^{1,k} \cdot t = (v \cdot t)^{2,k-1} + \beta (\mathcal{T} \cdot n)^{2,k-1} \cdot t, \quad (8)$$

where the index k denotes the step level of the iterative Schwarz algorithm. It can be seen that when a converged state is reached, both linear combination expressions are continuous across the interface.

As for the projection step, it can be shown in a similar manner that the pressure and its flux must be continuous across the interface. Once again, instead of enforcing each condition on one of the two faces of the interface, a linear combination of these two conditions is used. Combined with the iterative Schwarz technique, we get:

$$p^{1,k} + \gamma (\nabla p)^{1,k} \cdot n = p^{2,k-1} + \gamma (\nabla p)^{2,k-1} \cdot n. \quad (9)$$

It must be noted that the coefficient γ , as well as α and β , are chosen in order to optimize the convergence rate of the Schwarz algorithm.

3.2 Sliding Meshes

The case for which the subdomains are sliding one relatively to the other is now considered. For the sake of simplicity, it is assumed that subdomain 1 is attached to the absolute frame of reference, and that subdomain 2 slides along the surface of subdomain 1 with respect to the moving frame velocity vector v_0 . The absolute velocity of a fluid particle in the absolute frame of reference is denoted by v^a , whereas the relative velocity of a particle viewed from the reference frame attached to subdomain 2 by v^r . Both velocities are related by the usual reference frame transformation rule:

$$v^a = v^r + v_0.$$

The equations are solved for the absolute velocity in both subdomains as follows. In the fixed subdomain 1, equation (1) reads:

$$\frac{\partial v^a}{\partial t} + \nabla \cdot (v^a \otimes v^a) = -\nabla p + \frac{1}{Re} \nabla \cdot \mathcal{T},$$

the pressure and the viscous tensor being frame-independent. In the moving subdomain 2, the momentum equation expressed in the relative frame

of reference reads:

$$\frac{\partial v^r}{\partial t} + \nabla \cdot (v^r \otimes v^r) + \frac{\partial v_0}{\partial t} = -\nabla p + \frac{1}{Re} \nabla \cdot \mathcal{T},$$

where $\partial/\partial t$ denotes a time derivative with respect to the moving frame. The time derivative of the moving frame velocity can be integrated in the first time derivative, since the moving frame velocity is frame-independent. In the end, the following equation has to be solved:

$$\frac{\partial v^a}{\partial t} + \nabla \cdot (v^r \otimes v^r) = -\nabla p + \frac{1}{Re} \nabla \cdot \mathcal{T}.$$

3.3 Data Exchange Strategy

Conservation is a key issue in multidomain computations. It is however difficult to achieve when non-matching sliding grids are used. In our case, conservation is a direct consequence of the interpolation technique at interfaces as described below.

All quantities in equations (7-8-9) are integrated over every faces of the subdomains, yielding their respective "integrated" functions. These latter functions are interpolated and exchanged from one subdomain to the other by means of an interpolation operator preserving the order of accuracy of the actual discretisation. The transmitted integrated functions are then derived in the receiving subdomain in order to recover the fields of interest.

This technique ensures that the integral of any field is the same on the two sides of an interface. Thereby, conservation is necessarily satisfied provided that the Schwarz iterative technique has reached a converged state, which turns out to be easily met thanks to the above mentioned optimisation of the coefficients α , β and γ .

4. NUMERICAL TEST CASE

In order to assess the validity of the present methodology, a 2D wind turbine-like configuration has been simulated. The problem consists of a tower represented by a circular cylinder of radius one, and a NACA-63-215 airfoil of unit length moving in front of the tower, perpendicularly to the main flow direction (see figure 1). The incoming wind speed is set equal to 1 at the bottom of the domain. Zero-shear stress BC ($\mathcal{T} \cdot n = 0$) is enforced at the outlet of the domain. Periodicity is assumed on the two lateral sides of the domain in the direction crosswise to the flow. The Reynolds number of the flow based on the airfoil chord and its velocity is 400. The width of the domain is equal to 11, so that the time-period for the airfoil motion is 2.75. At time $t = 0$, the airfoil is impulsively started right in front of the tower.

The isocontours of the crosswise velocity component at time $t = 3$ are plotted on figure 1.

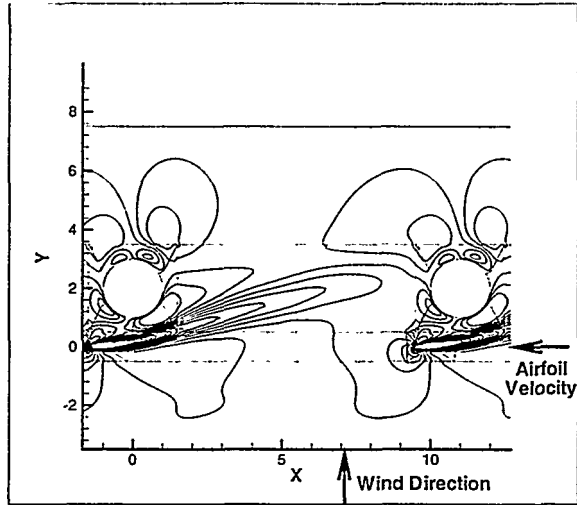


Figure 1: Isovalues of the crosswise velocity component

The boundaries of the several subdomains are also shown. For the purpose of visualisation, the tower and airfoil have been depicted two times. The wake of the airfoil can be clearly observed, which was expected for this relatively low Reynolds number.

The history of the pressure and viscous forces exerted on the bodies are reported on figure 2 and fig. 3, respectively. The drag on the airfoil is defined as the force in the direction crosswise to the main flow (the lift corresponds to the main flow direction). Conversely, the drag on the tower is the force in the streamwise direction. As it can be seen, the influence of the airfoil passing by the tower is quite high, especially when looking at the pressure forces.

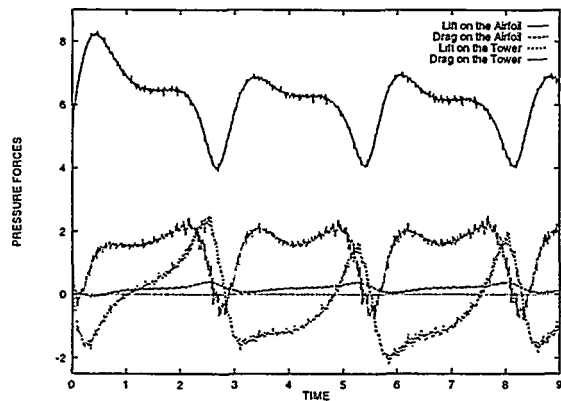


Figure 2: Pressure forces exerted on the bodies versus time

High-frequency oscillations can be observed on the curves of the pressure forces. They are believed to originate from the discrete motion of the sliding meshes, which may introduce numerical in-

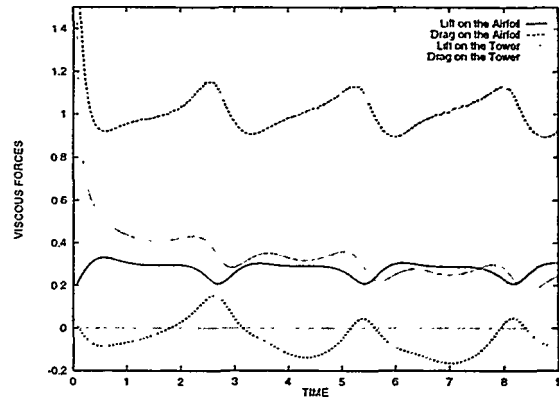


Figure 3: Viscous forces exerted on the bodies versus time

accuracies in the computed results.

5. CONCLUSION AND PERSPECTIVES

A numerical method for solving the Navier-Stokes equations for an incompressible fluid on several independent subdomains, possibly sliding relatively to each other, has been described. This methodology has been successfully applied to the simulation of a blade-tower interaction test-case. However, some further improvements are still required. Implementation of the numerical code on a parallel computer is in progress. A turbulence model will be implemented next in order to simulate high-Reynolds number flow.

In the future, comparisons of the computational data with experimental ones would also be relevant.

REFERENCES

- [1] F. Bertagnolio, O. Daube, *J. Comp. Phys.*, **138**, (1997), 121.
- [2] F. Bertagnolio, O. Daube, *Int. J. Numer. Meth. Fluids*, **28**, (1998), 917.
- [3] A. J. Chorin, *Math. Comput.*, **22**, (1968), 745.
- [4] A. Quarteroni, *Surv. Math. Ind.*, **1**, (1991), 75.

WHEN REAL LIFE WIND SPEED EXCEEDS DESIGN WIND ASSUMPTIONS

Martin Winther-Jensen
 Erik R. Jørgensen
 Risø National Laboratory
 P.O. Box 49
 DK-4000 Roskilde
 Denmark
 Phone: +45 4677 5035
 Fax: +45 4677 5083

E-mail: martin.winther@risoe.dk, erik.r.joergensen@risoe.dk

ABSTRACT: Most modern wind turbines are designed according to a standard or a set of standards to withstand the design loads with a defined survival probability. Mainly the loads are given by the wind conditions on the site defining the "design wind speeds", normally including extreme wind speeds given as an average and a peak value.

The extreme wind speeds are normally (e.g. in the upcoming IEC standard for wind turbine safety) defined as having a 50-year recurrence period. But what happens when the 100 or 10.000 year wind situation hits a wind turbine? Results on wind turbines of wind speeds higher than the extreme design wind speeds are presented based on experiences especially from the State of Gujarat in India.

A description of the normal approach of designing wind turbines in accordance with the standards is briefly given in this paper with special focus on limitations and built-in safety levels. Based on that, other possibilities than just accepting damages on wind turbines exposed for higher than design wind speeds are mentioned and discussed. The presentation does not intend to give the final answer to this problem but is meant as an input to further investigations and discussions.

Keywords: Extreme Wind Conditions , Failures , Load

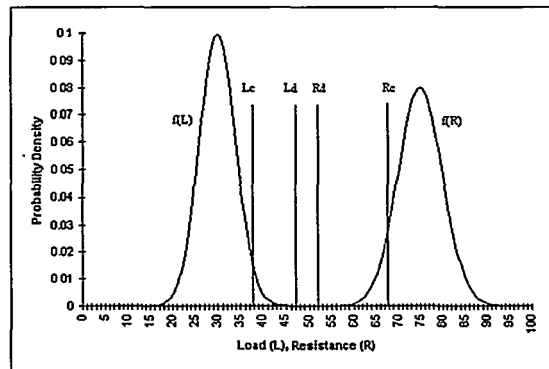
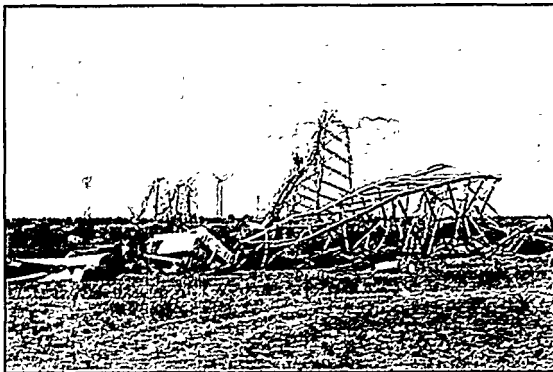


Figure 1: Load- and resistance-functions and characteristic and design values for load and resistance.

1 NORMAL DESIGN APPROACH (IEC-61400-1)

1.1 General

The normal way of designing wind turbines is to follow a set of standards and prove that the wind turbine can withstand the design loads with a defined survival probability. The standards can be national or international as e.g. the international standard IEC 61400-1, Ed. 2: Wind Turbine Generator Systems - Part 1: Safety Requirements [1]. This standard uses the principles of ISO 2394 defining the limit states and partial coefficients for loads, materials etc., which have to be applied to obtain the corresponding design values.

1.2 The Principles

The determination of the actual margins to the limit states is desirable because such margins can provide a measure of the actual safety obtained for the resistance. Interpretation of such values is not straightforward and presumable probabilistic methods have to be applied. It can be done combining the ultimate limit states and probability density functions for e.g. load and resistance.

The principles can be explained with reference to Figure 1. The probability density functions for load and resistance $f(L)$ and $f(R)$ are shown and the characteristic values for the same two functions are denoted L_c and R_c . These two values usually (as in ref. 1) correspond to 5 % fractile values of the involved variables. By applying the

appropriate partial coefficients on the variables the corresponding design values of the functions are obtained as L_d and R_d . The partial coefficients will normally be chosen to obtain the defined survival probability (if defined – in ref. 1 no survival probability is defined!) The difference between L_d and R_d is the reserve factor for the construction.

The probability density functions for the load and resistance respectively are here assumed as more or less well known, which is a qualified truth especially regarding the full resistance density function for the total construction. But this is not to be discussed in this paper.

1.3 Wind Conditions

Mainly the loads are defined by the wind conditions on the site. Normally these "design wind speeds" will among others include some extreme wind speeds given as an average value (e.g. a 10 minute value plus a turbulence level) and a peak value (e.g. a value of a few seconds).

In many standards - including ref. 1 - these extreme wind speeds are normally defined as having a 50-year recurrence period.

In Table 1 the extreme wind speed gusts are calculated according to ref. 1 and the national Danish Standard DS472: Loads and Safety on Wind Turbines [2]. Further the assumed peak wind speed value for the cyclone damaging the wind turbines in the Porbandar wind farms in the state of Gujarat in India is given.

Table 1 Wind Speeds 20 m above the ground based on a wind turbine with 40m-hub height.

According to	Extreme gust	
IEC 61400-1	64.9 m/s	WTG class I
	55.1 m/s	WTG class II
	48.6 m/s	WTG class III
DS 472 Danish Code	49.8 m/s	Roughness class 0
	48.7 m/s	Roughness class 1
Gujarat site	> 70.0 m/s	

1.4 Load Situations

In most standards including ref. 1 and ref. 2 it is normal practice only to combine an unusual load situation with normal operational modes for the wind turbine (except in case of common course failures).

To force the constructors to think about also unexpected situations some standards are defining "accidental load cases", normally defined as very unusual cases with an associated partial load factor on 1.0.

In neither ref. 1 nor ref. 2 the exceeding of the extreme design wind speeds is defined as an accidental load case. In fact ref. 1 does not define any accidental load cases at all.

2 INDIAN EXPERIENCES

2.1 General

During a mission to the State of Gujarat in India Oct./Nov. 1998 an expert team from Risø National Laboratory investigated the damages on wind turbines

located on the coast of Gujarat. The damages were caused by the passage of a tropical cyclone June 8 – 9 1998.

The objective of the mission was to investigate the accidents on the wind turbines on the Lamba, Navadra and Bhogat sites in Gujarat and to try to find explanations and top events of the incidents.

2.2 The Cyclone

In June 1998 the west coast of the Indian State of Gujarat was hit by a tropical cyclone. More than 2000 persons were killed and the damages on harbours, houses, roads, electrical grids etc. exceed 1 billion dollars.

The cyclone came from the Arabian Sea and passed among others through the three large wind turbine farms located near the city of Porbandar (Figure 2).

Measurements of wind speeds during the cyclone were done by MNES (Ministry of Non-Conventional Energy Sources) on six met-stations.

According to readings on the MNES met-mast in Haripar (located approx. 60 km to the NE of the wind turbine sites) an hourly mean wind speed of 42 m/s (152 km/h) was measured in 20 m height at 8 a.m. June 9 -98. At approx. 10 a.m. a gust wind speed of 65 m/s (232 km/h) were reached before the collapse of the met mast. It is assumed that the wind speeds on the wind turbine have been even higher.

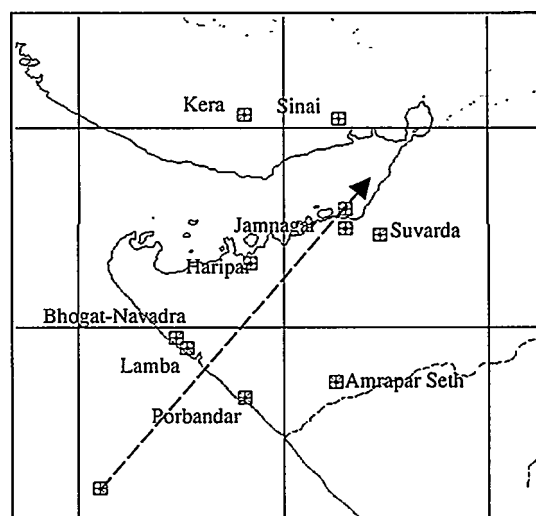


Figure 2 Track of Cyclone and location of MET-stations

Based on this reading and other evidence it is obvious that the wind speed at the coast has exceeded even 70m/s as a gust value.

It is also obvious that the wind speeds during the cyclone hereby have exceeded the design wind speeds for at least most of the turbines located in the wind farms. In general most of the turbines are designed to sustain a 10 minute mean wind speed (20 m above ground level) of approx. 37 m/s (133 km/h) and a 2 second gust wind speeds of approx. 50 m/s (179 km/h).

2.3 The Damages

In the three large wind farms close to Porbandar, (having an installed capacity of 85 MW in total) many

damages were reported. Out of 331 wind turbines in total 125 wind turbines were totally damaged. Further 29 wind turbines had serious damages (as broken blades or damages on major machine components) and 82 wind turbines had minor damages (as e.g. damages repairable at the site, minor cracks in the blades etc.).

It looks as if all wind turbines stopped as expected when the grid was cut off before the cyclone arrived. Some of the turbines started freewheeling during the passage of

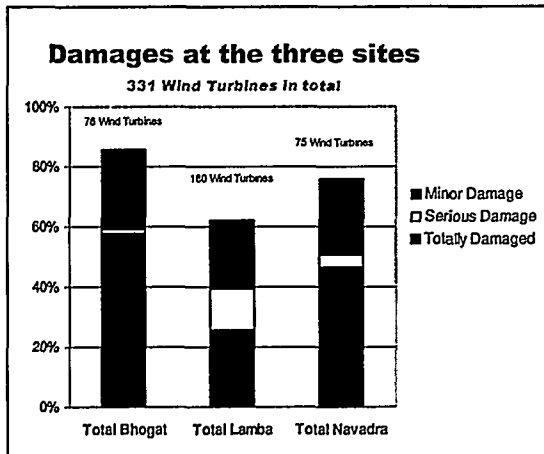


Figure 3 Damages at the three sites

the cyclone and failed because of that. Other turbines having no evidence of freewheeling during the passage of the cyclone failed probably because of too high trusts caused by the extreme high wind speeds. The wind farm location near Porbandar is normally defined as a low wind speed area often with annual capacity factors of less than 10%.

Assuming quadratic relationship between wind speed and loading, a lot of the turbines located at the sites were subjected to an increase in the loads of up to approx. 100% related to the design loads. This has to be compared with the partial load coefficient, which in ref. 1 is defined as 1.35 and in ref. 2 as 1.3.

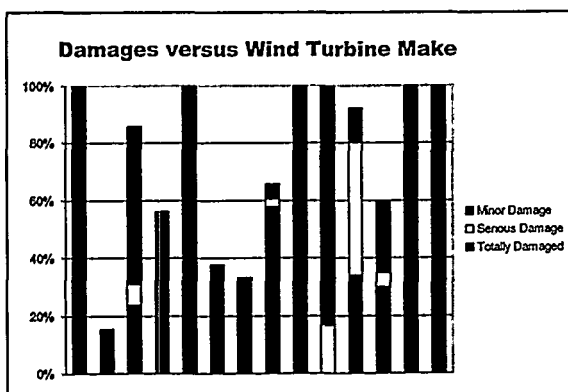


Figure 4 Damages versus make

3 RECOMMENDATIONS

3.1 General

In many standards - including ref. 1 - the extreme wind speeds are normally defined as having a 50-year recurrence period. Further it is normal practice only to combine an unusual load situation with normal operational modes for the wind turbine and vice versa.

Together with the acceptance of a 5 % fractile value for the materials, it shows that a certain level of failures and/or incidents are acceptable in the lifetime of a population of wind turbines even if the design assumptions including partial coefficients are fulfilled.

This attitude is generally accepted not only for wind turbines but also for most constructions. But in our opinion there is a big difference in just calculating in accordance with the standards and to include considerations on events just outside the "standardised" scope, as: what happens if the 100 or 10.000 year situation hits a wind turbine?

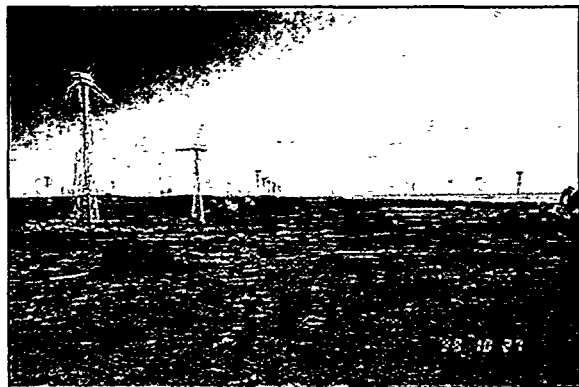
It doesn't necessarily mean to include new normal load cases. The load cases can e.g. be defined as accidental load cases or the wind turbines can be equipped with systems securing it against dangerous situations. But the considerations about this kind of situations are important and have to include the exact possibility of a given situation.

In some standards other values than the 50-year situation for the loads are defined as the reference (e.g. some offshore standards use the 100-year situation instead). It is also known that big constructions as bridges etc. are often calculated with a higher recurrence period than 50 years.

3.2 Site Assessment

The Porbandar area has not been defined as an area with high cyclone risk so the incident was unexpected. But the incident shows the importance of accurate site assessments.

3.3 If Cyclones are Expected



In areas where cyclones are expected normally the choice will be not to erect wind turbines. But if the possibility of cyclones is acceptable the wind turbines have to be designed to withstand the expected loads with a given

possibility. Here considerations regarding e.g. installation of extra devices to secure the wind turbine during very high wind speeds, or a definition of a special accidental load case as mentioned above can be relevant.

4 CONCLUSIONS

The reason for the damages on the wind turbines located on the Porbandar sites was wind speeds much higher than the design values. Some of the protection systems (as mechanical and/or aerodynamic brakes) were not sufficient at these wind speeds and because of that a lot of turbines began freewheeling resulting in - for most of the turbines - serious failures. Other turbines collapsed or failed during stand still because of too high wind pressure.

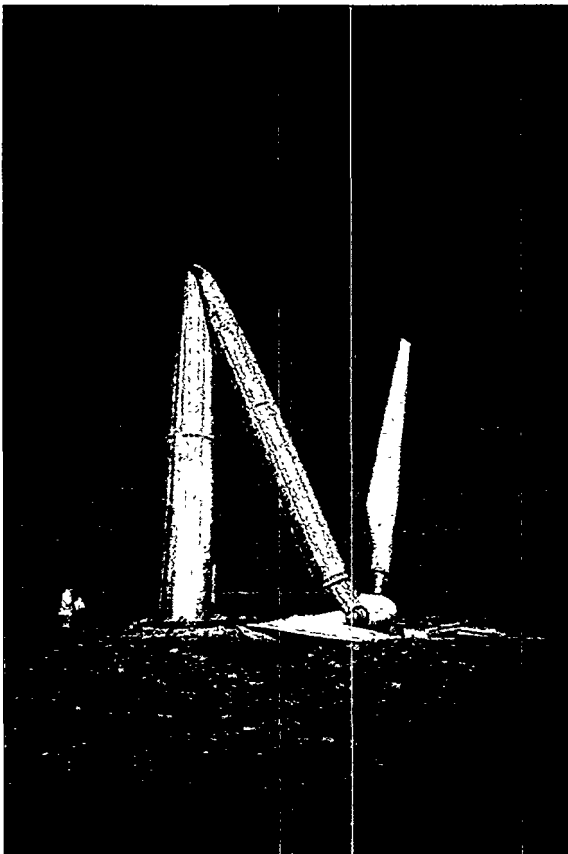
To ensure that wind turbines are not brought in unexpected situation e.g. because of cyclones, accurate site assessments are very important.

In areas with "acceptable cyclone risks" consideration on definition of special load cases (e.g. including accidental load cases) or installation of special devices to prevent the turbines being brought in unexpected situations are recommended.

The same arguments can be used for wind turbines erected on more normal sites (as e.g. offshore sites) to insure that the all assumptions are fulfilled.

REFERENCES

- [1] IEC 61400-1, Ed. 2 Wind Turbine Generator Systems - Part 1: Safety Requirements, FDIS 1998-12-15
- [2] Danish Standard DS472, Loads and safety on Wind turbines, DS, May 1992
- [3] European Wind Turbine Standards II, EUREC-Agency's, Draft issued June 1998



VARIABILITY OF EXTREME FLAP LOADS DURING TURBINE OPERATION

Knut O. Ronold
Det Norske Veritas
P.O. Box 300
N-1322 Høvik, NORWAY
phone: +47-67577311
e-mail: knut.ronold@dnv.com

Gunner C. Larsen
Wind Energy and Atmospheric Physics Dept.
Risø National Laboratory
DK-4000 Roskilde, DENMARK
phone: +45-46775056
e-mail: gunner.larsen@risoe.dk

ABSTRACT: The variability of extreme flap loads is of utmost importance for design of wind-turbine rotor blades. The flap loads of interest consist of the flapwise bending moment response at the blade root whose variability in the short-term, for a given wind climate, can be represented by a stationary process. A model for the short-term bending moment process is presented, and the distribution of its associated maxima is derived. A model for the wind climate is given in terms of the probability distributions for the 10-minute mean wind speed and the standard deviation of the arbitrary wind speed. This is used to establish the distribution of the largest flapwise bending moment in a specific reference period, and it is outlined how a characteristic bending moment for use in design can be extracted from this distribution. The application of the presented distribution models is demonstrated by a numerical example for a site-specific wind turbine.

KEYWORDS: Wind climate – wind speed variability – extreme response

1. INTRODUCTION

The verification of the structural integrity of a wind turbine involves analyses of fatigue loading as well as extreme loading of the different structural components. With the trend of persistently growing turbines, the extreme loading seems to become relatively more important. Hence, also the natural variability of such extreme loads gain in importance as a topic that needs thorough attention to ensure an acceptably low failure probability.

Several extreme failure modes need consideration, of which the extreme loading under turbine operation is one of significant importance. During operation, the turbine loading consists of a periodic deterministic part and a superimposed stochastic part. The mean wind field and gravity cause the deterministic part. The stochastic part originates from the natural variability of the wind turbulence components.

A methodology for representation of the extreme flapwise loading of a rotor blade and its natural variability is proposed. The procedure is based on extensive measurements on a turbine sited in a flat and homogeneous terrain, and it provides probabilistic models for the wind loading and its transfer to extreme responses, conditional on the wind climate. The wind climate is parameterized by only two wind field characteristics - the 10-minute mean wind speed and the standard deviation of the wind speed, both referring to the hub height of the wind turbine. The distribution of the global extreme in a 1-year reference period is finally established by assuming the mean wind speed to be Weibull-distributed in the long term with parameters as given in the IEC-61400 code.

2. THEORY

The wind climate that governs the loading of a wind turbine and its rotor blades is commonly described by the 10-minute mean wind speed U_{10} at the site in conjunction with the standard deviation σ_U of the wind speed. The

long-term distribution of the 10-minute mean wind speed can be taken as a Weibull distribution

$$F_{U_{10}}(u) = 1 - \exp\left(-\left(\frac{u}{A}\right)^k\right) \quad (1)$$

in which k and A are site- and height-dependent coefficients. Only normal operation of the wind turbine is considered. The turbine will stop whenever the cut-out wind speed u_C is exceeded. For analysis of failure in ultimate loading in the normal operating condition, it is therefore of interest to represent the 10-minute mean wind speed by a Weibull distribution, whose upper tail is truncated at the cut-out speed,

$$F_{U_{10}}(u) = \frac{1 - \exp\left(-\left(\frac{u}{A}\right)^k\right)}{1 - \exp\left(-\left(\frac{u_C}{A}\right)^k\right)}; \quad 0 < u < u_C \quad (2)$$

This is the cumulative distribution function of the 10-minute mean wind speed in an arbitrary 10-minute period whose mean wind speed does not exceed the threshold u_C . Ideally, also the lower tail of the distribution should have been truncated, viz. at the cut-in wind speed, below which the turbine is not operated. However, such a lower-tail truncation would not have any practical significance in an extreme loading analysis and it has therefore been left out. The 10-minute mean wind speed may be interpreted as a measure of the intensity of the wind climate. The higher the 10-minute mean wind speed, the more severe is the wind climate.

The standard deviation σ_U of the wind speed depends on the 10-minute mean wind speed U_{10} . The distribution of σ_U conditioned on U_{10} can be well represented by a log-normal distribution

$$F_{\sigma_U}(s) = \Phi\left(\frac{\ln s - b_0}{b_1}\right) \quad (3)$$

in which $\Phi()$ denotes the standard Gaussian cumulative distribution function, and the coefficients b_0 and b_1 depend on U_{10} as follows

$$b_0 = c_0 + c_1 \ln U_{10} \quad (4)$$

$$b_1 = d_0 + d_1 \exp(-d_2 U_{10})$$

One rotor blade is considered in the following. Let X denote the bending moment at the blade root in flapwise bending. The bending moment process X is characterized by its mean value μ , standard deviation σ , skewness α_3 , kurtosis α_4 , and regularity factor α . Based on the first four moments, the marginal distribution of X can be represented by a Hermite moment transformation (fourth-moment Hermite polynomial expansion) of a standard Gaussian variable U . Reference is made to Winterstein (1988). For kurtosis $\alpha_4 > 3$, the transformation reads

$$X = \mu + \kappa \sigma (U + c_3 (U^2 - 1) + c_4 (U^3 - 3U))$$

$$c_4 = \frac{\sqrt{1+36h_4}-1}{18}; \quad h_4 = \frac{\alpha_4-3}{24} \quad (5)$$

$$c_3 = \frac{h_3}{1+6c_4}; \quad h_3 = \frac{\alpha_3}{6}$$

$$\kappa = \frac{1}{\sqrt{1+2c_3^2+6c_4^2}}$$

For kurtosis $\alpha_4 < 3$, the transformation reads

$$X = \mu + \sigma ((\sqrt{c^2+k}+c)^{1/3} - (\sqrt{c^2+k}-c)^{1/3} - a)$$

$$c = 1.5b(a+U) - a^3 \quad (6)$$

$$b = -\frac{1}{3h_4}; \quad h_3 = \frac{\alpha_3}{6}$$

$$a = \frac{h_3}{3h_4}; \quad h_4 = \frac{\alpha_4-3}{24}$$

$$k = (b-1-a^2)^3$$

In either case, the transformation is monotonous, which in particular implies that local maxima of the underlying Gaussian process U are transformed to local maxima of X . Note that the processes X and U will have the same number of local maxima and the same regularity factor. Consider now an arbitrary 10-minute period during which the 10-minute mean wind speed can be considered constant equal to a realization of the distribution in Eq. (2). The largest maximum X_{\max} in an arbitrary 10-minute period is dealt with in the following. Consider now the corresponding maximum U_{\max} of the underlying standard Gaussian process U . The distribution of local maxima of U is a Rice distribution, see Rice (1944). This implies that the distribution of U_{\max} is an extreme-value distribution, which can be approximated by

$$F_{U_{\max}}(u) = \exp(-\alpha N_{\max} \exp(-\frac{u^2}{2})) \quad (7)$$

where α is the regularity factor and N_{\max} is the number of local maxima in 10 minutes. Reference is made to Ronold (1993). Once U_{\max} has been determined from this distribution, X_{\max} can be found from U_{\max} through the transformations in Eqs. (5) and (6). Note in the present context that U is a standard notation for a normally distributed variable or a Gaussian process and is not to be confused with any wind speed.

3. NUMERICAL EXAMPLE

Wind climate data are available from an on-shore location at Lammefjord in Denmark and are used in conjunction with load measurement data from a 600 kW wind turbine with three 21.5 m long rotor blades.

The wind loading regime at the chosen location is characterized by a scale parameter $A=9.1$ m/sec and a shape parameter $k=1.9$. The cut-out wind speed for the turbine is $u_c=25$ m/sec. A reference period of one year is considered in the following. There are 52560 10-minute periods during this time span. Provided no operational failures occur, the turbine will be in its operating condition during $N=52503$ of these 10-minute periods as determined from the frequency of wind speeds beyond the cut-out speed.

As described in a previous section, the distribution of the standard deviation σ_U of the wind speed, conditioned on the 10-minute mean wind speed U_{10} , can be represented by a lognormal distribution

$$F_{\sigma_U}(s) = \Phi\left(\frac{\ln s - b_0}{b_1}\right) \quad (8)$$

Based on the available wind climate data from the considered location, the coefficients b_0 and b_1 are represented as functions of U_{10} as follows

$$b_0 = -2.1601 + 1.0326 \ln U_{10} \quad (9)$$

$$b_1 = 0.0579 + 0.6169 \exp(-0.1709 U_{10})$$

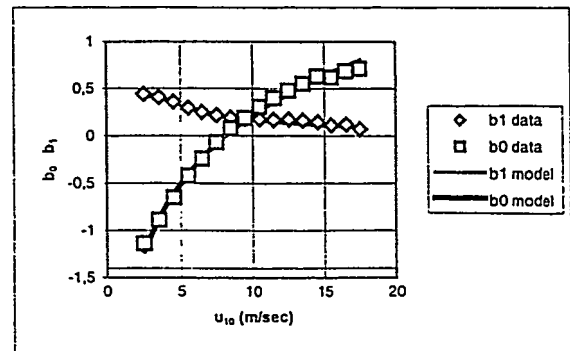


Figure 1 Data and model for distribution parameters b_0 and b_1 for distribution of standard deviation of wind speed

Figure 1 shows the data points, which are condensed from fits of the empirical distributions conditional on the 10-minute mean wind speed, and which support the two relationships of Eq. (9). Figure 2 gives an example of such a conditional empirical distribution.

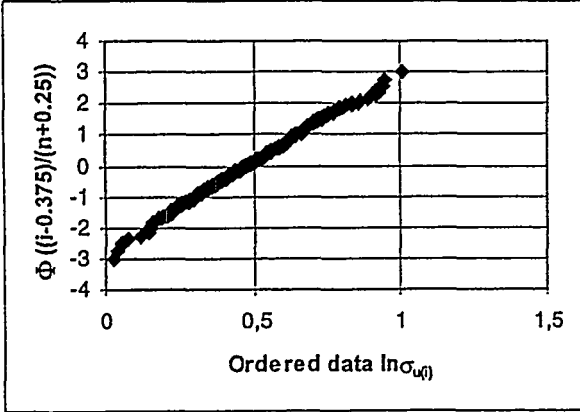


Figure 2 Normal scores plot for natural logarithm of observations of standard deviation of wind speed for $u_{10}=12-13$ m/sec. The straight line indicates a normal distribution of the logarithm, and the coefficients of the line provide one set (b_0, b_1) in Figure 1.

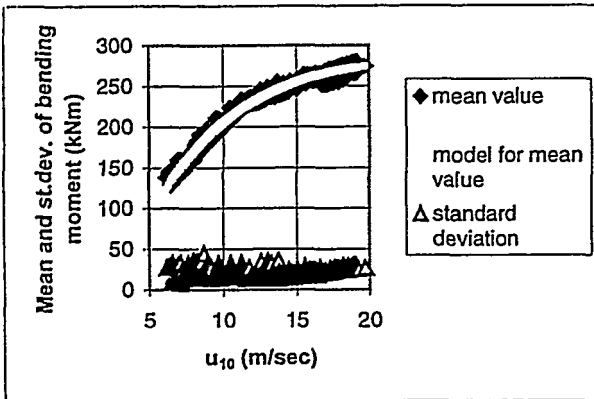


Figure 3 Mean value and standard deviation of bending moment response process vs. 10-minute mean wind speed

A total of 642 10-minute records of the flapwise bending moment response process X at the blade root for various realizations of the 10-minute mean wind speed U_{10} are available from this campaign. Based on these data, the mean value μ and the standard deviation σ of the response process conditional on U_{10} are represented as functions of U_{10} and σ_U .

$$\mu = -156.77 + 213.45\sqrt{U_{10} - 2.1796} - 23.488U_{10} \quad (10)$$

$$\sigma = 17.545 - 1.9038U_{10} + 0.0939U_{10}^2 + 76.478\frac{\sigma_U}{U_{10}} + 335.87\left(\frac{\sigma_U}{U_{10}}\right)^2 \quad (11)$$

These functions were selected as the ones that give the best fits to available measurement data. Reference is made

to Figure 3. For 10-minute mean wind speeds in excess of 15 m/sec, which is of practical interest here, the data indicate very stable and well-determined values of the skewness α_3 and the kurtosis α_4 of the bending moment response process X , and they can both be modelled as constants

$$\alpha_3 = -0.0066 \quad \text{and} \quad \alpha_4 = 2.8174 \quad (13)$$

Note that these values for skewness and kurtosis indicate a response process whose marginal distribution is very close to a Gaussian distribution in the high wind speed range. This may be reasonable for flapwise bending, which is considered here. For edgewise bending, where the response has a significant sinusoidal term owing to the effects of gravity, the marginal distribution of the response process will be far from any Gaussian distribution, in particular because its kurtosis will be much smaller than 3.0. Based on available data, the regularity factor of the bending moment response process is represented as a function of U_{10} as follows,

$$\alpha = 0.02954 \arctan(1.1541(U_{10} - 11.701)) + 0.16636 \quad (14)$$

and the number of local maxima of this process in 10 minutes is

$$N_{\max} = 336.86 \arctan(0.4857(U_{10} - 11.609)) + 2016.0 \quad (15)$$

These functions were selected as the ones that gave the best fits to available measurement data. The above suffices to produce the distribution of the maximum bending moment response in 10 minutes, cfr. Eqs. (5), (6), and (7).

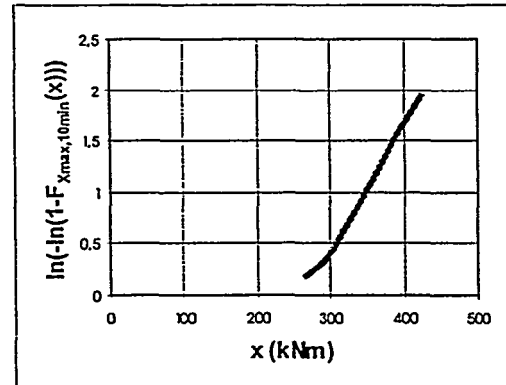


Figure 4 Upper tail of distribution of maximum flapwise bending moment in arbitrary 10-minute period

The distribution of the maximum bending moment response X_{\max} in an arbitrary 10-minute period can be determined on the basis of the distribution models, which are described above, i.e. the distribution models for

- the 10-minute mean wind speed U_{10}
 - the wind speed standard deviation σ_U conditional on U_{10}
 - the bending moment X_{\max} conditional on U_{10} and σ_U .
- The distribution of X_{\max} can best be achieved by means of a Monte-Carlo simulation that capitalizes on these three

distribution models. This in particular gives the upper tail of the unconditional distribution of X_{\max} , denoted $F_{X_{\max},10\min}(x)$, as shown in Figure 4. It appears that this upper tail is well represented by a Weibull distribution for $\exp(X_{\max})$, since Figure 4 shows a straight line in a Weibull probability plot for $\exp(X_{\max})$.

Under an assumption of independence between the $N=52503$ 10-minute bending moment response maxima during one year of operation, the distribution of the annual maximum of the bending moment response can be found as

$$F_{X_{\max},1\text{yr}}(x) = F_{X_{\max},10\min}(x)^N \quad (16)$$

and its upper tail can be represented as shown in Figure 5. For design in ultimate loading, the 98% quantile of the annual maximum load is traditionally used as the characteristic bending moment value, $X_{\max,c}$, see Madsen et al. (1986). The 98% quantile can be read off from this figure, and gives the following characteristic bending moment

$$X_{\max,c} = X_{\max,1\text{yr},98\%} = 482.5 \text{ kNm} \quad (17)$$

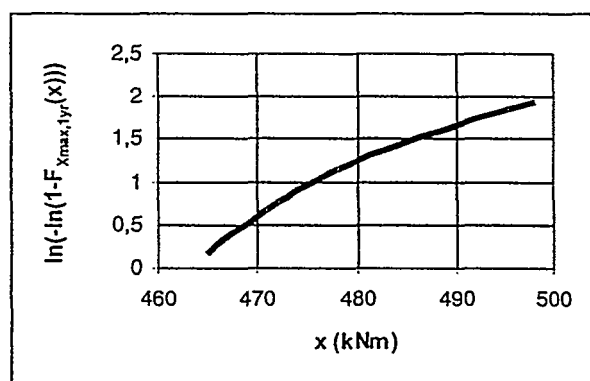


Figure 5 Upper tail of distribution of annual maximum of flapwise bending moment

4. CONCLUSIONS

A model for the distribution of the extreme value of the flapwise bending moment response of a rotor blade during turbine operation has been established. The wind climate

as expressed in terms of the 10-minute mean wind speed and the standard deviation of the wind speed has been modelled in terms of their respective probability distributions. Further, the bending moment response process in the rotor blades, conditioned on the wind climate, has also been modelled. This has been used to establish a model for the extreme load, i.e. the distribution of the largest bending moment response in an arbitrary 10-minute period with an approximately stationary wind climate. The model has been used to establish the distribution of the largest bending moment response in a specified reference period, and it has been demonstrated how the characteristic bending moment response for design can be extracted from such a distribution. The application of the presented distribution models has been illustrated by a numerical example for a site-specific wind turbine of prescribed make.

5. ACKNOWLEDGMENTS

The work presented herein is partly funded by the European Commission within the framework of the Non-Nuclear Energy Program Joule III, under contract no. JOR3-CT95-0026, and partly by the Danish Energy Agency. These contributions are gratefully acknowledged.

6. REFERENCES

- [1] Madsen, H.O., S. Krenk, and N.C. Lind, *Methods of Structural Safety*, Prentice-Hall Inc., Englewood Cliffs, N.J., 1986.
- [2] Rice, S.O., "Mathematical Analysis of Random Noise", *Bell System Technical Journal*, Vol. 23, pp. 282-332, and Vol. 24, pp. 46-156, 1944, reprinted in *Selected Papers in Noise and Stochastic Processes*, ed. N. Wax, Dover, N.Y., 1954.
- [3] Ronold, K.O., "Reliability of Marine Clay Foundations in Cyclic Loading", *Ph.D. thesis*, Stanford University, Stanford, Cal., 1993.
- [4] Winterstein, S.R., "Nonlinear Vibration Models for Extremes and Fatigue", *Journal of Engineering Mechanics*, ASCE, Vol. 114, No. 10, pp. 1772-1790, 1988.

GRID IMPACT OF VARIABLE-SPEED WIND TURBINES

Åke Larsson

Chalmers University of Technology
Dept. of Electric Power Engineering
S-412 96 Göteborg
SWEDEN
phone: +46 31 772 1642
fax: +46 31 772 1633
mail: ake.larsson@elkraft.chalmers.se

Poul Sørensen

Risø National Laboratory
P.O.Box 49
DK-4000 Roskilde
DENMARK
phone: +45 4677 5075
fax: +45 4677 5083
mail: poul.e.soerensen@risoe.dk

Fritz Santjer

German Wind Energy Institute, DEWI
Ebertstr. 96
D-6382 Wilhelmshaven
GERMANY
phone: +49 44 21 48 08 22
fax: +49 44 21 48 08 43
mail: f.santjer@dewi.de

ABSTRACT: In this paper the power quality of variable-speed wind turbines equipped with forced-commutated inverters is investigated. Measurements have been taken on the same type of variable-speed wind turbines in Germany and Sweden. The measurements have been analysed according to existing IEC standards. Special attention has been paid to the aggregation of several wind turbines on flicker emission and harmonics. The aggregation has been compared with the summation laws used in the draft IEC 61400-21 "Power Quality Requirements for Grid Connected Wind Turbines".

The methods for calculating and summing flicker proposed by IEC Standards are reliable. Harmonics and interharmonics are treated in IEC 61000-4-7 and IEC 61000-3-6. The methods for summing harmonics and interharmonics in IEC 61000-3-6 are applicable to wind turbines. In order to obtain a correct magnitude of the frequency components, the use of a well-defined window width, according to IEC 61000-4-7 Amendment 1 is of a great importance.

Keywords: Power Quality, Variable-Speed Operation, Grid, Power Factor

1 INTRODUCTION

The grid interaction and grid impact of wind turbines has been put into focus during the last few years. The reason behind this interest is that wind turbines are among utilities considered being potential sources of bad power quality. Measurements show that the power quality impact at wind turbines has been improved in the last years. Especially variable-speed wind turbines have advantages concerning flicker. But a new problem is faced with variable-speed wind turbines. Modern forced-commutated inverters used in variable-speed wind turbines produce not only harmonics but also interharmonics.

The purpose of this work is to investigate the power quality of variable-speed wind turbines equipped with forced-commutated inverters. The measurements have been analysed according to IEC standards. Special attention has been paid to the aggregation of several wind turbines on flicker emission and harmonics.

2 SITES

Measurements have been taken on a wind farm consisting of five variable-speed wind turbines in Germany, and at one variable-speed wind turbine in Gotland, Sweden.

In Germany measurements at the Emden wind park have been performed by DEWI. The measurements were taken simultaneously at the low voltage side of two Enercon E-40 wind turbines. The measurements are divided into two different types:

1. Flicker measurements performed at a sampling frequency of 800 Hz. From the measured voltages and currents, active power and phase angle has been calculated. The sampling frequency of the calculated values is 50 Hz and the length of each measurement is 10 minutes.
2. Harmonics measurements performed at a sampling frequency of 12 800 Hz.

Chalmers University of Technology has performed measurements at the island of Gotland in Sweden. At Gotland the site consists of two Enercon E-40, but measurements were taken only at one Enercon. The measurements are divided into two different types:

1. Flicker measurements performed at a sampling frequency of 500 Hz. The cut-off frequency of the anti-alias filter is 104 Hz and the length of each measurement is 10 minutes.
2. Harmonics measurements performed at a sampling frequency of 5 000 Hz.

3 FLICKER

In order to determine the flicker emission produced by a wind turbine, measurements must be performed. IEC 61400-21 warns that flicker emission should not be determined from voltage measurements, as this method will be influenced by the background flicker of the grid [1]. Two methods are proposed to overcome this problem. One is based on the measurement of active and reactive power, and the other method is based on the measurement of current and voltage. The short-term flicker emission from the wind turbine should be calculated by means of a reference grid using the measured active and reactive power as the only load on the grid.

The flicker is calculated using a PC-program developed by Risø National Laboratory [2]. This program uses IEC 60868, Amendment 1 to calculate the P_{st} [3-4]. The input to the program are time series of active and reactive power, short circuit power and the phase angle of the grid.

Figure 1 shows the short-term flicker emission P_{st} from a Enercon E-40 at different mean values of the produced power. In this particular case, a short-circuit power of 20 times the rated power of the wind turbine and a grid angle of 45 degrees are used. As can be seen in Figure 1, the flicker emission P_{st} is increasing at higher wind speeds due to higher turbulence in the wind. The flicker level is low, almost 4 times lower than the

flicker produced by the fixed-speed Wind World 600 kW. Measurements performed on the fixed-speed turbine using the same equipment and flicker algorithm gives a short-time flicker emission $P_{st}=0,46$.

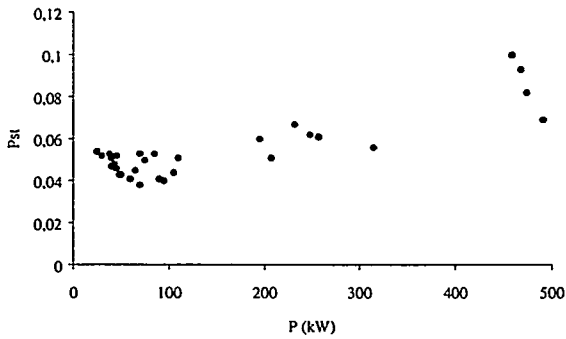


Figure 1: Short term flicker emission P_{st} from an E-40 at different mean value of the produced power.

3.1 Flicker Coefficient

According to IEC 61400-21, the flicker coefficient from wind turbines shall be determined by applying:

$$c(\psi_k) = P_{st, fic} \frac{S_{k, fic}}{S_{ref}} \quad (1)$$

where $c(\psi_k)$ is the flicker coefficient and S_{ref} is the rated active power of the wind turbine. $P_{st, fic}$ is the flicker emission level calculated at the short-circuit power of a fictitious reference grid $S_{k, fic}$ with grid angle ψ_k .

The flicker emission produced by a wind turbine connected to a grid with an arbitrary short-circuit power may then be recalculated by:

$$P_{st} = c(\psi_k) \frac{S_k}{S_{ref}} \quad (2)$$

3.2 Summation of Flicker

According to IEC 61400-21, the following equation applies for determining the flicker contribution from several wind turbines connected to a common point:

$$P_{st \Sigma} = \sqrt{\sum P_{st, i}^2} \quad (3)$$

where $P_{st, i}$ is the flicker emission from the individual single wind turbine.

Figure 2 shows the calculated short-term flicker emission from ten different measured time series of two Enercon E-40. The P_{st} is calculated in two different ways:

1. Directly by using the sum of the time series of power from the wind turbines.
2. By the use of equation 3.

As can be seen in the figure, the short-term flicker emission varies due to variations in the wind, i.e. turbulence. The mismatch of the two different ways of calculating the flicker (i.e. deviation from the dotted line) is although small.

4 HARMONICS AND INTERHARMONICS

Harmonics and interharmonics are defined in IEC 61000-4-7 and Amendment 1 [5][6]. The definition of harmonics is components at frequencies which are multiples of the supply frequency, i.e. 100 Hz, 150 Hz, 200 Hz etc. Interharmonics are in a similar way defined as components of frequencies located between the harmonics of the supply frequency.

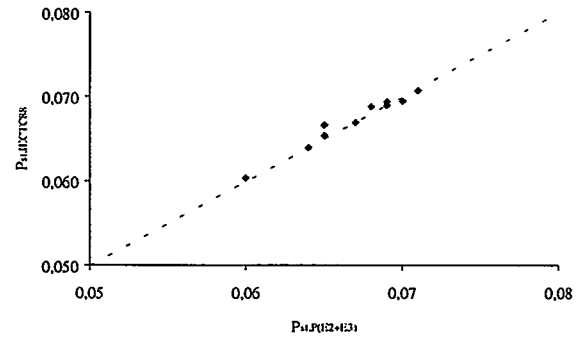


Figure 2: Calculated short term flicker emission from ten different measured time series of two Enercon E-40.

The signal, which is to be analysed, is sampled, A/D-converted and stored. These samples form a window of time ("window width") on which discrete Fourier transform is performed. The window width shall, according to the standard, be 10 line-periods in a 50 Hz system. This window width will give a distance between two consecutive interharmonic components of 5 Hz. Figure 3 shows the interharmonic components in the measured current from an Enercon E-40 at Gotland. The current is analysed in accordance with IEC 61000-4-7.

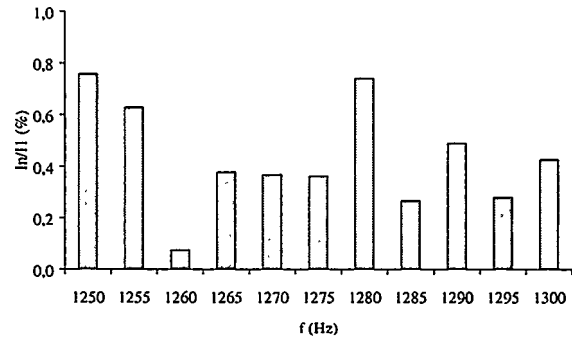


Figure 3: Current interharmonics content between 1250-1300 Hz.

The rms value of all interharmonics components between two consecutive harmonic frequencies forms an interharmonic group. The interharmonic group frequency is the centre frequency of the harmonic frequency between which the group is situated. That is, a group between the harmonic orders n and $n+1$ is designated with $n+0.5$, i.e. the group between $n=5$ and $n=6$ is designated $n=5.5$.

Figure 4 shows the harmonics and interharmonic groups of order 20 to 25 of the measured current from an Enercon E-40 at Gotland.

4.1 Impact of window size

The window width shall according to IEC 61000-4-7 be 10 line-periods in a 50 Hz system. A 10 line-period window width gives, as illustrated in Figure 4, a distance between two consecutive interharmonic components of 5 Hz.

If a window width of 16 lineperiods is used, the distance between two consecutive interharmonic components will be 3.125 Hz. The use of the larger window decreases the distance between two consecutive interharmonic components. As a

consequence, each interharmonic component will have a lower content.

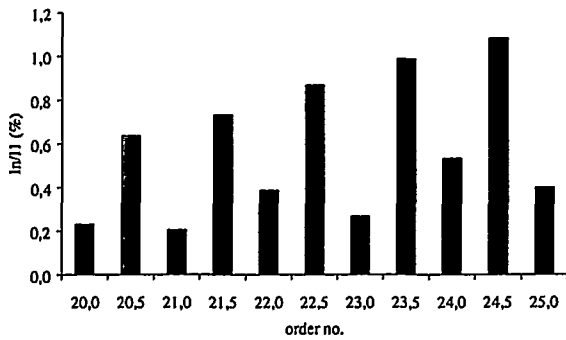


Figure 4: Current harmonics and interharmonic group.

Figure 5 shows the harmonics content in the same current using a window width of 10 and 16 lineperiods. As can be seen, the harmonic content will be larger in the smaller window. Note: an exact comparison can not be made since one window is 16 line-periods and the other just 10 line-periods.

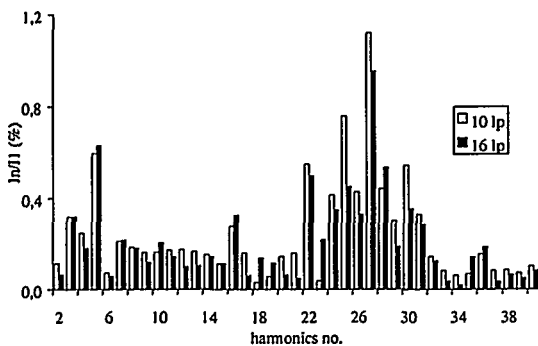


Figure 5: Harmonics content in current using a window width of 10 and 16 line-periods, respectively.

4.2 Harmonics

The Enercon wind turbine is equipped with a 12-pulse inverter using IGBT valves. This implies that the first harmonics should appear around the switching frequency of the IGBT. The switching frequency of IGBTs can be rather high (5-10 kHz). The switching frequency must not be fixed, the controller could either employ a PWM pattern or it could be of the simple on off type having a small histories band which creates a lower limit for the time interval between two subsequent switching operations.

Figure 6 shows the harmonics content on the low voltage side of Enercon E-40. The measurements originate from two different sites, Emden in Germany and Gotland in Sweden. As can be seen in the figure, the harmonics content in the current from the two sites are almost identical. The largest discrepancy is on the 2:nd-order harmonic, where the content at Gotland is 0,65% while it only is 0,2% at Emden. The large 2:nd order harmonic at Gotland does most likely depend on lack of phase-lock on the measurement equipment used at Gotland. The switching frequency of the IGBTs is, as mentioned earlier, not fixed and it seems to be around 1 to 1,5 kHz, i.e. harmonics of order 20 – 30. In the figure a whole range of harmonics between 20 and 30 can be noticed. The harmonics content in Figure 6 is calculated as a mean value over several seconds. The current also contains lower harmonics, for example 3rd, 5th and 7th order. These harmonics may originate from two different sources. A simple control of an inverter is simply to generate a current with the same shape as the voltage. If the voltage

contain lower order harmonics, the current will also contain lower order harmonics. In the Enercon, there are also other control equipment's and inverters used. For example, each blade has an electrical pitch mechanism by means of an electrical drive system. Grid-commutated inverters generate harmonics of order 5th, 7th, 11th, 13th, etc. and single phase switched equipment generates harmonics of 3rd order.

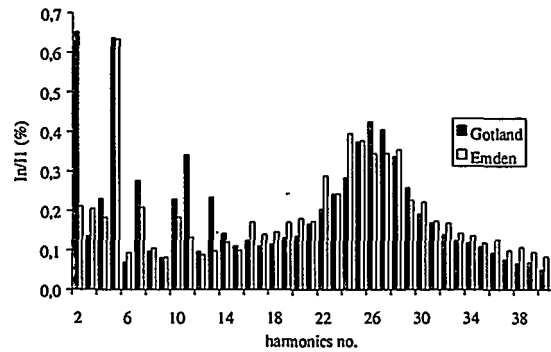


Figure 6: Current harmonics content on low side of transformer.

4.3 Summations of Harmonics

According to the IEC 61000-4-7, the following equation applies for determining the harmonic currents from more than one source connected to a common point [7]:

$$I_{n,tot} = \sqrt{\sum_i I_{n,i}^a} \quad (4)$$

where i_n is the harmonic current of the order n , $i_{n,k}$ is the harmonic current of the order n from source number k and α is an exponent chosen from Table 3.1.

Table 3.1: Summation exponents for harmonics.

a	harmonic order
1	$h < 5$
1,4	$5 \leq h \leq 10$
2	$h > 10$

Figure 7 shows the harmonics content from the sum of two Enercon and the calculated content. The harmonics content from the sum of the two Enercon is derived from the sum of the measured time series of the current. The calculated harmonics content has been performed by equation 4 and the harmonics content of each Enercon.

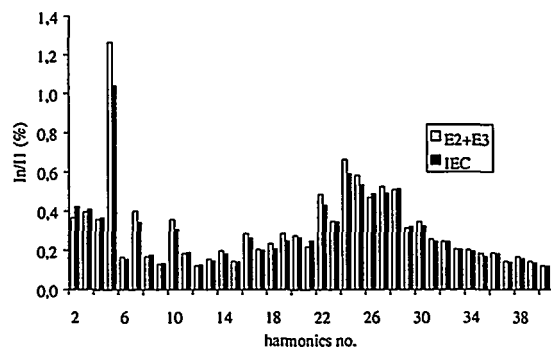


Figure 7: Calculated harmonics content from two different Enercon E-40 by means of the time series of current and by means of equation 4.

4.4 Interharmonics

Enercon wind turbines do not only produce harmonics, they also produce interharmonics, i.e. harmonics which are not a multiple of 50 Hz. Since the switching frequency of the inverter is not constant but varies, the harmonics will also vary. Consequently, since the switching frequency is arbitrary the harmonics are also arbitrary. Some times they are a multiple of 50 Hz and some times they are not. Figure 8 shows the total harmonics spectrum from one Enercon. As can be seen in the figure, at lower frequencies there are only pure harmonics but at higher frequencies there are a whole range of harmonics and interharmonics. This whole range of harmonics and interharmonics represents variations in the switching frequency of the Enercon inverter.

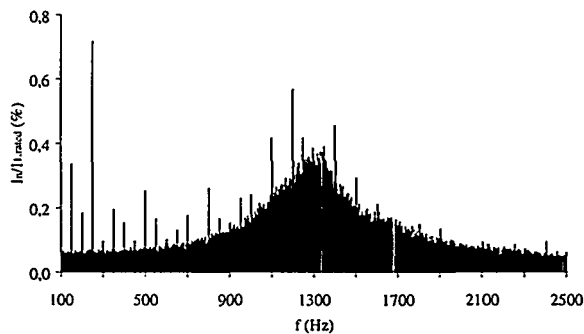


Figure 8: Harmonics and interharmonics content in current.

5 START

Figure 9 shows the active and reactive power during start of the

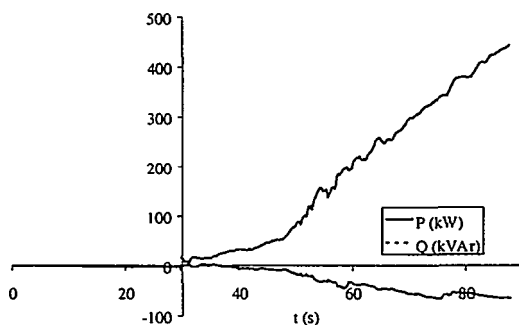


Figure 9: Active and reactive power during. The upper (positive) curve is the active power and the lower (negative) curve is the reactive power.

Enercon E-40 located in Gotland at high wind speed conditions. At the time, $t=30$ s., the generator is connected to the grid via the converter. The active power rises smooth and gently from a standstill to rated power. The whole process takes approximately 50 s. During the time the active power rises, the reactive power is controlled in order to keep the power factor constant.

6 CONCLUSIONS

The power quality of the variable-speed wind turbine shows a low flicker contribution, a controllable power factor and a smooth start/stop, which give minor impact on the grid. One drawback with variable-speed wind turbine is the injection of current harmonics into the grid. This variable-speed wind turbine is equipped with a forced-commutated inverter. The current harmonics produced by the inverter is low compared with wind turbines equipped with grid-commutated inverters. Since the switching frequency of the inverter is not fixed the wind turbine not only produces harmonics but also interharmonics.

The methods for calculating and summing flicker proposed by IEC Standards are reliable. Harmonics and interharmonics are treated in IEC 61000-4-7 and IEC 61000-3-6. The methods for summing harmonics and interharmonics in IEC 61000-3-6 are applicable to wind turbines. In order to obtain a correct magnitude of the frequency components, the use of a well-defined window width, according to IEC 61000-4-7 Amendment 1 is of a great importance.

REFERENCES

- [1] International Electrotechnical Commission, IEC Standard, Draft 61400-21: Power Quality Requirements for Grid Connected Wind Turbines, 1998.
- [2] Sørensen, P., Methods for Calculation of the Flicker Contribution from Wind Turbines, Risø National laboratory, Roskilde, Denmark, Risø-I-939, December 1995.
- [3] International Electrotechnical Commission, IEC Standard, Publication 60868, Flickermeter – Functional and Design Specifications, 1990.
- [4] International Electrotechnical Commission, IEC Standard, Amendment 1 to Publication 60868, Flickermeter – Functional and Design Specifications, 1990.
- [5] International Electrotechnical Commission, IEC Standard, Publication 61000-4-7, Electromagnetic Compatibility, General Guide on Harmonics and Interharmonics Measurements and Instrumentation, 1991.
- [6] International Electrotechnical Commission, IEC Standard, Amendment 1 to Publication 61000-4-7, Electromagnetic Compatibility, General Guide on Harmonics and Interharmonics Measurements and Instrumentation, 1997.
- [7] International Electrotechnical Commission, IEC Standard, Publication 61000-3-6, Electromagnetic Compatibility, Assessment of Emission Limits for Distorting Loads in MV and HV Power Systems, 1996.

LIGHTNING PROTECTION OF WIND TURBINES

T. Soerensen and M.H. Brask, DEFU[#]; F.V. Jensen and N. Raben, SEAS;
Saxov, J., Nordjyllandsvaerket; Nielsen, L., Vestkraft and
Soerensen, P. E.; Risoe
[#]DEFU, P.O. Box 259, DK-2800 Lyngby (Denmark).
Tel: +45 4588 1400 – Fax: +45 4593 1288 – E-mail: info@defu.dk

ABSTRACT: Lightning damage to wind turbines is a serious problem for Danish power companies, who have experienced some cases with very costly lightning damage and a large number of cases with minor damage. The most costly cases include one catastrophic damage to an entire wind turbine, and several cases of destruction of blades, main bearings, generators and control systems. Over the years there have been several hundreds of cases with minor damage - typically damage and interruptions of the control and communication systems, or the power systems.

The Danish power companies anticipate that the lightning threat will be even bigger for the large off-shore wind turbine installations that are currently being planned in Denmark. Furthermore, it is known from the off-shore wind turbines at Vindeby in Denmark that the costs of inspection and particularly repair work must be expected to be much higher off-shore as compared to wind turbines on land.

These considerations was the background for a two year project concerned with investigation of lightning damages and with the formulation of a DEFU Recommendation for lightning protection of wind turbines, which was published in January 1999. The project was funded by the Danish power companies Elsam, Eltra, Elkraft and by DEFU.

Keywords: Lightning, protection, safety

1. THE DEFU RECOMMENDATION 25 LIGHTNING PROTECTION OF WIND TURBINES

DEFU Recommendations are technical guides for power company personnel working with planning, procurement, installation, operation and maintenance of power system components. Rekommandation 25 *Lightning Protection of Wind Turbines* is aimed at the land and off-shore located wind turbines, considered relevant for Danish power companies. It therefore describes lightning protection for three bladed wind turbines with horizontal axis, and nominal power of 500 kW or more. Methods and principles, however, may also be applied to other sizes and types of wind turbines.

In the recommendation are outlined appropriate methods for evaluating the risk of lightning damage to wind turbines, and the risk for people present inside and in the vicinity of the wind turbines. It is required of the wind turbine manufacturer that a documented total concept of lightning protection for the wind turbine is prepared. Guidelines describing how the required concept may be developed,

checklists for the required documentation, and checklists to be used for inspection of the lightning protection system are included.

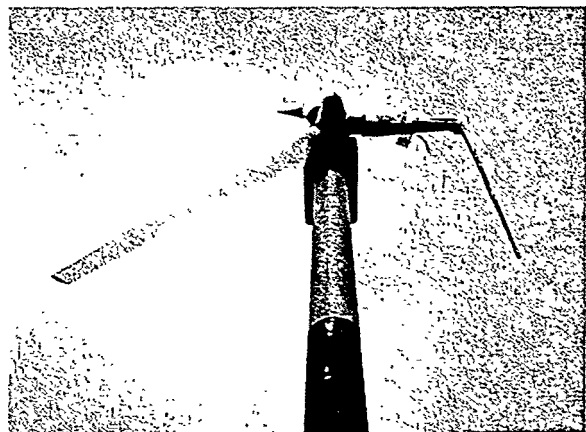


Figure 1: Wind turbine struck in one blade, which was completely destroyed. Another blade was damaged by debris.

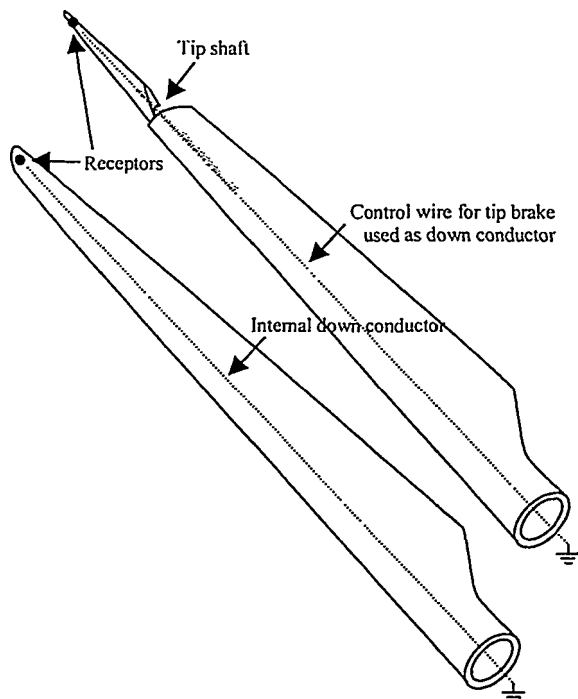


Figure 2: Example of lightning protection of blades by air-termination receptors at the blade tip and an internal down conductor. The lightning down conductor is terminated to the hub.

2. OUTLINE OF CONTENT

- Basic statistical information about lightning conditions in Denmark
- Simple methods for risk evaluation and selection of protection level
- Determination of lightning attachment points with the Rolling Sphere method
- Documented total concept of lightning protection
- Protection of specific components
 - Rotor blades
 - Nacelle
 - Tower
 - Earthing system
 - Machine components
 - Generator
 - Electrical system
 - Control system
 - Sensors and signal connections
 - External communication systems
- Choice and dimensioning of materials
- Requirements of documentation and testing
- Inspection – periodical and after lightning strikes

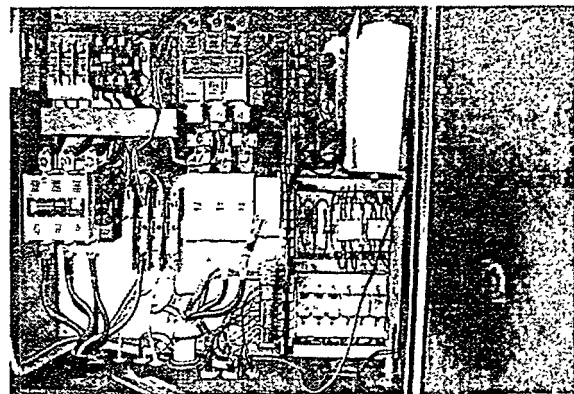


Figure 3: Extensive damages to power and control systems of wind turbine struck in lightning rod on the nacelle.

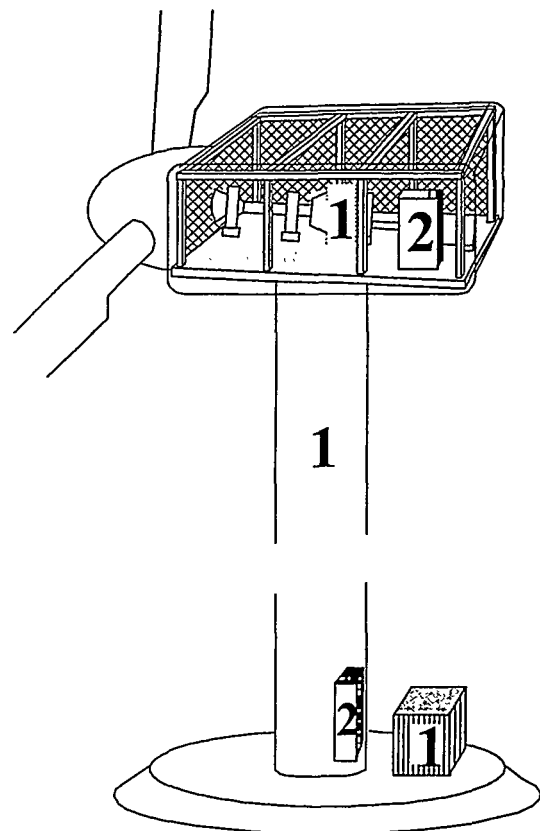


Figure 4: The wind turbine is divided into lightning protection zones, according to the IEC 61312-1. The most sensitive equipment e.g. the control system is placed in zone 2.

3. MAJOR PROBLEMS AND SOLUTIONS

Experiences with lightning damage to wind turbines in Denmark in the years 1985-1997 show, that the average damage occurrence was 4.1 % per wind

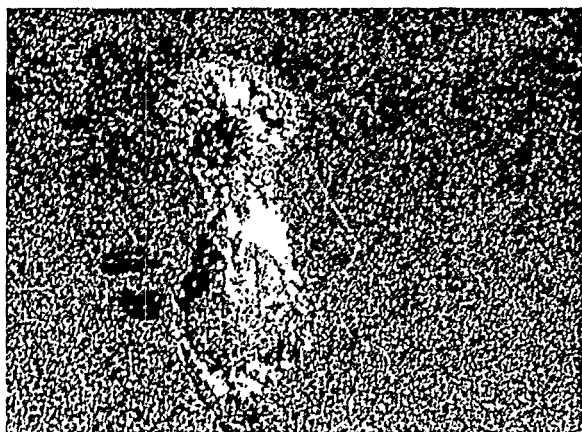


Figure 5: Damage to a roller from a main bearing on a wind turbine struck by lightning.

turbine year. About 50 % of the reported damages are damages to the control system, 20 % are damages and interruptions in the power system, and 18 % are damages to mechanical components [3].

Lightning damages to wind turbine blades are particularly important, as unprotected blades are literally destroyed when struck by lightning (fig. 1). Blades were damaged to a smaller or larger extent in 10.4 % of the cases reported in the period 1985-1997. In DEFU recommendation 25 it is required that blades are protected against lightning. E.g. with a lightning protection system such as the one shown in figure 2, which was developed by Danish blade manufactures. In this system air-termination receptors are placed at the tip of the blade and an internal down conductor leads the lightning current to the hub. Further documentation of the effectiveness of this system is needed, however, especially for blades longer than 20 m.

Damages to the control and power systems constitute the majority of the cases (fig. 3). In DEFU recommendation 25 it is required that a total lightning protection concept is developed, in which the turbine is divided into lightning protection zones as defined in IEC 61312-1. In each zone it must be secured with equipotential bonding, shielding and surge protective devices at the zone boundaries that no wind turbine components are subjected to excessive lightning influences (fig. 4).

The mechanical drive train represent a special problem, as lightning currents entering the nacelle from the blades are led into the nacelle and have to pass through bearings and gear to the nacelle bed plate. In figure 5 is shown a damage to a bearing roller where material is molten due to lightning current passing through the bearing. In DEFU

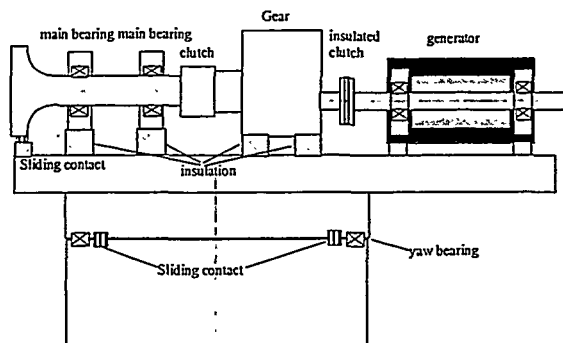


Figure 6: Lightning protection of the main bearings can be made by a sliding contact in front of the bearings, and insulation of the other current paths.

recommendation 25 it is required that bearings, gear etc. in the drive train are protected against excessive lightning currents e.g. by diverting the current with sliding contacts and increasing the impedance of the current paths through bearings etc. with resistive or insulating layers (fig. 6).

4. HOW TO GET A COPY ?

The DEFU Recommendation 25 *Lightning Protection of Wind Turbines* can be obtained from DEFU, either in Danish or in an English translation.

5. ADDRESSES OF AUTHORS

T. Soerensen, DEFU - Research Institute of Danish Electric Utilities, P.O. Box 259, DK-2800 Lyngby, Denmark.

Tel: +45 4588 1400, Fax: +45 4593 1288,
E-mail: trs@defu.dk

M.H. Brask, DEFU - Research Institute of Danish Electric Utilities, P.O. Box 259, DK-2800 Lyngby, Denmark.

Tel: +45 4588 1400, Fax: +45 4593 1288,
E-mail: mhb@defu.dk

F.V. Jensen, SEAS, Slagterivej 25, DK-4690 Haslev, Denmark.

Tel: +45 5631 2700, Fax: +45 5631 5042,
E-mail: Flemming.Vagn.Jensen@seas.dk

N. Raben, SEAS, Slagterivej 25, DK-4690 Haslev, Denmark.

Tel: +45 5631 2700, Fax: +45 5631 5042,
E-mail: Niels.Raben@seas.dk

J. Saxov, Nordjyllandsvaerket, P.O. Box 51, DK-9310 Vodskov, Denmark.
Tel: +45 9954 5454, Fax: +45 9954 5455,
E-mail: jsa@nv.dk

L. Nielsen, Vestkraft, P.O. Box 508, DK-6701 Esbjerg, Denmark.
Tel: +45 7512 4700, Fax: +45 7512 5132,
E-mail: ln@vestkraft.dk

Soerensen, P. E.; The Test Station for Wind Turbines, Risoe National Laboratory, P.O. Box 49, DK-4000 Roskilde, Denmark.
Tel: +45 4677 4677, Fax: +45 4677 5075
E-mail: poul.e.soerensen@risoe.dk

REFERENCES

1. DEFU: *Technical Report no. 394, part 1 to 8, Lightning Protection of Wind Turbines (in danish)*. DEFU - Research Institute of Danish Electric Utilities, P.O. Box 259, DK-2800 Lyngby, Denmark, 1998.
2. DEFU: *Recommandation no. 25, Lightning Protection of Wind Turbines (in danish)*. DEFU - Research Institute of Danish Electric Utilities, P.O. Box 259, DK-2800 Lyngby, Denmark, 1999.
3. Soerensen T. Brask, M.H.; Grabau, P.; Olsen, K.O.; Olsen, M.L.: *Lightning Damages to Power Generating Wind Turbines*. 24th ICLP. Int. Conf. on Lightning Protection, Birmingham UK, September 14-18, 1998.
4. IEC 61024-1: *Protection of Structures against Lightning – Part 1: General Principles*, IEC 1990.
5. IEC 61024-1-1: *Protection of Structures against Lightning – Guide A – Selection of Protection Levels for Lightning Protection Systems*, 1993.
6. IEC 61312-1: *Protection against lightning electromagnetic impulse - Part 1 General principles*, 1995.

IMPROVING TRANSITION BETWEEN POWER OPTIMIZATION AND POWER LIMITATION OF VARIABLE SPEED/VARIABLE PITCH WIND TURBINES

Anca D. Hansen*, Henrik Bindner* and Anders Rebsdorf**

* VEA, Risø National Laboratory, 4000 Roskilde, Denmark.

** Vestas Wind Systems A/S, 6940 Lem, Denmark

ABSTRACT: The paper summarises and describes the main results of a recently performed study of improving the transition between power optimization and power limitation for variable speed/variable pitch wind turbines. The results show that the capability of varying the generator speed also can be exploited in the transition stage to improve the quality of the generated power.

Keywords: Variable speed operation, Pitch, Dynamic models, Control systems

1 INTRODUCTION

It is known that the combination of variable speed with variable pitch makes possible to operate the wind turbine at the maximum efficiency over a broad spectrum of wind speeds [1]. The impact of the wind speed variations on the drive-train loads is also reduced due to the fact that the changes in the aerodynamic power are absorbed as changes in the rotational speed instead of as changes in torque.

1.1 Variable speed/variable pitch concept

The variable speed/variable pitch concept is based on the idea that a maximum efficiency C_p^{\max} of the wind turbine can be achieved for as wide a range of wind speeds as possible. C_p^{\max} is reached at a certain pitch angle and tip speed ratio.

The considered control objective of a variable speed/variable pitch wind turbine is based on two tracking strategies:

- **power optimization strategy** (below rated wind speed) - where the energy capture is maximized by a controller causing the wind turbine to track the maximum efficiency C_p^{\max} curve. The pitch angle is kept constant, while the tip speed ratio $\lambda = \frac{\omega_r R}{u}$ is tuned to the optimal value λ_{opt} over different wind speeds u , by varying the rotor's speed ω_r . R is the rotor radius.
- **power limitation strategy** (above rated wind speed) - where the goal of the controller is to track the nominal power output of the wind turbine. The pitch angle is controlled in order to obtain the nominal rotational speed of the generator, while reference torque is chosen as nominal torque.

It is important to point out that these two strategies do not need a wind speed measurement. Only the rotor speed and generator reaction (air-gap) torque are required. The ability to vary the rotor speed ω_r with wind speed u is used in both strategies, but it is mostly exploited below rated wind speed, while the pitch action is mostly used above rated wind speed to prevent the rotor speed variation and power production becoming too large.

1.2 Scope of the paper

The purpose of the present paper is to analyze the possibility to limit the big fluctuations existing in the power production (power reference) in the transition stage between power optimization and power limitation, for a variable speed/variable pitch wind turbine. The goal is thus to improve the quality of the generated power.

2 SYSTEM MODELLING

A stochastic nonlinear dynamic model, appropriate for a variable speed/ variable pitch wind turbine has been established in order to analyze the performance and the loads of a wind turbine [1], [2]. It includes submodels for the most relevant components of the wind turbine from a control point of view: transmission system, generator, aerodynamic, frequency converter, rotational turbulence.

The model is implemented in Matlab/Simulink, a simulation program which provides a graphical interface for building models as block diagrams. In Figure 1, the connection between the component blocks of the wind turbine is illustrated. The model has as inputs the pitch angle and the torque reference, while the generator speed and the electrical power are used as outputs.

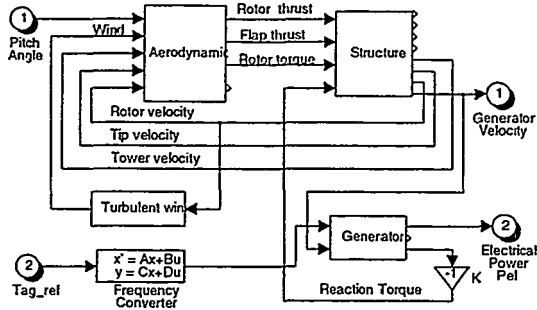


Fig. 1: Block diagram of the nonlinear dynamic model (open loop).

3 CONTROL-TRACKING PROBLEM

For variable speed wind turbines, the objective of the control system is formulated as a tracking problem. Below rated wind speed it must track the C_p^{\max} curve with minimum error, while above rated wind speed the wind turbine must track the nominal power curve. The idea is to keep the power coefficient C_p as close to its maximum C_p^{\max} as possible at a given wind speed u . Hence the tip-speed ratio must be kept constant to the optimal value: $\lambda = \lambda_{opt} = \frac{\omega_r R}{u}$. However, as no information about the wind speed u is available, the direct control of the tip-speed ratio λ is not possible. Therefore, instead of using wind speed measurement, a strategy to track C_p^{\max} is to use a predefined relation (called static characteristic) between the instantaneous power production (called power reference) and the generator speed (see Figure 2). This characteristic is based on aerodynamical data of the wind turbine's rotor and its points correspond to C_p^{\max} . Thus this strategy based on the predefined characteristic is that for each generator speed, an optimal power reference is determined.

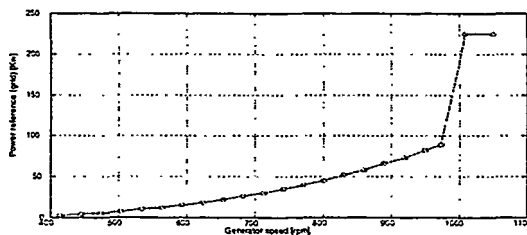


Fig. 2: Example of a grid power/generator speed characteristic.

The block diagram for the closed loop system is illustrated in Figure 3. Simulink offers the advantage of building hierarchical models, namely

to have the possibility to view the system at different levels. Thus each block can contain other blocks, other levels. For example, the internal "hidden" structure of the block "Turbine Plant" in Figure 3 is represented in Figure 1.

The control system contains two loops which cross-couple significantly:

- a speed control loop (up-left loop) - which controls the generator speed. It has as input the difference between the generator speed and the reference of the generator speed. The pitch angle is generated in such a way that a maximum power is produced for the certain reference generator speed.
- a power control loop (down-right loop) - which controls the power signal. It has as input the difference between the electrical power (from the wind turbine) and the reference of the electrical power (from the static characteristic - see Figure 2). It determines the reference torque, which is further applied to the frequency converter. The characteristic shown in Figure 2 is implemented as an interpolating table, i.e. in the "Power_ref" block illustrated in Figure 3.

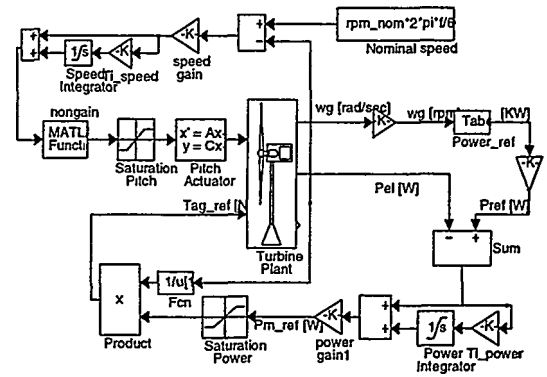


Fig. 3: Block diagram of the closed loop system.

Both control loops are active in the power limitation strategy, while only the power control loop is active in the optimization power strategy. Two continuous PI-controllers are used. For example, if the wind speed is less than the rated wind speed, the pitch angle is adjusted to that value, which yields the maximal power to the certain instantaneous generator speed. If now a wind gust appears, the rotor speed is increased due to an increased aerodynamical torque, and the power control loop reacts by increasing the power reference. If the wind speed increases further over the rated wind speed, then the speed

control loop reacts by increasing the pitch angle in order to prevent the rotor speed and power generation becoming too large, while the power control loop tries to keep the power to the nominal power.

4 LIMITATION OF THE POWER REFERENCE FLUCTUATIONS IN THE TRANSITION STAGE

The problem is that in the static characteristic (see Figure 2) the transition between the two strategies, described in Section 1, is reflected by a sharp curve and a discontinuity in the first derivative around the nominal generator speed. Thus even small changes in the generator speed create large changes in the power reference. This fact implies large fluctuations in the power production when, due to the wind speed variations, the generator speed decreases from over nominal speed to under nominal speed. This phenomenon is observed both in measurements and in simulation results.

The aim to improve the transition between the two control strategies is indirectly to make the sharp shape of the characteristic, near the nominal generator speed, to have a soft gradient.

Limitation of the changes in the generator speed ω_g is not an attractive option as it is quite difficult to control the large changes in the power signal, which appear even for small changes in generator speed - near the nominal generator speed. Therefore, limitations on the changes of the power reference seem to be a more attractive solution. In order to do that a slope limiter is applied on the power reference signal, the output of the "Power_ref" block in Figure 3. This solution has the advantage that different limitations on the rising and falling of the power reference signal can be imposed in the same time. For example, the variation of the power reference signal $\frac{dP_{ref}}{dt}$ can be limited as following:

$$F \leq \frac{dP_{ref}}{dt} \leq R \quad (1)$$

where the parameters F ("falling") and R ("rising") refer to how much the signal (power reference) maximally can fall and rise per second, respectively. The choice of these two parameters is very important for the performance of the whole system. It was found that a big positive value is suitable for the "rising" parameter R , because it is not necessary and it is undesirable to limit how fast the power reference should rise and eventually become equal to the nominal power. On the another hand the choice of "falling" parameter

F is quite sensitive to the operating point. The size of F has to ensure that the power fluctuations are limited by limiting the rate of change of the power reference, while at the same time to ensure that the power reference is allowed to change fast enough to ensure that the wind turbine is not brought to a stand still if the wind speed continues to decrease fast. F should not be chosen as a fixed value, but as a function of the state of the wind turbine, as for example:

$$F = func(\theta, \omega_g, \dot{\omega}_g), \text{ for } \dot{\omega}_g < 0 \quad (2)$$

This allows that both requirements are fulfilled, namely that the power fluctuations are effectively reduced and at the same time they have a sufficiently fast response to large changes in the wind speed. It is easy to implement and it has the advantage to not need a wind speed measurement.

5 SIMULATION RESULTS

Different investigations on the limitation of the power reference are done based on simulation results. The wind turbine is simulated in several operating points. The imposed limitation on the changes of the power reference is performed and the result is primarily evaluated by its capability to limit the power fluctuations, by its influence on the energy production of the wind turbine.

Figure 4 shows a simulation result at an average of a wind speed 15 m/s. The turbulence intensity is 0.2 and no slope limiter is used. It is observed that there exist fluctuations in power reference bigger than 100 kW. The standard deviation of the power is 27.56 [kW], while the total produced energy is $6.353 \cdot 10^4$ [kJ].

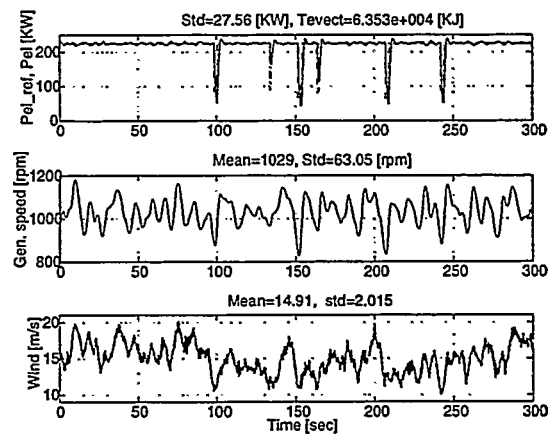


Fig. 4: Power, generator speed for 15 m/s without slope limiter.

The same wind sequence is further used in a simulation where the slope limiter is applied - see Figure 5. Some fluctuations are now reduced, while others are completely removed. This time the standard deviation is smaller, namely 15.56 [kW], while a larger amount of energy is produced $6.394 \cdot 10^4$ [kJ]. It is observed that the cost of smaller fluctuations in the power reference is increased fluctuations in the generator speed (more than 20 %).

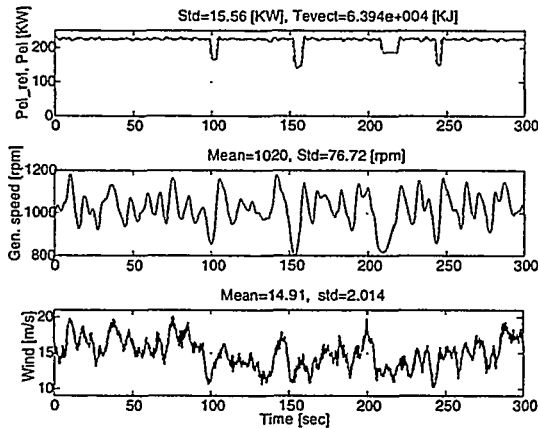


Fig. 5: Power, generator speed for 15 m/s with slope limiter.

In order to get a general idea about the influence of the slope limiter on the power reference, a set of simulations for average wind speeds between 5m/s and 20 m/s with turbulence intensity 0.2 has been performed. The situations with and without slope limiter are illustrated and compared. A general remark is that the slope limiter does not change the performances for low wind speed ($v \leq 9$ m/s).

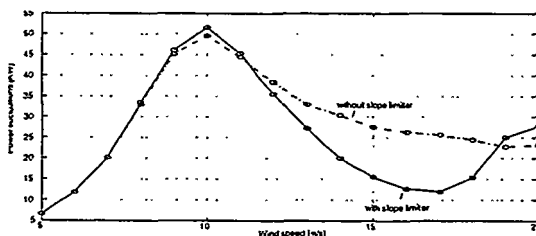


Fig. 6: Fluctuations in power.

Figure 6 shows that using a slope limiter on the power reference implies smaller fluctuations in power production at high wind speeds. The fluctuations are calculated as the standard deviation in the power reference.

The simulations show that this approach decreases the fluctuations of the power reference,

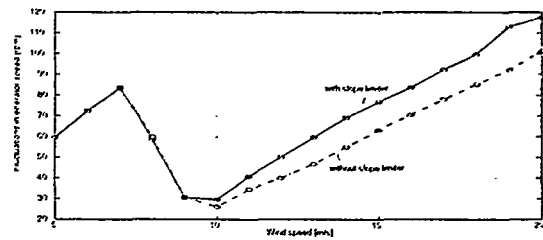


Fig. 7: Fluctuations in the generator speed.

while it increases the fluctuations of the generator speed (see Figure 7), a fact which reflects that it is allowed for the wind turbine to operate and to exploit the possibility of varying the generator speed.

The influence of the slope limiter is also investigated on the pitch angle and air-gap torque. It is observed that when the slope limiter is used, the fluctuations of the pitch angle are increased while the fluctuations of the air-gap torque are decreased at high wind speeds. The changes in the gearbox loads are therefore also reduced.

6 CONCLUSION

The transition between power optimization and power limitation can be dominated by large fluctuations in the power production. One way of making these fluctuations smaller is to apply a slope limiter on the power variations. The solution has the advantage to exploit the possibility of varying the generator speed.

The model simulations show that the cost of smaller fluctuations in the power production is bigger fluctuations in generator speed and pitch angle and smaller fluctuations in air-gap torque. The quality of the generated power is improved, while the changes in the gearbox loads are reduced.

7 ACKNOWLEDGEMENT

The work is partly funded by the Danish Energy Agency, jnr. 1363/96-0002.

References

- [1] H. Bindner, A. Rebsdorf, and W. Byberg. Experimental investigation of combined variable speed/variable pitch controlled wind turbine. *EWEC97*, Dublin, Oct 1997.
- [2] A. D. Hansen and H. Bindner. Dobbelt styrbar 3 - bladets vindmølle -regulering strategier-. Technical Report R-1071 (DA), Forskningscenter, Risø, 1998.

EXPERIENCES AND RESULTS FROM ELKRAFT 1 MW WIND TURBINE

Author: Niels Raben, SEAS Distribution A.m.b.A., Wind Power Dept., Slagterivej 25, DK-4690 Haslev, Denmark.

Telephone: (+45) 56 37 23 67, Telefax (+45) 56 31 50 42, e-mail: niels.raben@seas.dk

Co-author: Flemming Vagn Jensen, SEAS Distribution A.m.b.A., Wind Power Dept., Slagterivej 25, DK-4690 Haslev, Denmark. Telephone: (+45) 56 37 23 46, Telefax (+45) 56 31 50 42, e-mail: flemming.vagn.jensen@seas.dk

Co-author: Stig Øye, Institut for Energiteknik, DTU, bygn. 404, DK-2800 Lyngby, Denmark. Telephone: (+45) 45 25 43 11, Telefax (+45) 45 88 24 21, e-mail: s.oye@et.dtu.dk

Co-author: Søren Markkilde Petersen, Wind Energy & Atmospheric Physics Department, Risø National Laboratory, Building VEA-125, P.O. Box 49, DK-4000 Roskilde, Denmark. Telephone: (+45) 46 77 46 77, Telefax (+45) 42 36 06 09, e-mail: soeren.m.petersen@risoe.dk

Co-author: Ioannis Antoniou, Wind Energy & Atmospheric Physics Department, Risø National Laboratory, Building VEA-125, P.O. Box 49, DK-4000 Roskilde, Denmark. Telephone: (+45) 46 77 46 77, Telefax (+45) 42 36 06 09, e-mail: ioannis.antoniou@risoe.dk

ABSTRACT: The Elkraft 1 MW Demonstration wind turbine was at the time of installation in 1993 the largest stall controlled wind turbine in the world. It was constructed to allow accurate comparison of two different forms of operation: pitch control and stall control. A comprehensive programme for the investigation of the two operation modes was established. This paper presents the main experiences from five years of operation and measurements.

For a three-year period the wind turbine was in operation in stall controlled mode. During this period the wind turbine faced problems of various significance. Especially lightning strikes and unusually poor wind conditions caused delays of the project. In early 1997, the wind turbine was modified to enable pitch controlled operation. The gearbox ratio was changed in order to allow higher rotor speed, the hydraulic system was altered and new control software was installed. Tests were carried out successfully during the spring of 1997 and the wind turbine has since been operating as a pitch controlled wind turbine.

The most significant events and problems are presented and commented in this paper along with results from the measurement programme. The results cover both stall and pitch controlled operation and include power curves, annual energy production, structural loads, fatigue loads etc.

Keywords: 1 MW, stall control, vortex generators

1. INTRODUCTION

In September 1993 the 1 MW, 50 m diameter wind turbine was erected at Avedøre Holme, south of Copenhagen. SK Power Company, Project Division, was project manager and overall designer of the wind turbine on behalf of ELKRAFT. In 1996 management of the project was transferred to SEAS. The wind turbine is today owned by NESAs.

The wind turbine was located close to the dike at the South-eastern point of Avedøre Holme. A meteorological mast was erected south west of the wind turbine at a distance of approx. 128 metres.

The project was co-funded by the EU Commission (DG17) by DKK 6,7 mio and by the Danish Ministry of Energy by DKK 2 mio.

2. AIM OF THE PROJECT

Main objects of the Project were:

- Contribution to the development of large, reliable wind turbines suited for off-shore locations
- Introduction and test of stall control in the MW class

- Comparison between stall and pitch control
- Measurement and verification of power performance and structural loads
- Demonstration of a low noise emission design.

3. THE WIND TURBINE

The wind turbine was designed on basis of well-known and proven criteria's developed and used on Danish wind turbines. The wind turbine has bearings on the blade root for adjustable pitch setting of the blades. The blades may be fixed in a pitch setting for stall controlled operation or may be used with variable pitch setting thus enabling pitch controlled operation. The blades are designed for both operational modes but are optimised for stall control.

The dual-operation mode makes it possible to compare stall control and pitch control. At the time of erection it was considered uncertain whether a wind turbine of this size could be operated in stall controlled mode at all. The results from the measurement programme clearly proved that this was possible.

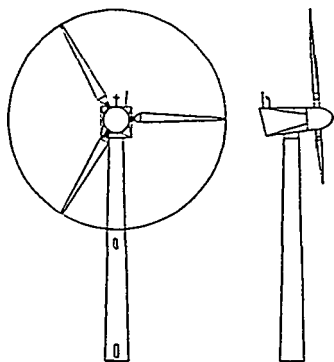


Figure 1: The 1 MW wind turbine

4. INSTALLATION AND OPERATION OF THE WIND TURBINE

Assembly of the nacelle was commenced in April 1993 at the Kyndby Power Station. The completed nacelle as well as the 53 metre tower was transported by sea to the site in early September 1993. After erection and completion of initial tests, the wind turbine started stall controlled operation in early 1994. In February 1997 the programme reached the next phase as the wind turbine was altered for pitch controlled operation. The gearbox ratio was changed for approx. 9% higher rotor speed, the hydraulic system was altered and new software was installed. Tests were carried out successfully during spring of 1997 and the wind turbine and the measurement programme was in full operation by summer of 1997. The measurement programme was completed by the end of 1998.

5. MEASUREMENT PROGRAMME

In order to verify and compare the two control strategies, a comprehensive measuring programme was carried out. The main objectives of the measurement programme were:

- Establishment of a better basis for the design of future wind turbines
- Description of the difference in loads for power regulation by stall and regulation by pitch
- Measurement of power curves, yaw efficiency, efficiency of the safety system, eigen-frequencies etc. both for stall and pitch controlled operation
- Investigation of the possibilities of reducing noise emission and vibrations from the main gear
- Verification of the design principles for large wind turbine blades.

A comprehensive database was established. The Test and Measurements Group of the Wind Energy and Meteorology Dept., Risø, undertook the task of implementing and operating the database system while the Electronic Dept. of Risø was responsible for the delivery and maintenance of instruments, sensors and other hardware. Analysis, reporting and verification of models etc. was carried out by Risø and by the Danish Technical University.

During the years of operation, there has been some modifications in the measurement programme due to:

- Repetitions due to adjustments of the operational conditions of the wind turbine (e.g. new blade pitch, large yaw error)
- Deviations between the measured and the calculated power curve, which resulted in the repetition of the measurements after installation of vortex generators on the blades
- Configuration from stall to pitch-controlled operation.
- Lack of high winds
- Data transmission from the rotating system to the fixed one through the slip rings was changed from analogue to digital in order to improve the quality of the measurements.

6. MAIN RESULTS FROM THE MEASUREMENT PROGRAMME

Results will be presented for both stall- and pitch-controlled operation of the wind turbine. The stall-controlled operation includes measurements without and with vortex generators on the blades. Vortex generators were installed to improve the power production of the turbine. In Figure 2 the turbine's yaw error is shown for the three measurement periods. The yaw efficiency for the pitch-controlled operation is slightly improved relative to the previous cases

The power curves and the corresponding power coefficients are shown in Figures 3 and 4. The presence of the vortex generators has improved the original power curve, as more power is extracted for wind speeds higher than 8 m/s. Of the three phases, the pitch-controlled operation shows the best power curve as this is steeper relative to the other two and as a result the nominal value is reached at a lower wind speed. The improvement from the vortex generators at high wind speeds can also be seen in the C_p curve in Figure 4. For the pitch controlled operation the top of the curve becomes as expected more flat.

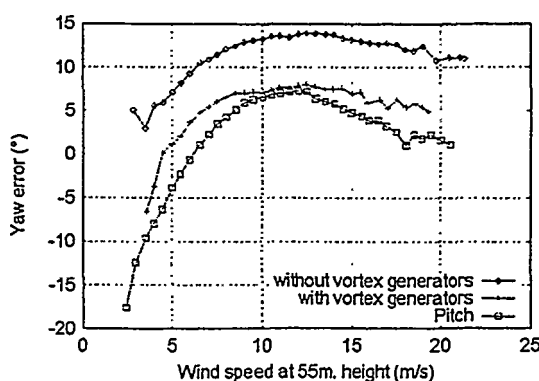


Figure 2: Yaw error

The improvement from the vortex generators can also be seen in the C_p curve in Figure 4. For the pitch controlled operation the top of the curve becomes as expected more flat.

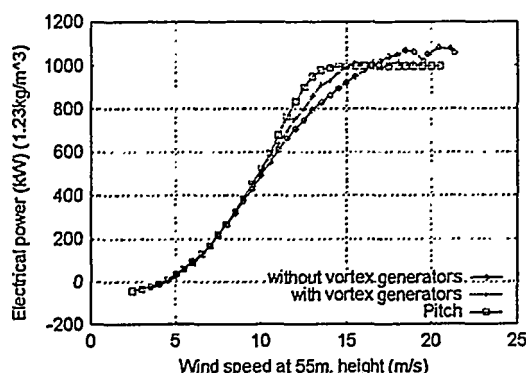


Figure 3: Electrical power curve

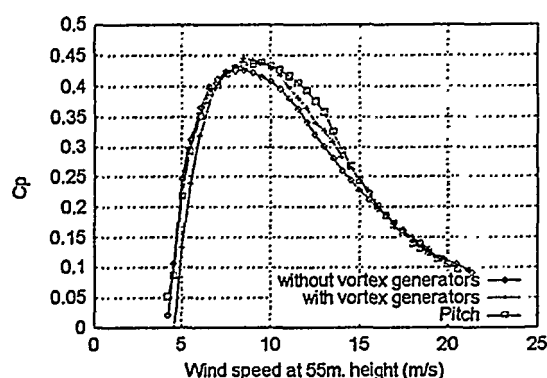


Figure 4: C_p -curve

The pitch angle during the pitch controlled operation as a function of the wind speed can be seen in Figure 5. The pitch angle becomes more negative at the wind speeds up to around 11 m/s in order to optimise the power output at the low wind speeds before the regulation begins.

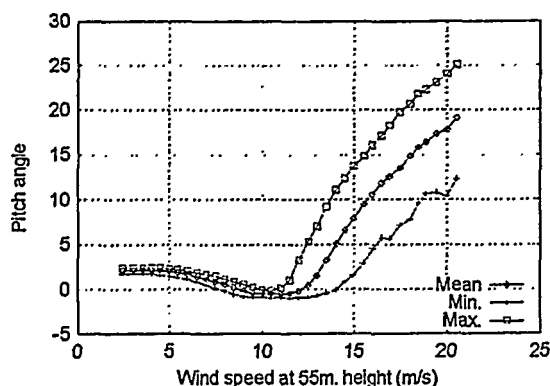


Figure 5: Pitch angle, pitch controlled operation

A very important part of the measurement programme has been the measurement of the structural loads and the calculation of the fatigue loads. The measurement of the structural loads is in many cases influenced by the presence of temperature drift experienced by the strain gauge sensors. Therefore the comparison of the fatigue loads is on many occasions more meaningful since these quantities are based on the dynamic content of the load signal and therefore they are not influenced by sensor drift. The fatigue loads are evaluated using the rainflow counting method (RFC). The RFC is here performed using 50 range levels between the minimum and the maximum of the signals and a jittery filter size of one level. The fatigue loads are expressed as a damage equivalent load range L_{eq} based on a rainflow spectrum $R_i(n_i)$. The damage equivalent load ranges L_{eq} are calculated from the load signals using an equivalent number of load cycles equal to 1 sec, thus $N_{eq}=600$ for a 10 minutes time history. The relation between the equivalent load range L_{eq} and the rainflow load spectrum is $L_{eq}=[(\sum R_i^m n_i)/N_{eq}]^{(1/m)}$ where n_i is the number of times a range level appeared and m the material SN curve exponent. Results are shown for $m=10$ and turbulence intensity between 7%-9%.

From Figure 6 to Figure 8, the mean load curves for the flap root bending, the tower root bending and the shaft torque are shown. The loads for the stall-controlled operation are comparable whereas they are reduced in the case of the pitch operation after regulation occurs

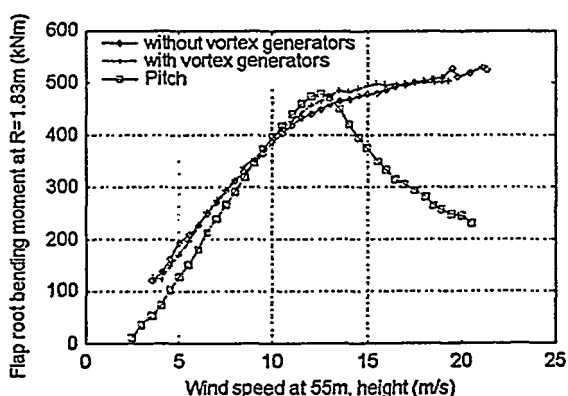


Figure 6: Flap root bending moment

The corresponding equivalent loads are shown in Figures 9 to 11 and in Figures 12 and 13, the equivalent loads for the edgewise root bending and the tower torsion are seen. As a general remark, the two stall controlled data sets exhibit the same behaviour. The presence of the vortex generators makes the fatigue loads little higher. The fatigue loads in the case of the pitch-controlled operation show a different behaviour above rated power due to the pitching of the blades.

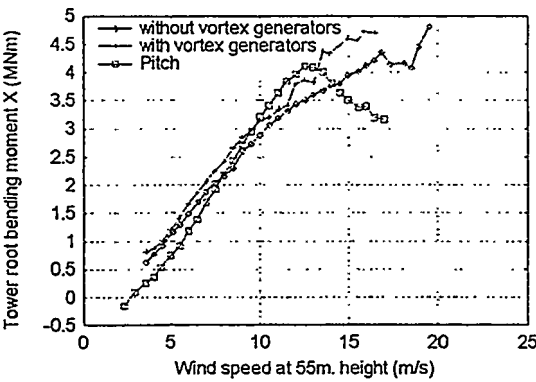


Figure 7: Tower root bending moment

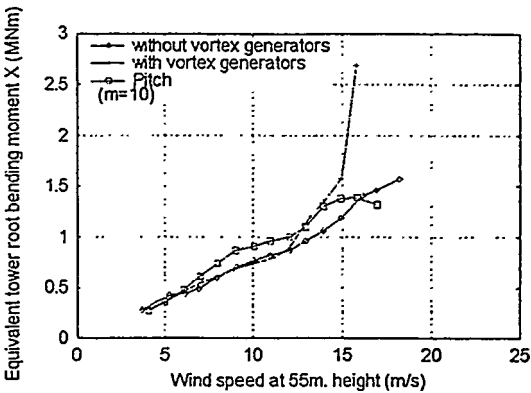


Figure 10: Equivalent tower root bending

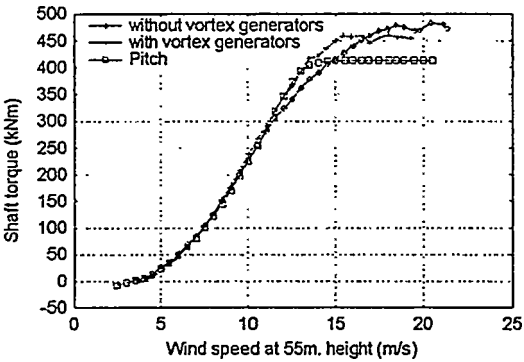


Figure 8: Shaft torque

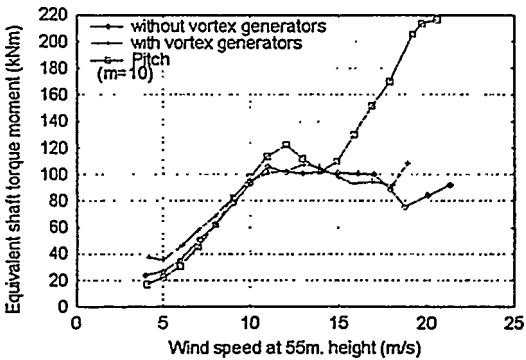


Figure 11: Equivalent shaft torque moment

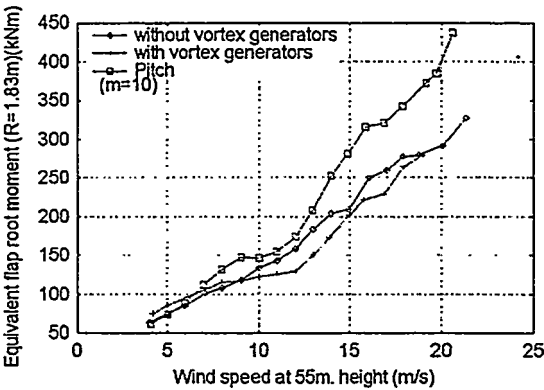


Figure 9: Equivalent flap root moment

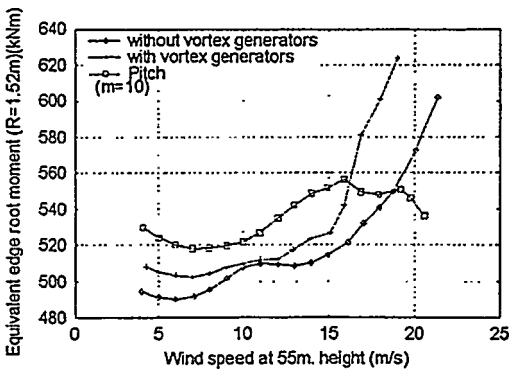


Figure 12: Equivalent edge root moment

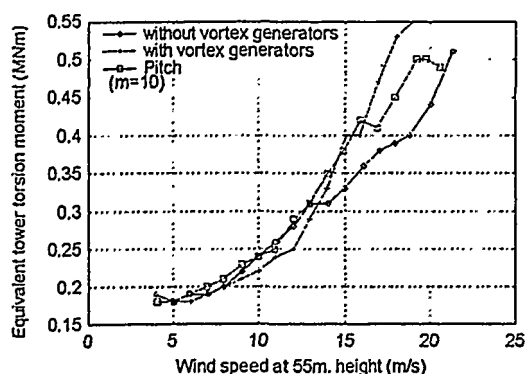


Figure 13: Equivalent tower torsion moment

7. OPERATION AND PRODUCTION EXPERIENCE

Production figures for 1994 - 1998 are listed in the table below.

Year	Production (kWh)
1994	1.394.781 kWh
1995	1.623.657 kWh
1996	1.165.978 kWh
1997	1.157.990 kWh
1998	1.773.473 kWh
Total	7.115.879 kWh

Table 1: Annual production from operation of the wind turbine

The estimated annual production is listed in table 2. In both operational modes this figure is approx. 2.200 MWh. The reason for the lower actual production in all of the years recorded is first of all more down time than expected, lower winds especially in the years 1995 and 1996 and a blade performance lower than anticipated. In mid 1995 a plan for improvement of the blades was devised. A row of vortex generators was mounted on the suction side of the inboard half of the blades.

Mean wind speed: 7 m/s		Form factor: 2
Test period	Calculated annual production (MWh)	Improvement since the first period (%)
Without vortex generators	2157	
With vortex generators	2216	2.74%
Pitch	2258	4.68%

Table 2: Calculated annual production at different operational conditions

Down-time of longer periods were experienced mainly due to the below listed reasons:

- Break-down of tip brake (1994 and 1998)
- Faults on the hydraulic system (1994)
- Lightning strikes on blade tip (1995)
- Bearing damage on gearbox (1995)
- Problems on yaw brake system (1995 - 1997)
- Low speed brake redesign (1995)
- Fitting of vortex-generators to blades (1995)
- Thorough blade inspection (1996)
- Arrangement for pitch controlled operation (1997)
- Gearbox oil contamination (1997)
- Major overhaul and labour conflict! (1998).

8. SUCCESS OF THE PROJECT AND PROSPECTS

Considering the results from this Project, including results from the measurements carried out and the implementation and operation experiences gained, it can be stated clearly that all expectations and contract objectives of this Project have been met. The investigations and analysis carried out in the measurement programme has given yet another good deal of insight and understanding of the behaviour and characteristics of large wind turbines. This has especially been to benefit for the partners in the Project: Risø and the Danish Technical University. The wind turbine is planned to proceed with electricity production for at least the next decade. The wind turbine will be operating in pitch controlled mode. Plans for investigations on up-grading the wind turbine are under consideration.

Construction costs totalled DKK 32.819.917,15. Measurement programme costs for the Project were by the end of 1998 DKK 5.075.554,00. The costs for the Project and specifically the costs for construction of the wind turbine should never be considered as an indication for the economics of wind turbines in the MW-class. It was never the intention of the Project to demonstrate state-of-the-art of cost optimised wind generated electricity. The Project first of all had objects of a technical nature. As commercial megawatt wind turbines have entered the market the recent years, it should be noted that these machines are presenting costs figures that are highly competitive to wind turbines of smaller size. The costs for these machines are about 20% of the costs for the wind turbine.

9. REFERENCES

- [1] Test Report. Static load test of wind turbine blade manufactured by LM Glasfiber A/S. Blade type: LM 24 m. Test performed: 24 June and 29 June 1993. Risø-I-xxx (EN). Forskningscenter Risø. January 1994.
- [2] General Design and First Experiences from Elkraft 1 MW Experimental wind turbine. F.V. Jensen, F.A. Olsen og N. Raben, ELKRAFT A.m.b.A. EWEC '94, 10 - 14 October 1994, Conference Proceedings.

- [3] Wind turbine Test: Power curve measurements ELKRAFT 1 MW (Stall regulated operation). Version no. 01. Risø-I-866 (EN). Risø National Laboratory. July 1995.
- [4] Wind turbine Test: Structural loads ELKRAFT 1 MW (Stall regulated operation). Risø-I-865 (EN). Risø National Laboratory. December 1995.
- [5] The effect of Vortex Generators on the performance of the ELKRAFT 1000 kW Turbine. Stig Øye, Dept. of Fluid Mechanics, Technical University of Denmark. Presented at the 9th IEA Symposium on the Aerodynamics of wind turbines. FFA, Stockholm, December 11-12, 1995.
- [6] The ELKRAFT 1 MW wind turbine: Results from the Test Program. Antoniou, Søren M. Petersen, Stig Øye, Carsten Westergaard, Niels Raben, Flemming V. Jensen, EUWEC Sweden, 1996
- [7] Wind turbine Test: Structural loads (new yaw conditions) ELKRAFT 1 MW (Stall regulated operation). Risø-I-866 (EN). Risø National Laboratory. August 1996.
- [8] Nacelle Anemometry on a 1 MW wind turbine: Comparing the power performance results by use of the nacelle or mast anemometer. Risø-R-941(EN), I. Antoniou, Troels Friis Pedersen, Risø National Laboratory, Denmark, August 1997.
- [9] Comparing the power performance results by using the nacelle and the mast anemometer. I. Antoniou, Troels Friis Pedersen, Søren Markkilde Petersen, Risø National Laboratory, Denmark. Paper presented at EWEC97, Dublin, Ireland, October 1997.
- [10] Wind turbine Test: Structural Loads (Vortex Generators on the Blades) ELKRAFT 1 MW (stall Regulated Operation). Risø-I-868(EN), I. Antoniou, Søren M. Petersen, Risø National Laboratory, Denmark, August 1998.

Information on the wind turbine can be found on a homepage:

<http://www.afm.dtu.dk/wind/ek1000.html>

KEYS TO SUCCESS FOR WIND POWER IN ISOLATED POWER SYSTEMS

Jens Carsten Hansen, Per Lundsager, Henrik Bindner, Lars Hansen, Sten Frandsen
Wind Energy and Atmospheric Physics Department
Risø National Laboratory
P.O. Box 49, DK-4000 Roskilde, Denmark

ABSTRACT: It is generally expected that wind power could contribute significantly to the electricity supply in power systems of small and medium sized isolated communities. The market for such applications of wind power has not yet materialized. Wind power in isolated power systems have the main market potentials in developing countries. The money available world-wide for this technological development is limited and the necessary R&D and pilot programmes have difficult conditions. Consequently, technology developed exclusively for developing countries rarely becomes attractive for consumers, investors and funding agencies. A Danish research project is aimed at studying development of methods and guidelines rather than "universal solutions" for the use of wind energy in isolated communities.

This paper reports on the findings of the project regarding barriers removal and engineering methods development, with a focus on analysis and specification of user demands and priorities, numerical modeling requirements as well as wind power impact on power quality and power system operation. Input will be provided on these subjects for establishing of common guidelines on relevant technical issues, and thereby enabling the making of trustworthy project preparation studies.

The Danish Energy Agency is funding the present work under contract as part of the Danish Energy Research Programme.

Keywords: Wind power, isolated power systems, high wind energy penetration, power system modeling, power quality

1 INTRODUCTION

The market for wind power applications in small and medium sized isolated communities has not yet materialized. Few pilot projects have been made and even fewer have been successful. A Danish research project is aiming at development of methods and guidelines rather than "universal solutions" for the use of wind energy in isolated communities. The main activities of this project, which forms the basis for this paper, are

- review of projects done, relevant literature on the subject and available computational methods and tools
- identification of barriers for use of wind power in isolated power systems
- user demands to isolated power systems
- development regarding operational engineering design and assessment methods
- application and verification of methods on sites in Egypt
- formulation of a guideline for project preparation

Wind power in isolated power systems have the main market potentials in developing countries. The amount of R&D and pilot projects world-wide for this technological development exclusively for the developing countries market is limited compared to large scale applications. Consequently, the technology offered has not yet reached the same level of maturity, and it has difficulties convincing consumers, investors and funding agencies that it offers commercially attractive solutions. The main barriers identified are

- lack of positive track records due to failures in too complex system designs applied in early pilot projects
- lack of institutional sustainability at the recipient in small remote communities with limited human resources
- lack of detailed knowledge of user demands and priorities and their development in time
- lack of project implementation models other than turnkey
- lack of financial sustainability and commercial market

- lack of funding for technological development
- lack of engineering tools for customizing systems
- lack of generalized reported experience and guidelines

In search for keys to success for wind power in isolated power systems, the focus of this paper is on the three selected issues

- consumer demands and priorities, e.g. in Egypt
- review of models availability and modeling requirements
- wind power impact on power quality and power system operation - some results from a measurement programme

Inputs are provided on these three subjects for establishing of common guidelines on relevant technical issues, and thereby enabling the making of trustworthy project preparation studies. For documentation, data on power supply conditions in Egypt are analysed. Some actions and methods to facilitate introduction on the markets in the developing countries are presented.

2 CONSUMER DEMANDS IN ISOLATED COMMUNITIES

Small isolated power systems with wind power should from a consumer's point of view meet demands exactly as is the case for conventional power system solutions. Wind power should as such be treated as just another option in accordance with priorities of relevant policies and plans. However, in order to be able to assess wind power in comparison with conventional options such as diesel, a supplementary set of information describing the community may be necessary.

Regarding consumer demands and community development, wind power feasibility in small isolated power systems may be particularly sensitive to

- variations in land use
- village/town expansions
- site availability – distance to grid

- grid interconnection costs
- electricity demand development
- diurnal consumer pattern – especially whether the power system offers electricity supply 24 hours a day or less

Furthermore, costs for consultants for special studies or power system design add to the investment, which may be unacceptable for such small communities.

In order for this potential market to develop, a simple approach should preferably be found, which can be applied at low cost and at a risk comparable to the risk involved when deciding and designing a diesel powered system.

Realizing this need and the fact that economics of scale apply, it was decided to try to acquire a general overview of the potential types of systems in which wind power could be an option in Egypt as an example. An overview splitting the communities in 3 categories is done in Table 1.

Table 1 Overview of isolated power systems in Egypt

Category	isolated power systems – brief description	estimated No. in Egypt
1	very small - not electrified or non-grid communities – which get electricity from buying or charging batteries or individual household systems	more than 100
2	small – micro or mini grids. p.t. power by diesel systems of sizes 50-1000 kW	50
3	medium size – isolated or end-of-line grids with 1-150MW installed capacity of diesel or gas-turbines fueled by oil or natural gas	5-10

Hurghada, which is studied more closely below, is Category 3 with about 100 MW installed gas turbines and already a 5 MW wind farm at Hurghada Wind Energy Technology Center (WETC). Hurghada has operated as a high-wind-energy-penetration system, and it has provided demonstration for Egypt of this technology, ref [11] and [12]. This technology may in certain cases be applied in Category 2 systems, for which reason an inventory of information of such systems was made by NREA. Some statistics are shown in Table 2.

Table 2 Selected key information - 50 communities of Category 2 in Egypt

	Average	st. dev.*
installed diesel capacity (kW)	165	170
distance to grid (km)	41	30
No. of households	145	235
persons/household	8	2
consumption/year (MWh/y)	450	750
Estimated annual growth rate (%)	4	
hours/day supply	7.5	3
tariff (USD/kWh)	~0.05	0.00
load factor on diesels	0.87	0.45

* distributions are not necessarily symmetric

Embarking on an approach with individual feasibility studies for each community, e.g. with demand-forecasting techniques similar to those used for urban systems of Category 3 or larger, rarely apply to remote rural isolated communities. An overview such as the one provided in Table 2, documents availability, conditions and similarities of the "market", on the other hand offers a possibility to assess, whether it could be developed as a common programme, enabling a reduction of effects of the economics of scale. Doing so, Table 2 also shows that such overview data should be treated carefully. E.g. systems

appear, according to the first draft of the data, which have load factors higher than 1, and distance to grid is in this context the distance to the existing substation of the national grid, which may be different from the actual future potential grid connection location. The finding of most immediate impact is that electricity in Category 2 communities is offered only part of the day and night, which is a major problem if wind power is to become economically competitive to other options.

A similar study providing an overview of the power supply situation and expected development could be made for Category 1 communities as well.

With such overviews in hand, consumer demands may be studied more thoroughly for selected types of communities. Load patterns for different key types of load can be used in the design phase for estimation of the total load and consequences of offering 24 hours power can be compared to the present situation.

3 NUMERICAL MODELING REQUIREMENTS – A REVIEW OF ISSUES AND MODELS

Numerical modeling is an important part of the design, assessment, implementation and evaluation of isolated power systems with wind power. Usually the performance of such systems are predicted in terms of

- technical performance (power and energy production)
- economical performance (COE or IRR)

Performance measures may also include

- power quality measures
- load flow criteria
- grid stability issues
- scheduling and dispatch of generating units, in particular diesel generators

Thus a large variety of features are needed to cover the numerical modeling needs for all contexts. No single numerical model is able to provide all features, as they often are in conflict with each other in terms of modeling requirements. This survey of modeling requirements is based on a review of relevant studies that was carried out as part of the present project, see [1].

3.1 Requirements & Applications

The requirements to the numerical models depend on the actual application of the modeling. Many factors influence the layout of a numerical model, and the main factors include

- The objectives of the simulations
- Time scale of the modeling
- Modeling principle (deterministic or probabilistic)
- Representation of the technical & economic scenarios
- System configurations, including dispersed vs. single system configurations

The objectives of the simulations depend on whether the simulations are done in a feasibility study as part of the decision process or by a manufacturer as part of the design process:

- Screening or optimization of possible system / grid configurations

- Overall annual performance of selected configurations
- Supervisory control including scheduling / dispatch of generating units
- Grid modeling, stability or load flow

Several time scales of modeling are used, depending on the context and purpose of the simulation

- Transient analysis of electrical transients due to switching, or certain power quality measures. Typically a few seconds at time step < 0.001 sec.
- Dynamic analysis of machine dynamics, power quality or grid stability. Typically around 1 minute at time steps around 0.01 sec.
- Dispatch analysis of supervisory control, including diesel dispatch. Typically a few minutes to 1 hour at time steps of 0.1 to 1 sec.
- Logistic analysis of power flows and seasonal / annual energy production. Days, weeks, months, seasons or one year at time steps 10 minutes to one hour

Probabilistic modeling, based on probability distributions such as load duration curves or wind speed probability curves, can work directly with the outputs of typical utility statistics and WASP analyses. Time series simulation can represent “memory” effects such as energy storage, diesel dispatch strategies and deferrable loads, but to obtain the same statistical significance as probabilistic models, ideally Monte Carlo techniques should be applied.

Most models represent technical performance by one year’s performance measures (fuel savings etc), and use an economic life cycle analysis to establish the economic indicators. This way the technical developments/extensions of the system during its lifetime are neglected. This is in fact inadequate to give a realistic representation of the rapid development of isolated systems during their entire technical/economic project life.

A realistic representation of both system configuration and control strategy in the modeling is essential for a reliable prediction of system performance. Several techniques have been applied to facilitate flexible modeling of system configuration/connectivity, while flexible modeling of supervisory control strategy appears to be even more challenging, cf. [2] and [3].

For dispersed systems the electric grid becomes part of the system. Deterministic load flow analysis is well established, but probabilistic load flow modeling is more in line with the stochastic nature of wind and loads in isolated systems, and the associated probabilistic power quality measures, [4].

Actual grid stability analysis requires real dynamic electromechanical models, and such analysis is frequently outside the scope of isolated system analysis.

3.2 A Review of Numerical Models

A number of numerical modeling techniques and models are reviewed in ref. 1, although the review does not claim to be complete. Selected models are briefly described below:

[5] HOMER is a fast & comprehensive village power systems screening model, now (1998) supplemented with the VIPOR model for optimal layout of a supply area into grid connected vs. independently supplied consumers. State of the art in this category, but not publicly available.

[6] INSEL Offers almost unlimited flexibility in specifying system configurations by allowing the user to specify the connectivity on a component level. Intended as an out-of-house-model.

[7] HYBRID2 The state-of-the-art (1998) time series model for prediction of technical-economical performance of hybrid wind/PV systems. Offers a very high flexibility in specifying the connectivity of systems. Publicly available and quite widely used.

[3] SIMENERG The only model so far with a very high degree of flexibility in the control / dispatch strategy, using a “market square” approach, where the economically optimal subset of power sources that satisfy the power demand is dispatched in each time step.

[8] WINSYS is a spreadsheet (QPW) based model implementing probabilistic representations of resources and demands. WINSYS incorporates the anticipated technical expansions during its lifetime in the technical performance measures, combined with a traditional economic life cycle cost assessment. Thus WINSYS represents a more real life cycle cost analysis than most other models.

[9] ENGINEERING DESIGN TOOLS FOR WIND DIESEL SYSTEMS, This package contains seven European logistic models: SOMES (NL), VINDEC (N), WDILOG (DK), RALMOD (UK) and TKKMOD (FIN). It also includes the modular electromechanical model JODYMOD.

[10] PROLOAD A probabilistic load flow analysis code, using Monte Carlo techniques, developed in co-operation with an electrical utility for dimensioning of distribution systems with wind turbines.

4 WIND POWER IMPACT ON POWER QUALITY AND POWER SYSTEM OPERATION – MEASUREMENTS AT HURGHADA

The varying of the power output from wind turbines has an impact on both the operation of the power system and on the power quality of the system. This impact increases as the level of penetration increases.

The influence on power quality is mainly on the level and fluctuations of voltage and frequency. The stability of voltage and frequency should not be degraded significantly as the controllers of systems are required to be able to prevent instability. Furthermore, the shape of the voltage should not be degraded by the inclusion of wind power in the system. If wind turbines or storage systems applying power electronics are included in the system, it should be ensured that the distortion of the voltage is within required limits.

4.1 Voltage levels

Isolated power systems considered in this context are usually characterised by having only one power station. The transmission and distribution network is usually quite simple and weak. When the wind turbines are connected to the grid, the situation will often be that they are connected at a point in the grid where consumers are also connected.

The voltage level at the point of common connection will depend on the output from the wind turbines and on the consumer load. Situations where the voltage becomes high due to a high wind power production and a low consumer load will quite often occur. Measurements illustrating the dependence of the voltage on the wind power production and the consumer load from Hurghada are shown in Figure 1, from [11]. It is clearly seen that the voltage level depends on the output from the wind farm, but also that the consumer load is important. In Figure 2, the estimated bus bar voltage as a function of the wind farm output for both the maximum and minimum consumer load is shown. The permitted voltage limit is $11\text{kV}+10\%$, and it is noticed that for the current size of the wind farm this limit is not reached. Care has to be taken that the voltage level at the wind turbines is not too high even when the voltage level at the bus bar is within limits.

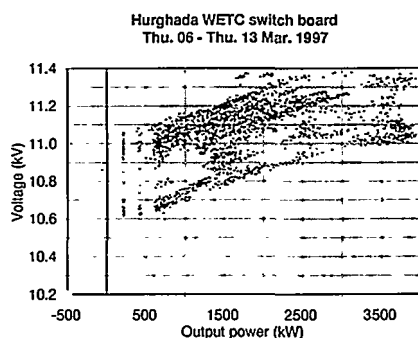


Figure 1 Measured instantaneous true RMS values of bus-bar voltage at WETC switch board versus measured instantaneous values of active power from the WETC.

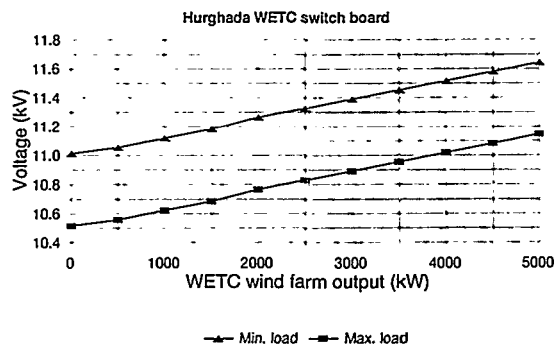


Figure 2 Estimated bus-bar voltage at the WETC switch board as a function of the output power from the WETC.

4.2 Power fluctuations

Another important aspect is the power fluctuations. The power fluctuations create fluctuations in the voltage and they impose fluctuations in the diesel output. The voltage fluctuations have to be low to avoid disturbances e.g. in the light intensity. The power fluctuations do not only depend on the amount of installed wind power capacity, but whether the wind farm consists of a few large wind turbines or correspondingly more, but smaller wind turbines. The dependence of the power fluctuations on the number of wind turbines is shown in Figure 3. The wind farm is made up from $4 \times 300\text{kW}$ (NTK) + $20 \times 100\text{kW}$ (WC) stall controlled wind turbines and $10 \times 100\text{kW}$ (V) pitch

controlled wind turbines. The number of wind turbines in the figure is a calculated as the equivalent number of wind turbines, see Table 3. It is noticed from Figure 3 that the relative power fluctuation level basically is decreasing as the number of wind turbines is increasing. Keeping power fluctuations small is a desirable feature in an isolated power system with a high penetration level. The decrease in power fluctuations is due to the stochastic nature of the turbulent wind. The power fluctuations from the individual wind turbines will to some extent be independent of each other and they will therefore even out some of the higher frequency fluctuations. The non-ideal decrease of the fluctuation levels for increasing number of wind turbines may be explained by the wind farm consisting of different types of wind turbines.

Table 3 Number of different types wind turbines, and the calculated equivalent number of wind turbines

No. NTK	No. WC	No. V	Neq
1	-	-	1
1	-	-	1
1	-	-	1
1	-	-	1
2	1	-	2.5
4	-	-	4
-	15	-	15
-	4	7	11.0
6	20	7	24.6

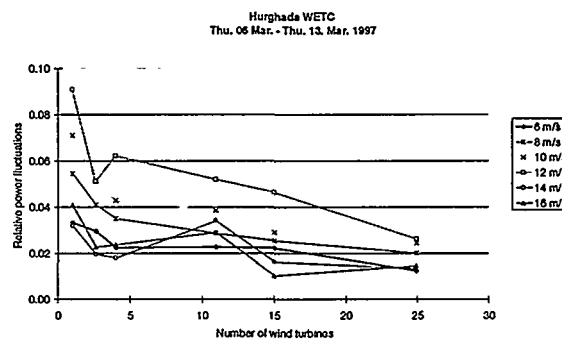


Figure 3 Measured relative power fluctuations.

4.3 Operation

The operation and performance of an isolated system with wind power depends on the characteristics of the load. The load is the sum of many individual loads. The load can to some extent be categorized. In Figure 5 and Figure 6, the load patterns of a hotel load and a residential load are shown for illustration. Both of the loads are measured as the load of a $10/0.4\text{kV}$ transformer. The figures show the diurnal pattern. It is clearly seen that there is a distinct diurnal pattern for the residential load whereas the hotel load is quite constant over the day. It is also seen that the pattern for the reactive power is very similar to that of the active power. Day-to-day variations of loads shown by the minimum to maximum band are small in the residential load case. In the hotel load case the variation is larger. This is also seen in the standard deviation of loads in Figure 4.

Due to their impact on the operation strategy of the diesels, several aspects of the load are important. Briefly summarizing, the minimum load, together with the allowed technical minimum load of the diesel, determines the amount of wind power that can be absorbed by the system.

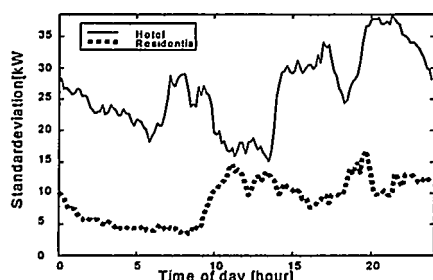


Figure 4 Standard deviation of hotel and residential load.

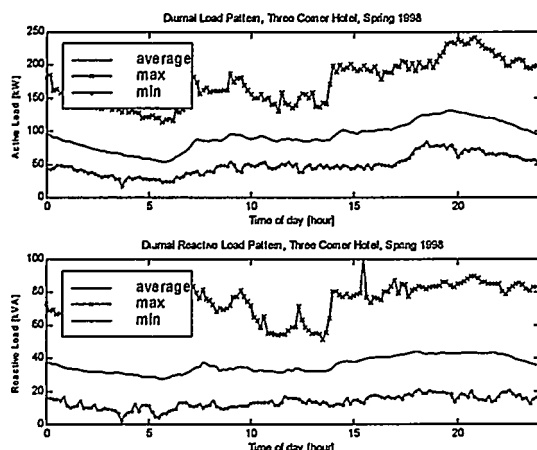


Figure 5 Diurnal load pattern for hotel load.

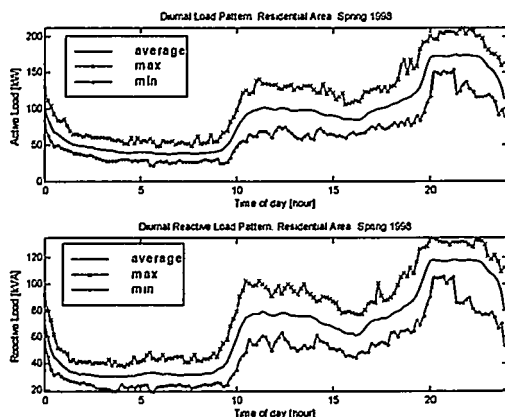


Figure 6 Diurnal load pattern for residential load.

The maximum load determines the necessary installed diesel capacity. The variations in loads and power – active and reactive – together with the rate of change of the load and the rate of change of the wind power, determine the necessary spinning capacity, in order to ensure adequate power quality and reliability in terms of loss of load probability.

5 CONCLUSIONS AND GUIDELINES

The main recommendations of this paper as keys to success for the further development of the use of wind power in isolated power systems are

- to develop the use of wind power in isolated systems as concerted actions in national and international programmes rather than as individual projects
- to develop wind power in small to medium size systems following the simple proven approaches, e.g. by repeating and/or downscaling pilot and demonstration systems with positive track records
- to invest research and development in very small and small systems to support development of rugged technology applicable for remote communities
- to use modeling assumptions from the hardware reality for the types of systems that will be applied
- to install experimental systems only at test benches prepared to serve as experimental facilities
- to develop a common best practice guideline as a living document, addressing at least key issues such as

Technology

Climate and wind resources

Site description

Consumer needs and community development

Scenario definitions

Technical performance

Economic performance and Finance

Institutional issues

Socioeconomic and sociological issues

Uncertainties and risk/sensitivity

Project implementation

Sustainability - operation and maintenance

REFERENCES

- [1] L.H. Hansen and P. Lundsager, *A Review of Relevant Studies of Isolated Power Systems*. Risø-R-1109, 1999.
- [2] A. Pereira, H. Bindner, P. Lundsager, and O. Jannerup, *Modeling Supervisory Controller for Hybrid Systems*. 1999. 1999 European Wind Energy Conference, Nice.
- [3] C. Briozzo, G. Casaravilla, R. Chaer, and J.P. Oliver, *SIMENERG: The Design of Autonomous Systems*. pp. 2070-2073, 1996. WREC 1996.
- [4] H. Bindner and P. Lundsager, *On Power Quality Measures for Wind-diesel Systems: A Conceptual Framework and A Case Study*. 1994. EUWEC'94, Thessaloniki, Greece.
- [5] P. Lilienthal, L. Flowers, and C. Rossmann, *HOMER: The Hybrid Optimization Model for Electric Renewable*. pp. 475-480, 1995. Windpower '95 - Proceedings AWEA.
- [6] Renewable Energy Group. *INSEL Reference Manual - Version 4.80*, Dept. of Physics, Univ. of Oldenburg, 1993.
- [7] H.J. Green and J. Manwell, *HYBRID2 - a versatile model of the performance of hybrid power systems*. pp. 437-446, 1995. Windpower '95 - Proceedings of AWEA.
- [8] J.C. Hansen and J.O.G. Tande, *High Wind Energy Penetration Systems Planning*. pp. 1116-1120, 1994. EUWEC'94, Thessaloniki, Greece.
- [9] D. Infield. *Engineering Design Tools for Wind Diesel Systems. Volume 6 - Logistic Package: User documentation*. Energy Research Unit, Rutherford Appleton Laboratory, 1994.
- [10] J.O.G. Tande et al, *Power Quality and Grid Connection of Wind Turbines. Part 1: Stationary Voltages*. 1999.
- [11] J.O.G. Tande et al, *Hurghada Wind Energy Technology Center, Demonstration Wind Farm Studies - Power Quality Assessment*. NREARisø-I-1141(EN) 1997.
- [12] J.O.G. Tande et al, *Hurghada Wind Energy Technology Center, Demonstration Wind Farm Studies - Power System Operation*. NREARisø-I-1142(EN) 1997.

MODELLING SUPERVISORY CONTROLLER FOR HYBRID POWER SYSTEMS

Alexandre Pereira¹, Henrik Bindner¹, Per Lundsager¹ and Ole Jannerup²

¹Risø National Laboratory, P.O.Box 49, Roskilde, 4000 Denmark

Phone: +45 4677 5035, fax: +45 4677 5083, E-mail: *@risoe.dk

* = alexandre.pereira, henrik.bindner, per.lundsager

²Technical University of Denmark – DTU, Department of Automation

Building 326, Lyngby, 2800 Denmark

Phone: +45 4525 3580, fax: +45 4588 1295, E-mail: oej@iau.dtu.dk

ABSTRACT: Supervisory controllers are important to achieve optimal operation of hybrid power systems. The performance and economics of such systems depend mainly on the control strategy for switching on/off components. The modular concept described in this paper is an attempt to design standard supervisory controllers that could be used in different applications, such as village power and telecommunication applications. This paper presents some basic aspects of modelling and design of modular supervisory controllers using the object-oriented modelling technique. The functional abstraction hierarchy technique is used to formulate the control requirements and identify the functions of the control system. The modular algorithm is generic and flexible enough to be used with any system configuration and several goals (different applications). The modularity includes accepting modification of system configuration and goals during operation with minor or no changes in the supervisory controller.

Keywords: Wind-Diesel Systems, Control Systems, Models (Mathematical)

1. INTRODUCTION

Supervisory controllers play an important role in the performance and economics of hybrid power systems. Although the standard components used in hybrid systems have some kind of controller that allow safe operation, the optimal operation of a hybrid system can only be achieved through the use of a supervision process that analyses the system as a whole and decides the best mode of operation based on the specific goals of each application.

The task of supplying power to an isolated system (often remote places where technical assistance – operation and maintenance – is limited) is not elementary. In addition, the operation of weak grids, a prevalent characteristic of isolated systems, with large penetration of renewable power may face several technical problems [1].

In fact, hybrid power systems are still not popular because of the inherent difficulties associated to the power supply problem. The partial success of several pilot projects around the world showed some points that needed to be improved. Supervisory controllers are fundamental for integrating renewable energy into diesel power plants. The authors consider that there is a lack of robust and feasible control systems in the market that can be applied by designers into isolated systems with different characteristics.

The modular controller, a new concept described in this paper, is able to operate a hybrid power system in different applications, where the goals are distinct, without changing the control software. Furthermore it is not limited to any particular system configuration; it can connect any number of components of different sizes and types. The modularity includes accepting modification of system configuration – e.g. adding or removing components – during operation with minor or no changes in the supervisory controller.

This work presents the basis for the development and implementation of an intelligent and autonomous supervisory control system for hybrid power systems that

fulfils the developers/designers needs contributing to the success of future isolated systems projects. The paper describes the modelling of modular supervisory controllers and the use of object-oriented modelling technique as a methodology for developing the control system software.

2. THE MODULAR SUPERVISORY CONTROLLER

The term supervisory controller is not well defined and various interpretations exist. In this context, supervision refers to operation overview, planning & scheduling, co-ordination and execution of actions that improve performance and reliability. The dynamic control, i.e. the dynamic regulation of system variables, is not a task of the supervisory controller.

The following definition is general and compatible to the viewpoint described above: "A supervisory controller continuously monitors the operating state of the system and keeps it within the specified target domain. The supervisory controller takes actions to ensure that the system's operating goals are achieved and maintained in spite of uncertainties and resource constraints. It can also prevent safety critical system states and/or alleviate consequences of failures in system components."

The modular concept is an attempt to design supervisory controllers that are flexible enough to be included in very different applications, such as village power and telecommunication applications, without significant changes. This is possible because the modular controller can work with any hybrid power system configuration.

Standard input/output interfaces are the keys to build up different configurations with theoretically no limitations in number of components, type and size. The controller uses the common characteristics of the hybrid power systems components to implement a modular way of building a system. This can be understood as an abstraction

of the components' functions. A wind turbine and a diesel generator are both sources of power and can be grouped as a class of components. In the highest level of abstraction all components (loads, wind turbines, storage systems, etc.) have the same behaviour – they exchange electric power – and can be treated as identical objects.

Different applications may have distinct goals. The modular controller allows the designer/operator to define the main objective, for example: minimise generation costs, save fuel, supply firm power uninterruptedly. The definition of a main goal leads to the selection of a suitable operational strategy. The modular controller contains several control strategies that can be used to achieve different goals. Therefore an eventual modification of the main goal during system operation will not require new control software.

The modular concept provides the controller the capability to adapt to configuration changes as well as operation strategy changes which need to be performed when upgrading the system or when components' failures occur. This is an important feature when considering village power applications where load characteristics tend to change fast from year to year and system upgrade is often needed.

Designers will benefit from the modular controller by reducing development time and uncertainties related to the performance of the controller in applications with different characteristics.

The modular characteristics of the supervisory controller are presented below as features of the new concept:

- Flexible enough to control any hybrid power system architecture
- Accepts unlimited number of components (hardware limitation only)
- No restrictions on type or size of components.
- Different goals can be selected modifying automatically the control strategy
- No software modification is needed when changing system configuration (removing, adding or upgrading components)

3. MODELLING THE MODULAR CONTROLLER

The methodology used for designing the supervisory controller is based on the Object-Oriented Modelling Technique [2]. The first step is to carry out an analysis of the problem in order to obtain a concise and understandable model of the real world. The description of the physical system is usually a detailed representation of the physical mechanisms, their behaviour and interactions. In this work the system is described in a higher level of abstraction because the modular concept is not linked to any specific configuration.

On a high level of abstraction the physical system (a hybrid power system) comprises several units that exchange power with each other using a common network (grid). A supervisory controller can optionally be included. Rated power, instantaneous electrical power (produced or consumed) and operational status are some of the common characteristics belonging to all units of the superclass *component*.

Figure 1 shows part of the object diagram representing the hybrid power system and the specialisation of the superclass *component*. The power sources compose the class *generator*, the sinks are grouped into the class *consumer* and the storage devices are in the class *storage*. This high level representation of the hybrid power system is essential for the modularity of the controller. Part of the control logic is developed using abstract models – generators, consumers and storages – instead of real components (wind turbines, dump load, etc.) creating conditions for a generic code construction.

The real components are implemented as subclasses of generators, consumers and storage. Fig. 1 illustrates the specialisation of the class *consumer*. Consumers are classified as random and deterministic type. The former type includes the primary and deferrable loads, loads that are stochastic by nature. Deterministic consumers are well-defined loads – size and duration – usually used as dump load or as part of the load management strategy.

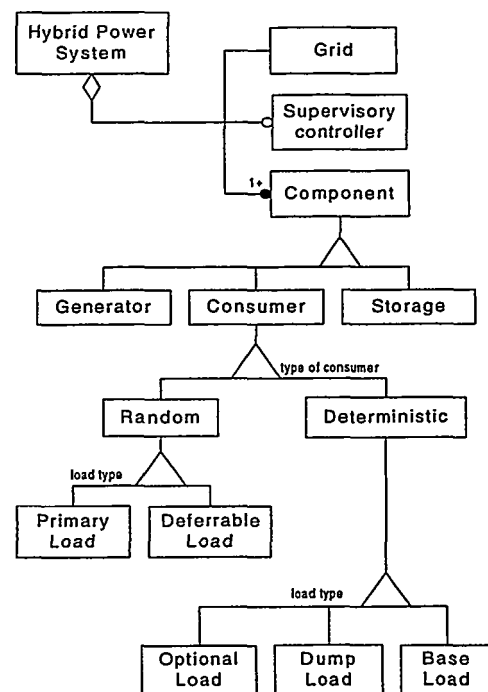


Figure 1: Partial object diagram representing a hybrid power system. Grid, component and supervisory controller are all part of a hybrid power system. There are three types of components: generator, consumer and storage. The generalisation of the class consumer is presented. The actual object model has much detail that is not shown.

The generator class is also specialised into two abstract classes: random and deterministic. Random generators are components whose power output are totally unpredictable and vary according to the current available energy resource. Wind turbines and photovoltaic panels are examples of random generators. Deterministic generators can attend constant or variable demand by adjusting their power output. Diesel generators are instances of this class.

3.1 Goals and Functions of the Supervisory Controller

Another important step of the analysis is to determine the control requirements, which are derived from the relations between the possible system states, the specified target domains and the actions required for maintaining system control.

The functional abstraction hierarchy technique [3] is used to formulate the control requirements and identify the functions (to be implemented as control algorithms) of the supervisory controller. The combination of whole-parts & means-ends abstraction hierarchy is used to investigate the supervisory controller goals and functions. In the highest hierarchical level the goal is "Optimise electricity supply". This goal is decomposed (whole-parts decomposition) into five sub-goals: "Maximise fuel savings", "Provide uninterrupted power supply", "Minimise generation costs", "Maintain good power quality" and "Reduce environmental impact". Each sub-goal can be decomposed in terms of a means-ends abstraction hierarchy describing bottom-up what components and functions can be used for, and, top-down, how purposes can be implemented by functions and components.

3.2 High Level Architecture of the Supervisory Controller

The basic modular structure of the supervisory controller as suggested in [4] is presented in Figure 2. The architecture is based on an organised collection of subsystems called modules, which can work independently and communicate with other modules. The arrows in the figure show the control flow from one module to another, it does not indicate the actual information flow in the decision making, i.e. it can not be implied from the diagram what would be the sequence of tasks executed by the controller.

The *input interface* module reads data from sensors, regulators and receives messages from other controllers (for example: wind turbine controller). It also allows the operator to supply information to the control system. The *data base* module is responsible for collecting, processing and storing data that can be analysed by an operator and/or accessed by another module of the control system. The *system identification* module interprets the information available from the *data base* and identifies the current status of the system based on state variables values and operational constraints.

The *scenario selection* determines the best control strategy that meets the goal without violating any constraints. This includes choosing the system mode of operation, which components to be switched on/off and changes of control parameters. The *planning and scheduling* module elaborates a plan of actions, i.e., a scheduled list of actions to achieve the mode of operation (strategy) determined by the *scenario selection*. The *dispatch management* executes the planned actions while dealing with the disturbances that were not predicted by the *planning and scheduling* module. The *output interface* module has an interface with the system components and sends commands to actuators, regulators and controllers.

The *critical situations planning* module contains pre-defined rules (actions) to compensate large disturbances in the system. It bypasses the basic decision model when safety critical system states are identified. The *expert systems* module is used to improve efficiency of the control algorithm.

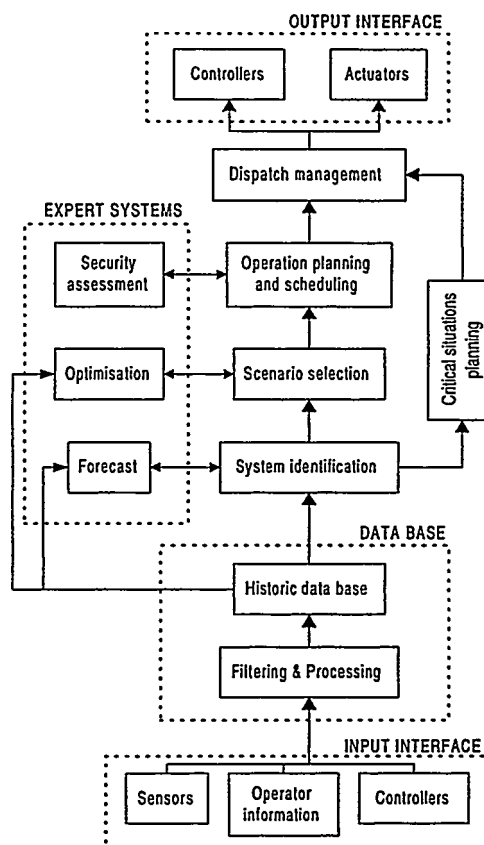


Figure 2: Block diagram of the supervisory controller architecture. Each block is a module, a subsystem that is implemented individually with weak links to other modules so it can be replaced without affecting the entire system.

3.3 Tasks of the Supervisory Controller

The decision model of Fig. 2 is the framework for classification and allocation of the controller tasks. The system goals and the model of the hybrid power system (object model) constitute the basic information used to define the control tasks. For each controller module (blocks of Fig. 2) a series of state diagrams is created describing the dynamic behaviour of the system, i.e., the pattern of activity for the controller, the relation between states and events.

Figure 3 presents part of the state diagram for the module *scenario selection*. This example shows the dynamic behaviour of the controller when an event "high frequency alarm" occurs. The "power surplus" state measures the alarm severity (alarm level) and points to the next state. The select actions diagram showed in the figure, which is the state activated by a first level alarm, starts with the "available components" state. A selection of component objects is made based on the status attribute. A status OK means that the component is either operating at normal conditions or ready to start. A status ERROR represents a condition of failure, SERVICE means it was stopped for maintenance, and so on.

The next state "listing possible actions" builds up a list of possible actions to compensate the alarm. Note that a rule-based system can be used to determine the strategy based on the alarm type. In this example, the high

frequency alarm indicates power surplus and defines two basic strategies: a) connect a consumer and b) switch off a generator. This exemplifies how the modular control algorithm can be implemented using the high-level object information included in the abstract superclasses.

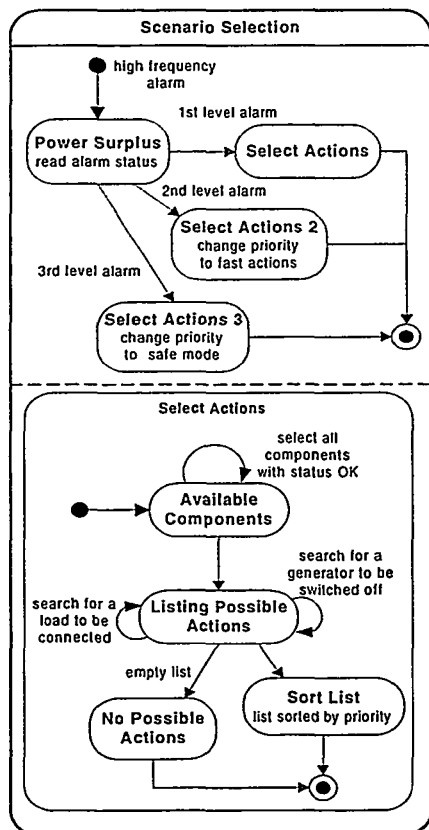


Figure 3: Part of the state diagram for the module Scenario Selection. The input is the alarm information from the system identification and the output is a list of possible actions to compensate the alarm.

The "sort list" state receives the complete list of possible actions and sort it by priority based on the system main goal. For example, considering the goal save fuel the action *switch off diesel generator 3* would have priority over *switch off wind turbine B* and also over *connect optional load 2*. Using another goal for the system the action *switch off wind turbine B* could have received the first priority and the diesel generator, requested to be running as spinning reserve, would be the last priority. Therefore the same control algorithm can be used in different applications having different goals.

4. MODULAR ALGORITHM

The program structure models the structure of the real world problem. A hybrid power system consists of distinct components that interact with each other, and the control software comprises a number of different objects that represent the real world components. Each object encapsulates information (characteristics) about a real component in its computational model that enables it to

perform operations (for example: start-up, power generation, etc.) and interact with the entire system. Knowledge about the dynamics of the components can be included in the object models and used by the supervisory controller to reason about starting/stopping procedures.

The control logic is developed using the high-level abstractions of components and several system goals. The result is a generic algorithm that can control any hybrid power system and achieve different goals. The algorithm remains unchanged also when adding components with different characteristics of those already implemented. The new objects, representing the new components, inherit the attributes, operations and relations of their superclasses which is the necessary information for the controller reasoning.

5. CONCLUSION

The present study focused on basic aspects of modelling modular control systems. The results described in this paper delineate the first phase of a project to design and implement an intelligent, autonomous and modular supervisory controller for hybrid power systems.

The object-oriented modelling technique is an adequate tool for developing control software with modular characteristics. It allows the construction of pre-defined classes that interact with each other in a high level while all detailed information about the real world is encapsulated in the objects. The modular algorithm is generic and flexible enough to be used with any system configuration and several goals (different applications). The modularity includes accepting modification of system configuration and goals during operation with minor or no changes in the hardware and software of the supervisory controller.

Computer simulations are currently being conducted to demonstrate the effectiveness of the modular design. This work will be reported later. The development process will be concluded with the hardware implementation and experimental tests at Risø National Laboratory.

6. ACKNOWLEDGMENT

The research activities of Alexandre Pereira are sponsored by the Brazilian Research Council - CNPq. The support provided by Risø National Laboratory, Technical University of Denmark - DTU and the Brazilian Wind Energy Centre is acknowledged.

7. REFERENCES

- [1] J.A.Pecas Lopes, Operation of Isolated Systems with a Large Penetration of Wind Power Generation, Proceedings 5th Symposium of Specialists in Electric Operational and Expansion Planning, (1996) IP-43.
- [2] J.Rumbaugh et al., Object-Oriented Modeling and Design, Prentice Hall International, (1991).
- [3] M.Lind, Modelling Goals and Functions of Complex Industrial Plants, Applied Artificial Intelligence, 8, (1994) 259-283.
- [4] A.L.Pereira, Supervisory Controller for Hybrid Power Systems, Report of Seminar Modelling for Intelligent and Supervisory Control, Technical University of Denmark, (1998).

ASSESSMENT OF WIND TURBINE LOAD MEASUREMENT INSTRUMENTATION

E.Morfiadakis¹, K..Papadopoulos¹, N. van der Borg², S.M.Petersen³, H.Seifert⁴

1. CRES, 19th Km Marathonos Ave., GR-190 09, Greece, Tel. +301 6039 900, Fax +301 60 39 905
2. ECN, Petten 1755 ZG, P.O. Box 1, The Netherlands, Tel. +31 (0) 224 56 4233, Fax. +31 (0) 224 56 3214
3. RISO, P.O.Box49, 4000 Roskilde, Denmark, Tel. +(45) 46775042, Fax. +(45) 4677 5083
4. DEWI, Ebertstr. 96, Wilhelmshaven 26384, Germany Tel. +49 4421 4808 – 0, Fax. +49 4421 4808 – 43

ABSTRACT: In the framework of Sub-Task3 "Wind turbine load measurement instrumentation" of EU-project "European Wind Turbine Testing Procedure Development", the load measurement techniques have been assessed by laboratory, full scale and numerical tests. The existing methods have been reviewed with emphasis on the strain gage application techniques on composite materials and recommendations are provided for the optimisation of load measurement techniques.

Keywords: Test methods, strain gages applications, composite materials, standards.

1.INTRODUCTION

Load measurements on wind turbines (WT) have become an important tool in the development of wind turbine design. The load measurements are used by European certifying authorities, becoming mandatory in some cases. The adjustment of several wind turbine model inputs strongly depends on the accuracy of load measurements.

Considerable effort and resources have been spent in a number of national and European Union projects with the objective of performing load measurements on wind turbines. In the framework of the Joule II project "European Wind Turbine Standards" [1], adequate guidelines were developed for load measurements and the IEC TC-88 has initiated a working group for the same purpose. The acquired experience has shown that there are a number of drawbacks in the procedure for measuring the loads on the various wind turbine components and in the evaluation technique.

The "European Wind Turbine Testing Procedure Development" project (SMT4-CT96-2116) aims to develop and improve specific measurements and testing methods for WT within the European Community supplementing the standardisation work in CENELEC BTTF83-2, IEC TC88 and the EWTS-II-JOULE-III project. The objective of the project sub-task 3 "Wind turbine load measurement instrumentation" addressed by CRES, DEWI, ECN and RISOE is to provide a qualitative assessment of wind turbine load measurements and suggest improved measuring and interpretation methods with emphasis on the strain gage application techniques on composite materials. The goals of this work assist in a better understanding and a more careful realisation of WT load measurements:

- comprehensive inventory of error sources in the common load measurement techniques,
- documentation of the cross talk and temperature effects (blade, hub, tower and shaft load measurements) based on the laboratory, simulation and full-scale work performed by the participants,
- general methodology for determining the combined uncertainty of load measurements.
- empirical methodology for correcting the zero-drift of load signals,
- recommendations and guidelines for improvement of measuring methodologies and of data processing.

2.REVIEW OF PROBLEMS IN LOAD MEASUREMENTS

The standard technique is based on strain gage configurations properly selected to resolve the desired load component. It has proven successful for measurements on metal components (tower, blade extender, and shaft). However, problems arise for strain measurements on composite materials. The transformation from the measured strain to the estimated load involves a chain of assumptions and error sources.

2.1. Strain measurement

The strain measurement is sensitive to the choice of location of strain gages, their bonding and protection method, misalignment errors and transverse sensitivity, temperature/humidity effects, errors associated to the performance of the Wheatstone bridge. The strain gages should be applied at a point with a measurable strain level, in a uniform area avoiding stress concentration regions (steel preferable to composite materials). The strain gage selection criteria [2] relate to the definition of the measurement problem, the identification of both the electrical and mechanical conditions at the point of measurement and the application conditions (component material, access, cabling). Due to the specific mechanical, thermal and chemical properties of composite materials, some of the aforementioned errors which can be neglected in strain measurements on metal components become significant in composite material measurements ([3] and [4]). In this case, the non-homogeneity of the strain field, the low thermal conductivity of composites, the variation of the thermal expansion coefficient of the composite with direction and location should be considered. Methods for overcoming the temperature effect involve properly selected self-temperature compensated strain gages, use of dummy strain gages and pre-calibration of strain gage output vs. temperature changes.

2.2. Stress/Strain relations on measuring section

In orthotropic materials, the stress-strain relation is described by the thermoelastic constitutive relation that includes the temperature and moisture concentration effects. Problems are related to hygrothermal stresses in the measured material and to the spatial and directional sensitivity of strains in stress concentration regions.

2.3. Translation of loads to stresses

Configurations for measuring tensile, bending and torsion loads are summarised in [5]. The proper selection of strain gage configurations may eliminate the temperature effect of load measurements in isotropic materials. A critical point is that the stress field of the measuring section depends on the load distribution, the material and geometric properties (including the relative location of elasticity, shear and mass centres). Misalignment of these centres results to coupling of loading stresses, e.g. axial forces may produce bending moments. These effects introduce errors in the interpretation of the calibration results.

2.4. Calibration procedures

The mechanical calibration of strain gage load transducers is performed on-site as described in [1]. It has been noted that loads in other parts of the hub structure may affect the validity of blade load measurements and an improved method has been proposed [6]. The calibration uncertainty is associated with the regression procedure of calibration data, the force measurement or estimation (magnitude, point and direction of application), the contamination of the calibration load from aerodynamic forces, and the applicability of static calibration results to the dynamic measurements.

The electrical (shunt) calibration can be used either as a frequent offset verification of strain gage bridges, or as the main calibration procedure. The latter case is applicable only for metal structures and well-defined material and geometric characteristics so that the stress/strain relations are unambiguously defined. The uncertainty is associated with the shunt resistor value, gage factor, the material stiffness data and the geometry of the measuring section.

2.5. Measurement uncertainties

It has been realised that the ISO guide [7] does not provide sufficient information for dealing with all aspects of the load measurements (i.e., calibration, time series, equivalent loads, rainfall matrices).

3. ASSESSMENT OF BLADE LOAD MEASUREMENTS

An error assessment of strain gage signal interpretation in common experimental practices has been performed based on laboratory tests, numerical simulations and existing data from full-scale campaigns to address the cross talk effects (axial force, shear forces, edgewise/flapwise bending moment, torsional moment), aspects of the measurement configuration, calibration practices and temperature effects (loading under different ambient temperature levels, loading with temperature difference between opposite blade surfaces, correction methodologies).

Laboratory tests have been performed by CRES [8] on an AERPAC APX25 glass reinforced epoxy blade (length 12.05m) and by ECN on the inner 6-m section of a DEBRA prototype blade provided by DEWI [9].

Simulation tests have been performed by CRES for a 10m-prototype FRP blade of the WINCON 110 kW wind turbine using a finite element model (EMRC-NISA II). ECN applied the finite element modelling code ANSYS-linear plus on the DEBRA blade [10] to investigate the

possibility of selecting a suitable location for applying strain gages where cross talk is minimised and to compare with the laboratory results.

Four full-scale blade load databases were analysed by CRES (TACKE 500kW stall, HMZ-Windmaster 300 kW pitch free yaw, AOA 100 variable speed) and RISO (VESTAS V27 pitch) to compare the order of magnitude of errors with the simulation and laboratory tests results [11].

Although the quantitative estimates differ according to the blade tested or between laboratory and simulation tests, it is verified that the basic error source for blade load measurements on the composite material is the temperature effect. The following refer to measurements on the blade composite material unless otherwise stated.

Temperature effect. Strain gage measurements are contaminated by temperature variations due to thermal stresses from differential thermal expansion of different parts of the construction and to apparent strains caused by the mismatch of the thermal expansion coefficient between the strain gage and the measured material. The temperature effect is affected by the loading and thermal conditions of the blade and the time scale of the temperature variations. The errors are caused by the diurnal temperature cycle and most importantly by the direct solar heating of the blade surface. Although the numerical simulations indicate that the first effect is negligible, this is due to the assumption of a homogenous blade temperature distribution. The actual conditions encountered by the wind turbine blades indicate that the development of temperature gradients along the blade may induce load errors of 1% to 10% per degree of temperature deviation from the reference calibration temperature (parallel configuration). The errors are more important for the edge than for the flap bending moment increasing with the intensity of the solar radiation.

For measurements on the blade extender using the parallel bridge configuration, zero drift is reported due to the solar radiation effect (differential blade heating). The errors are minimised for T-bridges.

For measurements on the composite blade material, the use of T-rosettes gives larger temperature-induced errors than the parallel configuration due to the anisotropy of the material. The temperature effect is equally important for the flap/edge and the +/-45 degrees configurations.

The temperature effect may be significantly reduced through pre-calibration of the load transducer response against the ambient or blade skin temperature. An empirical, but more effective, methodology to correct for the zero-drift of the strain gage bridges irrespective of its source is to determine the reference 'mean load vs. power' curve against which all measurements should be corrected. The reference curves can be determined from measurements over a short time period characterised by acceptable small variations of the ambient temperature and of humidity conditions [11].

Cross-talk effects. The cross talk of the flap bending moment on the edge bridge signal and vice versa should be always quantified in calibration practices, especially for the +/-45 arrangement. The axial and shear forces do not induce errors in the flap and edgewise signals. The cross talk effect of the torsion moment on the flapwise and edgewise signals cannot be definitely excluded. However, in view of the severity of the temperature effect, any

suggestions for including the measurement of the torsion in blade load measurements would be premature.

Calibration practice. The on-site blade load calibration can be reliably performed by applying external loads to define the response matrix. The offsets may be derived by continuous sampling of calibration data during slow rotor revolutions at low wind [12]. A practical and economic calibration procedure is the use of the blade weight as the unique calibrating load provided that accurate data on blade weight and centre of mass are available and that the rotor cone angle is non-zero. The latter requirement is important when the blade bending moment strain gage bridges are aligned with the blade global co-ordinate system.

Assessing the calibration reproducibility in the fully controlled laboratory conditions, it has been found that an overall standard deviation of calibration coefficients compiled from several calibration sessions involving differences in ambient temperature and humidity, point and direction of load application is on the order of 2-3% of their average values [11]. The position of the calibrating forces does not definitely affect the calibration reliability.

4. ASSESSMENT OF HUB LOAD MEASUREMENTS

The error assessment in relation to material and geometric properties has been numerically performed by RISO for a standard spherical hub using the finite element model COSMOS/M version 1.75A [13].

The analysis verified experimental findings indicating that loads from the other legs of the hub can be transferred through the complex hub geometry to the measurement location. The cross talk errors are more important for the edgewise than for the flapwise load measurements and are enhanced by the presence of a hole close to the measurement region. The parallel bridge configuration performs better than the T-configuration, as far as cross talk errors are concerned.

The change of load distribution, i.e. due to one bolt in the blade-to-hub flange not being well tightened, does not result to significant errors in the bending moment measurements. The measurements are practically insensitive to a doubling of the stiffness of the flange for the parallel configuration. The application of T-rosettes would result to increased errors for a less stiff flange.

The "stiffness of the hole" is very important. Therefore, measurements on a "soft" hub could give even larger errors in the bending moments.

5. ASSESSMENT OF TOWER LOAD MEASUREMENTS

Strain gages for measuring the tower base bending moment in two perpendicular directions are normally applied at some distance above the access door, the distance being dictated by the maximum door width. The unfavourable condition of measuring at a horizontal level passing through the mid-height of the door due to space or access limitations has been numerically addressed by CRES [11]. Full-scale tower load measurements performed by CRES on two wind turbines (AOA 100 kW stall, variable speed and TACKE 500 kW stall) were further analysed to assess temperature effects, cross-talk effects and calibration practices.

Temperature effects. Existing full-scale measurements have not indicated significant errors when using parallel bridges for measuring the bending moment components. However, the use of T-rosettes effectively compensates the temperature effects.

Cross-talk effects. The errors for the case of measurements near the tower access door using the results of a finite element numerical code are negligible for the main bending moment component, while larger errors are calculated for the lateral component of the bending moment depending on the direction of load application [11]. Therefore, valid measurements for the tower bottom bending moment components can be performed even at a level intersecting the door opening. Based on the available full-scale database, the values for the cross talk effects between the two bending moment signals have been found smaller than the uncertainty due to an error of 1 degree in the direction of the load application.

Calibration practice. The calibration of strain gages for measuring bending moment components is performed by applying external loads on the tower. The zero-load readings are evaluated by slowly rotating the nacelle over one complete revolution.

6. SHAFT LOAD MEASUREMENTS

No measurable cross talk or temperature effect has been estimated from the analysis performed by CRES on its extensive database from a WINCON 110 kW stall wind turbine [11].

7. GUIDELINES-RECOMMENDATIONS

7.1. Review of current available guidelines

Guidelines on the mechanical load measurements have been developed in the course of the EWTS-Joule II programme [1] addressing the general issues of sensor types, choice of location, strain gage practice and arrangement and calibration procedures providing general guidance. The missing items of the available information refer to the systematic quantification of the errors related to the cross talk effects, the temperature effects, the zero-drift, the uncertainty analysis procedure and methods for improving the current measuring methodologies. Additional information is provided by the numerical simulation, laboratory and full-scale tests performed within this subtask.

7.2. Sensor selection and measurement configurations

The general requirements outlined in [1] should be followed. The use of T-rosettes should be avoided for blade load measurements on the composite material (due to the combination of temperature effect with the orthotropic nature of reinforced composite laminates) and for hub load measurements (due to the complex geometry that induces cross talk), but are recommended for tower load measurements and blade root measurements on the extender.

7.3. Calibration practice

The calibration of load sensors can be performed by applying external loads (measured loads, blade weight, tower head weight) and verified by frequently repeated slow rotations of the rotor or nacelle at calm winds. The corresponding procedures are well documented. The

processing should include the calculation of the off-diagonal elements of the calibration matrix, at least for blade load measurements. These 'cross-talk coefficients' should be included in the interpretation of load signals, if they are statistically significant against the calibration uncertainties.

7.4. Cross-talk and temperature effects

The cross-talk effects are significant for load measurements on the hub and on the composite blade material. They can be neglected in the shaft, tower and blade extender load measurements.

For measurements on the composite blade material, the cross talk between the flap and edge bending moments should always be considered. The parallel bridge configuration for bending moment measurement should be preferred to T-rosettes.

Hub measurements should not be performed by strain gages on one hub leg only, due to the existence of cross talks from the bending moments at the other two legs. The parallel bridge configuration for bending moment measurement should be preferred to T-rosettes.

The most important error source for measurements on the blade composite material is the temperature effect induced by the differential heating of opposite blade surfaces and by changes in the environmental temperature and humidity. Measurements performed in a wide range of environmental conditions may become inconclusive unless proper clipping of the database is done. The two best correction methodologies are the calibration of sensor sensitivity against temperature changes and the compilation of the 'reference' mean load vs. power curves from measurements performed during a short time period, when the ambient conditions are practically constant. The second methodology implies that, once the reference load vs. wind speed curve has been established, all future measurements are shifted accordingly to force their mean value to conform with the reference curve. This approach assumes that the sensitivity coefficients are unaffected and that turbulence effects on the mean loading are negligible.

The observation that the larger temperature errors are found in T-rosettes is an additional reason for discouraging their use in all blade measurements except when performed on the blade extender.

The T-rosettes should be preferred in tower bending moment load measurements, because they offer adequate temperature compensation. However, the temperature errors for parallel bridges appear tolerable.

In concluding, data should be carefully examined to reveal the effect of ambient temperature and humidity variations. Validity criteria should be defined and zero-drift correction schemes need to be developed even for measurements on the blade extender, otherwise only data for a narrow, well-defined range of environmental conditions should be used.

7.5. Uncertainty estimation for load measurements

The uncertainty sources to be taken into account are the calibration uncertainty (due to uncertainties in the measurement of the distances, direction and value of calibration loads), the signal uncertainty and the wind speed uncertainty. A procedure has been developed [14] involving numerical combination of standard uncertainties

for the case of equivalent loads and rainflow matrices through Monte-Carlo calculations.

The procedure applies when temperature/humidity and zero-drift effects have been eliminated through proper clipping of the database or application of correction schemes. However, either of the two approaches contributes to the combined uncertainty.

Acknowledgements. The authors are indebted to EU/DGXII and the Greek General Secretariate for Research and Technology for co-funding the SMT4-CT96-2116 project.

REFERENCES

- [1] Seifert H. et al.: 'Mechanical load measurements', EWTS J0U2-CT93-0387 final report, vol.6 (1996).
- [2] Hoffmann K.: 'An introduction to measurements using strain gages', HBM GmbH (1989)
- [3] Manual on experimental methods for mechanical testing of composites, SEM (1989)
- [4] Perry C.C.: 'Strain gage measurements on Plastics and Composites', Measurements Group, Technical Note.
- [5] Hoffmann K.: "Applying the Wheatstone bridge circuit", HBM vd72001e.
- [6] Dahlberg J., Johansson H.: 'Calibration procedures for improved accuracy of wind turbine blade load measurements', Proceedings EWEC'96, Goteborg Sweden, pp.1023 (1996).
- [7] ISO 1993 'Guide to the expression of uncertainty in measurement' (ISBN 92-67-10188-9)
- [8] Papadopoulos K., Morfiadakis E.: "Laboratory test for blade load measurements", CRES.WE.SMT4T3.04 (1998)
- [9] N.J.C.M. van der Borg and J.J.D. van Dam: "The experimental quantification of specific uncertainty sources in wind turbine blade load measurements"; ECN-C-98-105.
- [10] Hamelink, J.J. Heijdra, N.vanderBorg: "Numerical quantification of cross talk in load measurements on the DEBRA blade", ECN-C-98-073 report.
- [11] Papadopoulos K., ed. 'Wind turbine load measurement instrumentation'-Final Report Sub-Task3 of SMT4-CT96-2116. (1998)
- [12] Foussekis D., P.Chaviaropoulos: "On-site calibration of strain gauges for blade load measurements", CRES.WE.SMT4T3.08 Report (1998)
- [13] Jørgensen E.R., S.M. Pedersen: "Validation of Strain Gauge Measurements Using Finite Element Modelling", RISO report (1998)
- [14] N.J.C.M. van der Borg and J.J.D. van Dam: "Procedure for the evaluation of uncertainties in load measurements in wind turbines, ECN-C-98-006.

Bibliographic Data Sheet**Risø-R-1114(EN)**

Title and author(s)

Contributions from the Department of Wind Energy and Atmospheric Physics to EWEC'99 in Nice, France

Edited by Gunner C. Larsen, Kirsten Westermann and Per Nørgård

ISBN

87-550-2542-0

ISSN

0106-2840

Dept. or group

Department of Wind Energy and atmospheric Physics

Date

March 1999

Groups own reg. number(s)**Project/contract No.**

Pages

256

Tables**Illustrations****References**

Abstract (Max. 2000 char.)

The first conference following the merger of the series of European Union Wind Energy Conferences and the European Wind Energy Conferences – EWEC'99 – was held in Nice, France during the period 1–5 March 1999. About 600 delegates, mainly from Europe but also from other parts of the world, attended the conference. The conference contributions included 96 oral presentations and 305 posters.

The Department of Wind Energy and Atmospheric Physics contributed with 29 oral presentations and 36 posters with members of the department as authors or co-authors. The present report contains the set of these papers available at the deadline 19 March 1999. The contributions cover a wide spectrum of subjects including wind resources, aerodynamics, reliability and load assessment, grid connection, measurement methods, innovative wind turbines and market aspects.

Descriptors INIS/EDB

AERODYNAMICS; MEETINGS; RISØE NATIONAL LABORATORY; TURBULENCE; WIND; WIND LOADS; WIND POWER; WIND TURBINES

Available on request from:

Risø Library, Risø National Laboratory (Risø Bibliotek, Forskningscenter Risø)

P.O. Box 49, DK-4000 Roskilde, Denmark

Phone (+45) 46 77 46 77, ext. 4004/4005 · Telefax (+45) 46 77 40 13